Okinawa Institute of Science and Technology
Graduate University

Thesis submitted for the degree

Doctor of Philosophy

Spin–1 Magnets and Their Excitations

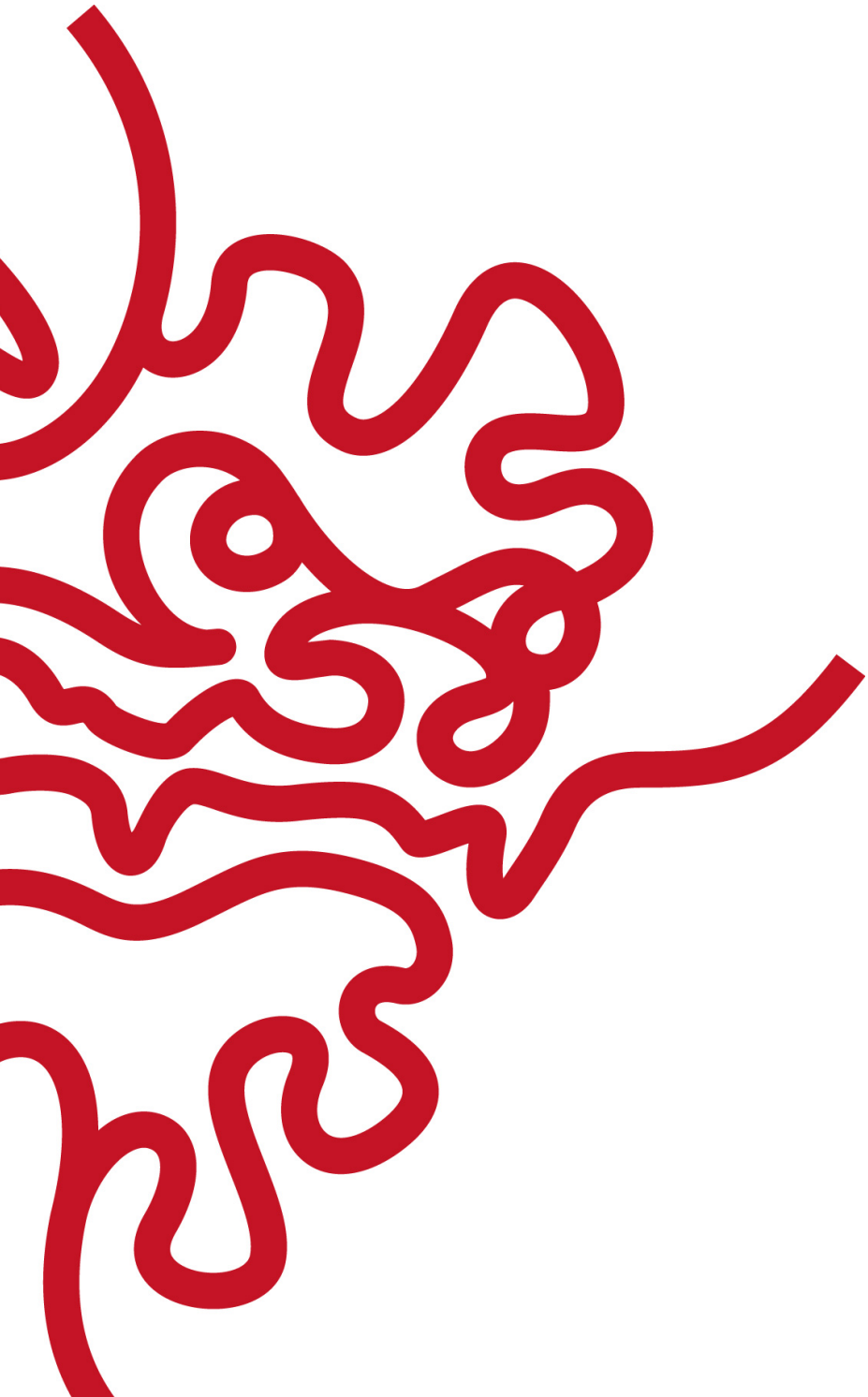

by

Kimberly Remund

Supervisor: **Nic Shannon**

November 2022

Declaration of Original and Sole Authorship

I, Kimberly Remund, declare that this thesis entitled *Spin–1 Magnets and Their Excitations* and the data presented in it are original and my own work.

I confirm that:

- No part of this work has previously been submitted for a degree at this or any other university.
- References to the work of others have been clearly acknowledged. Quotations from the work of others have been clearly indicated, and attributed to them.
- In cases where others have contributed to part of this work, such contribution has been clearly acknowledged and distinguished from my own work.
- None of this work has been previously published elsewhere, with the exception of [201] K. Remund, R. Pohle, Y. Akagi, J. Romhányi, and N. Shannon, *Semiclassical simulation of spin-1 magnets*, Phys. Rev. Research, **4** 033106 (2022).

Date: November 2022
Signature:

Abstract

Nature sometimes arranges itself in extremely curious ways, sowing the seed of very intriguing physics. Magnetic systems offer a rich variety of interesting features. They are traditionally studied in either their classical ($S \to \infty$), or their extreme quantum limit ($S = \frac{1}{2}$). However, magnetic degrees of freedom in spin systems span within a whole spectrum range and do not necessarily reduce to the specific case found at the extremities. Spin–1 magnets provide a good example of what happens to ground state and excitations properties for such instance. Indeed, a spin–1 is special, in the sense that, besides displaying dipolar degrees of freedom, a spin–1 can also exhibit on-site quadrupolar degrees of freedom, while retaining its quantum characteristics. Therefore, spin–1 systems are often used as examples to refer to spin-nematic order in magnetic insulators, Fe-based superconductors, or cold atoms. Unlike for spin–$\frac{1}{2}$, which in the classical limit can be represented by an O(3) vector, for spin–1, an O(3) vector does not completely describe all of what a spin–1 can do, namely intrinsically exhibiting quadrupoles. In this Thesis, I develop a united framework that enables us to treat dipolar and quadrupolar degrees of freedom of a spin–1 moment on an equal footing. My method is based on the extension of the usual $su(3)$ algebra describing a quantum spin–1 into the $u(3)$ algebra. Within the $u(3)$ formalism, I derive equations of motion (EoM) for the objects living in the $u(3)$ algebra. The u(3) approach enables the appropriate formulation for both classical and quantum derivations. Moreover, the EoM take a simple form suitable for numerical implementation. I illustrate this method by applying it to the well-known Bilinear-Biquadratic model on the triangular lattice for the ferroquadupolar state. This study is supported through classical low-temperature expansion in order to probe the thermodynamical properties, as well as quantum multi-bosons theory that allows to access dynamics. These results are validated by comparison with numerical simulations classical Monte Carlo (MC) and Molecular Dynamics (MD) respectively, both expressed in terms of $u(3)$ objects. I show that at sufficiently low temperature numerical simulations can be corrected for the classical statistics, and the fully quantum zero-temperature analytical results are retrieved. Additionally, I confirm that our method is also applicable to anisotropic models, which is of experimental relevance. Finally, some new ideas, including the description of topological defects in spin–1 magnets and the generalization of the commonly used Self-Consistent Gaussian Approximation to the degrees of freedom of a spin–1 expressed within our $u(3)$ framework are explored.

Acknowledgment

I would like to first express my gratitude to all my friends that I am lucky to have encountered during my time at OIST. There are too many of them to be listed here, but I would like to especially thank my dear friends Nishtha and Chrispy who have always shown support and with whom I will recall many exceptional memories including all the interesting adventures we spent together in Okinawa, in its surrounding islands, as well as various parts of Japan.

I also want to acknowledge my successive roommates, Yaz, Dani, and Amy for sharing not only furniture but also a great sense of camaraderie. And even though, neither Yaz nor Dani share the same roof as me right now, I am honored that we are still very good friends. I am especially thankful to Miso and Taro, Dani's and Amy's respective cat, for always agreeing with me, despite all the unphysical nonsense I sometimes divulge about. They have shown unbetrayed loyalty and are an exceptional source of encouragement.

I also would like to thank Momo, my favourite neighbor, who provided the needed fuel to finish this Thesis in forms of Haribos and Lindt chocolate.

I am also thankful to Yuka, Joel, Makoto, and Darshini who are always happy to dance and train, despite also being busy Ph.D. students. I am glad we had many cycling trips, which often started before sunrise, and that will stay engraved in my memory. Besides sports, I am happy to have shared various and tasty culinary experiences with them as well, including the monthly tradition of Big Dip Day Blue Seal ice cream, as well as our less regular but always fun cooking events in the community kitchen.

I also wish to thank all the members of the OIST street dance club for trusting me and allowing me to share my passion for dance and body motion. These classes have been a great support, especially during times when social gatherings were more difficult due to the global pandemic.

I am very grateful to the Ishikawa Dojo, where I was able to learn an Okinawan style of Karate under the leadership of Sakumoto sensei, Shimizu sensei, and more recently Ryusei Sensei. Every practice brings me joy and allows me to forget the equations for 3 hours a week, which without a doubt helps preserve my mental sanity.

Nic Shannon, my supervisor, to whom I am deeply thankful for guiding me on the path to Ph.D., and hopefully beyond it as well, has been of great support. His enthusiasms about physics and his caring for all unit members are a source of inspiration.

Academically, I have become the scientist I am today thanks to all the people I was lucky to work with, including my collaborators, Prof. Yutaka Akagi and Dr. Rico Pohle, whom scientific expertise and valuable simulation results have been an important pillar to support the work presented in this thesis.

Judit, my friend and collaborator, has always been an inspiring model and also had an important impact in my academic life.

I am also grateful I have come to meet all wonderful former and current TQM members and befriended many of them, including Leilee and Ananya, as well as Geet.

I wish to acknowledge our research admin, who solves many important and impactful problems for us, so we can focus on solving different, hopefully still important and impactful problems ourselves, and who is also responsible for deserving snacks, which consumption has definitely increased since the beginning of the writing of this thesis, and therefore played an important role at keeping me functional.

Lastly, I am glad I was able to carry out my Ph.D. at OIST in Okinawa. It is a beautiful island, and despite its relatively small size, it is quite dynamic and there is always something that awaits to be discovered.

Abbreviations

AFM	anti–ferromagnetic
AFQ	anti–ferroquadruploar
AKTL	Affleck–Kennedy–Lieb–Tasaki
BBQ	bilinear biquadratic
DMRG	density matrix renormalization group
DTF	density functional theory
ED	exact diagonalization
EoM	equations of motion
FM	ferromagnetic
FQ	ferroquadruploar
FW	flavor–wave
KT	Kosterlitz–Thouless or Berezinskii–Kosterlitz–Thouless
LCs	liquid crystals
LSW	linear spin–wave
MF	mean–field
MC	Monte Carlo
MD	molecular dynamics
NMR	nuclear magnetic resonance
SOC	spin–orbit coupling
SCGA	self–consistent Gaussian approximation
QMC	quantum Monte Carlo
TR	time–reversal
u3MC	Monte Carlo based on a $u(3)$ representation
u3MD	molecular dynamics based on a $u(3)$ representation
VBS	valence bond solid

Nomenclature

$\hbar$	Planck constant ($1.054\ 572\ 66 \times 10^{-34}$ Js)
k_B	Boltzmann constant ($1.380\ 658 \times 10^{-23}$ JK^{-1})

To Miso and Taro, for their unconditional feline
support and unscrupulous biting.

Contents

Declaration of Original and Sole Authorship iii

Abstract v

Acknowledgment vii

Abbreviations ix

Nomenclature xi

Contents xv

List of Figures xix

List of Tables xxix

1 Introduction: Why am I Even Doing This? 1
- 1.1 The Advent of Quantum Mechanics and Magnetism . . . 1
  - 1.1.1 Historical Prelude . . . 1
  - 1.1.2 Origin of Magnetic Moments . . . 5
  - 1.1.3 Origin of Magnetic Interactions . . . 6
- 1.2 What Makes Spin–1 Special . . . 14
  - 1.2.1 Single Spin–$\frac{1}{2}$ . . . 14
  - 1.2.2 Single Spin–1 . . . 16
  - 1.2.3 Polygamous Spin–1 . . . 18
  - 1.2.4 Spin Nematics . . . 19
  - 1.2.5 Spin–1 1D–Chains . . . 23
- 1.3 Spin–1 Nowadays . . . 24
  - 1.3.1 Spin–1 in the Wild . . . 24
  - 1.3.2 Spin–1 in the Zoo . . . 32
- 1.4 And us in All That? . . . 37

2 U(3) as an Algebra for Spin–1 45
- 2.1 A Little Bit of Group Theory . . . 45
- 2.2 A Little Bit of $su(2)$ . . . 48
  - 2.2.1 Description of a Single Quantum Spin–$\frac{1}{2}$ . . . 48

2.2.2 SO(3) vs SU(2): Both Describe a Spin–$\frac{1}{2}$ 49
2.3 A Bit More to Make $su(3)$ 51
2.4 From $su(3)$ to $u(3)$ 55
2.4.1 Description in Terms of $u(3)$ 55
2.4.2 Relationship Between $U(3)$ and $SU(3)$ Representations 56
2.4.3 Mathematical Properties of A–matrices 58
2.4.4 Representation of the BBQ Model Within a $u(3)$ Formalism . . 59
2.4.5 BBQ Hamiltonian and Equations of Motion in u(3) 61
2.5 $u(3)$ as a Basis for Analytical Theory 62
2.6 $u(3)$ as a Basis for Numerical Simulation of Spin–1 70
2.6.1 Monte Carlo Simulations Within $u(3)$ Framework 71
2.6.2 Molecular Dynamics Simulations Within $u(3)$ Framework 74

3 Classical Thermodynamics of the FQ-State of the BBQ Model on the Triangular Lattice 79
3.1 Expansion of Small Fluctuations 79
3.2 Classical Theory of Fluctuations 84
3.3 Classical Low Temperature Expansion 87
3.3.1 Expression for Free Energy 88
3.3.2 Specific Heat 89
3.3.3 Classical Structure Factors 90
3.3.4 Structure Factors Classically at $\mathbf{q} = 0$ 94
3.3.5 Structure Factor for Dipole Moments 96
3.3.6 Structure Factor for Quadrupole Moments 97
3.3.7 Structure Factor for A–matrices 98
3.3.8 Sum Rule for Structure Factors 98
3.3.9 Ordered Moments 99
3.4 Comparison with $u(3)$ Monte Carlo Simulations 99
3.4.1 Heat Capacity 100
3.4.2 Ordered Moment 101
3.4.3 Equal–Time Structure Factor 103

4 Semi-Classical Dynamics of the FQ State of the BBQ Model on the Triangular Lattice 107
4.1 Quantum Fluctuations 107
4.1.1 Quantum Thermodynamic Quantities 110
4.1.2 Comparison of Dispersion Relations Between Quantum and Classical Theories of Fluctuations 113
4.2 Dynamical Structure Factors Within Zero–Temperature Quantum Theory 115
4.2.1 Quantum Structure Factors at General Values of $\mathbf{q}$ 116
4.2.2 Quantum Structure Factors: Contribution of the Ground State at $\mathbf{q} = 0$ 118
4.2.3 Dynamical Structure Factor for Dipole Moments 122
4.2.4 Dynamical Structure Factor for Quadrupole Moments 123
4.2.5 Dynamical Spin Structure Factor for A–Matrices 124

4.2.6 Sum Rule on Quantum Structure Factors . . . 126
4.2.7 Comparison of Structure Factors Between Quantum and Classical Theories of Fluctuations . . . 126
4.3 Comparison with "Raw" $u(3)$ Molecular Dynamics . . . 127

5 Classical-Quantum Correspondence in Molecular Dynamics Simulations 133
5.1 Relationship Between Classical and Quantum Theories of Equal–Time Correlations . . . 133
5.2 Relationship Between Numerical Methods and Quantum Theory of Dynamical Correlations . . . 139
5.3 Comparison with Corrected Molecular Dynamics . . . 143

6 Spin–1 Magnets with Anisotropic Interactions 147
6.1 Generalization of the $u(3)$ Approach to Anisotropic Interactions . . . 147
6.2 Application to the FQ State with Single–Ion, Easy–Plane Anisotropy . 149
6.2.1 Analytical Quantum Theory for the FQ state with Single–Ion, Easy–Plane Anisotropy . . . 149
6.2.2 Comparison to Molecular Dynamics Simulations . . . 151
6.3 Application to an Easy–Plane Ferromagnet with both Single–Ion and Exchange Anisotropy . . . 152

7 Outlook and Conclusion 161
7.1 Thesis Panorama . . . 161
7.2 New Horizons . . . 163
7.2.1 Topological Defects in Spin Nematics . . . 164
7.2.2 Generalization to Self-Consistent Gaussian Approximation Within the $u(3)$ Algebra . . . 172
7.3 Concluding Remarks . . . 180

Bibliography 183

Appendix A Spin Fluctuation Probability 209

Appendix B Properties of A–Matrices 211
B.1 Properties of a Single A–Matrix . . . 211
B.2 Properties of Quadratric Terms of A–Matrices . . . 212

Appendix C Bogolioubov Transformation 215

Appendix D Conventions for the Triangular Lattice 221

Appendix E Numerical Simulation of Spin–1 223
E.1 u3MC . . . 223
E.1.1 Phase Diagram and Comparison with Published Results . . . 224
E.2 Molecular Dynamics Simulations Within $u(3)$ Framework . . . 226

E.2.1 Implementation of u3MD Update 226
E.2.2 Calculation of Dynamical Structure Factors 228

Appendix F Useful Gaussian Integrals **231**

Appendix G Classical Structure Factors **235**
G.1 Dipole Moments: Classical Structure Factor for $\mathbf{q} \neq 0$ 235
G.2 Dipole Moments: Classical Structure Factor at $\mathbf{q} = 0$ 237
G.3 Quadrupole Moments: Classical Structure Factor for $\mathbf{q} \neq 0$ 238
G.4 Quadrupole Moments: Classical Structure Factor at $\mathbf{q} = 0$ 239
G.5 A-matrices: Classical Structure Factor $\mathbf{q} \neq 0$ 241
G.6 A-Matrices: Classical Structure Factor at $\mathbf{q} = 0$ 242

Appendix H System Size Dependence of the Ordered Moment **245**

Appendix I Dynamical Structure Factors Within Zero–Temperature Quantum Theory **249**
I.1 Dipole Moments: Quantum Structure Factor at General Values of $\mathbf{q}$ . . 249
I.2 Dipole Moments: Contribution of the Ground State to the Quantum Structure Factor at $\mathbf{q} = 0$ 250
I.3 Quadrupole Moments: Quantum Structure Factor at General Values of $\mathbf{q}$ 252
I.4 Quadrupole Moments: Contribution of the Ground State to the Quantum Structure Factor at $\mathbf{q} = 0$ 253
I.5 A–Matrices : Quantum Structure Factors at General Values of $\mathbf{q}$ 256
I.6 A-matrices: Contribution of the Ground State to the Quantum Structure Factor at $\mathbf{q} = 0$ 257

List of Figures

1.1 Mariner's compass. Drawing by Thomas Dawson (public domain). . . 2

1.2 Bloch Sphere representing the spin–coherent states of a spin–$\frac{1}{2}$ moment according to Eq. (1.39). 15

1.3 Usual, "magnetic" basis for a spin–$\frac{1}{2}$. [(a)] and a spin–1 [(b)] moment, formed by eigenstates of S^z. (a) States representing a spin–$\frac{1}{2}$ moment with $S^z = \pm\frac{1}{2}$, labeled $|\uparrow\rangle$ and $|\downarrow\rangle$ (b) States representing a spin–1 moment. Those with $S^z = \pm 1$, labeled $|1\rangle$ and $|\overline{1}\rangle$ break time–reversal symmetry and have a finite spin–dipole moment (blue arrow). While, the state with $S^z = 0$, which is only present for a spin–1 and labeled $|0\rangle$, posses a quadrupolar magnetic moment, which can be represented through a director (red bar). Figure is reproduced from [201]. 16

1.4 Liquid crystals are made of rod-shaped molecules invariant under inversion symmetry, such that the order parameter space is given by $\mathbb{RP}^n$, where n+1 is the dimension of the space in which the molecules are embedded. For this figure, $n = 2$. In certain Liquid Crystals, it can happen that these molecules align themselves with each other along a given axis. The resulting order is characterized by a vector without an orientation, called a director. 20

1.5 Order parameter space for a dipole moment and a director. An O(3)–spin dipole moment of length 1 can be characterized by two angles which represent a point on the unit sphere $\mathbb{S}^2$. Therefore the order parameter is given by the sphere $\mathbb{S}^2$. While for a (purely real) director of length 1, a point on half of the sphere with opposite edge point being identified suffice to determine it because of its non-orientability. This space is called the real projective space and is noted $\mathbb{RP}^2$. 21

1.6 Representation of the Valence Bond Solid (VBS) state on a spin–1 chain. The orange-red spheres represent the spin–1 moments consisting of two spin–$\frac{1}{2}$ moments in a triplet state. The colored boxes encapsulating the two individual neighboring "sub"–spin–$\frac{1}{2}$ illustrate a singlet state. At both extremities of the chain are found the two edge spin–$\frac{1}{2}$ degrees of freedom. 24

1.7 (a) $NiGa_2S_4$ crystal grown by chemical vapor transport method, reproduced from [162]. (b) Crystal and spin structures of $NiGa_2S_4$, consisting of layers stacked along the c axis and separated from each other by a van der Waals gap. Each layer of $NiGa_2S_4$ consists of an undistorted triangular lattice of Ni^{2+} ions in the ab–plane formed by the central edge-sharing NiS_6 octahedra (red) sandwiched between sheets of nonmagnetic GaS_4 tetrahedra (green), also illustrated in the inset of Fig. 1.8(b). Figures are reproduced from [159]. 25

1.8 Thermodynamic properties of for $NiGa_2S_4$. (a) Magnetic specific heat C_M under different magnetic fields in function of temperature. The solid lines show the T^2 dependence of C_M suggesting the existence of long–range correlations. Inset: $\frac{C_M}{T}$ in function of temperature under zero magnetic field for $NiGa_2S_4$ and $NiGa_2S_{4.2}$ which has a sulfur doping of excess of 5%. Reproduced from [159]. (b) Spin correlation length ξ in function of temperature. No abnormal behavior is observed as one would expect from a conventional phase transition. Inset: crystal structure of $NiGa_2S_4$. Reproduced from [165]. 26

1.9 (a) $NaCaNi_2F_7$ crystal grown by a modified Bridgman-Stockbarger method, reproduced from [125]. (b) Pyrochlore lattice consisting of corner–sharing tetrahedra, reproduced from [267]. 28

1.10 Comparison of experimental and results obtained by Linear Spin-Wave theory, Molecular Dynamics for $O(3)$-spin dipole moments and a self–consistent Gaussian approximation for the dynamics of $NaCaNi_2F_7$. The spin–dipole dynamical structure factor is shown along momentum cuts [22L] and [HH2]. First row shows the neutron scattering intensity is in absolute units. Second, third and fourth row show the predictions from Linear Spin-Wave (LSW) theory, rescaled Molecular Dynamics (MD) and a self–consistent Gaussian approximation extended to a stochastic model labeled SLN, respectively. LSW and MD results qualitatively reproduce the shape of the broad dispersive continuum but disagree at the lowest energies; SLN fails to capture the structure of the experimental data at high energies. Figure is reproduced from [267]. 30

1.11 Mean–field phase diagram of the spin–1 bilinear–biquadratic (BBQ) model on the triangular lattice [Eq. (1.48)] at $T = 0$, adapted from [229] and reproduced from [201]. The model shows four distinct ordered ground states: ferromagnet (FM); three–sublattice antiferromagnet (AFM); ferroquadrupolar (FQ); and three–sublattice antiferroquadrupolar (AFQ). For $J_1 = J_2$, the model exhibits an enlarged $SU(3)$ symmetry. 33

1.12 Dynamical spin dipole $S_{\mathsf{S}}(\mathbf{q}, \omega)$ and quadrupole $S_{\mathsf{Q}}(\mathbf{q}, \omega)$ structure factors obtained by Quantum Monte Carlo simulations. Results are shown for the BBQ model [Eq. (1.48)] on the triangular lattice with parameters $J = 1, \theta = -\frac{\pi}{2}$ [Eq. (1.50)] at a temperature $T = \frac{1}{32}\ J$, and are reproduced from [255]. The intensities of the dynamical spin dipole $S_{\mathsf{S}}(\mathbf{q}, \omega)$ and quadrupole structure factors $S_{\mathsf{Q}}(\mathbf{q}, \omega)$ are given in function of the irreducible wedge along the points $\mathbf{\Gamma}$–$\mathbf{K}$–$\mathbf{M}$–$\mathbf{\Gamma}$ given in Eq. (D.3) in abscissa, and the energy ω in ordinate. 36

1.13 Finite–temperature phase diagram obtained from Monte Carlo simulation of $\mathcal{H}_{\mathsf{BBQ}}$ [Eq. (1.69)] in the space of $u(3)$ matrices (u3MC) for the spin–1 bilinear–biquadratic (BBQ) model on the triangular lattice, performed by my collaborator Dr. Rico Pohle. Circles correspond to the location of peaks in the heat capacity. The phases are labeled according to their dominant correlations at the ordering vector. Figure is reproduced from [201]. 40

1.14 Dynamical spin–dipole structure factor $S_{\mathrm{S}}(\mathbf{q},\omega)$ for the ferroquadrupolar (FQ) phase of the BBQ model Eq. (1.69) with $J_1 = 0.0; J_2 = -1.0$ on the triangular lattice, reproduced from [201]. (a) Raw results of "molecular dynamics" (u3MD) simulation at finite T. We observe a dispersing band of excitations, which is linearly dispersive for small vectors in the reciprocal space. These are the Goldstone modes of the FQ order. The spectral weight in these excitations is governed by the classical statistics inherited from Monte Carlo (u3MC) simulations. (b) Predictions of quantum multi-boson theory at $T = 0$. (c) MD results corrected for the effects of classical statistics, showing agreement with $T = 0$ quantum results. The u3MD method was implemented by my collaborator Dr. Rico Pohle using a Runge-Kutta algorithm of order 4. 42

2.1 Time–reversal invariant basis for a spin–1 moment. The three states $|\alpha\rangle$, with $\alpha = x, y, z$, are invariant under time–reversal, and have vanishing dipole moments $\langle\alpha|S^{\mu}|\alpha\rangle = 0$, for $\mu = x, y, z$ referring to the usual spacial spin components. The red rods represent their respective directors whose components are given by Eq. (2.35) Their spin fluctuations exhibit the characteristic "donuts–shaped" profile [Appendix A]. These states can be expressed in terms of the usual magnetic basis [Fig. 1.3] through Eq. (2.33). 53

2.2 Evidence for the stability of the numerical integration of equations of motion for "A-matrices". (a) Time–dependence of Tr $\mathcal{A}$ [Eq. (2.57)], shows the conservation of spin length up to numerical precision, implying that if the time evolution originates from a proper spin configuration with Tr $\mathcal{A}$=1, we never leave the $su(3)$ sub–algebra of $u(3)$. This implies that we properly describe the spin–1 system trough out the time evolution. (b) Time–dependence of the energy $E = \langle\mathcal{H}_{\mathsf{BBQ}}\rangle$, shows that the energy is preserved to the level expected for a 4^{th}–order Runge–Kutta (RK–4) algorithm. Simulations were computed by my collaborator Dr. Rico Pohle, for the spin–1 bilinear–biquadratic model [Eq. (2.72)], using the equation of motion Eq. (2.74) for a triangular–lattice cluster with linear dimension L = 24 (N = 2304 spins), for parameters $J_1 = 0$, $J_2 = -1$, at a temperature $T = 0.1\ J$ and with a time–step $\delta t = 0.4\ J^{-1}$. Figures are reproduced from [201]. 76

3.1 Ferroquadrupolar (FQ) ground state of a spin–1 magnet on a triangular lattice consisting of all magnetic moments having their director [Eq. (2.35)] aligned with each other. Each magnetic moment has been drawn in the state $|y\rangle$. Their corresponding director representation $d^x = 0,\ d^y = 1,\ d^z = 0,$ [Eq. (2.35)] is shown as a red bar, and their corresponding spin probability distribution [Eq. (A.3)] is shown in grayish blue. Figure is reproduced from [201]. 80

3.2 Effect of the four generators creating fluctuations about the ferroquadrupolar (FQ) ground state $|y\rangle$, computed for each generator separately according to Eq. (2.87), and drawn here for an angle of $\phi = \frac{\pi}{8}$. The generators $\hat{\mathcal{A}}^1{}_2$ (acting on the right from the application of $\hat{R}^\dagger(\vec{\phi})$) and $\hat{\mathcal{A}}^2{}_1$ (acting on the left from the application of $\hat{R}(\vec{\phi})$) introduce a complex component of the director $\mathbf{d}$ along the x–axis, inducing a complex rotation of the directors about the z–axis. This deforms the quadrupole "donut" about the same axis and promotes a small but finite spin dipole moment along the z–axis [Eq. (2.44)]. The generators $\hat{\mathcal{A}}^2{}_3$ and $\hat{\mathcal{A}}^3{}_2$ produce a complex component of the director $\mathbf{d}$ along the z–axis, corresponding to a complex rotation of the director about the x–axis, reshape the quadrupole "donut" about the x–axis, and induce a spin dipole moment along the z–axis. The red bar represents the real part $\mathbf{u}$ of the coefficients d^α [Eq. (2.37)] in Eq. (2.35), and the orange bar represents the imaginary part $\mathbf{v}$. Figure is reproduced from [201]. 83

3.3 Spectral representation of structure factors found in a classical theory of fluctuations about a ferroquadrupolar (FQ) ground state of the BBQ model. (a) Spectral representation of dipole structure factor, $S_{\mathrm{S}}^{\mathsf{CL}}(\mathbf{q},\omega)$ [Eq. (3.86)], within the classical low–temperature expansion developed in Section 3.2, at temperature $T = J$. (b) Equivalent result the for the quadrupole structure factor, $S_{\mathrm{Q}}^{\mathsf{CL}}(\mathbf{q},\omega)$ [Eq. (3.91)]. (c) Equivalent results for the A–matrix structure factor, $S_{\mathrm{A}}^{\mathsf{CL}}(\mathbf{q},\omega)$ [Eq. (3.94)]. All results are shown for parameters Eq. (3.87), and have been convoluted with Gaussian of FWHM 0.35 J. Bragg peaks have been omitted for simplicity. 97

3.4 Temperature dependence of the specific heat per spin $c(T)$, obtained by $U(3)$ Monte Carlo (u3MC) simulations of the BBQ model $\mathcal{H}_{\mathsf{BBQ}}$ [Eq. (2.72)], for a ferroquadrupolar (FQ) ground state. Results are illustrated for different system sizes L. The peak at $c(T)$ at $T^* \sim 0.43$ reflects the onset of fluctuations of FQ order, as depicted in Fig. 3.5 (a). The low temperature limit $c(T \to 0) \to 2$ agrees with the prediction obtained from the analytical theory of thermal fluctuations, which is based on the existence of four independent classical excitations about the the FQ ground state, as discussed in Section 3.3.2. All simulations were carried out by my collaborator Dr. Rico Pohle using the MC scheme described in Section 2.6.1 for parameters given in Eq. (3.87) and consistent with a FQ ground state. Figure is reproduced from [201]. 101

3.5 Temperature and system size dependence of the order moment $\mathbf{Q}$ for a ferroquadrupolar (FQ) ground state of the BBQ model $\mathcal{H}_{\mathsf{BBQ}}$ [Eq. (2.72)]. (a) Results for $\mathbf{Q}^2$ found in $U(3)$ Monte Carlo (u3MC) simulations for different system sizes, L. The temperature $T^* \sim 0.43$ of the onset of fluctuations of FQ order at $\mathbf{Q}^2$ corresponds to the one found in the peak of the heat capacity, shown in Fig. 3.4. At low temperatures, $\mathbf{Q^2}$ tends to the ordered moment of the FQ ground state, Q_0^2 [Eq. (3.105)]. (b) Finite–size scaling of the coefficient $\alpha(L)$ [Eq. (3.106)], showing a logarithmic divergence for large L. This implies a correction of the leading order in temperature $\alpha(L)$ to the ordered moment which suppresses any quadrupole moments at finite temperate in the thermodynamic limit [Eq. (3.108)], consistent with the Mermin–Wagner Theorem. Results are shown for both u3MC simulations (blue circle), and the analytic theory (red points) [Eq. (3.107)], developed in Section 3.3. All u3MC simulations were carried out by my collaborator Dr. Rico Pohle using the u3MC scheme described in Section 2.6.1, for parameters Eq. (3.87) consistent with a FQ ground state. Figures are reproduced from [201]. 102

3.6 Results for equal–time structure factors $S_\lambda^{\mathsf{CL}}(\mathbf{q})$ obtained from the analytical theory of thermal fluctuations (solid line) [cf. Section 3.3.3 and Section 3.3.4] and compared with $U(3)$ Monte Carlo (u3MC) simulations results [Eq. (2.124)] of $\mathcal{H}_{\mathsf{BBQ}}$ [Eq. (2.72)], for parameters consistent with a ferroquadrupolar (FQ) ground state [Eq. (3.87)] (a) Dipole structure factor, $S_{\mathsf{S}}^{\mathsf{CL}}(\mathbf{q})$ [Eq. (3.85)], exhibiting a spectral weight peak around $\mathbf{K}$, reflecting AFM correlations . (b) Quadrupole structure factor, $S_{\mathsf{S}}^{\mathsf{CL}}(\mathbf{q})$ [Eq. (3.89)], showing divergence associated with fluctuations of FQ order for $\mathbf{q} \to \mathbf{\Gamma}$. (c) A–matrix structure factor, $S_{\mathsf{A}}^{\mathsf{CL}}(\mathbf{q})$ [Eq. (3.93)], which shows behavior associated with both dipolar and quadrupolar fluctuations. In all cases, the structure factors have been divided by temperature T, and agree perfectly with the predictions of low–temperature analytic theory (line). All simulations were performed by my collaborator Dr. Rico Pohle with parameters Eq. (3.87), for a cluster with linear dimension $L = 96$ ($N = 9216$ spins), at T ≈ 0.03, using the u3MC scheme described in Section 2.6.1. Figures are reproduced from [201]. 104

4.1 Quantum excitations about a ferroquadrupolar (FQ) ground state of the BBQ model [Eq. (2.72)] on the triangular lattice as resolved in quantum dynamical structure factors compared with equivalent results obtained from a classical theory. (a) Dynamcial dipole structure factor $S_{\mathrm{S}}^{\mathsf{QM}}(\mathbf{q},\omega)$ [Eq. (4.71)], within $T=0$ quantum theory of Section 3.2. (b) Equivalent results for the quadrupole structure factor, $S_{\mathrm{Q}}^{\mathsf{QM}}(\mathbf{q},\omega)$ [Eq. (4.78)]. (c) Equivalent results for the A–matrix structure factor, $S_{\mathrm{A}}^{\mathsf{QM}}(\mathbf{q},\omega)$ [Eq. (4.86)]. (d) Spectral representation of dipole structure factor, $S_{\mathrm{S}}^{\mathsf{CL}}(\mathbf{q},\omega)$ [Eq. (3.86)], within the classical low–temperature expansion developed in Section 3.2, at temperature $T=J$. (e) Equivalent result the for the quadrupole structure factor, $S_{\mathrm{Q}}^{\mathsf{CL}}(\mathbf{q},\omega)$ [Eq. (3.91)]. (f) Equivalent results for the A–matrix structure factor, $S_{\mathrm{A}}^{\mathsf{CL}}(\mathbf{q},\omega)$ [Eq. (3.94)]. We also note that the quantum dispersion corresponds to the geometrical mean of the two classical dispersions for dipolar and quadrupolar excitations Eq. (4.33). All results are shown for parameters Eq. (3.87), and have been convoluted with Gaussian of FWHM 0.35 J. Bragg peaks have been omitted for simplicity. Details of the quantum theory are given in Section 4.1. 114

4.2 Comparison between "raw" results of $u(3)$ Molecular Dynamics (u3MD) simulations of excitations about the FQ state and the predictions of a $T=0$ quantum analytical theory. "Raw" simulation results offer a good account of the dispersions of the excitations, but not of their spectral intensities. (a) Dynamical structure factor associated with dipole moments, $S_{\mathrm{S}}^{\mathsf{MD}}(\mathbf{q},\omega)$. Dipolar fluctuations exhibit relatively high spectral weight near the top of the band, where excitations have more of a spin–wave character. (b) Dynamical structure factor associated with quadrupole moments, $S_{\mathrm{Q}}^{\mathsf{MD}}(\mathbf{q},\omega)$. (c) Dynamical structure factor associated with A–matrices, $S_{\mathrm{A}}^{\mathsf{MD}}(\mathbf{q},\omega)$. (d) Prediction for $S_{\mathrm{S}}^{\mathsf{QM}}(\mathbf{q},\omega)$ from $T=0$ quantum theory [Eq. (4.71)]. (e) Equivalent prediction for $S_{\mathrm{Q}}^{\mathsf{QM}}(\mathbf{q},\omega)$ [Eq. (4.78)]. (f) Equivalent prediction for $S_{\mathrm{A}}^{\mathsf{QM}}(\mathbf{q},\omega)$ [Eq. (4.86)]. Simulations were carried out by my collaborator Dr. Rico Pohle, using the u3MD simulation scheme described in Section 2.6.2, for $\mathcal{H}_{\mathsf{BBQ}}$ [Eq. (2.72)] with parameters Eq. (3.87), at a temperature $T=0.05\ J$, in a cluster of linear dimension $L=96$ ($N=9216$ spins). $T=0$ quantum analytical predictions have been calculated using the quantum theory of fluctuations developed in Section 4.2. All the results have been convoluted with a Gaussian envelope of FWHM = 0.35 J. Bragg peaks are not plotted for simplicity. The individual panels are reproduced from [201]. 128

4.3 Temperature dependence of "raw" results obtained by $U(3)$ Molecular Dynamics (u3MD) simulation at fixed wave vector $\mathbf{q} = \mathbf{K}$. Results are shown for the dynamical structure factor associated with A–matrices, $S_{\mathrm{A}}^{\mathsf{MD}}(\mathbf{q} = \mathbf{K}, \omega)$ [Eq. (2.130)], obtained from u3MD simulations for temperatures between $T = 0.01\ J$ to $T = 0.15\ J$. The $T = 0$ prediction obtained by a quantum theory, $S_{\mathrm{A}}^{\mathsf{QM}}(\mathbf{q}, \omega)$ [Eq. (4.86)], is shown by the red dashed line. Solid lines correspond to fits of u3MD data using a Voigt function [Eq. (4.93)]. For $T \to 0$, the energy of the associated excitations for "raw" u3MD simulation results converge towards the energy predicted by the quantum theory. But the spectral weight of the structure factor suffers a dramatic loss of intensity. Indeed, the intensities of the peak fail to converge to the predictions of a $T = 0$ quantum theory for $T \to 0$. Simulations of $\mathcal{H}_{\mathsf{BBQ}}$ [Eq. (2.72)] were carried out by my collaborator Dr. Rico Phole, using the u3MD simulation scheme described in Section 2.6.2, for parameters given in Eq. (3.87), and for a system size $L = 96$ ($N = 9216$ spins). Simulation results and analytic prediction have both been convoluted with a Gaussian of FWHM $= 0.02\ J$. Figure is reproduced from [201]. 130

5.1 Comparison between dynamical structure factors obtained from $U(3)$ Molecular Dynamics (u3MD) simulations [Section 2.6.2] and $T = 0$ quantum theory results [Section 4.2] for a ferroquadrupolar (FQ) state. (a) Simulation results for dynamical structure factor associated with dipole moments, $S_{\mathrm{S}}^{\mathsf{MD}}(\mathbf{q}, \omega)$. Dipolar fluctuations exhibit relatively high spectral weight near the top of the band, where excitations have more of a spin–wave character. (b) Equivalent results for quadrupole moments, $S_{\mathrm{Q}}^{\mathsf{MD}}(\mathbf{q}, \omega)$. (c) Equivalent results for associated with A–matrices, $S_{\mathrm{A}}^{\mathsf{MD}}(\mathbf{q}, \omega)$. (d) Simulation results for dynamical structure factor associated with dipole moments, $\tilde{S}_{\mathrm{S}}^{\mathsf{MD}}(\mathbf{q}, \omega)$, corrected for classical statistics, following Eq. (5.32). (e) Equivalent results for quadrupole moments, $\tilde{S}_{\mathrm{Q}}^{\mathsf{MD}}(\mathbf{q}, \omega)$. (f) Equivalent results for A–matrices, $\tilde{S}_{\mathrm{Q}}^{\mathsf{MD}}(\mathbf{q}, \omega)$. (g) Prediction for $S_{\mathrm{S}}^{\mathsf{QM}}(\mathbf{q}, \omega)$ from $T = 0$ quantum theory [Eq. (4.71)]. (h) Equivalent prediction for $S_{\mathrm{Q}}^{\mathsf{QM}}(\mathbf{q}, \omega)$ [Eq. (4.78)]. (i) Equivalent prediction for $S_{\mathrm{A}}^{\mathsf{QM}}(\mathbf{q}, \omega)$ [Eq. (4.86)]. Simulations were carried out by my collaborator Dr. Rico Pohle, using the u3MD simulation scheme described in Section 2.6.2, for $\mathcal{H}_{\mathsf{BBQ}}$ [Eq. (2.72)] with parameters Eq. (3.87) at a temperature $T = 0.05\ J$, in a cluster of linear dimension $L = 96$ ($N = 9216$ spins). All results have been convoluted with a Gaussian in frequency of FWHM $= 0.35$ J. Figures are reproduced from [201]. 144

5.2 Temperature dependence of results of $U(3)$ Molecular Dynamics (u3MD) simulation corrected for classical statistics according to Eq. (5.32) and demonstrating successful convergence as $T \to 0$ towards the $T = 0$ quantum predictions. (a) u3MD results for dynamical structure factor associated with A–matrices, $S_{\mathrm{A}}^{\mathsf{MD}}(\mathbf{q}, \omega)$, at wave vector $\mathbf{q} = \mathbf{K}$, for temperatures between $T = 0.01\ J$ and $T = 0.15\ J$. u3MD simulation results are represented by circles. They have computed with an energy resolution $0.02\ J$, and have been corrected for classical statistics using Eq. (5.32). Solid lines are the fits of the u3MD results using a Voigt profile, Eq. (4.93). The prediction of the $T = 0$ quantum theory, Eq. (4.86), convoluted with a Gaussian of FWHM = 0.02 J, is shown with a solid red line. (b) Shift in peak energy $\Delta\omega(T)$, obtained by fitting using a Voigt profile, showing convergence of the peak position on the prediction of the $T = 0$ quantum theory. (c) Equivalent results for the inverse lifetime $\Gamma(T)$. (d) Equivalent results for the peak height, $I(T)$. u3MD simulations have been performed by my collaborator Dr. Rico Pohle, for parameters identical to those used in Fig. 5.1 and given by Eq. (3.87). Panels are reproduced from [201]. 145

6.1 Comparison of u3MD simulation results and $T = 0$ analytical quantum prediction for the dynamical structure factors of a ferroquadrupolar (FQ) state in the spin–1 bilinear–biquadratic (BBQ) model with easy–plane anisotropy $\mathcal{H}_{\mathsf{D}}$ [Eq. (6.7)]. (a) Dipole dynamical structure factor, $S_{\mathrm{S}}^{\mathsf{QM}}(\mathbf{q}, \omega)$, predicted by $T = 0$ quantum theory of Section 6.2.1. (b) Equivalent results for quadrupole moments, $S_{\mathrm{Q}}^{\mathsf{QM}}(\mathbf{q}, \omega)$. (c) Equivalent results for A–matrices, $S_{\mathrm{A}}^{\mathsf{QM}}(\mathbf{q}, \omega)$. (d) Dipole dynamical structure factor $S_{\mathrm{S}}^{\mathsf{MD}}(\mathbf{q}, \omega)$ found in molecular dynamics simulations within $u(3)$ representation (u3MD) . (e) Equivalent results for quadrupole moments, $S_{\mathrm{Q}}^{\mathsf{MD}}(\mathbf{q}, \omega)$. (f) Equivalent results for A–matrices, $S_{\mathrm{A}}^{\mathsf{MD}}(\mathbf{q}, \omega)$. Numerical simulations were carried out by my collaborator Rico Pohle for $\mathcal{H}_{\mathsf{D}}$ [Eq. (6.7)], with parameters given in Eq. (6.15), at a temperature $T = 0.05\ J$, for system size of dimension $L = 96$ ($N = 9216$ spins). u3MD results have been corrected for classical statistics by multiplication by a prefactor $\omega/2T$ following Eq. (5.32). All results have been convoluted with a Gaussian in frequency of FWHM = 0.35 J. Figures are reproduced from [201]. 151

6.2 Eigenstates of $\hat{\mathrm{S}}_i^x$ forming the basis states of $\mathcal{B}^x$ [Eq. (6.24)]. Figure is reproduced from [201]. 153

6.3 Fluctuations created by the generators $\hat{\mathcal{A}}^x{}_y$, $\hat{\mathcal{A}}^x{}_z$, $\hat{\mathcal{A}}^y{}_x$, and $\hat{\mathcal{A}}^z{}_x$, according to Eq. (2.86), for an angle $\phi_{\alpha\beta} = \frac{\pi}{8}$, around the FM ground state given in Eq. (6.23). Figure is reproduced from [201]. 155

6.4 Dynamical structure factors predicted by $T = 0$ quantum theory of fluctuations for the ferromagnetic (FM) phase of the BBQ model on the triangular lattice (Eq. (1.69)) with J_1 being considered as Heisenberg anisotropic exchange interactions [Eq. (6.19)] and $J_2 = 0$, and with an additional single ion anisotropic exchange Hamiltonian [Eq. (6.20)]. (a)–(c) Dynamical structure factors for $S_{\rm A}(\mathbf{q},\omega)$ (A-matrices), $S_{\rm Q}(\mathbf{q},\omega)$ (quadrupoles) and $S_{\rm S}(\mathbf{q},\omega)$ (dipoles) obtained for the isotropic FM state of the Heisenberg Hamiltonian [Eq. (6.19)] where $J^{xx} = J^{yy} = J^{zz} = -1$ without any single–ion anisotropy [Eq. (6.20)], $D^{\perp} = D^{x} = 0$. (d)–(f) Equivalent results for the easy-plane anisotropic FM state of the Heisenberg Hamiltonian [Eq. (6.19)] where $J^{yy} = J^{zz} = 0.8J^{xx}$ and $J^{xx} = -1$ without any single–ion anisotropy [Eq. (6.20)], $D^{\perp} = D^{x} = 0$. (g)–(i) Equivalent results for the isotropic FM state of the Heisenberg Hamiltonian [Eq. (6.19)] where $J^{yy} = J^{zz} = J^{xx} = -1$ with single–ion anisotropy [Eq. (6.20)], $D^{\perp} = 0.5D^{x}$ and $D^{x} = J^{xx}$. (j)–(l) Equivalent results for the easy-plane anisotropic FM state of the Heisenberg Hamiltonian [Eq. (6.19)] where $J^{zz} = 0.8J^{xx}$ and $J^{yy} = J^{xx} = -1$ with single–ion anisotropy [Eq. (6.20)], $D^{\perp} = 0.8D^{x}$ and $D^{x} = J^{xx}$. Figures are reproduced from [201] 160

7.1 Configuration of directors $\mathbf{n}$ [Eq. (7.11)] in a vortex defined by $k = \frac{1}{2}$ and $\phi_0 = \frac{\pi}{4}$ according to Eq. (7.10) 167

7.2 Configuration of directors $\mathbf{n}$ [Eq. (7.11)] in a vortex defined by $k_1 = \frac{1}{2}$, $\phi_0^1 = 0$and $k_2 = \frac{1}{2}$ $\phi_0^2 = \frac{\pi}{2}$ according to Eq. (7.10). 168

7.3 Directors in the KT-regime obtained by u3MC Monte Carlo simulations at T=0.036J, described in Section 2.6.1, for the BBQ model [Eq. (2.72)] in the FQ phase. Numerical simulations were carried out by my collaborator Dr. Rico Pohle. 169

7.4 Topological defects for a spin–1 system in the FQ phase on the triangular lattice. Directors configuration for a (a) point–like Π_1 topological excitation, (b) Skyrmion–type Π_2 topological excitation, (c) SU(3) Π_2 topological excitation. The background intensities represent the normalized value of the quadrupole component $Q^{xx2} - Q^{yy2}$. Pictures are reproduced from [5]. 170

7.5 (a)-(f) Snapshots at different time during time evolution obtained by u3MD scheme, described in Section 2.6.2, of the BBQ model [Eq. (2.72)] in the FQ phase with topological defects. The x– and y–axis represent the real space variables of the 2 dimensional triangular lattice, and the intensities corresponds to the total quadrupolar weight $\sum_{\alpha,\beta} Q_i^{\alpha\beta}(t)$. Numerical simulations were carried out by my collaborator Dr. Rico Pohle. 171

E.1 Statistical independence of points randomly generated a 5–dimensional sphere, using Eq. (2.120). The second moment $\langle x_m^2 \rangle$ of the variables x_m, $m = 1, ..., 6$ is plotted as a function of the number of points, N_{dot} and converges towards $\langle x_m^2 \rangle \to 1/6$ (middle black solid line) as $N_{\mathsf{dot}} \to \infty$. Statistical errors respect the central–limit theorem and decrease as $1/\sqrt{N_{\mathsf{dot}}}$ (dashed lines). Sampling was performed by my collaborator Dr. Rico Pohle. Figure is reproduced from [201]. 223

E.2 Comparison of the $U(3)$ Monte Carlo (u3MC) method with published results for the spin–1 bilinear—biquadratic (BBQ) model on the triangular lattice for parameters $J_1 = 1$, $J_2 = -1.5$, which corresponds to the AFM phase [Fig. 1.11]. Specific heat C/N shows a double–peak structure. Results obtained from MC simulation, based on a $u(3)$ matrices, $\hat{\mathcal{A}}^{\alpha}{}_{\beta}$ description, for an u3MC update based on a 5–dimensional sphere [Eq. (2.120)] and 4–dimensional sphere by eliminating the gauge freedom on the phase [Eq. (2.120) with Eq. (2.122)] are represented by squares and triangles symbols, respectively. u3MC simulations were performed by my collaborator Dr. Rico Pohle. While, circles correspond to results from "sSU(3)" MC simulations in the space of the complex vector $\mathbf{d}$, following Stoudenmire *et al.*. The three different approaches agree within statistical errors. Figure is reproduced from [201]. 225

E.3 Phases occurring in the spin–1 BBQ model on a triangular lattice at finite temperature, as found in classical Monte Carlo simulation in the space of $u(3)$ matrices (u3MC). (a) Dipolar structure factor $S_{\mathrm{S}}(\mathbf{q})$ [Eq. (2.124)], representing ferromagnetic (FM) correlations for $\mathbf{q} = \Gamma$ (red circles) and 3–sublattice antiferromagnetic (AFM) correlations for $\mathbf{q} = K$ (blue triangles). (b) Quadrupolar structure factor $S_{\mathrm{Q}}(\mathbf{q})$ [Eq. (2.124)], showing ferroquadrupolar (FQ) correlations for $\mathbf{q} = \Gamma$ (red circles) and 3–sublattice antiferroquadrupolar (AFQ) correlations for $\mathbf{q} = K$ (blue triangles). Simulations of Eq. (1.48) were performed using the u3MC method described in Section 2.6.1, for a system size with linear dimension $L = 48$ ($N = 2304$ spins), at a temperature $T = 0.01\ J$ and for the FQ phase with parameters given by Eq. (E.1). The phases found are in direct correspondence with known results for the mean–field ground state [131, 183, 229], summarised in Fig. 1.11. In each case, the temperature associated with the onset of fluctuations corresponds to the peak found in specific heat, cf. Fig. 1.13. Simulations were carried out by my collaborator Dr. Rico Pohle. Figures are reproduced from [201]. 226

List of Tables

7.1 Constraints counting on the A–matrix describing a spin–1 moment. Naively, an A–matrix contains 18 real degrees of freedom. However, a spin–1 moment is fully characterized by 4 parameters. Here, we show that by accounting for the properties of the A–matrix, in particular, the constraint on the trace, its Hermitian nature, and the fact that it is a projection, reduces back to 4 independent real parameters. 179

H.1 Temperature intervals used for fitting the parameter $\alpha(L)$ according to Eq. (3.108). 245

Chapter 1

Introduction: Why am I Even Doing This?

In this Thesis, I present the new method I developed for studying spin–1 magnets. This is based on the embedding of the usual $su(3)$ algebra describing a spin–1 moments within the larger $u(3)$ algebra. In this Chapter, I provide an overview of the context in which my work fits and summarize my key results.

I start in Section 1.1, where I first explain how the discovery of Quantum Mechanics allowed scientists to understand Magnetism. I provide a historical summary about the scientific discoveries from the beginning of the 20^{th} that led to the discovery of spin angular moments of electrons. I illustrate qualitatively how the laws of Quantum Mechanics govern the behavior of the electrons on a single atom, how they interact, and how this gives rise to magnetic moments. I then endeavor to explain how magnetic atoms within a crystal interact, and how this gives rise to Magnetism and permits the bloom of emergent and sometimes unexpected magnetic properties.

Section 1.2 set outs some motivations as why we should care about spin–1 magnets and what makes a spin–1 moment so special. I give first a basic introductory description of a single spin–1 and what happens when we describe them as interacting spin-moments on a lattice described by a Hamiltonian. Then I give two interesting and non-trivial examples of what spin–1 moments are capable of: nematic order and symmetry-protected states in 1D Haldane chains.

In Section 1.3, I give an overview of modern research of spin–1 magnets that are relevant to our investigation for both experimental and theoretical studies.

Finally, in Section 1.4, I summarize the results I have obtained and how they relate to published work.

1.1 The Advent of Quantum Mechanics and Magnetism

1.1.1 Historical Prelude

Magnetism has been studied for thousands of years. According to written sources, magnets were first discovered in ancient Greece. Indeed, Greek philosophers described

that they observed how iron was attracted to a specific type of stone, now called magnetite [12, 219, 261]. There is even a "legend" where a shepherd named Magnes got his nail toe stuck to a piece of magnetite. In China, the mention of magnetism can also be linked back to 400 B.C.E [225]. Historically, the use of the proprieties of magnetite is known for being used as a compass. The first mention of magnetized needles used for navigation purposes happened in China and is relatively recent (1117 C.E) [166]. A little bit later, in 1190 C.E, Europe also discovered the utility of compasses [124]. In certain ways, magnets shaped history by allowing humans to navigate in capricious

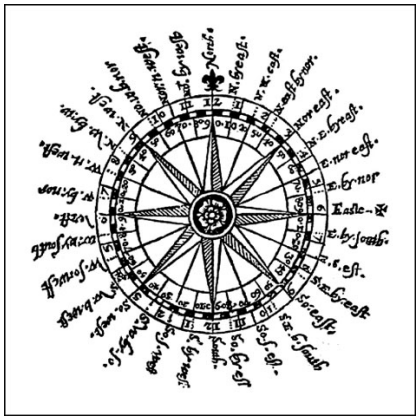

Figure 1.1: Mariner's compass. Drawing by Thomas Dawson (public domain).

weather conditions. Nowadays, the applications of magnets are prodigious and very diverse, spanning from fridge magnets to medical devices, including our understanding of plate tectonics. But it wasn't before the discovery of Quantum Mechanics at the beginning of the 20^{th} century, that the mysteries of Magnetism were elucidated.

In the 19^{th} century, thanks to Faraday's [85, 246] and Maxwell's [31, 144, 158] contributions, properties of magnetic fields were well understood. But the microscopic origin of Magnetism remained a mystery to the laws of classical physics. Indeed, the existence of quantized spin degrees of freedom, as well as exchange interactions was indispensable to fully explain the origin of magnetism. Luckily, by the end of the nineteenth century, these missing concepts started to gear together in such a way that allowed for a fundamental breakthrough in the history of science.

With the advent of Quantum Mechanics [45, 128, 205, 216], which began with the black body radiation problem solved by Max Plank in 1900 and the explanation of the photoelectric effect explained by Albert Einstein in 1905, a new whole world burgeoned.

Quantum Mechanics offers various mathematical formalisms to describe the world at the atomic and subatomic scale. In one of its formulations, called the Schrödinger picture, Quantum Mechanics describes particles as wave–functions that evolve in time. At each point in the phase–space, a wave function dictates a probability amplitude of finding the particle in a given state. The states are described as vectors living in a linear vector space called the Hilbert space. The time evolution of the states constituting the systems is governed by the Schrödinger equation.

Despite being a fully deterministic theory, Quantum Mechanics relies deeply on probability amplitudes and can only predict outcomes with certain probabilities. A famous consequence of this is the uncertainty principle [130, 216]. It states that for

two canonically conjugated variables, such as the position and the momentum of a particle for instance, the accuracy for measuring these quantities is limited by the Planck constant. This leads to important repercussions, even in magnetic systems, where electrons may decrease their kinetic energy by delocalizing themselves.

A surprising feature of the Quantum Mechanics formalism is that it naturally leads to a quantization of the physical quantities. This is in particular true for the angular momentum and spin degrees of freedom. Another remarkable property of Quantum Mechanics classifies the particle as either bosons or fermions [130, 205]. Additionally, the spin-statistic theorem requires all particles with half–integer spin to behave as fermions and all particles with integer spin to behave as bosons [54, 182].

Historically, the first evidence for the existence of spin degrees of freedom was first discovered in spectral lines of alkali metals. In spectrum experiments, electrons make transitions between different states, having different energies. The difference in energy of the transition results in the absorption or emission of a photon. From Rutherford's experiments, also called Geiger–Marsden experiments, in the early 1900s, physicists knew that atoms consisted of a hard, relatively small, positively charged nucleus surrounded by a diffuse cloud of negatively charged electrons [203]. Spectral emission lines for the Hydrogen atom seemed to follow a particular pattern, known as the Balmer series, a specific case of the Rydberg formula applied to the Hydrogen atom [204].

The Hydrogen atom is the simplest model consisting of 2 quantum particles interacting, with the electron being bound to the proton. To explain the spectral emission pattern, Niels Bohr built a model for the Hydrogen atom named after him, where he assumed that the angular momentum of the electron is quantized [28]. When a magnetic field is added, the main spectral lines split further apart into two (Zeeman effect). However, Bohr's model was not able to explain this. Wolfgang Pauli then introduced a "two-valuedness not describable classically" [181] to account for the additional degrees of freedom. This allowed him to formulate Pauli's exclusion principle. At approximately the same time, George Uhlenbeck and Samuel Goudsmit emitted the hypothesis that electrons have an intrinsic angular momentum called spin, which is quantized and two-valued, in order to explain the fine-structure splits in spectral lines.

In 1922, this was experimentally tested with the Stern–Gerlach experiment [71, 72], which is now considered the first experimental evidence of the spin of an electron. In this experiment, a beam of silver atoms is sent through an inhomogeneous magnetic field. The spin angular momentum interacts with the magnetic field, and this interaction deviates the atom. Stern and Gerlach observed that the beam splits into 2, demonstrating the quantized two-valued possible outcomes for the spin angular momentum.

Of course, the energy levels of the electrons in the Hydrogen atoms can be found by solving the Shrödringer equation of motion [61]. One founds that the energy levels are quantized and that the electron can be described by three quantum numbers: n, l, and m. However, this does not still explain the existence of spin degrees of freedom. It is only with the advance of Quantum Mechanics, in 1928 when Paul Dirac introduced the Dirac equation, that spin magnetic moments were correctly predicted and naturally arise as an intrinsic property of matter [55]. Indeed, by solving the Dirac equation for the Hydrogen atom, the electron's energy levels are adequately described by four

quantum numbers, n,l, m, and s. This has made the previous theories based on a classical picture of the electron, such as the Bohr model, obsolete. However, they still provide helpful pedagogical insights.

Before explaining the physics of magnets, we need to borrow from Quantum Mechanics, the fact that observables are described by operators. The total angular momentum is then an operator $\hat{\mathbf{J}}$ and follows commutations relations given by

$$\left[J^\alpha, J^\beta\right] = i\hbar\epsilon^{\alpha\beta\gamma}J^\gamma \ . \tag{1.1}$$

It follows that the spectrum of $\hat{\mathbf{J}}^2$ is given by the eigenvalues:

$$\hat{\mathbf{J}}^2|\psi_j\rangle = \hbar j(j+1)|\psi_j\rangle \ , \quad j = 0, \frac{1}{2}, 1, \dots \ , \tag{1.2}$$

and that the possible eigenvalues of $\hat{J}^z$ for the eigenvectors $|\psi_j\rangle$ of $\hat{\mathbf{J}}^2$ are given by

$$\hat{J}^z|\psi_j\rangle = \hbar m_j|\psi_j\rangle \ , \quad m_j = -j, -j+1, \dots, j \ , \tag{1.3}$$

which results are valid for any operators satisfying Eq. (1.1).

For now, we assume that the electrons are independent particles and are evolving around the nucleus in a central potential $V(|\hat{\mathbf{x}}|)$. We then can restrict ourselves at describing a single electron by the Hamiltonian

$$\hat{\mathcal{H}} = -\frac{\hat{\mathbf{p}}^2}{2m_e} + V(|\hat{\mathbf{x}}|) \ . \tag{1.4}$$

The electrostatic field perceived by the electrons is then just an instance of a central potential.

The results obtained for $\hat{\mathbf{J}}^2$ are also valid for the orbital angular moment $\hat{\mathbf{L}}$, defined by

$$\hat{\mathbf{L}} = \hat{\mathbf{x}} \times \hat{\mathbf{p}} \ , \tag{1.5}$$

which also follows commutations relations given by Eq. (1.1). In analogy with classical mechanics where the total angular momentum $\mathbf{L}$ is conserved, $\hat{\mathbf{L}}$ is also preserved, which follows from the fact that its components commute with the Hamiltonian [Eq. (1.4)]

$$\left[L^\alpha, \hat{\mathcal{H}}\right] = 0 \ . \tag{1.6}$$

This implies that $\hat{\mathbf{L}}^2$ also commutes with $\hat{\mathcal{H}}$. Therefore, $\hat{\mathbf{L}}^2$ and $\hat{\mathcal{H}}$ can be diagonalized within a common basis. The problem consists in finding the eigenvalues and eigen–functions for $\hat{\mathbf{L}}^2$, and then in solving the eigensystem for $\hat{\mathcal{H}}$ with the eigen–functions we obtained for $\hat{\mathbf{L}}^2$.

For $\hat{\mathbf{L}}^2$, we then find that the solutions are given by

$$\hat{\mathbf{L}}^2|\psi_l\rangle = \hbar l(l+1)|\psi_l\rangle \ , \quad l = 0, 1, 2 \dots \ , \tag{1.7}$$

and that the possible eigenvalues of $\hat{L}^z$ for the eigenvectors $|\psi_l\rangle$ of $\hat{\mathbf{L}}^2$ are given by

$$\hat{L}^z|\psi_l\rangle = \hbar m_l|\psi_l\rangle \ , \quad m = -l, -l+1, \ldots, l \ . \tag{1.8}$$

We conclude by noticing that the angular momentum is quantized, and for a given eigenvalue of $\hat{\mathbf{J}}^2$ characterized by j, the operator $\hat{J}^z$ splits these into $2j+1$ levels labeled m_j. Armed with theses considerations, and the fact the electrons have an intrinsic angular degree of freedom, called the spin of the electron, we can now explain what happens when electrons interact. As we will see in the next section, Section 1.1.2, this will lead to selections rules, called Hund's rules that dictated how the electrons organize themselves within atoms, and how this allows for atoms to have a magnetic moment.

1.1.2 Origin of Magnetic Moments

From the spin-statistic theorem, we know that because electrons have spin–$\frac{1}{2}$, they are fermions, and this has major consequences on how electrons of an atom interact at the microscopic level and how this leads to macroscopic properties [54, 182]. Indeed, from the fermionic character of electrons ensue interaction exchanges, due to the fact that the wave function describing electrons needs to be anti–symmetric (in spatial coordinates as well as in spin coordinates) under the exchange of 2 of the electrons. These resulting "exchange forces" shape the way electrons organize themselves at the atomic level [54]. They interact in such a way that emergent properties, otherwise not predictable by considering independent electrons, arise and are even described as observables. This led to two considerable consequences.

The first one is that atoms/ions have emergent spin moments, which arise from the collective interplay between electrons. Hund's rules and Pauli's principle allow to summarize theseexchange interactions and to predict the electronic ground state configuration for an independent atom/ion [134]. Pauli's principle ensures that they can only be 2 electrons within the same orbital, one with spin up $m_s^1 = +\frac{1}{2}$ and one with spin down $m_s^2 = +\frac{1}{2}$. The first of Hund's rules, known as the rule for maximum multiplicity, states that given a certain electronic configuration, electrons will maximize their total spin magnetic moments $\hat{\mathbf{S}}$.

Concretely, this means that electrons will first singly occupy the different orbital levels of a shell while all the electrons have their spin being up $m_s^i = +\frac{1}{2}$, before doubly occupying them. When a shell is more than half-filled, i.e there is one or more doubly occupied orbitals, the 2 electrons within the same orbital have opposite spin in accordance with Pauli's principle. The reason for electrons within a shell to maximize their total spin moment and have their spin parallel (and therefore by Pauli's principle to lay in different orbitals) is generally thought as the fact of having parallel spins and being in different orbital ensures that the electrons are further apart from each other and that their Coulomb repulsion is less important.

However, this turns out to be a wrong explanation. As explained in [134], considering the two following configurations of a helium atom : $1s2s$ with both spin pointing up noted ^3S, and $1s2s$ with spin being anti–parallel designated by ^1S, calculations based on quantum wave functions have shown that the average spacing between the

2 electrons is smaller for ${}^3S$ and that the inter-electronic repulsion is greater for ${}^3S$. Therefore the electron-electron interaction should favor a configuration with opposite spin. However, it turns out that the nucleus-electron interaction is more important for the ${}^3S$ and therefore reduces the potential energy of ${}^3S$ compared to the ${}^1S$ configuration. Taking into account the potential energy due to electron-electron interaction and electron-nucleus interaction imposes a lower energy state for the ${}^3S$ configuration. This is explained by the fact that the screening from the nucleus is less important for parallel spin due to their Pauli "repulsion" which induces a greater average angle between the electrons. Less screening from the nucleus allows the electrons to lower their potential energy by getting closer to the nucleus [29, 110, 134, 179, 220].

The second rule says that for a given multiplicity, the lowest energy configuration is given by the one with the largest value of orbital momentum $\hat{\mathbf{L}}$. The third and last rule expresses the effect of spin-orbit coupling and affirms that the lowest energy configuration happens for a total angular momentum $\hat{\mathbf{J}} = \hat{\mathbf{L}} + \hat{\mathbf{S}}$. Hund's rules have important repercussion on the magnetic properties of materials as it governs how the electrons are arranged. They are the reason for the existence of atoms/ions with effective spin–1 moments. Indeed, for instance, the nickel ion Ni^{2+} has an electronic structure given by $[Ar]3d^8$, where the 8 outer-electrons on the d shell will arrange themselves such that 3 of the 5 d orbitals will be doubly occupied, while 2 of them will each support an electron. Because of Hund's rules, the 2 unpaired electrons will have parallel spin summing up to a total spin magnetic moment $\hat{\mathbf{S}} = 1$.

We conclude by stating that the key point of the repercussions of how electrons interact via the laws of quantum electrodynamics allows for the total magnetic moment of an atom to take on different values, including $\hat{\mathbf{S}} = 1$.

The second consequence is that it impacts the way atoms interact with each other, which is mostly explained by how the outer electrons on each atom interact with the neighboring ones. Indeed, Magnetism usually arises from the collective behavior of outer electrons, even though its origin can also sometimes be due to the nuclei. This topic is discussed in the next Section, Section 1.1.3.

1.1.3 Origin of Magnetic Interactions

In bulk materials, magnetic properties result from the interaction between its constituents, which is described by quantum electrodynamics. It is, however, usually impossible to solve the systems exactly by taking into account all of its possible degrees of freedom. We, therefore, simplify the systems to an effective model that compasses the relevant degrees of freedom. For magnets, we commonly assume that the atoms are isolated and consist of ions (formed by the nucleus and the core electrons) which form a solid-state system of tight-bidding orbitals, and the outer electrons, which are the ones that we usually assume to mediate between the atoms.

Indeed, the exchange interactions arise from the interplay between Pauli's exclusion principle and the Coulomb interaction [55]. A simple example where this is at play is given by H_2 molecules, which consist of 2 electrons with 2 orbital degrees of freedom. Electrons are fermions and their total wave-function should be anti-symmetric (symmetric in real space and anti-symmetric in spin components or vice-versa). Considering 2 electrons a and b, if ϕ represents the single electron spacial wave function, their total

spatial wave function can be described by

$$\psi_{\pm} = \frac{1}{\sqrt{2}}(\phi_a(\mathbf{r}_1)\phi_b(\mathbf{r}_2) \pm \phi_b(\mathbf{r}_1)\phi_a(\mathbf{r}_2)) \ , \tag{1.9}$$

such that when permuting the 2 electrons, ψ_+ is symmetric in space but anti-symmetric in spin components and corresponds to an anti-parallel spin-singlet with anti–ferromagnetic (AFM) spin configurations, while ψ_- is anti-symmetric in space but symmetric in spin components and correspond to a parallel spin-triplet with ferromagnetic (FM) spin configurations.

We can estimate the energy due to exchanging the positions of two particles as

$$\mathcal{H}_{\mathbf{r}_1\mathbf{r}_2} = \tilde{J}\hat{P}_{\mathbf{r}_1\mathbf{r}_2} \ , \tag{1.10}$$

where $\tilde{J}$ sets out the strength of the interaction, such that when $\tilde{J} > 0$, ψ_- is favored, corresponding to a parallel spin-triplet state and when $\tilde{J} < 0$, ψ_+ is favored, corresponding to an anti-parallel spin-singlet state.

Additionally, we note that permuting the positions of the electrons can be equivalently described as permuting the spin–components

$$\hat{P}_{\mathbf{r}_1\mathbf{r}_2}\psi_{\pm} = \pm\hat{P}_{ab}\psi_{\pm} \ . \tag{1.11}$$

Instead of characterizing Eq. (1.10), we can consider the exchange of the spin of the 2 electrons and study the operator $\hat{P}_{ab}$

$$\mathcal{H}_{ab} = J\hat{P}_{ab} \ , \tag{1.12}$$

where J correspond to the energy due to the permutation $\hat{P}_{ab}$ of the spin components of particle b with particle a, which acts on the four states made out of the two electrons and their spin, namely $\{|\uparrow\uparrow\rangle \ , |\uparrow\downarrow\rangle \ , |\downarrow\uparrow\rangle \ , |\downarrow\uparrow\rangle\}$. The permutation operator $\hat{P}_{ab}$ rearranges these basis states into its eigenstates consisting of a singlet state with eigenvalue $\lambda = -1$ and 3 states forming a triplet with eigenvalues $\lambda = 1$.

$$\begin{aligned} &\text{singlet state:} && |s\rangle = \tfrac{1}{\sqrt{2}}(|\uparrow\downarrow\rangle - |\downarrow\uparrow\rangle) && \lambda = -1 \ , \\ &\text{triplet state:} && \begin{aligned} |t_1\rangle &= |\uparrow\uparrow\rangle \\ |t_2\rangle &= \tfrac{1}{\sqrt{2}}(|\uparrow\downarrow\rangle + |\downarrow\uparrow\rangle) \\ |t_3\rangle &= |\downarrow\uparrow\rangle \end{aligned} && \lambda = 1 \ . \end{aligned} \tag{1.13}$$

For a positive $J > 0$, the state that lowers the energy is the singlet state, and for a negative $J < 0$, the triplet state is favored. It follows that there is a sign difference between $\mathcal{H}_{\mathbf{r}_1\mathbf{r}_2}$ and $\mathcal{H}_{ab}$, such that we should consider the negative sign version of Eq. (1.11).

Additionally, applying the permutation operator twice should always project us back onto the same initial state

$$\hat{P}_{ab}^2 = \mathbb{I} \ . \tag{1.14}$$

Following [55, 90], we consider the operator

$$\hat{O}_{ab} = \frac{1}{2}(\hat{\mathbf{S}}_a \cdot \hat{\mathbf{S}}_b + \mathbb{I}) \,, \tag{1.15}$$

where $\hat{\mathbf{S}}$ represents the spin angular momentum of the electron and encodes the Pauli matrices as

$$\hat{\mathbf{S}}_\alpha = \frac{1}{2}\hbar \begin{pmatrix} \sigma_\alpha^x \\ \sigma_\alpha^y \\ \sigma_\alpha^z \end{pmatrix} \,. \tag{1.16}$$

Using the fact that the Pauli matrices satisfy

$$\left[\sigma_\alpha^\mu, \sigma_\beta^\nu\right] = 2i\epsilon^{\mu\nu\lambda}\delta_{\alpha\beta}\sigma_\alpha^\lambda \,, \tag{1.17}$$

to obtain

$$(\hat{\mathbf{S}}_a \cdot \hat{\mathbf{S}}_b)^2 = 3\mathbb{I} - 2\hat{\mathbf{S}}_a \cdot \hat{\mathbf{S}}_b \,, \tag{1.18}$$

we see that

$$\begin{aligned} \hat{O}_{ab}^2 =& \frac{1}{2}(\hat{\mathbf{S}}_a \cdot \hat{\mathbf{S}}_b + \mathbb{I}) \\ =& \frac{1}{4}((\hat{\mathbf{S}}_a \cdot \hat{\mathbf{S}}_b)^2 + 2\hat{\mathbf{S}}_a \cdot \hat{\mathbf{S}}_b + \mathbb{I}) \\ =& \mathbb{I} \,. \end{aligned} \tag{1.19}$$

It follows that

$$\hat{O}_{ab}\hat{\mathbf{S}}_a\hat{O}_{ab}^{-1} = \hat{\mathbf{S}}_b \,, \tag{1.20}$$

$$\hat{O}_{ab}\hat{\mathbf{S}}_b\hat{O}_{ab}^{-1} = \hat{\mathbf{S}}_a \,, \tag{1.21}$$

where we see that the operator $\hat{O}_{ab}$ exchanges the electrons the same way $\hat{P}_{ab}$ does. Therefore we write

$$\hat{P}_{ab} = \hat{O}_{ab} \,. \tag{1.22}$$

The energy associated with this permutation is given by

$$\mathcal{H}_{ab} = J\frac{1}{2}(\hat{\mathbf{S}}_a \cdot \hat{\mathbf{S}}_b + \mathbb{I}) \,, \tag{1.23}$$

where we see that a positive $J > 0$ favors an anti–parallel alignment of $\hat{\mathbf{S}}_a$ and $\hat{\mathbf{S}}_b$, while $J < 0$ favors a parallel alignment. We note that this is the opposite behavior of Eq. (1.10), and that, as previously mentioned, we need to consider the minus sign in Eq. (1.11), such that we obtain

$$\mathcal{H}_{\mathbf{r}_1\mathbf{r}_2} = -J\frac{1}{2}(\hat{\mathbf{S}}_a \cdot \hat{\mathbf{S}}_b + \mathbb{I}) \,, \tag{1.24}$$

which up to a proportional term and a constant term is known as the Heisenberg

Hamiltonian

$$\mathcal{H}_{\mathsf{Heis}} = J \sum_{\langle i,j \rangle} \hat{\mathbf{S}}_{\boldsymbol{i}} \cdot \hat{\mathbf{S}}_{\boldsymbol{j}} \ , \tag{1.25}$$

with J being the Heisenberg exchange interaction and where $\langle i, j \rangle$ represents nearest neighbor sites, and where $\hat{\mathbf{S}}_{\boldsymbol{i}}$ is the spin dipole moment defined through

$$\hat{\mathbf{S}}_{\boldsymbol{i}} = \begin{pmatrix} \hat{\mathrm{S}}_i^x \\ \hat{\mathrm{S}}_i^y \\ \hat{\mathrm{S}}_i^z \end{pmatrix} \ . \tag{1.26}$$

Its components satisfy the commutation relation

$$[\hat{\mathrm{S}}_i^\alpha, \hat{\mathrm{S}}_i^\beta] = 2i\epsilon_\gamma^{\alpha\beta} \hat{\mathrm{S}}_i^\gamma \ , \tag{1.27}$$

where a sum over repeated indices is assumed, and the spin length constraint

$$\hat{\mathbf{S}}_{\boldsymbol{i}}{}^2 = s(s+1) = \frac{3}{4} \ , \tag{1.28}$$

for spin–$\frac{1}{2}$. In what follows, we shall follow the Einstein convention of assuming sums on repeated indices of tensors, if not indicated explicitly. The Heisenberg Hamiltonian [Eq. (1.25)] is one of the simplest effective models.

The Origin of Exchange Interactions

Generally, the exchange interaction J can be positive or negative and favor configurations with anti-parallel or parallel dipole spin moments, leading to anti-ferromagnetism or ferromagnetism, respectively. In materials, whether the ground state is a ferromagnet (FM) or an anti-ferromagnet (AFM) depends on the case. For example, coming back to H_2 molecules, the ground state is found to be the singlet spin state favoring AFM order where the wave function corresponds to a bonding state between the two Hydrogen atoms [91, 133]. This, however, results in a zero total magnetic moment since the electrons share the same orbital quantum state. If, on the other hand, electrons are on two degenerate and orthogonal orbitals, an FM triplet ground state is favored.

Another mechanism that can lead to ferromagnetism is the double exchange [9, 49, 263]. There the interaction between two magnetic ions (usually in different hybridization states) happens through the exchange of an electron, but instead of directly being exchanged between the two magnetic ions, the exchange occurs via the intercourse of another atom. Typically, the atom mediating the interaction can give an electron to one of the magnetic ions and then receive an electron from the other ion. Delocalization reduces the energy, and transition from one atom to the other is facilitated if the electrons keep their spin value. Therefore double exchange usually leads to FM exchange [9, 263].

Another example of indirect exchange processes is the superexchange [9, 49]. In the superexchange mechanism, the interactions between two transition-metal ions happen via the coupling of the spin of 2 electrons belonging to a non-magnetic ligand. Different mechanisms have been proposed to explain this type of interaction, known as

Anderson's mechanism [8, 123], and Goodenough's mechanism [75, 77].

The nature of the interaction, FM or AFM, can generally be found using the Goodenough-Kanamori rules, which depend on the symmetry of the crystal and the electron occupancy of the involved orbitals [75, 76, 108]. If more than one ligand is involved so that the magnetic ions do not share the same ligand, we then refer to super-superexchange. Other types of interaction exchanges exist, such as the Ruderman-Kittel-Kasuya-Yoshida (RKKY) interaction [109, 202, 262], where the coupling happens via conduction electrons, or dipole-dipole interaction, which is usually much smaller than the exchange interactions but might not be negligible for a system where the exchange interactions are particularly weak, as it can be the case in some single-molecule magnets [266].

When corrections to relativistic phenomena are taken into account, they can lead to anisotropic exchange interaction. For instance Spin-Orbit Coupling (SOC) [$\mathcal{H}_{SO} = \lambda \hat{\mathbf{S}} \cdot \hat{\mathbf{L}}$] is a consequence of relativistic effects [134]. SOC can lead to single-ion anisotropy, or result in Kitaev-type exchange interactions [136, 184, 249]. If the spatial inversion symmetry is broken, SOC can also lead to Dzyaloshinski-Moriya interactions [56, 154, 155]. The origin of SOC is derived properly from Dirac's relativistic treatment of electrons. However, we can try to intuitively think about SOC as being the result of the electron's movement around the nucleus. In the electron's referential frame, the nucleus appears moving around the electrons. The nucleus being a positively charged moving object, it induces a magnetic field $\mathbf{B}$ which interacts with the magnetic moment of the electron μ as $\mathbf{B} \cdot \mu$. The apparent magnetic field is proportional to the electron's orbital moment $\mathbf{B} \propto \mathbf{L}$ and the electron's magnetic moment of the electron is proportional to its spin $\mu \propto \mathbf{S}$. This indeed results in a term proportional to $\mathbf{S} \cdot \mathbf{L}$, which depends on the relative angle between $\mathbf{S}$ and $\mathbf{L}$. And so does the total angular momentum $\mathbf{J} = \mathbf{L} + \mathbf{S}$. The effect of SOC is to split each atomic term into levels with different $\mathbf{J}$ and, therefore different energies and to induce interactions which are anisotropic in spin–space.

On general symmetry grounds, the Hamiltonian should stay invariant under time-reversal symmetry. This mean that only terms formed by the product of two spin dipole moments are allowed: $\hat{\mathbf{S}}_i \cdot \hat{\mathbf{S}}_j$, $(\hat{\mathbf{S}}_i \cdot \hat{\mathbf{S}}_j)(\hat{\mathbf{S}}_k \cdot \hat{\mathbf{S}}_l)$, etc. Unless a magnetic field is applied, which would result in a term proportional to $\hat{\mathbf{S}}_i \cdot \mathbf{B}_\mathrm{i}$, terms with odd numbers of spin components are forbidden [136].

As we will see in Section 1.2, higher orders interactions of spin components also sometimes need to be taken into account, especially when larger spin moments or itinerant electrons are involved. This is particularly true for a spin–1 system, for which the most general form of the Hamiltonian respecting $SU(2)$ symmetry is given by the bilinear-biquadratic Hamiltonian [Eq. (1.48)]. Indeed, the Hubbard model with multi-orbitals degrees of freedom gives rise to new terms besides the Heisenberg model, namely allowing biquadratic terms in case of a spin–1 [95, 140].

Thermodynamics of Magnets

Another important concept is the notion of spontaneous symmetry breaking, which happens when the order parameter breaks the symmetry allowed by the Hamiltonian. When the value of the order parameter, characterizing the order of the system, changes

value, we refer to a phase transition. Within Landau's theory, it is assumed that above a critical temperature the order parameter is zero, and non-zero under the critical temperature [129]. The free energy is considered to be an analytical function of the order parameter, and in the vicinity of the phase transition, the free energy can be expanded in powers of the order parameter.

For instance, considering the FM case, no specific type of order of the spin moments can be observed at high temperatures. However, as the temperature decreases, the local interaction between the spins starts favoring a parallel alignment. Below a certain critical temperature, all the spins are perfectly aligned with each other, and by selecting a specific orientation, the FM state spontaneously breaks the $SU(2)$ (or equivalently O(3)) spin-rotational continuous symmetry. From the local interactions, the system then acquires long-range correlations. Systems in which spontaneous symmetry occurs always exhibit Goldstone modes. The number of Goldstone-mode depends on the number of generators that have been broken.

This can be related to ferromagnetism in iron alloys, for example, where the magnetism comes from unpaired electrons in the 3d–shell of the iron atoms. Because of the interactions at play between the unpaired electrons, a parallel alignment of their magnetic moments is favored, and all the individual magnetic moments sum up to give rise to a macroscopic finite magnetization. Typically, for magnetite, which is an iron–oxide, and is generally formed by geophysical processes such as volcanic eruptions, the magnetic moments will align themselves and induce a finite magnetization along the earth's local magnetic field [167]. This finite magnetization is defined as a vector and will be pointing in a certain direction, breaking the continuous rotational symmetry of all possible configurations the magnetization could take. Small magnetic single domains of magnetite in many rocks are the main reason of their remanent magnetization [16, 88].

Also related to spontaneous symmetry breaking, we can mention the Mermin-Wagner theorem [146]. The Mermin-Wagner theorem states that for space dimensions $d \leq 2$, no phase transition in the isotropic Heisenberg model due to the spontaneous breaking of a continuous symmetry can happen at finite temperature.

When different types of interactions are competing, this usually results in frustration. Generally, frustration appears when the interaction between the agents involved is such that all of them can not be satisfied. Frustration can also find its origin in the lattice symmetry, such as in the famous AFM Ising model on the triangular lattice, where the lattice geometry forbids all the bonds to minimize their energy. This results in the fact that the system shows an absence of phase transition into the ground state and that there isn't a unique ground state, but a degenerate manifold of ground states [257]. Moreover, the degeneracy of the ground state scales exponentially with system size leading to a finite zero-temperature entropy [257]. Indeed, frustration is known as being a fruitful ground to explore rich physics.

Beyond The Theory of Bands

Many properties of the electrons in solids can be described by assuming the electrons to be free independent fermions in a periodic potential. This led to the band theory developed by Felix Bloch in 1928, which consists in solving the Schrödinger equations

for the wave function of an electron in the presence of a period potential [26]. In this approach, the interactions between the electrons are neglected. However, the Coulomb interaction between the electrons is not negligible. The band theory alone fails at explaining why certain materials with an odd number of electrons per unit site are insulators. Such metals are called Mott insulators [157]. Moreover, despite the physicists' intense efforts, the band theory failed at explaining superconductivity [132].

To explain why some metals with non-filled bands were insulating rather than conducting, Nevill Mott considered the difference in energy between the energy cost of having a doubly occupied site due to the Coulomb repulsion and the energy gain due to the kinetic energy obtained by delocalization of the "hole" and the double occupied state [156]. Indeed, electrons are negatively charged particles with spin–$\frac{1}{2}$. This means that they will repulse each other due to the Coulomb interaction. The behavior of the electrons will then also depend on the energy cost of having 2 electrons on the same site. This results in an insulator-conductor phase transition. The nature of such a transition is different from the conventional metal described by bands theory, as the gap is due to the Coulomb interaction. If the orbitals on different sites overlap sufficiently (typically by applying pressure), then conduction can happen.

Indeed, if the Coulomb interaction is prevailing, charge fluctuations are suppressed, electrons can be localized and only spin fluctuations stay relevant. Suppose we further assume that the Coulomb interaction between all the electrons is screened. In that case, we only need to account for the Coulomb repulsion when two or more electrons are on the same orbital at the same site, and we consider only one orbital per site. This can be seen through a simple model, called the Hubbard Model [97],

$$\mathcal{H}_{\mathsf{Hub}} = -t \sum_{\langle i,j\rangle,\sigma} \left(\hat{\mathrm{c}}^{\dagger}_{i,\sigma} \hat{\mathrm{c}}_{j,\sigma} + \hat{\mathrm{c}}_{i,\sigma} \hat{\mathrm{c}}^{\dagger}_{j,\sigma} \right) + U \sum_{i} \hat{n}_{i,\downarrow} \hat{n}_{i,\uparrow} \, , \tag{1.29}$$

where the sum $\langle i,j\rangle$ runs over nearest neighbors, $\sigma = \{\uparrow,\downarrow\}$ represents the spin of the electrons and $\hat{\mathrm{c}}^{\dagger}_{i,\sigma}/\hat{\mathrm{c}}_{i,\sigma}$, creates/annihilate an electron with spin σ on site i, $\hat{n}_{i,\sigma} = \hat{\mathrm{c}}^{\dagger}_{i,\sigma}\hat{\mathrm{c}}_{i,\sigma}$ counts the number of electrons on site i, such that t is the hopping parameter, and U represents the Coulomb repulsion due of having 2 spins with opposite spins (Pauli's exclusion principle). Electrons are fermions and the creation/annihilation operators $\hat{\mathrm{c}}^{\dagger}_{i,\sigma}/\hat{\mathrm{c}}^{\dagger}_{i,\sigma}$ satisfy fermionic commutation relations

$$\{\hat{\mathrm{c}}_{i,\sigma}, \hat{\mathrm{c}}^{\dagger}_{i,\sigma}\} = 1 \, . \tag{1.30}$$

The Hubbard model also allows explaining the physics described in Mott insulators. Indeed, as $\frac{U}{t}$ increases, the system undergoes a metal-insulator phase transition.

Moreover, in the limit $t \ll U$, for 2$^{\text{nd}}$ order in perturbation and for half-filling, the Hubbard model can be mapped to the anti-ferromagnetic (AFM) Heisenberg Hamiltonian [Eq. (1.25)] with

$$J = 4\frac{t^2}{U} > 0 \, . \tag{1.31}$$

Again, the exchange interaction J arises from quantum phenomena. In the example that we just saw, the way electrons interact is dictated by an interplay between the Coulomb interaction and Pauli's exclusion principle [55]. The interaction exchange

$J = 4\frac{t^2}{U}$ is positive and favors a configuration with anti-parallel dipole spins. This can be understood by noticing that with one electron on each site (half-filled single orbital), the electrons can hop on neighboring orbital only if they have opposite spins and that these delocalizing processes can lower the energy. However, it can be shown that when orders in perturbation are being taken up to 4^{th}, this leads to a correction of $J = 4\frac{t^2}{U} - 16\frac{t^4}{U^3}$ [95]. The correction term $-16\frac{t^4}{U^3}$ is valid when assuming hopping between two neighboring sites but is shown to increase as the number of involved sites is extended. This may eventually result in FM interactions, but as previously mentioned, other mechanisms, such as double exchange, can also lead to ferromagnetism. Moreover, when considering 4 sites or more, biquadratic terms of the form $(\hat{\mathbf{S}}_{\boldsymbol{i}} \cdot \hat{\mathbf{S}}_{\boldsymbol{j}})(\hat{\mathbf{S}}_{\boldsymbol{k}} \cdot \hat{\mathbf{S}}_{\boldsymbol{l}})$ also appear [95, 140].

Modern applications stemming from considering only the Coulomb interaction and Pauli's exclusion principle appear in ab–initio quantum chemistry methods. A recent illustration of such considerations is used to derive effective models for a family of trihalide materials: RuX_3, where X stands for Cl, Br, or I atoms [107]. These materials appear to be possible candidates for exhibiting honeycomb Kitaev–like physics at finite temperature and to be modeled by magnetic effective spin–$\frac{1}{2}$ moments interacting via anisotropic Kitaev–type couplings [259]. Indeed, for $RuCl_3$ the spin excitations show a broad continuum above the ordering temperature, which is interpreted as an indication for hosting the short–range order of the Kitaev spin liquid [15]. Below the ordering temperatures $T \simeq 7$ K [15] and $T \simeq 34$ K [99], for $RuCl_3$ and $RuBr_3$,respectively, the system exhibit a zigzag anti–ferromagnetic order. Meanwhile, for RuI_3 no long–range magnetic ordering is observed down to a temperature of $T = 0.35$ K under zero–field [169].

Density functional theory (DFT) based on a multi–orbitals Hubbard model is used to extract electronic structures and an exact–diagonalization method based on prior ab–inito estimates is used to derive an effective low-temperature magnetic model for all three compounds $RuCl_3$, $RuBr_3$, and RuI_3. As explained in [107], these techniques suggest that the three trihalide materials are Mott insulators, with a gap that is shown to decrease as the ligand size increases, suggesting that RuI_3 is close to a metal–insulator transition, which is consistent with its reduced resistivity compare to the two other compounds $RuCl_3$ and $RuBr_3$, accounting for the fact that sample purity might also affect the observed resistivity. Results also show that these trihalide materials have predominant FM Kitaev and FM Heisenberg nearest–neighbor interactions, where the latter nearly vanishes for RuI_3. Additionally, spin–orbit coupling is shown to be a necessary ingredient in order to restore agreement with experimental data, suggesting that $RuCl_3$, $RuBr_3$, and RuI_3 are spin–orbit Mott insulators. The DFT calculations show that $RuCl_3$ and $RuBr_3$ exhibit a zigzag magnetic order, while RuI_3 is subject to high frustration, for which ab–initio calculations applied to the effective low–temperature magnetic model suggest that RuI_3 hosts a quantum spin–liquid ground state, which is however possibly different from the $\mathbb{Z}_2$ Kitaev spin liquid [169].

1.2 What Makes Spin–1 Special

In this Section, I review some basic knowledge about spin–1 physics, what is special about a spin-1 on a single site, what interesting repercussions does this have for interacting spin–1 on a lattice, and what are the exotic features arising from the previous considerations.

However, before presenting the needed mathematical description of a spin–1 moment, in Section 1.2.1, I review how the conceptual math framework applies to a spin–$\frac{1}{2}$ moment and its (semi–)classical "large–S" limit. This will allow us to have a hopefully insightful comparison with spin-1 moments. In Section 1.2.2, I explain how spin–1 moments differ from both classical spin and spin–1/2 moments, by describing some special characteristics which arise for spin–1 moments. In Section 1.2.3, I describe how spin–1 moments interact in magnetic materials. In Section 1.2.4 and Section 1.2.5, I present two interesting features of spin–1 magnets in spin nematics and in 1–dimensional chain.

1.2.1 Single Spin–$\frac{1}{2}$

Generally, a quantum spin can be completely described by the eigenstates of the operator $\hat{\mathrm{S}}^z$

$$\hat{\mathrm{S}}^z|m\rangle = m|m\rangle \ , \tag{1.32}$$

where m is the spin projection quantum number specifying the quantization of the spin angular momentum and can take $2s+1$ values given by $m = -s, -s+1, \ldots, s-1, s$. The $2s+1$ states $|m\rangle$ form a closed orthogonal basis [130].

In the case of spin–$\frac{1}{2}$, $s = \frac{1}{2}$, and there are only two such eigenstates of $\hat{\mathrm{S}}^z$ with $m = \pm\frac{1}{2}$ as shown in Fig. 1.3(a)

$$\mathcal{B}_{\frac{1}{2}} = \{|\uparrow\rangle, |\downarrow\rangle\} \ . \tag{1.33}$$

These two states have both finite spin–dipole moments, and form a Kramers pair, related by time–reversal (TR) symmetry. A spin–$\frac{1}{2}$ moment can generally be described by a generic state consisting of a linear combination of the basis state $\mathcal{B}_{\frac{1}{2}}$

$$\left|\psi_{\frac{1}{2}}\right\rangle = c_\uparrow|\uparrow\rangle + c_\downarrow|\downarrow\rangle \ , \quad c_{\uparrow,\downarrow} \in \mathbb{C} \ , \tag{1.34}$$

subject to the constraint

$$|c_\uparrow|^2 + |c_\downarrow|^2 = 1 \ . \tag{1.35}$$

A spin–$\frac{1}{2}$ can be represented by a vector in a 2D Hilbert space, and any operation that ce be effectuated on a spin–$\frac{1}{2}$ while satisfying Eq. (1.35) can be represented by a $SU(2)$ matrix. The generators of $SU(2)$ are also the generators of $O(3)$. To be exact, $SO(3)$ is the universal cover of $SU(2)$, and this means that their algebra is the same. The generators belonging to the Lie algebra $su(2)$ can be used to generate both the Lie group $SU(2)$ and the Lie group $SO(3)$.

This implies a spin–$\frac{1}{2}$ can very well be represented by 2-dimensional complex vector subject to $SU(2)$ transformation, or equivalently by a $O(3)$-vector subject to $SO(3)$ transformations. For this reason, representing a "classical" spin–$\frac{1}{2}$ by an $O(3)$-vector

works really well and makes all classical methods that rely on the representation of a spin by an $O(3)$-vector powerful tools for studying systems with dipolar degrees of freedom.

This can also be understood in terms of a coherent state on the Bloch sphere. For a spin–$\frac{1}{2}$, coherent states are formed by transforming the maximum polarized state with SU(2) elements expressed in terms of the generators of SU(2). As basis for the generators, we use the Pauli matrices σ_i, and we can characterize a general rotation within $su(2)$ as [13]

$$\begin{aligned}|\Omega\rangle &= e^{-\frac{1}{2}\phi\sigma_z} e^{-\frac{1}{2}\theta\sigma_y} e^{-\frac{1}{2}\xi\sigma_z} |\uparrow\rangle \\ &= \begin{pmatrix} e^{-i\frac{\phi-\xi}{2}}\cos(\frac{\theta}{2}) & -e^{i\frac{\phi+\xi}{2}}\sin(\frac{\theta}{2}) \\ e^{i\frac{\phi-\xi}{2}}\sin\frac{\theta}{2}) & e^{i\frac{\phi+\xi}{2}}\cos(\frac{\theta}{2}) \end{pmatrix} \begin{pmatrix} 1 \\ 0 \end{pmatrix} \\ &= e^{-i\frac{\phi-\xi}{2}}\cos(\frac{\theta}{2})|\uparrow\rangle + e^{i\frac{\phi-\xi}{2}}\sin(\frac{\theta}{2})|\uparrow\rangle \quad \phi,\theta,\xi \in [0,2\pi] \,, \end{aligned} \tag{1.36}$$

where we used

$$e^{-\frac{1}{2}\theta\sigma_\alpha} = \cos(\frac{\theta}{2})\mathbb{I} - i\sigma_\alpha \sin(\frac{\theta}{2}) \,, \tag{1.37}$$

which is obtained by expanding the exponential in its Taylor series, and using the fact that $\sigma_\alpha^2 = \mathbb{I}$. In Eq. (1.36), we can then define

$$\psi = \phi - \xi \,, \tag{1.38}$$

and using the fact that $|\Omega\rangle$ is defined up to a phase, we consider

$$|\Omega\rangle = e^{-i\psi}\sin(\frac{\theta}{2})|\uparrow\rangle + \cos(\frac{\theta}{2})|\downarrow\rangle = \cos(\psi)\sin(\frac{\theta}{2})|\uparrow\rangle - i\sin(\psi)\sin(\frac{\theta}{2})|\uparrow\rangle + \cos(\frac{\theta}{2})|\downarrow\rangle \,, \tag{1.39}$$

that we can represent as a 3–dimensional vector on the 2–dimensional sphere as illustrated by the Bloch sphere shown in Fig. 1.2.

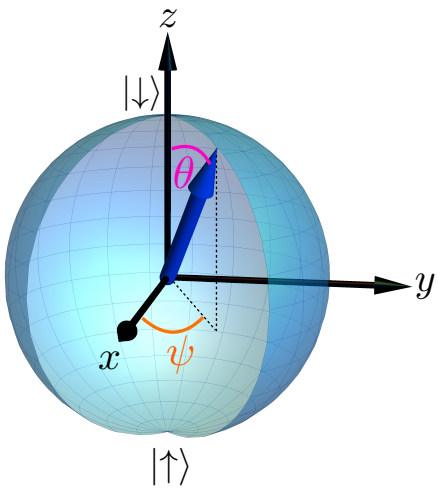

Figure 1.2: Bloch Sphere representing the spin–coherent states of a spin–$\frac{1}{2}$ moment according to Eq. (1.39).

More details on the representation of a spin–$\frac{1}{2}$ are given in Section 2.2.2.

1.2.2 Single Spin–1

For a spin–1, several new features appear. The quantum number m can take 3 different values $m = 1, 0, -1$. The associated eigenstates of $\hat{\mathrm{S}}^z$

$$\mathcal{B}_1 = \left\{|1\rangle, |0\rangle, \left|\overline{1}\right\rangle\right\} \ , \tag{1.40}$$

form the "magnetic" basis illustrated in Fig. 1.3(b). The two states $|1\rangle$ and $\left|\overline{1}\right\rangle$ are said

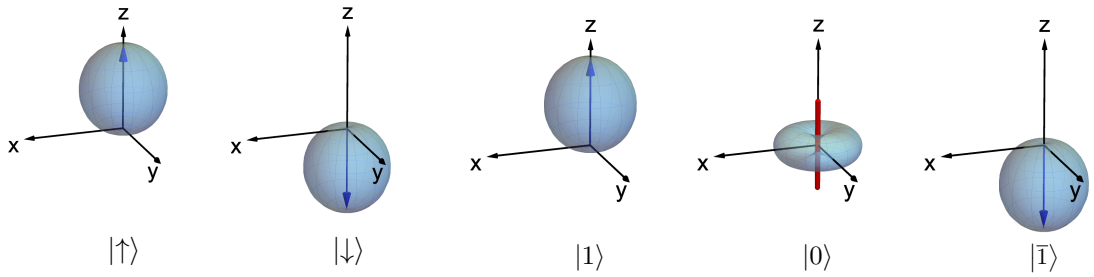

(a) Magnetic basis for a spin–$\frac{1}{2}$. **(b)** Magnetic basis for a spin–1.

Figure 1.3: Usual, "magnetic" basis for a spin–$\frac{1}{2}$. [(a)] and a spin–1 [(b)] moment, formed by eigenstates of S^z. (a) States representing a spin–$\frac{1}{2}$ moment with $S^z = \pm\frac{1}{2}$, labeled $|\uparrow\rangle$ and $|\downarrow\rangle$ (b) States representing a spin–1 moment. Those with $S^z = \pm 1$, labeled $|1\rangle$ and $|\overline{1}\rangle$ break time–reversal symmetry and have a finite spin–dipole moment (blue arrow). While, the state with $S^z = 0$, which is only present for a spin–1 and labeled $|0\rangle$, posses a quadrupolar magnetic moment, which can be represented through a director (red bar). Figure is reproduced from [201].

to be magnetic in the sense that the expectation value of at least one of the spin-dipole components is finite, namely

$$\langle 1|\hat{\mathrm{S}}^z|1\rangle = 1 \ , \quad \left\langle\overline{1}\right|\hat{\mathrm{S}}^z\left|\overline{1}\right\rangle = -1 \ ,$$

and null for the other components. Similarly to the two dipolar states of the spin–$\frac{1}{2}$, the states $|1\rangle$ and $\left|\overline{1}\right\rangle$ are also related by TR symmetry and from a Kramers pair. However, the same is not true for $|0\rangle$. Indeed, we have

$$\langle 0|\hat{\mathrm{S}}^x|0\rangle = \langle 0|\hat{\mathrm{S}}^y|0\rangle = \langle 0|\hat{\mathrm{S}}^z|0\rangle = 0 \ . \tag{1.41}$$

This can be understood from the fact that even though $|0\rangle$ is not TR invariant, $|0\rangle$ is proportional to $-i|0\rangle$, which is TR invariant

$$\hat{T}|0\rangle = -|0\rangle \quad \Rightarrow \quad \hat{T}(-i|0\rangle) = -i|0\rangle \ . \tag{1.42}$$

This implies that $|0\rangle$ cannot possess a finite dipole moment. However, expectation values of products of two spin-dipole moments can still take on a finite value:

$$\langle 0|\hat{\mathrm{S}}^x\hat{\mathrm{S}}^x|0\rangle = \langle 0|\hat{\mathrm{S}}^y\hat{\mathrm{S}}^y|0\rangle = 1 \quad , \quad \langle 0|\hat{\mathrm{S}}^z\hat{\mathrm{S}}^z|0\rangle = 0 \; . \tag{1.43}$$

We call these quantities, which are of second order in spin-dipole moments, quadrupoles. The quadrupole tensor is defined as

$$\hat{\mathrm{Q}}^{\alpha\beta} = \hat{\mathrm{S}}^\alpha\hat{\mathrm{S}}^\beta + \hat{\mathrm{S}}^\beta\hat{\mathrm{S}}^\alpha - \frac{2}{3}\delta^{\alpha\beta}s(s+1) \; . \tag{1.44}$$

And, we say that the state $|0\rangle$ has a finite spin–quadrupole moment, even though it does not possess a finite spin-dipole moment.

Being able to support a quadrupole moment is a property that distinctively differentiates a spin–1 from a spin–$\frac{1}{2}$. A spin–1 is special because it is the smallest spin that is able to support a quadrupole moment on a single site. This makes spin–1 systems good candidates to investigate magnetism, including higher spin order–moments as well as quantum effects. The fact that a spin–1 is able to be a state characterized by vanishing spin-dipole moments, being TR invariant, and having finite second order spin-dipole (i.e. quadrupole) moments, motivates the introduction of the quadrupole tensor defined by Eq. (1.44). It is a traceless, symmetric rank–2 tensor. This means that there are only five linearly independent components (given below in Eq. (1.47)). Being the product of two spin-dipole components, we note that a quadrupole moment is TR invariant.

A general state of a spin–1 moment can generally be described by a generic state consisting of a linear combination of the basis state $\mathcal{B}_1$

$$|\psi_1\rangle = c_1|1\rangle + c_2|0\rangle + c_3|\overline{1}\rangle \; , \quad c_\alpha \in \mathbb{C} \; , \tag{1.45}$$

subject to the constraint

$$|c_1|^2 + |c_2|^2 + |c_3|^2 = 1 \; . \tag{1.46}$$

Abstractly, a spin–1 is represented by a vector belonging to a 3D-Hilbert space, where the components of the vector expressed in the the "magnetic" basis $\mathcal{B}_1$ are given by the complex coefficients c_α. Anything that can happen to such a vector, while satisfying the normalization constraint in Eq. (1.46), can be described by a matrix of $SU(3)$. To generate the $SU(3)$ group, which dimension is 8, we need the eight generators belonging to the algebra $su(3)$ to describe a spin–1 properly [180, 183, 229].

As explained in Section 2.2, for a spin–$\frac{1}{2}$, the 3 spin-dipole components in Eq. (1.26) and their commutation relations [Eq. (1.27)] suffice to generate $SU(2)$ (that describes anything that can happen to a 2D complex vector representing a spin–$\frac{1}{2}$) which is 3–dimensional. However, they fail at describing a spin–1 moments. Indeed, we need five additional generators to construct the $su(3)$ algebra. Luckily, these can be found to be

the 5 linearly independent spin–quadrupole moments

$$\mathbf{Q}_i = \begin{pmatrix} Q^{x^2-y^2} \\ Q^{3z^2-r^2} \\ Q^{xy} \\ Q^{yz} \\ Q^{xz} \end{pmatrix}_i = \begin{pmatrix} (S^x)^2 - (S^y)^2 \\ \frac{1}{\sqrt{3}}(3((S^z)^2 - S(S+1)) \\ S^xS^y + S^yS^x \\ S^yS^z + S^zS^y \\ S^xS^z + S^zS^x \end{pmatrix}_i . \tag{1.47}$$

Moreover, when considering the classical limit $S \to \infty$, we might think that larger spins are more classical. Indeed as the length of the spin increases s, so does the possible $2s+1$ value of the quantum number $m = -s, -s+1, \ldots, s$, partitioning the z-axis into the discrete allowed m values. And in the classical limit $S \to \infty$, the allowed m values become continuous, and representing a spin in its classical limit by an $O(3)$–vector seems legitimate. But this is not necessarily true for an integer-spin, such as spin–1, which can lack any finite dipole-moment and support quadrupoles. Indeed a spin–1, and any integer spin in general, will have a state with $m = 0$ such that its associated dipole moment is not pointing anywhere. This means that for a spin–1, the classical limit as an $O(3)$–vector is not valid, since it is obvious that an $O(3)$–vector can not describe the "dipole-less-ness" of a spin–1 moments.

To summarize, what makes a spin–1 unique is its ability to support quadrupole on a single site, but at the same time also allow for large quantum fluctuations [87, 131, 180, 183, 250]. A detail explanation of the comparison between a spin–$\frac{1}{2}$ and spin–1, their corresponding algebra and representations is given in Section 2.2 and Section 2.3, respectively.

1.2.3 Polygamous Spin–1

We now extend this analysis of a single spin–1 moment to a model of many interacting spin–1 moments. The questions we endeavor to answer in this section are: what can happen if we consider spin–1 moment interacting on a lattice and how does this make spin–1 systems different from their little siblings consisting of spin–$\frac{1}{2}$?

Generally for a spin of length s, terms up to $(\hat{\mathbf{S}}_i \cdot \hat{\mathbf{S}}_j)^{2s}$ can contribute to the Hamiltonian. Higher order can always be rewritten in $(\hat{\mathbf{S}}_i \cdot \hat{\mathbf{S}}_j)^{2s}$ terms, which is a consequence of the algebra structure describing a spin–s. For instance, because of the structure of the $SU(2)$ algebra (i.e. the properties of the Pauli matrices), the $(\hat{\mathbf{S}}_i \cdot \hat{\mathbf{S}}_j)^2$ can be rewritten as a bilinear term [185, 210]. And, we insist on the fact that this precise biquadratic term $(\hat{\mathbf{S}}_i \cdot \hat{\mathbf{S}}_j)^2$ is not allowed for a spin–$\frac{1}{2}$.

In contrast, for a spin–1 system, the first crucial observation is that higher order terms of spin components interactions, besides the Heisenberg term, are allowed. Indeed, for a spin-1, besides the Heisenberg term, a biquadratic term $(\hat{\mathbf{S}}_i \cdot \hat{\mathbf{S}}_j)^2$ is also expected. We note for now that a biquadratic dipole term $(\hat{\mathbf{S}}_i \cdot \hat{\mathbf{S}}_j)^2$ will include a term proportional to a quadratic quadrupole term $\hat{\mathbf{Q}}_\mathbf{i} \cdot \hat{\mathbf{Q}}_\mathbf{j}$ [Eq. (1.47)]. The additional presence of the biquadratic term can be intuitively understood by considering the exchange interaction of electrons between 2 spin–1 atoms, which should affect their quadrupolar as well as dipolar moments. Thus, the resulting effective interaction should also depend on both dipolar and quadrupolar interactions.

Taking these considerations into account, the most general $SU(2)$ invariant Hamiltonian describing a system of spin-1 moments is known as the Bilinear Biquadratic (BBQ) Hamiltonian:

$$\mathcal{H}_{\mathsf{BBQ}} = \sum_{\langle i,j \rangle} \left[J_1 \hat{\mathbf{S}}_{\boldsymbol{i}} \cdot \hat{\mathbf{S}}_{\boldsymbol{j}} + J_2 (\hat{\mathbf{S}}_{\boldsymbol{i}} \cdot \hat{\mathbf{S}}_{\boldsymbol{j}})^2 \right] , \tag{1.48}$$

where we do not consider SOC and any type of anisotropy, yet. Extending the single orbital Hubbard model [Eq. (1.29)] to two orbitals, and considering 2 sites leads to terms proportional to $(\hat{\mathbf{S}}_{\boldsymbol{i}} \cdot \hat{\mathbf{S}}_{\boldsymbol{j}})^2$. Indeed, it can be shown that by considering the Hubbard model [Eq. (1.29)] for a spin–1, with two orbital degrees of freedom per site, up to 4^{th} order in perturbation, it can be mapped onto the BBQ Hamiltonian [4, 17, 23, 59, 95, 150, 244]. Recently, a four-site Hubbard model has been shown to reproduce the physics of spin–1 chains described by the BBQ Hamiltonian [35].

In terms of the 5 linearly independent quadrupole moments [Eq. (1.47)], the BBQ Hamiltonian [Eq. (1.48)] can be expressed as

$$\mathcal{H}_{BBQ} = \sum_{\langle i,j \rangle} \left(J_1 - \frac{J_2}{2} \right) \hat{\mathbf{S}}_{\boldsymbol{i}} \cdot \hat{\mathbf{S}}_{\boldsymbol{j}} + \frac{J_2}{2} \, \hat{\mathbf{Q}}_{\mathbf{i}} \cdot \hat{\mathbf{Q}}_{\mathbf{j}} + \frac{J_2}{3} s^2 (s+1)^2 , \tag{1.49}$$

where for convenience, we parameterize the interaction couplings J_1 and J_2 as

$$J_1 = J \cos\theta \quad , \; J_2 = J \sin\theta \, . \tag{1.50}$$

In the form of Eq. (1.49), it becomes clear that it is the biquadratic interaction exchange J_2 that endorses for quadrupole moments to interact. We also note that from the above explanation, and in concordance with the discussion in Section 1.1, biquadratic term for a spin–$\frac{1}{2}$ (i.e. electron with one orbital) are not allowed.

1.2.4 Spin Nematics

An interesting feature of spin–1 systems is that they can support nematic order. This comes from the fact that a spin–1 allows for on-site quadrupole moments. Nematic order happens when quadrupoles rather than dipole order. The word nematic originates from the Liquid Crystals' (LCs) nomenclature [37, 62]. LCs are formed of rod-shaped molecules. At high temperatures, these molecules are simply disordered and from a kind of liquid. They are homogeneous and isotropic, and therefore invariant under $SO(3)$ symmetry. It can happen that, for some LCs, under a certain temperature, they become anisotropic while staying homogeneous. The rod-shaped molecules can align themselves along a given axis. However, the extremities of the molecules are indistinguishable, and it is not possible to assign an orientation to the axis along which they align, as shown in Fig. 1.4. We call this orientation-less axis a director. This type of order is characterized by being symmetric under $SO(2)$ (rotation around the axis of the molecule) and under O(1) (flipping the extremities). The order parameter space M is given by

$$M = SO(3)/(SO(2) + O(1)) = \mathbb{RP}^2 , \tag{1.51}$$

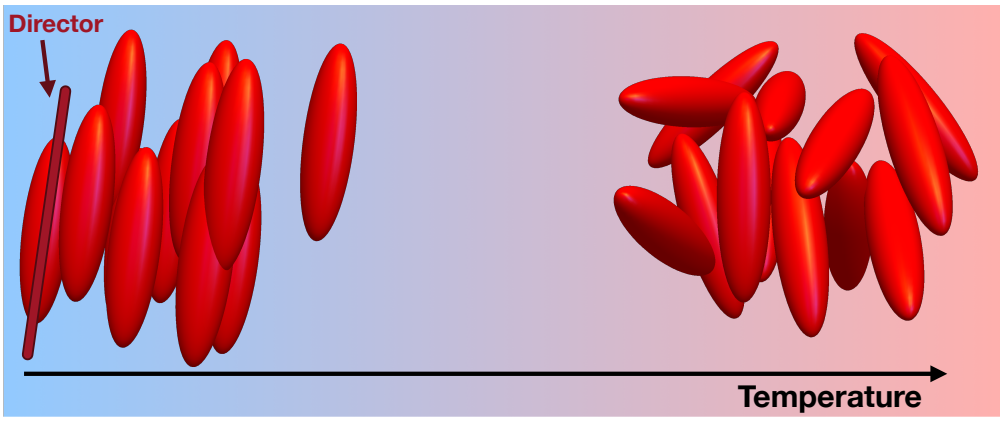

Figure 1.4: Liquid crystals are made of rod-shaped molecules invariant under inversion symmetry, such that the order parameter space is given by $\mathbb{RP}^n$, where n+1 is the dimension of the space in which the molecules are embedded. For this figure, $n = 2$. In certain Liquid Crystals, it can happen that these molecules align themselves with each other along a given axis. The resulting order is characterized by a vector without an orientation, called a director.

which is called the real projective space and represents half of a sphere where opposite points on the edge are identified as illustrated in Fig. 1.5. When the order parameter takes a well-defined value in $\mathbb{RP}^2$, it is said to be nematic.

The same type of order can happen in spin systems. This is easily illustrated by considering a spin–1. Indeed, the $|0\rangle$ state, which posses quadrupole moments, can also be represented by a (complex) director [Eq. (2.35)] (red rod in Fig. 1.3(b)) which does not possess an orientation, as can be inferred from the symmetric donut-shape of its spin fluctuation probability. This can also be understood by the fact that for the $|0\rangle$ state, the spin dipole moment is not pointing anywhere, but it still represents a spin of length 1 and therefore exhibits finite spin-quadrupole moments. These spin-quadrupole moments are products of two spin-dipole moments, such that the information on the orientation of the spin is lost. The spin analog of the nematic state in LCs can then be built up by considering quadrupolar states characterized by vanishing spin-dipole moments. If their directors, or rods, align themselves with each other, we obtain what we call the ferro-quadrupolar state. This state does not possess any spin-dipole moment and does not break TR symmetry but exhibits spin-quadrupole moments. The fact that the spin nematic preserves TR symmetry makes its static properties quite challenging to probe in commonly used experimental techniques, such as neutron scattering experiments or splitting of spectral lines in NMR spectroscopy [229–231]. The spin nematic state is therefore sometimes referred to as a hidden order.

Spin nematic order for the BBQ Hamiltonian was recognized by Blume in 1969 [27]. Fifteen years later, it was theoretically discussed [10] and gained interest among scientists as being this unconventional order where spin-space isotropy is broken but time–reversal invariance is preserved. Only recently have some material emerged as experimental candidate for spin–nematic such as $NiGa_2S_4$[159, 161, 253], $LiCuVO_4$ [70, 80, 177], Volborthite [119] and $BaCdVO(PO_4)_2$ [192, 227]. Spin–1 models provide a rich and fruitful playground to investigate the spin analogue nematic order found in

LCs and have been studied as a prototype for spin–nematic (i.e. quadrupolar) order in various physical systems such as magnetic insulators [87, 131, 180, 229, 250], Fe–based superconductors [60, 74, 126, 139, 256], and cold atoms [52, 53, 100, 232, 270].

From Eq. (1.45), a spin–1 can be represented by 3 complex numbers, which can be collected into a vector. Expressed within a special basis, that is TR–invariant in order to describe the symmetries of a spin–nematic. This vector is referred to as director and is formally introduced later [Eq. (2.35)]. Similar to the LCs, the order parameter phase of spin-nematics can also be represented by the complex projective plane $\mathbb{CP}^n$, since the components of the vector describing a spin–1 are complex. We note that for a 3–dimensional complex vector, the vector is normalized and defined up to phase. Using the constraint on the length and the gauge freedom on the phase, we can restrict to a 2–dimensional director which takes on value on the 2–dimensional complex projective plane $\mathbb{CP}^2$. We further mention that if the considered phase is fully quadrupolar, such that the director (vector in the TR–invariant basis) is purely real (such that it stays TR–invariant), then the order parameter phase is given by the 2–dimensional real projective plane $\mathbb{RP}^2$, which is illustrated in Fig. 1.5.

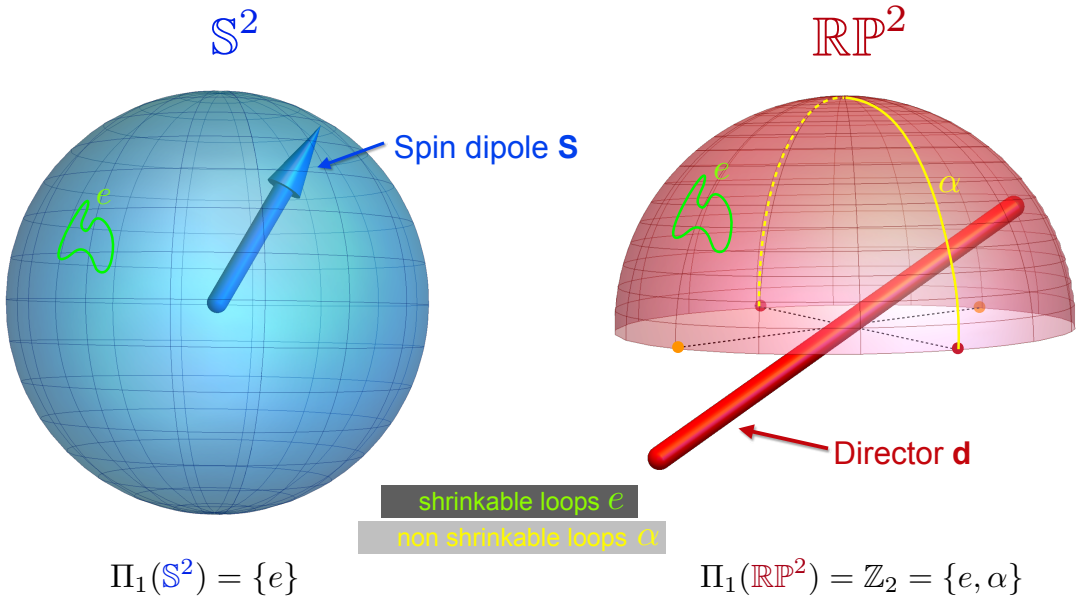

Figure 1.5: Order parameter space for a dipole moment and a director. An O(3)–spin dipole moment of length 1 can be characterized by two angles which represent a point on the unit sphere $\mathbb{S}^2$. Therefore the order parameter is given by the sphere $\mathbb{S}^2$. While for a (purely real) director of length 1, a point on half of the sphere with opposite edge point being identified suffice to determine it because of its non-orientability. This space is called the real projective space and is noted $\mathbb{RP}^2$.

The study of "shape" taken by the order parameter manifold can lead to important repercussions. Namely, studying its topology, and how it transforms under smooth deformations can provide useful insights regarding non-trivial, topological excitations [145]. A convenient way to investigate the "forms and shape" of groups and spaces consists in studying their homotopy groups by classifying their homotopy classes. For

this, we consider the mapping of closed n-loops from the n-sphere $\mathbb{S}^n$ onto the order-parameter space. We then study what happens to these loops under smooth deformations and classify all the loops that "behave identically" into the same equivalence classes. For instance, for the first homotopy group, i.e. n=1, this means that we map closed strings defined on the circle $\mathbb{S}^1$ onto the order-parameter space and observes what happens as we continuously deform the closed strings.

As we will see shortly, this feature also drastically differentiates a spin-$\frac{1}{2}$ from a spin–1. In the classical limit, a spin-$\frac{1}{2}$ can be represented by $O(3)$-vector which can take any value on the sphere $\mathbb{S}^2$, and therefore the order-parameter space is the sphere $\mathbb{S}^2$, as shown in Fig. 1.5. We also know that for a classical spin–1, an $O(3)$-vector does not suffice, but, in the case of a nematic ground state, a director can depict the "dipole-less-ness" of a classical spin–1. We just saw that the order-parameter space for a 3-dimensional complex or real director is the complex or real projective space, $\mathbb{CP}^2$ or $\mathbb{RP}^2$. We then study how closed loops transform under continuous deformation when mapped to the sphere $\mathbb{S}^2$ for a spin-$\frac{1}{2}$ and (for simplicity reasons) to the real protective plane $\mathbb{RP}^2$ for a purely quadrupolar (i.e TR invariant) spin–1, respectively.

As shown in Fig. 1.5, we can intuitively note that for the sphere $\mathbb{S}^2$, all the closed loops are trivially equivalent and all can be continuously shrunk into a single point. We say that the first homotopy group of the $\mathbb{S}^2$ is trivial [Eq. (1.52a)]. However, for the real projective plane $\mathbb{RP}^2$, we observe that there are two kinds of loops, one type that does not go through the edge and that is shrinkable; and the second type of loops that goes through the edge and that is not shrinkable. We also note that a loop that goes through the edge and winds twice around becomes a shrinkable loop. Therefore, there are only two first homotopy classes for the real projective space $\mathbb{RP}^2$ [Eq. (1.52b)]. Symbolically, we write [30]

$$\Pi_1(\mathbb{S}^2) = \{e\} \,, \tag{1.52a}$$

$$\Pi_1(\mathbb{RP}^2) = \mathbb{Z}_2 \,, \tag{1.52b}$$

where $\{e\}$ is the identity element.

Characterizing homotopy groups for order-parameter spaces allows identifying what type of topological defects are allowed [145]. The first homotopy group gives information about point-like defects. This means that there are no point-like defects in systems consisting of classical $O(3)$-vectors, but that there can be topological defects (sometimes called vortices) for spin–1 magnets. For spin nematic characterized by quadrupolar order, the fact that its first homotopy class is given by the group $\mathbb{Z}_2$ implies that there are there is the trivial element (which corresponds to the shrinkable loops) and one type of non–trivial topological elements (which corresponds to non–shrinkable loops). This means that there is one kind of vortex and that a vortex is also its anti–vortex. This can be seen that by combing a non–shrinkable loop with its "anti–loop" (i.e. the inverse loop), we are back to a trivial shrinkable loop. Higher homotopy groups can also be computed, bringing knowledge about higher orders of topological defects, such as skyrmions for dipolar spins.

1.2.5 Spin–1 1D–Chains

A famous example that emphasizes the importance of the value of the spin in quantum magnetism is the 1D Haldane chain. Originally, Haldane's claim stems from considering the non-linear σ model for the 1-D Heisenberg chain. This leads to a formulation of the Lagrangian (or the action) in terms of a topological quantity that depends on the value of the spin. This resulted in the fact that in 1D-chains, spin fluctuations lead to different physics for integer and half-integer spin [82, 83].

For the 1D Heisenberg anti-ferromagnetic chain, Haldane predicted that for half-integer spins, the system is gapless, mimicking the fact that it has Goldstone modes and breaks a continuous symmetry, but in fact, it is exhibiting incipient order with algebraic correlations. [82, 83]. For spin–$\frac{1}{2}$, the Lieb-Schultz-Mattis theorem [137] gave a solid proof for the non-existence of the gap and has been shown to be extendable to higher half-integer spins.[1]

For a spin-1, however, Haldane conjectured that the excitations are gapped [82, 83]. This was unexpected because it was believed that they were gapless too, similarly to spin–$\frac{1}{2}$. Indeed, quantum fluctuations for $s > \frac{1}{2}$ are even weaker, and there were no apparent reasons as to why the quantum fluctuation would wash out the "quasi"-long-range order. This seemed even to violate the Mermin-Wagner theorem [146], as it would mean that one would have a phase transition at a temperature equivalent to the gap. It was then believed that the gapped ground state of the 1-D Heisenberg chain consisted simply of a product state of spin-1 in their $S^z = 0$ state, not breaking any symmetries and any display of order. However, it turns out that the nature of the ground state goes beyond the Landau theory.

Affleck showed that for the BBQ model [Eq. (1.48)] for a 1D–chain, with parameters $\frac{J_2}{J_1} = \frac{1}{3}$, called the AKTL model, the ground state is gapped and exhibits a Valence Bond Solid (VBS) nature, while correlations show exponential decay [2, 3]. In the VBS ground state, each spin–1 can be viewed as a triplet state formed by two spin–$\frac{1}{2}$, where each individual "sub"–spin–$\frac{1}{2}$ forms a singlet state with the "sub"–spin–$\frac{1}{2}$ of the neighboring spin–1. The VBS ground state then has dangling free spin–$\frac{1}{2}$ on each extremity. These gapless spin–$\frac{1}{2}$ excitations have also been observed in experiments [79]. It turns out that the edge spin–$\frac{1}{2}$ degrees of freedom are topologically protected only if the integer spin value is odd and the topological phase is protected by a set of global symmetries (dihedral group of π rotations about the x–, y–, and z–axes, time-reversal symmetry and bond inversion symmetry) [39, 191]. The VBS is depicted in Fig. 1.6. Since in the VBS ground state, each "sub"–spin-$\frac{1}{2}$, is involved in a singlet-state, two adjacent spin-1, can only be in a superposition with total spin either equal to 1 or 0.

It can be shown that the AKTL model in fact represents the projector operator of a spin-2. Therefore, the VBS state is an eigenstate of the AKTL model, and it turns out to be the unique ground state [2, 3]. Moreover, using DMRG, the VBS ground state of the AKTL model is shown to extend to the pure Heisenberg Hamiltonian [209] (see reference [209] for a detailed description of the phase diagram of the BBQ model for a 1D spin-chain). Therefore the ground state of the 1D AFM spin–1 Heisenberg chain is the VBS state, which is gapped, shows short-range order, and exponentially decaying correlations [209]. This ground state is sometimes called a non-degenerate disordered

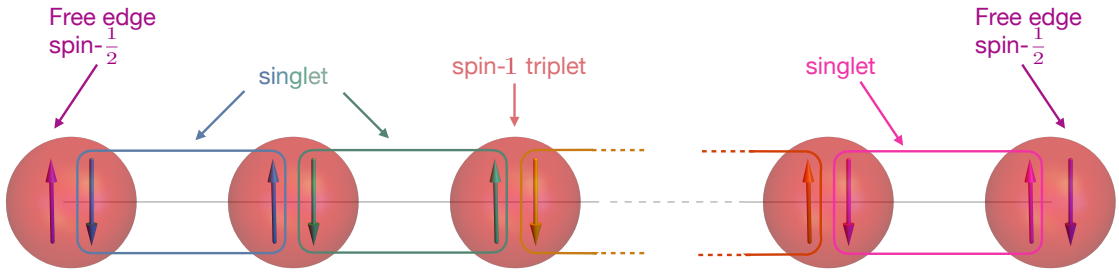

Figure 1.6: Representation of the Valence Bond Solid (VBS) state on a spin–1 chain. The orange-red spheres represent the spin–1 moments consisting of two spin–$\frac{1}{2}$ moments in a triplet state. The colored boxes encapsulating the two individual neighboring "sub"–spin–$\frac{1}{2}$ illustrate a singlet state. At both extremities of the chain are found the two edge spin–$\frac{1}{2}$ degrees of freedom.

one because it is unique and does not break spin symmetry. This is why it is also sometimes referred to as a hidden state. This type of order was the first example of symmetry protected topological state (SPT) [84, 191, 213]. Different physical characteristics of systems can be linked to SPT, such as the quantization of magnetization plateau [178, 241, 243] Spin–1 quasi–1–D chains have also been studied to explore extension of 1–D chains physics. For instance, the zig–zag 1D–chain reproduces a type of 1-dimensional triangular structure and is used as a prototype to investigate the BBQ model on a simple, yet closer to 2–dimensional real material systems, such as the triangular lattice compounds $NiGa_2S_4$ [159]. For this model a trimerized state is also found [48].

Spin-1 chains provide a particular example that spin-1 is different and can lead to unexpected and exotic physics.

1.3 Spin–1 Nowadays

Here, I present the current understanding and interest of spin–1 magnets, and I will mainly focus on the experimental history of two spin–1 materials, $NiGa_2S_4$ and $NaCaNi_2F_7$, and I illustrate how modern theoretical techniques have been applied to understand their physics better. This allows me to introduce important concepts and methods that motivate the development of my own formalism.

1.3.1 Spin–1 in the Wild

A Triangular Lattice Example: $NiGa_2S_4$

A well–studied example of a spin–1 material is $NiGa_2S_4$, whose crystal image and crystalline structure are shown in Fig. 1.7(a) and Fig. 1.7(b). In this material, Magnetism is associated with the Nickel ions Ni^{2+}, which form a triangular lattice. $NiGa_2S_4$ special's characteristic is to exhibit gapless excitations at low temperatures in the absence of long-range magnetic order.

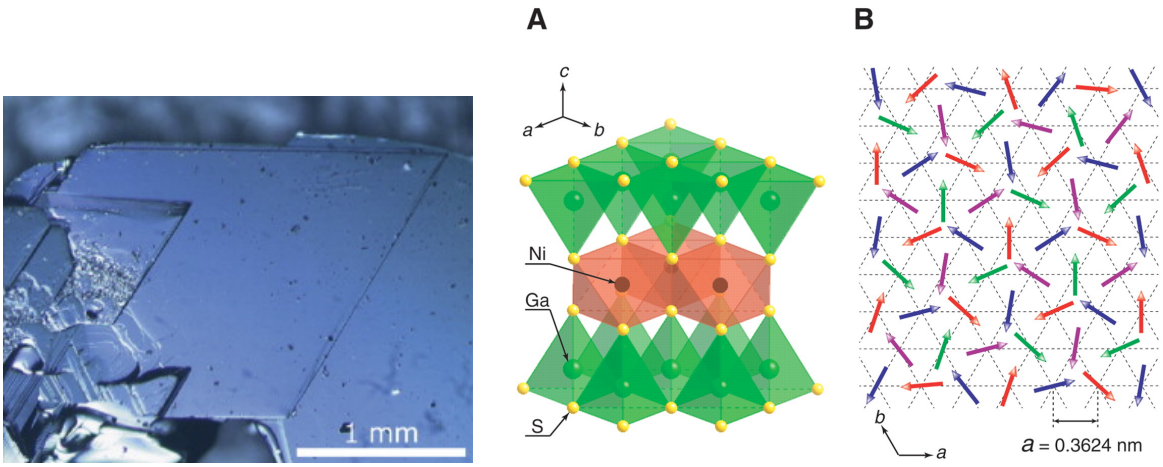

(a) $NiGa_2S_4$ crystal **(b)** $NiGa_2S_4$ structure

Figure 1.7: (a) $NiGa_2S_4$ crystal grown by chemical vapor transport method, reproduced from [162]. (b) Crystal and spin structures of $NiGa_2S_4$, consisting of layers stacked along the c axis and separated from each other by a van der Waals gap. Each layer of $NiGa_2S_4$ consists of an undistorted triangular lattice of Ni^{2+} ions in the ab–plane formed by the central edge-sharing NiS_6 octahedra (red) sandwiched between sheets of nonmagnetic GaS_4 tetrahedra (green), also illustrated in the inset of Fig. 1.8(b). Figures are reproduced from [159].

The electronic structure of Nickel ions Ni^{2+} is given by $[Ar]3d^8$. The crystal field subsequently splits the d-orbital states into two: t_{2g}^6 and e_g^2, and the two electrons in e_g^2 give the Ni^{2+} ion an effective spin–1. $NiGa_2S_4$ is an example of a bulk material exhibiting 2D physics. $NiGa_2S_4$'s neutrons scattering data suggests strong AFM correlations [159, 161] appearing for a wave vector near $\mathbf{q} = (\frac{1}{6}, \frac{1}{6}, 0)$ which are explained to arise from a competition between FM 1st nearest neighbor interaction exchange J_1 due to the ∼97° Ni-S-Ni bond angle and AFM 3rd neighbor interaction exchange J_3 due to superexchange [159, 234, 242]. Values of the different interaction exchange couplings can vary depending on the methods [193].

In reference [159], susceptibility measurements imply a Weiss temperature $\theta_W = -80$ K, which indicates strong AFM correlations but doesn't show any signature of a conventional phase transition. Nor is any evidence of a phase transition found in specific heat measurements. This indicates the existence of a disordered state and, therefore an absence of conventional AFM order.

Magnetic specific heat data for $NiGa_2S_4$ show a double peak structure [159, 161], presented in Fig. 1.8(a), which is reproduced from [159]. As temperature is decreased, the first peak appears around $T = |\theta_W|$[159, 161], and the second one around $T_{peak} = 10$ K [159–161]. The entropy obtained by integrating the magnetic specific heat exhibits a plateau at approximately $\frac{1}{3}$ of its high temperature limit $R\log(3)$. This indicates a highly degenerate low-temperature state due to the frustrated nature of the material. At low temperatures, magnetic specific heat measurements show a quadratic dependence with temperature, which in 2–dimensions indicates gapless linearly dispersive excitations [197], which in turn signal the existence of long-range correlations

[159–161]. However, the magnetic specific heat seems independent of the applied magnetic field. This means that the low–temperature peak does not arise due to AFM ordering of individual spin–1 moments but is associated with short–range correlation due to degrees of freedom that are insensitive to static uniform magnetic fields.

Moreover, no long-range magnetic order is seen in neutron scattering experiments [159, 165, 234]. From a conventional second order phase, one would expect a scaling anomaly of the spin correlation length. However in $NiGa_2S_4$, the spin correlation length is on the scale of the *nm* order and does not exhibit any finite temperature abnormal feature [159, 165, 234], as shown in Fig. 1.8(b) reproduced from [165].

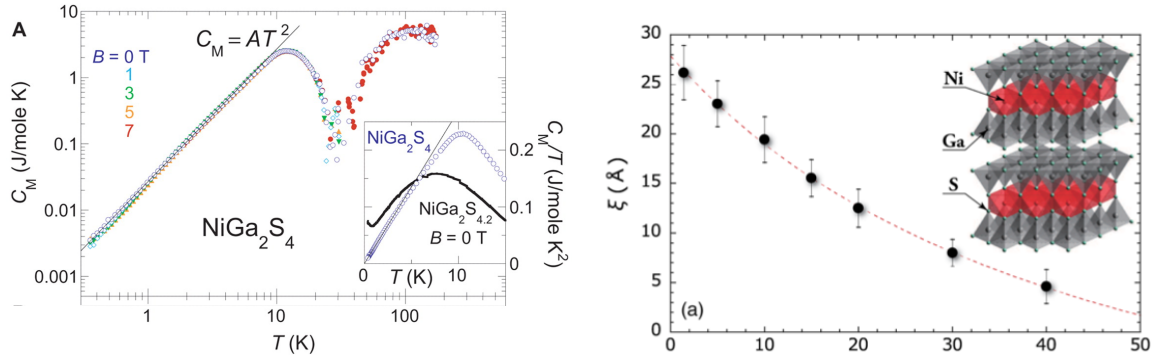

(a) Magnetic specific heat **(b)** In-plane correlation length

Figure 1.8: Thermodynamic properties of for $NiGa_2S_4$. (a) Magnetic specific heat C_M under different magnetic fields in function of temperature. The solid lines show the T^2 dependence of C_M suggesting the existence of long–range correlations. Inset: $\frac{C_M}{T}$ in function of temperature under zero magnetic field for $NiGa_2S_4$ and $NiGa_2S_{4.2}$ which has a sulfur doping of excess of 5%. Reproduced from [159]. (b) Spin correlation length ξ in function of temperature. No abnormal behavior is observed as one would expect from a conventional phase transition. Inset: crystal structure of $NiGa_2S_4$. Reproduced from [165].

Additionally, no canonical bulk freezing is observed. Despite weak filed dependence and hysteresis of the susceptibility below the freezing temperature $T_f = 8.5$ K, this feature is attributed to impurities [159, 161]. Substitution of the magnetic Ni^{2+} ions by non-magnetic Zn^{2+} ions indeed suggests that the defect spins freeze and not the bulk spins [161]. Because of their interplay with the bulk, it seems that the spin defects freeze in response to a change happening in the bulk. A substitution of the Ni^{2+} ions ($S = 1$) by Zn^{2+} ($S = 0$), Co^{2+} ($S = \frac{3}{2}$), Fe^{2+} ($S = 2$), or Mn^{2+} ($S = \frac{5}{2}$) highlights the dependence of the value of the spin in the low-temperature physical properties [162, 163]. For Co^{2+} ($S = \frac{3}{2}$) and Mn^{2+} ($S = \frac{5}{2}$) substitutions, specific heat data exhibit a conventional spin glass state below 1K which is expected due to the random nature of the impurities and the geometrical frustration of the triangular lattice, while for Zn^{2+} ($S = 0$) and Fe^{2+} ($S = 2$) substitutions, the specific heat data show similar behavior as the pure compounds [163]. This is quite surprising and suggests that these low-temperature properties emerge for integer spin values only, and that $NiGa_2S_4$'s unique features emanate from its integer spin value.

$NiGa_2S_4$ seems to be evading conventional magnetic order and exhibits unique low

temperature properties. To explain these, scientists have suggested that this material may be in a spin–liquid phase [159, 161] , experiencing a KT-type phase [94, 113–117, 159–161, 163, 165, 269], or be in a spin-nematic phase [24, 131, 159–161, 163, 165, 234, 235, 240, 250, 253, 269].

The fact that $NiGa_2S_4$ may specifically realize a spin–nematic phase has been studied in numerous works [24, 131, 135, 235, 240, 250, 253, 269] but mostly relies on the existence of a biquadratic exchange interaction, which is not clearly motivated by experimental measurements [159, 161, 234], or theoretical calculations [193]. In the most recent study [253], Raman scattering measurements, which have been theoretically suggested to detect quadrupolar order [148], indicate the existence of magnetoelastic couplings as well as random Dzyaloshinskii-Moriya interactions. It has been shown that a biquadratic exchange can originate from the displacement of atoms (i.e. phonons) responsible for magnetic exchange or super-exchange [18, 245]. In $NiGa_2S_4$ a biquadratic term could arise from the FM J_1 coupling which is due to the $\sim 97^\circ$ Ni-S-Ni bond angle [235, 253]. In [253], Raman scattering data shows the existence of such a phonon. Moreover, data also exhibit evidence for loss of local symmetry inversion that increases as temperature is decreased, which is associated with sulfur vacancies [164, 253]. This allows for Dzyaloshinskii-Moriya interactions. Dzyaloshinskii-Moriya interactions have not been investigated in the context of $NiGa_2S_4$, but they are known to affect magnetic order.

Raman scattering data [253] show 3 different regimes which are in accordance with specific heat measurements [159, 161]. In the high temperature regime, $T > 160$ K, there seems to be no AFM nor magneto-elastic couplings. In the intermediate regime $50\ \mathrm{K} < \mathrm{T} < 160\ \mathrm{K}$, a phonon responsible for magneto-elastic coupling is observed, and the magnetic susceptibility stays isotropic. The asymmetry of the peak associated with the phonon indicates that the phonon couples with the continuum of excitations. This suggests a spin nematic state. In the low-temperature phase, $50\ \mathrm{K} < \mathrm{T}$, Raman scattering data [253] and neutron scattering data [234] show an increase of anisotropy of the susceptibility as well as an increase of anisotropy of the correlation length. This suggests an increase of in-plan AFM couplings, which are accompanied by an increase of the magneto-elastic coupling, as temperature is decreased. The phonon observed by Raman scattering data is therefore potentially responsible for biquadratic exchange, which can lead to a spin-nematic phase in the intermediate temperature range $50\ \mathrm{K} < \mathrm{T} < 160\ \mathrm{K}$ [253].

In summary, $NiGa_2S_4$ unique low temperature properties makes it an interesting material exhibiting long–range correlations without apparent magnetic order [159, 161, 165, 234]. And recent experimental data juge $NiGa_2S_4$ as a realistic candidate for holding spin–nematic order [253]. This makes $NiGa_2S_4$ a good instance for studying dynamical properties of spin-nematics. Ground state and thermodynamic properties have already been theoretically studied in connection with $NiGa_2S_4$ [24, 131, 135, 235, 240, 250, 269], a theoretical model able to access dynamics would allow to better understand $NiGa_2S_4$'s unique low temperature spin dynamics [269]. Additionally, investigating the effect of Dzyaloshinskii-Moriya interactions in the context of $NiGa_2S_4$, which result in anti–symmetric interactions between the spin dipole components can also lead to rich and hopefully consequential insights about $NiGa_2S_4$ particular phenomenology.

A Pyrochlore Lattice Example: $NaCaNi_2F_7$

Pyrochlore systems are known to exhibit exotics physics. Namely, the classical AFM Heisenberg model on the pyrochlore lattice is known to be a spin liquid and was first discussed by Villain [254]. The classical AFM Heisenberg Hamiltonian is minimized for configurations of spin with a vanishing total magnetization on each tetrahedron. This results in a ground state manifold of a microscopically degenerate ensemble of spin configurations which are highly correlated. This leads to a rich physics in magnetic pyrochlore oxides [69, 199]. However, most of the efforts are directed into classical pyrochlore spin-liquids [92, 101, 151, 152] and less investigated are their quantum counterpart [33, 34, 93].

Pyrochlore spin–1 magnets have also recently attracted attention [64]. Among which, $NaCaNi_2F_7$ shows exciting features. In this material, the Ni^{2+} ions also carry an effective spin–1 and form a pyrochlore lattice where the Na and Ca atoms are randomly distributed on the A sublattice, and the Ni and F sublattices are fully ordered [125]. A $NaCaNi_2F_7$ crystal is shown in Fig. 1.9(a) and the pyrochlore structure is shown in Fig. 1.9(b).

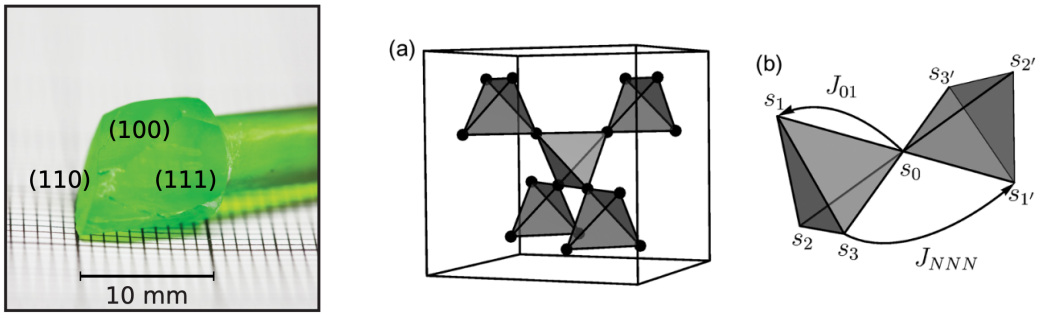

(a) $NaCaNi_2F_7$ crystal **(b)** In $NaCaNi_2F_7$, the Ni^{2+} form a pyrochlore lattice

Figure 1.9: (a) $NaCaNi_2F_7$ crystal grown by a modified Bridgman-Stockbarger method, reproduced from [125]. (b) Pyrochlore lattice consisting of corner–sharing tetrahedra, reproduced from [267].

For $NaCaNi_2F_7$, susceptibility measurements display a Curie-Weiss temperature $\theta_W = -129$ K suggesting AFM correlations. The susceptibility remains isotropic from 300K down to 5K. Susceptibility data show that the system undergoes a spin freezing at 3.6 K, which is also consistent with specific heat data [125]. The reason for the spin freezing might be explained by weak bond disorder in the Ni-Ni interactions induced by the disorder of Na and Ca atoms. This type of disorder has been shown to cause a freezing into a spin glass state [207]. However, under the freezing temperature, specific heat measurements display a quadratic temperature dependence which seems incompatible with the usual linear temperature dependence of the specific heat for spin glass states but seems to be related to high frustration [196, 198]. Neutron scattering data exhibit spin–liquid–like properties above the freezing temperature and display a continuum of excitations, signaling the existence of a spin-liquid state [188].

In order to describe $NaCaNi_2F_7$, Neutron scattering data have been modeled by using a Hamiltonian with weakly anisotropic AFM 1^{st} nearest neighbor interaction

and isotropic next nearest neighbors interactions:

$$\mathcal{H}_{\mathsf{Ani}} = \sum_{\langle i,j\rangle} J_{ij}^{\alpha\beta} \hat{\mathrm{S}}_i^{\alpha} \hat{\mathrm{S}}_j^{\beta} + \sum_{\langle\langle i,j\rangle\rangle} J_{NNN} \hat{\mathrm{S}}_i^{\alpha} \hat{\mathrm{S}}_j^{\alpha} \ , \tag{1.53}$$

where the $J^{\alpha\beta}$ allows for anisotropy in the spin space compared to the isotropic model [Eq. (1.25)], and J_{NNN} is the next nearest neighbor interaction coupling. A symmetry analysis [50] allows for 4 different interaction couplings

$$\mathbf{J}_{01} = \begin{pmatrix} J_2 & J_4 & J_4 \\ -J_4 & J_1 & J_3 \\ -J_4 & J_3 & J_1 \end{pmatrix} \ . \tag{1.54}$$

In reference [188], the values of the couplings are extracted from the best match given by a Self-Consistent Gaussian Approximation (SCGA) [47] compared to the experimental data of neutron scattering experiments. According to [188], the values obtained are

$$\begin{array}{ccc} J_1 = J_2 = 3.2(1) \text{ meV} & , & J_3 = 0.019(3) \text{ meV} \ , \\ J_4 = -0.070(4) \text{ meV} & \text{and} & J_{NNN} = -0.025(5) \text{ meV} \ . \end{array} \tag{1.55}$$

Considering the agreement between the model proposed for $NaCaNi_2F_7$ [Eq. (1.55) and Eq. (1.53)] with its neutron scattering data implies that Eq. (1.53) delivers a satisfactory modeling. Even though the effective moment $3.7(1)\mu_B$ implies a contribution of an orbital moment to the magnetism [125], the fact that the Heisenberg model describes neutron scattering data well enough suggests that the spin-orbit coupling is very small [188]. Therefore, $NaCaNi_2F_7$ provides an example of a Heisenberg pyrochlore lattice material with only anisotropic symmetric and anti–symmetric nearest neighbor as well as next nearest neighbor interactions.

Reference [267] compares with neutron scattering measurements 3 different methods (Linear Spin-Wave (LSW) theory, Molecular Dynamics (MD) simulations and a SCGA method extended to a stochastic model labeled SLN) applied to the previous AFM Heisenberg model on the pyrochlore lattice. The 3 methods give approximately satisfying comparison at high energies but seem at fail at reproducing experimental features at low energy. This can been seen in Fig. 1.10, where there seems to be a loss of spectral weight in the dipole structure factor at (2,2,0) in the experimental data when compared to the others methods. In Linear Spin-Wave (LSW), fluctuations are expanded around an ordered ground state, but only contain dipole excitation $\Delta S = 1$, and quadrupole excitations with $\Delta S = 2$ are disregarded (see Supplemental Material in [267]). Molecular Dynamics (MD) are based on the integration of the classical Landau-Lifshitz equations of motion for $O(3)$-spin dipole moments for an ensemble of thermalized states obtained by classical Monte Carlo for a temperature of 1.8 K, which also relied on the $O(3)$ description of a spin–dipole moment. Same applies to the SCGA, which is also described in terms of classical $O(3)$-vectors and which was extended for frustrated models [68] and supplemented by a stochastic model to allow for dynamics [46].

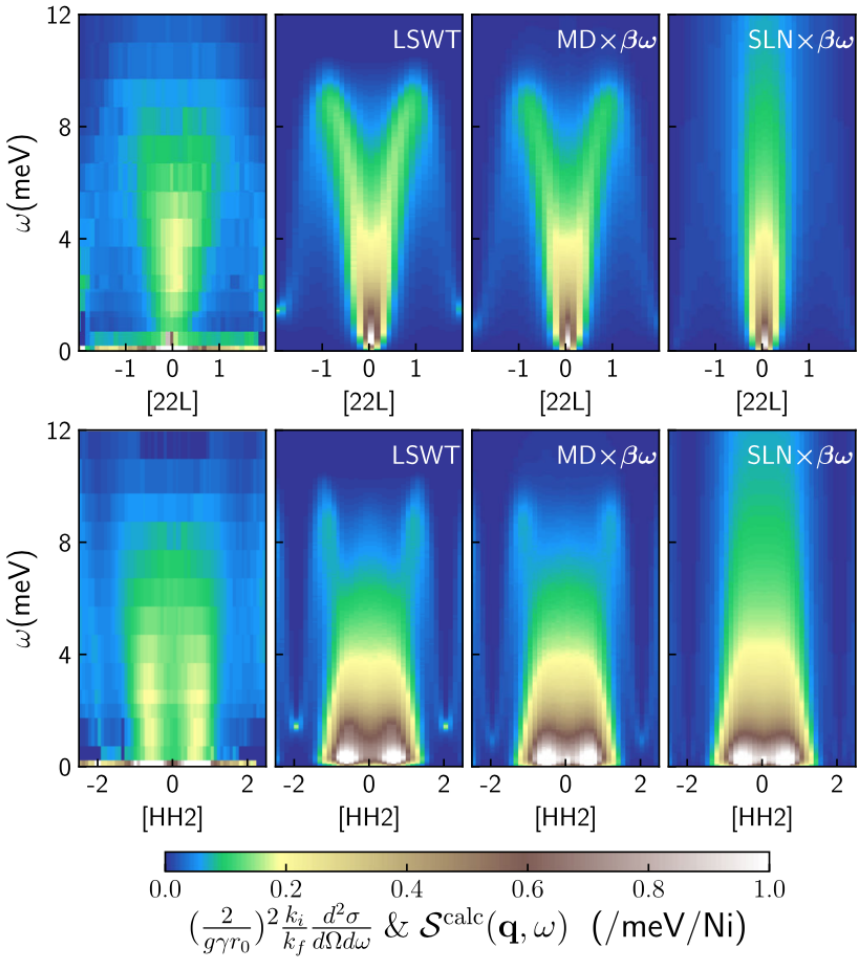

Figure 1.10: Comparison of experimental and results obtained by Linear Spin-Wave theory, Molecular Dynamics for $O(3)$-spin dipole moments and a self–consistent Gaussian approximation for the dynamics of $NaCaNi_2F_7$. The spin–dipole dynamical structure factor is shown along momentum cuts [22L] and [HH2]. First row shows the neutron scattering intensity is in absolute units. Second, third and fourth row show the predictions from Linear Spin-Wave (LSW) theory, rescaled Molecular Dynamics (MD) and a self–consistent Gaussian approximation extended to a stochastic model labeled SLN, respectively. LSW and MD results qualitatively reproduce the shape of the broad dispersive continuum but disagree at the lowest energies; SLN fails to capture the structure of the experimental data at high energies. Figure is reproduced from [267].

Therefore, all these 3 methods rely on a description of spin–1 moment as an $O(3)$-vector. However, an $O(3)$-vector does not properly represent a spin–1. The disagreement of these 3 methods with experiments is likely to come from the fact that an $O(3)$-vector does not properly describe a spin–1 moment.

Moreover the Hamiltonian [Eq. (1.53)] used to describe $NaCaNi_2F_7$ has originally been derived for $Tb_2Ti_2O_7$, which also is a pyrochlore material but consists of effective spin–$\frac{1}{2}$ moments. For a spin–1, additional terms, such as biquadratic term, are also

allowed. It seems that this material cannot be fully explained within a framework based on $O(3)$ moments [267].

A Few Other Interesting Examples

Another interesting spin–1 magnet is the compound $Ba_3NiSb_2O_9$ [40, 224]. It has been shown to exhibit 2 structural phases displaying spin–liquid–like behaviors with AFM couplings: the 6H-B phase which has a quasi-2-dimensional triangular lattice formed by Ni^{2+} ions, and the C3 phase consisting of $Ni_{\frac{2}{3}}Sb_{\frac{1}{3}}$-three-dimensional edge- shared tetrahedral lattice. Both phases show AFM interactions, and no sign of magnetic ordering is shown to appear in magnetic susceptibility data and specific heat measurements [40]. Specific heat data display a different temperature dependence for the two phases. Namely, it scales as T^2 for the 6H-B phase, and as T for the C3 phase. For the 6H-B phase, muon spin rotation experiments [195] are also consistent with previous measurements [40] and show no ordering down to a temperature of $T = 0.02$ K. Among different explanations given to explain the experimental observations, there is the formation of a 3-dimensional nematic spin liquid [98], or a consequence of an interplay between intra– and inter–layer interactions leading to a critical point [38], or lastly, the presence of a Femi liquid [40]. Indeed Fermi Spin liquid states have also been suggested theoretically, where Ni^{2+} ions fractionalize into 3 [138, 214, 215, 260] or 4 [25] fermionic spinons. Recent neutron scattering data suggests that the experimental data are best explained by 3 flavors of unpaired spinons forming a Fermi-surface [58].

The spin–1 Kagome–lattice material $YCa_3(VO)_3(BO_3)_4$ [149] shows interesting low–temperature properties. Neutron scattering data show an absence of long–range magnetic order, but specific heat measurements suggest the existence of short–range correlations. This short–range magnetic order seems to be frustrated by the geometrical structure of the Kagome lattice and the competition between AFM and FM interactions. $YCa_3(VO)_3(BO_3)_4$ exhibits broad and non–dispersive excitation features [226] and is discussed as a possible example of a $S = 1$ quantum spin liquid.

An interesting occurrence for exotic physics in quasi–1 dimensional model is illustrated by the compound CaV_2O_4. In this material, V^{+3} ions have an effective spin–1 and form two different but equivalent zigzag–chains of edge-sharing octahedra VO_6, forming a chain of almost equilateral triangles, resulting in apparent competing nearest and next–nearest interactions [170, 186]. The octahedral structure partially lifts the degeneracy of the 3d orbitals of the V^{+3} ions, such that the two outer electrons occupy the t_{2g} levels. The remarkable phenomena observed in CaV_2O_4 comes from its orbital degrees of freedom which order in such a way to reduce frustration. Because of the slightly shorter distance between spins along the chain, compared to the distance between spins across the zigzag path, the 3 t_2 levels are separated into one lower level and two degenerate higher levels. CaV_2O_4 undergoes a structural phase transition at $T_s \simeq 141$ K, where the zigzag bonds become inequivalent. This results in an additional lifting of the two degenerate higher t_2 levels. At high temperature, $T > T_s$, one electron fully occupies the lowest t_2 level, and partially occupies two degenerate higher levels. This selection of orbitals results in the 1D-Haldane chain. Whereas at low temperature, both electrons occupy fully 2 discting levels resulting in a spin–1 ladder configuration [186].

Recently, systems considering higher spin–moments have attracted attention. Systems where conduction electrons scatter with magnetic impurities can be described by the Kondo model. For instance, an anisotropic 1–dimensional Kondo lattice model with S=1 impurities studied using density matrix renormalization group (DMRG) has been proposed to explain the coexistence of ferromagnetism and superconductivity in some materials such as URhGe [236, 237]. And very recently, a 1–dimensional Kondo lattice model with $S \geq 1$ impurities has been generalized to also include direct Heisenberg exchange interactions between the localized spin–1 moments and has been investigated by mean of analytical calculation in the strong Kondo—coupling regime and by DMRG simulations [142].

1.3.2 Spin–1 in the Zoo

Here, I give an overview of the "domesticated" methods used to study spin–1 systems, focusing namely on the theoretical tools employed to examine the models describing the materials presented above.

BBQ Hamiltonian as Playground for Spin–1 Animals

The material $NiGa_2S_4$ motivated much theoretical and computational work on the BBQ model [Eq. (1.48)]. Particularly, a lot of efforts has been invested on the theoretical side with calculations based on multi-boson theory [131, 176, 183, 250], and continuum field theory, [102–104, 221–223, 228–231, 251], and computational side with Monte Carlo simulations [235], and Quantum Monte Carlo simulations [78, 111, 255].

In order to better understand the low temperature features of $NiGa_2S_4$, intense investigations on the BBQ model [Eq. (1.48)] (which is the most general Hamiltonian for a spin–1 moment) on the triangular lattice have been carried out. In reference [131], the mean-field phase diagram is obtained by minimization of a variational wave function consisting in the product of single site wave–functions. The mean-field phase diagram of the BBQ model on the triangular lattice is shown in Fig. 1.11. It is represented in term of the parameter θ [Eq. (1.50)] such that $\tan(\theta) = \frac{J_2}{J_1}$. We can distinguish four distinct ground states: ferromagnet (FM); three–sublattice antiferromagnet (AFM); ferroquadrupolar (FQ); and three–sublattice antiferroquadrupolar (AFQ). All these phases have been studied theoretically. Namely, the ferromagnetic phase of the Heisenberg model [Eq. (1.25)] on the triangular lattice with single–ion anisotropy has been studied through multi-boson theory [176]. Its anti-ferromagnetic phase has been investigated using Linear Spin–Wave theory and taking into account magnon interactions [42]. The anti-ferromagnetic phase of BBQ model [Eq. (1.48)] with single–ion anisotropy on the triangular lattice has also been studied via a representation of spin in terms of fermionic operators [214] as well as bosonic operators (Multi-boson theory) with additional Heisenberg next–nearest neighbors interactions [187].

The anti-ferroquadrupolar phase of the BBQ model on the triangular lattice has been examined by means of a multi-boson theory [250]. The anti-ferroquadrupolar and ferroquadupolar phase of the BBQ model on the triangular was also investigated by a lattice bond–operator mean–field theory expressed in the bosonic representation [135]. Continuum field theories have also been applied to study the anti-ferroquadrupolar

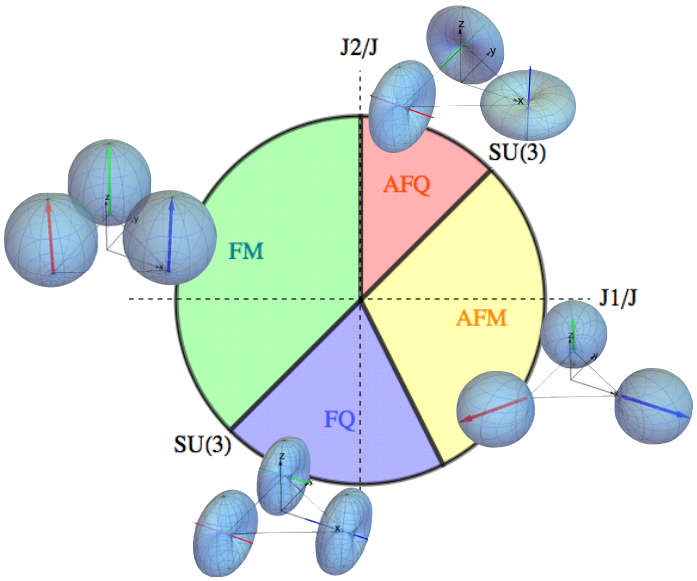

Figure 1.11: Mean–field phase diagram of the spin–1 bilinear–biquadratic (BBQ) model on the triangular lattice [Eq. (1.48)] at $T = 0$, adapted from [229] and reproduced from [201]. The model shows four distinct ordered ground states: ferromagnet (FM); three–sublattice antiferromagnet (AFM); ferroquadrupolar (FQ); and three–sublattice antiferroquadrupolar (AFQ). For $J_1 = J_2$, the model exhibits an enlarged $SU(3)$ symmetry.

phase of the BBQ model on the triangular lattice [228–231] as well as to the ferroquadrupolar phase [102–104]. The ferroquadupolar phase of the BBQ model on the triangular was investigated by mean of multi-boson theory supplemented by exact diagonalization [24, 131, 183]. A recent study of the BBQ model on the triangular lattice with XXZ anisotropy also makes use of multi-boson theory to derive the anisotropic phase diagram [212].

The BBQ model has also been applied to different type of lattices, namely the square lattice, where exact diagonalization and multi-boson theory have been applied and have shown that for a certain region of the phase diagram, there is a tri-sublatice ordering despite the bipartite nature of the square lattice [247, 248]. This model has also been studied via linked cluster perturbation expansions method [174].

An approach to classical spin dynamics of the BBQ Hamiltonian based on an $SU(3)$ representation of a spin–1 moments has been previously investigated [14, 200]. However, because of the complex structure of the $su(3)$ algebra, the associated equations of motion take a very intricated form, which prevents a smooth implementation for numerical investigations [14, 200]. Recently, a general description based on a representation of $SU(n)$ coherent states has also been derived by computing equations of motion for the generators of $SU(n)$ [51, 264]. Applied to a spin–1 system and therefore based on $SU(3)$, the associated equations of motion take nevertheless a very intricated from [14, 51, 200, 264]. Until now, the $SU(n)$ coherent states have been illustrated for a relatively simple model consisting of a Heisenberg Hamiltonian and single–ion anisotropy [51, 264]. A general description for the full BBQ Hamiltonian is however

missing.

Topological excitations within the BBQ model have also been studied [104, 252]. From [252], it is known that not all solitons are equivalent, and solitons of higher charges decay into elementary solitons. Why and how this happens remains a mystery. Magnetic $\mathbb{CP}^2$ skyrmions in spin–1 systems have also been recently reported for the easy-axis anisotropic Heisenberg Hamiltonian with ferromagnetic first nearest neighbor interactions and anti-ferromagnetic second-nearest neighbor interactions supplemented by a Zeeman coupling to an external magnetic field as well as single–ion anisotropy [265].

Multi–Boson Theory

From this non-exhaustive, yet still representative list of theoretical and mostly analytical studies applied to the BBQ model on the triangular, we note that the multi-boson theory is particularly useful to characterize the different ground states of the BBQ model. Moreover, because I show that within our $u(3)$ formalism, the analytical approach leads to qualitatively similar results as the one obtained by multi-boson theory, following the pedagogical overview provided in [212], I shortly introduce this method below. The multi-boson theory is valid for ordered systems, where the ordered ground state is known, as it relies on expanding orthogonal fluctuation around the ground states. This method was already applied to describe a spin–1 almost 50 years ago [143], and remains of relevance in nowadays research, testifying of its powerful importance. Conceptually, in order to perform multi-boson theory, after identifying a suitable basis to represent the considered spin moment (2 basis states for a spin–$\frac{1}{2}$, 3 for a spin–1, etc), one introduce bosons operators that are responsible for creating or annihilating these states. For concreteness, let us consider a spin–1 moments describe by 3 orthogonal states $\{|1\rangle, |2\rangle, |3\rangle\}$, which satisfy the closure relation

$$|1\rangle\langle 1| + |2\rangle\langle 2| + |3\rangle\langle 3| = \mathbb{I} \, . \tag{1.56}$$

The bosonic operators $\hat{\mathrm{b}}^\dagger_\alpha$ are introduced such that

$$\hat{\mathrm{b}}^\dagger_\alpha |GS\rangle = |\alpha\rangle \, , \tag{1.57}$$

for $|\alpha\rangle$ being one of the 3 orthogonal states $\{|1\rangle, |2\rangle, |3\rangle\}$. From Eq. (1.56), we obtain

$$\sum_\alpha \hat{\mathrm{b}}^\dagger_\alpha \hat{\mathrm{b}}_\alpha = 1 \, , \tag{1.58}$$

which enforces the number of bosons per site to 1. For simplicity, we assume that the ground state is $|3\rangle$. Generally, it could be any linear combination of the 3 orthogonal states $\{|1\rangle, |2\rangle, |3\rangle\}$, but one can then always perform a basis change by mean of a linear transformation and recover a basis where one state is the ground state and the others two are orthogonal to it. We then "condense" the ground state bosons $\hat{\mathrm{b}}^\dagger_3$ by expressing it in terms of the 2 orthogonal bosons $\hat{\mathrm{b}}^\dagger_1$ and $\hat{\mathrm{b}}^\dagger_2$. To this end, one can

generalize Eq. (1.58) to allow for M_b bosons per sites

$$\sum_{\alpha} \hat{\mathrm{b}}_{\alpha}^{\dagger}\hat{\mathrm{b}}_{\alpha} = M_b \ . \tag{1.59}$$

This allows to perform an expansion in terms of $\frac{1}{M_b}$ similarly to a Holstein–Primakoff transformation

$$\hat{\mathrm{b}}_3^{\dagger} = \hat{\mathrm{b}}_3 = \sqrt{M_b - \hat{\mathrm{b}}_1^{\dagger}\hat{\mathrm{b}}_1 - \hat{\mathrm{b}}_2^{\dagger}\hat{\mathrm{b}}_2} \simeq \sqrt{M_b}\left(1 - \frac{1}{2}\frac{\hat{\mathrm{b}}_1^{\dagger}\hat{\mathrm{b}}_1}{M_b} - \frac{1}{2}\frac{\hat{\mathrm{b}}_2^{\dagger}\hat{\mathrm{b}}_2}{M_b} + \mathcal{O}(\frac{1}{M_b^2})\right) \ , \tag{1.60}$$

where we should keep in mind that $M_b = 1$ only has physical meaning, and that this approach is valid as long as we can assume that $\langle \hat{\mathrm{b}}_{\alpha}^{\dagger}\hat{\mathrm{b}}_{\alpha}\rangle \ll M_b = 1$. We also note that the classical limit $M_b \to \infty$ suppresses all quantum fluctuations. It is then possible to transcribe any operators (usually directly represented in the $\{|1\rangle, |2\rangle, |3\rangle\}$) in terms of the $\hat{\mathrm{b}}_{\alpha}^{\dagger}$ bosons and to expand them as terms in $\frac{1}{M_b}$. This is in particular true for the Hamiltonian

$$\mathcal{H}_{tot} = M_b^2\mathcal{H}^0 + M_b^{\frac{3}{2}}\mathcal{H}^1 + M_b\mathcal{H}^2 + \sqrt{M_b}\mathcal{H}^3 + \dots \ , \tag{1.61}$$

where $\mathcal{H}^n$ represents the n-order term in function of the bosons. This means that $\mathcal{H}^1 = 0$, since no linear terms in bosons should subsist in the ground state. Usually, we consider up to second order and write

$$\mathcal{H}_{tot} = M_b^2\mathcal{H}^0 + M_b\mathcal{H}^2 + \mathcal{O}(\sqrt{M_b}) \ . \tag{1.62}$$

The problem is solved by diagonalizing $\mathcal{H}^2$ using a Bogoliubov transformation. All the quantities of interest can then be expressed in terms of the Bogoliubov bosons diagonalizing the Hamiltonian. For a spin–1, we will always expect 2 modes associated with the 2 orthogonal excitations. If only one type of excitation around the ground state is considered, then we usually refer to this method as linear spin–wave. This is for instance the case for a spin–$\frac{1}{2}$, which only has one state available to create fluctuation, once the ground state is set. But linear spin-waves theory can also be applied to a spin–1 moments, if the relevant degrees of freedom only include excitations to one of the two available states. Unfortunately, the application of multi-boson theory is redistricted to problems where the knowledge of an ordered ground state is at least guessable, leaving many exotic physics not available for this type of analytical study, despite being a very powerful method for applications where we do know the nature of the ordered ground state.

Numerical Methods for Spin–1 Animals

On the numerical side, exact diagonalization (ED) has been applied to the FQ state of the BBQ Hamiltonian on the triangular lattice, but leads to a different value of the critical angle a which the FQ-AFM transition happens: Mean-fields predict a transition at $\frac{J_2}{J_1} \approx -2$ (see also Fig. 1.11), while exact diagonalization finds $\frac{J_2}{J_1} \approx -0.4$ [131]. A cluster mean–field approach has also been used to investigate the uniaxial anisotropic BBQ Hamiltonian on the triangular lattice [153]. This approach relies on

exact diagonalization of small clusters which are mean-field coupled to each other. In the isotropic case, the FQ-AFM transition is predicted to happen at $\frac{J_2}{J_1} \approx -0.6$. In the presence of anisotropy, the existence of a spin liquid phase is discussed [153]. However, the application of this method seems limited, as when the 3–sublattice symmetry is broken, results strongly depend on the size and the geometry of the clusters. Additionally, exact diagonalization has the merit of indeed being exact, but is numerically very heavy and therefore restricted to small system sizes, which might be problematic in case of exotic excitations such as topological defects.

The ferro-quadrupolar state of the BBQ model has been investigated using Classical Monte-Carlo (MC) simulations [235], Quantum Monte Carlo (QMC) simulations [86, 87, 111, 255] as well as tensor-network simulations [171–173]. The classical Monte Carlo simulation presented in [235] is applied to the the BBQ model [Eq. (1.48)] on the triangular lattice for anti-ferromagnetic $J_1 > 0$, and ferro-nematic $J_2 < 0$ and based on a description of the spin–1 moments in terms of d–vectors (see Eq. (2.35) in Section 2.3) that the authors called sSU(3). This indeed allows to properly describe a spin–1 moment, since $O(3)$–vectors can not represent quadrupolar order. In order to explain $NiGa_2S_4$, third-nearest neighbor interactions are also taken into account in order to explain its freezing behavior. Classical Monte Carlo based on the sSU(3) representation allows to access semi–classical finite temperature thermodynamics of spin–1 systems. However, dynamical properties remain out of reach.

Quantum Monte Carlo simulations have been performed for the BBQ model [Eq. (1.48)] on the square lattice [86, 87] and on the triangular lattice for the purely biquadratic case $J_1 = 0$ [111], as well as for the ferromagnetic and ferroquadrupolar phase $\theta \in [-\pi, -\frac{\pi}{2}]$ [255], giving insight into the quadrupolar quantum nature of spin–1 moments. Quantum Monte Carlo simulation results reproduced form [255] for the FQ phase of the BBQ model on the triangular lattice with parameters $J = 1, \theta = -\frac{\pi}{2}$ are shown in Fig. 1.12. These studies enable the investigations of the quantum characteris-

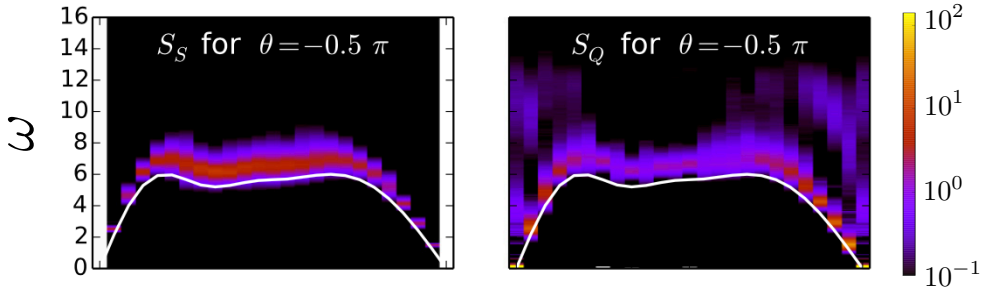

Figure 1.12: Dynamical spin dipole $S_{\mathsf{S}}(\mathbf{q}, \omega)$ and quadrupole $S_{\mathsf{Q}}(\mathbf{q}, \omega)$ structure factors obtained by Quantum Monte Carlo simulations. Results are shown for the BBQ model [Eq. (1.48)] on the triangular lattice with parameters $J = 1, \theta = -\frac{\pi}{2}$ [Eq. (1.50)] at a temperature $T = \frac{1}{32}\ J$, and are reproduced from [255]. The intensities of the dynamical spin dipole $S_{\mathsf{S}}(\mathbf{q}, \omega)$ and quadrupole structure factors $S_{\mathsf{Q}}(\mathbf{q}, \omega)$ are given in function of the irreducible wedge along the points **Γ**–**K**–**M**–**Γ** given in Eq. (D.3) in abscissa, and the energy ω in ordinate.

tics of thermodynamics properties [86, 87, 111] as well as dynamics through analytical

continuations [255]. However, Quantum Monte Carlo simulations are only applicable to a restricted number of sign-free problems [112], and dynamics are only accessible via analytic continuation for relatively small system sizes, and might not be applicable to systems with complex excitations.

The BBQ model on the square lattice has also been studied via tensor network [171, 268] allowing to investigate a generalization of the Haldane phase in 2D. The tensor network was also applied to the BBQ model on the triangular lattice, which allowed to predict the FQ-AFM transition for $\frac{J_2}{J_1} \approx -0.42$ [173] confirming exact diagonalization results [131]. Rapid advances in numerical methods, namely the density-matrix renormalization group method, have suddenly allowed access to almost any 1D quantum system [258], but their generalization to higher dimension beyond ground state properties remains problematic [208].

1.4 And us in All That?

All these various and abundant examples of spin-1 peculiarities motivate the need for good theoretical tools to investigate spin–1 magnets. The characteristic and interesting features of spin-1 systems are precisely what makes them challenging to study. Classical Monte Carlo simulations based on an $O(3)$ representation are not able to describe quadrupolar ground states nor quadrupolar excitations. Quantum Monte Carlo is able to reproduce quadrupolar order [87, 111], and dynamics from its associated excitations [255]. However, Quantum Monte Carlo can only be used for a restricted number of cases that do not suffer from a sign problem [21]. Its dynamics are only accessible through analytic continuation and might prove itself problematic for systems where complex excitations are present. Additionally, the dynamic proprieties are also restricted to relatively small system sizes.

Exact Diagonalization (ED) is also capable of properly representing a spin–1 moment and its quadrupolar nature. But because the Hilbert space grows rapidly with system size, ED is typically restricted to calculations for systems of 20 sites or less [52, 131]. Variational calculations methods, where the wave functions are represented by a matrix– or tensor–product well describe the dynamics in 1D [208, 258], but their extensions to higher dimensions have been challenging when investing further than ground-state properties [171, 173, 268]. Despite all the efforts involved in these methods, most of our knowledge of the exotic phenomena in spin–1 magnets is restricted to mean–field (MF) theory. MF theory is based on the assumption of a total product wave function of single–site wave functions, and the knowledge of an (ordered) ground state around which it is possible to expand fluctuations linearly. These drawbacks leave many important questions out of reach.

In this Thesis, appealed by all the formidable science that has been undertaken in order to study spin–1 magnets, I would like to motivate our work by asking ourselves, in link with what we learned about the existing methods and their limitations, the following questions:

- ⋆ Is there a general method to study spin–1 systems?
- ⋆ A method based on a truthful representation of a spin–1 moment?

- ⋆ A method that can describe the quantum proprieties of a spin–1 moment?
- ⋆ A method that would also allow us to treat a spin–1 moment at the classical level while still retaining its quadrupolar degrees of freedom?
- ⋆ A method that would allow us to describe thermodynamics?
- ⋆ as well as dynamical properties?
- ⋆ A method that could be easily implemented on a computer in order to simulate spin–1 system?
- ⋆ A method that would allow us to access conventional ordered magnets and systems with more exotic properties? Such as spin-liquids or topological defects?

In this Thesis, I develop a method based on the embedding of spin–1 moments in the group $U(3)$ [180], which allows to treat both dipolar and quadrupolar order on an equal basis and which treats quantum aspects of the problem exactly, at the level of a single site. This leads to a formulation in terms of the generators of $u(3)$, which is suitable for MC and molecular dynamics (MD) simulations, as well as analytical methods. The nice simple structure of the group $U(3)$ also makes it possible to derive very compact equations of motion (EoM), in a form that can easily be integrated numerically. This allows to evaluate dynamical properties for both conventional and unconventional forms of order.

I demonstrate that this approach reproduces known results for the excitations of ferroquadrupolar (FQ) order of the bilinear biquadratic (BBQ) model [Eq. (1.48)] on the triangular lattice, where both QMC simulations [255] and analytic multi-boson theory calculations [131] are available for comparison. Moreover, the FQ state is the simplest yet not trivial example to exhibit the particular features of a spin–1 (quadrupoles). In order to build $SU(3)$, which is the natural group to describe a spin–1 moment, as briefly discussed in Section 1.2.2, but also explained in details in Chapter 2, we consider the 3 linearly independent dipole moments [Eq. (1.26)] and the 5 linearly independent quadrupole moments [Eq. (1.47)] that make the 8 generators of the $su(3)$ algebra. Although the $su(3)$ algebra faithfully represents a spin–1 moment, its complicated structure makes it a challenging starting point for describing its dynamics [14, 200, 264]. However, we can escape these tedious efforts by adding one more generator, the spin-length $\hat{\mathbf{S}}_{\boldsymbol{i}}{}^2$, and constraining its length via

$$\hat{\mathbf{S}}_{\boldsymbol{i}}{}^2 = s(s+1) = 2\ . \tag{1.63}$$

This allows a transcription of a spin–1 moment in terms of the $u(3)$ algebra, where the addition of the spin-length $\hat{\mathbf{S}}_{\boldsymbol{i}}{}^2$ to the 8 generators of $su(3)$ extends to compose the 9

generators of the $u(3)$ algebra, as illustrated in Eq. (1.64).

$$
\begin{array}{l}
su(3) \\ \text{algebra}
\end{array}
\left\{
\begin{array}{l}
\text{Spin length} \\
\\
\text{3 linearly independent} \\ \text{dipole components} \\
\\
\\
\text{5 linearly independent} \\ \text{quadrupole} \\ \text{components}
\end{array}
\right.
\left\{
\begin{array}{c}
\\
\\
\\
\\
\\
\\
\\
\\
\\
\end{array}
\right.
\begin{pmatrix}
\hat{\mathbf{S}}_{\boldsymbol{i}}{}^2 \\
\hat{\mathrm{S}}_i^x \\
\hat{\mathrm{S}}_i^y \\
\hat{\mathrm{S}}_i^z \\
\hat{\mathrm{Q}}_i^{x^2-y^2} \\
\hat{\mathrm{Q}}_i^{3z^2-s^2} \\
\hat{\mathrm{Q}}_i^{xy} \\
\hat{\mathrm{Q}}_i^{xz} \\
\hat{\mathrm{Q}}_i^{yz}
\end{pmatrix}
\xrightarrow{\text{basis change}}
\begin{pmatrix}
\hat{\mathcal{A}}_{i\ x}^{x} \\
\hat{\mathcal{A}}_{i\ y}^{x} \\
\hat{\mathcal{A}}_{i\ z}^{x} \\
\hat{\mathcal{A}}_{i\ x}^{y} \\
\hat{\mathcal{A}}_{i\ y}^{y} \\
\hat{\mathcal{A}}_{i\ z}^{y} \\
\hat{\mathcal{A}}_{i\ x}^{z} \\
\hat{\mathcal{A}}_{i\ y}^{z} \\
\hat{\mathcal{A}}_{i\ z}^{z}
\end{pmatrix}
\begin{array}{l}
u(3) \\ \text{algebra}
\end{array}
\tag{1.64}
$$

In terms of the $u(3)$ generators $\hat{\mathcal{A}}_{i\ \alpha}^{\alpha}$, the length constraint [Eq. (1.63)] translates as a constraint on the trace

$$\hat{\mathcal{A}}_{i\ \alpha}^{\alpha} = \frac{1}{2}s(s+1) = 1 \ , \tag{1.65}$$

on each site in the lattice, where repeated indices are summed. Imposing this constraint restricts back to $su(3)$ and ensures that we are properly describing a spin–1 moment.

The tensors $\hat{\mathcal{A}}_i$ provide a convenient basis for $u(3)$, thanks to their simple form. They consist of a set of real, 3×3 matrices with only one single non–vanishing matrix element [180]. They are subject to the commutation relations given by

$$
\begin{aligned}
\left[\hat{\mathcal{A}}_{i\ \beta}^{\alpha}, \hat{\mathcal{A}}_{i\ \eta}^{\gamma}\right] &= \delta^{\gamma}{}_{\beta}\hat{\mathcal{A}}_{i\ \eta}^{\alpha} - \delta^{\alpha}{}_{\eta}\hat{\mathcal{A}}_{i\ \beta}^{\gamma} \ , \\
\left[\hat{\mathcal{A}}_{i\ \beta}^{\alpha}, \hat{\mathcal{A}}_{j\ \eta}^{\gamma}\right] &= 0 \ .
\end{aligned}
\tag{1.66}
$$

In terms of matrix elements of $\hat{\mathbf{A}}$, the spin–dipole moments are given by

$$\hat{\mathrm{S}}^{\alpha} = -i\epsilon^{\alpha}{}_{\beta}{}^{\gamma}\hat{\mathcal{A}}^{\beta}{}_{\gamma} \ , \tag{1.67}$$

and quadrupole–moments by

$$\hat{\mathrm{Q}}^{\alpha\beta} = -\hat{\mathcal{A}}^{\alpha}{}_{\beta} - \hat{\mathcal{A}}^{\beta}{}_{\alpha} + \frac{2}{3}\delta^{\alpha\beta}\hat{\mathcal{A}}^{\gamma}{}_{\gamma} \ . \tag{1.68}$$

The BBQ Hamiltonian [Eq. (1.48)], rewritten in terms of the $\hat{\mathbf{A}}$–matrices becomes

$$
\begin{aligned}
\mathcal{H}_{\mathsf{BBQ}} &= \sum_{\langle i,j\rangle}\left[J_1\hat{\mathcal{A}}_{i\ \beta}^{\alpha}\hat{\mathcal{A}}_{j\ \alpha}^{\beta} + (J_2 - J_1)\hat{\mathcal{A}}_{i\ \beta}^{\alpha}\hat{\mathcal{A}}_{j\ \beta}^{\alpha} + J_2\hat{\mathcal{A}}_{i\ \alpha}^{\alpha}\hat{\mathcal{A}}_{j\ \beta}^{\beta}\right] \\
&= \sum_{\langle i,j\rangle}\left[J_1\hat{\mathcal{A}}_{i\ \beta}^{\alpha}\hat{\mathcal{A}}_{j\ \alpha}^{\beta} + (J_2 - J_1)\hat{\mathcal{A}}_{i\ \beta}^{\alpha}\hat{\mathcal{A}}_{j\ \beta}^{\alpha} + \frac{J_2}{4}s^2(s+1)^2\right] \ ,
\end{aligned}
\tag{1.69}
$$

where we used the constraint on the trace [Eq. (1.65)] in the last line. From now on,

the adoption of the Einstein convention of summing over repeated indices prevails. We note that in terms of the $u(3)$ generators, the BBQ Hamiltonian takes on a quadratic form, while it is biquadratic in dipole moments. Details of the embedding of the algebra $su(3)$ into $u(3)$ and properties of $\hat{\mathbf{A}}$–matrices can be found in Chapter 2.

I then take the BBQ Hamiltonian written in terms of the $\hat{\mathbf{A}}$–matrices [Eq. (1.69)] as starting point for the analytical derivations. The generators of $u(3)$ are used to create fluctuations around a given ground state $\hat{\mathbf{A}}_0$–matrix. While a formulation in terms of classical $O(3)$–vectors does not allow for quadrupolar excitations, the fluctuations of $\hat{\mathbf{A}}$–matrices can be treated classically by simply diagonalizing the Hamiltonian. The representation as $u(3)$ $\hat{\mathbf{A}}$–matrices subject to the trace constraint [Eq. (1.65)] allows to correctly take the classical limit of a spin–1. I propose here to use the classical excitations as a basis to develop a new analytic theory for classical correlations. Performing a low-temperature expansion of the classical analytical results allows a direct comparison with Monte Carlo simulations. Additionally, I can also choose to quantize the fluctuations into bosons by enforcing them to have bosonic commutation relations. This can be done by performing a Bogoliubov transformation. Considering quantum fluctuations is shown to be equivalent to multi-boson theory and to exactly reproduce already well-known results.

I also propose to use the $u(3)$ representation to establish a numerical method to simulate spin-1 magnets through the characterization of dynamical structure factors. On the thermodynamic side of the simulations, we suggest to perform Monte-Carlo simulations, with an $\hat{\mathbf{A}}_i$–matrix defined at each lattice site as a starting point. I refer to the method as "u3MC". The $\hat{\mathbf{A}}_i$-matrices are updated according to Metropolis's argument. This allows us to access static thermodynamic quantities, such as the specific heat, equal-time structure factors, etc., In Fig. 1.13, we draw the finite-temperature phase diagram of the BBQ model on the triangular lattice obtained from the u3MC method, performed by my collaborator, Dr. Rico Pohle. Classical analytical derivations for the thermodynamic properties and comparison with u3MC simulations are detailed in Chapter 3.

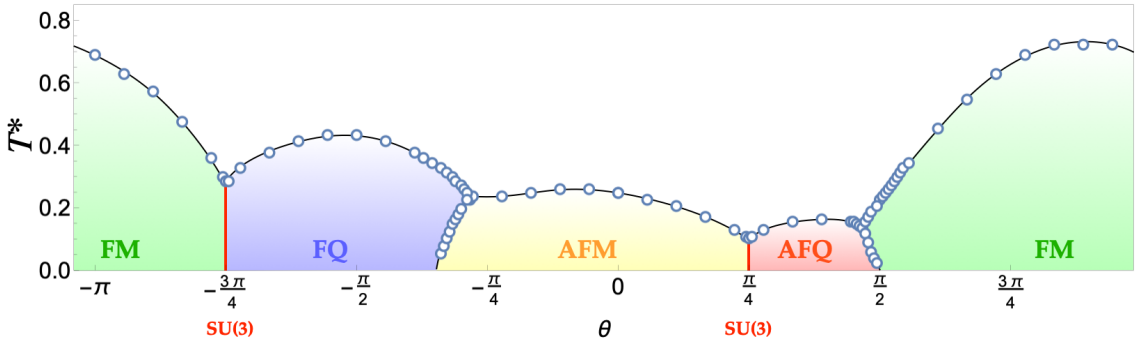

Figure 1.13: Finite–temperature phase diagram obtained from Monte Carlo simulation of $\mathcal{H}_{\mathsf{BBQ}}$ [Eq. (1.69)] in the space of $u(3)$ matrices (u3MC) for the spin–1 bilinear–biquadratic (BBQ) model on the triangular lattice, performed by my collaborator Dr. Rico Pohle. Circles correspond to the location of peaks in the heat capacity. The phases are labeled according to their dominant correlations at the ordering vector. Figure is reproduced from [201].

The simple form of the commutation relations [Eq. (1.66)] and the quadratic form of the BBQ Hamiltonian allows to easily derive the Heisenberg equation of motion (EoM) for $\hat{\mathcal{A}}_i$. I find

$$\begin{aligned}\partial_t \hat{\mathcal{A}}_{i\ \eta}^{\gamma} &= -i\Big[\hat{\mathcal{A}}_{i\ \eta}^{\gamma}, \mathcal{H}_{\mathsf{BBQ}}\Big] \\ &= -i\sum_{\delta}\big[\ J_1(\hat{\mathcal{A}}_{i\ \alpha}^{\gamma}\hat{\mathcal{A}}_{i+\delta\ \eta}^{\alpha} - \hat{\mathcal{A}}_{i\ \eta}^{\alpha}\hat{\mathcal{A}}_{i+\delta\ \alpha}^{\gamma}) \\ &\quad + (J_2 - J_1)(\hat{\mathcal{A}}_{i\ \alpha}^{\gamma}\hat{\mathcal{A}}_{i+\delta\ \alpha}^{\eta} - \hat{\mathcal{A}}_{i\ \eta}^{\alpha}\hat{\mathcal{A}}_{i+\delta\ \gamma}^{\alpha})\ \big]\ ,\end{aligned} \tag{1.70}$$

which takes on a simple quadratic form suitable for numerical integration, making the $u(3)$ representation an important advantage when considering dynamics. The EoM are fully quantum and correctly describe quantum dynamics. Moreover, they automatically preserve the length of the spin [Eq. (1.65)]. As long as the original representation obeys the spin-length constraint [Eq. (1.65)], we are properly describing the evolution of a spin–1 moment.

We also propose to combine classical MC with the integration of the EoM. From this emerges a numerical method similar to "molecular dynamics". The system is thermalized by means of the u3MC scheme. The evolution of the classical thermal ensemble of states obtained for the $\hat{\mathbf{A}}_i$-matrices is drawn by numerically integrating the EoM [Fig. 1.70], typically using a Runge-Kutta algorithm. We call this method "u3MD" and show that it can be used to calculate dynamical structure factors. This allows to support the quantum analytical results. Moreover, it can also be applied to disordered phases, or unconventional types of order such as vortices, or skyrmions in spin–1 magnets. In 2 dimensions, the Mermin-Wagner theorem forbids any phase transition due to the breaking of continuous symmetry to occur. But our formalism enables us to witness a different kind of phase transition, a topological one. Indeed the application of our method to the FQ state of the BBQ model on the triangular lattice allows us to discover and observe a KT–like type of topological phase transition due to the unbinding of $\mathbb{Z}_2$–vortices [190].

Although in the u3MD simulations, the EoM are fully quantum, they are originated from a classical thermal ensemble of states obtained by u3MC. The resulting excitations exhibit dynamics governed by Quantum Mechanics, but their classical spectral weight is controlled by classical statistics and is propagated by the time-integration. We find, however, that at low temperatures it is possible to correct for the effect of classical statistics inherited from u3MC simulations by a temperature–dependent prefactor. This enables us to link results obtained from finite-temperature numerical simulations and quantum zero–temperature analytical results, according to

$$S^{\mathsf{QM}}(\mathbf{q},\omega,T=0) = \lim_{T\to 0}\frac{\hbar\omega}{2k_BT}S^{\mathsf{MD}}(\mathbf{q},\omega,T)\ . \tag{1.71}$$

Using Eq. (1.71), we obtain a perfect agreement between the corrected simulation results and the semi–classical quantum results at $T = 0$, as summarized in Fig. 1.14 for the FQ phase . Detailed derivations of the quantum results, the classical-quantum correspondence and comparison with u3MD simulations are presented in Chapter 5.

Additionally, in Chapter 6, I show that our u(3) formalism is also valid for anisotropic

systems and delivers results for the FQ state on the triangular lattice for the BBQ model supplemented by single–ion anisotropy. We also show how one can apply the $u(3)$ formalism and its representation in terms of the $\hat{\mathbf{A}}$–matrices to the Heisenberg ferromagnetic easy-plane anisotropic model. The $\hat{\mathbf{A}}$–matrices are especially useful to work with on the TR-invariant basis and relatively easy to use when the ground state is quadrupolar. However, some attention is demanded when working with systems where dipoles rather than quadrupoles order. I additionally demonstrate how one can carefully apply our method for dipolar ordering, with anisotropic interactions.

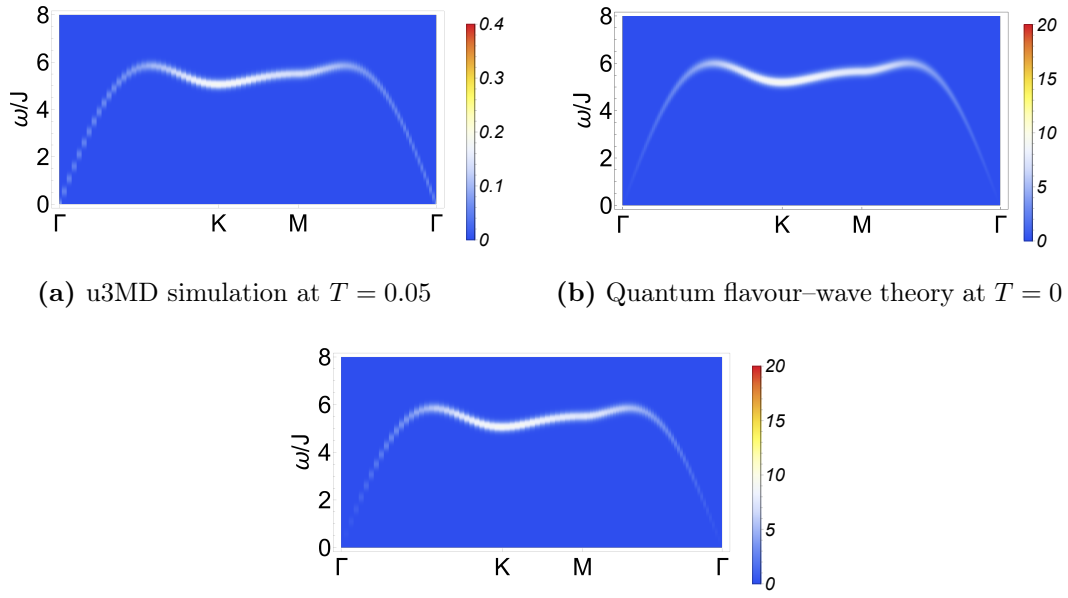

(a) u3MD simulation at $T = 0.05$

(b) Quantum flavour–wave theory at $T = 0$

(c) u3MD, corrected for classical statistics

Figure 1.14: Dynamical spin–dipole structure factor $S_{\mathrm{S}}(\mathbf{q}, \omega)$ for the ferroquadrupolar (FQ) phase of the BBQ model Eq. (1.69) with $J_1 = 0.0; J_2 = -1.0$ on the triangular lattice, reproduced from [201]. (a) Raw results of "molecular dynamics" (u3MD) simulation at finite T. We observe a dispersing band of excitations, which is linearly dispersive for small vectors in the reciprocal space. These are the Goldstone modes of the FQ order. The spectral weight in these excitations is governed by the classical statistics inherited from Monte Carlo (u3MC) simulations. (b) Predictions of quantum multi-boson theory at $T = 0$. (c) MD results corrected for the effects of classical statistics, showing agreement with $T = 0$ quantum results. The u3MD method was implemented by my collaborator Dr. Rico Pohle using a Runge-Kutta algorithm of order 4.

Finally, a summary and conclusion stating the advantages and limitations of our methods as well as future directions are provided in Chapter 7. I give a brief recapitulation of the work achieved during my Thesis, its repercussion and impacts on the understanding of spin–1 magnets as well as its consequences in the context of the recent endeavor in multi–polar phase. And I conclude with an outlook plan for the future possible applications our method is able to offer. The working progress for projects

descending from this Thesis is presented in Section 7.2. I discuss the application of our method to topological defects in spin–1 magnets and the generalization of the widely used Self-Consistent Gaussian Approximation to the degrees of freedom of a spin–1 expressed within our u(3) formalism.

The majority of the work presented in the Thesis has been published in an article Physical Review Research, Ref. [201]

Chapter 2

U(3) as an Algebra for Spin–1

In this Chapter, I provide the mathematical and conceptual baggage needed to describe a spin–1 moment using the group $U(3)$ together with the general methodology of the formalism that I derived. I start in Section 2.1 by introducing basic and useful definitions of notions coming from group theory that will turn out to be indispensable. In Section 2.2, I describe how a spin–$\frac{1}{2}$ moment can be represented within the $su(2)$ algebra, and how this implies that a classical valid representation can be accounted by an $O(3)$–vector. In Section 2.3, I explain how the $su(3)$ algebra can describe a spin–1 moment, and why the $O(3)$–vector is not a compatible classical limit for a spin–1. Because of the complicated structure of $su(3)$ algebra, in Section 2.4, I explain how we can simplify the mathematical derivation by instead considering the $u(3)$ algebra supplemented by a constraint. In Section 2.5, I develop a theory of fluctuations within the $u(3)$ formalism that can be treated at the classical or quantum level. Finally, in Section 2.6, I present how the $u(3)$ framework can be implemented to carry out numerical simulations by proposing a $u(3)$ classical Monte–Carlo and $u(3)$ Molecular Dynamics scheme.

2.1 A Little Bit of Group Theory

Before considering how we can represent a spin moment mathematically, I first provide some basic definitions, without attempting to give an extensive summary of group theory. Useful and pedagogic introductions can be found in [105, 211, 233]. Therefore, I here shortly introduce some important concepts and definitions that will reveal themselves as essential in understanding the next parts of this Chapter.

Lie groups are groups whose elements continuously depend on some parameters, they are manifolds and are very useful in physics in order to describe continuous symmetries. A group is an ensemble G equipped with a composition law $\cdot$, such that $\forall g_1, g_2, g_3 \in G$

1. $g_1 \cdot g_2 \in G$,
2. $g_1 \cdot (g_2 \cdot g_3) = (g_1 \cdot g_2) \cdot g_3$,
3. $\exists e \in G : e \cdot g_1 = g_1 \cdot e = g_1$,

4. $\exists g_1^{-1} \in G : g_1 \cdot g_1^{-1} = g_1^{-1} \cdot g_1 = e$.

Without entering too much into mathematical details, a Lie group L is a group. Therefore, it possesses a group structure, but is additionally characterized by the fact that the inverse and product operations between two elements of the group are differentiable:

- ⋆ Product: $L \times L \to L$, $(l_1, l_2) \to l_1 l_2$.
- ⋆ Inverse: $L \to L$, $l_1 \to l_1^{-1}$.

This implies that $l \in L$ continuously depends on n local coordinates $(x^1, \ldots, x^n)$, where n defines the dimension of L, such that $l = l(\mathbf{x})$:

1. $l(x)l(y) = l(f(x, y))$,
2. $l^{-1}(x) = l(g(x))$,
3. $l(0) = e$,

where e is the identity element of L. This way, the functions f and g are differentiable.

As examples of Lie groups, we consider $U(n)$ and $SU(n)$. This analysis will prove useful in Section 2.3 and Section 2.4.

$U(n)$ is the Lie group of unitary transformation in $\mathbb{C}^n$ defined by

$$U(n) = \left\{ M \in GL(n, \mathbb{C}) \mid MM^\dagger = \mathbb{I} \right\} . \tag{2.1}$$

The number of real independent components required to build up any element of a Lie group is called its dimension. It is the number of continuous parameters needed to describe them, and it is the dimension of its associated real manifold. $U(n)$'s dimension is n^2. $GL(n, \mathbb{C})$ denotes the group of general linear transformations in $\mathbb{C}^n$ consisting of $n \times n$ M matrices such that $\det(M) \neq 0$ (M is invertible), with elements M_{ij} belonging to $\mathbb{C}$. $GL(n, \mathbb{C})$'s dimension is $2n^2$.

$SU(n)$ is the Lie group of special unitary transformation in $\mathbb{C}^n$ defined by

$$SU(n) = \{ M \in U(u) \mid \det(M) = 1 \} . \tag{2.2}$$

Its dimension is $n^2 - 1$, because among the $U(n)$ matrices with $\det = e^{i\phi}$, $\phi \in [0, 2\pi]$, it selects the one with $\det = 1$.

As previously stated, Lie groups are groups whose elements continuously depend on some parameters. This continuity implies that we can construct the tangent space to any point. And this is in particular true for the identity element. From the tangent space at the identity arise a Lie algebra structure on its elements. The Lie algebra allows to generate with a finite number of elements, called generators, the neighborhood of the Lie group close to the identity. The generators of the associated Lie algebra are codified by composition laws usually given in terms of commutation relations. Indeed, Lie algebras are defined by their Lie bracket $[,]$ that tells us how to combine elements of the Lie algebra. Therefore, in order to describe a Lie group, we sometimes refer to its Lie algebra instead. As we will see, different Lie groups can have the same Lie algebra.

Lie algebras are linear vector spaces with a structure given by the Lie bracket $[\cdot,\cdot]$. Mathematically, we define a Lie algebra ℓ as the linear vector space V over a field F with a binary operation given by the Lie bracket $[\cdot,\cdot]$ such that for any $m,l,k \in \ell$ and any $a,b \in F$, the following properties are satisfied:

1. $[m,l] \in \ell \quad ,$
2. $[m,l] = -\,[l,m] \quad ,$
3. $[m, al+bk] = 2\,[m,l] + b\,[m,k] \quad ,$
4. $[[m,l],k] + [[l,k],m] + [[k,m],l] = 0 \quad .$

In a given basis $\{\mathbf{e}^i\}$ of ℓ, one can entirely characterize the algebra by the action of the Lie bracket on the basis element:

$$\left[\mathbf{e}^i, \mathbf{e}^j\right] = c^{ij}_{\ k}\mathbf{e}_k \ , \tag{2.3}$$

where $c^{ij}_{\ k} \in F$ are called the structure constants. More intuitively, we can choose to parametrize the elements l_i of the Lie group L in terms of parameters x_α as

$$l_i(\{x_\alpha\}) = e^{-i\sum_\beta x_\beta m_\beta} \ , \tag{2.4}$$

where m_β are the generators:

$$m_\beta = \left.\frac{\mathrm{d}l_i}{\mathrm{d}x_\beta}\right|_{\{x_\alpha\}=0} \ . \tag{2.5}$$

We see from Eq. (2.5), that all the m_β can be used as a basis to build the tangent space of the Lie group L at the identity. They also satisfy Eq. (2.3). This gives an alternative definition of Lie algebras, such as for any element m of the Lie algebra ℓ, $M = e^{tm}$ belongs to the Lie group $\mathcal{L}$, for any $t \in \mathbb{R}$. Additionally, if there is a neighborhood in the Lie group $\mathcal{L}$ around the identity $\mathbb{I}$, such that M is in this neighborhood, there is a unique element m of the Lie algebra ℓ in a neighborhood of 0, such that $M = e^m$. An important result states that there is a unique (up to an isomorphism) connected or simply connected Lie group $\widehat{\mathcal{L}}$ which has the same algebra as the Lie group $\mathcal{L}$ and is called the universal covering group of $\mathcal{L}$. We elucidate this point with an example below in Section 2.2.2.

The Lie algebra of the Lie group $U(n)$ is denoted by $u(n)$ and is given by

$$u(n) = \left\{m \in L(n,\mathbb{C}) \mid m + m^\dagger = 0\right\} \ , \tag{2.6}$$

where $L(n,\mathbb{C})$ simply represents the group of $n \times n$ square matrices with complex components. The dimension of the Lie algebra is the same as its Lie group, and for $u(n)$ we also have a dimension of n^2. The Lie algebra $su(n)$ of the Lie group $SU(n)$ is given by

$$su(n) = \left\{m \in L(n,\mathbb{C}) \mid m + m^\dagger = 0,\ \mathrm{Tr}(m) = 0\right\} \ . \tag{2.7}$$

Its dimension of $n^2 - 1$, meaning that as a basis for $su(n)$, we need to find $n^2 - 1$ independent generators.

Lastly, as mentioned above, Lie algebras generate only the group elements that are continuously connected to the identity element of that group. For instance, the group $O(3)$ consisting of all 3×3 orthogonal matrices in $\mathbb{R}^3$ is different from $SO(3)$ which is the group of all 3×3 orthogonal matrices with $\det = 1$, even though they have the same dimension. Indeed, $O(3)$matrices can have $\det = \pm1$, and among these, $SO(3)$ only selects those with $\det = 1$. O(3) matrices with $\det = 1$ are called proper matrices and they form a sub-group of $O(3)$, noted $O(3)^+ = SO(3)$, while those with $\det = -1$ do not from a group. (Indeed, if $M_1, M_2 \in O(3)^- = \{M \in O(3) \,|\, \det(M) = -1\}$ such that $\det(M_1) = \det(M_2) = -1$, then $M_3 = M_1M_2 \notin O(3)^-$ as $\det(M_3) = \det(M_1)\det(M_2) = 1$.) However, $O(3)$ and $SO(3)$ share the same algebra. Indeed,

$$o(3) = so(3) = \left\{m \in L(3, \mathbb{R}) \,|\, m + m^T = 0\right\} \ . \tag{2.8}$$

This algebra allows to generate all the elements that are continuously connected to the identity element, all of $O(3)^+ = SO(3)$ (since $\det(\mathbb{I}_3) = 1$), but not the elements with $\det = -1$. For the interested reader, a detailed introduction to these concepts can be found in [105, 211, 233].

2.2 A Little Bit of $su(2)$

2.2.1 Description of a Single Quantum Spin–$\frac{1}{2}$

As explained in the Introduction, Section 1.2.2, for a spin–$\frac{1}{2}$ moments there are only two eigenstates of the $\hat{\mathrm{S}}^z$ operators with eigenvalues $m = \pm\frac{1}{2}$ [Eq. (1.33)], illustrated in Fig. 1.3(a). These two states have both finite spin–dipole moments, and form a Kramers pair, related by time–reversal (TR) symmetry. We also saw that any possible quantum state for a spin–$\frac{1}{2}$ can be described in terms of two complex numbers $c_\uparrow, c_\downarrow \in \mathbb{C}$ which are the coefficients of the linear superposition of the two eigenstates [Eq. (1.33)]

$$\left|\psi_{\frac{1}{2}}\right\rangle = c_\uparrow|\uparrow\rangle + c_\downarrow|\downarrow\rangle \ , \quad c_{\uparrow,\downarrow} \in \mathbb{C} \ , \tag{2.9}$$

which was previously introduced as Eq. (1.34) and where the coefficients $c_\uparrow$ and $c_\downarrow$ are subject to the normalization constraint given Eq. (1.35). All the possible complex values for the 2 coefficients $c_\uparrow, c_\downarrow$ form a linear vector space, called the Hilbert space. For a spin–$\frac{1}{2}$, the Hilbert space is therefore 2-dimensional and denoted $\mathbb{H}_2$. Generally, two states in $\mathbb{H}_n$ can be linked by an $SU(n)$ transformation.

Coming back to spin–$\frac{1}{2}$, any two states in $\mathbb{H}_2$ can be connected via a $SU(2)$ transformation. Its dimension is 3, meaning one needs 3 independent parameters to describe it. The Lie group $SU(2)$ can also be parameterized by 2 complex numbers (i.e 4 real parameters) and 1 constraint. Indeed any $SU(2)$ matrix M can be written in the form of

$$M = \begin{pmatrix} z_1 & -z_2 \\ z_2 & z_1^* \end{pmatrix} \ , \ z_1, z_2 \in \mathbb{C} \ , \text{ such that } \ |z_1|^2 + |z_2|^2 = 1 \ , \tag{2.10}$$

where z_1^* denotes the complex conjugate of z_1. We can express the complex numbers

by their projection onto the real and complex axis of the complex plane:

$$z_1 = a + ib \, , z_2 = c + id \, , \tag{2.11}$$

such that

$$a^2 + b^2 + c^2 + d^2 = 1 \, . \tag{2.12}$$

From this picture arise a description in terms of quaternion

$$q = a + ib + jc + kd \, , \tag{2.13}$$

satisfying Eq. (2.12), which is the same constraint as the 3-dimensional sphere S^3. Therefore, $SU(2)$ can be thought of as the 3-dimensional sphere S^3.

The $su(2)$ algebra is also 3–dimensional and one also needs 3 independent parameters to describe it. A convenient basis for the Lie algebra $su(2)$ is given by the 3 Pauli matrices:

$$\sigma^x = \begin{pmatrix} 0 & 1 \\ 1 & 0 \end{pmatrix} \, , \; \sigma^y = \begin{pmatrix} 0 & -i \\ i & 0 \end{pmatrix} \, , \; \sigma^z = \begin{pmatrix} 1 & 0 \\ 0 & -1 \end{pmatrix} \, , \tag{2.14}$$

and the structure of the Lie algebra $su(2)$ is given by the commutation relations

$$[\sigma^\alpha, \sigma^\beta] = 2i\epsilon^{\alpha\beta}_{\;\;\gamma}\sigma^\gamma \, . \tag{2.15}$$

We can redefine the generators as $S^\alpha = \frac{1}{2}\sigma^\alpha$ and get rid of the 2 in the commutation relations:

$$[S^\alpha, S^\beta] = i\epsilon^{\alpha\beta}_{\;\;\gamma}S^\gamma \, . \tag{2.16}$$

2.2.2 SO(3) vs SU(2): Both Describe a Spin–$\frac{1}{2}$

An interesting result from group theory is that the universal covering group of the rotation group $SO(3)$ is $SU(2)$, and we write

$$\widehat{SO(3)} = SU(2) \, . \tag{2.17}$$

This implies that $SO(3)$ and $SU(2)$ share the same algebra. In order to make this more explicit, we quickly consider the $SO(3)$ group by defining

$$SO(n) = \left\{ M \in GL(n, \mathbb{R}) \,|\, MM^T = \mathbb{I}, \; \det(M) = 1 \right\} \, . \tag{2.18}$$

Its dimension is $\frac{n(n-1)}{2}$. $GL(n, \mathbb{R})$ denotes the group of general linear transformations in $\mathbb{R}^n$, i.e $n \times n$ M invertible matrices, with real components. Its algebra is given by

$$so(n) = \left\{ m \in L(n, \mathbb{R}) \,|\, m + m^\dagger = 0 \right\} \, . \tag{2.19}$$

This means that $SO(3)$ and its algebra are 3–dimensional. For the algebra $so(3)$, a convenient basis is given by

$$J^1 = \begin{pmatrix} 0 & 0 & 0 \\ 0 & 0 & -i \\ 0 & i & 0 \end{pmatrix} , \; J^2 = \begin{pmatrix} 0 & 0 & -i \\ 0 & 0 & 0 \\ i & 0 & 0 \end{pmatrix} , \; J^3 = \begin{pmatrix} 0 & -i & 0 \\ i & 0 & 0 \\ 0 & 0 & 0 \end{pmatrix} , \tag{2.20}$$

which satisfy the commutation relation:

$$[J^i, J^j] = i\epsilon^{ij}{}_k J^k , \tag{2.21}$$

which is the same as for the generators of $su(2)$ [Eq. (2.16)]. The Lie algebras are defined by their Lie brackets, and therefore the Lie groups $SO(3)$ and $SU(2)$ have the same algebra. This has drastic repercussions on the way we can represent a spin–$\frac{1}{2}$ moment. Indeed, valid representations of a spin–$\frac{1}{2}$ moment include both pictures: as a 2-dimensional complex vector (spinor) in $\mathbb{H}_2$ subject to $SU(2)$ transformations, or as a 3-dimensional real unit vector (O(3)-vector) prone to $SO(3)$ rotations ($O(3)$ since they have the same algebra $o(3) = so(3)$). There is actually a (local) isomorphism between $su(2)$ and $o(3) = so(3)$. And we write

$$su(2) \simeq so(3) . \tag{2.22}$$

In terms of the Lie groups, this isomorphism is local, in the sense that it concerns elements of the groups that can only be continuously connected to the identity element, as we saw previously. The mapping in Eq. (2.22) is actually 2 onto 1. This means that while we can think about $SU(2)$ as the sphere S^3, we can think of $SO(3)$ as "half" the sphere, namely the protective space $\mathbb{RP}^3$.

Because $SU(2)$ is connected, and simply connected (i.e $\Pi_1(S^3) = \{e\}$, all loops are shrinkable on the sphere S^3), as representation of $su(2)$ for a spin–s corresponds to a true representation of $SU(2)$. But, since $\Pi_1(SO(3)) = \Pi_1(\mathbb{RP}^3) = \mathbb{Z}_2$, any representation of $so(3)$ for a spin–s does not necessarily give a true representation of $SO(3)$. It turns out that a representation of $so(3)$ for a spin–s is a true representation of $SO(3)$ if s is an integer, but a protective one if s is a half-integer.

Because of this mathematical luck, we can equally well represent a spin–$\frac{1}{2}$ by a 2–dimensional complex vector subject to $SU(2)$ transformations as by a 3–dimensional real vector prone to $SO(3)$ rotations. Therefore, representing a spin–$\frac{1}{2}$ moment by a "classical" real O(3)-vector on the S^2 sphere (unit vector)

$$\mathbf{S} = (S^x, S^y, S^z) , \; \mathbf{S}^2 = 1 , \tag{2.23}$$

works very well. Indeed, for a spin–$\frac{1}{2}$, all higher-order terms of spin moments vanish, because of the very structure of the Lie algebra $su(2)$, and an O(3)-vector on the S^2 sphere suffice to describe all the degrees of freedom of a spin–$\frac{1}{2}$. All the degrees of freedom are encoded in what can plausibly happen to the spin–$\frac{1}{2}$ moment, which is dictated by the generators, i.e. the algebra.

This is very fortunate as we can then use the representation of a spin–$\frac{1}{2}$ in terms of an O(3)-vector on the S^2 sphere as a starting point for numerical simulations, such as

Monte Carlo algorithm [127] or analytic methods such as the Self-Consistent Gaussian Approximation (SCGA) [68] for calculating thermodynamic properties. The description of a spin–$\frac{1}{2}$ in terms of a unit O(3)-vector also allows to describe the dynamics at a (semi–)classical level from the Heisenberg equation of motion (EoM)

$$\frac{d\mathbf{S}_i}{dt} = -i\big[\mathbf{S}_i, \mathcal{H}\big] = \frac{d\mathcal{H}}{d\mathbf{S}_i} \times \mathbf{S}_i \ . \tag{2.24}$$

Using classical Monte Carlo simulation to draw thermalized spin configurations and then numerically integrating the EoM for spin–dipole moments [Eq. (2.24)] provides a (semi–)classical approach to spin dynamics. This approach has been referred to as "Molecular Dynamics" (MD)[152, 189, 267], and is similar to simulations based on the (phenomenological) Landau–Lifshitz–Gilbert equations [73]. However, the standard MD approach for spins will break down when $O(3)$–vector representation fails. This can happen when considering higher spin moments, as we will see below, or if one were to consider entanglement or additional orbital degrees of freedom [106]. Indeed, even two entangled spin–$\frac{1}{2}$ requires a description in terms of $su(4)$, which is 15–dimensional. While two independent spin–$\frac{1}{2}$ moments, each represented by $su(2) \simeq so(3)$ which is 3–dimensional, need a total of six parameters.

2.3 A Bit More to Make $su(3)$

As explained in the introduction, a spin–1 moment is described by 3 basis states. These can be chosen as the eigenstates of the $\hat{\mathrm{S}}^z$ operators with eigenvalues $m = 1, 0, -1$ [Eq. (1.40)] as illustrated in Fig. 1.3(b). Any state representing a spin–1 can be expressed as a linear combination of these 3 basis states

$$|\psi_1\rangle = c_1|1\rangle + c_2|0\rangle + c_3|\overline{1}\rangle \ , \quad c_\alpha \in \mathbb{C} \ , \tag{2.25}$$

which was previously introduced as Eq. (1.45), and where the coefficients c_1, c_2, c_3 are constrained by Eq. (1.46) and fully determine any spin–1 (provided the knowledge of basis in which we represent it). We then collect the coefficients c_1, c_2, c_3 describing any spin–1 and constrained by Eq. (1.46) into a 3–dimensional complex vector, living in the 3–dimensional Hilbert space $\mathbb{H}_3$. Any transformation allowed for a spin–1 such that Eq. (1.46) is preserved is given by the Lie group $SU(3)$, which has dimension 8.

The 3-dimensional representation of $SU(2)$ can be used to describe a spin–1, but it would only describe its rotations in R^3, i.e. only its dipolar moments. However, we saw that a spin–1 can do more, namely not "point" anywhere, and instead exhibit a quadrupole moment. In order to describe the features of a spin–1 beyond dipolar moments, one needs $SU(3)$. Moreover, the fundamental representation of $SU(3)$ is the one of a spin–1, while the fundamental representation of $SU(2)$ is the "two–state" one of a spin–$\frac{1}{2}$.

The eight generators of the Lie algebra $su(3)$ allow to generate any transformation of $SU(3)$ around the identity. A convenient basis for these is given by the eight Gell-Mann matrices

$$\begin{aligned}
\lambda^1 &= \begin{pmatrix} 0 & 1 & 0 \\ 1 & 0 & 0 \\ 0 & 0 & 0 \end{pmatrix} , \ \lambda^2 = \begin{pmatrix} 0 & -i & 0 \\ i & 0 & 0 \\ 0 & 0 & 0 \end{pmatrix} , \ \lambda^3 = \begin{pmatrix} 1 & 0 & 0 \\ 0 & -1 & 0 \\ 0 & 0 & 0 \end{pmatrix} , \\
\lambda^4 &= \begin{pmatrix} 0 & 0 & 1 \\ 0 & 0 & 0 \\ 1 & 0 & 0 \end{pmatrix} , \ \lambda^5 = \begin{pmatrix} 0 & 0 & -i \\ 0 & 0 & 0 \\ i & 0 & 0 \end{pmatrix} , \ \lambda^6 = \begin{pmatrix} 0 & 0 & 0 \\ 0 & 0 & 1 \\ 0 & 1 & 0 \end{pmatrix} , \\
\lambda^7 &= \begin{pmatrix} 0 & 0 & 0 \\ 0 & 0 & -i \\ 0 & i & 0 \end{pmatrix} , \ \lambda^8 = \frac{1}{\sqrt{3}} \begin{pmatrix} 1 & 0 & 0 \\ 0 & 1 & 0 \\ 0 & 0 & -2 \end{pmatrix} .
\end{aligned} \tag{2.26}$$

They satisfy commutation and anti-commutation relations

$$[\lambda^i, \lambda^j] = 2i f^{ij}_{\ k} \lambda^k \ , \quad f^{ij}_{\ k} = -\frac{i}{4} \mathrm{Tr}(\lambda^i [\lambda^j, \lambda^k]) \ , \tag{2.27a}$$

$$\{\lambda^i, \lambda^j\} = \frac{4}{3} \delta^{ij} \mathbb{I} + 2 g^{ij}_{\ k} \lambda^k \ , \quad g^{ij}_{\ k} = \frac{1}{4} \mathrm{Tr}(\lambda^i \{\lambda^j, \lambda^k\}) \ . \tag{2.27b}$$

It is clear that because it has 8 generators the $su(3)$ algebra describing a spin–1 is much richer than $su(2)$ describing a spin–$\frac{1}{2}$. As previously mentioned, the 3 generators needed to describe a spin–$\frac{1}{2}$ ($S^i = \frac{1}{2}\sigma^i$),

$$\mathbf{S} = (S^x, S^y, S^z) \ , \tag{2.28}$$

correspond to the rotation generators and form a sub-algebra of $su(3)$. The remaining 5 generators to construct $su(3)$ can then be identified as the 5 linearly independent quadrupole moments

$$\hat{\mathbf{Q}} = \begin{pmatrix} \hat{\mathrm{Q}}^{x^2-y^2} \\ \hat{\mathrm{Q}}^{3z^2-s^2} \\ \hat{\mathrm{Q}}^{xy} \\ \hat{\mathrm{Q}}^{xz} \\ \hat{\mathrm{Q}}^{yz} \end{pmatrix} = \begin{pmatrix} \frac{1}{2}(\hat{\mathrm{Q}}^{xx} - \hat{\mathrm{Q}}^{yy}) \\ \frac{1}{\sqrt{3}}(\hat{\mathrm{Q}}^{zz} - \frac{1}{2}(\hat{\mathrm{Q}}^{xx} + \hat{\mathrm{Q}}^{yy})) \\ \hat{\mathrm{Q}}^{xy} \\ \hat{\mathrm{Q}}^{xz} \\ \hat{\mathrm{Q}}^{yz} \end{pmatrix} = \begin{pmatrix} (\hat{\mathrm{S}}^x)^2 - (\hat{\mathrm{S}}^y)^2 \\ \frac{1}{\sqrt{3}}(2(\hat{\mathrm{S}}^z_i)^2 - (\hat{\mathrm{S}}^x)^2 - (\hat{\mathrm{S}}^y)^2) \\ \hat{\mathrm{S}}^x \hat{\mathrm{S}}^y + \hat{\mathrm{S}}^y \hat{\mathrm{S}}^x \\ \hat{\mathrm{S}}^x \hat{\mathrm{S}}^z + \hat{\mathrm{S}}^z \hat{\mathrm{S}}^x \\ \hat{\mathrm{S}}^y \hat{\mathrm{S}}^z + \hat{\mathrm{S}}^z \hat{\mathrm{S}}^y \end{pmatrix} , \tag{2.29}$$

as previously defined in Eq. (1.47).

The vector notation [Eq. (2.29)], and tensor notation [Eq. (1.44)] are linked to each other by

$$\hat{\mathbf{Q}} \cdot \hat{\mathbf{Q}} = \sum_\alpha \hat{\mathrm{Q}}^\alpha \hat{\mathrm{Q}}^\alpha = \mathbf{\frac{1}{2}} \sum_{\alpha\beta} \hat{\mathrm{Q}}^{\alpha\beta} \hat{\mathrm{Q}}^{\alpha\beta} \ . \tag{2.30}$$

Spin moments are commonly represented in their magnetic basis formed by the eigenstates of the $\hat{\mathrm{S}}^z$ operators. However, this choice is not unique. Indeed, any linear combination of these states that form 3 new orthogonal states can be used just as well. We saw that what makes a spin–1 special includes the fact that it can exhibit quadrupole moments on a single site, which are time–reversal (TR) invariant. For a

spin–1 moment, it turns out to be convenient to work in a basis that respects the symmetries of the quadrupole moments, such that

$$\hat{T}|\phi\rangle = |\phi\rangle \ , \tag{2.31}$$

where $\hat{T}$ is the TR–operator. Such a TR–invariant basis is given by

$$\mathcal{B}_2 = \{|x\rangle, |y\rangle, |z\rangle\} \ , \tag{2.32}$$

where

$$|x\rangle = \tfrac{i}{\sqrt{2}}(|1\rangle - |\overline{1}\rangle), \quad |y\rangle = \tfrac{1}{\sqrt{2}}(|1\rangle + |\overline{1}\rangle), \quad |z\rangle = -i|0\rangle \quad . \tag{2.33}$$

These states are illustrated in Fig. 2.1 and are subject to the closure relation

$$|x\rangle\langle x| + |y\rangle\langle y| + |z\rangle\langle z| = \mathbb{I} \ . \tag{2.34}$$

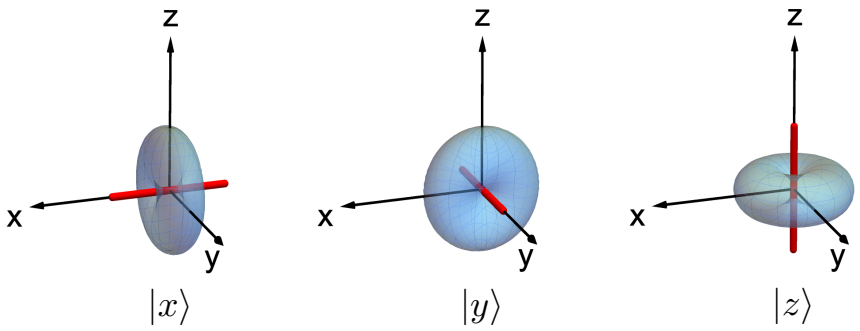

Figure 2.1: Time–reversal invariant basis for a spin–1 moment. The three states $|\alpha\rangle$, with $\alpha = x, y, z$, are invariant under time–reversal, and have vanishing dipole moments $\langle\alpha|S^\mu|\alpha\rangle = 0$, for $\mu = x, y, z$ referring to the usual spacial spin components. The red rods represent their respective directors whose components are given by Eq. (2.35) Their spin fluctuations exhibit the characteristic "donuts–shaped" profile [Appendix A]. These states can be expressed in terms of the usual magnetic basis [Fig. 1.3] through Eq. (2.33).

Any state describing a spin–1 can be expressed as a linear combination of the TR–invariant basis states as

$$|\mathbf{d}\rangle = \sum_{\alpha=x,y,z} d^{*\alpha}|\alpha\rangle, \quad d^{*\alpha} \in \mathbb{C} \ . \tag{2.35}$$

The coefficients $d^{*\alpha}$ are collected in a complex vector (director) $\mathbf{d}$, of unit length

$$\mathbf{d}^* \cdot \mathbf{d} = 1 \ . \tag{2.36}$$

We note that the spin fluctuations of the 3 TR–invariant basis states [Eq. (2.33)] shown in Fig. 2.1 take the characteristic donuts-shape, do not have any dipole moments, and are represented by their director $\mathbf{d}$ shown in red. The real and imaginary parts can be

explicitly separated as

$$\mathbf{d}^* = \mathbf{u} + i\mathbf{v} \; . \tag{2.37}$$

This provides a representation of a spin–1 in terms of 2 real 3–dimensional vectors, subject to the constraint

$$\mathbf{u} \cdot \mathbf{u} + \mathbf{v} \cdot \mathbf{v} = 1 \; . \tag{2.38}$$

A spin–1 moment can be entirely characterized by the 3 complex coefficients of its decomposition within an orthogonal basis, that we can choose to be the TR invariant basis [Eq. (2.33)], such that the 3 complex coefficients correspond to the components of the director $\mathbf{d}$, subject to the normalization constraint [Eq. (2.36)]. Additionally, a quantum state is defined up to a phase, and therefore so is $\mathbf{d}$ [Eq. (2.35)]. We therefore have the freedom of fixing the gauge of $\mathbf{d}$. It is sometimes convenient [229] to choose it such that $\mathbf{u}$ and $\mathbf{v}$ are perpendicular to each other

$$\mathbf{u}.\mathbf{v} = 0 \; . \tag{2.39}$$

A spin–1 moment can then be represented by a 3–dimensional complex vector, 6 real parameters, subject to a length constraint and a gauge degree of freedom for the phase. This implies that ultimately a spin–1 moment can be described by 4 independent real–degrees of freedom. The length constraint and the gauge freedom can also be chosen such that we can get rid of one of the 3 complex coefficients, and a spin–1 moment is then simply represented by a 2–dimensional complex vector, 4 real parameters. This explains why the parameter phase of a spin–1 moment is given by the 2–dimensional complex projective space $\mathbb{CP}^2$.

The 8 operators needed to represent a spin–1 moment can also be expressed in the TR–invariant basis. The dipole moments become

$$\hat{\mathrm{S}}^\alpha = -i\epsilon^{\alpha\beta\gamma}|\beta\rangle\langle\gamma| \; , \tag{2.40}$$

and correspond to the anti–symmetric contraction of TR–invariant basis states, while the quadrupoles moments are given by

$$\hat{\mathrm{Q}}^{\alpha\beta} = -|\alpha\rangle\langle\beta| - |\beta\rangle\langle\alpha| + \frac{2}{3}\delta^{\alpha\beta}|\gamma\rangle\langle\gamma| \; , \tag{2.41}$$

and correspond to the symmetric contraction. Given a general state represented by its director [Eq. (2.35)], its expected dipole–moments and quadrupole–moments in terms of $\mathbf{d}$ and in terms of $\mathbf{u}$ and $\mathbf{v}$ [Eq. (2.37)] yield

$$\begin{aligned} \langle\mathbf{d}|\hat{\mathrm{S}}^\alpha|\mathbf{d}\rangle &= -i\epsilon^{\alpha\beta\gamma}d^{*\beta}d^\gamma \\ &= \; 2\epsilon^{\alpha\beta\gamma}\mathrm{u}^\beta\mathrm{v}^\gamma \; , \end{aligned} \tag{2.42}$$

$$\begin{aligned} \langle\mathbf{d}|\hat{\mathrm{Q}}^{\alpha\beta}|\mathbf{d}\rangle &= -d^{*\alpha}d^\beta - d^{*\beta}d^\alpha + \frac{2}{3}\delta^{\alpha\beta}d^{*\gamma}d^\gamma \\ &= -2(\mathrm{u}^\alpha\mathrm{u}^\beta + \mathrm{v}^\alpha\mathrm{v}^\beta) + \frac{2}{3}\delta^{\alpha\beta}(\mathrm{u}^\gamma\mathrm{u}^\gamma + \mathrm{v}^\gamma\mathrm{v}^\gamma) \; . \end{aligned} \tag{2.43}$$

The equation for the dipole moment [Eq. (2.42)] can be rewritten in its vector form

$$\langle \mathbf{S} \rangle = 2\mathbf{u} \times \mathbf{v} \ . \tag{2.44}$$

We see that if the director $\mathbf{d}$ is either purely real ($\mathbf{v} = 0$), or purely imaginary ($\mathbf{u} = 0$), the associated dipole moments will be zero. This is, of course, in particular the case for the TR–invariant basis [Eq. (2.33)].

2.4 From $su(3)$ to $u(3)$

2.4.1 Description in Terms of $u(3)$

From the form of the expressions for spin– [Eq. (2.40)] and quadrupole–moments [Eq. (2.41)], we see that it is convenient to introduce an object with matrix elements

$$\hat{\mathcal{A}}^{\alpha}_{\ \gamma} = |\alpha\rangle\langle\gamma| \ , \tag{2.45}$$

i.e.

$$\hat{\mathbf{A}} = \begin{pmatrix} |x\rangle\langle x| & |x\rangle\langle y| & |x\rangle\langle z| \\ |y\rangle\langle x| & |y\rangle\langle y| & |y\rangle\langle z| \\ |z\rangle\langle x| & |z\rangle\langle y| & |z\rangle\langle z| \end{pmatrix} \ , \tag{2.46}$$

that we referred to as the " A–matrix" [180] . Given a general state represented by its director $\mathbf{d}$ [Eq. (2.35)], the expected value of the A-matrix components is given by

$$\langle \mathbf{d}|\hat{\mathcal{A}}^{\alpha}_{\ \beta}|\mathbf{d}\rangle = d^{*\alpha}d^{\beta} = \mathrm{u}^{\alpha}\mathrm{u}^{\beta} + \mathrm{v}^{\alpha}\mathrm{v}^{\beta} + \mathrm{i}(\mathrm{u}^{\alpha}\mathrm{v}^{\beta} + \mathrm{u}^{\beta}\mathrm{v}^{\alpha}) \ , \tag{2.47}$$

where $\mathbf{u}$ and $\mathbf{v}$ are defined through Eq. (2.37).

We call it " A–matrix", but to be mathematically correct, $\hat{\mathbf{A}}$ is a tensor, as described in Section 2.4.3. The matrix $\hat{\mathbf{A}}$ is subject to the constraint

$$\mathrm{Tr}\ \hat{\mathbf{A}} = 1 \ , \tag{2.48}$$

which follows from the closure relation [Eq. (2.34)] of the TR–invariant basis states [Eq. (2.33)]. The component of the matrix $\hat{\mathbf{A}}$ also satisfy

$$\hat{\mathcal{A}}^{\alpha\dagger}_{\ \beta} = \hat{\mathcal{A}}^{\beta}_{\ \alpha} \ , \tag{2.49}$$

which follows from the definition Eq. (2.45). In terms of the components of the matrix $\hat{\mathbf{A}}$ [Eq. (2.45)], the dipole– and quadrupole–moments become

$$\hat{\mathrm{S}}^{\alpha} = -i\epsilon^{\alpha}_{\ \beta\ \gamma}\hat{\mathcal{A}}^{\beta}_{\ \gamma} \ , \tag{2.50}$$

$$\hat{\mathrm{Q}}^{\alpha\beta} = -\hat{\mathcal{A}}^{\alpha}_{\ \beta} - \hat{\mathcal{A}}^{\beta}_{\ \alpha} + \frac{2}{3}\delta^{\alpha\beta}\hat{\mathcal{A}}^{\gamma}_{\ \gamma} \ , \tag{2.51}$$

which were previously introduced in Eq. (1.67) and Eq. (1.68).

A convenient basis for $\hat{\mathbf{A}}$ is provided by the representation of components of the matrix $\hat{\mathbf{A}}$ in the TR–invariant basis, giving nine matrices with a single non–zero element

[180]

$$\begin{aligned}
\hat{\mathcal{A}}^1{}_1 &= \begin{pmatrix}1&0&0\\0&0&0\\0&0&0\end{pmatrix}\ ,\ \hat{\mathcal{A}}^1{}_2 = \begin{pmatrix}0&1&0\\0&0&0\\0&0&0\end{pmatrix}\ ,\ \hat{\mathcal{A}}^1{}_3 = \begin{pmatrix}0&0&1\\0&0&0\\0&0&0\end{pmatrix}\ ,\\
\hat{\mathcal{A}}^2{}_1 &= \begin{pmatrix}0&0&0\\1&0&0\\0&0&0\end{pmatrix}\ ,\ \hat{\mathcal{A}}^2{}_2 = \begin{pmatrix}0&0&0\\0&1&0\\0&0&0\end{pmatrix}\ ,\ \hat{\mathcal{A}}^2{}_3 = \begin{pmatrix}0&0&0\\0&0&1\\0&0&0\end{pmatrix}\ ,\\
\hat{\mathcal{A}}^3{}_1 &= \begin{pmatrix}0&0&0\\0&0&0\\1&0&0\end{pmatrix}\ ,\ \hat{\mathcal{A}}^3{}_2 = \begin{pmatrix}0&0&0\\0&0&0\\0&1&0\end{pmatrix}\ ,\ \hat{\mathcal{A}}^3{}_3 = \begin{pmatrix}0&0&0\\0&0&0\\0&0&1\end{pmatrix}\ .
\end{aligned} \tag{2.52}$$

These matrices close the algebra $u(3)$, with commutation relations

$$\begin{aligned}
\left[\hat{\mathcal{A}}^\alpha_{i\ \beta}, \hat{\mathcal{A}}^\gamma_{i\ \eta}\right] &= \delta^\gamma{}_\beta \hat{\mathcal{A}}^\alpha_{i\ \eta} - \delta^\alpha{}_\eta \hat{\mathcal{A}}^\gamma_{i\ \beta}\ ,\\
\left[\hat{\mathcal{A}}^\alpha_{i\ \beta}, \hat{\mathcal{A}}^\gamma_{j\ \eta}\right] &= 0\ ,
\end{aligned} \tag{2.53}$$

previously introduced in Eq. (1.66). Any complex linear combination of the basis matrices as represented in Eq. (2.52) can be used to generate transformations of $U(3)$. However, we saw that in order to describe a spin–1 moment, we need $SU(3)$, and don't require all of $U(3)$. In the next sections, we will see that we can effectively describe all possible states of a spin–1 moment using $U(3)$, and use a constraint to restrict back to $SU(3)$. We will also see that because of the nice commutation relations of the $\hat{\mathbf{A}}$–matrices Eq. (2.53), it is more convenient to work with $u(3)$, rather than $su(3)$.

2.4.2 Relationship Between $U(3)$ and $SU(3)$ Representations

Compared to the eight generators of $SU(3)$ [Eq. (2.26)], the description of a spin–1 moment in terms of the nine matrices $\hat{\mathcal{A}}^\alpha{}_\beta$ [Eq. (2.52)], contains one additional operator. This additional operator is the spin–length $\hat{\mathbf{S}}^2$.

Indeed, we note that the spin–length $\hat{\mathbf{S}}^2$ is represented by a diagonal matrix, with eigenvalues $s(s+1)$ and therefore commutes with any other matrix. Under a basis change $\Lambda \in SU(n)$, the spin–length $\hat{\mathbf{S}}^2$ remains unchanged as $\Lambda\hat{\mathbf{S}}^2\Lambda^\dagger = \hat{\mathbf{S}}^2\Lambda\Lambda^\dagger = \hat{\mathbf{S}}^2$. And therefore, its trace also stays invariant under a basis change

$$\mathrm{Tr}(\hat{\mathbf{S}}^2) = n \times s(s+1) > 1\ , \tag{2.54}$$

where n is the dimension of the Hilbert space, since already for a spin–$\frac{1}{2}$, we have $n = 2$ and $s = \frac{1}{2}$ which leads to $\mathrm{Tr}(\hat{\mathbf{S}}^2) = \frac{3}{2}$. Since $\mathrm{Tr}(\hat{\mathbf{S}}^2) \neq 0$, $\hat{\mathbf{S}}^2$ does not belong to the algebra $su(n)$, but can be used as the additional generator to build o basis for $u(n)$.

Consequently, we can use the 3 linearly independent dipole moments $\hat{\mathrm{S}}$ [Eq. (2.28)], which represents the $SO(3)$ rotations and the 5 linearly independent quadrupole mo-

ments $\hat{\mathrm{Q}}$ [Eq. (2.29)], which together make a representation of $SU(3)$, to which we add the additional spin–length $\hat{\mathbf{S}}^2$ operator in order to build a representation of $U(3)$. We can then map the representation of $SU(3)$ in terms of dipole [Eq. (2.28)] and quadrupole [Eq. (2.29)] moments, plus the spin–length $\hat{\mathbf{S}}^2$ operator, with the representation of $U(3)$ in terms of the nine generators $\hat{\mathbf{A}}^{\alpha}_{\beta}$ [Eq. (2.52)]

$$\begin{pmatrix} \hat{\mathbf{S}}^2 \\ \hat{\mathrm{S}}^x \\ \hat{\mathrm{S}}^y \\ \hat{\mathrm{S}}^z \\ \hat{\mathrm{Q}}^{x^2-y^2} \\ \hat{\mathrm{Q}}^{3r^2-s^2} \\ \hat{\mathrm{Q}}^{xy} \\ \hat{\mathrm{Q}}^{xz} \\ \hat{\mathrm{Q}}^{yz} \end{pmatrix} = C \begin{pmatrix} \hat{\mathcal{A}}^1{}_1 \\ \hat{\mathcal{A}}^1{}_2 \\ \hat{\mathcal{A}}^1{}_3 \\ \hat{\mathcal{A}}^2{}_1 \\ \hat{\mathcal{A}}^2{}_2 \\ \hat{\mathcal{A}}^2{}_3 \\ \hat{\mathcal{A}}^3{}_1 \\ \hat{\mathcal{A}}^3{}_2 \\ \hat{\mathcal{A}}^3{}_3 \end{pmatrix} , \tag{2.55}$$

where C is the 9×9 matrix.

$$C = \begin{pmatrix} 2 & 0 & 0 & 0 & 2 & 0 & 0 & 0 & 2 \\ 0 & 0 & 0 & 0 & 0 & -i & 0 & i & 0 \\ 0 & 0 & i & 0 & 0 & 0 & -i & 0 & 0 \\ 0 & -i & 0 & i & 0 & 0 & 0 & 0 & 0 \\ -1 & 0 & 0 & 0 & 1 & 0 & 0 & 0 & 0 \\ \frac{1}{\sqrt{3}} & 0 & 0 & 0 & \frac{1}{\sqrt{3}} & 0 & 0 & 0 & -\frac{2}{\sqrt{3}} \\ 0 & -1 & 0 & -1 & 0 & 0 & 0 & 0 & 0 \\ 0 & 0 & -1 & 0 & 0 & 0 & -1 & 0 & 0 \\ 0 & 0 & 0 & 0 & 0 & -1 & 0 & -1 & 0 \end{pmatrix} , \tag{2.56}$$

previously shown schematically as Eq. (1.64).

This means that within $U(3)$, the length of the spin is not fixed, it is one of the possible degrees of freedom encoded by $U(3)$. Luckily, we can pin down the spin sector by imposing the constraint Eq. (2.48) as

$$\mathrm{Tr}\mathcal{A} = \sum_{\alpha} \hat{\mathcal{A}}^{\alpha}_{i\ \alpha} = \sum_{\alpha} \tfrac{1}{2} \hat{\mathrm{S}}^{\alpha}_{i} \hat{\mathrm{S}}^{\alpha}_{i} = \tfrac{1}{2} s(s+1) = 1 \ , \tag{2.57}$$

where we have used the property

$$\sum_{\alpha} \hat{\mathrm{Q}}^{\alpha\alpha}_{i} = 0 \ . \tag{2.58}$$

This way we restrict fluctuations to only the smaller group $SU(3)$, which is the group that properly describes a spin–1 moment.

From this observation follows that we can work directly with the matrices $\hat{\mathbf{A}}$, as long as these satisfy the constraint Eq. (2.57). This will turn out to be very useful for numerical simulations of spin–1 moment.

2.4.3 Mathematical Properties of A–matrices

We mentioned that for convenience we might refer to the operators $\hat{\mathcal{A}}^{\alpha}{}_{\beta}$ as matrices, while in fact, they are tensors. Details on the tensor nature of the operators $\hat{\mathcal{A}}^{\alpha}{}_{\beta}$ are given in Appendix B. Here, I simply present the way in which $\hat{\mathcal{A}}^{\alpha}{}_{\beta}$ transforms under a linear map, a property that will turn out to be useful later.

According to its definition[Eq. (2.45)], the operator $\hat{\mathcal{A}}^{\alpha}{}_{\beta}$ is given by matrix elements of the TR–invariant basis [Eq. (2.32)], we directly introduced a contravariant index α, and a covariant index β, such that the index α corresponds to a bra vector, while the index γ relates to a ket vector. Because the Bra–vector space is the dual of the ket–vector space, covariant and contravariant indexes transform differently under a linear transformation of basis vectors.

We consider a general linear transformation

$$\Lambda : V \to V \ , \tag{2.59}$$

with

$$\det \Lambda \neq 0 \ , \tag{2.60}$$

such that Λ is invertible. We then define

$$\tilde{\Lambda} = \left(\Lambda^{-1}\right)^{T} \ . \tag{2.61}$$

Under such a transformation, the components of $\hat{\mathcal{A}}^{\alpha}{}_{\beta}$ will transform as

$$(\hat{\mathcal{A}}^{\alpha}{}_{\beta})^{\mu}{}_{\nu} = \Lambda^{\mu}{}_{\gamma}\tilde{\Lambda}_{\nu}{}^{\kappa}(\hat{\mathcal{A}}^{\alpha}{}_{\beta})^{\gamma}{}_{\kappa} = \Lambda^{\mu}{}_{\gamma}(\Lambda^{-1})^{\kappa}{}_{\nu}(\hat{\mathcal{A}}^{\alpha}{}_{\beta})^{\gamma}{}_{\kappa} \ , \tag{2.62}$$

where we once again assume the Einstein convention of summing over repeated indices.

Mathematically, $\hat{\mathcal{A}}^{\alpha}{}_{\beta}$ is a $(1,1)$–tensor, implying that it can be viewed as a linear map that takes one element in the vector space V, and a second one in the dual vector space V^*, and assigns then a number in the field F.We also note that the only non-zero component of $(\hat{\mathcal{A}}^{\alpha}{}_{\beta})^{\gamma}{}_{\kappa}$ in the TR–invariant basis is simply

$$(\hat{\mathcal{A}}^{\alpha}{}_{\beta})^{\alpha}{}_{\beta} \equiv 1 \ . \tag{2.63}$$

Two other useful mathematical properties of the operators $\hat{\mathbf{A}}$ which will prove useful in later calculations are shortly presented below. Firstly, any state $|\alpha = x, y, z\rangle$ in the basis $\mathcal{B}_2$ [Eq. (2.32)] can be constructed as

$$|\alpha\rangle = \mathrm{d}^{\dagger\alpha}|\mathrm{vac}\rangle \ , \tag{2.64}$$

where $\hat{\mathrm{d}}_{\alpha}$ satisfies the bosonic commutation relation

$$[\hat{\mathrm{d}}_{\alpha}, \mathrm{d}^{\dagger\alpha}] = \delta_{\alpha\beta} \ , \tag{2.65}$$

and $|\mathrm{vac}\rangle$ is the vacuum. This implies that the matrix $\hat{\mathbf{A}}$ can be built as the exterior product of the operators $\hat{\mathrm{d}}_{\alpha}$

$$\hat{\mathcal{A}}^{\alpha}{}_{\beta} = \mathrm{d}^{\dagger\alpha}\hat{\mathrm{d}}_{\beta} \ . \tag{2.66}$$

The fact that $\hat{\mathrm{d}}_\alpha$ satisfies the Bosonic commutation relation ensures that the structure of the $u(3)$ algebra is preserved [Eq. (2.53)] This representation will in particular prove itself useful when we come to construct the quantum theory of excitations in Section 4.1.

Secondly, we note that the dipole moments, the quadrupole moments and the $\hat{\mathcal{A}}^\alpha{}_\beta$ operators are linked to each other via

$$\sum_{\alpha,\beta} \hat{\mathcal{A}}^\alpha_{i\ \beta}\hat{\mathcal{A}}^\beta_{j\ \alpha} = \sum_{\alpha,\beta} \frac{1}{4}\hat{\mathrm{Q}}^{\alpha\beta}_i\hat{\mathrm{Q}}^{\beta\alpha}_j + \sum_\alpha \frac{1}{2}\hat{\mathrm{S}}^\alpha_i\hat{\mathrm{S}}^\alpha_j + \frac{1}{12}s^2(s+1)^2 \ . \tag{2.67}$$

We will especially rely on this result in Section 3.3.3 and Section 4.2 as it states a sum rule on the structure factors.

2.4.4 Representation of the BBQ Model Within a $u(3)$ Formalism

We have previously encountered the spin–1 bilinear–biquadratic (BBQ) model [Eq. (1.48)], which is reproduced here for clarity

$$\mathcal{H}_{\mathsf{BBQ}} = \sum_{\langle i,j\rangle}\left[J_1\hat{\mathbf{S}}_{\boldsymbol{i}}\cdot\hat{\mathbf{S}}_{\boldsymbol{j}} + J_2(\hat{\mathbf{S}}_{\boldsymbol{i}}\cdot\hat{\mathbf{S}}_{\boldsymbol{j}})^2\right] \ . \tag{2.68}$$

We have also seen that the BBQ Hamiltonian, which is the most general, $SU(2)$ symmetric, nearest–neighbour Hamiltonian allowed for a spin–1 magnet, has been extensively studied [10, 87, 111, 131, 143, 180, 183, 229, 250, 255]. As previously introduced in Eq. (1.49), when written down in terms of the nine generators of $SU(3)$, which includes both dipole and quadrupoles,

$$\mathcal{H}_{BBQ} = \sum_{\langle i,j\rangle}\left(J_1 - \frac{J_2}{2}\right)\hat{\mathbf{S}}_{\boldsymbol{i}}\cdot\hat{\mathbf{S}}_{\boldsymbol{j}} + \frac{J_2}{2}\ \hat{\mathbf{Q}}_{\mathbf{i}}\cdot\hat{\mathbf{Q}}_{\mathbf{j}}\ + \frac{4J_2}{3}\ , \tag{2.69}$$

the physical nature of the biquadratic term becomes apparent. Indeed, we note that a biquadratic interaction of dipoles induces a quadratic interaction of quadrupoles, which are not permitted for a single spin–$\frac{1}{2}$.

By noticing that, in Eq. (2.68) or Eq. (2.69), the vector products $\hat{\mathbf{S}}_{\boldsymbol{i}}\cdot\hat{\mathbf{S}}_{\boldsymbol{j}}$ and $\hat{\mathbf{Q}}_{\mathbf{i}}\cdot\hat{\mathbf{Q}}_{\mathbf{j}}$ are unchanged under an $O(3)$ transformation, the $SU(2)\simeq O(3)$ invariance of the BBQ Hamiltonian is also obvious.

Moreover in the special case where $J_1 = J_2 = J$, the symmetry of the model is enlarged to $SU(3)$ [180, 183, 229]. Indeed, when $J_1 = J_2 = J$, the BBQ model can be rewritten

$$\mathcal{H}_{\mathsf{BBQ}} = \frac{J}{2}\sum_{\langle i,j\rangle}\mathbf{T}_i\cdot\mathbf{T}_j + \frac{4J}{3}\ , \tag{2.70}$$

where $\mathbf{T}_i$ is the eight–dimensional vector

$$\mathbf{T}_i = (\hat{\mathrm{S}}^x_i, \hat{\mathrm{S}}^y_i, \hat{\mathrm{S}}^z_i, \hat{\mathrm{Q}}^{x^2-y^2}_i, \hat{\mathrm{Q}}^{3r^2-s^2}_i, \hat{\mathrm{Q}}^{xy}_i, \hat{\mathrm{Q}}^{xz}_i, \hat{\mathrm{Q}}^{yz}_i)\ , \tag{2.71}$$

and dipoles and quadrupoles appear on an equal level. In this case, it becomes pos-

sible to transform dipole moments into quadrupoles (or vice versa) within the $SU(3)$ group, without any energy cost [229]. As shown in Fig. 1.11, these $SU(3)$-symmetry points are located at the zero–temperature boundaries between phases with dipolar and quadrupolar nature.

We can rewrite $\mathcal{H}_{\mathsf{BBQ}}$ in terms of generators of $U(3)$ using Eq. (2.69), Eq. (1.67) and Eq. (1.68) (or, equivalently, Eq. (2.55)). We obtain

$$\mathcal{H}_{\mathsf{BBQ}} = \sum_{\langle i,j \rangle} \left[J_1 \hat{\mathcal{A}}_{i\ \beta}^{\alpha} \hat{\mathcal{A}}_{j\ \alpha}^{\beta} + (J_2 - J_1) \hat{\mathcal{A}}_{i\ \beta}^{\alpha} \hat{\mathcal{A}}_{j\ \beta}^{\alpha} + J_2 \right] , \tag{2.72}$$

where we use Einstein's convention on the summation of repeated indices. The $\mathcal{A}_i$–matrices are subject to the constraint

$$\mathrm{Tr}\ \mathcal{A}_i = \sum_{\alpha} \hat{\mathcal{A}}_{i\ \alpha}^{\alpha} = 1 . \tag{2.73}$$

Eq. (2.72) and Eq. (2.73) were previously introduced in Eq. (1.69) and Eq. (1.65) (and Eq. (2.57)), respectively. Again Eq. (2.73) restricts the $u(3)$ algebra to $su(3)$, such that we are indeed properly representing a spin–1 system [Eq. (2.57)].

We note that in terms of $\hat{\mathcal{A}}^{\alpha}_{\ \beta}$, the BBQ model [Eq. (2.72)] retains the same symmetry properties as the one discussed for the BBQ model in terms of dipoles [Eq. (2.68)] (and quadrupoles [Eq. (2.69)]).

Indeed, the BBQ model in terms of $\hat{\mathcal{A}}^{\alpha}_{\ \beta}$ [Eq. (2.72)] consists of 2 terms which transform differently. The second term,

$$\hat{\mathcal{A}}_{i\ \beta}^{\alpha} \hat{\mathcal{A}}_{j\ \beta}^{\alpha}$$

has its indices which are contracted either convariantly on both sides or contravariantly on both sides. And, using results of Section 2.4.3 , we can show that it is invariant under $O(3) \simeq SU(2)$ rotations. This results is also derived in Appendix B.1 in Eq. (B.13). While the first term

$$\hat{\mathcal{A}}_{i\ \beta}^{\alpha} \hat{\mathcal{A}}_{j\ \alpha}^{\beta}$$

has indices α and β which transform contravariantly on one site, and covariantly on the other, and therefore possesses $U(3)$ symmetry. However, because of the constraint on the $\mathcal{A}_i$–matrices [Eq. (2.73)], the $U(3)$ symmetry is broken down to $SU(3)$. Therefore, Eq. (2.72) possesses $SU(2)$ symmetry for general values of the parameters J_1, J_2. But for $J_1 = J_2$, the second term vanishes, and as previously noted, the symmetry is enlarged to $SU(3)$. Further details of this analysis can be found in Appendix B.1 in Eq. (B.11).

As previously noted, written in terms of generators of $U(3)$ [Eq. (2.72)], the BBQ model takes on a form quadratic in $\hat{\mathcal{A}}^{\alpha}_{i\ \beta}$, which treats dipole and quadrupole moments on an equal footing. This contrasts with the biquadratic term in dipole moments from Eq. (2.68). Since it allows to straightforwardly decouple the interactions, the quadratic form is well–suited to develop any analytic, mean–field methods [180].

The BBQ Hamiltonian is also be expressed in a quadratic form, using dipole $\hat{\mathrm{S}}$ and quadrupole $\hat{\mathrm{Q}}$ moments, which form the $su(3)$ algebra, as in Eq. (2.69). However, the

clutter nature of the commutation relations of generators of $SU(3)$ [Eq. (2.27a)] makes derivations difficult [14, 51, 200, 264]. As we will see in Section 2.4.5, the simple form of the commutation relations for the $\mathcal{A}_i$–matrices [Eq. (2.53)] permits an easy derivation of the equations of motion. Additionally, in Section 2.6.1, we show how the quadratic form of the BBQ Hamiltonian, written in terms of generators of $U(3)$ [Eq. (2.72)], can also be used to develop classical Monte Carlo simulations, which allow to access classical thermodynamic properties of spin–1 magnets, while taking into account the fact that the (semi–)classical limit of a spin–1 moment is not an $O(3)$ vector. This permits us to classically simulate spin–1 systems by respecting all the allowed degrees of freedom of a single spin–1.

2.4.5 BBQ Hamiltonian and Equations of Motion in u(3)

The quadratic form of the BBQ Hamiltonian in terms of the $\mathcal{A}_i$–matrices [Eq. (2.72)], and their clean commutation relations [Eq. (2.53)] make it straightforward to derive Heisenberg equations of motion (EoM) for a spin–1 magnets. The Heisenberg EoM are derived by explicit calculation of the commutators of the $\mathcal{A}_i$–matrices components with the BBQ Hamiltonian. Using Eq. (2.53) and Eq. (2.72), we find

$$\begin{aligned}
\partial_t \hat{\mathcal{A}}_{i\ \eta}^{\gamma} &= -i\Big[\hat{\mathcal{A}}_{i\ \eta}^{\gamma}, \mathcal{H}_{\mathsf{BBQ}}\Big] \\
&= -i\sum_{\delta}\big[\, J_1(\hat{\mathcal{A}}_{i\ \alpha}^{\gamma}\hat{\mathcal{A}}_{i+\delta\ \eta}^{\alpha} - \hat{\mathcal{A}}_{i\ \eta}^{\alpha}\hat{\mathcal{A}}_{i+\delta\ \alpha}^{\gamma}) \\
&\quad +(J_2 - J_1)(\hat{\mathcal{A}}_{i\ \alpha}^{\gamma}\hat{\mathcal{A}}_{i+\delta\ \alpha}^{\eta} - \hat{\mathcal{A}}_{i\ \eta}^{\alpha}\hat{\mathcal{A}}_{i+\delta\ \gamma}^{\alpha})\,\big]\ ,
\end{aligned} \tag{2.74}$$

where we set $\hbar = 1$. This result was previously introduced in Fig. 1.70.

The EoM for $\mathcal{A}_i$–matrices Eq. (2.74), just like the Hamiltonian it is derived from, treats dipole and quadrupole moments on an equal footing and also takes a quadratic form, which is well–suited for numerical integration, as discussed below in Section 2.6.2. However, because this EoM is written in terms of a representation of the $u(3)$ algebra, it also describes the dynamics of the operator $\hat{\mathbf{S}}^2$, the total spin–length, which should remain constant. Therefore, in order to correctly describe the dynamics of a spin–1 magnet, we need to enforce Eq. (2.57). To this end, we require that

$$s = 1 \ \Rightarrow\ \mathrm{Tr}\ \hat{\mathcal{A}} = 1\ . \tag{2.75}$$

We further note that the EoM for the $\mathcal{A}$–matrices conserves the trace of $\mathcal{A}$,

$$\begin{aligned}
\partial_t\left(\mathrm{Tr}\ \hat{\mathcal{A}}_{\mathrm{i}}\right) &= -i\ \mathrm{Tr}\sum_{\delta}\big[\,\mathrm{J}_1(\hat{\mathcal{A}}_{\mathrm{i}\ \alpha}^{\gamma}\hat{\mathcal{A}}_{\mathrm{i}+\delta\ \eta}^{\alpha} - \hat{\mathcal{A}}_{\mathrm{i}\ \eta}^{\alpha}\hat{\mathcal{A}}_{\mathrm{i}+\delta\ \alpha}^{\gamma}) \\
&\quad +(J_2 - J_1)(\hat{\mathcal{A}}_{i\ \alpha}^{\gamma}\hat{\mathcal{A}}_{i+\delta\ \alpha}^{\eta} - \hat{\mathcal{A}}_{i\ \eta}^{\alpha}\hat{\mathcal{A}}_{i+\delta\ \gamma}^{\alpha})\,\big] \\
&\equiv 0\ ,
\end{aligned} \tag{2.76}$$

which follows from Eq. (2.74), and which ensures that Eq. (2.75) is satisfied trough out.

This implies that as long as the EoM Eq. (2.74) originate from a valid configuration

of $\mathcal{A}$–matrices (with Tr $\mathcal{A}_i \equiv 1$, so that we properly describe spin–1 moments), the time–evolution of the operators $\hat{\mathcal{A}}_i^{\alpha}{}_{\beta}$ will respect the constraint on spin length, meaning that it remains a proper representation of spin–1 moments throughout time evolution, which is happening within $u(3)$! Additionally, in Chapter 6 will see that this remains also true for systems with interactions that are anisotropic in spin–space. This makes the EoM in terms of a representation of the $u(3)$ algebra, a powerful tool for the exploration of the dynamics of spin–1 magnets. Indeed, in Section 2.6.1, we explain how to apply these EoM to a numerical integration scheme in order to make predictions for semi–classical dynamical properties of spin–1 systems.

2.5 $u(3)$ as a Basis for Analytical Theory

In this Section, we use the $u(3)$ formalism that we introduced in Section 2.4 to develop a theory of fluctuations. We will see that this method allows to treat fluctuations at both the classical and quantum level. We here present the general concepts, and then give two explicit examples through the application of our method to the FQ-state of the BBQ model on the triangular lattice which is extensively discussed in Chapter 3 and Chapter 4, as well as to the FM-state with easy–plane anisotropy which is presented in Section 6.3. We first show here how small fluctuations about a given ground state can be described using four of the nine generators of $U(3)$.

We start by assuming that we can find a mean-field (MF) ground state in the form of a product wave function

$$|\Psi_0\rangle_{\mathsf{GS}}^{\mathsf{MF}} = \prod_{i=1}^{N} |\mathbf{d}_{\mathbf{i}}^{\mathsf{GS}}\rangle \ . \tag{2.77}$$

For simplicity, we further assume that the single-site MF ground state is the same on every site, and disregard sub–lattice orders. Ultimately, this has no significant implications, as then the ground–state is just defined on the extended unit–cell instead. The single–site ground state wave function can be expressed in an orthogonal basis of our choice, as long as it is a valid basis for a spin–1 (i.e. any 3 orthogonal basis states built from the magnetic basis [Eq. (1.40)] or the TR basis [Eq. (2.32)])

$$|\mathbf{d}_{\mathbf{i}}^{\mathsf{GS}}\rangle = \sum_{\alpha} d_{\alpha} |\alpha\rangle \ , \tag{2.78}$$

where $|\alpha\rangle$ are the 3 orthogonal basis states. We can then express this total wave function as a product state of single–site wave functions as given in Eq. (2.77), where $|\mathbf{d_i}\rangle$ is defined through Eq. (2.78).

The choice of the basis that we use to represent the ground state will depend on the nature of the order. For instance, if the system is ferromagnetically ordered, then the magnetic basis [Eq. (1.40)] seems like a good option. When we explicitly apply it to the FQ order, we will choose the TR invariant basis [Eq. (2.32)] which naturally exhibits quadrupole moments as illustrated in Fig. 2.1. For convenience, we choose a basis such that the ground state is one of these basis states, and the two others basis states are orthogonal states. This way, we express the ground state as a 3–dimensional vector with "1" on one of its components (corresponding to the ground state basis

state), and "0" everywhere else.

For concreteness, let's assume that our ground state is given by

$$\left|\mathbf{d}_i^{\mathsf{GS}}\right\rangle = |\alpha_1\rangle \ , \tag{2.79}$$

where $|\alpha_1\rangle, |\alpha_2\rangle$ and $|\alpha_3\rangle$ form an orthogonal basis

$$\mathcal{B}_\alpha = \{|\alpha_1\rangle, |\alpha_2\rangle, |\alpha_3\rangle\} \ . \tag{2.80}$$

Therefore we write:

$$\mathbf{d}^{\mathsf{GS}} = \begin{pmatrix} 1 \\ 0 \\ 0 \end{pmatrix} \ . \tag{2.81}$$

We express our ground state as an $\mathcal{A}$–matrix ground state using Eq. (2.45)

$$\left\langle \mathbf{d}_i^{\mathsf{GS}} \middle| \mathcal{A} \middle| \mathbf{d}_i^{\mathsf{GS}} \right\rangle = \mathbf{A_i^{GS}} = \begin{pmatrix} 1 & 0 & 0 \\ 0 & 0 & 0 \\ 0 & 0 & 0 \end{pmatrix} \ . \tag{2.82}$$

In the space of $\mathcal{A}$–matrices, the product state becomes

$$|\Psi_0\rangle_{\mathsf{FQ}}^{\mathsf{MF}} = \prod_{i=1}^{N} \left|\mathbf{A_i^{GS}}\right\rangle \ . \tag{2.83}$$

We now derive a framework that allows us to describe fluctuations around the ground state in terms of generators belonging to the Lie algebra $u(3)$. The corrections to mean–field theory due to the fluctuations will induce either thermal and/or quantum fluctuations within the product state, and a reduction of the expectation value of the order parameter. Because of the convenience of expressing the BBQ Hamiltonian [Eq. (2.72)] in terms $\mathcal{A}$–matrix represented in the TR invariant basis [Eq. (2.45)], it is useful to define the basis change transformation $\Lambda \in SU(3)$ between the TR invariant basis [Eq. (2.32)] and the ground state basis [Eq. (2.80)]

$$\begin{pmatrix} |\alpha_1\rangle \\ |\alpha_2\rangle \\ |\alpha_3\rangle \end{pmatrix} = \Lambda \begin{pmatrix} |x\rangle \\ |y\rangle \\ |z\rangle \end{pmatrix} \ . \tag{2.84}$$

Under such a transformation, an operator given in the TR invariant basis $\mathcal{B}_2$ is expressed as

$$\hat{\mathrm{O}}_{\mathcal{B}_\alpha} = \Lambda \hat{\mathrm{O}}_{\mathcal{B}_2} \Lambda^\dagger \ , \tag{2.85}$$

in the ground state basis $\mathcal{B}_\alpha$.

We start working in the ground state basis $\mathcal{B}_\alpha$ [Eq. (2.80)], where representations are simple, and where creations of orthogonal fluctuations are naturally arising by application of the nine generators of $U(3)$. As explained in Section 2.1, we can construct transformations belonging to $U(3)$ using the exponential map and the generators of $u(3)$. We use the $\mathcal{A}$–matrices as generator to construct an element of $U(3)$,

parametrized by the nine complex parameters $\phi_{\alpha,\beta}$

$$\hat{R}(\vec{\phi}) = e^{i\sum_{\alpha\beta}\phi_{\alpha,\beta}\hat{\mathcal{A}}^{\alpha}{}_{\beta}} \ , \tag{2.86}$$

where $\alpha, \beta = 1, 2, 3$.

Under this operation a state $|\mathbf{d}\rangle$ transforms as

$$\left|\mathbf{d}(\vec{\phi})\right\rangle = \hat{R}(\vec{\phi})|\mathbf{d}\rangle \ , \tag{2.87}$$

and $\mathcal{A}$–matrices transform as

$$\mathbf{A}(\vec{\phi}) = \hat{R}(\vec{\phi})\mathbf{A}^{GS}\hat{R}(\vec{\phi})^{\dagger} \ , \tag{2.88}$$

as determined by Eq. (2.62) [cf. Appendix B]. $\hat{R}(\vec{\phi})$ allows to create the fluctuations around the identity as explained in Section 2.1. This can also be understood by expanding the exponential as its power series

$$e^{X} = \sum_{n=0}^{\infty}\frac{X^{n}}{n!} = \mathbb{I} + X + \frac{X^{2}}{2!} + \frac{X^{3}}{3!} + \dots \ . \tag{2.89}$$

By assuming small fluctuations ($\phi_{\alpha,\beta} \ll 1$), the expansion can be truncated and only consider terms up to the second order

$$\hat{R}(\vec{\phi}) = e^{i\sum_{\alpha\beta}\phi_{\alpha,\beta}\hat{\mathcal{A}}^{\alpha}{}_{\beta}} = \mathbb{I} + i\sum_{\alpha\beta}\phi_{\alpha,\beta}\hat{\mathcal{A}}^{\alpha}{}_{\beta} - \frac{1}{2}\sum_{\alpha\beta}\phi^{2}_{\alpha,\beta}(\hat{\mathcal{A}}^{\alpha}{}_{\beta})^{2} + \mathcal{O}(\phi^{3}) \ . \tag{2.90}$$

An important technical point worth mentioning here is the fact that we can treat the fluctuation at the quantum or at the classical level results from the ability to treat the parameters $\phi_{\alpha,\beta}$ as bosons $\hat{\phi}_{\alpha,\beta}$ (i.e. a complex field) related by

$$\hat{\phi}^{\dagger}_{\alpha,\beta} = \hat{\phi}_{\beta,\alpha} \ , \tag{2.91}$$

in the quantum case, or as numbers

$$\phi^{*}_{\alpha,\beta} = \phi_{\beta,\alpha} \ , \tag{2.92}$$

in the classical case. These implications follow directly from the Hermitian nature of the matrix$\hat{\mathbf{A}}$ [Eq. (2.49)]. Considering the action of $\hat{R}(\vec{\phi})$ on the FQ ground state, as characterised by the matrix $\mathbf{A_{GS}}$ [Eq. (2.82)], the only $\hat{\mathcal{A}}^{\alpha}{}_{\beta}$ that will give a non–zero result are $\hat{\mathcal{A}}^{1}{}_{1}$, $\hat{\mathcal{A}}^{1}{}_{2}$, $\hat{\mathcal{A}}^{1}{}_{3}$, $\hat{\mathcal{A}}^{2}{}_{1}$, and $\hat{\mathcal{A}}^{3}{}_{1}$. However, we need to ensure that the spin–length constraint Eq. (2.57) is satisfied. This implies that we only really need to keep the 4 generators $\hat{\mathcal{A}}^{1}{}_{2}$, $\hat{\mathcal{A}}^{1}{}_{3}$, $\hat{\mathcal{A}}^{2}{}_{1}$, and $\hat{\mathcal{A}}^{1}{}_{3}$.

This can also be noted by explicitly considering the non–vanishing terms of $\hat{R}(\vec{\phi})$

and $\hat{R}(\vec{\phi})^\dagger$ in Eq. (2.88)

$$\begin{aligned}\hat{R}(\vec{\phi}) &= \mathbb{I} + i\phi_{2,1}\hat{\mathcal{A}}^2{}_1 + i\phi_{3,1}\hat{\mathcal{A}}^3{}_1 + i\phi_{1,1}\hat{\mathcal{A}}^1{}_1 - \frac{1}{2}\phi_{1,1}^2(\hat{\mathcal{A}}^1{}_1)^2 \\ &= \begin{pmatrix} 1 + i\phi_{1,1} - \frac{1}{2}\phi_{1,1}^2 & 0 & 0 \\ i\phi_{2,1} & 1 & 0 \\ i\phi_{3,1} & 0 & 1 \end{pmatrix} , \qquad (2.93a) \\ \hat{R}(\vec{\phi})^\dagger &= \mathbb{I} - i\phi_{1,2}\hat{\mathcal{A}}^1{}_2 - i\phi_{1,3}\hat{\mathcal{A}}^1{}_3 - i\phi_{1,1}\hat{\mathcal{A}}^1{}_1 - \frac{1}{2}\phi_{1,1}^2(\hat{\mathcal{A}}^1{}_1)^2 \\ &= \begin{pmatrix} 1 - i\phi_{1,1} - \frac{1}{2}\phi_{1,1}^2 & -i\phi_{1,2} & -i\phi_{1,3} \\ 0 & 1 & 0 \\ 0 & 0 & 1 \end{pmatrix} . \qquad (2.93b)\end{aligned}$$

Because $\hat{R}(\vec{\phi})$ should belong to $SU(3)$, its determinant should be equal to 1 [Eq. (2.2)], but we observe that

$$\det(\hat{R}(\vec{\phi})) = 1 + i\phi_{1,1} - \tfrac{1}{2}\phi_{1,1}^2 , \qquad \det(\hat{R}(\vec{\phi})^\dagger) = 1 - i\phi_{1,1} - \tfrac{1}{2}\phi_{1,1}^2 , \qquad (2.94)$$

and that the generator $\hat{\mathcal{A}}^1{}_1$ does not preserve the ground state and even takes the ground state out of $SU(3)$. This can be seen by considering the effect of $\hat{R}(\vec{\phi})$ on the ground state vector $\mathbf{d}^{\mathsf{GS}}$ [Eq. (2.81)]

$$\hat{R}(\vec{\phi})\mathbf{d}^{\mathsf{GS}} = \begin{pmatrix} 1 + i\phi_{1,1} - \frac{1}{2}\phi_{1,1}^2 \\ i\phi_{2,1} \\ i\phi_{3,1} \end{pmatrix} . \qquad (2.95)$$

Here, the effect of the generator $\hat{\mathcal{A}}^1{}_1$ is to induce a longitudinal fluctuation, which violates the constraint on the spin length. We, therefore, discard the term in $\phi_{1,1}$ as nonphysical. Consequently we only consider the 4 generators $\hat{\mathcal{A}}^1{}_2$, $\hat{\mathcal{A}}^1{}_3$, $\hat{\mathcal{A}}^2{}_1$, and $\hat{\mathcal{A}}^1{}_3$.

The action of these 4 broken generators on the ground state *Eq.* (2.82)] characterized by inducing non-zero contribution (i.e. not preserving the ground state), according to Eq. (2.88), are shown explicitly later in Chapter 3 in Fig. 3.2 for a ferroquadrupolar ground state, and in Chapter 6 in Fig. 6.3 for the ferromagnetic ground state.

For the quantum case, because of the "hermicity" property on the components of the matrix $\hat{\mathbf{A}}$ [Eq. (2.49)], we have

$$\hat{\mathcal{A}}^{1\dagger}{}_2 = \hat{\mathcal{A}}^2{}_1 \qquad \hat{\mathcal{A}}^{1\dagger}{}_3 = \hat{\mathcal{A}}^1{}_3 . \qquad (2.96)$$

So really, we only need 2 generators, and we expect 2 quantum modes associated with the 2 bosonic fluctuations [Eq. (2.91)], which is consistent with a description in terms of multi–boson theory for a spin–1, as explained in Section 1.3.2, where the bosons, defined as creation annihilation operators acting on the ground state and generating the states which are orthogonal to it, are then treated as quantum fluctuations.

In the classical case, we treat the 4 fluctuations as complex numbers which are related by Eq. (2.92). Consequently, the 4 complex fluctuations are described by only 4 independent real numbers. Therefore we expect 4 classical modes associated with

these 4 real–valued fluctuations.

This can also be understood by considering the ordered ground state in Eq. (2.81). For an arbitrary state describing a spin–1, it would consist of 3 complex numbers or equivalently 6 real numbers, which would correspond to the coefficients of the linear combination of the basis states [Eq. (2.78)]. However, when we impose an ordered ground state, 2 of these 3 complex numbers, i.e., 4 out of the 6 reals numbers, are set to zero. The last non zero complex coefficients $d_{\neq 0}$ needs to satisfy the norm constraint $|d_{\neq 0}| = 1$, which allows for the freedom of the choice of the phase, i.e. Eq. (2.81) is defined up to a phase transformation. By forcing the other components to zero, we break the symmetry of the space in which the state lives, namely the 3–dimensional Hilbert space $\mathbb{H}^3$.

Recall that any states in $\mathbb{H}^3$ can be linked by an $SU(3)$ transformation. This means there will be only some transformations of $SU(3)$ that will preserve the ground state (or modify its phase, but we saw that this does not change the ground state), and some transformations that will not preserve the ground state. The $SU(3)$ transformations can be generated from its algebra (generators). Therefore, there will be generators associated with transformations preserving the ground state, and with transformations modifying the ground state. We say that the generators modifying the ground state are broken (by the symmetry breaking of the ordered state).

At the quantum level, this means that the symmetry breaking of the ground state, i.e., the enforcement of 2 out of the 3 complex degrees of freedom, induces the breaking of two generators of $SU(3)$. These two broken generators will each induce a quantum excitation $\hat{\phi}^{\dagger}_{\alpha,\beta}$ and generate a total of 2 quantum modes. Meanwhile, a classical treatment assumes that we froze 4 out of the 6 reals numbers, and there will be 4 associated generators in order to create the fluctuations, implying the existence of 4 modes. These modes emanating due to the continuous symmetry breaking of the ground state are called Goldstone modes.

We restrict Eq. (2.90) to the four relevant generators, and by retaining terms up to order ϕ^2, we obtain a general expression for infinitesimal fluctuations about the ordered ground state. We can now write $\mathbf{A}(\vec{\phi})$ [Eq. (2.88)] in terms of these 4 fluctuations.

$$\begin{aligned}\hat{\mathbf{A}}(\vec{\phi}) &= \hat{R}(\vec{\phi})\mathbf{A}^{GS}\hat{R}(\vec{\phi})^{\dagger} \\ &= \begin{pmatrix} 1-\phi_{1,2}\phi_{2,1}-\phi_{1,3}\phi_{3,1} & i\phi_{2,1} & i\phi_{3,1} \\ -i\phi_{1,2} & \phi_{1,2}\phi_{2,1} & \phi_{1,2}\phi_{3,1} \\ -i\phi_{1,3} & \phi_{2,1}\phi_{1,3} & \phi_{1,3}\phi_{3,1} \end{pmatrix} ,\end{aligned} \tag{2.97}$$

where we ensured that the constraint over the trace is satisfied [Eq. (2.57)]. However, $\mathbf{A}(\vec{\phi})$ is still expressed in the ground state basis $\mathcal{B}_\alpha$ [Eq. (2.80)], to make this explicit, we write $\mathbf{A}(\vec{\phi})_{\mathcal{B}_\alpha}$. In order to plug it in the BBQ Hamiltonian [Eq. (2.72)] written down in terms of the $\mathcal{A}$–matrices expressed in the TR basis $\mathcal{B}_2$ [Eq. (2.32)], we need to make a basis change to obtain $\mathbf{A}(\vec{\phi})_{\mathcal{B}_2}$. Inverting Eq. (2.85), we get

$$\mathbf{A}(\vec{\phi})_{\mathcal{B}_2} = \Lambda^{\dagger}\mathbf{A}(\vec{\phi})_{\mathcal{B}_\alpha}\Lambda \, , \tag{2.98}$$

where we used the fact that $\Lambda \in SU(3) \Rightarrow \Lambda^{-1} = \Lambda^{\dagger}$.

We can finally express the BBQ Hamiltonian in terms of the 4 relevant fluctuations

$\phi_{\alpha,\beta}$, up to second order by inserting Eq. (2.98) into Eq. (2.72). After performing a Fourier transform (see Eq. (2.100) below), we obtain a Hamiltonian which can then be written in the form

$$\mathcal{H}'_{\mathsf{BBQ}} = E_0 + \frac{1}{2}\sum_{\mathbf{k}} \left[\vec{\phi}^T_{\mathbf{k}} M_{\mathbf{k}} \vec{\phi}_{-\mathbf{k}}\right] + \mathcal{O}(\phi^3) \ , \tag{2.99}$$

where E_0 the energy of the MF ground state, and where linear order in $\phi_{\alpha,\beta}$ should vanish, as the MF ground state should minimize the energy. The 4 fluctuations are encoded by

$$\vec{\phi}_{\mathbf{k}} = \begin{pmatrix} \phi_{\mathbf{k}1,2} \\ \phi_{\mathbf{k}2,1} \\ \phi_{\mathbf{k}1,3} \\ \phi_{\mathbf{k}3,1} \end{pmatrix} = \frac{1}{\sqrt{N}} \sum_i \begin{pmatrix} e^{i\mathbf{k}\cdot\mathbf{r}_i}\phi_{\mathbf{r}_i 1,2} \\ e^{i\mathbf{k}\cdot\mathbf{r}_i}\phi_{\mathbf{r}_i 2,1} \\ e^{i\mathbf{k}\cdot\mathbf{r}_i}\phi_{\mathbf{r}_i 1,3} \\ e^{i\mathbf{k}\cdot\mathbf{r}_i}\phi_{\mathbf{r}_i 3,1} \end{pmatrix} \ , \tag{2.100}$$

and the energy determined by $M_{\mathbf{k}}$, which will depend on the nature of the ground state and the parameter of the BBQ model, as well as the geometry of the lattice. We also note that the transpose vector for the fluctuations has the property

$$\phi^{T\mu,\nu}_{\mathbf{k}} = \phi^{\nu,\mu}_{\mathbf{k}} \ . \tag{2.101}$$

At the Gaussian (i.e. non–interacting) level, all possible fluctuations about the MF ground state are well described by the Hamiltonian $\mathcal{H}'_{\mathsf{BBQ}}$ [Eq. (2.99)], which can be used as a starting point for both classical and quantum theories of its excitations. The first step for both derivations is to find the eigenmodes and "eigen-fluctuations", i.e., the eigenvalues and eigenvectors of the Hamiltonian $\mathcal{H}'_{\mathsf{BBQ}}$.

For the classical case, solving the eigensystem is obtained by simply diagonalizing the energy matrix $M_{\mathbf{k}}$. The obtained eigenmodes and eigen–fluctuations can be used to derive the free energy for the considered model. Classical thermodynamic quantities are computed by taking the appropriate functional derivative of the free energy. We show explicit calculations for the specific heat, equal–time structure factors, and the order moment of the FQ state of the BBQ Hamiltonian [Eq. (2.72)] in Section 3.3

Meanwhile, for the quantum case, we need to "bosonify" the fluctuations in order to ensure that the structure of the $u(3)$ algebra is preserved [Eq. (2.53)] To understand why the quantum excitations have a bosonic nature, we start by considering that the generators create quantum fluctuations $\hat{\phi}_{\alpha,\beta}$

$$\hat{R}(\hat{\phi}) = e^{\sum_{\alpha\beta} \hat{\phi}_{\alpha,\beta} \hat{\mathcal{A}}^{\alpha}{}_{\beta}} \ , \tag{2.102}$$

where for simplicity the imaginary number i is encapsulated into $\hat{\phi}_{\alpha,\beta}$. Ultimately, this makes no difference as the fluctuations $\hat{\phi}_{\alpha,\beta}$ still satisfy Eq. (2.91). In the basis that we chose [Eq. (2.80)], and for the chosen ground state [Eq. (2.79)], following the same argument as above, the quantum excitations that will contribute are the one associated with the generators $\hat{\mathcal{A}}^1{}_1$, $\hat{\mathcal{A}}^1{}_2$, $\hat{\mathcal{A}}^1{}_3$, $\hat{\mathcal{A}}^2{}_1$, and $\hat{\mathcal{A}}^3{}_1$. And Eq. (2.93a) and

Eq. (2.93b) become

$$\begin{aligned}\hat{R}(\hat{\phi}) &= \mathbb{I} + \hat{\phi}_{2,1}\hat{\mathcal{A}}^2{}_1 + \hat{\phi}_{3,1}\hat{\mathcal{A}}^3{}_1 + \hat{\phi}_{1,1}\hat{\mathcal{A}}^1{}_1 + \frac{1}{2}\hat{\phi}^2_{1,1}(\hat{\mathcal{A}}^1{}_1)^2 \\ &= \begin{pmatrix} 1+\hat{\phi}_{1,1}+\frac{1}{2}\hat{\phi}^2_{1,1} & 0 & 0 \\ \hat{\phi}_{2,1} & 1 & 0 \\ \hat{\phi}_{3,1} & 0 & 1 \end{pmatrix} = \begin{pmatrix} 1+\hat{\phi}^\dagger_{1,1}+\frac{1}{2}\hat{\phi}^{\dagger 2}_{1,1} & 0 & 0 \\ \hat{\phi}^\dagger_{1,2} & 1 & 0 \\ \hat{\phi}^\dagger_{1,3} & 0 & 1 \end{pmatrix}, \end{aligned} \tag{2.103a}$$

$$\begin{aligned}\hat{R}(\hat{\phi})^\dagger &= \mathbb{I} + \hat{\phi}_{1,2}\hat{\mathcal{A}}^1{}_2 + \hat{\phi}_{1,3}\hat{\mathcal{A}}^1{}_3 + \hat{\phi}_{1,1}\hat{\mathcal{A}}^1{}_1 + \frac{1}{2}\hat{\phi}^2_{1,1}(\hat{\mathcal{A}}^1{}_1)^2 \\ &= \begin{pmatrix} 1+\hat{\phi}_{1,1}+\frac{1}{2}\hat{\phi}^2_{1,1} & \hat{\phi}_{1,2} & \hat{\phi}_{1,3} \\ 0 & 1 & 0 \\ 0 & 0 & 1 \end{pmatrix}, \end{aligned} \tag{2.103b}$$

where we used Eq. (2.91). We note that using Eq. (2.49) it is easily seen that $\hat{R}(\hat{\phi})^\dagger$ is indeed the conjugate transposed of $\hat{R}(\hat{\phi})$. Following the same argument as before on the determinant of $\hat{R}(\hat{\phi})^\dagger$ and $\hat{R}(\hat{\phi})$, and using Eq. (2.49) or equivalently Eq. (2.91), we only need to consider 2 creation/annihilation pairs: $(\hat{\phi}^\dagger_{1,2}/\hat{\phi}_{1,2})$ and $(\hat{\phi}^\dagger_{1,3}/\hat{\phi}_{1,3})$ This can also be understood by applying $\hat{R}(\hat{\phi})$ to the ground state the ground state vector $\mathbf{d}^{\mathsf{GS}}$ [Eq. (2.81)]

$$\mathbf{d} = \hat{\mathbf{R}}(\hat{\phi})\mathbf{d}^{\mathsf{GS}} = \begin{pmatrix} 1+\hat{\phi}^\dagger_{1,1}+\frac{1}{2}\hat{\phi}^{\dagger 2}_{1,1} \\ \hat{\phi}^\dagger_{1,2} \\ \hat{\phi}^\dagger_{1,3} \end{pmatrix}, \tag{2.104}$$

where we see that the operators $\hat{\phi}_{1,2}$ and $\hat{\phi}_{1,3}$ act as the operators $\hat{\mathrm{d}}^{\dagger\alpha}$ of Eq. (2.64). Therefore in order to preserve the structure of the $u(3)$ algebra [Eq. (2.53)], we require the fluctuations $\phi^\dagger$ to satisfy bosonic commutation relations

$$\left[\hat{\phi}_{\alpha,\beta}, \hat{\phi}^\dagger_{\mu\nu}\right] = \delta_{\alpha\nu}\delta_{\beta,\mu}\,. \tag{2.105}$$

We again emphasize, that by construction, the bosons are orthogonal to the ground state in $U(3)$, in order to restrict to orthogonal fluctuations in $SU(3)$, we disregard the "longitudinal" boson (which excites the ground state into itself!) We restrict Eq. (2.90) to the 2 relevant generators, $\hat{\mathcal{A}}^1{}_2$ and $\hat{\mathcal{A}}^1{}_3$ and by retaining terms up to order $\hat{\phi}^2$, we obtain a general expression for infinitesimal quantum fluctuations about the ordered ground state. We can now write $\mathbf{A}(\hat{\phi})$ [Eq. (2.88)] in terms of the 2 bosons

$$\begin{aligned}\hat{\mathbf{A}}(\hat{\phi}) &= \hat{R}(\hat{\phi})\mathbf{A}^{GS}\hat{R}(\hat{\phi})^\dagger \\ &= \begin{pmatrix} 1-\hat{\phi}_{1,2}\hat{\phi}^\dagger_{1,2}-\hat{\phi}_{1,3}\hat{\phi}^\dagger_{1,3} & \hat{\phi}^\dagger_{1,2} & \hat{\phi}^\dagger_{1,3} \\ \hat{\phi}_{1,2} & \hat{\phi}_{1,2}\hat{\phi}^\dagger_{1,2} & \hat{\phi}_{1,2}\hat{\phi}^\dagger_{1,3} \\ \hat{\phi}_{1,3} & \hat{\phi}^\dagger_{1,2}\hat{\phi}_{1,3} & \hat{\phi}_{1,3}\hat{\phi}^\dagger_{1,3} \end{pmatrix}. \end{aligned} \tag{2.106}$$

After effectuating the basis change [Eq. (2.98)], we can express the BBQ Hamiltonian

[Eq. (2.72)] in the form

$$\mathcal{H}'_{\mathsf{BBQ}} = E_0 + \frac{1}{2}\sum_{\mathbf{k}} \left[\vec{\hat{\phi}}^{\dagger}_{\mathbf{k}} M_{\mathbf{k}} \vec{\hat{\phi}}_{\mathbf{k}}\right] + \mathcal{O}(\hat{\phi}^3) \ , \tag{2.107}$$

where E_0 the energy of the MF ground state, and where linear order in $\hat{\phi}$ should vanish, as the MF ground state should minimize the energy. The 4 fluctuations are encoded by

$$\vec{\hat{\phi}}_{\mathbf{k}} \ = \ \begin{pmatrix} \hat{\phi}_{\mathbf{k}1,2} \\ \hat{\phi}^{\dagger}_{-\mathbf{k}1,2} \\ \hat{\phi}_{\mathbf{k}1,3} \\ \hat{\phi}^{\dagger}_{-\mathbf{k}1,3} \end{pmatrix} \ . \tag{2.108}$$

Because of how the fluctuations are encoded into the vectors given in Eq. (2.100) and Eq. (2.108), the interaction matrix $M_{\mathbf{k}}$ in Eq. (2.99) is the same as in Eq. (2.107). In the quantum case, we simply require the fluctuations to satisfy commutations relations given by Eq. (2.105) and rewritten in terms of the components of $\vec{\hat{\phi}}_{\mathbf{k}}$ as

$$\left[(\vec{\hat{\phi}}_{\mathbf{k}})^{\alpha}, (\vec{\hat{\phi}}^{\dagger}_{\mathbf{q}})^{\beta}\right] = {\gamma_0}^{\alpha\beta}\delta_{\mathbf{k},\mathbf{q}} \ , \tag{2.109}$$

where

$$\gamma_0 = \begin{pmatrix} 1 & 0 & 0 & 0 \\ 0 & -1 & 0 & 0 \\ 0 & 0 & 1 & 0 \\ 0 & 0 & 0 & -1 \end{pmatrix} \ . \tag{2.110}$$

Diagonalizing the Hamiltonian [Eq. (2.107)] while accounting for bosonic commutation relations [Eq. (2.109)] is equivalent to solving the eigensystem given by

$$\gamma_0 M_{\mathbf{k}} \hat{\phi}_{\mathbf{k},\lambda} = \epsilon_{\mathbf{k},\lambda}\hat{\phi}_{\mathbf{k},\lambda} \qquad \lambda = 1,2,3,4 \ , \tag{2.111}$$

and is straightforwardly obtained by diagonalizing the matrix $\gamma_0 M_{\mathbf{k}}$. As explained in Appendix C, this allows to automatically enforce bosonic commutations relations [Eq. (2.109)] and is equivalent to performing a Bogolioubov transformation.

Additionally, considering that the ground state is given by $\mathbf{d}^{\mathsf{GS}} = \hat{\phi}^{\dagger}_{1,1}|vac\rangle$, we rewrite Eq. (2.104) as

$$\mathbf{d}^{\dagger} = \begin{pmatrix} \hat{\phi}^{\dagger}_{1,1} \\ \hat{\phi}^{\dagger}_{1,2} \\ \hat{\phi}^{\dagger}_{1,3} \end{pmatrix} \ . \tag{2.112}$$

Using Eq. (2.112) and requiring $\mathbf{d}^{\dagger}\cdot\mathbf{d} = \mathbf{1}$ [Eq. (2.36)], naturally leads to a mutli-boson theory as described in Section 1.3.2, where the boson $\hat{\phi}^{\dagger}_{1,1}$ is "condensed". Indeed, by expressing $\hat{\phi}^{\dagger}_{1,1}, \hat{\phi}_{1,1}$ in terms of the other boson, and assuming $\hat{\phi}^{\dagger}_{1,2}\hat{\phi}_{1,2}$, $\hat{\phi}^{\dagger}_{1,3}, \hat{\phi}_{1,3} \ll 1$,

we obtain,

$$\mathbf{d}^\dagger = \begin{pmatrix} 1 - \frac{1}{2}(\hat{\phi}^\dagger_{1,2}\hat{\phi}_{1,2} + \hat{\phi}^\dagger_{1,3}, \hat{\phi}_{1,3}) \\ \hat{\phi}^\dagger_{1,2} \\ \hat{\phi}^\dagger_{1,3} \end{pmatrix} . \tag{2.113}$$

Using Eq. (2.66) to build the corresponding A–matrix, we see that we find exactly Eq. (2.106). This confirms that the creation of the quantum fluctuations within our $u(3)$ formalism is equivalent to a multi-boson type expansion.

To summarize, we developed an approach that allows us to generate orthogonal fluctuations about an ordered state by using the generators of $U(3)$. This permits us to express the Hamiltonian in terms of these fluctuations. The interaction energy matrix $M_{\mathbf{k}}$ encompasses all we need to know about the fluctuations. A classical treatment is obtained by simply diagonalizing the matrix $M_{\mathbf{k}}$, while a quantum approach requires to diagonalize the matrix $\gamma_0 M_{\mathbf{k}}$ where the multiplication by γ_0 [Eq. (4.8)] ensures that the quantum fluctuations satisfy bosonic commutation relations [Eq. (2.109)]. This offers the subsequent possibility to calculate thermodynamical and dynamical properties as explained in Chapter 3 and Chapter 4

Here, I presented a somewhat abstract derivation of how to implement an analytical theory within our formalism, but recall that explicit applications are provided in Chapter 3 and Chapter 4 for the FQ state and might be more enlightening that the general description. Moreover, because the ground state is one of the TR invariant basis, the derivation is much more straightforward. I also provide an application to the ferromagnetic Heisenberg model with easy-plane and single–ion anisotropy in Section 6.3, where the formalism shown here will turn out to be useful.

2.6 $u(3)$ as a Basis for Numerical Simulation of Spin–1

In Section 2.4, we developed the technical framework needed to describe a spin–1 magnet. We introduced it in terms of a representation of $u(3)$, $\mathcal{A}^\alpha{}_\beta$ [Eq. (2.46)] which allowed us to treat dipolar and quadrupolar degrees of freedom on an equal footing. This enabled us to derive an expression for both the BBQ model, $\mathcal{H}_{\mathsf{BBQ}}$ [Eq. (2.72)], and the associated equation of motion [Eq. (2.74)] for $\mathcal{A}^\alpha{}_\beta$–objects, the generators of $U(3)$ $\mathcal{A}^\alpha{}_\beta$. The obtained derivations took a simple form which is quadratic in $\mathcal{A}^\alpha{}_\beta$, and do not involve any approximation to its physical meaning.

Here, we format these results into a practical formulation for numerical simulations of spin–1 magnets. We will consider a classical Monte Carlo (MC) scheme and (semi-)classical Molecular Dynamics (MD) simulations, both carried out in the space of the "A-matrices", $\mathcal{A}^\alpha{}_\beta$. We will refer to these approaches as "u3MC" and "u3MD", respectively. Technical details regarding the updates needed for both classical Monte Carlo (MC) and (semi-)classical Molecular Dynamics (MD) simulations, are provided in Appendix E.

The detailed application of the method to the thermodynamics and dynamics of the ferroquadrupolar (FQ) phase will be described in Section 3.4 and Section 4.3.

2.6.1 Monte Carlo Simulations Within $u(3)$ Framework

Implementation of u3MC Update

We start by expressing a single wave function in the space of $\mathcal{A}$–matrices. By using Eq. (2.45) or equivalently Eq. (2.66), we see that the wave function for a spin–1 moment expressed in terms of $\mathcal{A}$–matrices is exactly equivalent to one be expressed in terms of a $\mathbf{d}$–vector

$$|\mathcal{A}_i\rangle \;=\; \sum_{\alpha,\beta} \hat{\mathcal{A}}_{i\ \beta}^{\alpha}|\beta\rangle = \sum_{\alpha,\beta} \mathrm{d}_i^{\dagger\alpha}\hat{\mathrm{d}}_{i\beta}\mathrm{d}_i^{\dagger\beta}|vac\rangle = \sum_{\alpha} \mathrm{d}_i^{\dagger\alpha}|vac\rangle \equiv |\mathbf{d_i}\rangle \;, \tag{2.114}$$

where $\mathcal{A}_i$ denotes the nine parameters $\mathcal{A}_{i,\beta}^{\alpha}$, $|\beta\rangle$ is the basis of TR–invariant states [Eq. (2.32)], and $|\mathbf{d_i}\rangle$ is defined through Eq. (2.35). We also note that the nine complex parameters $\mathcal{A}_{i,\beta}^{\alpha}$ can be built from the 3 complex components of the $\mathbf{d}$–vector [Eq. (2.66)] subject to the constraint [Eq. (2.36)], i.e. from 5 independent degrees of freedom:

$$\mathcal{A}_{i\ \beta}^{\alpha} = (\mathrm{d}_i^{\alpha})^*\ \mathrm{d}_{i,\beta}\,. \tag{2.115}$$

The hermicity of the $\mathcal{A}$–matrix implies the diagonal components $\mathcal{A}_{i,\beta}^{\alpha}$ are real, and off–diagonal terms satisfy $\mathcal{A}_{i,\beta}^{\alpha,*} = \mathcal{A}_{i,\alpha}^{\beta}$. Additionally, the trace of the $\mathcal{A}$–matrix is constrained to 1 [Eq. (2.57)], such that there are only 5 real degrees of freedom needed to build an $\mathcal{A}$–matrix.

We then express the total wave function as a product wave function written in the space of $\mathcal{A}$–matrices

$$|\Psi_{\mathcal{A}}\rangle \;=\; \prod_{i=1}^{N}|\mathcal{A}_i\rangle = \prod_{i=1}^{N}\sum_{\alpha,\beta}\hat{\mathcal{A}}_{i,\beta}^{\alpha}|\beta\rangle \equiv \prod_{i=1}^{N}|\mathbf{d_i}\rangle\;. \tag{2.116}$$

This will be the starting point for both u3MC and u3MD simulations of spin–1 magnets.

According to Eq. (2.72), the average (classical) energy of such a state yields

$$\begin{aligned} E[\mathcal{A}_i] \;&=\; \langle\Psi_{\mathcal{A}}|\mathcal{H}_{\mathsf{BBQ}}|\Psi_{\mathcal{A}}\rangle \\ &=\; \sum_{\langle i,j\rangle}\sum_{\alpha\beta}\Big[J_1\mathcal{A}_{i,\beta}^{\alpha}\mathcal{A}_{j,\alpha}^{\beta} + (J_2-J_1)\mathcal{A}_{i,\beta}^{\alpha}\mathcal{A}_{j,\beta}^{\alpha} + J_2\Big]\;. \end{aligned} \tag{2.117}$$

Such a product wave function does not take into account entanglement and cannot describe quantum effects from interacting spins. However, it does account for quantum effects on a single site, such as quadrupolar degrees of freedom. And it represents a semi–classical approximation in the sense that the quantum mechanical properties are treated exactly at the level of a single site for each spin–1 moment independently. According to Eq. (2.116), it follows that u3MC simulations can just as well be carried out in the space of $\mathbf{d}$–vectors, with energy [183, 229]

$$\begin{aligned} E[\mathbf{d}_i] \;&=\; \langle\Psi_{\mathbf{d}}|\mathcal{H}_{\mathsf{BBQ}}|\Psi_{\mathbf{d}}\rangle \\ &=\; \sum_{\langle i,j\rangle}\big[J_1|\mathbf{d}_i\cdot\overline{\mathbf{d}}_j|^2 + (J_2-J_1)|\mathbf{d}_i\cdot\mathbf{d}_j|^2 + J_2\big]\;. \end{aligned} \tag{2.118}$$

This approach has been studied in reference [235], and is referred to as "semiclassical $SU(3)$" or "s$SU(3)$" simulation. However, just as for various analytic calculations, $\mathcal{A}$–matrices representation is more convenient for MD simulations as well. Therefore, we here propose a simple description in terms of $\mathcal{A}$–matrices.

In order to convert Eq. (2.116) and Eq. (2.117) into a practical MC scheme, we require an update that is capable of generating spin configurations $\{\mathcal{A}_i\}$ corresponding to states drawn from a thermal ensemble. This is done by constructing a Metropolis–like [147] update for a single matrix $\mathcal{A}_i$, representing spin–1 moment. We could also choose to implement our formalism for more general cluster– [127] or worm– [168] updates, but we will not consider these here.

Using the expression of an individual A–matrix given by Eq. (2.115) in terms of the director $\mathbf{d}$

$$\mathbf{d} = \begin{pmatrix} x_1 + i\ x_2 \\ x_3 + i\ x_4 \\ x_5 + i\ x_6 \end{pmatrix}; \qquad \mathbf{d}^*\mathbf{d} = |\mathbf{d}|^2 = 1\,. \tag{2.119}$$

Expressed this way, it is clear that any matrix $\mathcal{A}^\alpha{}_\beta$ [Eq. (2.115)] can be written down in terms of 5 linearly–independent real variables, coming from the six real coefficients of $\mathbf{d}$, $x_1, x_2, \ldots x_6$, and the constraint on its length.

The construction of a general update capable of describing a single spin–1 moment requires the ability to sample over statistically–independent, equally–distributed points on a 5–dimensional sphere, embedded within a 6–dimensional space. We generalize the Marsaglia construction [141], and write

$$x_1 = \theta_2^{1/4}\ \theta_1^{1/2}\ \sin\phi_1\ , \tag{2.120a}$$
$$x_2 = \theta_2^{1/4}\ \theta_1^{1/2}\ \cos\phi_1\ , \tag{2.120b}$$
$$x_3 = \theta_2^{1/4}\ \sqrt{1-\theta_1}\ \sin\phi_2\ , \tag{2.120c}$$
$$x_4 = \theta_2^{1/4}\ \sqrt{1-\theta_1}\ \cos\phi_2\ , \tag{2.120d}$$
$$x_5 = \sqrt{1-\theta_2^{1/2}}\ \sin\phi_3\ , \tag{2.120e}$$
$$x_6 = \sqrt{1-\theta_2^{1/2}}\ \cos\phi_3\ , \tag{2.120f}$$

where $0 \leq \theta_1, \theta_2 \leq 1$ and $0 \leq \phi_1, \phi_2, \phi_3 < 2\pi$ are parameters which are randomly sampled from a uniform distribution. Because we restrict the $\mathbf{d}$–director to a 5–dimensional sphere, we have $|\mathbf{d}|^2 = 1$ by construction. From Eq. (2.115), this implies that $\mathrm{Tr}\,\mathcal{A} = 1$, and therefore directly ensures that all states generated remain within $\mathbb{H}^3$, the Hilbert space for a spin–1 moment [Eq. (2.48)].

We show evidence that the generalised Marsaglia approach proposed in Eq. (2.120), randomly generates the variable $x_1, \cdots, x_6$ as points on a 5-dimensional sphere, and properly and independently selects them as shown in Appendix E.1 in Fig. E.1. However, as explained in Section 2.3, the state of a spin–1 moment, represented by 3 complex numbers $\mathrm{d}_{\alpha=x,y,z}$, is defined up to a phase, and ultimately characterized by 4 real parameters From Eq. (2.115), it is easily seen that the elements $\mathcal{A}^\alpha{}_\beta$ of the A–matrix are independent of the phase of $\mathbf{d}$. This leads to a gauge–redundancy in the 5–dimensional spherical parametrization in Eq. (2.120). The fact that it is possible to

take into account the gauge freedom of phase, and parameterize the $\mathbf{d}$ by 4 independent angles can also be seen from another important result [7]

$$\frac{S^5}{S^1} \simeq \mathbb{CP}^2 \,, \tag{2.121}$$

which means that the 5–dimensional sphere with the gauge freedom $U(1) \simeq S^1$ is homeomorphic to the 2–dimensional complex projective space, which is the space that characterizes completely a spin–1 moment.

It therefore should be possible to generate a Marasaglia construction for an update based on 4–dimension real subspace of the 5–dimensional sphere defined by Eq. (2.120). There is however no unique choice of fixing the gauge, but a convenient way is to choose the z–component of $\mathbf{d}$ to be purely real, i.e $x_6 = 0$ according to Eq. (2.119), implying that

$$\phi_3 \equiv \pi/2 \,, \tag{2.122}$$

in Eq. (2.120). This is, however, a specific choice, and a different implementation of the method is of course also possible. We have confirmed that simulations based on 4 independent parameters yield the same results.

Whether we choose to select a new update on a 4– or 5–dimensional sphere, our u3MC scheme is defined by randomly selecting a site within the lattice. Using Eq. (2.120) a new configuration of the $\mathcal{A}$–matrix is generated at that site. The new configuration is accepted or rejected by following the standard Metropolis argument [147]. We accept the new state μ if

$$r_0 \leq e^{-\beta(E_\mu - E_\nu)} \,, \tag{2.123}$$

where r_0 is number randomly chosen within the interval $r_0 \in (0, 1)$, $\beta = \frac{1}{k_B T}$ (we set $k_B = 1$), and E_ν is the energy of the initial configuration. The energies of the different states are computed according to Eq. (2.117).

The u3MC method has been implemented by my collaborator, Dr. Rico Pohle. And for completeness and later comparison with analytic derivations, we give here some details about the implementation of the numerical methods. Within a single MC step, N such local updates are performed, where N is the total number of sites in the system. Additionally, we also use the replica–exchange method (parallel tempering), which allows to reduce auto–correlation within the resulting Markov chain obtained from the MC sampling [57, 238]. An exchange of replicas is performed every 100 MC steps.

The simulations can be initialized by randomly choosing a $\mathcal{A}$–matrix on every site, mimicking a high–temperature paramagnet. The system is then thermalized by cooling the system adiabatically to the target temperature over 10^6 MC steps (simulated annealing), followed by a further 10^6 MC steps of thermalization at that target temperature. Thermodynamic quantities are calculated by averaging over 5×10^5 statistically–independent samples. Among thermodynamic quantities, the equal–time structure

factors allow access to correlations properties

$$S_\lambda(\mathbf{q}) = \left\langle \sum_{\alpha\beta} |m_\lambda{}^\alpha{}_\beta(\mathbf{q})|^2 \right\rangle , \tag{2.124}$$

where $\langle \ldots \rangle$ means that the quantity is averaged over statistically–independent states (Monte Carlo averaging).

We consider dipole, $\lambda = S$; quadrupole, $\lambda = Q$; and A–matrices, $\lambda = A$ structure factors. It is convenient to work with the lattice Fourier transform of $\mathcal{A}_i^\alpha{}_\beta$,

$$m_A{}^\alpha{}_\beta(\mathbf{q}) = \frac{1}{\sqrt{N}} \sum_i^N e^{i\mathbf{r}_i\mathbf{q}} \mathcal{A}_i^\alpha{}_\beta \, , \tag{2.125}$$

which can be found by fast Fourier transform (FFT). This allows us to obtain the structure factors for dipole moments, using Eq. (1.67),

$$m_S{}^\alpha{}_\alpha(\mathbf{q}) = -i \sum_{\beta,\gamma} \epsilon^\alpha{}_\beta{}^\gamma m_A{}^\beta{}_\gamma(\mathbf{q}) \, , \tag{2.126}$$

as well as for quadrupole moments, using Eq. (1.68),

$$m_Q{}^\alpha{}_\beta(\mathbf{q}) = -m_A{}^\alpha{}_\beta(\mathbf{q}) - m_A{}^\beta{}_\alpha(\mathbf{q}) + \frac{2}{3}\delta^{\alpha\beta} \sum_\gamma m_A{}^\gamma{}_\gamma(\mathbf{q}) \, , \tag{2.127}$$

by directly substituting these expressions in Eq. (2.124).

In Appendix E.1.1, I show results obtained by my collaborator, Dr. Rico Pohle, using the u3MC method and compare the obtained thermodynamic properties with published results [131, 229, 235]. This allows us to benchmark simulations based on the representation for a spin–1 in terms of "A-matrices". We present results for the heat capacity and structures factors for the BBQ model Eq. (2.68) on a triangular lattice and compare them with published results [131, 229, 235].

From our analysis in Appendix E.1.1, we conclude that our study of correlations at finite temperature, summarised in Fig. 1.13 and Fig. E.3, provides a strong evidence that the u3MC approach introduced in Section 2.6.1 can properly describe the thermodynamic properties of spin–1 magnets. Additionally, in Section 3.4 we present an exhaustive comparison for the thermodynamic properties of the FQ phase at low temperatures, between analytic predictions and numerical results obtained from a description in terms of "A-matrices".

2.6.2 Molecular Dynamics Simulations Within $u(3)$ Framework

Numerical integration of the equations of motion, combined with classical Monte Carlo simulation provides a powerful tool to investigate the (semi–)classical dynamics properties of quantum magnets. This approach has been referred to as "molecular dynamics" (MD) simulation [46, 151, 152, 239, 267]. Usually, this type of method starts from the Heisenberg equation of motion for an $O(3)$ spin, Eq. (2.24), providing a microscopic

description and quite surprisingly have shown to effectively describe dynamics of quantum magnets [41, 189, 206, 267]. This success relies on the fact that a (semi–)classical description of a spin–1/2 moment is appropriately provided by an $O(3)$ vector.

However, as already discussed, for spin–1 magnets, a representation in terms of $O(3)$ vectors fails, since an $O(3)$ vector does not properly account for the allowed quadrupole degrees of freedom of a spin–1 moment. [cf. Section 2.3 and Section 2.4.2]. This problem has a long history within the analytic theory of nematic phases [143, 180]. Generally, the excitations of spin–1 magnets include both spin waves and quadrupole waves [6]. And analytically, excitations can be studied through a multi–boson expansion, also sometimes referred to as "flavour–wave" theory [183].

On the numerical side, equations of motion in terms of spin– and quadrupole–operators have also been developed to study the dynamics of spin–1 magnets [14, 51, 200, 264]. However, these approaches rely on a description in terms of generators belonging to the $su(3)$ algebra are quite complicated due to the nature of the structure constants of the algebra $su(3)$ Eq. (2.27a). In contrast, for the $u(3)$ framework established in Section 2.4.2 we obtained a simple and compact form of the EoM for $\mathcal{A}$–matrices, Eq. (2.74), which makes this method ideally–suited for numerical integration. Moreover, the fact that these EoM can be combined with the MC method developed in Section 2.6.1 strengthen their applicability potential. Indeed, similarly to the $O(3)$ methods applied to spin–1/2 magnets, they provide an "$u(3)$ molecular dynamics" (u3MD) approach to spin–1 magnets.

Just like the u3MC simulations described in Section 2.6.1, our u3MD approach relies on a description in terms of a basis of $\mathcal{A}$–matrices product states [Eq. (2.116)]. We choose to implement the simulations using a 4^{th} order Runge-Kutta (RK–4) algorithm [81, 194], in order to numerically integrate Eq. (2.74). This is done for each component of $\mathcal{A}^{\alpha}_{i,\beta}$, using a fixed timestep δt_{RK}.

We iteratively apply the RK–4–integration of the equations of motion for the $\mathcal{A}$–matrices [Eq. (2.74)],

$$\{\mathcal{A}^{\alpha}_{i,\beta}(t)\} \mapsto \{\mathcal{A}^{\alpha}_{i,\beta}(t+\delta t_{\mathsf{RK}})\} + \mathcal{O}(\delta t^{5}_{\mathsf{RK}}) \ , \tag{2.128}$$

where δt_{RK} defines the RK–time step. This generates a time series

$$\{\mathcal{A}^{\alpha}_{\beta}(i,t_n)\} \ , \quad t_n = n\ \delta t \ , \quad n = 1 \ldots N_{\mathsf{t}} \ . \tag{2.129}$$

More details about the implementation of the RK–4–integration are provided in Appendix E.2.1.

We here simply note that the validity of this MD approach depends on the assertion that the constraint on spin–length, i.e. the trace of the $\mathcal{A}$–matrices, [Eq. (2.73)] is preserved, and that the total energy of the system, $E[\mathcal{A}_i]$ [Eq. (2.117)] is conserved. In Fig. 2.2 we show evidence that both are satisfied, within controlled errors, for simulations of a triangular–lattice cluster of linear dimension L = 24 (N = 2304 spins), with model parameters Eq. (E.11), and time–step Eq. (E.8), at a temperature $T = 0.1\ J$.

Additionally, the dynamics associated with the time evolution of the $\mathcal{A}$–matrices can be investigated by computation of dynamical structure factors. From the time–series generated by the RK–4–integration $\{\mathcal{A}^{\alpha}_{\beta}(i,t_n)\}$, we can define structure factors

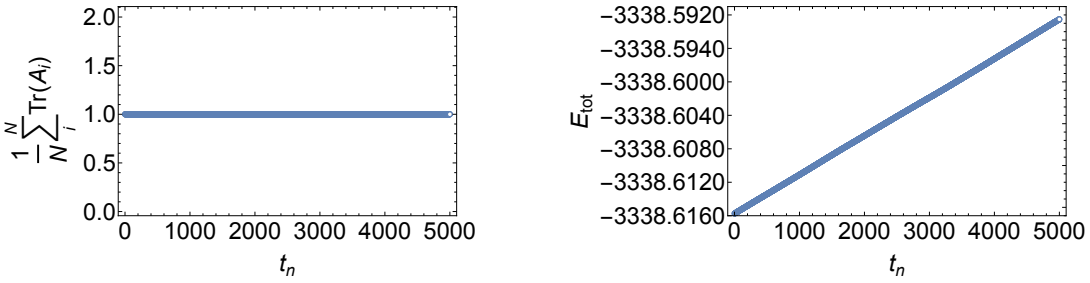

(a) time-dependence of Tr $\mathcal{A}$ **(b)** time-dependence of total energy

Figure 2.2: Evidence for the stability of the numerical integration of equations of motion for "A-matrices". (a) Time–dependence of Tr $\mathcal{A}$ [Eq. (2.57)], shows the conservation of spin length up to numerical precision, implying that if the time evolution originates from a proper spin configuration with Tr $\mathcal{A}$=1, we never leave the $su(3)$ sub–algebra of $u(3)$. This implies that we properly describe the spin–1 system trough out the time evolution. (b) Time–dependence of the energy $E = \langle \mathcal{H}_{\mathsf{BBQ}} \rangle$, shows that the energy is preserved to the level expected for a 4^{th}–order Runge–Kutta (RK–4) algorithm. Simulations were computed by my collaborator Dr. Rico Pohle, for the spin–1 bilinear–biquadratic model [Eq. (2.72)], using the equation of motion Eq. (2.74) for a triangular–lattice cluster with linear dimension L = 24 (N = 2304 spins), for parameters $J_1 = 0$, $J_2 = -1$, at a temperature $T = 0.1\ J$ and with a time–step $\delta t = 0.4\ J^{-1}$. Figures are reproduced from [201].

similar to Eq. (2.124), where the associated Fourier transformed moments in Eq. (2.125) defined in reciprocal space will also depend on time. Consequently, we define the time–Fourier transform, which allows us the resolve the dynamical structure factors in reciprocal space $\mathbf{q}$ and energy ω

$$S_\lambda(\mathbf{q}, \omega_m) = \left\langle \sum_{\alpha\beta} |\overline{m}_\lambda{}^\alpha{}_\beta(\mathbf{q}, \omega_m)|^2 \right\rangle \ , \tag{2.130}$$

where

$$\overline{m}_\lambda{}^\alpha{}_\beta(\mathbf{q}, \omega_m) \ = \ \frac{1}{\sqrt{N_t}} \sum_{n=1}^{N_t} e^{i\omega_m t_n} \sqrt{\overline{g}(t_n)}\ m_\lambda{}^\alpha{}_\beta(\mathbf{q}, t_n)\,, \tag{2.131}$$

with $\overline{g}(t_n)$ being a Gaussian envelope necessary to avoid numerical artifacts due to discontinuities at the beginning and the end of the time–series. Detailed explanations about the computation of the dynamical structure factors are given in Appendix E.2.2.

The approach presented here in order to compute dynamical structure factors from an MD scheme has been applied to the FQ phase of the BBQ model on the triangular lattice. An example of results obtained using this approach has been presented in Fig. 1.14. In Section 3.4, Section 4.3 and in Chapter 5, we use these results to compare with the analytic theory of the excitations about the FQ ground state.

Additional details regarding the implementation of the "u3MD" method can be found in Appendix E.2

Chapter 3

Classical Thermodynamics of the FQ-State of the BBQ Model on the Triangular Lattice

In this Chapter, I use the $u(3)$ formalism introduced in Section 2.4 and Section 2.5 to develop a classical theory of fluctuations about a ferroquadrupolar (FQ) ground state and compare its predictions with results from numerical simulations carried out using the u3MC scheme introduced in Section 2.6.1. I chose to illustrate our method for the FQ order because it is the simplest of the non–trivial phases found in the BBQ model, and it is already relatively well characterized.

A FQ ground state for the spin–1 BBQ model on a triangular lattice was predicted by mean–field (MF) calculations [131, 229] and by exact–diagonalisation [131], for a broad range of parameters [Fig. 1.11], and has since been confirmed by QMC [111, 255] and tensor–network approaches [173]. Its dynamic properties have also been explored using "flavour wave" (multi-bosons) theory [131, 143, 176, 183] and QMC simulations [255]. With many published results which are available for comparison, the FQ state is indeed a convenient starting point on which to bench-mark our method. Despite the rich literature around nematic order and more specifically FQ order, a classical theory of its low–temperature properties is missing.

In Section 3.1, I show how the expansion of small fluctuations about the FQ ground state is derived within our u(3) formalism following Section 2.5. In Section 3.2, I characterize the eigen–excitations of the system within the classical theory of fluctuations, and in Section 3.3 I further develop it into a classical low–temperature expansion and derive thermodynamic quantities. In Section 3.4, I compare the analytical predictions of the classical theory of excitations with classical Monte Carlo simulations carried out using the u3MC scheme [Section 2.6.1]. Additionally, these results will also serve for our derivation of the quantum–classical correspondence in Chapter 5.

3.1 Expansion of Small Fluctuations

Following the methodology developed in Section 2.5, we choose as our starting point the FQ ground state found in mean–field calculations. We assume $\left|\mathbf{d}_{\mathbf{i}}^{\mathsf{FQ}}\right\rangle$ to be the

single–site quadrupolar order, such that the total ground state wave function is given by a product wave function of on–site quadrupolar moments $\left|\mathbf{d}_\mathbf{i}^{\mathsf{FQ}}\right\rangle$ with a common orientation

$$|\Psi_0\rangle_{\mathsf{FQ}}^{\mathsf{MF}} = \prod_{i=1}^{N} \left|\mathbf{d}_\mathbf{i}^{\mathsf{FQ}}\right\rangle . \tag{3.1}$$

We choose the TR invariant basis [Eq. (2.32)] to describe the ferroquadrupolar state. For simplicity, we consider the director to be along the y-axis

$$\left|\mathbf{d}_i^{\mathsf{FQ}}\right\rangle = |y\rangle \quad \text{or equivalently} \quad \mathbf{d}^{\mathsf{FQ}} = \begin{pmatrix} 0 \\ 1 \\ 0 \end{pmatrix} , \tag{3.2}$$

for all lattice sites i. The state $|y\rangle$ is the time–reversal invariant state defined in Eq. (2.33). An illustration of the FQ ground state on the triangular lattice with all directors aligned along the y-axis is shown in Fig. 3.1. We note that it does not have the exact form of Eq. (2.81), but is just a reordering of the basis states, and the arguments presented in Section 2.5 still apply, such that we expect four generators to be broken by the FQ ground state.

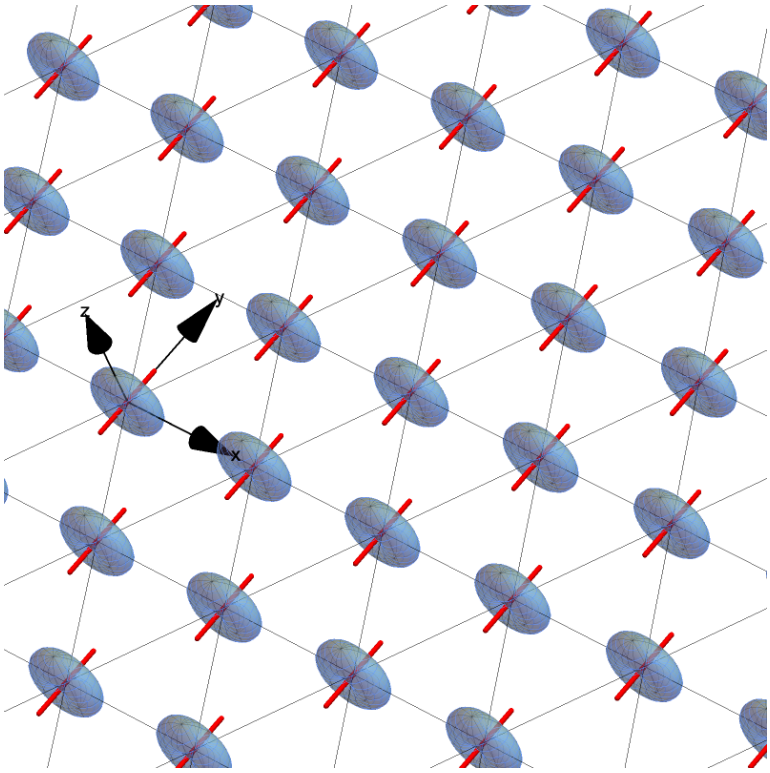

Figure 3.1: Ferroquadrupolar (FQ) ground state of a spin–1 magnet on a triangular lattice consisting of all magnetic moments having their director [Eq. (2.35)] aligned with each other. Each magnetic moment has been drawn in the state $|y\rangle$. Their corresponding director representation $d^x = 0$, $d^y = 1$, $d^z = 0$, [Eq. (2.35)] is shown as a red bar, and their corresponding spin probability distribution [Eq. (A.3)] is shown in grayish blue. Figure is reproduced from [201].

The corrections to mean–field theory due to taking into account excitations will introduce thermal and/or quantum fluctuations within the product state, as well as a reduction in the strength of the quadrupolar order. Following the procedure depicted in Section 2.5, we now derive a framework for describing these fluctuations in terms of generators of $U(3)$.

Using Eq. (2.45), we represent the MF ground state, Eq. (3.1), in terms of $\mathcal{A}$–matrices.

$$\left\langle \mathbf{d}_i^{\mathsf{FQ}} \middle| \mathcal{A} \middle| \mathbf{d}_i^{\mathsf{FQ}} \right\rangle = \mathbf{A_0} = \begin{pmatrix} 0 & 0 & 0 \\ 0 & 1 & 0 \\ 0 & 0 & 0 \end{pmatrix} . \tag{3.3}$$

In the space of $\mathcal{A}$–matrices, the product state reads

$$|\Psi_0\rangle_{\mathsf{FQ}}^{\mathsf{MF}} = \prod_{i=1}^{N} |\mathbf{A_0}\rangle . \tag{3.4}$$

Within the $u(3)$ Lie algebra, local fluctuations about any state $|\psi_0\rangle$ can be written using Eq. (2.87), where $\hat{R}(\vec{\phi})$ allows to create the fluctuations around the identity as explained in Section 2.1. Under this operation, $\mathcal{A}$–matrices transform as

$$\mathbf{A}(\vec{\phi}) = \hat{R}(\vec{\phi}) \mathbf{A} \hat{R}(\vec{\phi})^\dagger , \tag{3.5}$$

as determined by Eq. (2.62) [cf. Appendix B], where

$$\hat{R}(\vec{\phi}) = e^{i \sum_{\alpha\beta} \phi_{\alpha,\beta} \hat{\mathcal{A}}^\alpha{}_\beta} \tag{3.6a}$$

$$= \mathbb{I} + i \sum_{\alpha\beta} \phi_{\alpha,\beta} \hat{\mathcal{A}}^\alpha{}_\beta - \frac{1}{2} \sum_{\alpha\beta} \phi_{\alpha,\beta}^2 (\hat{\mathcal{A}}^\alpha{}_\beta)^2 + \mathcal{O}(\phi^3) , \tag{3.6b}$$

with $\alpha, \beta = 1, 2, 3$ as previously introduced in Eq. (2.86) and Eq. (2.90).

By expanding the exponential in Eq. (3.6a), and assuming small fluctuations, i.e. $\phi_{\alpha,\beta} \ll 1$, we restrict ourselves to quadratic order in $\phi_{\alpha,\beta}$ and obtain Eq. (3.6b). Considering the action of $\hat{R}(\vec{\phi})$ on the FQ ground state, as characterised by the matrix $\mathbf{A_0}$ [Eq. (3.4)], we note that the only $\hat{\mathcal{A}}^\alpha{}_\beta$ which do not preserve the ground state and will give a non–zero contribution are $\hat{\mathcal{A}}^1{}_2, \hat{\mathcal{A}}^3{}_2$ on the left by the application of $\hat{R}(\vec{\phi})$, $\hat{\mathcal{A}}^2{}_1, \hat{\mathcal{A}}^2{}_3$ on the right by the application of $\hat{R}^\dagger(\vec{\phi})$, and $\hat{\mathcal{A}}^2{}_2$ for both $\hat{R}(\vec{\phi})$ and $\hat{R}^\dagger(\vec{\phi})$

$$\begin{aligned} \hat{R}(\vec{\phi}) &= \mathbb{I} + i\phi_{1,2} \hat{\mathcal{A}}^1{}_2 + i\phi_{3,2} \hat{\mathcal{A}}^3{}_2 + i\phi_{2,2} \hat{\mathcal{A}}^2{}_2 - \frac{1}{2} \phi_{2,2}^2 (\hat{\mathcal{A}}^2{}_2)^2 \\ &= \begin{pmatrix} 1 & i\phi_{1,2} & 0 \\ 0 & 1 + i\phi_{2,2} - \frac{1}{2}\phi_{2,2}^2 & 0 \\ 0 & i\phi_{3,2} & 1 \end{pmatrix} , \end{aligned} \tag{3.7a}$$

$$\hat{R}(\vec{\phi})^\dagger = \mathbb{I} - i\phi_{2,1}\hat{\mathcal{A}}^2{}_1 - i\phi_{2,3}\hat{\mathcal{A}}^2{}_3 - i\phi_{2,2}\hat{\mathcal{A}}^2{}_2 - \frac{1}{2}\phi_{2,2}^2(\hat{\mathcal{A}}^2{}_2)^2$$
$$= \begin{pmatrix} 1 & 0 & 0 \\ -i\phi_{2,1} & 1 - i\phi_{2,2} - \frac{1}{2}\phi_{2,2}^2 & -i\phi_{2,3} \\ 0 & 0 & 1 \end{pmatrix} . \tag{3.7b}$$

For now, we simply note that

$$\det(\hat{R}(\vec{\phi})) = 1 + i\phi_{2,2} - \tfrac{1}{2}\phi_{2,2}^2 , \qquad \det(\hat{R}(\vec{\phi})^\dagger) = 1 - i\phi_{2,2} - \tfrac{1}{2}\phi_{2,2}^2 . \tag{3.8}$$

However, $\hat{R}(\vec{\phi})$ should belong to $SU(3)$, and therefore its determinant should equal unity [Eq. (2.2)]. The generator $\hat{\mathcal{A}}^2{}_2$ is therefore the one that takes the ground state out of $SU(3)$. This can also be seen by considering the effect of $\hat{R}(\vec{\phi})$ on the ground state vector $\mathbf{d}^{\mathsf{FQ}}$ [Eq. (3.1)]

$$\hat{R}(\vec{\phi})\mathbf{d}^{\mathsf{FQ}} = \begin{pmatrix} i\phi_{1,2} \\ 1 + i\phi_{2,2} - \frac{1}{2}\phi_{2,2}^2 \\ i\phi_{3,2} \end{pmatrix} , \tag{3.9}$$

where the generator $\hat{\mathcal{A}}^2{}_2$ induces a longitudinal fluctuation, which changes the length of the spin. But we only want to include orthogonal fluctuations that leave the length of the spin invariant. Therefore, we can disregard the nonphysical fluctuation $\phi_{2,2}$. Inserting Eq. (3.7a) and Eq. (3.7b) into Eq. (3.5), we get

$$\hat{\mathbf{A}}(\vec{\phi}) = \hat{R}(\vec{\phi})\mathbf{A}_0\hat{R}(\vec{\phi})^\dagger$$
$$= \begin{pmatrix} \phi^{1,2}\phi^{2,1} & i\phi^{1,2} & \phi^{1,2}\phi^{2,3} \\ -i\phi^{2,1} & 1 - \phi^{1,2}\phi^{2,1} - \phi^{2,3}\phi^{3,2} & -i\phi^{2,3} \\ \phi^{2,1}\phi^{3,2} & i\phi^{3,2} & \phi^{2,3}\phi^{3,2} \end{pmatrix} , \tag{3.10}$$

where we ensured that the spin–length constraint Equation 2.57 is satisfied. As a result, we only need to keep the four generators $\hat{\mathcal{A}}^1{}_2, \hat{\mathcal{A}}^3{}_2, \hat{\mathcal{A}}^2{}_1, \hat{\mathcal{A}}^2{}_3$ in order to describe fluctuations about the FQ ground state [Eq. (3.3) or equivalently Eq. (3.2)] The effect of the four generators $\hat{\mathcal{A}}^1{}_2, \hat{\mathcal{A}}^3{}_2, \hat{\mathcal{A}}^2{}_1, \hat{\mathcal{A}}^2{}_3$ is illustrated in Fig. 3.2.

The effect of the four generators $\hat{\mathcal{A}}^1{}_2, \hat{\mathcal{A}}^3{}_2, \hat{\mathcal{A}}^2{}_1, \hat{\mathcal{A}}^2{}_3$ on the state $|y\rangle$ can now be quantified directly. Inserting Eq. (3.10) into Eq. (1.68), and keeping terms up to $\mathcal{O}(\phi^2)$, we obtain

$$\hat{\mathbf{Q}}(\vec{\phi}) = \begin{pmatrix} \frac{2}{3} - 2\phi^{1,2}\phi^{2,1} & i(\phi^{2,1} - \phi^{1,2}) & -\phi^{1,2}\phi^{2,3} - \phi^{2,1}\phi^{3,2} \\ i(\phi^{2,1} - \phi^{1,2}) & -\frac{4}{3} + 2\phi^{1,2}\phi^{2,1} + 2\phi^{2,3}\phi^{3,2} & i(\phi^{2,3} - \phi^{3,2}) \\ -\phi^{1,2}\phi^{2,3} - \phi^{2,1}\phi^{3,2} & i(\phi^{2,3} - \phi^{3,2}) & \frac{2}{3} - 2\phi^{2,3}\phi^{3,2} \end{pmatrix} . \tag{3.11}$$

Similarly, for Eq. (1.67), up to $\mathcal{O}(\phi^2)$ we find

$$\hat{\mathbf{S}}(\vec{\phi}) = \begin{pmatrix} -\phi^{2,3} - \phi^{3,2} \\ i(\phi^{1,2}\phi^{2,3} - \phi^{2,1}\phi^{3,2}) \\ \phi^{1,2} + \phi^{2,1} \end{pmatrix} . \tag{3.12}$$

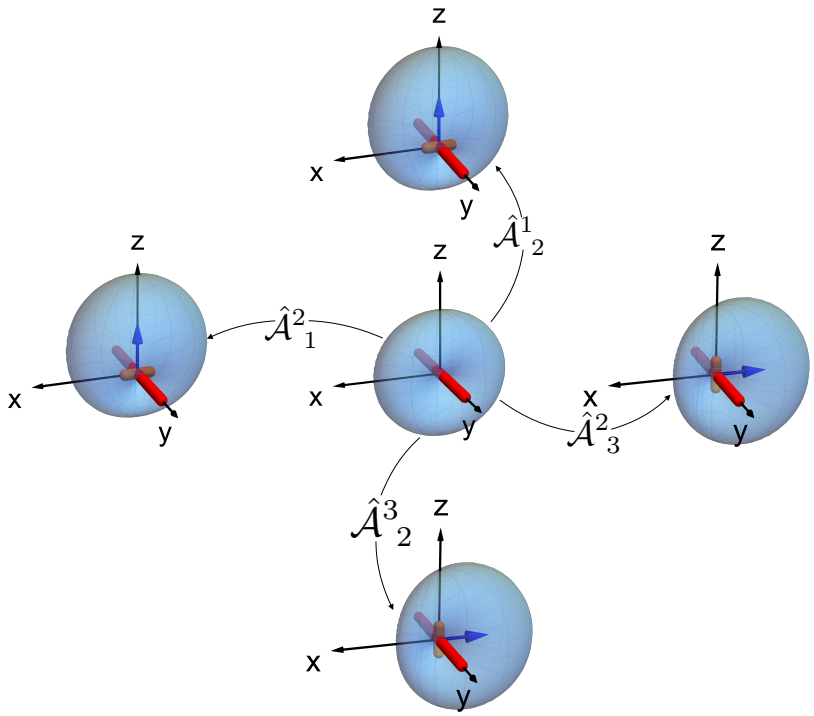

Figure 3.2: Effect of the four generators creating fluctuations about the ferro-quadrupolar (FQ) ground state $|y\rangle$, computed for each generator separately according to Eq. (2.87), and drawn here for an angle of $\phi = \frac{\pi}{8}$. The generators $\hat{\mathcal{A}}^1{}_2$ (acting on the right from the application of $\hat{R}^\dagger(\vec{\phi})$) and $\hat{\mathcal{A}}^2{}_1$ (acting on the left from the application of $\hat{R}(\vec{\phi})$) introduce a complex component of the director $\mathbf{d}$ along the x–axis, inducing a complex rotation of the directors about the z–axis. This deforms the quadrupole "donut" about the same axis and promotes a small but finite spin dipole moment along the z–axis [Eq. (2.44)]. The generators $\hat{\mathcal{A}}^2{}_3$ and $\hat{\mathcal{A}}^3{}_2$ produce a complex component of the director $\mathbf{d}$ along the z–axis, corresponding to a complex rotation of the director about the x–axis, reshape the quadrupole "donut" about the x–axis, and induce a spin dipole moment along the z–axis. The red bar represents the real part $\mathbf{u}$ of the coefficients d^α [Eq. (2.37)] in Eq. (2.35), and the orange bar represents the imaginary part $\mathbf{v}$. Figure is reproduced from [201].

From these results, we see that the fluctuations introduce a small imaginary part to the director $\mathbf{d}^{\mathsf{FQ}}$, either along the x– or the z–axis, and therefore introduce a rotation of the director $\mathbf{d}^{\mathsf{FQ}}$ in the Hilbert space $\mathbb{H}^3$ either about the z– or the x–axis. This introduces a small dipole moment and distorts the quadrupole "donut" about either the z– or the the x–axis. These changes are clearly visible in Fig. 3.2, where the real part to the director $\mathbf{d}^{\mathsf{FQ}}$ is shown as the red bar, and the small imaginary part induced as the fluctuation is shown by the orange bar. The dipole moment induced by each fluctuation is represented by a blue arrow and is also visible as a (small) distortion of the spin–probability distribution, i.e., the "donut" becomes more "spherical".

Since $\hat{\mathbf{A}}(\vec{\phi})$ in Eq. (3.10) is already expressed in the TR invariant basis, we are now able to derive a Hamiltonian describing fluctuations about FQ order. This is done by

substituting Eq. (3.10) in the expression for the BBQ Hamiltonian [Eq. (2.72)]

$$\mathcal{H}'_{\mathsf{BBQ}} = E_0 + \frac{1}{2}\sum_{\mathbf{k}} \left[\vec{\phi}^T_{\mathbf{k}} M_{\mathbf{k}} \vec{\phi}_{-\mathbf{k}}\right] + \mathcal{O}(\phi^4) \,, \tag{3.13}$$

where the energy of the MF ground state is

$$E_0 \;=\; NzJ_2 \,, \tag{3.14}$$

and where the fluctuations are encoded as

$$\vec{\phi}_{\mathbf{k}} = \begin{pmatrix} \phi^{2,1}_{\mathbf{k}} \\ \phi^{1,2}_{\mathbf{k}} \\ \phi^{3,2}_{\mathbf{k}} \\ \phi^{2,3}_{\mathbf{k}} \end{pmatrix} = \frac{1}{\sqrt{N}} \sum_i \begin{pmatrix} e^{i\mathbf{k}\cdot\mathbf{r}_i}\phi^{2,1}_{\mathbf{r}_i} \\ e^{i\mathbf{k}\cdot\mathbf{r}_i}\phi^{1,2}_{\mathbf{r}_i} \\ e^{i\mathbf{k}\cdot\mathbf{r}_i}\phi^{3,2}_{\mathbf{r}_i} \\ e^{i\mathbf{k}\cdot\mathbf{r}_i}\phi^{2,3}_{\mathbf{r}_i} \end{pmatrix} \,. \tag{3.15}$$

The energy matrix is

$$M_{\mathbf{k}} \;=\; \begin{pmatrix} A_{\mathbf{k}} & -B_{\mathbf{k}} & 0 & 0 \\ -B_{\mathbf{k}} & A_{\mathbf{k}} & 0 & 0 \\ 0 & 0 & A_{\mathbf{k}} & -B_{\mathbf{k}} \\ 0 & 0 & -B_{\mathbf{k}} & A_{\mathbf{k}} \end{pmatrix} \,, \tag{3.16}$$

where $A_{\mathbf{k}}$ and $B_{\mathbf{k}}$ are given by

$$A_{\mathbf{k}} \;=\; z(J_1\gamma(\mathbf{k}) - J_2) \,, \tag{3.17a}$$

$$B_{\mathbf{k}} \;=\; z\gamma(\mathbf{k})(J_2 - J_1) \,, \tag{3.17b}$$

with lattice structure factor

$$\gamma(\mathbf{k}) \;=\; \frac{1}{z}\sum_{\boldsymbol{\delta}} e^{-i\mathbf{k}\cdot\boldsymbol{\delta}} \,. \tag{3.18}$$

For the $z = 6$–coordinated triangular lattice, the vectors which connect neighbouring lattice sites, $\{\boldsymbol{\delta}\}$, are listed in Appendix D. We also note that the transpose vector for the fluctuations has the property given in Eq. (2.101), which implies

$$\vec{\phi}^T_{\mathbf{k}} = \begin{pmatrix} \phi^{1,2}_{\mathbf{k}}, & \phi^{2,1}_{\mathbf{k}}, & \phi^{2,3}_{\mathbf{k}}, & \phi^{3,2}_{\mathbf{k}} \end{pmatrix} \,. \tag{3.19}$$

We mention that the absence of terms linear in ϕ in Eq. (3.13) confirms that the MF ground state Eq. (3.4) is a valid starting point for describing FQ order, since it minimizes energy.

3.2 Classical Theory of Fluctuations

From the Hamiltonian [Eq. (3.13)] written in terms of fluctuations about the FQ ground state, we can obtain the classical eigenmodes $\omega_{\mathbf{k},\lambda}$ and the classical eigen–fluctuations $\mathbf{v}_{\mathbf{k},\lambda}$ by directly diagonalizing the energy matrix $M_{\mathbf{k}}$. This corresponds to solving the

following eigensystem

$$M_{\mathbf{k}}\mathbf{v}_{\mathbf{k},\lambda} = \omega_{\mathbf{k},\lambda}\mathbf{v}_{\mathbf{k},\lambda} \ . \tag{3.20}$$

The eigenvalues are found by solving

$$\det|M_{\mathbf{k}} - \omega_{\mathbf{k}}\mathbb{I}_4| = 0 \ . \tag{3.21}$$

The obtained eigenvalues are given by

$$\omega^{+}_{\mathbf{k}} = \omega_{\mathbf{k},1} = \omega_{\mathbf{k},3} = A_{\mathbf{k}} + B_{\mathbf{k}} \ , \tag{3.22a}$$
$$\omega^{-}_{\mathbf{k}} = \omega_{\mathbf{k},2} = \omega_{\mathbf{k},4} = A_{\mathbf{k}} - B_{\mathbf{k}} \ , \tag{3.22b}$$

and their associated eigenvectors, expressed in the basis

$$\{\phi^{2,1}_{\mathbf{k}},\ \phi^{1,2}_{\mathbf{k}},\ \phi^{3,2}_{\mathbf{k}},\ \phi^{2,3}_{\mathbf{k}}\} \ , \tag{3.23}$$

are given by

$$v_1 = \tfrac{1}{\sqrt{2}}\begin{pmatrix}-1\\1\\0\\0\end{pmatrix} \quad , \quad v_2 = \tfrac{1}{\sqrt{2}}\begin{pmatrix}1\\1\\0\\0\end{pmatrix} \quad , \quad v_3 = \tfrac{1}{\sqrt{2}}\begin{pmatrix}0\\0\\-1\\1\end{pmatrix} \quad , \quad v_4 = \tfrac{1}{\sqrt{2}}\begin{pmatrix}0\\0\\1\\1\end{pmatrix} \quad . \tag{3.24}$$

We note that the fluctuations v_1 and v_2 correspond to complex rotations of quadrupole moments in the ferroquadupolar ground state $\sim |y\rangle$ about the z–axis, while v_3 and v_4 correspond to complex rotations about the x–axis [cf. Fig. 3.2].

The fluctuations ϕ^{λ} orthogonal to the ground state $|y\rangle$, are related to the fluctuations v_λ that diagonalize the Hamiltonian [Eq. (3.13)], by an orthogonal basis change transformation O defined by

$$\begin{pmatrix}\phi^{2,1}\\ \phi^{1,2}\\ \phi^{3,2}\\ \phi^{2,3}\end{pmatrix} = O\begin{pmatrix}v_1\\v_2\\v_3\\v_4\end{pmatrix} \quad \text{where} \quad O = \tfrac{1}{\sqrt{2}}\begin{pmatrix}-1 & 1 & 0 & 0\\ 1 & 1 & 0 & 0\\ 0 & 0 & -1 & 1\\ 0 & 0 & 1 & 1\end{pmatrix} \ . \tag{3.25}$$

The orthogonality of O ensures that the eigen–fluctuations form an orthonormal set

$$v^{T}_{\mathbf{k},\lambda} v_{-\mathbf{k},\lambda'} = \delta_{\lambda\lambda'} \ . \tag{3.26}$$

Indeed the transpose eigenvectors $v^{T}_{\mathbf{k},\lambda}$ have the property that when expressed in the basis

$$\vec{\phi}^{T}_{\mathbf{k}} = \begin{pmatrix}\phi^{1,2}_{\mathbf{k}}, & \phi^{2,1}_{\mathbf{k}}, & \phi^{2,3}_{\mathbf{k}}, & \phi^{3,2}_{\mathbf{k}} & \end{pmatrix} \ , \tag{3.27}$$

they take the same form as $v_{\mathbf{k},\lambda}$ [Eq. (3.24)]. For instance,

$$v^{T}_{\mathbf{k},1} = \left(\frac{1}{\sqrt{2}}(\phi^{1,2}_{\mathbf{k}} - \phi^{2,1}_{\mathbf{k}})\right)^{T} = \frac{1}{\sqrt{2}}(\phi^{2,1}_{\mathbf{k}} - \phi^{1,2}_{\mathbf{k}}) \ , \tag{3.28}$$

which expressed in the basis $\vec{\phi}^T_{\mathbf{k}}$ [Eq. (3.27)] yields

$$v_1^T = \frac{1}{\sqrt{2}} \begin{pmatrix} -1 \\ 1 \\ 0 \\ 0 \end{pmatrix} . \tag{3.29}$$

We also note that considering a similar argument as Eq. (3.28) for all the components, we have

$$v^T_{\mathbf{k},1} = -v_{\mathbf{k},1} \ , \quad v^T_{\mathbf{k},2} = v_{\mathbf{k},2} \ , \quad v^T_{\mathbf{k},3} = -v_{\mathbf{k},3} \ , \quad v^T_{\mathbf{k},4} = v_{\mathbf{k},4} \ . \tag{3.30}$$

The coordinate system in terms of the eigenvectors $\mathbf{v_k}$ will turn out to be useful in the calculation of correlation functions and ordered moments, as described below in Section 3.3.

This also implies that the energy matrix $M_{\mathbf{k}}$ and the diagonal matrix consisting of eigenvalues on the diagonal are related by the similarity transformation defined by O

$$\tilde{M}_{\mathbf{k}} = O^T M_{\mathbf{k}} O = \begin{pmatrix} \omega_{\mathbf{k},1} & 0 & 0 & 0 \\ 0 & \omega_{\mathbf{k},2} & 0 & 0 \\ 0 & 0 & \omega_{\mathbf{k},3} & 0 \\ 0 & 0 & 0 & \omega_{\mathbf{k},4} \end{pmatrix} . \tag{3.31}$$

Then, to $\mathcal{O}(v^2)$, the Hamiltonian $\mathcal{H}'_{\mathsf{BBQ}}$ is diagonal in the basis,

$$\vec{v}^T_{\mathbf{k}} = (v_{\mathbf{k},1}, v_{\mathbf{k},2}, v_{\mathbf{k},3}, v_{\mathbf{k},4},) \ , \tag{3.32}$$

by construction, and can be written as

$$\begin{aligned} \mathcal{H}'_{\mathsf{BBQ}} &= E_0 + \frac{1}{2} \sum_{\mathbf{k}} \vec{v}^T_{\mathbf{k}} \tilde{M}_{\mathbf{k}} \vec{v}_{-\mathbf{k}} + \mathcal{O}(\vec{v}^4) \\ &= E_0 + \frac{1}{2} \sum_{\mathbf{k}} \sum_{\lambda=1}^{4} \omega_{\mathbf{k},\lambda} v^T_{\mathbf{k},\lambda} v_{-\mathbf{k},\lambda} + \mathcal{O}(\vec{v}^4) \ . \end{aligned} \tag{3.33}$$

Inserting Eq. (3.25) into Eq. (3.10) and keeping terms up to $\mathcal{O}(v^2)$, the A–matrix becomes

$$\hat{\mathbf{A}}(\vec{v}) = \begin{pmatrix} \frac{1}{2}(v_2^2 - v_1^2) & \frac{i}{\sqrt{2}}(v_1 + v_2) & \frac{1}{2}(v_1 v_3 + v_1 v_4 + v_2 v_3 + v_2 v_4) \\ \frac{i}{\sqrt{2}}(v_1 - v_2) & 1 - \frac{1}{2}(v_2^2 + v_4^2 - v_1^2 - v_3^2) & -\frac{i}{\sqrt{2}}(v_3 + v_4) \\ \frac{1}{2}(v_1 v_3 - v_1 v_4 - v_2 v_3 + v_2 v_4) & \frac{i}{\sqrt{2}}(-v_3 + v_4) & \frac{1}{2}(v_4^2 - v_3^2) \end{pmatrix} , \tag{3.34}$$

where thanks to Eq. (3.30), the hermicity of the A–matrix is preserved. Similarly, for

quadrupole moments [Eq. (3.11)], we obtain

$$\hat{\mathbf{Q}}(\vec{v}) = \begin{pmatrix} \frac{2}{3} - (v_2^2 - v_1^2) & -i\sqrt{2}v_1 & -v_1v_3 - v_2v_4 \\ -i\sqrt{2}v_1 & -\frac{4}{3} + (v_2^2 + v_4^2 - v_1^2 - v_3^2) & i\sqrt{2}v_3 \\ -v_1v_3 - v_2v_4 & i\sqrt{2}v_3 & \frac{2}{3} - (v_4^2 - v_3^2) \end{pmatrix} . \tag{3.35}$$

And, finally for dipole moments [Eq. (3.12)], we find

$$\hat{\mathbf{S}}(\vec{v}) = \begin{pmatrix} -\sqrt{2}v_4 \\ i(v_1v_4 + v_2v_3) \\ \sqrt{2}v_2 \end{pmatrix} . \tag{3.36}$$

Considering now up to linear order in the fluctuations, $\mathcal{O}(v)$, we note that the fluctuations v_2 and v_4 induce a correction to the dipole moments, while v_1 and v_3 induce a correction to the quadrupole moments. And for the A-matrices, all 4 fluctuations contribute [cf. Fig. 3.2].

These effects will also visible in Section 3.3.3 in Fig. 3.3, when computing the structure factors. We will see that the spin dipole spectral intensities of the excitations v_2 and v_4 are associated with their respective eigen–mode $\omega_{\mathbf{k}}^-$, and similarly for the quadrupole spectral intensities of the excitations v_1 and v_3 only contribute to their corresponding eigen–mode $\omega_{\mathbf{k}}^+$. Again for the A-matrix, their spectral weight encompasses all 4 fluctuations and shows intensities for both eigen–modes $\omega_{\mathbf{k}}^-$ and $\omega_{\mathbf{k}}^+$.

3.3 Classical Low Temperature Expansion

In this Section, the analytic framework of classical fluctuations developed in Section 3.1 is used to explore thermodynamic properties of the ferroquadrupolar (FQ) order at low temperatures. I describe how we can derive thermodynamic quantities within the framework of Section 3.1 by developing a classical theory of thermal fluctuations about FQ order at low temperature, which allows to calculate thermodynamic quantities for comparison with u3MC simulations. I will consider thermal corrections up to linear order in T (i.e. quadratic in fluctuations).

In Section 3.3.1, I will first consider the expression of the partition function and the free energy described in terms of the orthogonal fluctuations about the FQ ground state. This allows me to calculate the specific heat in Section 3.3.2. In Section 3.3.3 and Section 3.3.9, I calculate correlation functions by taking the appropriate functional derivative of the free energy. In particular, I will show results for the spin dipole, quadrupole, and A-matrix structure factors in Section 3.3.3. Ordered moments are calculated in Section 3.3.9 and will prove indispensable in explaining thermodynamic features arising in u3MC simulations. Finally, I compare the analytic classical calculations with classical simulation results obtained by the u3MC scheme presented in Section 2.6.1.

3.3.1 Expression for Free Energy

The partition function describing the FQ order and its fluctuation is given by

$$Z_0 \;=\; \int \mathrm{d}\vec{\phi}_{\mathbf{k}}\; e^{-\beta \mathcal{H}'_{\mathsf{BBQ}}[\vec{\phi}_{\mathbf{k}}]} \;, \tag{3.37}$$

where the measure of integration is

$$\mathrm{d}\vec{\phi}_{\mathbf{k}} = \mathrm{d}\phi_{\mathbf{k}}^{1,2}\mathrm{d}\phi_{\mathbf{k}}^{2,1}\mathrm{d}\phi_{\mathbf{k}}^{2,3}\mathrm{d}\phi_{\mathbf{k}}^{3,2} \;, \tag{3.38}$$

the inverse temperature is defined through

$$\beta = \tfrac{1}{k_B T} \;, \tag{3.39}$$

and $\mathcal{H}'_{\mathsf{BBQ}}[\vec{\phi}_{\mathbf{k}}]$ is given by Eq. (3.13). Neglecting $\mathcal{O}(\phi^4)$ terms, (all $\mathcal{O}(\phi^3)$ terms vanish), we compute

$$Z_0 \;=\; \prod_{\mathbf{k}}^{N} \int e^{-\beta \frac{1}{2}\vec{\phi}_{\mathbf{k}}^{T} M_{\mathbf{k}} \vec{\phi}_{-\mathbf{k}}} e^{-\beta \frac{E_0}{N}} \mathrm{d}\vec{\phi}_{\mathbf{k}} \tag{3.40a}$$

$$\;=\; e^{-\beta E_0} \prod_{\mathbf{k}}^{N} \left[\sqrt{\frac{(2\pi)^n}{\beta^n \det M_{\mathbf{k}}}} \right] \;, \tag{3.40b}$$

where E_0 is the MF ground state energy [Eq. (3.14)], the 4×4 matrix $M_{\mathbf{k}}$ is defined through Eq. (3.16), N is the number of lattice sites, n is the number of fluctuations, i.e., the dimension of $M_{\mathbf{k}}$ (in this case, $n = 4$), and where we used Eq. (F.1d) to calculate the Gaussian integral. The free energy of the system is given by

$$F_0 = -\frac{\log(Z_0)}{\beta} \;. \tag{3.41}$$

The free energy per site is consequently given by

$$\begin{aligned} f_0 &= \frac{F_0}{N} \\ &= \frac{E_0}{N} + \frac{k_B T}{2N} \sum_{\mathbf{k}} \sum_{\lambda=1}^{N_\lambda} \log\!\left(\frac{\omega_{\mathbf{k},\lambda}}{2\pi k_{\mathsf{B}} T}\right) + \mathcal{O}(T^2) \;, \end{aligned} \tag{3.42}$$

where $\omega_{\mathbf{k},\lambda}$ are the eigenvalues of $M_{\mathbf{k}}$ given in Eq. (3.22), and where we have used Eq. (3.39) and the fact that

$$\log[\det M_{\mathbf{k}}] = \mathrm{Tr} \log M_{\mathbf{k}} = \sum_{\lambda=1}^{N_\lambda} \log \omega_{\mathbf{k},\lambda} \;, \tag{3.43}$$

with N_λ counting the number of eigenmodes. Here

$$N_\lambda = 4 \;. \tag{3.44}$$

The free energy, Eq. (3.42), represents the leading order correction due to the fluctuation in the framework of a classical low–temperature expansion. Up to $\mathcal{O}(T)$, the thermodynamic properties of the FQ ground state of the BBQ model are entirely determined by the eigensystem defined by $M_{\mathbf{k}}$ and its solutions.

It is possible to calculate all thermodynamic properties of the FQ state, which can be obtained by taking the relevant (functional) derivatives of the free energy f_0 [Eq. (3.42)], as the leading term in a perturbative expansion series about $T = 0$.

We can also calculate the energy E_0 given by

$$\begin{aligned} E_0^{\mathsf{CL}} &= -\frac{\partial \log(Z_0)}{\partial \beta} \\ &= E_0 + \frac{1}{2}\sum_{\mathbf{k}}\sum_{\lambda=1}^{N_\lambda} k_B T \qquad (3.45a) \\ &= E_0 + 2N k_B T \ , \qquad (3.45b) \end{aligned}$$

where we use Eq. (3.39). We see that each classical fluctuations $\lambda = 1, 2, 3, 4$, contributes $\frac{1}{2}k_B T$ to the energy per site, for a total energy per site given $2k_B T$.

3.3.2 Specific Heat

The specific heat is defined as

$$c_v = \frac{C_v}{N} = -T\left(\frac{\partial^2 f_0}{\partial T^2}\right)_V \ , \qquad (3.46)$$

and represents the simplest thermodynamic property computable from the free energy. Using Eq. (3.42), we obtain

$$c_v = -T\frac{-k_B N_\lambda}{2T} = k_B\frac{N_\lambda}{2} \ , \qquad (3.47)$$

where $N_\lambda = 4$ as given in Eq. (3.44) and represents the number of eigenmodes for a spin–1 moment, i.e. the number of generators broken by the ordered ground state. For simplicity, we set

$$k_B = 1 \ , \qquad (3.48)$$

and it follows that,

$$c_v \to 2 \qquad [u(3) \text{ matrix}] \ , \qquad (3.49)$$

in the limit $T \to 0$.

In contrast, the usual result for classical fluctuations about an ordered state composed of $O(3)$ vectors, where the ground state breaks 2 $so(3)$ generators. Consequently, only two orthogonal fluctuations are possible for a single spin–1 moment, implying $N_\lambda = 2$ [218]:

$$c_v \to 1 \qquad [O(3) \text{ vector}] \ . \qquad (3.50)$$

We will find out that the zero–temperature limit of the specific heat is important for the interpretation of the u3MC simulation results, as discussed in Section 3.4.

3.3.3 Classical Structure Factors

I now present how the calculation of the classical structure factors associated with dipole moments, quadrupole moments, and A–matrices are obtained within our framework of classical thermal fluctuations. We start by introducing a source term $\Delta\mathcal{H}[h^{\alpha}_{i,\beta}]$ to the BBQ Hamiltonian

$$\mathcal{H} = \mathcal{H}_{\mathbf{BBQ}} + \Delta\mathcal{H}[h^{\alpha}_{i,\beta}] \, , \tag{3.51}$$

where

$$\Delta\mathcal{H}[h^{\alpha}_{i,\beta}] \;\; = \;\; -\sum_{i,\alpha} h^{\alpha}_{i,\beta}\hat{O}^{\alpha}_{i,\beta} \, , \tag{3.52}$$

describes the coupling of a ficticious field $h^{\alpha}_{i,\beta}$ to the observable $\hat{O}^{\alpha}_{i,\beta}$. In the following sections, we will replace

$$\hat{O}^{\alpha}_{i,\beta} \;\; \rightarrow \;\; \hat{\mathrm{S}}^{\alpha}_{i} \; \delta_{\alpha\beta} \, , \; \hat{\mathrm{Q}}^{\alpha\beta}_{i} \, , \; \hat{\mathcal{A}}^{\alpha}_{i \;\beta} \, , \tag{3.53}$$

to make explicit calculations for the dipole moment, quadrupole moment, and A–matrix structure factors.

The introduction of the source term $\Delta\mathcal{H}[h^{\alpha}_{i,\beta}]$ allows us to calculate correlations functions for the variables $\hat{O}^{\alpha}_{i,\beta}$ by taking the appropriate derivatives of the free energy with respect to the fictitious field $h^{\alpha}_{i,\beta}$, evaluated at zero field.

Explicit calculations are computed by expanding the observable $\hat{O}^{\alpha}_{i,\beta}$ in terms of the orthogonal eigenmodes $v_{\mathbf{k},\lambda}$ [Eq. (3.25)], which allows us to calculate the partition function by integrating out the fluctuations. Finally, as mentioned above, the relevant thermodynamic averages are obtained through functional derivatives of the free energy [Eq. (3.42)] with respect to $h^{\alpha}_{i,\beta}$.

I will first present the general framework needed to calculate the structure factors for an unspecified observable $\hat{O}^{\alpha}_{i,\beta}$. We will then simply apply the obtained results to the relevant operators [Eq. (3.53)]. Details for the specific cases are provided in Appendix G.

The structure factors involve contributions from both the ground state and thermal excitations, and below I present how to compute both. The calculation for the structure factors is therefore divided into two parts. The first part is valid for $\mathbf{q} \neq 0$. It consists of taking into account up to linear order in the expansion of fluctuations and is presented below. I provide details of the calculation for $\mathbf{q} \neq 0$ for dipole moments in Appendix G.1, quadrupole moments in Appendix G.3, and A–matrices in Appendix G.5. The second part captures the ground state contribution at $\mathbf{q} = 0$ and consists in taking into account up to quadratic order in the expansion of fluctuations. The general steps of the calculation at $\mathbf{q} = 0$ are given in Section 3.3.4. The details at $\mathbf{q} = 0$ are provided in Appendix G.2 for the dipole moments, in Appendix G.4 for the quadrupole moments, in Appendix G.6 for the A–matrices.

In order to compare with results obtained from a quantum theory of the fluctuations in Section 4.1, we introduce a spectral decomposition of the structure factors, defined in Eq. (3.72), which allows us to resolve contributions from the different eigenmodes

at different energies.

We start by assuming that the field-dependent part of the Hamiltonian is given by Eq. (3.52), and that the moment $\hat{O}^{\alpha}_{i,\beta}$ can be written down in terms of the fluctuations ϕ_i. Considering up to second order in fluctuations, the moments $\hat{O}^{\alpha}_{i,\beta}$ becomes

$$\hat{O}^{\alpha}_{i,\beta} = q^{\alpha}{}_{\beta\,\mu\nu}\phi^{\mu}_i\phi^{\nu}_i + l^{\alpha}{}_{\beta\,\mu}\phi^{\mu}_i + c^{\alpha}{}_{\beta} + \mathcal{O}(\phi^3) \ , \tag{3.54}$$

where we implicitly sum over μ and ν, and where $q^{\alpha}{}_{\beta\,\mu\nu}$, $l^{\alpha}{}_{\beta\,\mu}$ and $c^{\alpha}{}_{\beta}$, are respectively the quadratic, linear, and constant coefficients from the expansion of $\hat{O}^{\alpha}_{i,\beta}$ in terms of the fluctuations ϕ_i. The field dependent part of the Hamiltonian then becomes

$$\Delta\mathcal{H}[\mathbf{h}_i] = -\sum_i h^{\alpha}_{i,\beta}q^{\alpha}{}_{\beta\,\mu\nu}\phi^{\mu}_i\phi^{\nu}_i + h^{\alpha}_{i,\beta}l^{\alpha}{}_{\beta\,\mu}\phi^{\mu}_i + h^{\alpha}_{i,\beta}c^{\alpha}{}_{\beta} \ , \tag{3.55}$$

where we also implicitly sum over α, β, and where we neglect terms in $\mathcal{O}(\phi^3)$, which will from now on be disregarded. We now perform a Fourier transform according to Eq. (3.15), and obtain

$$\Delta\mathcal{H}[\mathbf{h}_{\mathbf{q}}] = -\sum_{\mathbf{q}}\left[l^{\alpha}{}_{\beta\,\mu}h^{\alpha}_{\mathbf{q},\beta}\phi^{\mu}_{-\mathbf{q}} + \sqrt{N}c^{\alpha}{}_{\beta}h^{\alpha}_{\mathbf{q},\beta}\delta_{\mathbf{q},0}\right] - \sum_{\mathbf{q}}\sum_{\mathbf{k}}\frac{1}{\sqrt{N}}q^{\alpha}{}_{\beta\,\mu\nu}h^{\alpha}_{\mathbf{q},\beta}\phi^{\mu}_{\mathbf{k}}\phi^{\nu}_{-\mathbf{q}-\mathbf{k}} \ , \tag{3.56}$$

where N is the number of lattice sites. We notice that if we were to include this in the total Hamiltonian Eq. (3.51) and write it down in the same form as Eq. (3.13), the interaction matrix $M_{\mathbf{k}}$ would take the same dimension as the number of lattice sites, because of the form of quadratic term in Eq. (3.56). We can then calculate it for a fixed $\mathbf{q}$. Namely for $\mathbf{q} = 0$, we find

$$\Delta\mathcal{H}[\mathbf{h}_{\mathbf{q}=0}] = -\,l^{\alpha}{}_{\beta\,\mu}h^{\alpha}_{\mathbf{q}=0,\beta}\phi^{\mu}_{-\mathbf{q}=0} - \sqrt{N}c^{\alpha}{}_{\beta}h^{\alpha}_{\mathbf{q}=0,\beta} - \sum_{\mathbf{k}}\frac{1}{\sqrt{N}}q^{\alpha}{}_{\beta\,\mu\nu}h^{\alpha}_{\mathbf{q}=0,\beta}\phi^{\mu}_{\mathbf{k}}\phi^{\nu}_{-\mathbf{k}} \ . \tag{3.57}$$

We note that the form of Eq. (3.57) is compatible with the form of Eq. (3.13). Indeed, for $\mathbf{q} = 0$, the contribution of the second order in fluctuations will enter the interaction matrix $M_{\mathbf{k}}$, modifying its eigenvalues, i.e., its dispersion relations, which will also depend on the field $\mathbf{h}$. For $\mathbf{q} = 0$, the interaction matrix $M_{\mathbf{k}}$ can be easily diagonalized. Therefore, we decide to only take into account up to second order in fluctuations for $\mathbf{q} = 0$, since it is exactly solvable and since we will need it when comparing the ordered moments at $\mathbf{q} = 0$, and to neglect them for $\mathbf{q} \neq 0$. To make the fact that we are taking up to second order in fluctuations into account only at $\mathbf{q} = 0$ more obvious, we write

$$\Delta\mathcal{H}[\mathbf{h}_{\mathbf{q}}] = -\sum_{\mathbf{q}} l^{\alpha}{}_{\beta\,\mu}h^{\alpha}_{\mathbf{q},\beta}\phi^{\mu}_{-\mathbf{q}} - \sum_{\mathbf{q}}\left(\sqrt{N}c^{\alpha}{}_{\beta}h^{\alpha}_{\mathbf{q},\beta} + \sum_{\mathbf{k}}\frac{1}{\sqrt{N}}q^{\alpha}{}_{\beta\,\mu\nu}h^{\alpha}_{\mathbf{q},\beta}\phi^{\mu}_{\mathbf{k}}\phi^{\nu}_{-\mathbf{k}}\right)\delta_{\mathbf{q},0} \ . \tag{3.58}$$

We then rewrite the field dependent part of the Hamiltonian such that the Hamiltonian is symmetric in $\vec{\phi}_{\mathbf{q}}$ and $\vec{\phi}^{T}_{\mathbf{q}}$ [Eq. (3.19)], which will be necessary when calculating

the structure factors at $\mathbf{q} = 0$. We have

$$\Delta\mathcal{H}[\mathbf{h_q}] = -\sum_{\mathbf{q}} \mathbf{N}_1[\mathbf{h_q}]^T \vec{\phi}_{-\mathbf{q}} + \vec{\phi}_{\mathbf{q}}^T \mathbf{N}_2[\mathbf{h}_{-\mathbf{q}}] + \tilde{C}[\mathbf{h_q}]\delta_{\mathbf{q},0} \ , \tag{3.59}$$

where we define

$$\mathrm{N}_1[\mathbf{h_q}]^\mu = \tfrac{1}{2}\mathrm{l}^\alpha{}_{\beta\,\mu}\mathrm{h}^\alpha_{\mathbf{q},\beta} \ , \qquad \mathrm{N}_2[\mathbf{h}_{-\mathbf{q}}]^\mu = \tfrac{1}{2}\mathrm{l}^\alpha{}_{\beta\,\mu}\mathrm{h}^\alpha_{-\mathbf{q},\beta} \ , \tag{3.60}$$

and

$$\tilde{C}[\mathbf{h_q}] = \sqrt{N} c^\alpha{}_\beta h^\alpha_{\mathbf{q},\beta} + \sum_{\mathbf{k}} \frac{1}{\sqrt{N}} q^\alpha_{\mu\nu} h^\alpha_{\mathbf{q}=0,\beta} \phi^\mu_{\mathbf{k}} \phi^\nu_{-\mathbf{k}} \ . \tag{3.61}$$

$\mathbf{N}_{1,2}[\mathbf{h_q}]$ are n–dimensional vectors whose components depend linearly on the fields $h^\alpha_{\mathbf{q},\beta}$ and represent the linear terms in $\phi_{\mathbf{q}}$ of the moments $\hat{O}_{\mathbf{q}}$. $\tilde{C}[\mathbf{h_q}]$ represents the zeroth order term and the second order contribution in $\phi_{\mathbf{q}}$ of the moments $\hat{O}_{\mathbf{q}}$ at $\mathbf{q} = 0$. $\tilde{C}[\mathbf{h_q}]$ is also linear in the fields $h^\alpha_{\mathbf{q},\beta}$. Plugging Eq. (3.59) in Eq. (3.51), using the definition of the partition function in Eq. (3.37), and using Eq. (F.1e) to perform the integral, we get

$$Z[\mathbf{h_q}] = e^{-\beta E_0} \prod_{\mathbf{q}}^{N} \left[\sqrt{\frac{(2\pi)^n}{\beta^n \det(M_{\mathbf{q}})}} e^{2\beta \mathbf{N}_1[\mathbf{h_q}]^T M_{\mathbf{q}}^{-1} \mathbf{N}_2[\mathbf{h_q}]} \ e^{\beta(\tilde{C}[\mathbf{h_q}]\delta_{\mathbf{q},0})} \right] \ , \tag{3.62}$$

where E_0 is given in Eq. (3.14), and the $n \times n$ square matrix $M_{\mathbf{q}}$ is given by Eq. (3.16). n is the dimension of $M_{\mathbf{q}}$, i.e., the number of independent classical fluctuations. In our case, we have $n = 4$. N is the number of lattice sites.

The free energy then becomes

$$\begin{aligned} F[\mathbf{h_q}] =& -\frac{\log(Z[\mathbf{h_q}])}{\beta} \\ =& E_0 - \sum_{\mathbf{q}}^{N} \tilde{C}[\mathbf{h_q}]\delta_{\mathbf{q},0} - 2\sum_{\mathbf{q}}^{N} \mathbf{N}_1[\mathbf{h_q}]^T M_{\mathbf{q}}^{-1} \mathbf{N}_2[\mathbf{h}_{-\mathbf{q}}] \\ &+ \frac{n}{2\beta}\sum_{\mathbf{q}} \log(\frac{\beta}{2\pi}) + \frac{1}{2\beta}\sum_{\mathbf{q}} \log(\det(M_{\mathbf{q}})) + \mathcal{O}(T^2) \ . \end{aligned} \tag{3.63}$$

The first derivative of the free energy with respect to field components $\mathbf{h_q}$ gives

$$\langle \hat{O}^\mu_{\mathbf{q},\nu} \rangle = -\left.\frac{\partial F}{\partial h^\mu_{\mathbf{q},\nu}}\right|_{\mathbf{h}=0} = \left.\frac{\partial \tilde{C}[\mathbf{h_q}]}{\partial h^\mu_{\mathbf{q},\nu}}\right|_{\mathbf{h}=0} \delta_{\mathbf{q},0} \ . \tag{3.64}$$

The second derivative of the free energy with respect to field components $\mathbf{h_q}$ corre-

sponds to

$$\langle \hat{O}^{\alpha}_{\mathbf{q},\beta}\hat{O}^{\mu}_{-\mathbf{q},\nu}\rangle - \langle \hat{O}^{\alpha}_{\mathbf{q},\beta}\rangle\langle \hat{O}^{\mu}_{-\mathbf{q},\nu}\rangle = -\frac{1}{\beta}\frac{\partial^2 F}{\partial h^{\alpha}_{\mathbf{q},\beta}\partial h^{\mu}_{-\mathbf{q},\nu}}\bigg|_{\mathbf{h}=0} \tag{3.65a}$$

$$= \frac{2}{\beta}\frac{\partial^2}{\partial h^{\alpha}_{\mathbf{q},\beta}\partial h^{\mu}_{-\mathbf{q},\nu}}\sum_{\mathbf{q}}^{N}(\mathbf{N}_1[\mathbf{h_q}]^T M_{\mathbf{q}}^{-1}\mathbf{N}_2[\mathbf{h_{-q}}])\bigg|_{\mathbf{h}=0}, \tag{3.65b}$$

where we have used the fact that $\tilde{C}[\mathbf{h_q}]$ is linear in the field components $h^{\alpha}_{\mathbf{q},\beta}$. For $\mathbf{q}\neq 0$, it turns out to be more convenient to work with $\tilde{M}_{\mathbf{q}}$ [Eq. (3.31)] which is diagonal, and hence the inverse is

$$(\tilde{M_{\mathbf{q}}}^{-1})^{\lambda\lambda} = \frac{1}{\tilde{M_{\mathbf{q}}}^{\lambda\lambda}} = \frac{1}{\omega_{\mathbf{q},\lambda}}\,. \tag{3.66}$$

We are allowed to do this because for $\mathbf{q}\neq 0$, the interaction matrix stays unchanged. However, we need to be more careful for $\mathbf{q}=0$ as explained in Section 3.3.4. Then, $\mathbf{N}_{1,2}[\mathbf{h_q}]$ become $\tilde{\mathbf{N}}_{1,2}[\mathbf{h_q}]$

$$\tilde{\mathbf{N}}_1[\mathbf{h_q}]^T = \mathbf{N}_1[\mathbf{h_q}]^T O\,, \tag{3.67a}$$

$$\tilde{\mathbf{N}}_2[\mathbf{h_{-q}}] = O^T\mathbf{N}_2[\mathbf{h_{-q}}]\,, \tag{3.67b}$$

such that $\tilde{\mathbf{N}}_{1,2}[\mathbf{h_q}]$ corresponds to the linear term when expressing the operators $\hat{O}^{\alpha}_i$ in terms of the fluctuations $\vec{v}_{\mathbf{q}}$ that diagonalize the BBQ Hamiltonian as shown in Eq. (3.32). Indeed, we then obtain

$$\Delta\mathcal{H}[\mathbf{h_q}] = -\sum_{\mathbf{q}}\tilde{\mathbf{N}}_1[\mathbf{h_q}]^T\vec{v}_{-\mathbf{q}} + \vec{v}_{\mathbf{q}}^T\tilde{\mathbf{N}}_2[\mathbf{h_{-q}}] + \tilde{C}[\mathbf{h_q}]\delta_{\mathbf{q},0}\,. \tag{3.68}$$

Therefore, we can simply write

$$\begin{aligned} F[\mathbf{h_q}] =& E_0 + \sum_{\mathbf{q}}^{N}\tilde{C}[\mathbf{h_q}]\delta_{\mathbf{q},0} - 2\sum_{\mathbf{q}}^{N}\sum_{\lambda=1}^{N_\lambda}\frac{(\tilde{\mathbf{N}}_1[\mathbf{h_q}]^T)^{\lambda}\tilde{\mathbf{N}}_2[\mathbf{h_{-q}}]^{\lambda}}{\omega_{\mathbf{q},\lambda}} \\ &+ \frac{N_\lambda}{2\beta}\sum_{\mathbf{q}}\log(\frac{\beta}{2\pi}) + \frac{1}{2\beta}\sum_{\mathbf{q}}\sum_{\lambda=1}^{N_\lambda}\log(\omega_{\mathbf{q},\lambda}) + \mathcal{O}(T^2)\,, \end{aligned} \tag{3.69}$$

where we have used Eq. (3.43) and where $N_\lambda = 4$ is the number of modes. Eq. (3.64) stays unchanged, but Eq. (3.65b) takes the simple form given by

$$\langle \hat{O}^{\alpha}_{\mathbf{q},\beta}\hat{O}^{\mu}_{-\mathbf{q},\nu}\rangle - \langle \hat{O}^{\alpha}_{\mathbf{q},\beta}\rangle\langle \hat{O}^{\mu}_{-\mathbf{q},\nu}\rangle = \frac{2}{\beta}\frac{\partial}{\partial h^{\alpha}_{\mathbf{q},\beta}\partial h^{\mu}_{-\mathbf{q},\nu}}\left(\sum_{\lambda=1}^{N_\lambda}\frac{(\tilde{\mathbf{N}}_1[\mathbf{h_q}]^T)^{\lambda}\tilde{\mathbf{N}}_2[\mathbf{h_{-q}}]^{\lambda}}{\omega_{\mathbf{q},\lambda}}\right)\bigg|_{\mathbf{h}=0}. \tag{3.70}$$

The dynamical factor associated with the operator $\hat{O}$ is defined by

$$S_{\mathrm{O}}^{\mathsf{CL}}(\mathbf{q}) = \sum_{\alpha,\beta} \langle \hat{O}^{\alpha}_{\mathbf{q},\beta} \hat{O}^{\beta}_{-\mathbf{q},\alpha} \rangle \ . \tag{3.71}$$

We also introduce a spectral decomposition of the structure factor as

$$S_{\mathrm{O}}^{\mathsf{CL}}(\mathbf{q},\omega) \ = \ \sum_{\alpha,\beta,\lambda} \langle \hat{O}^{\alpha}_{\mathbf{q},\beta} \hat{O}^{\beta}_{-\mathbf{q},\alpha} \rangle_{\lambda} \delta(\omega - \omega_{\mathbf{q},\lambda}) \ , \tag{3.72}$$

which we calculate as

$$S_{\mathrm{O}}^{\mathsf{CL}}(\mathbf{q},\omega) \ = \ \sum_{\alpha,\beta,\lambda} \left[\langle \hat{O}^{\alpha}_{\mathbf{q}=0,\beta} \rangle_{\lambda} \langle \hat{O}^{\beta}_{-\mathbf{q}=0,\alpha} \rangle_{\lambda} \delta(\omega) + \chi_{\lambda}^{\alpha\beta\beta\alpha}(\mathbf{q}) \delta(\omega - \omega_{\mathbf{q},\lambda}) \right] \ , \tag{3.73}$$

where the generalized susceptibility

$$\begin{aligned} \chi_{\lambda}^{\alpha\beta\mu\nu}(\mathbf{q}) &= \langle \hat{O}^{\alpha}_{\mathbf{q},\beta} \hat{O}^{\mu}_{-\mathbf{q},\nu} \rangle_{\lambda} - \langle \hat{O}^{\alpha}_{\mathbf{q},\beta} \rangle_{\lambda} \langle \hat{O}^{\mu}_{-\mathbf{q},\nu} \rangle_{\lambda} \\ &= \frac{2}{\beta} \frac{\partial}{\partial h^{\alpha}_{\mathbf{q},\beta} \partial h^{\mu}_{-\mathbf{q},\nu}} \left(\frac{(\tilde{\mathbf{N}}_1[\mathbf{h}_{\mathbf{q}}]^T)^{\lambda} \tilde{\mathbf{N}}_2[\mathbf{h}_{-\mathbf{q}}]^{\lambda}}{\omega_{\mathbf{q},\lambda}} \right) \Bigg|_{\mathbf{h}=0} \end{aligned} \tag{3.74}$$

is diagonal in λ. From Eq. (3.64), we note that the first moments $\langle \hat{O}^{\alpha}_{\mathbf{q},\beta} \rangle$ will only contribute at $\mathbf{q} = 0$, which is explicitly taken in account in Eq. (3.73). Therefore, for $\mathbf{q} \neq 0$, we can neglect the $\langle \hat{O}^{\alpha}_{\mathbf{q},\lambda} \rangle \langle \hat{O}^{\beta}_{-\mathbf{q},\lambda} \rangle$ term and we obtain

$$S_{\mathrm{O}}^{\mathsf{CL}}(\mathbf{q} \neq 0) \ = \ \sum_{\alpha\beta\lambda} \chi_{\lambda}^{\alpha\beta\beta\alpha}(\mathbf{q}) + \mathcal{O}(T^2) \ . \tag{3.75}$$

3.3.4 Structure Factors Classically at $\mathbf{q} = 0$

Here we present the calculation for the structure at $\mathbf{q} = 0$. At $\mathbf{q} = 0$, the structure factor associated with the operator $\hat{O}$ is defined by

$$S_{\mathrm{O}}^{\mathsf{CL}}(\mathbf{q} = 0) = \sum_{\alpha,\beta} \langle \hat{O}^{\alpha}_{\mathbf{q}=0,\beta} \hat{O}^{\beta}_{\mathbf{q}=0,\alpha} \rangle \ . \tag{3.76}$$

The relevant source term is given by Eq. (3.52). By expanding Eq. (3.52) in terms of the fluctuations, we obtained Eq. (3.58). We see that the contribution of the second order in fluctuations has the same form as the Hamiltonian expressed as Eq. (3.13) and will enter the interaction matrix $M_{\mathbf{k}}$, modifying its eigenvalues, i.e., dispersion relations, which will all also depend on the field $\mathbf{h}$. We can therefore assume that, at $\mathbf{q} = 0$, the total Hamiltonian [Eq. (3.51)] has the following form

$$\begin{aligned} \mathcal{H} =& E_0 + \frac{1}{2} \sum_{\mathbf{k}} \left[\vec{\phi}^T_{\mathbf{k}} M_{\mathbf{k}}[\mathbf{h}_{\mathbf{q}=0}] \vec{\phi}_{-\mathbf{k}} \right] + \sum_{\mathbf{k}} \left[N_1^T[\mathbf{h}_{\mathbf{k}}] \vec{\phi}_{-\mathbf{k}} + \vec{\phi}^T_{\mathbf{k}} N_2[\mathbf{h}_{-\mathbf{k}}] \right] \delta_{\mathbf{k},0} \\ &+ \sum_{\mathbf{k}} C[\mathbf{h}_{\mathbf{q}=0}] \delta_{\mathbf{k},0} + \mathcal{O}(\phi^3) \ , \end{aligned} \tag{3.77}$$

where $C[\mathbf{h}_{\mathbf{q}=0}]$ represents the zeroth order term in $\phi_{\mathbf{q}}$ of the moments $\hat{O}_{\mathbf{q}}$. The second order contribution at $\mathbf{q}=0$ is now included in $M_{\mathbf{k}}[\mathbf{h}_{\mathbf{q}=0}]$. As before, $\mathbf{N}_{1,2}[\mathbf{h}_{\mathbf{k}}]$ are n–dimensional vectors whose components depend linearly on the fields $h^{\alpha}_{\mathbf{k},\beta}$ and represent the linear terms in $\phi_{\mathbf{k}}$ of the moments $\hat{O}_{\mathbf{k}}$. Neglecting terms in $\mathcal{O}(\phi^3)$, and using Eq. (F.1e) to perform the integral, we find

$$Z = e^{-\beta E_0}\prod_{\mathbf{k}}^{N}\left[\int e^{-\beta\frac{1}{2}\vec{\phi}^T_{\mathbf{k}}M_{\mathbf{k}}[\mathbf{h}_{\mathbf{q}=0}]\vec{\phi}_{\mathbf{k}}}e^{-\beta\left[N_1^T[\mathbf{h}_{\mathbf{k}}]\vec{\phi}_{-\mathbf{k}}+\vec{\phi}^T_{\mathbf{k}}N_2[\mathbf{h}_{-\mathbf{k}}]\right]\delta_{\mathbf{k},0}}e^{-\beta C[\mathbf{h}_{\mathbf{q}=0}]\delta_{\mathbf{k},0}}\mathrm{d}\vec{\phi}_{\mathbf{k}}\right] \quad (3.78a)$$

$$= e^{-\beta E_0}\prod_{\mathbf{k}}^{N}\left[\sqrt{\frac{(2\pi)^n}{\beta^n\det M_{\mathbf{k}}[\mathbf{h}_{\mathbf{q}=0}]}}e^{2\beta N_1^T[\mathbf{h}_{\mathbf{k}}]M^{-1}_{\mathbf{k}}[\mathbf{h}_{\mathbf{q}=0}]N_2[\mathbf{h}_{-\mathbf{k}}]\delta_{\mathbf{k},0}}e^{-\beta C[\mathbf{h}_{\mathbf{q}=0}]\delta_{\mathbf{k},0}}\right], \quad (3.78b)$$

where E_0 is defined through Eq. (3.14), and the $n\times n$ matrix $M_{\mathbf{k}}[h^{\alpha}_{\mathbf{q}=0\beta}]$ through Eq. (3.77) that includes up to second order in fluctuations. n is the dimension of $M_{\mathbf{k}}[h^{\alpha}_{\mathbf{q}=0\beta}]$, i.e., the number of independent classical fluctuations. In our case, we have $n=4$. N is the number of lattice sites. It follows that the free energy is

$$\begin{aligned}F =& -\frac{\log(Z)}{\beta}\\ =& E_0+\sum_{\mathbf{k}}C[\mathbf{h}_{\mathbf{q}=0}]\delta_{\mathbf{k},0}-\frac{n}{2\beta}\sum_{\mathbf{k}}\log(\frac{(2\pi)}{\beta})+\frac{1}{2\beta}\sum_{\mathbf{k}}\sum_{\lambda=1}^{N_\lambda}\log(\omega_{\mathbf{k},\lambda}[\mathbf{h}_{\mathbf{q}=0}])\\ &-2\sum_{\mathbf{k}}N_1^T[\mathbf{h}_{\mathbf{k}}]M^{-1}_{\mathbf{k}}[\mathbf{h}_{\mathbf{q}=0}]N_2[\mathbf{h}_{-\mathbf{k}}]\delta_{\mathbf{k},0}+\mathcal{O}(T^2)\,,\end{aligned} \quad (3.79)$$

where $\omega_{\mathbf{k},\lambda}[\mathbf{h}_{\mathbf{q}=0}]$ are the eigenvalues of $M_{\mathbf{k}}[\mathbf{h}_{\mathbf{q}=0}]$, and we have used Eq. (3.43). The moments are given by

$$\langle\hat{O}^{\alpha}_{\mathbf{q}=0,\beta}\rangle = -\left.\frac{\partial F}{\partial h^{\alpha}_{\mathbf{q}=0,\beta}}\right|_{\mathbf{h}=0}, \quad (3.80)$$

and

$$\langle\hat{O}^{\alpha}_{\mathbf{q}=0,\beta}\hat{O}^{\mu}_{\mathbf{q}=0,\nu}\rangle = \langle\hat{O}^{\alpha}_{\mathbf{q}=0,\beta}\rangle\langle\hat{O}^{\mu}_{\mathbf{q}=0,\nu}\rangle-\frac{1}{\beta}\left.\frac{\partial^2 F}{\partial h^{\alpha}_{\mathbf{q}=0,\beta}\partial h^{\mu}_{\mathbf{q}=0,\nu}}\right|_{\mathbf{h}=0}. \quad (3.81)$$

Using Eq. (3.79), Eq. (3.80) yields

$$\begin{aligned}\langle\hat{O}^{\alpha}_{\mathbf{q}=0,\beta}\rangle =& -\left.\frac{\partial C[\mathbf{h}_{\mathbf{q}=0}]}{\partial h^{\alpha}_{\mathbf{q}=0,\beta}}\right|_{\mathbf{h}=0}-\frac{1}{2\beta}\sum_{\mathbf{k}}\sum_{\lambda=1}^{N_\lambda}\frac{1}{\omega_{\mathbf{k},\lambda}[\mathbf{h}_{\mathbf{q}=0}]}\left.\frac{\partial\omega_{\mathbf{k},\lambda}[\mathbf{h}_{\mathbf{q}=0}]}{\partial h^{\alpha}_{\mathbf{q}=0,\beta}}\right|_{\mathbf{h}=0}\\ &+2\left.\frac{\partial\left[N_1^T[\mathbf{h}_{\mathbf{q}=0}]M^{-1}_{\mathbf{q}=0}[\mathbf{h}_{\mathbf{q}=0}]N_2[\mathbf{h}_{\mathbf{q}=0}]\right]}{\partial h^{\alpha}_{\mathbf{q}=0,\beta}}\right|_{\mathbf{h}=0}+\mathcal{O}(T^2)\,,\end{aligned} \quad (3.82)$$

where the last derivative turns out to be null when evaluated at $\mathbf{h} = 0$, for dipoles, quadrupoles and A-matrices. Eq. (3.81) becomes

$$\langle \hat{O}^{\alpha}_{\mathbf{q}=0,\beta} \hat{O}^{\mu}_{\mathbf{q}=0,\nu} \rangle = \langle \hat{O}^{\alpha}_{\mathbf{q}=0,\beta} \rangle \langle \hat{O}^{\mu}_{\mathbf{q}=0,\nu} \rangle - \frac{1}{\beta} \left. \frac{\partial^2 C[\mathbf{h}_{\mathbf{q}=0}]}{\partial h^{\alpha}_{\mathbf{q}=0,\beta} \partial h^{\mu}_{\mathbf{q}=0,\nu}} \right|_{\mathbf{h}=0} + \frac{2}{\beta} \left. \frac{\partial^2 \left[N_1^T[\mathbf{h}_{\mathbf{q}=0}] M^{-1}_{\mathbf{q}=0}[\mathbf{h}_{\mathbf{q}=0}] N_2[\mathbf{h}_{\mathbf{q}=0}] \right]}{\partial h^{\alpha}_{\mathbf{q}=0,\beta} \partial h^{\mu}_{\mathbf{q}=0,\nu}} \right|_{\mathbf{h}=0} + \mathcal{O}(T^2) \, , \tag{3.83}$$

where the terms including second derivatives of $C[\mathbf{h}_{\mathbf{q}=0}]$ are zero, since $C[\mathbf{h}_{\mathbf{q}=0}]$ is linear in $h^{\alpha}_{\mathbf{q}=0,\beta}$ by definition. Finally, Eq. (3.76) can be calculated by using Eq. (3.82) and Eq. (3.83). For each type of moments, dipole, quadrupole or A-matrix, the interaction matrix $M_{\mathbf{k}}[\mathbf{h}_{\mathbf{q}=0}]$, the source terms $N_1^T[\mathbf{h}_{\mathbf{q}}]$ and $N_2[\mathbf{h}_{\mathbf{q}}]$ and the constant term will be different. They are given in Appendix G. In what follows, we present the results that we need in order to compare with numerical simulations of the FQ state in Section 3.4.

3.3.5 Structure Factor for Dipole Moments

We first consider the structure factor for spin dipole moments

$$S_{\mathrm{S}}^{\mathsf{CL}}(\mathbf{q}) \;=\; \sum_{\alpha} \langle \hat{\mathrm{S}}^{\alpha}_{\mathbf{q}} \hat{\mathrm{S}}^{\alpha}_{-\mathbf{q}} \rangle \, . \tag{3.84}$$

Within the classical low–temperature expansion for structure factors developed in Section 3.3.3 and Section 3.3.4, and to leading order in T, we find

$$S_{\mathrm{S}}^{\mathsf{CL}}(\mathbf{q}) \;=\; \frac{4}{\beta} \frac{1}{\omega^{-}_{\mathbf{q}}} + \mathcal{O}(T^2) \, , \tag{3.85}$$

where $\omega^{\pm}_{\mathbf{q}}$ are given in Eq. (3.22). We observe that the fluctuations restore a finite value of $S_{\mathrm{S}}^{\mathsf{CL}}(\mathbf{q})$ at finite temperature. Indeed, as can be seen in Eq. (3.36), the eigen–fluctuations v_2 and v_4 induce a (small) dipolar moment along the z– and x–axis respectively. The absence of terms in $\omega^{+}_{\mathbf{q}}$ reflects the fact that only the "odd" modes $\lambda = 2, 4$ corresponding to $\omega^{-}_{\mathbf{q}}$ contribute to dipolar fluctuations. However, all ground–state averages of dipole moments vanish as the FQ phase does not break time–reversal symmetry.

The spectral decomposition of the structure factor, Eq. (3.85), is given by

$$S_{\mathrm{S}}^{\mathsf{CL}}(\mathbf{q}, \omega) \;=\; \frac{4}{\beta} \frac{1}{\omega^{-}_{\mathbf{q}}} \delta(\omega - \omega^{-}_{\mathbf{q}}) + \mathcal{O}(T^2) \, . \tag{3.86}$$

Eq. (3.86) is plotted in Fig. 3.3 (a), for a temperature $T/J = 1$ and for parameters corresponding to a FQ ground state given by

$$J_1 = 0.0 \, , \; J_2 = -1.0 \, . \tag{3.87}$$

We observe that within the classical theory, excitations which are dipolar in nature are gapped and form a dispersing band with spectral intensity concentrated at $\mathbf{q} = \mathbf{K}$.

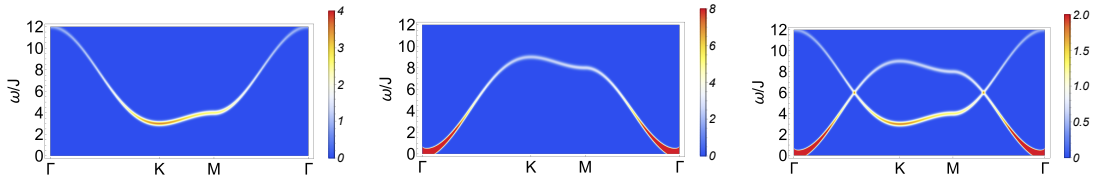

(a) $S_{\mathrm{S}}^{\mathsf{CL}}(\mathbf{q},\omega)$ (b) $S_{\mathrm{Q}}^{\mathsf{CL}}(\mathbf{q},\omega)$ (c) $S_{\mathrm{A}}^{\mathsf{CL}}(\mathbf{q},\omega)$

Figure 3.3: Spectral representation of structure factors found in a classical theory of fluctuations about a ferroquadrupolar (FQ) ground state of the BBQ model. (a) Spectral representation of dipole structure factor, $S_{\mathrm{S}}^{\mathsf{CL}}(\mathbf{q},\omega)$ [Eq. (3.86)], within the classical low–temperature expansion developed in Section 3.2, at temperature $T = J$. (b) Equivalent result the for the quadrupole structure factor, $S_{\mathrm{Q}}^{\mathsf{CL}}(\mathbf{q},\omega)$ [Eq. (3.91)]. (c) Equivalent results for the A–matrix structure factor, $S_{\mathrm{A}}^{\mathsf{CL}}(\mathbf{q},\omega)$ [Eq. (3.94)]. All results are shown for parameters Eq. (3.87), and have been convoluted with Gaussian of FWHM 0.35 J. Bragg peaks have been omitted for simplicity.

Further details of these calculations can be found in Appendix G.1 [$\mathbf{q} \neq 0$] and Appendix G.2 [$\mathbf{q} = 0$].

3.3.6 Structure Factor for Quadrupole Moments

The structure factor for quadrupole moments is defined as

$$S_{\mathrm{Q}}^{\mathsf{CL}}(\mathbf{q}) \;=\; \sum_{\alpha\beta} \langle \hat{\mathrm{Q}}_{\mathbf{q}}^{\alpha\beta} \hat{\mathrm{Q}}_{-\mathbf{q}}^{\beta\alpha} \rangle \;, \tag{3.88}$$

where the sum on α, β makes sure that $SU(2)$ symmetry is respect for the defined scalar contraction. To leading order in T, we obtain

$$S_{\mathrm{Q}}^{\mathsf{CL}}(\mathbf{q}) \;=\; \frac{8}{\beta}\frac{1}{\omega_{\mathbf{q}}^{+}}(1-\delta_{\mathbf{q},0}) + \frac{8}{3}\left[N - \frac{\Delta}{\beta}\right]\delta_{\mathbf{q},0} + \mathcal{O}(T^2) \;, \tag{3.89}$$

where

$$\Delta \;=\; 3\sum_{\mathbf{k}\neq 0}\left[\frac{1}{\omega_{\mathbf{k}}^{+}} + \frac{1}{\omega_{\mathbf{k}}^{-}}\right] + \frac{1}{\omega_{\mathbf{q}}^{-}} \;. \tag{3.90}$$

Unlike dipole moments, fluctuations associated with the FQ ground state contribute to the structure factor for quadrupole moments. This is encoded in the term Δ/β, which describes the corrections to ground state averages for $T > 0$. The absence of terms in $\omega_{\mathbf{q}}^{-}$ for $q \neq 0$ comes from the fact that only the "even" modes $\lambda = 1, 3$ contribute to quadrupolar fluctuations. Indeed, as can be seen in Eq. (3.35), the eigen–fluctuations v_1 and v_3 induce (small) quadupolar moments. However, through Eq. (3.90), all 4 modes, $\lambda = 1, 2, 3, 4$, contribute to the reduction of the ordered moment coming from the ground state averages.

The spectral decomposition of the structure factor, Eq. (3.89), yields

$$S_{\rm Q}^{\sf CL}(\mathbf{q},\omega) \;=\; \frac{8}{\beta}\frac{1}{\omega_{\mathbf{q}}^{+}}(1-\delta_{\mathbf{q},0})\delta(\omega-\omega_{\mathbf{q}}^{+}) + \frac{8}{3}\left[N-\frac{\Delta}{\beta}\right]\delta_{\mathbf{q},0}\delta(\omega)+\mathcal{O}(T^2)\;. \quad (3.91)$$

Eq. (3.91) is illustrated in Fig. 3.3 (b), where for simplicity we suppressed the Bragg peak at $\mathbf{q}=\mathbf{\Gamma}$. The classical excitations which have a quadrupolar character form a gapless dispersing band, with spectral weight concentrated at $\mathbf{q}=\mathbf{\Gamma}$.

Further details of these calculations are provided in Appendix G.3 [$\mathbf{q}\neq 0$] and Appendix G.4 [$\mathbf{q}=0$].

3.3.7 Structure Factor for A–matrices

Here we calculate the structure factor for the A-matrices $\hat{\mathcal{A}}^{\alpha}{}_{\beta}$, which in our theory is the most fundamental object describing a spin–1. The structure factor of the A-matrices is given by

$$S_{\rm A}^{\sf CL}(\mathbf{q}) \;=\; \sum_{\alpha\beta}\langle \hat{\mathcal{A}}^{\alpha}_{\mathbf{q}\ \beta}\hat{\mathcal{A}}^{\beta}_{-\mathbf{q}\ \alpha}\rangle\;, \quad (3.92)$$

where the contraction over α, β allows to preserve the full $U(3)$ symmetry of the representation. Uo to linear order in T, we have

$$S_{\rm A}^{\sf CL}(\mathbf{q}) \;=\; \frac{2}{\beta}\frac{1}{\omega_{\mathbf{q}}^{-}} + \frac{2}{\beta}\frac{1}{\omega_{\mathbf{q}}^{+}}(1-\delta_{\mathbf{q},0}) + \left[N-\frac{2}{3}\frac{\Delta}{\beta}\right]\delta_{\mathbf{q},0}+\mathcal{O}(T^2)\;. \quad (3.93)$$

Because the A-matrices $\hat{\mathcal{A}}^{\alpha}{}_{\beta}$ include both dipoles and quadrupoles moments, so does its structure factor, and all 4 modes, $\lambda=1,2,3,4$, contribute to the reduction of the A–moments coming from ground state averages. All four modes, $\omega_{\mathbf{q}}^{\pm}$, contribute to fluctuation terms for $\mathbf{q}\neq 0$, as can be seen from Eq. (3.34).

The spectral decomposition of the structure factor, Eq. (3.93), is given by

$$S_{\rm A}^{\sf CL}(\mathbf{q},\omega) = \frac{2}{\beta}\frac{1}{\omega_{\mathbf{q}}^{-}}\delta(\omega-\omega_{\mathbf{q}}^{-}) + \frac{2}{\beta}\frac{1}{\omega_{\mathbf{q}}^{+}}(1-\delta_{\mathbf{q},0})\delta(\omega-\omega_{\mathbf{q}}^{+}) + \left[1-\frac{2}{3}\frac{\Delta}{\beta}\right]\;\delta_{\mathbf{q},0}\;\delta(\omega)+\mathcal{O}(T^2)\;. \quad (3.94)$$

This is shown in Fig. 3.3 (c), where again we suppressed the Bragg peak at $\mathbf{q}=\mathbf{\Gamma}$, for simplicity. The contribution of both dipolar and quadrupolar fluctuations to the A-matrix structure factors $S_{\rm A}^{\sf CL}(\mathbf{q},\omega)$ become apparent and can be seen as independent, dispersing bands.

Further details of these calculations are given in Appendix G.5 and [$\mathbf{q}\neq 0$] Appendix G.6 [$\mathbf{q}=0$].

3.3.8 Sum Rule for Structure Factors

The sum rule associated with A–matrices, Eq. (2.67), implies a sum rule on the structure factors $S_{\rm S}^{\sf CL}(\mathbf{q})$, $S_{\rm Q}^{\sf CL}(\mathbf{q})$ and $S_{\rm A}^{\sf CL}(\mathbf{q})$, Indeed by performing a Fourier transform on

Eq. (2.67), we obtain

$$\hat{\mathcal{A}}^{\alpha}_{\mathbf{k}\ \beta}\hat{\mathcal{A}}^{\beta}_{-\mathbf{k}\ \alpha} = \frac{1}{4}\hat{\mathrm{Q}}^{\alpha\beta}_{\mathbf{k}}\hat{\mathrm{Q}}^{\beta\alpha}_{-\mathbf{k}} + \sum_{\alpha}\frac{1}{2}\hat{\mathrm{S}}^{\alpha}_{\mathbf{k}}\hat{\mathrm{S}}^{\alpha}_{-\mathbf{k}} + \frac{1}{12}s^2(s+1)^2 N\delta_{\mathbf{k},0}\ . \tag{3.95}$$

By using the respective definition of the dipole moments, quadrupole moments, and A–matrices structure factors given in Eq. (3.84), Eq. (3.88), and Eq. (3.92), we find

$$S^{\mathsf{CL}}_{\mathrm{A}}(\mathbf{q}) = \frac{1}{4}S^{\mathsf{CL}}_{\mathrm{Q}}(\mathbf{q}) + \frac{1}{2}S^{\mathsf{CL}}_{\mathrm{S}}(\mathbf{q}) + \frac{1}{3}N\delta_{\mathbf{q},0}\ . \tag{3.96}$$

This sum rule is easily checked by directly substituting Eq. (3.85),Eq. (3.89), and Eq. (3.93), into Eq. (3.96). It is then easily seen that the results of the low–temperature expansion satisfy the sum rule of Eq. (3.96). It can also be checked visually in Fig. 3.3.

3.3.9 Ordered Moments

Finally, we consider the quadrupole moment which characterizes the FQ state,

$$\langle\mathbf{Q}\rangle := \sqrt{\langle\mathbf{Q}^2\rangle}\ , \tag{3.97}$$

which acts as an order parameter for the FQ phase. For non–sublattice order, the associated Bragg peak appears at the ordering vector given by $\mathbf{q} = \mathbf{\Gamma}$. And, indeed, the quadrupole structure factor exhibits a Bragg peak at the $\mathbf{\Gamma}$–point, scaling linearly with N, the number of lattice sites. Therefore as a measure of the FQ state, we consider

$$\langle\mathbf{Q}^2_{\mathsf{CL}}\rangle = \frac{S^{\mathsf{CL}}_{\mathrm{Q}}(\mathbf{q}=\mathbf{\Gamma})}{N}\ , \tag{3.98}$$

where N denotes the number of lattice sites, such that $\langle\mathbf{Q}^2\rangle$ takes on a finite value. From Eq. (3.89), we simply find

$$\langle\mathbf{Q}^2_{\mathsf{CL}}\rangle = \frac{8}{3} - \frac{8}{N\beta}\sum_{\mathbf{k}\neq 0}\left[\frac{1}{\omega^{+}_{\mathbf{k}}} + \frac{1}{\omega^{-}_{\mathbf{k}}}\right]\ . \tag{3.99}$$

We note that at zero temperature the expected ground–state value of the order parameter is given by

$$Q^2_0 = \frac{8}{3}\ . \tag{3.100}$$

We compare these results with MC simulation in Section 3.4.2.

3.4 Comparison with $u(3)$ Monte Carlo Simulations

In this Section, I compare the analytic theory of classical fluctuations developed in Section 3.2 and Section 3.3 with the $U(3)$ Monte Carlo (u3MC) simulation schemes developed in Section 2.6.1. I start in Section 3.4.1 by analyzing the heat capacity,

which for simulations is also shown to satisfy the correct classical limit $c(T \to 0) \to 2$. In Section 3.4.2, I consider the low–temperature properties of the ordered moment $\langle \mathbf{Q^2} \rangle$. In simulations, the ordered moment is shown to take on a finite value at a finite temperature, which seems like a direct violation of the Mermin–Wagner theorem. But I show that it exhibits a finite–size scaling consistent with the Mermin–Wagner theorem. Then, I consider the equal–time structure factors associated with dipole moments, quadrupole moments, and A-matrices. In Section 3.4.3, I show that at low temperature, equal–time structure factors from the classical analytic theory [Section 3.2] are conforming with u3MC simulation results. This analysis confirms that the simulations based on the u3MC accurately describe the classical low–temperature properties, such as correlations, within the FQ state.

3.4.1 Heat Capacity

In Fig. 3.4, we present u3MC results for the temperature dependence of the heat capacity per spin defined as

$$c(T) = C(T)/N = \frac{1}{N}\frac{1}{T^2}\left[\langle E(T)^2\rangle - \langle E(T)\rangle^2\right] . \tag{3.101}$$

Results were obtained using the $U(3)$ Monte Carlo (u3MC) formalism developed in Section 2.6.1, applied to the BBQ Hamiltonian $\mathcal{H}_{\mathsf{BBQ}}$ [Eq. (2.72)], for the parameter values given in Eq. (3.87), and for clusters of linear dimension given by $L = 12, 24, 48, 96$ ($N = 144, 576, 2304, 9216$ spins).

At low temperatures, we find

$$c(T \to 0) \to 2 , \tag{3.102}$$

as can be observed from Fig. 3.4. This is in agreement with the result predicted by the classical theory developed in Section 3.3 [cf. Eq. (3.49)]. It implies that the $u(3)$ formalism implemented within the u3MC scheme also correctly describes the four orthogonal generators of fluctuations about the FQ ground state. As already discussed in Section 3.3.2, each of the four fluctuations contribute $1/2$ to $c(T)$ in the limit $T \to 0$ leading to Eq. (3.102). Meanwhile, for classical MC simulations based on an $O(3)$ representation, only two generators per spin are broken and $c(T \to 0) \leq 1$ [218].

We note that the onset of fluctuations of FQ order is indicated by the pronounced peak at $T^* \sim 0.43$. As system size is increased, the peak gradually shifts towards lower temperatures and sharpens simultaneously. However, because of the Mermin–Wagner theorem [146], long–range FQ order is not expected to occur at finite temperature in a two–dimensional system. The scaling of this peak does not conform with a conventional phase transition described by Landau's theory. Meanwhile, we saw that point–like topological defects are possible in a spin–1 systems with ferroquadrupolar correlations. Indeed, the order parameter is described by a real director, which takes on values on the 2–dimensional protective space $\mathbb{RP}^2$ (cf. Fig. 1.5). Homotopy analysis predicts the existence of vortices consisting of directors

$$\pi_1(\mathbb{RP}^2) = \mathbb{Z}_2 , \tag{3.103}$$

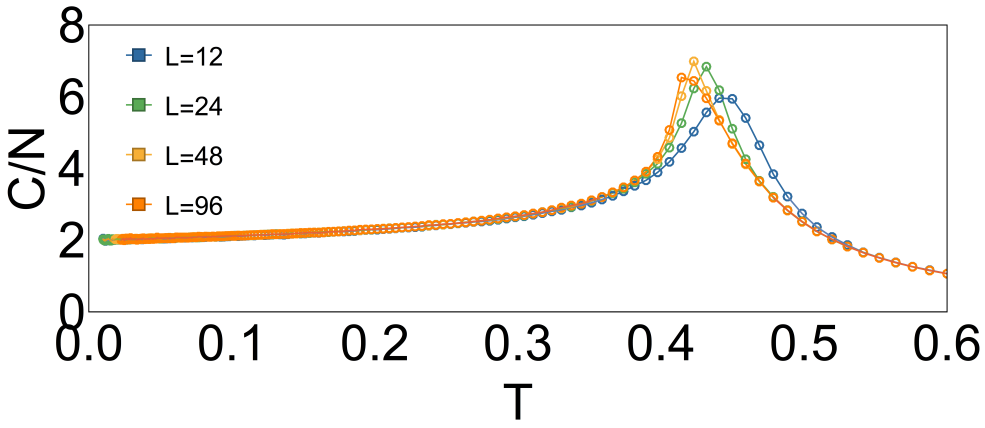

Figure 3.4: Temperature dependence of the specific heat per spin $c(T)$, obtained by $U(3)$ Monte Carlo (u3MC) simulations of the BBQ model $\mathcal{H}_{\text{BBQ}}$ [Eq. (2.72)], for a ferroquadrupolar (FQ) ground state. Results are illustrated for different system sizes L. The peak at $c(T)$ at $T^* \sim 0.43$ reflects the onset of fluctuations of FQ order, as depicted in Fig. 3.5 (a). The low temperature limit $c(T \to 0) \to 2$ agrees with the prediction obtained from the analytical theory of thermal fluctuations, which is based on the existence of four independent classical excitations about the the FQ ground state, as discussed in Section 3.3.2. All simulations were carried out by my collaborator Dr. Rico Pohle using the MC scheme described in Section 2.6.1 for parameters given in Eq. (3.87) and consistent with a FQ ground state. Figure is reproduced from [201].

previously introduced in Eq. (1.52b). These topological defects can mediate a phase transition into a phase with algebraic FQ correlations in a mechanism similar to the BKT-phase transition of the XY–model. Indeed, such a BKT–like topological phase transition is permitted at finite temperature and would be signaled by a peak in heat capacity. This type of unconventional phase transition has been observed in previous MC simulations of the $O(3)$ BBQ model on the triangular lattice [116]. A detailed analysis of topological phase transitions in the spin–1 BBQ model goes beyond the scope of this Thesis but is kept as a future investigation plan [Section 7.2.1].

3.4.2 Ordered Moment

Here we consider the behavior of the quadrupole–moment $\mathbf{Q}$, which defines an order parameter for the FQ state. The ordered moment is computed through the equal–time structure factor [cf. Eq. (3.98)] obtained by u3MC simulations developed in Section 2.6.1.

$$\langle \mathbf{Q}^2_{\text{MC}} \rangle = \frac{S^{\text{MC}}_{\text{Q}}(\mathbf{q} = \mathbf{\Gamma})}{N} \,. \tag{3.104}$$

In Fig. 3.5, we show simulation results obtained for our usual parameter set, Eq. (3.87). The ordered moment obtained from u3MC simulations takes on a finite value in finite–size clusters, as shown in Fig. 3.5 (a). At low temperatures, the u3MC

results agree with the expected ground–state value [Eq. (3.100)]

$$\langle \mathbf{Q}^2_{\mathsf{MC}} \rangle \big|_{T\to 0} = Q_0^2 = \frac{8}{3} \,. \tag{3.105}$$

For low but finite temperature, the order moment is well–described by polynomial function with respect to temperature.

$$\langle \mathbf{Q}^2 \rangle = Q_0^2 + \alpha(L) T + \beta(L) T^2 + \cdots \,, \tag{3.106}$$

where the coefficients $\alpha(L)$ and $\beta(L)$ are determined by fits to simulation results. This expansion is consistent with the result obtained from low–temperature expansion of the analytic theory of classical fluctuations [Eq. (3.99)]. At a temperature corresponding to the peak in heat capacity, $T \approx T^* \sim 0.43$ [Fig. 3.4], the value of $\langle \mathbf{Q}^2_{\mathsf{MC}} \rangle$ drops, and above this temperature, rapidly tends to zero with increasing system size. The fact that the order moment $\langle \mathbf{Q}^2_{\mathsf{MC}} \rangle$ take on a finite value for temperatures lower than $T \approx T^* \sim 0.43$ seems to contradict the Mermin–Wagner theorem, which forbids $\langle \mathbf{Q}^2 \rangle \neq 0$ at finite temperature for 2–dimensional systems [146].

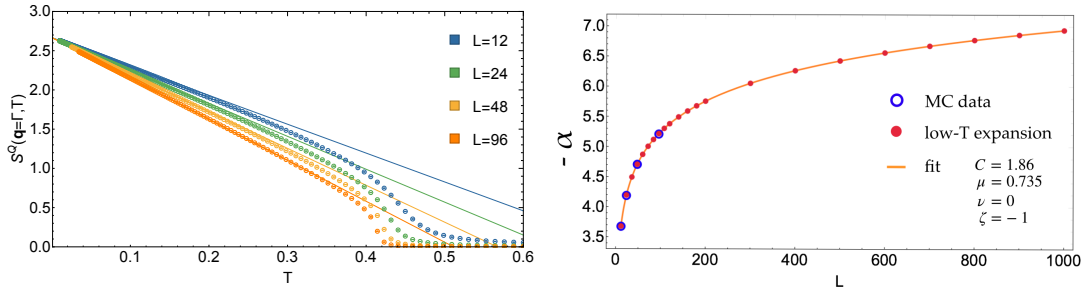

(a) Temperature dependence of ordered moment $\langle \mathbf{Q}^2_{\mathsf{MC}} \rangle$

(b) Coefficient $-\alpha(L)$ of the leading temperature correctio to $\langle \mathbf{Q}^2 \rangle$

Figure 3.5: Temperature and system size dependence of the order moment $\mathbf{Q}$ for a ferroquadrupolar (FQ) ground state of the BBQ model $\mathcal{H}_{\mathsf{BBQ}}$ [Eq. (2.72)]. (a) Results for $\mathbf{Q}^2$ found in $U(3)$ Monte Carlo (u3MC) simulations for different system sizes, L. The temperature $T^* \sim 0.43$ of the onset of fluctuations of FQ order at $\mathbf{Q}^2$ corresponds to the one found in the peak of the heat capacity, shown in Fig. 3.4. At low temperatures, $\mathbf{Q}^2$ tends to the ordered moment of the FQ ground state, Q_0^2 [Eq. (3.105)]. (b) Finite–size scaling of the coefficient $\alpha(L)$ [Eq. (3.106)], showing a logarithmic divergence for large L. This implies a correction of the leading order in temperature $\alpha(L)$ to the ordered moment which suppresses any quadrupole moments at finite temperate in the thermodynamic limit [Eq. (3.108)], consistent with the Mermin–Wagner Theorem. Results are shown for both u3MC simulations (blue circle), and the analytic theory (red points) [Eq. (3.107)], developed in Section 3.3. All u3MC simulations were carried out by my collaborator Dr. Rico Pohle using the u3MC scheme described in Section 2.6.1, for parameters Eq. (3.87) consistent with a FQ ground state. Figures are reproduced from [201].

We first note that in order to obey the Mermin–Wagner theorem, in the thermodynamic limit, we must have $\langle \mathbf{Q}^2 \rangle \equiv 0$ at any finite temperature [146]. The coefficient

$\alpha(L)$ in Eq. (3.106) describes the rate at which thermal fluctuations destroy the order. Therefore, the Mermin–Wagner theorem implies that the coefficient $\alpha(L)$ in Eq. (3.106) must diverge as $L \to \infty$. For $\langle \mathbf{Q}^2_{\mathsf{MC}} \rangle$, the dependence of $\alpha_{\mathsf{MC}}(L)$ with system size L is obvious from Fig. 3.5 (a), where we see that $\alpha_{\mathsf{MC}}(L)$ monotonically increases with L, as the slope become sharper with increasing system size L. The slope $\alpha_{\mathsf{MC}}(L)$ is obtained by fitting the simulations results over temperature intervals given in Table (H.1), as explained in Appendix H. This is plotted against system sizes L as blue circles in Fig. 3.5 (b). However, for all system sizes accessible to simulation, the ordered moment still takes on a finite value at low temperatures, seemingly contradicting the Mermin–Wagner theorem.

This is resolved by considering the analytic theory developed in Section 3.3. The analytic estimate of $\alpha_{\mathsf{CL}}(L)$ is found by evaluating numerically the sum on $\mathbf{k}$ found in the ordered moments [Eq. (3.99)] obtained analytically. Namely, we compute

$$\alpha_{\mathsf{CL}}(L) = -\frac{8}{L^2} \sum_{\mathbf{k} \neq 0}^{L^2} \left[\frac{1}{\omega^+_{\mathbf{k}}} + \frac{1}{\omega^-_{\mathbf{k}}} \right] , \tag{3.107}$$

where we set $k_B = 1$. The sum on $\mathbf{k}$ is performed by numerically summing over the reciprocal space of the triangular lattice accordingly partitioned with the number of lattice sites. This is computed for different values of system sizes, including the ones accessible to simulation. Details are provided in Appendix H. The values of $\alpha_{\mathsf{CL}}(L)$ are plotted as the red dots in Fig. 3.5 (b) and are well described by

$$-\alpha(L) = \alpha_0 + \mu \log L + \nu \frac{1}{L} + \xi \frac{1}{L^2} , \tag{3.108}$$

with fit parameters

$$\alpha_0 = 1.86 \ , \ \mu = 0.735 \ , \ \nu = 0 \ , \ \xi = -1 \ . \tag{3.109}$$

Additionally, by evaluating this sum as an integral, we can extract the leading contribution to $\alpha_{\mathsf{CL}}(L)$ in function of L. A logarithmic divergence in $\alpha_{\mathsf{CL}}(L)$ for large L is identified [Eq. (H.12)], which agrees with the estimated value μ obtained by the fit [Eq. (3.108)] of the sum given in Eq. (3.107).

To summarize, in Fig. 3.5 (b), the values of $\alpha(L)$ obtained from u3MC simulations and from analytic low–temperature expansion results for systems of size up to $L = 1000$ ($N = 10^6$ spins) are plotted. We find that $-\alpha(L \to \infty) \to \infty$, and that consequently, the Mermin–Wagner Theorem is respected. Indeed $-\alpha(L \to \infty) \to \infty$, implies $\langle \mathbf{Q}^2 \rangle \to 0$ for any $T > 0$. Additionally, we confirm from these results that, at $\mathbf{q} = 0$, the structure factors obtained from u3MC simulations and from analytic theory are in perfect agreement, at low temperatures. Further details of this analysis can be found in Appendix H.

3.4.3 Equal–Time Structure Factor

Finally, we investigate the low–temperature properties of correlations between magnetic moments. We compare equal–time structure factors $S^{\mathsf{CL}}_{\lambda}(\mathbf{q})$ obtained from the analyt-

ical theory of thermal fluctuations [cf. Section 3.3.3 and Section 3.3.4] with results $S_\lambda^{\mathsf{MC}}(\mathbf{q})$ found in u3MC simulations [Eq. (2.124)] for the BBQ model $\mathcal{H}_{\mathsf{BBQ}}$ [Eq. (2.72)]. In Fig. 3.6, structure factors associated with dipole moments, $S_{\mathrm{S}}(\mathbf{q})$, quadrupole moments $S_{\mathrm{Q}}(\mathbf{q})$, and A–matrices, $S_{\mathrm{A}}(\mathbf{q})$ obtained from analytic and numerical results are plotted along the irreducible wedge $\mathbf{\Gamma}$–$\mathbf{K}$–$\mathbf{M}$–$\mathbf{\Gamma}$ [cf. Appendix D].

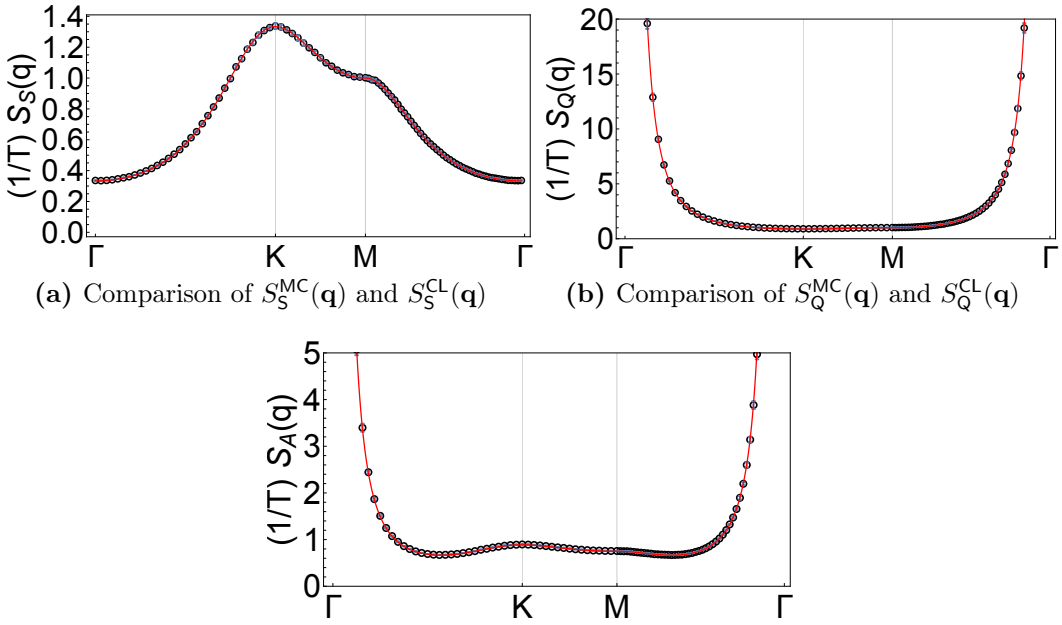

(a) Comparison of $S_{\mathsf{S}}^{\mathsf{MC}}(\mathbf{q})$ and $S_{\mathsf{S}}^{\mathsf{CL}}(\mathbf{q})$

(b) Comparison of $S_{\mathsf{Q}}^{\mathsf{MC}}(\mathbf{q})$ and $S_{\mathsf{Q}}^{\mathsf{CL}}(\mathbf{q})$

(c) Comparison of $S_{\mathsf{A}}^{\mathsf{MC}}(\mathbf{q})$ and $S_{\mathsf{A}}^{\mathsf{CL}}(\mathbf{q})$

Figure 3.6: Results for equal–time structure factors $S_\lambda^{\mathsf{CL}}(\mathbf{q})$ obtained from the analytical theory of thermal fluctuations (solid line) [cf. Section 3.3.3 and Section 3.3.4] and compared with $U(3)$ Monte Carlo (u3MC) simulations results [Eq. (2.124)] of $\mathcal{H}_{\mathsf{BBQ}}$ [Eq. (2.72)], for parameters consistent with a ferroquadrupolar (FQ) ground state [Eq. (3.87)] (a) Dipole structure factor, $S_{\mathsf{S}}^{\mathsf{CL}}(\mathbf{q})$ [Eq. (3.85)], exhibiting a spectral weight peak around $\mathbf{K}$, reflecting AFM correlations . (b) Quadrupole structure factor, $S_{\mathsf{S}}^{\mathsf{CL}}(\mathbf{q})$ [Eq. (3.89)], showing divergence associated with fluctuations of FQ order for $\mathbf{q} \to \mathbf{\Gamma}$. (c) A–matrix structure factor, $S_{\mathsf{A}}^{\mathsf{CL}}(\mathbf{q})$ [Eq. (3.93)], which shows behavior associated with both dipolar and quadrupolar fluctuations. In all cases, the structure factors have been divided by temperature T, and agree perfectly with the predictions of low–temperature analytic theory (line). All simulations were performed by my collaborator Dr. Rico Pohle with parameters Eq. (3.87), for a cluster with linear dimension $L = 96$ ($N = 9216$ spins), at $\mathrm{T} \approx 0.03$, using the u3MC scheme described in Section 2.6.1. Figures are reproduced from [201].

Structure factors obtained from simulations have all been divided by temperature, T. Considering $S_\lambda^{MC}(\mathbf{q})/T$ allows to extract their leading temperature dependence. However, the Bragg peak will show up more pronounced due to the division by T. In the case of the structure factors obtained analytically, $S_\lambda^{\mathsf{CL}}(\mathbf{q})$, in order to only account for the terms linear in temperature, we only consider $S_\lambda^{\mathsf{CL}}(\mathbf{q} \neq 0)$, This implies that we voluntarily disregard the Bragg peak and contributions due to ground state fluctuations. We then simply plot the terms linear in temperature. For instance, for

the quadrupole structure factors given in Eq. (3.89), we consider

$$S_{\rm Q}(\mathbf{q} \neq 0) = \frac{1}{T} 8 k_B T \frac{1}{\omega^+_{\mathbf{q}}} = 8 k_B \frac{1}{\omega^+_{\mathbf{q}}} \ , \tag{3.110}$$

where we set $k_B = 1$.

In the FQ state, the Bragg peak and the contributions coming from ground state fluctuations arise only for $\mathbf{q} = 0$. Therefore, we only expect a discrepancy between the simulations and the analytical results at the origin $\mathbf{q} = 0$, due to the fact that in simulations, the Bragg peak depends on the lattice sites, and only becomes a Bragg peak in the thermodynamic limit $N \to \infty$, and obviously, because we simply neglected $\mathbf{q} = 0$ contribution for the analytical structure factor. Simulations were carried out for parameters consistent with a FQ ground state [Eq. (3.87)], at a temperature T ≈ 0.03, in a cluster of linear dimension $L = 96$ ($N = 9216$ spins).

Fig. 3.6 (a) shows results for the spin dipole equal–time structure factors $S_{\rm S}(\mathbf{q})/T$. We note that at low temperatures u3MC simulations results (points) are perfectly described by the low–temperature analytic prediction (solid line), given in Eq. (3.85). Even though fluctuations of dipole moments are suppressed in the FQ ground state at zero temperature, they take on a finite value at finite temperature, and contribute to a finite weight of the spin dipole equal–time structure factors as shown in Fig. 3.6 (a). For the structure factor associated with dipole moments, the perfect match between analytic and numeric results is due to the fact that no ground state fluctuations contribute nor any Bragg peak arises at $\mathbf{q} = 0$.

The broad peak in $S_{\rm S}(\mathbf{q})$ for $\mathbf{q} = \mathsf{K}$, which corresponds to the 3–sublattice ordering vector, is explained by the fact that due to the proximity of the FQ order with 3–sublattice antiferromagnetic order (AFM) (cf. Fig. 1.11 or Fig. 1.13), some remnant AFM correlations persists within the FQ phase at finite temperature, as discussed in Appendix E.1.1.

The quadrupolar structure factor $S_{\rm Q}(\mathbf{q})/T$ shows a divergence for $\mathbf{q} \to 0$ as illustrated in Fig. 3.6 (b). For the analytic results, this is simply due to the fact that Eq. (3.110) shows a $\mathbf{q}$–dependent contribution that diverges for $\mathbf{q} \to 0$, since $\omega^+_{\mathbf{q}=0} = 0$. This divergence is however canceled out exactly at $\mathbf{q} = 0$ by the fluctuations coming from the ground state [Eq. (3.89)], but they are not taken into account here. For the simulation result, the divergence for $\mathbf{q} \to 0$ has the same origin as in the analytical case. But at exactly $\mathbf{q} = 0$, the divergence occurs because of the Bragg peak. It is so pronounced that, for clarity reasons, the Bragg peak is not shown in Fig. 3.6 (b). This way the emphasis is held on the $\mathbf{q} \neq 0$ part of the spectrum. Once again, at low temperatures , results for $S_{\rm Q}(\mathbf{q})/T$ for u3Mc simulations (points) and prediction of the low–temperature analytic theory, Eq. (3.110), (solid line), agree perfectly for $\mathbf{q} \neq 0$.

Finally, in Fig. 3.6 (c), the structure factor for A–matrices $S_{\rm A}(\mathbf{q})$ is shown. Because it is sensitive to both quadrupolar and dipolar fluctuations, it exhibits both a diverging contribution for $\mathbf{q} \to 0$, and a small peak at $\mathbf{q} = \mathsf{K}$. Once again, at low temperatures and for $\mathbf{q} \neq 0$, we find a perfect agreement between u3MC simulation results for $S_{\rm A}(\mathbf{q})/T$ (points) and analytic results obtained from the low–temperature expansion of classical fluctuations, [Eq. (3.93)], (solid line).

From our study, we note that the analytical theory of thermal fluctuations and the

u3MC scheme developed in Section 2.6.1, agree perfectly at $\mathbf{q} \neq 0$. For $\mathbf{q} = 0$, we have shown, in our study of the ordered moment in Section 3.4.2, that the quadrupole structure factors from u3MC simulation and analytic theory also demonstrate perfect agreement at low temperatures. Combining these results for $S_\lambda^{\mathsf{CL}}(\mathbf{q})$, we confirm that our analytical theory of thermal fluctuations and the u3MC scheme developed in Section 2.6.1, are able to correctly describe classical correlations of spin–1 magnets at low temperature. As we will see in Chapter 5, these results will turn out to be important when exploring the quantum–classical correspondence between the quantum dynamics predicted by a quantum theory of bosonic excitations and the (semi–)classical dynamics of u3MD simulation scheme introduced in Section 2.6.2.

Lastly, the same numerical approach based on the u3MC scheme [Section 2.6.1] can be applied to different values of parameters J_1 and J_2 of the BBQ model [Eq. (2.72)]. This allows to characterize a classical finite temperature phase diagram of the BBQ model on the triangular lattice as shown in Fig. 1.13. On the analytic side, I here presented a detailed study of the classical thermodynamic properties of the FQ state. Similar investigations for the three other ordered phases, (FM, AFM, and AFQ), are also possible by following the same strategy as developed in this Chapter for the FQ phase or following the general prescription detailed Section 2.5, but go beyond the scope of this Thesis.

Chapter 4

Semi-Classical Dynamics of the FQ State of the BBQ Model on the Triangular Lattice

In this Chapter, I construct a quantum theory of fluctuations about the FQ order by following the analysis of the $u(3)$ formalism introduced in Section 2.5. To this end, we use the results obtained from expanding small fluctuations around the FQ state in Section 3.1.

In Section 4.1, I show how these fluctuations, introduced in Section 3.1, can be quantized to lead to a quantum theory of fluctuations for the FQ state and that the quantization reproduces results from multiple–Boson expansion exactly equivalent to a published "flavor–wave" theory [131].

In Section 4.2, I provide explicit results for the dynamical structure factors associated with spin–dipole moments, quadrupole moments, and the A–matrices.

Finally, in Section 4.3, we compare the results predicted by the quantum theory of fluctuations with u3MD simulations performed in the space of A–matrices as explained in Section 2.6.2. We start by showing the "raw" u3MD results in Section 4.3 and emphasize its discrepancy with prediction from quantum theory [Section 4.2]. This is resolved in the next Chapter, Chapter 5, where we dig deeper into the mechanisms of MD simulations and obtain a classical–quantum correspondence that allows us to correct the u3MD simulations results, restoring a perfect agreement with $T = 0$ quantum results.

4.1 Quantum Fluctuations

We start by showing how we can apply the formalism used to generate the fluctuations around an ordered ground state [Section 2.5] to a quantum description of its excitations. We will see that this can be achieved by requiring that the fluctuations satisfy bosonic commutation relations. This step is explained here, where we use results obtained from expanding fluctuations around the FQ ground state [Section 3.1].

In Section 3.1, we saw that we can fully describe the fluctuations about the FQ order using the 4 generators $\hat{\mathcal{A}}^1{}_2$, $\hat{\mathcal{A}}^3{}_2$, $\hat{\mathcal{A}}^2{}_1$, $\hat{\mathcal{A}}^2{}_3$, which are related by Eq. (2.49),

naturally forming conjugate pairs [Fig. 3.2]. As explained in Section 2.5, this implies that fluctuations can be parameterized through two pairs of real fields $(\phi^{1,2}, \phi^{2,1})$, and $(\phi^{2,3}, \phi^{3,2})$. In the quantum case, the fluctuations in each pair are related by Eq. (2.91). And we can interpret each pair as a creation/annihilation pair, giving a total of two bosons per site, as discussed in Section 2.5. Indeed, the low–energy dynamics for these orthogonal excitations are identified with the Goldstone modes associated with the symmetry breaking of the FQ ground state. The creation/annihilation pairs represent then integer spin excitations about the ordered ground state and are therefore bosonic.

Consequently, we can simply impose the quantization of the fluctuations for each pair through the bosonic commutation relations

$$[\phi_i^{2,1}, \phi_j^{1,2}] = \delta_{ij} \ , \tag{4.1a}$$

$$[\phi_i^{2,3}, \phi_j^{3,2}] = \delta_{ij} \ . \tag{4.1b}$$

Using Eq. (2.91) explicitly, and considering how these fluctuations are linked with the image of the ground state after generating the fluctuations [Eq. (3.9)] each field $\phi^{\alpha,\beta}$ is associated with a creation or annihilation operator according to

$$\phi_i^{1,2} = (\phi_i^{2,1})^\dagger = -i\hat{\mathrm{a}}_i^\dagger \ , \tag{4.2a}$$

$$\phi_i^{2,3} = (\phi_i^{3,2})^\dagger = \ i\hat{\mathrm{b}}_i \ . \tag{4.2b}$$

In this basis, the state given by Eq. (3.9) which describes the effect of the fluctuations about the ground state vector $\mathbf{d}^{\mathsf{FQ}}$ [Eq. (3.1)]

$$\mathbf{d}_i = \begin{pmatrix} \hat{\mathrm{a}}_i^\dagger \\ 1 - \frac{1}{2}\hat{\mathrm{a}}_i^\dagger\hat{\mathrm{a}}_i - \frac{1}{2}\hat{\mathrm{b}}_i^\dagger\hat{\mathrm{b}}_i \\ \hat{\mathrm{b}}_i^\dagger \end{pmatrix} \ , \tag{4.3}$$

where we applied the arguments discussed at the end of Section 2.5, (i.e. Eq. (2.113) but with the permutation of the basis states).

In terms of the quantized fluctuations, the A–matrix state, given by Eq. (3.10) and describing the fluctuations about the state $|y_i\rangle$ [Eq. (3.4)], can be written as

$$\hat{\mathbf{A}}_i = \begin{pmatrix} \hat{\mathrm{a}}_i^\dagger\hat{\mathrm{a}}_i & \hat{\mathrm{a}}_i^\dagger & \hat{\mathrm{a}}_i^\dagger\hat{\mathrm{b}}_i \\ \hat{\mathrm{a}}_i & 1 - \hat{\mathrm{a}}_i^\dagger\hat{\mathrm{a}}_i - \hat{\mathrm{b}}_i^\dagger\hat{\mathrm{b}}_i & \hat{\mathrm{b}}_i \\ \hat{\mathrm{b}}_i^\dagger\hat{\mathrm{a}}_i & \hat{\mathrm{b}}_i^\dagger & \hat{\mathrm{b}}_i^\dagger\hat{\mathrm{b}}_i \end{pmatrix} \ , \tag{4.4}$$

and up to quadratic order in bosons, the BBQ model, Eq. (2.72), then becomes

$$\mathcal{H}'_{\mathsf{BBQ}} = E_0 + \frac{1}{2}\sum_{\mathbf{k}} \left[\hat{\mathbf{w}}_{\mathbf{k}}^\dagger M_{\mathbf{k}} \hat{\mathbf{w}}_{\mathbf{k}}\right] + \mathcal{O}(\vec{w}^4) \ , \tag{4.5}$$

with

$$\hat{\mathbf{w}}_{\mathbf{k}}^\dagger = \begin{pmatrix} \hat{\mathrm{a}}_{\mathbf{k}}^\dagger, & \hat{\mathrm{a}}_{-\mathbf{k}}, & \hat{\mathrm{b}}_{\mathbf{k}}^\dagger, & \hat{\mathrm{b}}_{-\mathbf{k}} \end{pmatrix} \ , \tag{4.6a}$$

and

$$\hat{\mathbf{w}}_{\mathbf{k}} = \begin{pmatrix} \hat{\mathrm{a}}_{\mathbf{k}} \\ \hat{\mathrm{a}}^{\dagger}_{-\mathbf{k}} \\ \hat{\mathrm{b}}_{\mathbf{k}} \\ \hat{\mathrm{b}}^{\dagger}_{-\mathbf{k}} \end{pmatrix} , \tag{4.6b}$$

where E_0 is the MF ground–state energy [Eq. (3.14)]. The matrix $M_{\mathbf{k}}$ governing the interactions of the fluctuations is the same as the one appearing in the classical theory [Eq. (3.13)] and is given by Eq. (3.16). The reasoning behind this is discussed at the end of Section 2.5.

The bosonic commutation relations [Eq. (4.2)], implies that

$$\left[\hat{\mathrm{w}}_{\mathbf{k}\alpha}, \hat{\mathrm{w}}^{\dagger\beta}_{\mathbf{q}}\right] = {\gamma_0}_{\alpha}{}^{\beta}\delta_{\mathbf{k},\mathbf{q}} , \tag{4.7}$$

where

$$\gamma_0 = \begin{pmatrix} 1 & 0 & 0 & 0 \\ 0 & -1 & 0 & 0 \\ 0 & 0 & 1 & 0 \\ 0 & 0 & 0 & -1 \end{pmatrix} . \tag{4.8}$$

And, as explained in Appendix C, it follows that the dispersion associated with these excitations can be found by solving the eigensystem

$$\gamma_0 M_{\mathbf{k}} u_{\mathbf{k},\lambda} = \epsilon_{\mathbf{k},\lambda} u_{\mathbf{k},\lambda} \qquad \lambda = 1, 2, 3, 4 , \tag{4.9}$$

with eigenvectors $u_{\lambda,\mathbf{k}}$, and associated eigenvalues given by $\epsilon_{\mathbf{k},\lambda}$. Solving Eq. (4.9) is equivalent to diagonalizing the matrix

$$\gamma_0 M_{\mathbf{k}} = \begin{pmatrix} A_{\mathbf{k}} & -B_{\mathbf{k}} & 0 & 0 \\ B_{\mathbf{k}} & -A_{\mathbf{k}} & 0 & 0 \\ 0 & 0 & A_{\mathbf{k}} & -B_{\mathbf{k}} \\ 0 & 0 & B_{\mathbf{k}} & -A_{\mathbf{k}} \end{pmatrix} , \tag{4.10}$$

where $A_{\mathbf{k}}$, $B_{\mathbf{k}}$ are given in Eq. (3.17). Diagonalizing $\gamma_0 M_{\mathbf{k}}$ can be performed numerically if needed. However, in our case, this is not necessary, and we can find an analytic solution. The corresponding eigenvalues read

$$\epsilon_{\mathbf{k},1} = -\epsilon_{\mathbf{k},2} = \epsilon_{\mathbf{k},3} = -\epsilon_{\mathbf{k},4} = +\sqrt{A_{\mathbf{k}}^2 - B_{\mathbf{k}}^2} , \tag{4.11}$$

where we note that only the two solutions with positive energy, $\epsilon_{\mathbf{k},1}$ and $\epsilon_{\mathbf{k},3}$ correspond to physical modes of the system. Indeed at zero temperature, negative modes solutions are forbidden as they correspond to the creations operators and would be associated with holes with energy lower than the ground state which are forbidden by construction. As expected, this implies that we have a total of two bosonic modes per site. Details about the calculation of these eigenvalues and associated bosonic excitations are provided in Appendix C, where we also explain that solving the quantum eigensystem,

Eq. (4.9), is equivalent to performing a generalized Bogoliubov transformation. The generalized Bogoliubov transformation consists in finding a new set of bosonic operators which diagonalize the Hamiltonian, Eq. (4.5), and allows for the correspondence between the bosons, [Eq. (4.2)], and Bogoliubov bosons.

The eigenvectors of the quantum eigensystem [Eq. (4.9)] associated with the eigenvalues [Eq. (4.11)] are given by

$$\hat{\mathbf{w}}_{\mathbf{k}}^{\dagger} = \frac{1}{\sqrt{\Delta_{\mathbf{k}}^2 - B_{\mathbf{k}}^2}} \begin{pmatrix} \Delta_{\mathbf{k}} & -B_{\mathbf{k}} & 0 & 0 \\ -B_{\mathbf{k}} & \Delta_{\mathbf{k}} & 0 & 0 \\ 0 & 0 & \Delta_{\mathbf{k}} & -B_{\mathbf{k}} \\ 0 & 0 & -B_{\mathbf{k}} & \Delta_{\mathbf{k}} \end{pmatrix} \hat{\mathbf{u}}_{\mathbf{k}}^{\dagger} , \tag{4.12}$$

where

$$\hat{\mathbf{w}}_{\mathbf{k}}^{\dagger} = \begin{pmatrix} \hat{\mathrm{a}}_{\mathbf{k}} \\ \hat{\mathrm{a}}_{-\mathbf{k}}^{\dagger} \\ \hat{\mathrm{b}}_{\mathbf{k}} \\ \hat{\mathrm{b}}_{-\mathbf{k}}^{\dagger} \end{pmatrix} \quad ; \quad \hat{\mathbf{u}}_{\mathbf{k}}^{\dagger} = \begin{pmatrix} \hat{\alpha}_{\mathbf{k}} \\ \hat{\alpha}_{-\mathbf{k}}^{\dagger} \\ \hat{\beta}_{\mathbf{k}} \\ \hat{\beta}_{-\mathbf{k}}^{\dagger} \end{pmatrix} \quad ; \quad \Delta_{\mathbf{k}} = A_{\mathbf{k}} + \sqrt{A_{\mathbf{k}}^2 - B_{\mathbf{k}}^2} . \tag{4.13}$$

By construction, the new set of Bogoliubov operators follow bosonic commutation rules

$$[\hat{\alpha}_{\mathbf{k}}, \hat{\alpha}_{\mathbf{k}'}^{\dagger}] = [\hat{\beta}_{\mathbf{k}}, \hat{\beta}_{\mathbf{k}'}^{\dagger}] = \delta_{\mathbf{k}\mathbf{k}'} , \tag{4.14}$$

and diagonalize the Hamiltonian Eq. (4.5). Indeed, in this new basis, the Hamiltonian reads

$$\mathcal{H}'_{\mathsf{BBQ}} \;=\; E_0 + \Delta E_0 + \sum_{\mathbf{k}} \epsilon(\mathbf{k}) \left[\hat{\alpha}_{\mathbf{k}}^{\dagger} \hat{\alpha}_{\mathbf{k}} + \hat{\beta}_{\mathbf{k}}^{\dagger} \hat{\beta}_{\mathbf{k}} \right] + [\text{higher order terms}] , \tag{4.15}$$

where

$$\epsilon(\mathbf{k}) = \epsilon_{\mathbf{k},1} = \epsilon_{\mathbf{k},3} = \sqrt{A_{\mathbf{k}}^2 - B_{\mathbf{k}}^2} , \tag{4.16}$$

and

$$\Delta E_0 \;=\; \sum_{\mathbf{k}} A_{\mathbf{k}} + \epsilon(\mathbf{k}) , \tag{4.17}$$

represents the contribution of the Bogoliubov ground state energy and E_0 is the MF ground state energy given in Eq. (3.14). We emphasize that in this form, this result is exactly equivalent to published results found using a multi-boson approach to the FQ order for the BBQ model [131, 183].

4.1.1 Quantum Thermodynamic Quantities

In analogy to our classical analysis in Chapter 3, we give here the expression of the free energy within the quantum theory of fluctuations. We consider the BBQ Hamiltonian in terms of Bogoliubov bosons given in Eq. (4.15), since its diagonal form makes the calculation much easier.

The canonical partition function for a quantum system is defined

$$Z = \mathrm{Tr}\left[e^{-\beta\hat{\mathcal{H}}}\right] , \tag{4.18}$$

where β is the inverse temperature given by Eq. (3.39), and $\hat{\mathcal{H}}$ is the operator Hamiltonian.

For quantum excitations of a FQ state of the BBQ model, its corresponding partition function yields

$$\begin{aligned} Z_0^{\mathsf{QM}} &= \mathrm{Tr}\left[e^{-\beta\mathcal{H}'_{\mathsf{BBQ}}}\right] \\ &= \mathrm{Tr}\left[e^{-\beta E_0 - \beta\Delta E_0}\prod_{\mathbf{k}} e^{-\beta\epsilon_{\mathbf{k}}\left[\hat{\alpha}^\dagger_{\mathbf{k}}\hat{\alpha}_{\mathbf{k}} + \hat{\beta}^\dagger_{\mathbf{k}}\hat{\beta}_{\mathbf{k}}\right]}\right] . \end{aligned} \tag{4.19}$$

Because the bosons $\hat{\alpha}^\dagger_{\mathbf{k}}$ and $\hat{\beta}^\dagger_{\mathbf{k}}$ follow bosonic commutation rules and commute between each other, the trace can be evaluated onto the Fock spaces $\{|n_\alpha\rangle\}$ and $\{|n_\beta\rangle\}$ associated with each Bogoliubov boson. We obtain

$$Z_0^{\mathsf{QM}} = e^{-\beta E_0 - \beta\Delta E_0}\prod_{\mathbf{k}} \frac{1}{1-e^{-\beta\epsilon_{\mathbf{k}}}}\frac{1}{1-e^{-\beta\epsilon_{\mathbf{k}}}} . \tag{4.20}$$

The corresponding free energy is then given by

$$\begin{aligned} F_0^{\mathsf{QM}} &= -\frac{\log(Z_0^{\mathsf{QM}})}{\beta} \\ &= E_0 + \Delta E_0 + \frac{1}{\beta}\sum_{\mathbf{k}}\log(1-e^{-\beta\epsilon_{\mathbf{k}}}) + \frac{1}{\beta}\sum_{\mathbf{k}}\log(1-e^{-\beta\epsilon_{\mathbf{k}}}) , \end{aligned} \tag{4.21}$$

where we keep the contributions coming from the different bosons in separate terms. The energy is given by

$$\begin{aligned} E_0^{\mathsf{QM}} &= -\frac{\partial\log(Z_0^{\mathsf{QM}})}{\partial\beta} \\ &= E_0 + \Delta E_0 + \sum_{\mathbf{k}}\frac{\epsilon_{\mathbf{k}}e^{-\beta\epsilon_{\mathbf{k}}}}{1-e^{-\beta\epsilon_{\mathbf{k}}}} + \sum_{\mathbf{k}}\frac{\epsilon_{\mathbf{k}}e^{-\beta\epsilon_{\mathbf{k}}}}{1-e^{-\beta\epsilon_{\mathbf{k}}}} \\ &= E_0 + \Delta E_0 + \sum_{\mathbf{k}}\epsilon_{\mathbf{k}}n_{\mathsf{BE}}(\epsilon_{\mathbf{k}}) + \sum_{\mathbf{k}}\epsilon_{\mathbf{k}}n_{\mathsf{BE}}(\epsilon_{\mathbf{k}}) , \end{aligned} \tag{4.22}$$

where $n_{\mathsf{BE}}(\epsilon_{\mathbf{k}})$ is the Bose–Einstein distribution

$$n_{\mathsf{BE}}(\epsilon_{\mathbf{k}}) = \frac{1}{e^{\beta\epsilon_{\mathbf{k}}}-1} . \tag{4.23}$$

At low temperature $\beta \gg \epsilon_{\mathbf{k}}$, we can approximate $n_{\mathsf{BE}}(\epsilon_{\mathbf{k}}) \simeq e^{-\beta\epsilon_{\mathbf{k}}}$, and the energy by

$$E_0^{\mathsf{QM}} \simeq E_0 + \Delta E_0 + \underbrace{\sum_{\mathbf{k}} \epsilon_{\mathbf{k}} e^{-\beta\epsilon_{\mathbf{k}}} + \sum_{\mathbf{k}} \epsilon_{\mathbf{k}} e^{-\beta\epsilon_{\mathbf{k}}}}_{\text{very small}} \ . \tag{4.24}$$

We see that, at low temperature, the energy is given by the ground state, and the fluctuations can contribute with $\epsilon_{\mathbf{k}}$ but that only happens with a probability $e^{-\beta\epsilon_{\mathbf{k}}}$ that becomes exponentially small temperature is decreased.

In the asymptotic high temperature limit of the quantum theory, $\beta \ll \epsilon_{\mathbf{k}}$, we can Taylor expand the exponential $e^{\beta\epsilon_{\mathbf{k}}}$, and approximate

$$n_{\mathsf{BE}}(\epsilon_{\mathbf{k}}) \simeq \frac{1}{\beta\epsilon_{\mathbf{k}}}(1 + \mathcal{O}(\beta\epsilon_{\mathbf{k}})) \ . \tag{4.25}$$

We obtain

$$\begin{aligned} E_0^{\mathsf{QM}} &\simeq E_0 + \Delta E_0 + \sum_{\mathbf{k}} \epsilon_{\mathbf{k}} \frac{1}{\beta\epsilon_{\mathbf{k}}}(1 + \mathcal{O}(\beta\epsilon_{\mathbf{k}})) + \sum_{\mathbf{k}} \epsilon_{\mathbf{k}} \frac{1}{\beta\epsilon_{\mathbf{k}}}(1 + \mathcal{O}(\beta\epsilon_{\mathbf{k}})) \\ &\simeq E_0 + \Delta E_0 + \sum_{\mathbf{k}} k_B T + \sum_{\mathbf{k}} k_B T + \mathcal{O}(\frac{\epsilon_{\mathbf{k}}}{k_B T}) \qquad (4.26) \\ &\simeq E_0 + \Delta E_0 + 2N k_B T \ , \qquad (4.27) \end{aligned}$$

where we use the expression for the inverse temperature β given in Eq. (3.39). We see that in the high temperature regime, for the quantum case, each fluctuation contributes $k_B T$ to the energy per site, for a total of $2k_B T$, such that the energy of the contribution of two quantum fluctuations tends to the low-T classical energy of the contribution of the four classical fluctuations [Eq. (3.45b)]. The specific heat can be calculated according to

$$C_v = \left(\frac{\partial E_0}{\partial T}\right)_V \ , \tag{4.28}$$

Using Eq. (4.22), we obtain,

$$\begin{aligned} C_v &= 2\sum_{\mathbf{k}} \epsilon_{\mathbf{k}} \frac{\partial n_{\mathsf{BE}}(\epsilon_{\mathbf{k}})}{\partial T} \\ &= 2\sum_{\mathbf{k}} k_B (\frac{\epsilon_{\mathbf{k}}}{\mathbf{k}_B T})^2 \frac{e^{\beta\epsilon_{\mathbf{k}}}}{(e^{\beta\epsilon_{\mathbf{k}}} - 1)^2} \ , \end{aligned} \tag{4.29}$$

where we added up the contributions coming from the two quantum excitations. At low temperature $\beta \gg \epsilon_{\mathbf{k}}$, we obtain

$$C_v \simeq 2\sum_{\mathbf{k}} k_B (\frac{\epsilon_{\mathbf{k}}}{\mathbf{k}_B T})^2 e^{-\beta\epsilon_{\mathbf{k}}} \ . \tag{4.30}$$

In order to calculate the leading order in temperature, we can then transform the sum over the reciprocal vectors $\mathbf{k}$ of the triangular lattice as an integral according to

Eq. (H.3) and separate in two a long wavelength, small $\mathbf{k}$ contribution and a short wavelength, big $\mathbf{k}$ contribution. In the long wavelength part, we can further approximate the dispersion relation $\epsilon_{\mathbf{k}} \simeq vk$, where v is the speed of the linearly dispersive Goldstone modes, which approximation is valid in the limit of small $\mathbf{k}$ values. The short wavelength is a contribution that vanishes exponentially for $\beta \gg \epsilon_{\mathbf{k}}$.

$$\begin{aligned} C_v &\simeq 2 * \frac{\sqrt{3}}{8\pi} 2\pi \int_0^{\Lambda} k (\frac{\epsilon_{\mathbf{k}}}{\mathbf{k}_B T})^2 k_B e^{-\beta\epsilon_{\mathbf{k}}} \mathrm{d}k + 2\int_{\Lambda}^{\infty} 2\pi k k_B (\frac{\epsilon_{\mathbf{k}}}{\mathbf{k}_B T})^2 e^{-\beta\epsilon_{\mathbf{k}}} \mathrm{d}k \\ &\simeq \frac{\sqrt{3}}{\pi} \int_0^{\Lambda} k_B k (\frac{vk}{\mathbf{k}_B T})^2 e^{-\beta v k} \mathrm{d}k \simeq \frac{\sqrt{3}}{\pi^2} \int_0^{\Lambda} \frac{k_B^2 T}{v} (\frac{vk}{\mathbf{k}_B T})^3 e^{-\beta v k} \mathrm{d}k \\ &\simeq \frac{\sqrt{3}}{\pi} \frac{k_B^3 T^2}{v^2} \underbrace{\int_0^{\infty} x^3 e^{-x} \mathrm{d}x}_{3\Gamma[3]} \simeq \frac{3\sqrt{3}\Gamma[3]}{\pi} k_B (\frac{k_B T}{v})^2 \, . \end{aligned} \tag{4.31}$$

We see that the specific heat in the low–temperature expansion of the non–interacting quantum theory shows a quadratic dependence with respect to temperature. This behaviour can be explained in terms of the two linearly dispersive Goldstone modes arising from the continuous symmetry breaking of the FQ state. This result is consistent with an earlier derivation for the J_1–J_2 antiferromagnetic Heisenberg model on the square lattice [217].

The quadratic term at low temperature is consistent with Quantum Monte Carlo simulations obtained for the FQ state of the BBQ model [255]. Indeed fits to QMC confirm the T^2 behaviour and provide a velocity v consistent with the analytical value obtained here [Eq. (4.16)] or from multi–bosons theory [131]. We note that an interaction theory predicts an additional term scaling as $T\ln(T)$ [19], but QMC might not be able to go to low enough temperature to capture this behaviour.

In the high temperature limit, $\beta \ll \epsilon_{\mathbf{k}}$, the specific heat yields

$$\begin{aligned} C_v &\simeq 2\sum_{\mathbf{k}} k_B (\frac{\epsilon_{\mathbf{k}}}{\mathbf{k}_B T})^2 \frac{1+\beta\epsilon_{\mathbf{k}}}{(\beta\epsilon_{\mathbf{k}})^2} \\ &\simeq 2\sum_{\mathbf{k}} k_B (1+\beta\epsilon_{\mathbf{k}}) \\ &\simeq 2\sum_{\mathbf{k}} k_B + \mathcal{O}(\frac{\epsilon_{\mathbf{k}}}{k_B T}) \, , \end{aligned} \tag{4.32}$$

where we see that each quantum excitation contributes k_B to the specific heat per site for a total of $2k_B$, the quantum theory in the high temperature limit reproduces the classical case in the limit $T \to 0$ [Eq. (3.47)].

4.1.2 Comparison of Dispersion Relations Between Quantum and Classical Theories of Fluctuations

In Fig. 4.1, we compare results obtained from a $T = 0$ quantum theory of fluctuations about a ferroquadrupolar (FQ) ground state with its corresponding classical treatment introduced in Section 3.2, where all the results have been convoluted with a Gaussian

in frequency of FWHM = 0.35 J.

First, we observe that the dispersion relations between quantum and classical theories are completely different, implied by the fact that the dispersion relations correspond to eigenvalues associated with different matrices. In the classical theory, we simply diagonalize the matrix $M_{\mathbf{k}}$ given in Eq. (3.16). While in the quantum case, we diagonalize the matrix $\gamma_0 M_{\mathbf{k}}$ given in Eq. (4.10), in order to ensure that the fluctuations follow bosonic commutation rules [Eq. (4.7)].

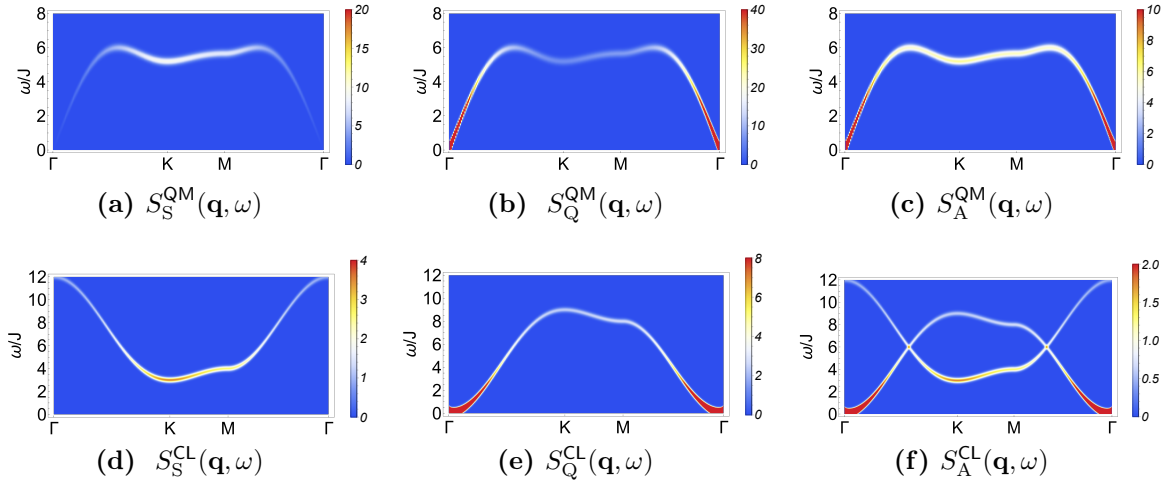

(a) $S_{\mathrm{S}}^{\mathsf{QM}}(\mathbf{q},\omega)$ (b) $S_{\mathrm{Q}}^{\mathsf{QM}}(\mathbf{q},\omega)$ (c) $S_{\mathrm{A}}^{\mathsf{QM}}(\mathbf{q},\omega)$

(d) $S_{\mathrm{S}}^{\mathsf{CL}}(\mathbf{q},\omega)$ (e) $S_{\mathrm{Q}}^{\mathsf{CL}}(\mathbf{q},\omega)$ (f) $S_{\mathrm{A}}^{\mathsf{CL}}(\mathbf{q},\omega)$

Figure 4.1: Quantum excitations about a ferroquadrupolar (FQ) ground state of the BBQ model [Eq. (2.72)] on the triangular lattice as resolved in quantum dynamical structure factors compared with equivalent results obtained from a classical theory. (a) Dynamcial dipole structure factor $S_{\mathrm{S}}^{\mathsf{QM}}(\mathbf{q},\omega)$ [Eq. (4.71)], within $T = 0$ quantum theory of Section 3.2. (b) Equivalent results for the quadrupole structure factor, $S_{\mathrm{Q}}^{\mathsf{QM}}(\mathbf{q},\omega)$ [Eq. (4.78)]. (c) Equivalent results for the A–matrix structure factor, $S_{\mathrm{A}}^{\mathsf{QM}}(\mathbf{q},\omega)$ [Eq. (4.86)]. (d) Spectral representation of dipole structure factor, $S_{\mathrm{S}}^{\mathsf{CL}}(\mathbf{q},\omega)$ [Eq. (3.86)], within the classical low–temperature expansion developed in Section 3.2, at temperature $T = J$. (e) Equivalent result the for the quadrupole structure factor, $S_{\mathrm{Q}}^{\mathsf{CL}}(\mathbf{q},\omega)$ [Eq. (3.91)]. (f) Equivalent results for the A–matrix structure factor, $S_{\mathrm{A}}^{\mathsf{CL}}(\mathbf{q},\omega)$ [Eq. (3.94)]. We also note that the quantum dispersion corresponds to the geometrical mean of the two classical dispersions for dipolar and quadrupolar excitations Eq. (4.33). All results are shown for parameters Eq. (3.87), and have been convoluted with Gaussian of FWHM 0.35 J. Bragg peaks have been omitted for simplicity. Details of the quantum theory are given in Section 4.1.

Additionally, in the classical case, we obtained two doubly-degenerate modes for a total of four modes associated with the four real orthogonal fluctuations. However, in the quantum case, these four fluctuations are combined into two bosonic fields through Eq. (2.91). When diagonalizing the matrix $\gamma_0 M_{\mathbf{k}}$, we did obtain four eigenvalues [Eq. (4.11)], but only two of them corresponding to the creations operators were physical, while the other two were non–physical and corresponded to negative energies associated with the annihilation operators. This led to a single doubly–degenerate dispersion relation for a total of two quantum modes associated with the two bosonic

fields. We also note that this results in the single doubly–degenerated quantum dispersion being expressed as the mean square to the two doubly-degenerate classical modes

$$\epsilon_{\mathbf{k}} = \sqrt{\omega^{+}_{\mathbf{k}}\omega^{-}_{\mathbf{k}}} \ . \tag{4.33}$$

This is consistent with the fluctuation–dissipation theorem which states that any mode ω contributes $\frac{1}{2}k_BT\log(\omega)$ to the classical free energy. This can be seen by considering the classical free energy given in Eq. (3.42).

$$\begin{aligned} F_0^{\mathsf{CL}} &= -\frac{\log(Z_0)}{\beta} \\ &= E_0 + \frac{k_BT}{2}\sum_{\mathbf{k}}\sum_{\lambda=1}^{N_\lambda}\left[\log(\omega_{\mathbf{k},\lambda}) - \log(2\pi k_{\mathsf{B}}T)\right] + \mathcal{O}(T^2) \ , \end{aligned} \tag{4.34}$$

where it is clear that all the four classical modes $\omega_{\mathbf{k},\lambda}$ where $\lambda = 1,2,3,4$ contribute $\frac{1}{2}k_BT\log(\omega_{\mathbf{k},\lambda})$. Considering the properties of the log function and Eq. (3.22), as well as Eq. (4.33), we see that we can rewrite F^{CL} as

$$\begin{aligned} F_0^{\mathsf{CL}} \sim \frac{k_BT}{2}\sum_{\mathbf{k}}\sum_{\lambda=1}^{N_\lambda}\log(\omega_{\mathbf{k},\lambda}) &= \frac{k_BT}{2}\sum_{\mathbf{k}}\log((\omega^{+}_{\mathbf{k}}\omega^{-}_{\mathbf{k}})^2) \\ &= \frac{k_BT}{2}\sum_{\mathbf{k}}\log((\epsilon_{\mathbf{k}})(\epsilon_{\mathbf{k}})) \\ &= \frac{k_BT}{2}\sum_{\mathbf{k}}\left[\log(\epsilon_{\mathbf{k}}) + \log(\epsilon_{\mathbf{k}})\right] \ , \end{aligned} \tag{4.35}$$

where we see that each of the two quantum modes also contribute $\frac{1}{2}k_BT\log(\epsilon_{\mathbf{k}})$. Thus, the four classical modes combine as two quantum modes such that the classical free energy is given by the same final expression, regardless of whether we consider the four classical modes or the two quantum ones.

The structure factors within the $T = 0$ quantum theory are derived in the next Section, Section 4.2, and their comparison with equivalent results obtained within classical theory is discussed later in Section 4.2.7.

4.2 Dynamical Structure Factors Within Zero–Temperature Quantum Theory

We now turn to investigate the dynamical properties of the FQ phase of the BBQ model [Eq. (1.48)]. For this, we calculate the dynamical structure factors which characterize the excitations about the FQ order. Dynamical structure factors are defined by

$$S_{\mathrm{O}}^{\mathsf{QM}}(\mathbf{q},\omega) = \int_{-\infty}^{\infty}\frac{\mathrm{d}t}{2\pi}e^{i\omega t}\sum_{\alpha,\beta}\langle\hat{O}^{\alpha}_{\mathbf{q},\beta}(t)\hat{O}^{\beta}_{-\mathbf{q},\alpha}(0)\rangle \ , \tag{4.36}$$

where

$$\hat{O}^{\alpha}_{\mathbf{q},\beta} = \frac{1}{\sqrt{N}} \hat{O}^{\alpha}_{i,\beta} e^{i\mathbf{q}\mathbf{r}_i} \ , \tag{4.37}$$

and the operator $\hat{O}^{\alpha}{}_{\beta}$ can describe dipole moments, $\hat{\mathrm{S}}^{\mu}$; quadrupole moments, $\hat{\mathrm{Q}}^{\mu\nu}$; or $u(3)$ A-matrices, $\hat{\mathcal{A}}^{\mu}{}_{\nu}$.

In analogy with Section 3.3.3, we divide the computation of the dynamical structure factors into two parts. Both of these approaches are generalized in such a way that we can use them to calculate structure factors for dipole moments, quadrupole moments, and A-matrices.

We divide the structure factors according to two different contributions to the structure factors: the dynamics of the excitations and the contribution of the ground state and zero–point energy

$$S^{\mathsf{QM}}_{\mathrm{O}}(\mathbf{q},\omega) = S^{\mathsf{EX}}_{\mathrm{O}}(\mathbf{q},\omega) + S^{\mathsf{GS}}_{\mathrm{O}}(\mathbf{q}=0)\delta(\omega) \ , \tag{4.38}$$

where $S^{\mathsf{EX}}_{\mathrm{O}}(\mathbf{q},\omega)$ represents the dynamical structure factors associated with the bosonic excitations and $S^{\mathsf{GS}}_{\mathrm{O}}(\mathbf{q}=0)\delta(\omega)$ accounts for the static contribution of the ground state and zero–point energy of the Bogoliubov excitations.

Accordingly, in Section 4.2.1, we derive a generalized form of the dynamical structure factors $S^{\mathsf{EX}}_{\mathrm{O}}(\mathbf{q},\omega)$ at finite energy ($\omega > 0$) and for arbitrary values of reciprocal lattice vectors $\mathbf{q}$. This is obtained by direct calculations of matrix elements within the FQ ground state, assuming transition to the basis of the 1$^{\mathrm{st}}$ excited states which are described by our bosons. We also compute static structure factors $S^{\mathsf{GS}}_{\mathrm{O}}(\mathbf{q}=0)\delta(\omega)$ ($\omega = 0$ and $\mathbf{q} = 0$) which are calculated through functional derivatives of the free energy, as explained in detail in Section 4.2.2. These encompass the contributions from the ground state and zero–point energy.

In the remaining part of the section, we show explicit computations at $T = 0$ specifically for the structure factors associated with dipole moments, quadrupole moments, and A-matrices, by using the results obtained in Section 4.2.1 and in Section 4.2.2. Subsequently, we will use these for the derivation of the relationship between quantum and classical results [Section 5.1] and for comparison with numerics [Section 3.4].

4.2.1 Quantum Structure Factors at General Values of q

Here, we derive how to calculate the structure factor $S^{\mathsf{EX}}_{\mathrm{O}}(\mathbf{q},\omega)$ at finite energy for an observable $\hat{O}^{\alpha}_{\mathbf{q},\beta}$. The definition of the structure factor is given by Eq. (4.36) and its components by

$$S^{\mathsf{QM}}_{\mathrm{O}}(\mathbf{q},\omega)^{\alpha\mu}_{\beta\nu} = \int_{-\infty}^{\infty} \frac{\mathrm{d}t}{2\pi} e^{i\omega t} \langle \hat{O}^{\alpha}_{\mathbf{q},\beta}(t) \hat{O}^{\mu}_{-\mathbf{q},\nu}(0) \rangle \ , \tag{4.39}$$

where in our case, the averages $\langle \hat{O}^{\alpha}_{\mathbf{q},\beta}(t) \hat{O}^{\mu}_{-\mathbf{q},\nu}(0) \rangle$ are taken on the ground state. We can rewrite the time dependency of $\hat{O}^{\alpha}_{\mathbf{q},\beta}(t)$ in the Heisenberg picture using the time evolution operator, and we obtain

$$\hat{O}^{\alpha}_{\mathbf{q},\beta}(t) = e^{\frac{i\hat{\mathcal{H}}t}{\hbar}} \hat{O}^{\alpha}_{\mathbf{q},\beta}(0) e^{\frac{-i\hat{\mathcal{H}}t}{\hbar}} \ . \tag{4.40}$$

For a complete basis $\{|\nu\rangle\}$ of Hilbert space, the closure relation holds

$$\sum_{\nu} |\nu\rangle\langle\nu| = 1 \, . \tag{4.41}$$

Using Eq. (4.40) and inserting the closure relation, Eq. (4.41), in Eq. (4.39) twice and considering only finite energy contribution, we obtain

$$\begin{aligned} S_{\mathrm{O}\ \beta\mu}^{\mathsf{EX}\,\alpha\mu}(\mathbf{q},\omega) &= \int_{-\infty}^{\infty} \frac{\mathrm{d}t}{2\pi} e^{i\omega t} \langle e^{\frac{i\hat{\mathcal{H}}t}{\hbar}} \sum_{\nu} |\nu\rangle\langle\nu| \hat{O}^{\alpha}_{\mathbf{q},\beta}(0) \sum_{\mu} |\mu\rangle\langle\mu| e^{\frac{-i\hat{\mathcal{H}}t}{\hbar}} \hat{O}^{\mu}_{-\mathbf{q},\nu}(0)\rangle \\ &= \sum_{\mu} \langle 0|\hat{O}^{\alpha}_{\mathbf{q},\beta}(0)|\mu\rangle\langle\mu|\hat{O}^{\mu}_{-\mathbf{q},\nu}(0)|0\rangle \delta(\omega - \epsilon_{\mu}) \, , \end{aligned} \tag{4.42}$$

where we assume that $|\nu\rangle$ is an eigenstate of the Hamiltonian of energy $E_{\nu} = \hbar\epsilon_{\nu}$ and where we have used

$$\begin{aligned} e^{\frac{i\hat{\mathcal{H}}t}{\hbar}}|\nu\rangle &= \sum_{n=0}^{\infty} \frac{(i\hat{\mathcal{H}}t)^n}{n}|\nu\rangle = \sum_{n=0}^{\infty} \frac{(iE_{\nu}t)^n}{n}|\nu\rangle \\ &= e^{\frac{iE_{\nu}t}{\hbar}}|\nu\rangle = e^{i\epsilon_{\nu}t}|\nu\rangle \, . \end{aligned} \tag{4.43}$$

In order to compute Eq. (4.42), we first note that, in our case, the excited states for all values of $\mathbf{k}$

$$|\alpha_{\mathbf{k}}\rangle = \hat{\alpha}^{\dagger}_{\mathbf{k}}|0_{\alpha}\rangle \, , \tag{4.44}$$

$$|\beta_{\mathbf{k}}\rangle = \hat{\beta}^{\dagger}_{\mathbf{k}}|0_{\beta}\rangle \, , \tag{4.45}$$

form a complete basis, where $|0_{\alpha}\rangle$ is the Bogoliubov ground state for the $\hat{\alpha}$ bosons, i.e., $\hat{\alpha}_{\mathbf{k}}|0_{\alpha}\rangle = 0$, and similarly for the $\hat{\beta}$ bosons. Since the Hilbert space consists of the direct product $|\alpha\rangle \oplus |\beta\rangle$, we can replace

$$\sum_{\mu} |\mu\rangle\langle\mu| \to \sum_{\mathbf{k}} \hat{\alpha}^{\dagger}_{\mathbf{k}}|0_{\alpha}\rangle\langle 0_{\alpha}|\hat{\alpha}_{\mathbf{k}} + \sum_{\mathbf{k}} \hat{\beta}^{\dagger}_{\mathbf{k}}|0_{\beta}\rangle\langle 0_{\beta}|\hat{\beta}_{\mathbf{k}} = 1 \tag{4.46}$$

in Eq. (4.42). We note that by replacing Eq. (4.41) by Eq. (4.46) in Eq. (4.42), we account for the 1$^{\mathrm{st}}$ excited states, and we therefore do not take into account the ground state and zero-point energy contribution to the structure factor. The ground state and zero-point energy only contribute at $\mathbf{q} = 0$ and $\omega = 0$. This is why it is expressed by a separate term $S_{\mathrm{O}}^{\mathsf{GS}}(\mathbf{q} = 0, \omega)$ in Eq. (4.38). We present how to calculate it in Section 4.2.2 below.

Finally, in order to compute Eq. (4.42), we need to express the operators $\hat{O}^{\alpha}_{\mathbf{q},\beta}$ in terms of the Bogoliubov bosons using Eq. (4.12). Then by inserting Eq. (4.46) in Eq. (4.42), the matrix elements are easily computed.

4.2.2 Quantum Structure Factors: Contribution of the Ground State at $\mathbf{q} = 0$

Here we present the zero-temperature correction to the ground state and the zero-point energy fluctuations' contribution to the quantum structure factors, which is expected to happen at $\mathbf{q} = 0$ and $\omega = 0$

$$S_{\mathrm{O}}^{\mathsf{GS}}(\mathbf{q} = 0)\delta(\omega) \; . \tag{4.47}$$

We, therefore, consider the zero–temperature quantum structure factor at $\mathbf{q} = 0$ to be given by

$$S_{\mathrm{O}}^{\mathsf{GS}}(\mathbf{q} = 0) = \sum_{\alpha\beta} \langle \hat{O}^{\alpha}_{\mathbf{q}=0,\beta} \hat{O}^{\beta}_{\mathbf{q}=0,\alpha} \rangle_{T=0} \; . \tag{4.48}$$

Calculating the contribution of the ground state and the zero-point energy fluctuations to the zero–temperature quantum structure factor can be achieved by adding a source term to the BBQ Hamiltonian that includes a fictitious field $\mathbf{h}$ coupled to the spin moments, similarly to what we did for the classical case [see Section 3.3.3 and Section 3.3.4]. The structure factors can then be calculated by taking the appropriate derivative of the free energy with respect to the field $\mathbf{h}$.

We consider the total Hamiltonian to be given by Eq. (3.51), and the source term to be of the form given in Eq. (3.52). We can then rewrite the operators $\hat{O}^{\alpha}_{\mathbf{q}\beta}$ of Eq. (3.52) as a function of the fluctuations orthogonal to the FQ ground state [Eq. (3.2)]. Section 3.1 provides details on the creation of orthogonal fluctuations. Expanding the source term Hamiltonian [Eq. (3.52)] up to second order in bosons, Fourier transforming it and considering its contribution for $\mathbf{q} = 0$, we can assume that it takes the following form :

$$\Delta\mathcal{H}[\mathbf{h_q}] = C[\mathbf{h_{q=0}}] + \frac{1}{2}\sum_{\mathbf{k}} \left[\hat{\mathbf{w}}^{\dagger}_{\mathbf{k}} m_{\mathbf{k}}[\mathbf{h_{q=0}}] \hat{\mathbf{w}}_{\mathbf{k}} + \left(\mathbf{N}[\mathbf{h_k}]^T \hat{\mathbf{w}}_{\mathbf{k}} + \hat{\mathbf{w}}^{\dagger}_{\mathbf{k}} \mathbf{N}[\mathbf{h_k}] \right) \delta_{\mathbf{k},0} \right] \; , \tag{4.49}$$

where $C[\mathbf{h_{q=0}}]$ is the coefficient for the zeroth order term of the source term expanded in terms of the fluctuations orthogonal to the FQ ground state, $\hat{\mathbf{w}}_{\mathbf{k}}$ represents these fluctuations orthogonal to the FQ ground state and is given Eq. (4.6b), $m_{\mathbf{k}}[\mathbf{h_{q=0}}]$ represents the interaction matrix for second order terms in fluctuations and depends on $\mathbf{h_{q=0}}$, and where $\mathbf{N}[\mathbf{h_k}]^{\dagger}$ and $\mathbf{N}[\mathbf{h_k}]$ are the coefficients for the linear terms in fluctuations. By definition of the source term Hamiltonian [Eq. (3.52)], all the coefficients $C[\mathbf{h_{q=0}}]$, $\mathbf{N}_1[\mathbf{h_k}]^T$, $\mathbf{N}_2[\mathbf{h_k}]$, and $m_{\mathbf{k}}[\mathbf{h_{q=0}}]$ depend linearly on the fictitious field $\mathbf{h}$ and will be different when considering a dipole, quadrupole, or A-matrix moment as the source term [Eq. (3.52)].

Using Eq. (4.5) for the BBQ Hamiltonian, we can assume that the total Hamiltonian [Eq. (3.51)] in terms of the bosons then takes the following form

$$\mathcal{H} = E_0 + C[\mathbf{h_{q=0}}] + \frac{1}{2}\sum_{\mathbf{k}} \left[\hat{\mathbf{w}}^{\dagger}_{\mathbf{k}} M_{\mathbf{k}}[\mathbf{h_{q=0}}] \hat{\mathbf{w}}_{\mathbf{k}} + \left(\mathbf{N}[\mathbf{h_k}]^{\dagger} \hat{\mathbf{w}}_{\mathbf{k}} + \hat{\mathbf{w}}^{\dagger}_{\mathbf{k}} \mathbf{N}[\mathbf{h_k}] \right) \delta_{\mathbf{k},0} \right] \; , \tag{4.50}$$

where E_0 is the mean-field ground–state given in Eq. (3.14), and where $M_{\mathbf{k}}[\mathbf{h_{q=0}}]$ is the

interaction matrix for the total Hamiltonian. It includes contributions from the BBQ Hamiltonian and the source term $m_{\mathbf{k}}[\mathbf{h}_{\mathbf{q}=0}]$, and, therefore, depends on $\mathbf{h}_{\mathbf{q}=0}$.

Following the method described in Appendix C , we perform a Bogoliubov transformation in order to diagonalize the total Hamiltonian. We assume that the new Bogoliubov bosons $\hat{\mathbf{v}}_{\mathbf{k}}$,

$$\hat{\mathbf{v}}_{\mathbf{k}} = \begin{pmatrix} \hat{\alpha}_{\mathbf{k}} \\ \hat{\alpha}^{\dagger}_{-\mathbf{k}} \\ \hat{\beta}_{\mathbf{k}} \\ \hat{\beta}^{\dagger}_{-\mathbf{k}} \end{pmatrix} , \tag{4.51}$$

are given in terms of the bosons orthogonal to the FQ ground state $\hat{\mathbf{w}}_{\mathbf{k}}$ by Eq. (C.2). We can then assume that the total Hamiltonian in terms of the Bogoliubov bosons $\hat{\mathbf{v}}_{\mathbf{k}}$ becomes

$$\begin{aligned} \mathcal{H} =& E_0 + \Delta E_0[\mathbf{h}_{\mathbf{q}=0}] + C[\mathbf{h}_{\mathbf{q}=0}] \\ &+ \frac{1}{2}\sum_{\mathbf{k}} \Big[\epsilon_{\mathbf{k},\alpha}[\mathbf{h}_{\mathbf{q}=0}]\hat{\alpha}^{\dagger}_{\mathbf{k}}\hat{\alpha}_{\mathbf{k}} + \epsilon_{\mathbf{k},\beta}[\mathbf{h}_{\mathbf{q}=0}]\hat{\beta}^{\dagger}_{\mathbf{k}}\hat{\beta}_{\mathbf{k}} \quad + \left(\tilde{\mathbf{N}}[\mathbf{h}_{\mathbf{k}}]^{\dagger}\hat{\mathbf{v}}_{\mathbf{k}} + \hat{\mathbf{v}}^{\dagger}_{\mathbf{k}}\tilde{\mathbf{N}}[\mathbf{h}_{\mathbf{k}}]\right)\delta_{\mathbf{k},0}\Big] , \end{aligned} \tag{4.52}$$

where $\epsilon_{\mathbf{k},\alpha}[\mathbf{h}_{\mathbf{q}=0}]$ and $\epsilon_{\mathbf{k},\beta}[\mathbf{h}_{\mathbf{q}=0}]$ are the two physical eigenvalues obtained by diagonalizing $M_{\mathbf{k}}[\mathbf{h}_{\mathbf{q}=0}]$ [see Eq. (C.6)], where $\Delta E_0[\mathbf{h}_{\mathbf{q}=0}]$ is the ground state contribution of the Bogoluibov bosons and where

$$\begin{aligned} \tilde{\mathbf{N}}[\mathbf{h}_{\mathbf{k}}]^{\dagger} &= \mathbf{N}[\mathbf{h}_{\mathbf{k}}]^{\dagger}U^{-1} , \\ \tilde{\mathbf{N}}[\mathbf{h}_{\mathbf{k}}] &= U^{\dagger^{-1}}\mathbf{N}[\mathbf{h}_{\mathbf{k}}] . \end{aligned} \tag{4.53}$$

Here, U is the Bogoliubov matrix change defined by Eq. (C.2) and remains to be determined. We also note that U^{-1} (and $U^{\dagger^{-1}}$) can be calculated from Eq. (C.3).

The canonical partition function is defined according to Eq. (4.18). However in order to compute the partition function and the free energy, we want to get rid of the linear terms $\tilde{\mathbf{N}}[\mathbf{h}_{\mathbf{k}}]^{\dagger}$ and $\tilde{\mathbf{N}}[\mathbf{h}_{\mathbf{k}}]$, which only contribute for $\mathbf{k} = 0$. The partition function [Eq. (4.18)] is then the one of a set of independent harmonic oscillators for the $\mathbf{k} \neq 0$ terms, but still contains linear terms with respect to the bosons for $\mathbf{k} = 0$:

$$\begin{aligned} Z =& \mathrm{Tr}\Big[e^{-\beta E_0 - \beta\Delta E_0[\mathbf{h}_{\mathbf{q}=0}] - \beta C[\mathbf{h}_{\mathbf{q}=0}]} \\ &\times \prod_{\mathbf{k}\neq 0} \left(e^{-\beta\epsilon_{\mathbf{k},\alpha}[\mathbf{h}_{\mathbf{q}=0}]\hat{\alpha}^{\dagger}_{\mathbf{k}}\hat{\alpha}_{\mathbf{k}}}\right)\left(e^{\beta\epsilon_{\mathbf{k},\beta}[\mathbf{h}_{\mathbf{q}=0}]\hat{\beta}^{\dagger}_{\mathbf{k}}\hat{\beta}_{\mathbf{k}}}\right) \\ &\times \left(e^{-\frac{1}{2}\beta\epsilon_{\mathbf{k}=0,\alpha}[\mathbf{h}_{\mathbf{q}=0}]\hat{\alpha}^{\dagger}_{\mathbf{k}=0}\hat{\alpha}_{\mathbf{k}=0} - \frac{1}{2}\beta n_1[\mathbf{h}_{\mathbf{k}=0}]\hat{\alpha}^{\dagger}_{\mathbf{k}=0} - \frac{1}{2}\beta n_2[\mathbf{h}_{\mathbf{k}=0}]\hat{\alpha}_{\mathbf{k}=0}}\right) \\ &\times \left(e^{-\frac{1}{2}\beta\epsilon_{\mathbf{k}=0,\beta}[\mathbf{h}_{\mathbf{q}=0}]\hat{\beta}^{\dagger}_{\mathbf{k}=0}\hat{\beta}_{\mathbf{k}=0} - \frac{1}{2}\beta n_3[\mathbf{h}_{\mathbf{k}=0}]\hat{\beta}^{\dagger}_{\mathbf{k}=0} - \frac{1}{2}\beta n_4[\mathbf{h}_{\mathbf{k}=0}]\hat{\beta}_{\mathbf{k}=0}}\right)\Big] , \end{aligned} \tag{4.54}$$

where

$$\begin{aligned} n_1[\mathbf{h}_{\mathbf{k}=0}] &= \tilde{N}[\mathbf{h}_{-\mathbf{k}=0}]^{\dagger,2} + \tilde{N}[\mathbf{h}_{\mathbf{k}=0}]^{1} , \\ n_2[\mathbf{h}_{\mathbf{k}=0}] &= \tilde{N}[\mathbf{h}_{\mathbf{k}=0}]^{\dagger,1} + \tilde{N}[\mathbf{h}_{-\mathbf{k}=0}]^{2} , \\ n_3[\mathbf{h}_{\mathbf{k}=0}] &= \tilde{N}[\mathbf{h}_{-\mathbf{k}=0}]^{\dagger,4} + \tilde{N}[\mathbf{h}_{\mathbf{k}=0}]^{3} , \\ n_4[\mathbf{h}_{\mathbf{k}=0}] &= \tilde{N}[\mathbf{h}_{\mathbf{k}=0}]^{\dagger,3} + \tilde{N}[\mathbf{h}_{-\mathbf{k}=0}]^{4} , \end{aligned} \tag{4.55}$$

with $\tilde{\mathbf{N}}[\mathbf{h_k}]^{\dagger,1}$ denoting the first component of $\tilde{\mathbf{N}}[\mathbf{h_k}]^{\dagger}$. To do this, we note that we can perform a change of variables by completing the square. For the $\mathbf{k}=0$ term, for the $\hat{\alpha}^{\dagger}_{\mathbf{k}}, \hat{\alpha}_{\mathbf{k}}$ bosons for instance, we have

$$\begin{aligned}
-\frac{1}{2}\beta\epsilon_{0,\alpha}[\mathbf{h_{q=0}}]\hat{\alpha}^{\dagger}_0\hat{\alpha}_0 - \frac{1}{2}\beta n_1[\mathbf{h_{k=0}}]\hat{\alpha}^{\dagger}_0 - \frac{1}{2}\beta n_2[\mathbf{h_{k=0}}]\hat{\alpha}_0 = \\
- \frac{1}{2}\beta\epsilon_{0,\alpha}[\mathbf{h_{q=0}}](\hat{\alpha}^{\dagger}_0 + \frac{n_1[\mathbf{h_{k=0}}]}{\epsilon_{0,\alpha}[\mathbf{h_{q=0}}]})(\hat{\alpha}_0 + \frac{n_2[\mathbf{h_{k=0}}]}{\epsilon_{0,\alpha}[\mathbf{h_{q=0}}]}) \\
+ \beta\frac{n_1[\mathbf{h_{k=0}}]n_2[\mathbf{h_{k=0}}]}{\epsilon_{0,\alpha}[\mathbf{h_{q=0}}]} \, .
\end{aligned} \tag{4.56}$$

We note that we have

$$n_1[\mathbf{h_{k=0}}] = n_2[\mathbf{h_{k=0}}]^{\dagger} \, , \tag{4.57}$$

so that we can define the change of variables

$$\begin{aligned}
\hat{\rho}^{\dagger}_{\mathbf{k}=0} &= \hat{\alpha}^{\dagger}_{\mathbf{k}=0} + \tfrac{n_1[\mathbf{h_{k=0}}]}{\epsilon_{\mathbf{k}=0,\alpha}[\mathbf{h_{q=0}}]} \, , \\
\hat{\rho}_{\mathbf{k}=0} &= \hat{\alpha}_{\mathbf{k}=0} + \tfrac{n_2[\mathbf{h_{k=0}}]}{\epsilon_{\mathbf{k}=0,\alpha}[\mathbf{h_{q=0}}]} \, ,
\end{aligned} \tag{4.58}$$

which ensures that $\hat{\rho}^{\dagger}_{\mathbf{k}=0}$ and $\hat{\rho}_{\mathbf{k}=0}$ have bosonic commutation relations and are associated with the eigenmode $\epsilon_{\mathbf{k}=0,\alpha}[\mathbf{h_{q=0}}]$. We follow the same argument for the $\hat{\beta}^{\dagger}_{\mathbf{k}=0}, \hat{\beta}_{\mathbf{k}=0}$ bosons, and get new bosons $\hat{\sigma}^{\dagger}_{\mathbf{k}=0}$ and $\hat{\sigma}_{\mathbf{k}=0}$:

$$\begin{aligned}
\hat{\sigma}^{\dagger}_{\mathbf{k}=0} &= \hat{\beta}^{\dagger}_{\mathbf{k}=0} + \tfrac{n_3[\mathbf{h_{k=0}}]}{\epsilon_{\mathbf{k}=0,\beta}[\mathbf{h_{q=0}}]} \, , \\
\hat{\sigma}_{\mathbf{k}=0} &= \hat{\beta}_{\mathbf{k}=0} + \tfrac{n_4[\mathbf{h_{k=0}}]}{\epsilon_{\mathbf{k}=0,\beta}[\mathbf{h_{q=0}}]} \, ,
\end{aligned} \tag{4.59}$$

associated with the eigenmode $\epsilon_{\mathbf{k}=0,\beta}[\mathbf{h_{q=0}}]$. The partition function is then the one of a set of independent harmonic oscillators. We obtain

$$\begin{aligned}
Z =& \mathrm{Tr}\left[e^{-\beta E_0 - \beta\Delta E_0[\mathbf{h_{q=0}}] - \beta C[\mathbf{h_{q=0}}]}\left(\prod_{\mathbf{k}\neq 0}(e^{-\beta\epsilon_{\mathbf{k},\alpha}[\mathbf{h_{q=0}}]\hat{\alpha}^{\dagger}_{\mathbf{k}}\hat{\alpha}_{\mathbf{k}}})(e^{-\beta\epsilon_{\mathbf{k},\beta}[\mathbf{h_{q=0}}]\hat{\beta}^{\dagger}_{\mathbf{k}}\hat{\beta}_{\mathbf{k}}})\right)\right. \\
&\left.\times (e^{-\beta\epsilon_{\mathbf{k}=0,\alpha}[\mathbf{h_{q=0}}]\hat{\rho}^{\dagger}_{\mathbf{k}}\hat{\rho}_{\mathbf{k}}})(e^{-\beta\epsilon_{\mathbf{k}=0,\beta}[\mathbf{h_{q=0}}]\hat{\sigma}^{\dagger}_{\mathbf{k}}\hat{\sigma}_{\mathbf{k}}})\, e^{\beta\frac{n_1[\mathbf{h_{k=0}}]n_2[\mathbf{h_{k=0}}]}{\epsilon_{\mathbf{k}=0,\alpha}[\mathbf{h_{q=0}}]}}\, e^{\beta\frac{n_3[\mathbf{h_{k=0}}]n_4[\mathbf{h_{k=0}}]}{\epsilon_{\mathbf{k}=0,\alpha}[\mathbf{h_{q=0}}]}}\right] \, .
\end{aligned} \tag{4.60}$$

We then perform the trace on the Fock space, and use the fact that the trace is independent of the choice of the basis. This means we can compute it separately for the $\hat{\alpha}^{\dagger}_{\mathbf{k}}$ bosons on their respective Fock basis $|n^{\alpha}_{\mathbf{k}}\rangle$ and for the $\hat{\rho}^{\dagger}_{\mathbf{k}=0}$ bosons on its respective Fock basis $|n^{\rho}_{\mathbf{k}=0}\rangle$, and similarly for $\hat{\beta}^{\dagger}_{\mathbf{k}}$ and $\hat{\sigma}^{\dagger}_{\mathbf{k}=0}$. Taking the trace over the Fock space as explained above, we obtain

$$\begin{aligned}
Z =& e^{-\beta E_0 - \beta\Delta E_0[\mathbf{h_{q=0}}] - \beta C[\mathbf{h_{q=0}}]} \\
&\times \prod_{\mathbf{k}} \frac{1}{1-e^{-\beta\epsilon_{\mathbf{k},\alpha}[\mathbf{h_{q=0}}]}}\frac{1}{1-e^{-\beta\epsilon_{\mathbf{k},\alpha}[\mathbf{h_{q=0}}]}} \\
&\times e^{\beta\frac{n_1[\mathbf{h_{k=0}}]n_2[\mathbf{h_{k=0}}]}{\epsilon_{\mathbf{k},\alpha}[\mathbf{h_{q=0}}]}}\, e^{\beta\frac{n_3[\mathbf{h_{k=0}}]n_4[\mathbf{h_{k=0}}]}{\epsilon_{\mathbf{k},\alpha}[\mathbf{h_{q=0}}]}} \, .
\end{aligned} \tag{4.61}$$

The free energy is given by

$$\begin{aligned} F &= -\frac{\log(Z)}{\beta} \\ &= E_0 + \Delta E_0[\mathbf{h}_{\mathbf{q}=0}] + C[\mathbf{h}_{\mathbf{q}=0}] \\ &+ \frac{1}{\beta}\sum_{\mathbf{k}} \log(1 - e^{-\beta\epsilon_{\mathbf{k},\alpha}[\mathbf{h}_{\mathbf{q}=0}]}) + \frac{1}{\beta}\sum_{\mathbf{k}} \log(1 - e^{-\beta\epsilon_{\mathbf{k},\beta}[\mathbf{h}_{\mathbf{q}=0}]}) \\ &- 2\frac{n_1[\mathbf{h}_{\mathbf{k}=0}]n_2[\mathbf{h}_{\mathbf{k}=0}]}{\epsilon_{\mathbf{k},\alpha}[\mathbf{h}_{\mathbf{q}=0}]} - 2\frac{n_3[\mathbf{h}_{\mathbf{k}=0}]n_4[\mathbf{h}_{\mathbf{k}=0}]}{\epsilon_{\mathbf{k},\alpha}[\mathbf{h}_{\mathbf{q}=0}]} + \mathcal{O}(T^2)\ . \end{aligned} \tag{4.62}$$

The moments are given by taking the appropriate derivative of the free energy. They are given by the same expression that we obtained for the classical case expressed in Eq. (3.80) and Eq. (3.81). We now note that we are interested in the zero temperature $T = 0$ structure factor, and we can disregard the terms with $\frac{1}{\beta}$ in the free energy. Eq. (3.80) then becomes

$$\begin{aligned} \langle \hat{O}^{\alpha}_{\mathbf{q}=0,\beta} \rangle_{T=0} = &- \left. \frac{\partial \left[\Delta E_0[\mathbf{h}_{\mathbf{q}=0}] + C[\mathbf{h}_{\mathbf{q}=0}] \right]}{\partial h^{\alpha}_{\mathbf{q}=0,\beta}} \right|_{\mathbf{h}=0} \\ &+ 2 \left. \frac{\partial \left[\frac{n_1[\mathbf{h}_{\mathbf{k}=0}]n_2[\mathbf{h}_{\mathbf{k}=0}]}{\epsilon_{\mathbf{k},\alpha}[\mathbf{h}_{\mathbf{q}=0}]} + \frac{n_3[\mathbf{h}_{\mathbf{k}=0}]n_4[\mathbf{h}_{\mathbf{k}=0}]}{\epsilon_{\mathbf{k},\alpha}[\mathbf{h}_{\mathbf{q}=0}]} \right]}{\partial h^{\alpha}_{\mathbf{q}=0,\beta}} \right|_{\mathbf{h}=0} . \end{aligned} \tag{4.63}$$

We also note that the terms with $n_1[\mathbf{h}_{\mathbf{k}=0}]n_2[\mathbf{h}_{\mathbf{k}=0}]$ and $n_3[\mathbf{h}_{\mathbf{k}=0}]n_4[\mathbf{h}_{\mathbf{k}=0}]$ are at least quadratic (if not of higher order, depending on $\epsilon_{\mathbf{k}}[\mathbf{h}_{\mathbf{q}=0}]$) in the field components $\mathbf{h}_{\mathbf{q}=0}$, as any of the $n_{i=1,2,3,4}$ is independently linear in $\mathbf{h}_{-\mathbf{k}=0}$ by definition. Therefore taking the first derivative of the terms with $n_1[\mathbf{h}_{\mathbf{k}=0}]n_2[\mathbf{h}_{\mathbf{k}=0}]$ and $n_3[\mathbf{h}_{\mathbf{k}=0}]n_4[\mathbf{h}_{\mathbf{k}=0}]$ and evaluating them at zero field will inevitably lead to a null contribution. We then are simply left with

$$\langle \hat{O}^{\alpha}_{\mathbf{q}=0,\beta} \rangle_{T=0} = - \left. \frac{\partial \Delta E_0[\mathbf{h}_{\mathbf{q}=0}] + C[\mathbf{h}_{\mathbf{q}=0}]}{\partial h^{\alpha}_{\mathbf{q}=0,\beta}} \right|_{\mathbf{h}=0} . \tag{4.64}$$

The second moments are given by Eq. (3.80) and disregarding again the term with $\frac{1}{\beta}$, it simply becomes

$$\langle \hat{O}^{\alpha}_{\mathbf{q}=0,\beta} \hat{O}^{\mu}_{\mathbf{q}=0,\nu} \rangle_{T=0} = \langle \hat{O}^{\alpha}_{\mathbf{q}=0,\beta} \rangle_{T=0} \langle \hat{O}^{\mu}_{\mathbf{q}=0,\nu} \rangle_{T=0} . \tag{4.65}$$

We can insert Eq. (4.65) into Eq. (4.48) to calculate the ground state contribution to the quantum structure factor. Therefore all we need to do is find the 0^{th} order contribution of the source term, i.e., find $C[\mathbf{h}_{\mathbf{q}=0}]$, and compute the zero–point energy of the Bogoliubov transformation $\Delta E_0[\mathbf{h}_{\mathbf{q}=0}]$.

4.2.3 Dynamical Structure Factor for Dipole Moments

First, we consider the dynamical spin structure factor associated with the dipole moments

$$S_{\mathrm{S}}^{\mathsf{QM}}(\mathbf{q},\omega) = \int_{-\infty}^{\infty} \frac{\mathrm{d}t}{2\pi} e^{i\omega t} \sum_{\mu} \langle \hat{\mathrm{S}}_{\mathbf{q}}^{\mu}(t) \hat{\mathrm{S}}_{-\mathbf{q}}^{\mu}(0) \rangle \ . \tag{4.66}$$

Following the procedure described in Section 4.2, we substitute Eq. (4.4) in the expression for spin dipole operators, Eq. (1.67). Keeping terms to linear order in the original bosons, we find

$$\hat{\mathrm{S}}_i^x \simeq i(\hat{\mathrm{b}}_i^\dagger - \hat{\mathrm{b}}_i) \ , \tag{4.67a}$$
$$\hat{\mathrm{S}}_i^y \simeq 0 \ , \tag{4.67b}$$
$$\hat{\mathrm{S}}_i^z \simeq -i(\hat{\mathrm{a}}_i^\dagger - \hat{\mathrm{a}}_i) \ . \tag{4.67c}$$

Then, we perform a Fourier transform and express the spin dipole operators in terms of the Bogoliubov bosons using Eq. (4.12). We obtain

$$\hat{\mathrm{S}}_{\mathbf{q}}^x \simeq i\xi_{\mathsf{S}}(\mathbf{q})(\hat{\beta}_{-\mathbf{q}}^\dagger - \hat{\beta}_{\mathbf{q}}) \ , \tag{4.68a}$$
$$\hat{\mathrm{S}}_{\mathbf{q}}^y \simeq 0 \ , \tag{4.68b}$$
$$\hat{\mathrm{S}}_{\mathbf{q}}^z \simeq -i\xi_{\mathsf{S}}(\mathbf{q})(\hat{\alpha}_{-\mathbf{q}}^\dagger - \hat{\alpha}_{\mathbf{q}}) \ , \tag{4.68c}$$

where $\xi_{\mathsf{S}}(\mathbf{q})$ is the coherence factor defined as

$$\xi_{\mathsf{S}}(\mathbf{q}) = \frac{\Delta_{\mathbf{q}} + B_{\mathbf{q}}}{\sqrt{\Delta_{\mathbf{q}}^2 - B_{\mathbf{q}}^2}} \ , \tag{4.69}$$

where $B_{\mathbf{q}}$ and $\Delta_{\mathbf{q}}$ are defined through Eq. (3.17) and Eq. (4.13).

We anticipate all the static averages of dipole moments to vanish, since FQ order does not break time–reversal symmetry, i.e

$$S_{\mathrm{S}}^{\mathsf{GS}}(\mathbf{q}=0,\omega) = 0 \ . \tag{4.70}$$

This is also explicitly calculated following Section 4.2.1 in Appendix I.2. Therefore all contributions to $S_{\mathrm{S}}^{\mathsf{QM}}(\mathbf{q},\omega)$ come from the excitations $S_{\mathrm{S}}^{\mathsf{EX}}(\mathbf{q},\omega)$. We find

$$S_{\mathrm{S}}^{\mathsf{QM}}(\mathbf{q},\omega) = 2\xi_{\mathsf{S}}(\mathbf{q})^2 \delta(\omega - \epsilon(\mathbf{q})) \tag{4.71a}$$
$$= 2\frac{\sqrt{A_{\mathbf{q}} + B_{\mathbf{q}}}}{\sqrt{A_{\mathbf{q}} - B_{\mathbf{q}}}} \delta(\omega - \epsilon(\mathbf{q})) \ , \tag{4.71b}$$

where we used Eq. (4.69) and Eq. (4.13) in the last line. This result is shown in Fig. 4.1 (d).

The associated equal–time structure factor is given by

$$\begin{aligned} S_{\mathrm{S}}^{\mathsf{QM}}(\mathbf{q}) &= \int d\omega \; S_{\mathrm{S}}^{\mathsf{QM}}(\mathbf{q},\omega) \\ &= 2\xi_{\mathsf{S}}(\mathbf{q})^2 \qquad (4.72a) \\ &= 2\frac{\sqrt{A_{\mathbf{q}}+B_{\mathbf{q}}}}{\sqrt{A_{\mathbf{q}}-B_{\mathbf{q}}}} \, , \qquad (4.72b) \end{aligned}$$

where $\xi_{\mathsf{S}}(\mathbf{q})$ given by Eq. (4.69), and $B_{\mathbf{q}}$ and $A_{\mathbf{q}}$ are defined through Eq. (3.17).

Details of these calculation are given in Appendix I.1 and in Appendix I.2 for $\mathbf{q}=0$.

4.2.4 Dynamical Structure Factor for Quadrupole Moments

Here we calculate the dynamical quadrupole structure factor

$$S_{\mathrm{Q}}^{\mathsf{QM}}(\mathbf{q},\omega) = \int_{-\infty}^{\infty} \frac{\mathrm{d}t}{2\pi} e^{i\omega t} \sum_{\mu\nu} \langle \hat{\mathrm{Q}}_{\mathbf{q}}^{\mu\nu}(t) \hat{\mathrm{Q}}_{-\mathbf{q}}^{\mu\nu}(0) \rangle \, . \tag{4.73}$$

Following the same steps as for the spin dipole structure factor, we express the quadrupole tensor in terms of the original fluctuations up to linear order by using Eq. (1.68) and Eq. (4.4). We find

$$\hat{\mathbf{Q}}_i \cong \begin{pmatrix} \frac{2}{3} & -\hat{\mathrm{a}}_i^\dagger - \hat{\mathrm{a}}_i & 0 \\ -\hat{\mathrm{a}}_i^\dagger - \hat{\mathrm{a}}_i & -\frac{4}{3} & -\hat{\mathrm{b}}_i^\dagger - \hat{\mathrm{b}}_i \\ 0 & -\hat{\mathrm{b}}_i^\dagger - \hat{\mathrm{b}}_i & \frac{2}{3} \end{pmatrix} \, . \tag{4.74}$$

After Fourier transform, transcribing in terms of the Bogoliubov bosons [Eq. (4.12)], the quadrupole tensor in Eq. (4.74) yields

$$\hat{\mathbf{Q}}_{\mathbf{q}} \cong \begin{pmatrix} \frac{2}{3}\sqrt{N}\delta(\mathbf{q}) & \xi_{\mathsf{Q}}(\mathbf{q})(\hat{\alpha}_{-\mathbf{q}}^\dagger + \hat{\alpha}_{\mathbf{q}}) & 0 \\ \xi_{\mathsf{Q}}(\mathbf{q})(\hat{\alpha}_{-\mathbf{q}}^\dagger + \hat{\alpha}_{\mathbf{q}}) & -\frac{4}{3}\sqrt{N}\delta(\mathbf{q}) & \xi_{\mathsf{Q}}(\mathbf{q})(\hat{\beta}_{-\mathbf{q}}^\dagger + \hat{\beta}_{\mathbf{q}}) \\ 0 & \xi_{\mathsf{Q}}(\mathbf{q})(\hat{\beta}_{-\mathbf{q}}^\dagger + \hat{\beta}_{\mathbf{q}}) & \frac{2}{3}\sqrt{N}\delta(\mathbf{q}) \end{pmatrix} \, , \tag{4.75}$$

where N is the number of sites, and $\xi_{\mathsf{Q}}(\mathbf{q})$ is the coherence factor for quadrupole moments defined as

$$\xi_{\mathsf{Q}}(\mathbf{q}) = \frac{B_{\mathbf{q}} - \Delta_{\mathbf{q}}}{\sqrt{\Delta_{\mathbf{q}}^2 - B_{\mathbf{q}}^2}} \, . \tag{4.76}$$

From Eq. (4.75), it is clear that the quadrupole moments at $\mathbf{q}=0$ take on a finite value in a FQ state. For convenience, we rescaled the coherence factor as

$$\tilde{\xi}_{\mathsf{Q}}(\mathbf{q}) = \sqrt{2}\xi_{\mathsf{Q}}(\mathbf{q}) \, . \tag{4.77}$$

Both the ground state and excitations contribute to the structure factor $S_{\mathrm{Q}}^{\mathsf{QM}}(\mathbf{q},\omega)$,

and we find

$$S_{\mathrm{Q}}^{\mathsf{QM}}(\mathbf{q},\omega) = \frac{8}{3}N(1-\Delta^{\mathsf{QM}})\delta(\mathbf{q})\delta(\omega) + 4\xi_{\mathrm{Q}}(\mathbf{q})^2\delta(\omega-\epsilon(\mathbf{q})) \tag{4.78a}$$

$$= \frac{8}{3}N(1-\Delta^{\mathsf{QM}})\delta(\mathbf{q})\delta(\omega) + 2\tilde{\xi}_{\mathrm{Q}}(\mathbf{q})^2\delta(\omega-\epsilon(\mathbf{q})) \tag{4.78b}$$

$$= \frac{8}{3}N(1-\Delta^{\mathsf{QM}})\delta(\mathbf{q})\delta(\omega) + 4\frac{\sqrt{A_{\mathbf{q}}-B_{\mathbf{q}}}}{\sqrt{A_{\mathbf{q}}+B_{\mathbf{q}}}}\delta(\omega-\epsilon(\mathbf{q}))\ , \tag{4.78c}$$

where we have used Eq. (4.76) and Eq. (4.13) in the last line, and where Δ^{QM} is given by

$$\Delta^{\mathsf{QM}} = \frac{3}{N}\sum_{\mathbf{k}}\frac{A_{\mathbf{k}}}{\sqrt{A_{\mathbf{k}}^2-B_{\mathbf{k}}^2}}\ . \tag{4.79}$$

The result obtained in Eq. (4.78) is shown in Fig. 4.1 (e), where the Bragg peak at $\mathbf{q}=\Gamma$ is suppressed for simplicity.

The corresponding equal–time structure factor yields

$$S_{\mathrm{Q}}^{\mathsf{QM}}(\mathbf{q}) = \frac{8}{3}N(1-\Delta^{\mathsf{QM}})\delta(\mathbf{q}) + 4\frac{\sqrt{A_{\mathbf{q}}-B_{\mathbf{q}}}}{\sqrt{A_{\mathbf{q}}+B_{\mathbf{q}}}}\ , \tag{4.80}$$

where $B_{\mathbf{q}}$ and $A_{\mathbf{q}}$ are defined through Eq. (3.17).

We provide details of these calculations in Appendix I.3 and in Appendix I.4 for $\mathbf{q}=0$.

4.2.5 Dynamical Spin Structure Factor for A–Matrices

We now consider the structure factors associated with the A–matrices. Within our formalism, the quantum state of the spin–1 moment is fully encapsulated by the A–matrix, and describing its corresponding structure factor is therefore useful

$$S_{\mathrm{A}}^{\mathsf{QM}}(\mathbf{q},\omega) = \int_{-\infty}^{\infty}\frac{\mathrm{d}t}{2\pi}e^{i\omega t}\sum_{\mu\nu}\langle\hat{\mathcal{A}}^{\mu}{}_{\nu}(t)\hat{\mathcal{A}}^{\nu}{}_{\mu}(0)\rangle\ . \tag{4.81}$$

Indeed this structure factor compasses all dynamics at the level of a two–point correlation function, and any other quantity can be computed by taking the appropriate index contractions. Up to linear order in terms of the fluctuations, Eq. (4.4) is rewritten as

$$\hat{\mathbf{A}}_i \cong \begin{pmatrix} 0 & \hat{\mathrm{a}}_i^\dagger & 0 \\ \hat{\mathrm{a}}_i & 1 & \hat{\mathrm{b}}_i \\ 0 & \hat{\mathrm{b}}_i^\dagger & 0 \end{pmatrix}\ . \tag{4.82}$$

After Fourier transforming, and transcribing into the Bogoliubov basis [Eq. (4.12)], we find

$$\hat{\mathbf{A}}_{\mathbf{q}} \cong \begin{pmatrix} 0 & \xi_{\mathsf{A}}^{-}(\mathbf{q})\hat{\alpha}^{\dagger}_{-\mathbf{q}} - \xi_{\mathsf{A}}^{+}(\mathbf{q})\hat{\alpha}_{\mathbf{q}} & 0 \\ -\xi_{\mathsf{A}}^{+}(\mathbf{q})\hat{\alpha}^{\dagger}_{-\mathbf{q}} + \xi_{\mathsf{A}}^{-}(\mathbf{q})\hat{\alpha}_{\mathbf{q}} & \sqrt{N}\delta_{\mathbf{q},0} & -\xi_{\mathsf{A}}^{+}(\mathbf{q})\hat{\beta}^{\dagger}_{-\mathbf{q}} + \xi_{\mathsf{A}}^{-}(\mathbf{q})\hat{\beta}_{\mathbf{q}} \\ 0 & \xi_{\mathsf{A}}^{-}(\mathbf{q})\hat{\beta}^{\dagger}_{-\mathbf{q}} - \xi_{\mathsf{A}}^{+}(\mathbf{q})\hat{\beta}_{\mathbf{q}} & 0 \end{pmatrix} , \quad (4.83)$$

where N is the number of sites, and $\xi_{\mathsf{A}}^{+}(\mathbf{q})$ and $\xi_{\mathsf{A}}^{-}(\mathbf{q})$ are the coherence factors for A–matrices given by

$$\xi_{\mathsf{A}}^{+}(\mathbf{q}) = \frac{\xi_{\mathsf{S}}(\mathbf{q}) + \xi_{\mathsf{Q}}(\mathbf{q})}{2} , \quad (4.84a)$$

$$\xi_{\mathsf{A}}^{-}(\mathbf{q}) = \frac{\xi_{\mathsf{S}}(\mathbf{q}) - \xi_{\mathsf{Q}}(\mathbf{q})}{2} , \quad (4.84b)$$

where $\xi_{\mathsf{S}}(\mathbf{q})$ and $\xi_{\mathsf{Q}}(\mathbf{q})$ are defined through Eq. (4.69) and Eq. (4.76) respectively. For convenience, we also define a total coherence factor for A–matrices given by

$$\tilde{\xi}_{\mathsf{A}}(\mathbf{q}) = \sqrt{\xi_{\mathsf{A}}^{+}(\mathbf{q})^2 + \xi_{\mathsf{A}}^{-}(\mathbf{q})^2} . \quad (4.85)$$

Like the structure factor for quadrupole moments, the A–matrices structure factor contains contributions from the ground state as well as the excitations. We obtain

$$\begin{aligned} S_{\mathrm{A}}^{\mathsf{QM}}(\mathbf{q},\omega) =& N(1 - \frac{2}{3}\Delta^{\mathsf{QM}})\delta(\mathbf{q})\delta(\omega) + 2(\xi_{\mathsf{A}}^{+}(\mathbf{q})^2 + \xi_{\mathsf{A}}^{-}(\mathbf{q})^2)\delta(\omega - \epsilon(\mathbf{q})) && (4.86a)\\ =& N(1 - \frac{2}{3}\Delta^{\mathsf{QM}})\delta(\mathbf{q})\delta(\omega) + 2\tilde{\xi}_{\mathsf{A}}(\mathbf{q})^2\delta(\omega - \epsilon(\mathbf{q})) && (4.86b)\\ =& N(1 - \frac{2}{3}\Delta^{\mathsf{QM}})\delta(\mathbf{q})\delta(\omega) + (\xi_{\mathsf{S}}(\mathbf{q})^2 + \xi_{\mathsf{Q}}(\mathbf{q})^2)\delta(\omega - \epsilon(\mathbf{q})) && (4.86c)\\ =& N(1 - \frac{2}{3}\Delta^{\mathsf{QM}})\delta(\mathbf{q})\delta(\omega) + (\xi_{\mathsf{S}}(\mathbf{q})^2 + \frac{1}{2}\tilde{\xi}_{\mathsf{Q}}(\mathbf{q})^2)\delta(\omega - \epsilon(\mathbf{q})) && (4.86d)\\ =& N(1 - \frac{2}{3}\Delta^{\mathsf{QM}})\delta(\mathbf{q})\delta(\omega) + 2\frac{A_{\mathbf{q}}}{\sqrt{A_{\mathbf{q}}^2 - B_{\mathbf{q}}^2}}\delta(\omega - \epsilon(\mathbf{q})) , && (4.86e) \end{aligned}$$

where we used Eq. (4.84) in the second line and Eq. (4.76), Eq. (4.69) and Eq. (4.13) in the last line, and where Δ^{QM} is defined in Eq. (4.79). This result is shown in Fig. 4.1 (f), where again we suppressed the Bragg peak at $\mathbf{q} = \Gamma$, for simplicity.

The equal–time structure factor is given by

$$S_{\mathrm{A}}^{\mathsf{QM}}(\mathbf{q}) = N(1 - \frac{2}{3}\Delta^{\mathsf{QM}})\delta(\mathbf{q}) + 2\frac{A_{\mathbf{q}}}{\sqrt{A_{\mathbf{q}}^2 - B_{\mathbf{q}}^2}} , \quad (4.87)$$

where $B_{\mathbf{q}}$ and $A_{\mathbf{q}}$ are defined through Eq. (3.17).

Details of these calculations can be found in and Appendix I.5 and in Appendix I.6 for $\mathbf{q} = 0$.

4.2.6 Sum Rule on Quantum Structure Factors

Like the sum rule for equal–time structure factors, Eq. (3.96), the sum rule on the moments, Eq. (2.67), implies that the quantum (semi–classical) dynamical structure factors must satisfy a sum rule of the same form, namely

$$S_{\mathrm{A}}(\mathbf{q},\omega) = \frac{1}{4}S_{\mathrm{Q}}(\mathbf{q},\omega) + \frac{1}{2}S_{\mathrm{S}}(\mathbf{q},\omega) + \frac{1}{3}N\delta(\omega)\ . \tag{4.88}$$

We confirm by direct substitution of the quantum results at $T = 0$ for $S_{\mathrm{S}}^{\mathsf{QM}}(\mathbf{q},\omega)$ [Eq. (4.72b)], $S_{\mathrm{Q}}^{\mathsf{QM}}(\mathbf{q},\omega)$ [Eq. (4.80)] and $S_{\mathrm{A}}^{\mathsf{QM}}(\mathbf{q},\omega)$ [Eq. (4.87)], into Eq. (4.88), that the sum rule is satisfied for $\mathbf{q} \neq 0$. This is easily seen by using the expressions that include the coherence factors. We also note that it is satisfied for $\mathbf{q} = 0$ by construction, since we used the sum rule to predict the quantum structure factor associated with the A–matrices, as explained in Section I.6. It is also useful to verify that the sum rule is visually satisfied, by directly looking at the spectral weight of the structure factors. This is simply done by multiplying the intensities with the correct prefactor according to the sum rule, and then "adding up" the intensities of the dipole moments [Fig. 4.1 (a)] and quadrupole moments [Fig. 4.1 (b)] to compare with the intensity for A–matrices [Fig. 4.1 (c)].

4.2.7 Comparison of Structure Factors Between Quantum and Classical Theories of Fluctuations

In Fig. 4.1, we compare results obtained from the quantum theory of fluctuations about a Ferroquadrupolar (FQ) ground state with its classical treatment. For clarity and aestheticism, all the results have been convoluted with a Gaussian in frequency of FWHM = 0.35 J. As discussed in Section 4.1.2, we observe that the dispersion relations are completely different, implied by the fact that the eigenvalues are associated with different matrices. Indeed, in the quantum case, we need to ensure that the fluctuations follow bosonic commutation rules.

In the classical case, we obtain two different modes, which are each two–fold degenerate, for a total of four modes. One of the modes is associated with the dipolar excitations v_2 and v_4 [Eq. (3.36)] and contribute to the dipolar channel. These excitations are gapped and form a dispersive band with intensities forming a broad peak centered around $\mathbf{q} = \mathbf{K}$. The other mode is characterized by the excitations v_1 and v_3 [Eq. (3.35)] which are of quadrupolar nature and therefore contributes to the quadrupole structure factor. The quadrupolar excitations are gapless and induce a spectral weight which is concentrated at $\mathbf{q} = \mathbf{\Gamma}$. Since the A–matrix encompasses both dipolar and quadrupolar moments[Eq. (3.34)], its structure factor is sensitive to both types of fluctuations. The spectral weights from dipole and quadrupole moments add up according to the sum rule [Eq. (4.88)] to produce the intensities for the A–matrices.

Meanwhile, in the quantum case, we have one doubly–degenerate mode. These two modes are the Goldstone modes associated with the continuous symmetry breaking of the FQ ground state. They describe the dispersion relations of the orthogonal quantum excitations $\hat{\alpha}^{\dagger}_{\mathbf{q}}$ and $\hat{\beta}^{\dagger}_{\mathbf{q}}$. Unlike the classical case, both these excitations enter dipoles and quadrupoles moments as can be seen from Eq. (4.68) and Eq. (4.75) as

well as the A-matrix [Eq. (4.83)]. The difference lies in the prefactor to which they are associated within the different expressions. This prefactor is determined by the coherence factor $\xi_\lambda(\mathbf{q})$ which controls the intensity of the quantum structure factors [Eq. (4.71),Eq. (4.78),Eq. (4.86)].

We note that the intensities of dipole structure factors are stronger at the top of the band and concentrated around $\mathbf{q} = \mathbf{K}$, similarly to the classical dipolar intensities. The quadrupole structure factors are highly localized around $\mathbf{q} = \mathbf{\Gamma}$, where the Goldstone modes emanate. And again, the A–matrices sum up both dipolar and quadrupolar weights. These features can be explained by remembering that the original fluctuations correspond to creating/annihilation of a boson along the x– or z– directions in the time–reversal invariant basis [Eq. (2.32)]. This is made obvious in Eq. (4.3). Therefore they are quadrupolar in nature, and, there is no reason why a fluctuation along the x–axis should behave differently from one along the z–axis. Additionally, they do not mix through the interactions of the BBQ Hamiltonian and therefore the two Bogoliubov excitations $\hat{\alpha}^\dagger_{\mathbf{q}}$ and $\hat{\beta}^\dagger_{\mathbf{q}}$ that diagonalize the BBQ Hamiltonian can independently be expressed in terms of only one single original fluctuation. Therefore, the Bogoliubov excitation $\hat{\alpha}^\dagger_{\mathbf{q}}$ is associated with fluctuations along the x–axis and $\hat{\beta}^\dagger_{\mathbf{q}}$ with fluctuations along the z–axis. They are independent and follow the same dynamics, hence, the doubly–degenerate dispersion relation.

We conclude by observing that the classical and quantum fluctuations follow different dispersion rules. They are associated with classical and quantum structure factors whose spectral weights seem to take on value at different orders of magnitude. However, the qualitative dependence of their spectral intensities with respect to momentum space seems consistent between classical and quantum theories, besides an important quantitative disagreement.

These analytical quantum results are also compared with u3MD simulations in Section 4.3.

4.3 Comparison with "Raw" $u(3)$ Molecular Dynamics

In this section, we complete our analysis of the excitations of the FQ phase of the spin–1 BBQ model by studying the dynamic properties found in the $U(3)$ Molecular Dynamics (u3MD) scheme developed in Section 2.6.2.

We present "raw" simulation results for dynamical structure factors obtained by numerical integration of the equations of motion expressed in our $u(3)$ framework. We find that these correctly portray the dispersion of the excitations in the limit $T \to 0$, but do not properly describe their spectral intensities. More specifically, by comparing u3MD simulation results with analytical zero–temperature quantum results for structure factors associated with dipole moments, quadrupole moments, and A–matrices, we show that u3MD simulation results reproduce the dispersion predicted by the zero–temperature quantum theory [Section 4.1], but that its spectral weights of the structure factors disagree with the analytical predictions. Nevertheless, as we will see in the next chapter, Chapter 5, this disagreement can be accounted for in the limit $T \to 0$.

In Fig. 4.2, we present "raw" u3MD simulation results obtained through numerical integration of the equations of motion as described in Section 2.6.2. $T = 0$ quantum results obtained within our expansion of fluctuation framework [Section 4.2] are shown for comparison. We show results for the dynamical structure factors $S^{\mathsf{MD}}_{\lambda}(\mathbf{q}, \omega)$ [Eq. (E.16)] for dipole moments ($\lambda = \mathsf{S}$), quadrupole moments ($\lambda = \mathsf{Q}$), and A–matrices ($\lambda = \mathsf{A}$). Results are plotted for our usual path in reciprocal space, given along the irreducible wedge **Γ**–**K**–**M**–**Γ** [cf. Appendix D]. For clarity, all the results shown in Fig. 4.2 have been convoluted with a Gaussian of FWHM $= 0.35\ J$.

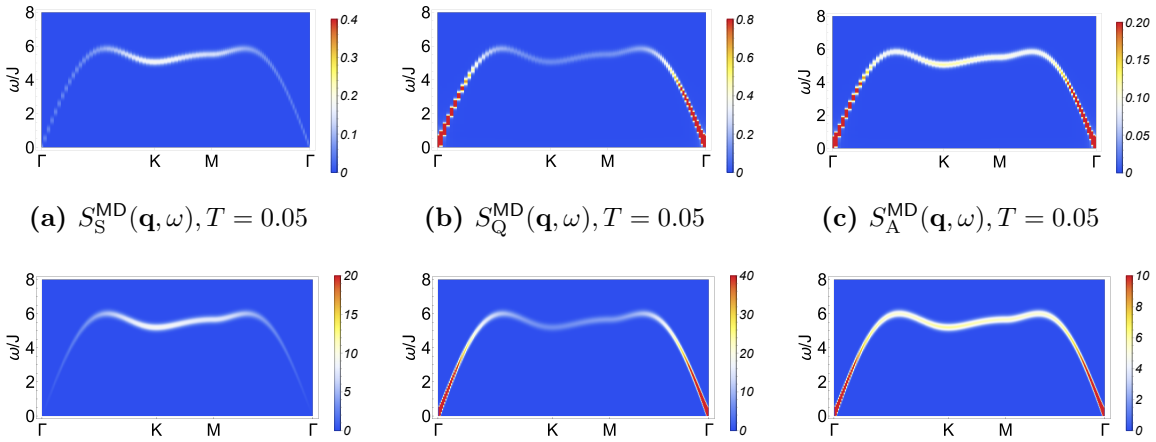

(a) $S^{\mathsf{MD}}_{\mathrm{S}}(\mathbf{q}, \omega), T = 0.05$ **(b)** $S^{\mathsf{MD}}_{\mathrm{Q}}(\mathbf{q}, \omega), T = 0.05$ **(c)** $S^{\mathsf{MD}}_{\mathrm{A}}(\mathbf{q}, \omega), T = 0.05$

(d) $S^{\mathsf{QM}}_{\mathrm{S}}(\mathbf{q}, \omega), T = 0$ **(e)** $S^{\mathsf{QM}}_{\mathrm{Q}}(\mathbf{q}, \omega), T = 0$ **(f)** $S^{\mathsf{QM}}_{\mathrm{A}}(\mathbf{q}, \omega), T = 0$

Figure 4.2: Comparison between "raw" results of $u(3)$ Molecular Dynamics (u3MD) simulations of excitations about the FQ state and the predictions of a $T = 0$ quantum analytical theory. "Raw" simulation results offer a good account of the dispersions of the excitations, but not of their spectral intensities. (a) Dynamical structure factor associated with dipole moments, $S^{\mathsf{MD}}_{\mathrm{S}}(\mathbf{q}, \omega)$. Dipolar fluctuations exhibit relatively high spectral weight near the top of the band, where excitations have more of a spin–wave character. (b) Dynamical structure factor associated with quadrupole moments, $S^{\mathsf{MD}}_{\mathrm{Q}}(\mathbf{q}, \omega)$. (c) Dynamical structure factor associated with A–matrices, $S^{\mathsf{MD}}_{\mathrm{A}}(\mathbf{q}, \omega)$. (d) Prediction for $S^{\mathsf{QM}}_{\mathrm{S}}(\mathbf{q}, \omega)$ from $T = 0$ quantum theory [Eq. (4.71)]. (e) Equivalent prediction for $S^{\mathsf{QM}}_{\mathrm{Q}}(\mathbf{q}, \omega)$ [Eq. (4.78)]. (f) Equivalent prediction for $S^{\mathsf{QM}}_{\mathrm{A}}(\mathbf{q}, \omega)$ [Eq. (4.86)]. Simulations were carried out by my collaborator Dr. Rico Pohle, using the u3MD simulation scheme described in Section 2.6.2, for $\mathcal{H}_{\mathsf{BBQ}}$ [Eq. (2.72)] with parameters Eq. (3.87), at a temperature $T = 0.05\ J$, in a cluster of linear dimension $L = 96$ ($N = 9216$ spins). $T = 0$ quantum analytical predictions have been calculated using the quantum theory of fluctuations developed in Section 4.2. All the results have been convoluted with a Gaussian envelope of FWHM $= 0.35$ J. Bragg peaks are not plotted for simplicity. The individual panels are reproduced from [201].

Compared with the predictions of the zero–temperature quantum theory, $S^{\mathsf{QM}}_{\lambda}(\mathbf{q}, \omega)$, we see that u3MD correctly reproduces a dispersing band of excitations, similar to the quantum modes obtained analytically. The intensities from u3MD structure factor results also show a predominant quadrupolar nature for $\omega \to 0$, and a predominant

dipolar character at the top of the band. However, a careful examination reveals small discrepancies in the energy of excitations, and important differences in the distribution of spectral weight across the band. For instance, analytic quantum results for the dipole dynamical structure factors [Fig. 4.2 (d), Eq. (4.71)], are predicted to show a characteristic linear loss of spectral weight at low energies [229]

$$S_{\mathsf{S}}^{\mathsf{QM}}(\mathbf{q}\to\mathbf{0},\omega) = 2\frac{\omega_{\mathbf{q}\to\mathbf{0}}}{A_{\mathbf{q}\to\mathbf{0}}-B_{\mathbf{q}\to\mathbf{0}}}\delta(\omega-\omega_{\mathbf{q}\to\mathbf{0}}) \propto \omega\times\delta(\omega-v|\mathbf{q}|)\ . \tag{4.89}$$

Meanwhile, numerical results for $S_{\mathsf{S}}^{\mathsf{MD}}(\mathbf{q},\omega)$ [Fig. 4.2 (a)] exhibit a roughly constant spectral weight as $\omega\to 0$. Additionally, the distribution of spectral weight of quadrupolar moments $S_{\mathsf{Q}}^{\mathsf{MD}}(\mathbf{q},\omega)$ [Fig. 4.2 (b)], is also clearly different from analytic quantum predictions [Fig. 4.1 (b), Eq. (4.78)]. The main disagreement lies in the order of magnitude of the spectral weights between the quantum predictions and u3MD simulations.

We note that "raw" simulation results for $S_{\lambda}^{\mathsf{MD}}(\mathbf{q},\omega)$ (where $\lambda=\mathrm{A},\mathrm{Q},\mathrm{S}$ whether we consider dynamical structure factors associated with A–matrices, quadrupole or dipole moments, respectively) exhibit two peaks centered around $-\epsilon(\mathbf{q})$ and $+\epsilon(\mathbf{q})$, where $\epsilon(\mathbf{q})$ is defined in Eq. (4.16). This is because the numerical time integration includes all four modes which are solutions of the eigensystem Eq. (4.9) given in Eq. (4.11). However, for the FQ state, two modes are doubly degenerate, and therefore contributions of the u3MD simulations in the spectral weight include only two peaks around $-\epsilon(\mathbf{q})$ and $+\epsilon(\mathbf{q})$. In other words, the u3MD simulations do not care whether the dynamics process one way $-\epsilon(\mathbf{q})$ or the other $+\epsilon(\mathbf{q})$.

The u3MD simulations are initiated from the configuration of spins obtained from the u3MC scheme as explained in Section 2.6. This implies that the spectral weight in inherited from the u3MC simulations and equally split into a contribution $S_{\lambda}^{\mathsf{MD}+}(\mathbf{q},\omega)$ around $+\epsilon(\mathbf{q})$ and a contribution $S_{\lambda}^{\mathsf{MD}-}(\mathbf{q},\omega)$ around $-\epsilon(\mathbf{q})$, that we symbolically write as

$$S_{\lambda}^{\mathsf{MD}+}(\mathbf{q},\omega) = S_{\lambda}^{\mathsf{MD}-}(\mathbf{q},\omega)\ . \tag{4.90}$$

Therefore, for "raw" simulation results for $S_{\lambda}^{\mathsf{MD}}(\mathbf{q},\omega)$, we choose to only consider the positive part of the energy spectrum, but multiplied by a factor two, to account for the fact that half of the spectral weight belongs in the negative part of the energy spectrum. More precisely, we consider the total spectral weight $S_{\lambda}^{\mathsf{MD}+}(\mathbf{q},\omega) + S_{\lambda}^{\mathsf{MD}-}(\mathbf{q},\omega)$

$$S_{\lambda}^{\mathsf{MD}}(\mathbf{q},\omega) = S_{\lambda}^{\mathsf{MD}+}(\mathbf{q},\omega) + S_{\lambda}^{\mathsf{MD}-}(\mathbf{q},\omega)\ , \tag{4.91}$$

that we artificially redefined only at positive energy as a single peak centered around $+\epsilon(\mathbf{q})$

$$S_{\lambda}^{\mathsf{MD}}(\mathbf{q},\omega) := 2S_{\lambda}^{\mathsf{MD}+}(\mathbf{q},\omega)\ . \tag{4.92}$$

The reason for this choice comes from the fact that it enables an easier comparison with zero–temperature analytical quantum predictions, which only allow for the positive modes $+\epsilon_{\mathbf{q}}$ given in Eq. (4.11). Indeed at zero temperature, negative modes solutions

are forbidden as they correspond to the creation of holes with energy lower than the ground state. This way, the "raw" simulation results for $S^{\mathsf{MD}}_{\lambda}(\mathbf{q}=\mathbf{K},\omega)$ show a single peak centered around an energy $+\epsilon(\mathbf{q}=\mathbf{K})=\omega_0$ which depends on temperature.

Indeed, we can characterize the "raw" u3MD results by investigating the temperature dependence of the dynamical structure factors at a fixed wave vector $\mathbf{q}$. In Fig. 4.3, we present results the intensities of the structure factors associated to the A–matrices, obtained from u3MD simulations $S^{\mathsf{MD}}_{\mathrm{A}}(\mathbf{q},\omega)$. These are shown at the specific wave vector $\mathbf{q}=\mathbf{K}$, $S^{\mathsf{MD}}_{\mathrm{A}}(\mathbf{q}=\mathbf{K},\omega)$ as a function of ω for different temperatures comprised between $T=0.01\ J$ to $T=0.15\ J$ and are represented as circles. The prediction obtained by the zero–temperature quantum theory, $S^{\mathsf{QM}}_{\mathrm{A}}(\mathbf{q}=\mathbf{K},\omega)$ [Eq. (4.86)], is shown for comparison by the red dashed line. The simulation results (circles) and the analytic one (dashed line) have been convoluted with a Gaussian of FWHM $=0.02\ J$.

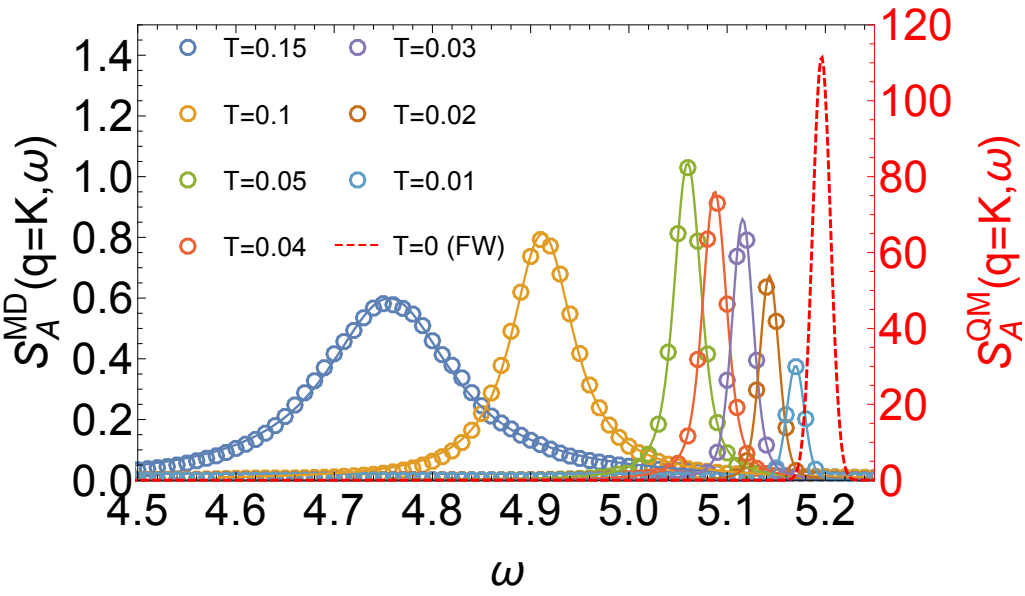

Figure 4.3: Temperature dependence of "raw" results obtained by $U(3)$ Molecular Dynamics (u3MD) simulation at fixed wave vector $\mathbf{q}=\mathbf{K}$. Results are shown for the dynamical structure factor associated with A–matrices, $S^{\mathsf{MD}}_{\mathrm{A}}(\mathbf{q}=\mathbf{K},\omega)$ [Eq. (2.130)], obtained from u3MD simulations for temperatures between $T=0.01\ J$ to $T=0.15\ J$. The $T=0$ prediction obtained by a quantum theory, $S^{\mathsf{QM}}_{\mathrm{A}}(\mathbf{q},\omega)$ [Eq. (4.86)], is shown by the red dashed line. Solid lines correspond to fits of u3MD data using a Voigt function [Eq. (4.93)]. For $T\to 0$, the energy of the associated excitations for "raw" u3MD simulation results converge towards the energy predicted by the quantum theory. But the spectral weight of the structure factor suffers a dramatic loss of intensity. Indeed, the intensities of the peak fail to converge to the predictions of a $T=0$ quantum theory for $T\to 0$. Simulations of $\mathcal{H}_{\mathsf{BBQ}}$ [Eq. (2.72)] were carried out by my collaborator Dr. Rico Phole, using the u3MD simulation scheme described in Section 2.6.2, for parameters given in Eq. (3.87), and for a system size $L=96$ ($N=9216$ spins). Simulation results and analytic prediction have both been convoluted with a Gaussian of FWHM $=0.02\ J$. Figure is reproduced from [201].

The peaks shown for $S_{\mathrm{A}}^{\mathsf{MD}}(\mathbf{q}=\mathbf{K},\omega)$ are well described by the Voigt function

$$V(\omega,\sigma,\Gamma)=\frac{\mathsf{Re}[w(z)]}{\sigma\sqrt{2\pi}}\,, \tag{4.93}$$

where the Faddeeva function $w(z)$ is given by

$$w(z)=e^{-z^2}\mathrm{erfc}(-iz)\,, \tag{4.94}$$

and is evaluated for

$$z=\frac{(\omega-\omega_0)+i\Gamma}{\sigma\sqrt{2}}\,. \tag{4.95}$$

The Voigt profile reflects then a Lorentzian lineshape convoluted with a Gaussian with full–width half–maximum (FWHM) determined by σ [Eq. (E.19)], where the Lorentzian lineshape is given by

$$f(\omega)=\frac{\Gamma}{2\pi}\frac{1}{(\omega-\omega_0)^2+\Gamma^2}\,, \tag{4.96}$$

and corresponds to a single excitation with energy ω_0 and inverse lifetime Γ.

Empirical fits of Eq. (4.93) to simulation data are shown with solid lines in Fig. 4.3. σ is entirely determined by the specifications of the u3MD simulation leaving the parameters ω_0, Γ, and the overall normalization (total spectral weight) as fit variables. These fits admirably correspond with the simulation data. This confirms that u3MD simulations describe a single type of excitations, with finite, temperature–dependent energy and lifetime. We recall that the mode associated with these excitations is nevertheless doubly–degenerate, and that there is technically a contribution at $-\epsilon(\mathbf{q}=\mathbf{K})$ and $+\epsilon(\mathbf{q}=\mathbf{K})$, but for convenient comparison with zero–temperature analytical quantum prediction, we consider the total spectral weight $2S_{\mathrm{A}}^{\mathsf{MD}+}(\mathbf{q}=\mathbf{K},\omega)$ around $+\epsilon(\mathbf{q}=\mathbf{K})$.

As temperature is decreased, the peak in $S_{\mathrm{A}}^{\mathsf{MD}}(\mathbf{q}=\mathbf{K},\omega)$ becomes sharper, and its center ω_0 tends to higher energies towards the predicted quantum dispersion relations $\epsilon(\mathbf{0})$, while retaining its underlying Lorentzian structure. However, at low temperatures, the spectral weight of u3MD results also exhibits a drastic loss of intensity, tending to zero as $T\to 0$. For instance, at $T\sim 0.1$, the difference in intensity between u3MD simulations and quantum predictions is at least of a factor of magnitude $\times$ 100. This is reflected in Fig. 4.3 by inspection of the different scales on the y–axes with values for $S_{\mathrm{A}}^{\mathsf{MD}}(\mathbf{q}=\mathbf{K},\omega)$ on the left hand side and valued for $S_{\mathrm{A}}^{\mathsf{QM}}(\mathbf{q}=\mathbf{K},\omega)$ on the right hand side. As $T\to 0$, we conclude that, except for having vanishing spectral weight, the simulation results approach the $T=0$ quantum result, where the spectral weight is concentrated in a delta function at $\epsilon(\mathbf{0})$, in the $\Gamma\to 0$ limit of Eq. (4.96). The reason for this discrepancy, and the way in which it can be corrected, will be discussed in Section 5.1.

Chapter 5

Classical-Quantum Correspondence in Molecular Dynamics Simulations

In Section 4.3, we compared the "raw" u3MD simulation results with predictions obtained from the $T = 0$ quantum (semi–classical) theory and noticed that the u3MD simulations appropriately captured the quantum (semi–classical) nature of the dynamics, but failed at reproducing the spectral weight of dynamical structure factors. In this Chapter, we dig deeper into the mechanisms of MD simulations by reviewing what we learned in the analysis of the "raw" u3MD simulations presented in Section 4.3. This permits us to analytically model the principles of MD simulations and obtain a classical–quantum correspondence that allows to correct the u3MD simulations results. Finally, we show that in the limit $T \to 0$, the corrected numerical simulations perfectly agree with the analytical zero–temperature quantum calculations.

In Section 5.1, we derive the relationship between the classical and quantum analytical theories of fluctuations that we developed in Chapter 3 and Chapter 4. In Section 5.2, we link the different quantities obtained from classical u3MC, quantum (semi–classical) u3MD, and the analytic theories, with each other. We then use these results in Section 5.3 where we construct a correspondence between u3MD simulations and a zero–temperature quantum theory. This allows us to correct the u3MD simulation results, restoring an excellent agreement with $T = 0$ quantum results.

5.1 Relationship Between Classical and Quantum Theories of Equal–Time Correlations

Here we investigate the relationship between classical and quantum theories of fluctuations for the FQ state of the BBQ Hamiltonian. The detailed reasoning was explained in Section 4.3 when we compared the "raw" dynamical structure factors obtained from u3MD simulations [Section 2.6.2] with analytical quantum predictions derived in Section 4.2.

For now, we simply summarize some of our observations, and the interested (or forgetful) reader is welcome to jump back to Chapter 4 before continuing here. In Section 4.3, we discussed why "raw" u3MD simulation results fail at reproducing zero–temperature analytical quantum results for the dynamical structure factors. The rea-

soning is summarized as follow:
u3MD simulations consist of thermalizing a system through classical u3MC simulations to a target temperature. Then the spin configurations drawn from this thermal ensemble of states are numerically time–evolved using the equations of motion for A–matrices [Eq. (2.74)]. u3MD simulations correctly capture the quantum (semi–classical, to be precise) dynamics of the excitations, since they are described by the quantum (semi-classical) equations of motion [Eq. (2.74)], which arise through commutation relations.

However, they fail to describe the spectral weight of the structure factors. The reason for this lies in the fact that the spectral intensities of the structure factors are not dictated by any type of quantization or quantum–like constraint. Instead, they are determined by the classical thermal fluctuations arising from the classical treatment of the fluctuations' statistics in classical MC simulations. This implies that as $T \to 0$, classical thermal fluctuations are eliminated and the corresponding spectral weights vanish, as illustrated in Fig. 4.3. In short, despite having quantum (semi–classical) dynamics, the u3MD simulations inherit the classical spectral weights induced by the classical statistics of u3MC simulation. This is because the dynamics originate from a classical thermal ensemble of states obtained by classical u3MC simulations.

However, the fact the spectral weight exhibits a peak described by a Lorentzian (cf. Fig. 4.3) that sharpens as $T \to 0$ suggests that we should be able to account for the low–temperature results within a single–mode approximation, in the sense that effects coming from interactions are negligible and that it is possible to resolve the spectrum for each of its spectral contributions. Recall that, technically, the spectrum of the u3MD simulations for $S^{\mathsf{MD}}_{\lambda}(\mathbf{q},\omega)$ posses two peaks at $-\omega_{\mathbf{q}}$ and $+\omega_{\mathbf{q}}$, but that we deliberately considered only one of them as expressed in Eq. (4.92).

Consequently, besides being encouraged by the analysis described above, with the ambition to free the u3MD simulations from their classical weights, the investigation of the relationship between the classical and the quantum (semi–classical) approaches allows also to fulfill our own curiosity and our endeavors for completeness. Indeed, this will lead us to a general classical–quantum correspondence that leads to a simple prescription that can rid the u3MD simulations of their classical affliction. This prescription comes in the form of

$$S^{\mathsf{QM}}(\mathbf{q},\omega,T=0) = \lim_{T\to 0} \frac{\hbar\omega}{2k_BT} S^{\mathsf{MD}}(\mathbf{q},\omega,T) \ , \tag{5.1}$$

which was previously introduced in Eq. (1.71). As we will see in Section 5.3, this allows us to rectify the structure factors obtained by u3MD simulations and perfectly retrieve zero–temperature quantum results, at the semi–classical level.

We now explore their classical–quantum correspondence in more detail. We start by modeling the u3MD simulations within our analytical framework of fluctuations about the FQ state. This is done by assuming that the fluctuations follow quantum dynamics while being described by classical statistics. This framework will be proved useful as it permits us to re–derive the classical results (previously calculated in Section 3.3) in a form that is suitable for comparison with the quantum results for the structure factors [Section 4.1]. We here focus on the dipole structure factor, as it is experimentally relevant, but this approach is also valid for quadrupole and A–matrices.

Then, we show that the u3MD simulations can be corrected and restore quantum zero–temperature structure factors.

We start our analysis from the quantum theory of excitations about the FQ state, with the Hamiltonian $\mathcal{H}'_{\mathsf{BBQ}}$ Eq. (4.15) described in terms of the Bogoliubov bosons. To this end, in analogy with the classical theory, we also include a source term $\Delta\mathcal{H}[\mathbf{h}]$ which couples dipole moments to a transverse field $\mathbf{h}$

$$\Delta\mathcal{H}[\mathbf{h_i}] \;=\; -\sum_i h_i^\alpha \hat{\mathrm{S}}_i^\alpha \;. \tag{5.2}$$

We then use the expression of the dipole in terms of the Bogoliubov bosons Eq. (4.68a)–Eq. (4.68c) to rewrite Eq. (5.2) up to linear order in bosons. The inclusion of $\Delta\mathcal{H}[\mathbf{h}]$ will allow us to compute correlations by taking the relevant functional derivative of the free energy. Using Eq. (4.15) as expression for $\mathcal{H}'_{\mathsf{BBQ}}$, the total Hamiltonian then reads

$$\begin{aligned}\mathcal{H} &= \mathcal{H}'_{\mathsf{BBQ}} + \Delta\mathcal{H}[\mathbf{h}] \\ &= E_0 + \Delta E_0 + \sum_{\mathbf{k}} \hbar\epsilon(\mathbf{k}) \left[\hat{\alpha}^\dagger_{\mathbf{k}}\hat{\alpha}_{\mathbf{k}} + \hat{\beta}^\dagger_{\mathbf{k}}\hat{\beta}_{\mathbf{k}}\right] \\ &\quad - \sum_{\mathbf{k}} \xi_{\mathsf{S}}(\mathbf{k}) \left[ih^x_{\mathbf{k}}(\hat{\beta}_{\mathbf{k}} - \hat{\beta}^\dagger_{-\mathbf{k}}) + ih^z_{\mathbf{k}}(\hat{\alpha}^\dagger_{-\mathbf{k}} - \hat{\alpha}_{\mathbf{k}})\right] \;,\end{aligned} \tag{5.3}$$

where E_0 is the classical MF ground state energy expressed in Eq. (3.14), the zero–point energy coming from the Bogoliubov transformation ΔE_0 is given in Eq. (4.17), the excitation energy $\epsilon(\mathbf{k})$ is defined through Eq. (4.16) and corresponds to the quantum dispersion bands of the Bogoliubov bosons, $\xi_{\mathsf{S}}(\mathbf{k})$ is the coherence factor defined in Eq. (4.69). All terms which are cubic or higher order in bosons have been explicitly neglected. We also point out that from now, we restore dimensional constants $\hbar$ and k_B, which have both been set to unity everywhere else.

Thanks to the diagonal and quadratic form of Eq. (5.3) in terms of the Bogoliubov bosons $\hat{\alpha}_{\mathbf{k}}$ and $\hat{\beta}_{\mathbf{k}}$, we recognize it as a set of N independent simple harmonic oscillators (SHO). This motivates the introduction of a new set of variables

$$\hat{\alpha}_{\mathbf{k}} \;=\; \sqrt{\frac{m\epsilon(\mathbf{k})}{2\hbar}}\hat{x}_{1,\mathbf{k}} + \frac{i}{\sqrt{2\hbar m\epsilon(\mathbf{k})}}\hat{p}_{1,\mathbf{k}} \;, \tag{5.4a}$$

$$\hat{\beta}_{\mathbf{k}} \;=\; \sqrt{\frac{m\epsilon(\mathbf{k})}{2\hbar}}\hat{x}_{2,\mathbf{k}} + \frac{i}{\sqrt{2\hbar m\epsilon(\mathbf{k})}}\hat{p}_{2,\mathbf{k}} \;, \tag{5.4b}$$

which satisfy the canonical commutation relation

$$[\hat{x}_{\lambda,\mathbf{k}}, \hat{p}_{\lambda',\mathbf{k}'}] = i\hbar\delta_{\mathbf{k}\mathbf{k}'}\delta_{\lambda\lambda'} \;, \tag{5.5}$$

with $\lambda = 1, 2$. The Hamiltonian [Eq. (5.3)] expressed in terms of these coordinates,

yields

$$\mathcal{H} = E_0 + \Delta E_0 + \sum_{\lambda,\mathbf{k}} \left[\frac{m\epsilon(\mathbf{k})^2}{2} \hat{x}^2_{\lambda,\mathbf{k}} + \frac{1}{2m} \hat{p}^2_{\lambda,\mathbf{k}} - \sqrt{\frac{2\xi_S^2(\mathbf{k})}{m\hbar\epsilon(\mathbf{k})}} \left(h^z_{\mathbf{k}} \delta_{1,\lambda} + h^x_{\mathbf{k}} \delta_{2,\lambda} \right) \hat{p}_{\lambda,\mathbf{k}} \right] . \tag{5.6}$$

The excitations of Eq. (5.6) follow well–defined, bosonic statistics, as long as they satisfy the commutation relation, Eq. (5.5). MD simulations consist of quantum (semi–classical) dynamics for spin configurations that are drawn from classical thermal ensembles obtained by classical MC simulations. Therefore the dynamics of the MD simulation are quantum (semi–classical) thanks to the commutation relations implied in the derivations of the EoM. But the dynamics are not subject to any quantization. Meanwhile, the thermal distribution of the states obtained by MC simulation at low temperatures is conditioned by a classical, and not a quantum band dispersion [cf. Fig. 4.1].

We can therefore mimic the classical statistics found in MD simulation by treating $x_{\lambda,\mathbf{k}}$ and $p_{\lambda,\mathbf{k}}$ as independent, classical, variables, disregarding the bosonic behavior of the excitations in Eq. (5.6). Neglecting the quantization rules of the variables in Eq. (5.6) is equivalent to treating the fluctuations classically. This will therefore lead back to the classical theory developed in Section 3.2. However, obtained this way, the results are expressed in a form that makes it easy to compare with the quantum results. Therefore, this framework makes it suitable to easily draw relationships between classical and quantum results.

Setting $[\hat{x}_{\lambda,\mathbf{k}}, \hat{p}_{\lambda,\mathbf{k}}] = 0$, the partition function associated with the SHO Hamiltonian [Eq. (5.6)] is given by

$$\begin{aligned} Z^{\mathsf{CL}'} = e^{-\beta(E_0+\Delta E_0)} \prod_{\lambda,\mathbf{k}} \Bigg[\left(\int \mathrm{d}x_{\lambda,\mathbf{k}} \; e^{-\frac{1}{2}\beta m\epsilon(\mathbf{k})^2 x^2_{\lambda,\mathbf{k}}} \right) \\ \times \left(\int \mathrm{d}p_{\lambda,\mathbf{k}} \; e^{-\frac{\beta}{2m} p^2_{\lambda,\mathbf{k}}} e^{\beta\sqrt{\frac{2\xi_S^2(\mathbf{k})}{m\hbar\epsilon(\mathbf{k})}} \left(h^z_{\mathbf{k}} \delta_{1,\lambda} + h^x_{\mathbf{k}} \delta_{2,\lambda} \right) p_{\lambda,\mathbf{k}}} \right) \Bigg] , \end{aligned} \tag{5.7}$$

where $\beta = 1/k_B T$. The integrals in Eq. (5.7) can be calculated exactly by using Eq. (F.1a) and Eq. (F.1b). We obtain

$$Z^{\mathsf{CL}'} = e^{-\beta(E_0+\Delta E_0)} \prod_{\mathbf{k}}^{N} \left[\frac{2\pi}{\beta\epsilon(\mathbf{k})} e^{\frac{\beta\xi_S^2(\mathbf{k})(h^z_{\mathbf{k}})^2}{\hbar\epsilon(\mathbf{k})}} \; \frac{2\pi}{\beta\epsilon(\mathbf{k})} e^{\frac{\beta\xi_S^2(\mathbf{k})(h^x_{\mathbf{k}})^2}{\hbar\epsilon(\mathbf{k})}} \right] . \tag{5.8}$$

The excitations described by Eq. (5.8) are subject to classical (i.e. Boltzmann) statistics, by construction, and therefore can be associated with the fluctuations of MC simulation. The next step is to calculate equal–time spin correlations using the same procedure as described in Section 3.3.3. This involves computing the free energy and taking functional derivatives with respect to the field components $\mathbf{h}_{\mathbf{q}}$. The free energy

is given by

$$\begin{aligned} F^{\mathsf{CL}'} =& -\frac{\log(Z^{\mathsf{CL}'})}{\beta} \\ =& E_0 + \Delta E_0 - \frac{2}{\beta}\sum_{\mathbf{k}} \log(\frac{2\pi}{\beta\epsilon(\mathbf{k})}) - \sum_{\mathbf{k}} \left[\frac{\xi_{\mathsf{S}}^2(\mathbf{k})(h_{\mathbf{k}}^z)^2}{\hbar\epsilon(\mathbf{k})} + \frac{\xi_{\mathsf{S}}^2(\mathbf{k})(h_{\mathbf{k}}^x)^2}{\hbar\epsilon(\mathbf{k})} \right] + \mathcal{O}(T^2) \ . \end{aligned} \tag{5.9}$$

The first dipole moments are given by

$$\langle \hat{S}_{\mathbf{q}}^{\mu} \rangle = -\left. \frac{\partial F}{\partial h_{\mathbf{q}}^{\mu}} \right|_{\mathbf{h}=0} = 0 \ , \tag{5.10}$$

which is anticipated since we expect all dipole moment expectation values to vanish ($\langle \hat{S}_{\mathbf{q}}^{\alpha} \rangle \equiv 0$) in the FQ ground state. The second derivatives of the free energy with respect to field components $\mathbf{h}_{\mathbf{q}}$ correspond to

$$\langle \hat{S}_{\mathbf{q}}^{\alpha} \hat{S}_{-\mathbf{q}}^{\mu} \rangle - \langle \hat{S}_{\mathbf{q},\beta}^{\alpha} \rangle \langle \hat{S}_{-\mathbf{q}}^{\mu} \rangle = -\left. \frac{1}{\beta} \frac{\partial^2 F}{\partial h_{\mathbf{q}}^{\alpha} \partial h_{-\mathbf{q}}^{\mu}} \right|_{\mathbf{h}=0} \ . \tag{5.11a}$$

Using Eq. (5.10) and Eq. (5.11a), we find

$$S_{\mathrm{S}}^{\mathsf{CL}'}(\mathbf{q}, T) \ = \ \sum_{\alpha} \langle \hat{S}_{\mathbf{q}}^{\alpha} \hat{S}_{\mathbf{q}}^{\alpha} \rangle = \frac{4\xi_{\mathsf{S}}^2(\mathbf{q})}{\beta\hbar\epsilon(\mathbf{q})} \ . \tag{5.12}$$

The presence of the quantum dispersion $\epsilon(\mathbf{q})$ and coherence factor $\xi_{\mathsf{S}}(\mathbf{q})$ in Eq. (5.12), is very evocative of the quantum theory developed in Section 4.1. This is because we started from the quantum Hamiltonian, then "classicalized" the fluctuations and calculated the associated classical partition function. And, by direct comparison with Eq. (4.72a), we obtain

$$S_{\mathrm{S}}^{\mathsf{CL}'}(\mathbf{q}, T) = 2\frac{S_{\mathrm{S}}^{\mathsf{QM}}(\mathbf{q}, T=0)}{\beta\hbar\epsilon(\mathbf{q})} \ . \tag{5.13}$$

This is a result that holds in the limit of low temperature. Additionally, we can see that $S_{\mathrm{S}}^{\mathsf{CL}'}(\mathbf{q})$ is equivalent to the earlier classical result $S_{\mathrm{S}}^{\mathsf{CL}}(\mathbf{q})$ [Eq. (3.86)]. To this end, we can simplify Eq. (5.12), using Eq. (4.69) and Eq. (4.13) , we first obtain

$$\xi_{\mathsf{S}}^2(\mathbf{q}) = \frac{\sqrt{A_{\mathbf{q}} + B_{\mathbf{q}}}}{\sqrt{A_{\mathbf{q}} - B_{\mathbf{q}}}} \ , \tag{5.14}$$

then using Eq. (4.16) leads to

$$S_{\mathrm{S}}^{\mathsf{CL}'}(\mathbf{q}, T) \ = \ \frac{4}{\beta(A_{\mathbf{q}} - B_{\mathbf{q}})} = S_{\mathrm{S}}^{\mathsf{CL}}(\mathbf{q}, T) \ , \tag{5.15}$$

where for the last equality we used Eq. (3.22). This result is also valid in the limit of low temperatures. Finally, by combining Eq. (5.15) with Eq. (5.13), we obtain a rela-

tionship that links classical correlations at finite temperature, to quantum correlations at $T = 0$:

$$S_{\mathrm{S}}^{\mathsf{QM}}(\mathbf{q}, T = 0) = \lim_{T\to 0} \frac{\hbar\epsilon(\mathbf{q})}{2k_B T} S_{\mathrm{S}}^{\mathsf{CL}}(\mathbf{q}, T) \ , \tag{5.16}$$

where we make temperature explicit [Eq. (3.39)]. The approach that we illustrated for dipole moments ($\lambda = \mathsf{S}$) can be generalised to quadrupole moments ($\lambda = \mathsf{Q}$), and A–matrices ($\lambda = \mathsf{A}$). We obtain the following general result

$$S_{\lambda}^{\mathsf{QM}}(\mathbf{q}, T = 0) = \lim_{T\to 0} \frac{\hbar\epsilon(\mathbf{q})}{2k_B T} S_{\lambda}^{\mathsf{CL}}(\mathbf{q}, T) \ . \tag{5.17}$$

We emphasize that the dispersion $\epsilon(\mathbf{q})$ in Eq. (5.17) reflects the quantum nature of the dynamics since it is obtained from quantum excitations [Eq. (4.16)]. It is not the dispersion band of a classical theory. We also point out that the quantum mechanics have been treated at the semi–classical level, i.e. Gaussian level. In the path integral formulation, this would be equivalent to taking into account quantization, but only considering one path, which would correspond to the classical trajectory. In the case of a SHO, this approximation is exact.

Following the analysis Section 4.2.2 for calculating structure factors at the origin $\mathbf{q} = 0$, in order to account for ground state energy and zero–point fluctuation contributions, one should consider an expansion of $\Delta\mathcal{H}[\mathbf{h_i}]$ up to second order in fluctuations, followed by a Bogoliubov transformation to find the new fluctuations which diagonalize the total Hamiltonian $\mathcal{H}$. This means that neglecting terms higher than linear order for the source term $\Delta\mathcal{H}[\mathbf{h_i}]$ corresponds to assuming that the Bogoliubov ground state, diagonalizing the BBQ Hamiltonian $\mathcal{H}'_{\mathsf{BBQ}}$, is not perturbed by the source term. This implies that Eq. (5.17) is valid for corrections at finite energy. In other words, it means that the thermal contribution to the classical structure factors, which is linear in temperature, can be re–scaled to correspond to zero–temperature quantum contribution induced by quantum fluctuations.

Additionally, we can interpret the factor $\frac{2k_B T}{\hbar\omega}$ as having the effect of mimicking thermal fluctuations, as can be seen by inverting Eq. (5.17)

$$S_{\lambda}^{\mathsf{CL}}(\mathbf{q}, T) = \frac{2k_B T}{\hbar\omega} S_{\lambda}^{\mathsf{QM}}(\mathbf{q}, T = 0) \ , \tag{5.18}$$

where we take out the limit $T \to 0$, and implicitly work within this limit. This is easily understood by considering the steps of our derivations in Section 5.1. Indeed, we start by assuming a quantum system with fluctuations governed by quantum dynamics. We then consider these fluctuations to follow classical (Boltzmann) statistics. The next step is to treat each quantum fluctuation as two independent real fluctuations. The effect of this procedure is to allow the quantum excitations to become classical thermal fluctuations.

Indeed, the splitting of each quantum mode into two real independent ones is the key for understanding the prefactor '2' of $\frac{2k_B T}{\hbar\omega}$. Indeed by closer inspection of our derivation, we note that this has the effect of doubling the number of integrals when calculating the partition function. For instance, in our example, we go from a "complex" integral over bosonic variables (which should technically, in the quantum case

be a discrete sum over the Fock space) onto two independent integrals over the real variables: position and momentum. This results in a contribution from both of these real degrees of freedom that adds up in the description of the free energy. Therefore, the prefactor '2' of $\frac{2k_BT}{\hbar\omega}$ accounts for the fact that each quantum bosonic excitation that contributes to $S_\lambda^{\mathsf{QM}}(\mathbf{q}, T=0)$ decouples into two real thermal fluctuations. When considering the zero–temperature quantum case, we explicitly get rid of the two negative non–physical energy solutions, $\epsilon_{\mathbf{q},2}$ and $\epsilon_{\mathbf{q},4}$ [Eq. (4.11)], and only account for contributions of the creation bosons, i.e. only considering half of the spectrum which corresponds to the two physical positive quantum eigenmodes, $\epsilon_{\mathbf{q},1}$ and $\epsilon_{\mathbf{q},3}$. Meanwhile, in the classical case, all four eigenmodes [Eq. (3.22)] are well defined and will contribute.

This can also be linked back to our description of the expansions of the fluctuations [Section 2.5], where we saw that in the case of classical fluctuations four generators are broken inducing four classical modes, while in the quantum case these fluctuations are linked via Eq. (2.49), and only two generators are broken, producing two modes. Consequently, a classical system will be described by double the number of quantum modes, hence, the prefactor '2'.

5.2 Relationship Between Numerical Methods and Quantum Theory of Dynamical Correlations

We now use the analytical results and transpose them to the numerical simulations.

The main issue in "raw" u3MD results for dynamical structure factors is the loss of spectral intensities at low temperatures, relatively to quantum intensities at $T=0$ [cf. Fig. 4.3]. Additionally, at low temperatures, the analytical classical structure factor $S_\lambda^{\mathsf{CL}}(\mathbf{q}, T)$ is equivalent to the structure factor found in u3MC simulation

$$\lim_{T\to 0} S_\lambda^{\mathsf{MC}}(\mathbf{q}, T) = \lim_{T\to 0} S_\lambda^{\mathsf{CL}}(\mathbf{q}, T)\ . \tag{5.19}$$

This implies

$$S_\lambda^{\mathsf{QM}}(\mathbf{q}, T=0) = \lim_{T\to 0} \frac{\hbar\epsilon(\mathbf{q})}{2k_BT} S_\lambda^{\mathsf{MC}}(\mathbf{q}, T)\ . \tag{5.20}$$

Therefore, we can use u3MC simulation to predict, at a given $\mathbf{q}$, the total spectral weight of the zero–temperature quantum theory, as long as we know what the quantum characteristic energy scale $\epsilon(\mathbf{q})$ is. However, the relationship between classical and quantum results in the absence of the prior knowledge of the quantum dispersion, is what remains to be understood.

u3MD simulation causes a redistribution of the classical spectral weight at a given $\mathbf{q}$ over a range of different energies ω. To be exact, at a given $\mathbf{q}$, the u3MD simulation redistributes the classical spectral weight around the two eigenmodes $\epsilon(\mathbf{q})$ and $-\epsilon(\mathbf{q})$ [Eq. (4.11)] governing the equations of motion [Fig. 1.70] for the FQ state. Since the

total spectral weight at a given $\mathbf{q}$ is conserved, we have the following sum rule

$$S_\lambda^{\mathsf{MC}}(\mathbf{q},T) = \int_{-\infty}^{\infty} d\omega \; S_\lambda^{\mathsf{MD}}(\mathbf{q},\omega,T) \; , \tag{5.21}$$

which ensures that the u3MD scheme preserves the total spectral weight inherited from u3MC simulations [Section 2.6]. The u3MD scheme equally redistributes it into a contribution $S_\lambda^{\mathsf{MD}+}(\mathbf{q},\omega)$ around $+\epsilon(\mathbf{q})$ and a contribution $S_\lambda^{\mathsf{MD}-}(\mathbf{q}=\mathbf{K},\omega)$ at $-\epsilon(\mathbf{q})$ as expressed in Eq. (4.90).

To estimate the zero–temperature quantum result $S_\lambda^{\mathsf{QM}}(\mathbf{q},\omega,T=0)$, we need to construct a model that describes this redistribution of spectral weight, and imposes dynamics to be treated at a semi–classical level. It is now helpful to return to the simulation results for fluctuations about FQ order. To this end, we shortly revise what is presented in Section 4.3. From the "raw" results, Fig. 4.2 and Fig. 4.3, we learn that

1. the characteristic energy scale of excitations converges on the exact quantum (semi–classical) result for $T \to 0$, and

2. peak of the spectral weight sharpens (resolution limited) as $T \to 0$.

Because, we considered only the positive energy contribution of the u3MD results [Eq. (4.92)], the FQ order studied here shows a single, two–fold degenerate band of excitations. However, more generally, there may be several excitations with different energies at a given $\mathbf{q}$. But they will all have a well–defined energy, at least at the semi–classical level, (i.e. treated as a set of independent oscillators) and in a finite–size system.

Consequently, we model MD simulation results as

$$\lim_{T\to 0} S_\lambda^{\mathsf{MD}}(\mathbf{q},\omega,T) = \sum_{\nu=1,3} A_{\lambda,\nu}(\mathbf{q},T)\delta(\omega-\epsilon_{\mathbf{q},\nu}) + A_{\lambda,\nu}(\mathbf{q},T)\delta(\omega+\epsilon_{\mathbf{q},\nu}) + \mathcal{O}(T^2) \; , \tag{5.22}$$

where the sum on ν runs over the physical quantum modes, with $\nu = 1, 3$ in our case, but where thanks to the delta functions at positive and negative energy, we account for all eigenmodes of the system, $\epsilon_{\mathbf{q},1}$, $\epsilon_{\mathbf{q},2}$, $\epsilon_{\mathbf{q},3}$ and $\epsilon_{\mathbf{q},4}$ as given Eq. (4.11). This can be explained from the Bogoliubov transformation used to solve the quantum problem, that associates, to each physical quantum mode, a negative solution corresponding to the annihilation operator, i.e., $\epsilon_{\mathbf{q},1} = -\epsilon_{\mathbf{q},2}$, and $\epsilon_{\mathbf{q},3} = -\epsilon_{\mathbf{q},4}$.

The spectral weight $A_{\lambda,\nu}(\mathbf{q},T)$ is defined through

$$A_{\lambda,\nu}(\mathbf{q},T) = \frac{k_B T}{\hbar\epsilon_{\mathbf{q},\nu}} \tilde{\xi}^2_{\lambda,\nu}(\mathbf{q}) \; , \tag{5.23}$$

with $\tilde{\xi}^2_{\lambda,\nu}(\mathbf{q})$ is the generalized coherence factor

$$\tilde{\xi}^2_{\lambda,\nu}(\mathbf{q}) \geq 0 \; , \tag{5.24}$$

characteristic of the relevant structure factor λ and the mode ν. The sum rule of

Eq. (5.21) implies that the equal time structure factor is given by

$$S_\lambda^{\mathsf{MC}}(\mathbf{q},T)=\int_{-\infty}^{\infty}d\omega\ S_\lambda^{\mathsf{MD}}(\mathbf{q},\omega,T)=\sum_{\nu=1,3}2A_{\lambda,\nu}(\mathbf{q},T)\ . \tag{5.25}$$

In order to compare with analytical quantum zero–temperature results, we consider only the quantum modes allowed at zero temperature, i.e, only positive energies. This implies that we only consider the contribution of the delta function $\delta(\omega-\epsilon_\nu(\mathbf{q}))$

$$\lim_{T\to 0}S_\lambda^{\mathsf{MD}}(\mathbf{q},|\omega|,T)=\sum_{\nu=1,3}A_{\lambda,\nu}(\mathbf{q},T)\delta(\omega-\epsilon_{\mathbf{q},\nu})+\mathcal{O}(T^2)\ . \tag{5.26}$$

However, we still want the structure factor to satisfy the sum rum in Eq. (5.21). Therefore, we artificially multiply the contribution in Eq. (5.26) by two, and we redefine

$$\lim_{T\to 0}S_\lambda^{\mathsf{MD}}(\mathbf{q},\omega,T):=\sum_{\nu=1,3}2A_{\lambda,\nu}(\mathbf{q},T)\delta(\omega-\epsilon_{\mathbf{q},\nu})+\mathcal{O}(T^2)\ , \tag{5.27}$$

such that when integrated over energies, we obtain Eq. (5.25). The zero–temperature quantum predictions are then generalized by

$$S_\lambda^{\mathsf{QM}}(\mathbf{q},\omega,T=0)=\sum_{\nu=1,3}\tilde{\xi}^2_{\lambda,\nu}(\mathbf{q})\delta(\omega-\epsilon_{\mathbf{q},\nu})\ , \tag{5.28}$$

where the sum over ν only allows for the physical quantum modes. In our case, these are given by $\epsilon_{\mathbf{q},1}$, and $\epsilon_{\mathbf{q},3}$. $\tilde{\xi}_{\lambda,\nu}(\mathbf{q})$ corresponds to the rescaled coherence factors $\tilde{\xi}_\lambda(\mathbf{q})$, which for the FQ state is independent of the mode, since the modes are degenerate, i.e., $\epsilon(\mathbf{q})=\epsilon_{\mathbf{q},1}=\epsilon_{\mathbf{q},3}$ [Eq. (4.16)]. However, this is not generally the case.

We note that, for the FQ state, the summation over both bosonic modes yields a total of

$$S_\lambda^{\mathsf{QM}}(\mathbf{q},\omega,T=0)=2\tilde{\xi}^2_\lambda(\mathbf{q})\delta(\omega-\epsilon(\mathbf{q}))\ , \tag{5.29}$$

which is consistent with the results obtained in Eq. (4.71), Eq. (4.78), Eq. (4.86), for the structure factors associated with dipole moments, quadrupole moments, and the A–matrices, respectively, recalling that the original result in Eq. (5.17) is valid at finite energy. For the dipole structure factor, the rescaled coherence factor is simply given by the coherence factor defined in Eq. (4.69).

The total spectral weight is constrained through Eq. (5.21), and for the FQ state, satisfies

$$S_\lambda^{\mathsf{QM}}(\mathbf{q},T=0)=2\tilde{\xi}^2_\lambda(\mathbf{q})\ . \tag{5.30}$$

Within the area of validity of this model, there is no requirement for knowing the excitation energies $\epsilon_{\mathbf{q},\nu}$ a priori. And we can correct for the effect of classical statistics

in MD simulations. Therefore, we write

$$S_{\lambda}^{\mathsf{QM}}(\mathbf{q},\omega,T=0) \;=\; \lim_{T\to 0}\frac{\hbar\omega}{2k_BT}S_{\lambda}^{\mathsf{MD}}(\mathbf{q},\omega,T)\;, \tag{5.31}$$

where we emphasize that "QM" should be understood as "semi–classical", i.e. modeling excitations with quantum statistics but treating fluctuations at the Gaussian level. In Section 5.3, we provide an empirical evidence for Eq. (5.31) and the validity of its application for the FQ state of the BBQ model on the triangular lattice.

The relationship in Eq. (5.31) might, at first sight, look empirical, but it is actually exact, in the sense that it is an analytical formulation, within its range of applicability. It is formally derived from Eq. (5.17), which we obtained by taking the classical limit of a set of independent Harmonic Oscillators, which is well–defined and well–understood. Therefore, the questionable approximation is whether it is a valid assumption to assume that the fluctuations can be treated as variables of a quantum Harmonic Oscillator. The answer to this depends on the form of the interactions governing the fluctuations and to which leading order in temperature the relevant quantities need to be estimated. As previously mentioned, if the physical properties can be characterized up to linear order in temperature, i.e. expanding fluctuations up to quadratic (Gaussian) level, then Eq. (5.17) prevails.

We conclude by noticing that multiplication of the dynamical structure factors by a prefactor $\propto \beta\omega \propto \frac{\omega}{T}$, in order to correct for classical statistics, has been anticipated previously, including for the spin–$\frac{1}{2}$ magnet $Ca_10Cr_7O_28$ [189], where equivalent results for a system with many bands can be found in [189]. In the Supplemental Material of [267], an outline of the derivation is provided, but we note that the result differs by a factor of $\frac{1}{2}$, compared to the prediction established by Eq. (5.31), which is possibly due to a different definition of the considered spectral weight of the dynamical structure factor. Indeed, the definition that we use here has been artificially multiplied by 2.

As previously explained, the MD simulations inherit the classical spectral weights from MC simulations at a given $\mathbf{q}$ and split them for the FQ state onto the two doubly degenerate quantum modes $+\epsilon(\mathbf{q})$ and $-\epsilon(\mathbf{q})$, where the mode $-\epsilon(\mathbf{q})$ is allowed because u3MD simulations are performed at finite temperature. While the zero–temperature quantum analytical theory, the $-\epsilon(\mathbf{q})$ is disregarded as the ground state represents the lowest energy, and excitations with negative energy are non–physical. We can then interpret Eq. (5.31) as follows: the spectral weight at a given $\mathbf{q}$ obtained by u3MD simulation, which is artificially multiplied by two to compile all the spectral weight into positive energies, such that it equals the classical equal time structure factor, and which then is divided by '2' to account for the fact that in the zero–temperature quantum case, we have half of the number of modes that we have in the classical case (i.e. two quantum modes associated with the two bosonic quantum excitations versus four classical modes associated to the four classical fluctuations), and which is finally corrected for its classical statistics by multiplication of $\frac{\hbar\omega}{k_BT}$.

5.3 Comparison with Corrected Molecular Dynamics

Using Eq. (5.31), we can revisit u3MD simulation results that we previously discussed in Section 4.3. In Fig. 5.1, we show a comparison between u3MD simulation results, corrected according to Eq. (5.31) and the predictions of the zero–temperature quantum theory developed in Section 4.1 for excitations around a FQ ground state. Following Eq. (5.31), the correction of simulation results is obtained by multiplying the "raw" structure factors by a prefactor $\omega/2T$,

$$\tilde{S}^{\mathsf{MD}}_{\lambda}(\mathbf{q},\omega,T) \;=\; \frac{\omega}{2T} S^{\mathsf{MD}}_{\lambda}(\mathbf{q},\omega,T)\;, \tag{5.32}$$

where we set the constants k_B and $\hbar$ back to unity.

In Fig. 5.1 (d)–(f), we present u3MD results obtained at $T = 0.05\ J$, and accordingly corrected using Eq. (5.32). For consistency, the u3MD simulations were carried out at a resolution of $\delta\omega = 0.02\ J$, further corrected according to Eq. (5.32), and then finally convoluted with a Gaussian of FWHM $= 0.33\ J$. This way the final energy resolution $0.35\ J$ is the same as used previously in Section 4.3.

This allows us to directly compare corrected u3MD simulations in Fig. 5.1 (d)–(f), with "raw" u3MD results Fig. 5.1 (a)–(c), previously illustrated in Fig. 4.2 (a)–(c). For dipole moments, the corrected results show a loss of spectral weight as $\omega \to 0$ similar to the quantum prediction, while this was not the case for "raw" simulation results.

Additionally, for an easy comparison, in Fig. 5.1 (i)–(g), we reproduce the $T = 0$ analytic theory results previously shown in Fig. 4.1 and Fig. 4.2. By direct human eye comparison of plots for the dynamical structure factors in Fig. 5.1, we observe that corrected simulation results essentially perfectly agree with $T = 0$ quantum predictions, and that no discrepancies in the dispersion or in the intensities are visible.

Similar to the "raw" structure factors, by plotting $\tilde{S}^{\mathsf{MD}}_{\lambda}(\mathbf{q},\omega,T)$ at fixed wave vector $\mathbf{q}$, for a series of temperature values tending towards $T = 0$, we can obtain a more precise analysis of the low temperature scaling and confirm the excellent comparison with $T = 0$ quantum theory. This is illustrated in Fig. 5.2 (a), where we plot results for corrected dynamical structure factors associated with A–matrices $\tilde{S}^{\mathsf{MD}}_{\mathsf{A}}(\mathbf{q} = \mathbf{K},\omega,T)$, for temperatures between $T = 0.15\ J$ and $T = 0.01\ J$. They are represented by circles.

For comparison, we additionally reproduce the result of the $T = 0$ analytic theory, Eq. (4.86), represented by the dashed red line. u3MD simulation and quantum analytic results have both been convoluted with a Gaussian envelope of FWHM $0.02\ J$. We now observe that the intensities of the u3MD simulations, unlike the "raw" results, do not vanish as $T \to 0$, but converge to the quantum analytic result. We can see from Fig. 5.2 (a), that the limit $T \to 0$ in Eq. (5.31) now makes sense. Indeed, in function of temperature, MD simulation results corrected according to Eq. (5.32) form a sequence that converges towards the $T = 0$ analytic prediction for $T \to 0$, establishing the validity of Eq. (5.31).

We now examine more precisely the convergence behavior of the corrected simulation results towards the zero–temperature quantum result. The dispersing peak of $\tilde{S}^{\mathsf{MD}}_{\lambda}(\mathbf{q},\omega,T)$ is also well–described by the Voigt function given by Eq. (4.93). The fits of the Voigt function for the numerical data shown in Fig. 5.1 (d)–(f) are represented as solid lines in Fig. 5.2.

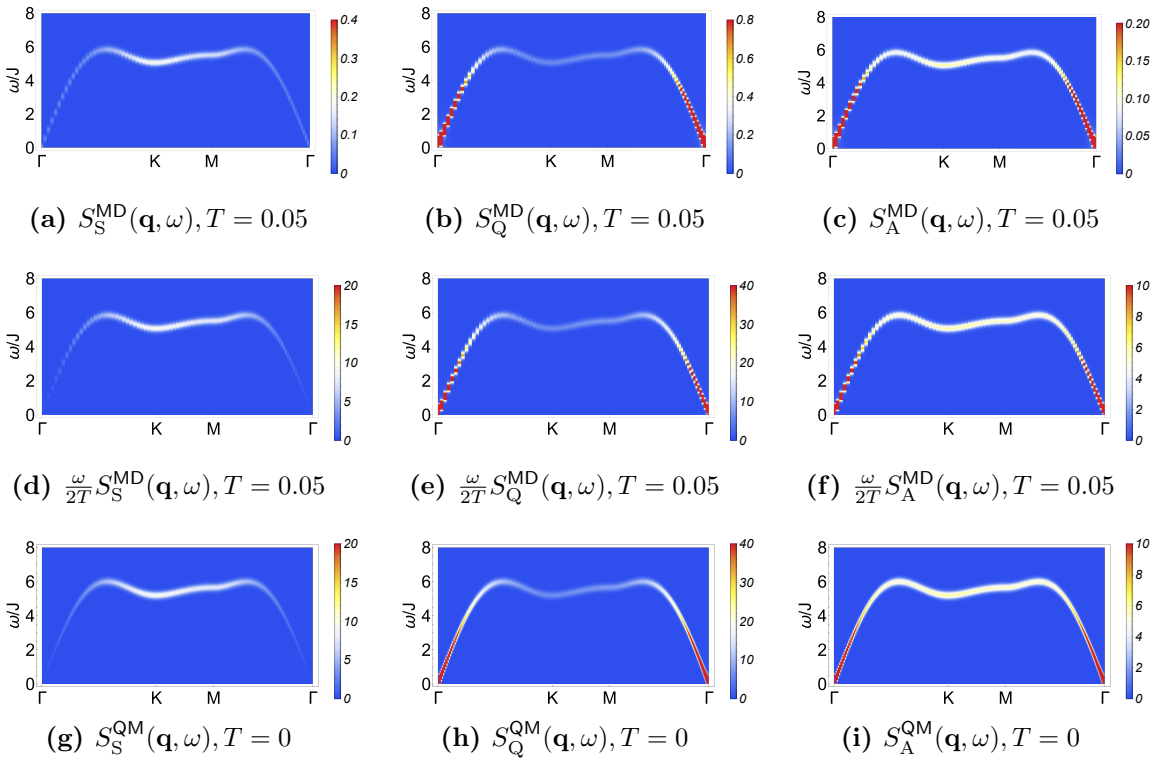

(a) $S_{\rm S}^{\rm MD}(\mathbf{q},\omega), T=0.05$ (b) $S_{\rm Q}^{\rm MD}(\mathbf{q},\omega), T=0.05$ (c) $S_{\rm A}^{\rm MD}(\mathbf{q},\omega), T=0.05$

(d) $\frac{\omega}{2T}S_{\rm S}^{\rm MD}(\mathbf{q},\omega), T=0.05$ (e) $\frac{\omega}{2T}S_{\rm Q}^{\rm MD}(\mathbf{q},\omega), T=0.05$ (f) $\frac{\omega}{2T}S_{\rm A}^{\rm MD}(\mathbf{q},\omega), T=0.05$

(g) $S_{\rm S}^{\rm QM}(\mathbf{q},\omega), T=0$ (h) $S_{\rm Q}^{\rm QM}(\mathbf{q},\omega), T=0$ (i) $S_{\rm A}^{\rm QM}(\mathbf{q},\omega), T=0$

Figure 5.1: Comparison between dynamical structure factors obtained from $U(3)$ Molecular Dynamics (u3MD) simulations [Section 2.6.2] and $T=0$ quantum theory results [Section 4.2] for a ferroquadrupolar (FQ) state. (a) Simulation results for dynamical structure factor associated with dipole moments, $S_{\rm S}^{\rm MD}(\mathbf{q},\omega)$. Dipolar fluctuations exhibit relatively high spectral weight near the top of the band, where excitations have more of a spin–wave character. (b) Equivalent results for quadrupole moments, $S_{\rm Q}^{\rm MD}(\mathbf{q},\omega)$. (c) Equivalent results for associated with A–matrices, $S_{\rm A}^{\rm MD}(\mathbf{q},\omega)$. (d) Simulation results for dynamical structure factor associated with dipole moments, $\tilde{S}_{\rm S}^{\rm MD}(\mathbf{q},\omega)$, corrected for classical statistics, following Eq. (5.32). (e) Equivalent results for quadrupole moments, $\tilde{S}_{\rm Q}^{\rm MD}(\mathbf{q},\omega)$. (f) Equivalent results for A–matrices, $\tilde{S}_{\rm Q}^{\rm MD}(\mathbf{q},\omega)$. (g) Prediction for $S_{\rm S}^{\rm QM}(\mathbf{q},\omega)$ from $T=0$ quantum theory [Eq. (4.71)]. (h) Equivalent prediction for $S_{\rm Q}^{\rm QM}(\mathbf{q},\omega)$ [Eq. (4.78)]. (i) Equivalent prediction for $S_{\rm A}^{\rm QM}(\mathbf{q},\omega)$ [Eq. (4.86)]. Simulations were carried out by my collaborator Dr. Rico Pohle, using the u3MD simulation scheme described in Section 2.6.2, for $\mathcal{H}_{\rm BBQ}$ [Eq. (2.72)] with parameters Eq. (3.87) at a temperature $T=0.05\ J$, in a cluster of linear dimension $L=96$ ($N=9216$ spins). All results have been convoluted with a Gaussian in frequency of FWHM $=0.35$ J. Figures are reproduced from [201].

From these fits, we can extract and estimate, within the limits set by the energy resolution of the simulations, the energy of the excitation $\omega(T)$, the inverse lifetime of the excitation, $\Gamma(T)$ and the intensity maximum $I(T)$.

In Fig. 5.2, we plot the shift in excitation energy $\Delta\omega(T)$ [Fig. 5.2 (b)], which is the energy difference between the zero–temperature prediction $\epsilon_{\mathbf{k}=0}$ and the energy of the excitation of the simulation. We also show the inverse lifetime of the excitation,

$\Gamma(T)$ [Fig. 5.2 (c)], and the intensity maximum $I(T)$ [Fig. 5.2 (d)], as a function of temperature.

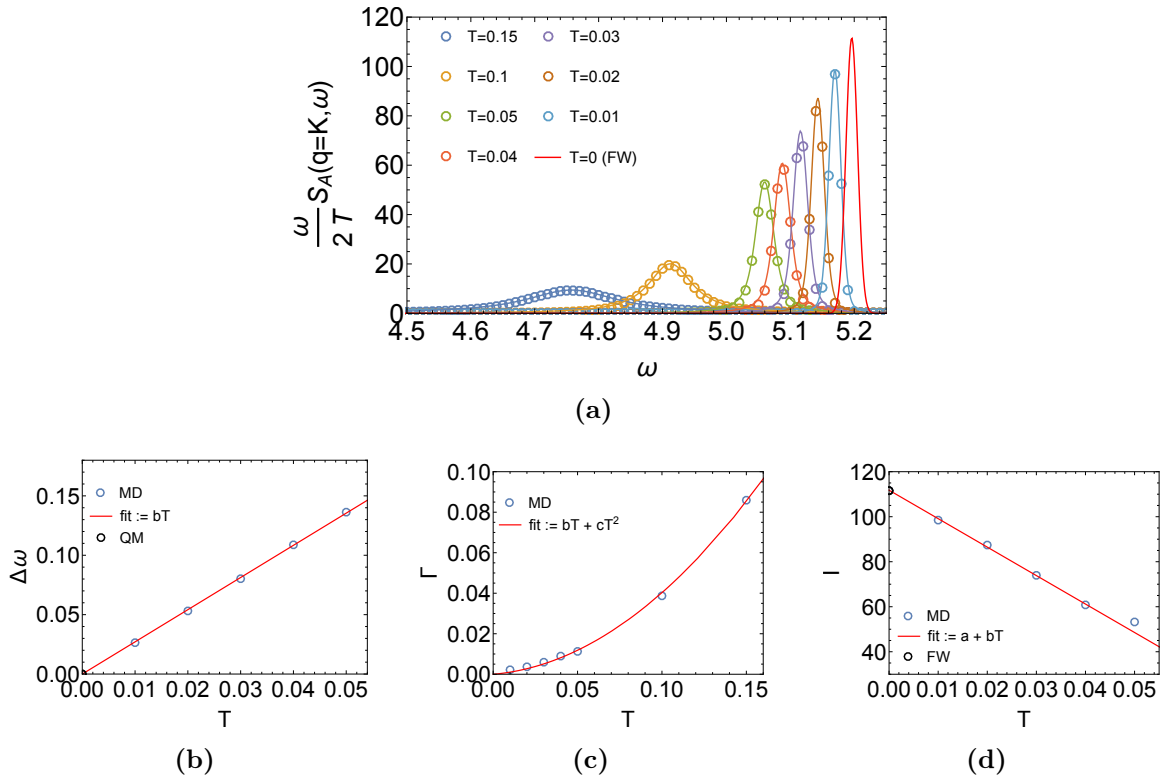

Figure 5.2: Temperature dependence of results of $U(3)$ Molecular Dynamics (u3MD) simulation corrected for classical statistics according to Eq. (5.32) and demonstrating successful convergence as $T \to 0$ towards the $T = 0$ quantum predictions. (a) u3MD results for dynamical structure factor associated with A–matrices, $S_{\rm A}^{\rm MD}(\mathbf{q}, \omega)$, at wave vector $\mathbf{q} = \mathbf{K}$, for temperatures between $T = 0.01\ J$ and $T = 0.15\ J$. u3MD simulation results are represented by circles. They have computed with an energy resolution $0.02\ J$, and have been corrected for classical statistics using Eq. (5.32). Solid lines are the fits of the u3MD results using a Voigt profile, Eq. (4.93). The prediction of the $T = 0$ quantum theory, Eq. (4.86), convoluted with a Gaussian of FWHM = 0.02 J, is shown with a solid red line. (b) Shift in peak energy $\Delta\omega(T)$, obtained by fitting using a Voigt profile, showing convergence of the peak position on the prediction of the $T = 0$ quantum theory. (c) Equivalent results for the inverse lifetime $\Gamma(T)$. (d) Equivalent results for the peak height, $I(T)$. u3MD simulations have been performed by my collaborator Dr. Rico Pohle, for parameters identical to those used in Fig. 5.1 and given by Eq. (3.87). Panels are reproduced from [201].

From [Fig. 5.2 (b)], we find that the characteristic energy of the excitations which corresponds to the peak position linearly converges towards the zero–temperature quantum result from below, according to

$$\Delta\omega(T) \quad = \quad bT + \mathcal{O}(T^3)\ , \ [\mathrm{b} = 2.71]\ . \tag{5.33}$$

The inverse lifetime of the excitation vanishes (approximately) quadratically as $T \to 0$

$$\Gamma(T) \;=\; bT + cT^2 + \mathcal{O}(T^3)\ ,\ [\text{b} = 0.07,\ \text{c} = 3.26]\ , \tag{5.34}$$

as illustrated in Fig. 5.2 (c). Finally, in Fig. 5.2 (d), we observe the maximum intensity of the peak $I(T)$ also converges linearly on the zero–temperature quantum result as

$$I(T) \;=\; a + bT + \mathcal{O}(T^3)\ ,\ [\text{a} = 111,\ \text{b} = \text{-}1230]\ , \tag{5.35}$$

where the value of coefficient a agrees with the prediction of the $T = 0$ quantum theory.

It is possible to derive a similar formalism in terms of Green's functions and to expand the self–energy diagrammatically for excitations within the mixed ensemble of states characteristic to MD simulations [22]. Such calculations go beyond the scope of this Thesis but, it should ultimately be possible to derive a schematic analytic interpretation of the trends observed in simulations.

Chapter 6

Spin–1 Magnets with Anisotropic Interactions

In Chapters 2 to 5, I have shown how the formalism based on the algebra $u(3)$ can be used to describe both the thermodynamic and dynamical properties of spin–1 magnets which preserves spin–rotation symmetry. In this Chapter, I extend this analysis to more general cases considering models with spin–anisotropic interactions.

I start in Section 6.1, by reviewing the condition needed for an $u(3)$ A–matrix to describe a spin–1 moment. Indeed, within our description of $u(3)$ generators, we can also allow for spin configuration with $s \neq 1$. This is resolved by enforcing the trace of the $u(3)$ A–matrices to unity [Eq. (2.57)]. Therefore, I here show that, at the level of single spin–1 moments, spin–anisotropic interactions do not mix sectors of $u(3)$ with different spin values, and that all of the general results of Chapter 2 hold in the presence of spin–anisotropy. This implies that, if started from valid spin–1 configuration with $\mathrm{Tr}(\mathcal{A}) = 1$ [Eq. (2.57)] being satisfied, both u3MC and u3MD simulations offer powerful tools to investigate properties of spin–1 systems with spin–anisotropic interactions.

In Section 6.2.1, I illustrate this result on the FQ order of the BBQ model with anisotropic nearest-neighbors interactions, supplemented by single–ion anisotropy. We show results obtained by a $T = 0$ analytical theory that I compare against u3MD simulations corrected for their classical statistics.

Finally, in Section 6.3, I consider the easy–plane, single–ion anisotropic, ferromagnetic order for the BBQ model on the triangular lattice. This will prove useful to explain how my analytical method applies when dipolar order rather than quadrupolar order is present. A–matrices are very useful for quadrupolar order, but when the ground state is not time–reversal symmetric, some extra care needs to be taken.

6.1 Generalization of the $u(3)$ Approach to Anisotropic Interactions

In this section, we generalize to spin–anisotropic models the arguments that we used as evidence for the validity of our method [Fig. 1.70 and Eq. (2.76)] when considering the BBQ Hamiltonian in Section 2.4.5.

Our aim is to model spin–1 moments on a lattice. In Section 2.4, we developed

an approach that allows us to represent a spin–1 moment by the algebra $u(3)$ supplemented by a constraint [Eq. (2.57)] that reduces back to $su(3)$, which is the correct representation for a spin–1. Therefore, for our $u(3)$ approach to properly describe spin–1 moments, the constraint [Eq. (2.57)] on the trace of the A–matrices which act as the generators of $u(3)$ must be preserved. In u3MC simulation [Section 2.6.1], because of sampling of states described on the 5–dimensional sphere, or as we saw, equivalently by fixing the gauge degree of freedom, on the 4–dimensional sphere, this condition is true by construction. However, this step is of crucial importance for the validity of the u3MD results and ensures that the simulations properly describe spin–1 moments of fixed length throughout time evolution. In Section 2.4.5, we showed that this was the case [Fig. 1.70 and Eq. (2.76)] for the $SU(2)$ symmetric BBQ model [Eq. (1.48)], implying that the length of the spin is conserved at each site.

We here show that the trace of the A–matrix defined at each site and representing a spin–1 is also preserved for models with spin–anisotropic interactions. To this end, let us consider the most general form of spin–anisotropic Hamiltonian which is allowed for a spin–1 moment

$$\mathcal{H}_\Delta = \sum_{\langle i,j \rangle} J^{\alpha\mu}_{\beta\nu} \hat{\mathcal{A}}^{\alpha}_{i\ \beta} \hat{\mathcal{A}}^{\mu}_{j\ \nu} + \sum_i L^{\alpha}_{\beta} \hat{\mathcal{A}}^{\alpha}_{i\ \beta} \ , \tag{6.1}$$

where the interaction couplings satisfy

$$J^{\alpha\mu}_{\beta\nu} = (J^{\beta\nu}_{\alpha\mu})^\dagger \qquad L^{\alpha}_{\beta} = (L^{\beta}_{\alpha})^\dagger \ , \tag{6.2}$$

as required from the fact that $\mathcal{H}_\Delta$ must remain Hermitian. From the Heisenberg equations of motion follows that

$$\begin{aligned} \partial_t \hat{\mathcal{A}}^{\gamma}_{i\ \eta} &= -\, i\, [\, \hat{\mathcal{A}}^{\gamma}_{i\ \eta}, \mathcal{H}_\Delta \,] \\ &= -\, \frac{i}{2} \sum_\delta \Big(J^{\eta\alpha}_{\mu\beta} \hat{\mathcal{A}}^{\gamma}_{i\ \mu} + J^{\alpha\eta}_{\beta\mu} \hat{\mathcal{A}}^{\gamma}_{i\ \mu} - J^{\mu\alpha}_{\gamma\beta} \hat{\mathcal{A}}^{\mu}_{i\ \eta} - J^{\alpha\mu}_{\beta\gamma} \hat{\mathcal{A}}^{\mu}_{i\ \eta} \Big) \hat{\mathcal{A}}^{\alpha}_{i+\delta\ \beta} \\ &\quad -\, \frac{i}{2} (\, L^{\eta}_{\alpha} \hat{\mathcal{A}}^{\gamma}_{i\ \alpha} - L^{\alpha}_{\gamma} \hat{\mathcal{A}}^{\alpha}_{i\ \gamma} \,) \ . \end{aligned} \tag{6.3}$$

By setting $\eta = \gamma$ and taking the trace, we find

$$\partial_t \mathrm{Tr}\ \mathcal{A}_i = -\frac{i}{2} \sum_\delta (\, J^{\alpha\gamma}_{\beta\mu} \hat{\mathcal{A}}^{\gamma}_{i\ \mu} - J^{\alpha\mu}_{\beta\gamma} \hat{\mathcal{A}}^{\mu}_{i\ \gamma} \,) \hat{\mathcal{A}}^{\alpha}_{i+\delta\ \beta} - \frac{i}{2} (\, L^{\gamma}_{\alpha} \quad \hat{\mathcal{A}}^{\gamma}_{i\ \alpha} - L^{\alpha}_{\gamma} \hat{\mathcal{A}}^{\alpha}_{i\ \gamma} \,) \ , \tag{6.4}$$

where we used the relationship

$$J^{\alpha\mu}_{\beta\nu} = J^{\mu\alpha}_{\nu\beta} \ , \tag{6.5}$$

which is implied from the fact that two components of $\mathcal{A}$ defined at different lattice sites commute [Eq. (1.66)]. By rearranging indices of Eq. (6.4), we obtain

$$\partial_t \mathrm{Tr}\ \hat{\mathcal{A}}_{\mathrm{i}}\ = 0 \ . \tag{6.6}$$

This implies that the trace of $\mathcal{A}$ is conserved through time evolution for arbitrary spin–anisotropic interactions and that within u3MD simulations the constraint on spin–

length is preserved. The implication of this result is that instead of solving the more complicated equations of motion for spin–1 moments found in the algebra $su(3)$ [14, 200, 264], we can equivalently solve the $u(3)$ equations of motion, Eq. (2.74), for a spin–1 moment, regardless of spin–anisotropy.

6.2 Application to the FQ State with Single–Ion, Easy–Plane Anisotropy

In this section, we concretely illustrate an example of a system with spin–anisotropic interactions by considering a simple expansion of the BBQ model, which was previously studied for the FQ phase and which we already obtained results for. This model was first studied in [176], with an additional Zeeman coupling term. In Section 6.2.1, we investigate this example by using the analytical quantum theory of fluctuations and compare these results against u3MD simulations in Section 6.2.2.

6.2.1 Analytical Quantum Theory for the FQ state with Single–Ion, Easy–Plane Anisotropy

We choose to apply our $u(3)$ framework to the spin–1 BBQ model with single–ion, easy–plane anisotropy

$$\mathcal{H}_{\mathsf{D}} = \mathcal{H}_{\mathsf{BBQ}} + \mathcal{H}_{\mathsf{SI}} \,, \tag{6.7}$$

where $\mathcal{H}_{\mathsf{BBQ}}$ is given in Eq. (1.48), and where $\mathcal{H}_{\mathsf{SI}}$ denotes the single–ion term defined as

$$\mathcal{H}_{\mathsf{SI}} = \sum_i D(\hat{\mathrm{S}}_i^y)^2 \,, \quad [D > 0] \,. \tag{6.8}$$

This model has previously been studied in [176]. Chosen this way, the anisotropic model $\mathcal{H}_{\mathsf{D}}$ springs from the BBQ model and for the triangular lattice, it therefore also displays a FQ phase for parameters $(J_1, J_2 < 0)$. Additionally, it is easily seen that the single–ion anisotropy term $\mathcal{H}_{\mathsf{SI}}$ [Eq. (6.8)] represents a quadrupole Q^{yy} [Eq. (1.44)], and for the considered coupling constant $D > 0$ favors a quadrupole moment characterized by its director being aligned along the y–axis [Eq. (2.43)]. This is consistent with our deliberate choice of expressing the FQ ground state by $|y\rangle$ [Eq. (3.2)]

Because we already have everything set up for the BBQ Hamiltonian and described in the form of A–matrices expressed in terms of quantum fluctuations [Eq. (4.4)], the next step is to write down the Hamiltonian in terms of $\mathcal{H}_{\mathsf{SI}}$ in terms of $\mathcal{A}$–matrices. Using Eq. (1.67), we find

$$\mathcal{H}_{\mathsf{SI}} = \sum_i D\left(-\frac{2}{3}\hat{\mathcal{A}}_{i\ y}^{y} + \frac{1}{3}\hat{\mathcal{A}}_{i\ x}^{x} + \frac{1}{3}\hat{\mathcal{A}}_{i\ z}^{z} + \frac{2}{3}\right) \,. \tag{6.9}$$

Expressed this way, it is obvious that $\mathcal{H}_{\mathsf{SI}}$ is a special case of the A-matrix single–ion term in Eq. (6.1).

Using Eq. (4.4), we can then express $\mathcal{H}_{\mathsf{SI}}$ in terms of the Bosonic excitations obtained by generating fluctuations around the FQ state as explained in Section 3.1, and by ensuring their quantum nature as discussed in Section 4.1. Using Eq. (4.5) with Eq. (3.16) for the BBQ term, the total Hamiltonian $\mathcal{H}_{\mathsf{D}}$ can then be written in a similar form as Eq. (4.5). We find

$$\mathcal{H}'_{\mathsf{D}} = E_0 + \frac{1}{2}\sum_{\mathbf{k}} \left[\hat{\mathbf{w}}^{\dagger}_{\mathbf{k}} M^{\mathsf{SI}}_{\mathbf{k}} \hat{\mathbf{w}}_{\mathbf{k}}\right] + \mathcal{O}(\vec{w}^4) \,, \tag{6.10}$$

where the bosons are encoded into $\hat{\mathbf{w}}_{\mathbf{k}}$ given by Eq. (4.6b) and where $M^{\mathsf{SI}}_{\mathbf{k}}$ yields

$$M^{\mathsf{SI}}_{\mathbf{k}} = \begin{pmatrix} A_{\mathbf{k}}+D & -B_{\mathbf{k}} & 0 & 0 \\ -B_{\mathbf{k}} & A_{\mathbf{k}}+D & 0 & 0 \\ 0 & 0 & A_{\mathbf{k}}+D & -B_{\mathbf{k}} \\ 0 & 0 & -B_{\mathbf{k}} & A_{\mathbf{k}}+D \end{pmatrix} , \tag{6.11}$$

with $A_{\mathbf{k}}$ and $B_{\mathbf{k}}$ being defined in Eq. (3.17). Compared to the pure BBQ case [Eq. (3.16)], we see that the effect of $\mathcal{H}_{\mathsf{SI}}$ is to introduce new diagonal terms in the interaction matrix governing the dispersion of excitations [Eq. (4.6b)]. We then perform a Bogoliubov transformation by solving the appropriate eigensystem [Eq. (4.9)]. We obtain two degenerate physical modes of excitation, whose dispersions are given by

$$\epsilon_{\mathbf{k}} = \sqrt{(A_{\mathbf{k}}+D)^2 - B^2_{\mathbf{k}}} \,. \tag{6.12}$$

This implies that the adjunction of the easy–plane anisotropy has the effect of opening a gap

$$\Delta = \sqrt{2A_0 D + D^2} \,, \tag{6.13}$$

and shifting the Goldstone modes of FQ order to higher energies. Because in the presence of single–ion, easy–plane anisotropy, the FQ state preserves the symmetry of the Hamiltonian, it no longer reflects a spontaneous symmetry breaking, and we expect the excitations to require finite energy.

We can also very easily generalize the derivation of structure factors calculated in Section 4.2 for the FQ state of the isotropic BBQ model. Indeed, by simply substituting

$$A_{\mathbf{k}} \longrightarrow A_{\mathbf{k}} + D \,, \tag{6.14}$$

into the results obtained for $S^{\mathsf{QM}}_{\mathrm{A}}(\mathbf{q},\omega)$ [Eq. (4.86)], $S^{\mathsf{QM}}_{\mathrm{Q}}(\mathbf{q},\omega)$ Eq. (4.78)] and $S^{\mathsf{QM}}_{\mathrm{S}}(\mathbf{q},\omega)$ [Eq. (4.71)], all these derivation can be adapted for the FQ state of the single–ion, easy–plane anisotropy model $\mathcal{H}_{\mathsf{D}}$ [Eq. (6.7)].

In Fig. 6.1 (a)–(c) , we show results for the parameter set

$$J_1 = 0 \,,\; J_2 = -1.0 \,,\; D = 0.2 \,. \tag{6.15}$$

These correspond to predictions obtained for the $T = 0$ quantum (semi–classical) analytical theory.

6.2.2 Comparison to Molecular Dynamics Simulations

Following the analysis of Section 6.1, we can also apply the u3MD simulation scheme [Section 2.6.2] to the easy–plane model $\mathcal{H}_{\mathsf{D}}$ [Eq. (6.7)]. In Fig. 6.1 (d)–(f), results obtained from u3MD simulation are shown.

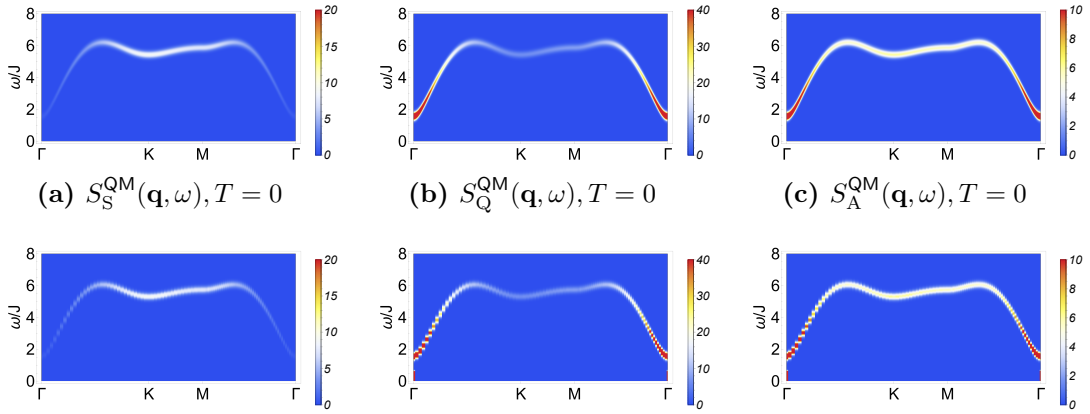

(a) $S_{\mathrm{S}}^{\mathsf{QM}}(\mathbf{q},\omega), T=0$ **(b)** $S_{\mathrm{Q}}^{\mathsf{QM}}(\mathbf{q},\omega), T=0$ **(c)** $S_{\mathrm{A}}^{\mathsf{QM}}(\mathbf{q},\omega), T=0$

(d) $\frac{\omega}{2T} S_{\mathrm{S}}^{\mathsf{MD}}(\mathbf{q},\omega), T/J=0.05$ **(e)** $\frac{\omega}{2T} S_{\mathrm{Q}}^{\mathsf{MD}}(\mathbf{q},\omega), T/J=0.05$ **(f)** $\frac{\omega}{2T} S_{\mathrm{A}}^{\mathsf{MD}}(\mathbf{q},\omega), T/J=0.05$

Figure 6.1: Comparison of u3MD simulation results and $T=0$ analytical quantum prediction for the dynamical structure factors of a ferroquadrupolar (FQ) state in the spin–1 bilinear–biquadratic (BBQ) model with easy–plane anisotropy $\mathcal{H}_{\mathsf{D}}$ [Eq. (6.7)]. (a) Dipole dynamical structure factor, $S_{\mathrm{S}}^{\mathsf{QM}}(\mathbf{q},\omega)$, predicted by $T=0$ quantum theory of Section 6.2.1. (b) Equivalent results for quadrupole moments, $S_{\mathrm{Q}}^{\mathsf{QM}}(\mathbf{q},\omega)$. (c) Equivalent results for A–matrices, $S_{\mathrm{A}}^{\mathsf{QM}}(\mathbf{q},\omega)$. (d) Dipole dynamical structure factor $S_{\mathrm{S}}^{\mathsf{MD}}(\mathbf{q},\omega)$ found in molecular dynamics simulations within $u(3)$ representation (u3MD) . (e) Equivalent results for quadrupole moments, $S_{\mathrm{Q}}^{\mathsf{MD}}(\mathbf{q},\omega)$. (f) Equivalent results for A–matrices, $S_{\mathrm{A}}^{\mathsf{MD}}(\mathbf{q},\omega)$. Numerical simulations were carried out by my collaborator Rico Pohle for $\mathcal{H}_{\mathsf{D}}$ [Eq. (6.7)], with parameters given in Eq. (6.15), at a temperature $T=0.05\ J$, for system size of dimension $L=96$ ($N=9216$ spins). u3MD results have been corrected for classical statistics by multiplication by a prefactor $\omega/2T$ following Eq. (5.32). All results have been convoluted with a Gaussian in frequency of FWHM = 0.35 J. Figures are reproduced from [201].

These were performed for the parameter set Eq. (6.15) consistent with a FQ ground state. u3MD results have been corrected for the effect of classical statistics using Eq. (5.32). We see that corrected simulation results show very good agreement with the $T=0$ quantum predictions of the analytic theory developed in Section 6.2.1.

These results provide an explicit demonstration of the ability of u3MD simulations to describe the excitations of spin–1 models with spin–anisotropic interactions.

6.3 Application to an Easy–Plane Ferromagnet with both Single–Ion and Exchange Anisotropy

Up to this point, all the explicit predictions for dynamical quantities have been computed for systems with a FQ ground state. Here, we show that the exact same methods can be applied to models with conventional dipolar magnetic order as well. To this end, we illustrate our $u(3)$ formalism and its representation in terms of the A-matrices to the Heisenberg ferromagnetic easy-plane anisotropic model. The A-matrices are especially useful to work with, when the relevant quantities are easily expressed in the TR-invariant basis, and are relatively easy to use when the ground state is quadrupolar. They can also equally well be applied to systems with dipolar order, but some additional care is required.

We demonstrate here how one can carefully apply our analytical theory of fluctuations developed in Section 2.5 to systems with dipolar order. Additionally, we make the interactions anisotropic. We show results for the zero–temperature quantum structure factors for dipole, quadrupole and A-matrix moments applied to the ferromagnetic (FM) state on the triangular lattice for the anisotropic Heisenberg Hamiltonian (BBQ Hamiltonian [Eq. (1.48)] with anisotropic J_1 and $J_2 = 0$), with single–ion anisotropy.

We consider the following Hamiltonian

$$\mathcal{H} = \mathcal{H}^{\mathrm{EP}} + \mathcal{H}^{\mathrm{SI}} \,. \tag{6.16}$$

$\mathcal{H}^{\mathrm{EP}}$ represents the Heisenberg Hamiltonian for spin-1 with easy–plane Heisenberg anisotropic exchange couplings $\mathbf{J}$

$$\mathcal{H}^{\mathrm{EP}} = \sum_{\langle i,j \rangle} \left[\hat{\mathbf{S}}_{\boldsymbol{i}} \cdot \mathbf{J} \cdot \hat{\mathbf{S}}_{\boldsymbol{j}} \right] \,, \tag{6.17}$$

where the spin dipole operator $\hat{\mathbf{S}}_{\boldsymbol{i}}$ is defined in Eq. (1.26), and where $\mathbf{J}$ corresponds to the usual nearest–neighbor spin–spin coupling tensor. $\mathcal{H}^{\mathrm{SI}}$ accounts for single–ion anisotropy and is given by

$$\mathcal{H}^{\mathrm{SI}} = \sum_{i} \hat{\mathbf{S}}_{\boldsymbol{i}} \mathbf{D} \hat{\mathbf{S}}_{\boldsymbol{i}} \,, \tag{6.18}$$

where $\mathbf{D}$ corresponds to the usual single site spin-spin coupling tensor. We assume the spin-spin coupling tensors $\mathbf{J}$ and $\mathbf{D}$ to only have diagonal components:

$$\mathcal{H}^{\mathrm{EP}} = \sum_{\langle i,j \rangle} \left[J^{xx} \hat{\mathrm{S}}_i^x \hat{\mathrm{S}}_j^x + J^{yy} \hat{\mathrm{S}}_i^y \hat{\mathrm{S}}_j^y + J^{zz} \hat{\mathrm{S}}_i^z \hat{\mathrm{S}}_j^z \right] \,, \tag{6.19}$$

$$\mathcal{H}^{\mathrm{SI}} = \sum_{i} \left[D^{xx} \hat{\mathrm{S}}_i^x \hat{\mathrm{S}}_i^x + D^{yy} \hat{\mathrm{S}}_i^y \hat{\mathrm{S}}_i^y + D^{zz} \hat{\mathrm{S}}_i^z \hat{\mathrm{S}}_i^z \right] \,. \tag{6.20}$$

We also assume the coupling constants to be negative and the order to be ferromagnetic:

$$J^{\alpha\alpha} < 0 \,, \tag{6.21}$$

$$D^{\alpha\alpha} < 0 \,, \text{ where } \; D^{\perp} = D^{yy} = D^{zz} \text{ with } \left| D^{\perp} \right| < |D^{xx}| \,. \tag{6.22}$$

This is consistent with the easy-plane FM order and the following choice of the ground state. We consider the ground state to have its spin dipole moment in the xy–plane. Without loss of generality we can choose it to be pointing along the x–axis:

$$|GS\rangle = |1^x\rangle \ . \tag{6.23}$$

As a basis to easily express the ground state $|1^x\rangle$, we choose the eigenstates of $\hat{\mathrm{S}}_i^x$:

$$\mathcal{B}^x = \left\{|1^x\rangle, |0^x\rangle, |\overline{1^x}\rangle\right\} \ , \tag{6.24}$$

which are illustrated in Fig. 6.2.

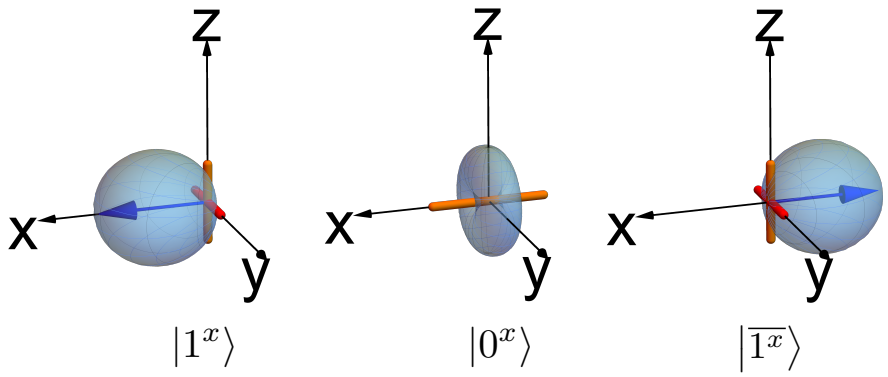

Figure 6.2: Eigenstates of $\hat{\mathrm{S}}_i^x$ forming the basis states of $\mathcal{B}^x$ [Eq. (6.24)]. Figure is reproduced from [201].

The basis states in Eq. (6.24) satisfy

$$\langle 1^x|\hat{\mathrm{S}}_i^x|1^x\rangle = 1 \ , \tag{6.25a}$$
$$\langle 0^x|\hat{\mathrm{S}}_i^x|0^x\rangle = 0 \ , \tag{6.25b}$$
$$\langle \overline{1^x}|\hat{\mathrm{S}}_i^x|\overline{1^x}\rangle = -1 \ , \tag{6.25c}$$
$$\langle \alpha|\hat{\mathrm{S}}_i^\mu|\alpha\rangle = 0 \quad \text{for } |\alpha\rangle \in \mathcal{B}^x \text{ and } \mu = y, z \ . \tag{6.25d}$$

Even though the A-matrices are deeply linked to the time-reversal (TR) invariant basis [Eq. (2.32)], we will here mostly focus on the basis $\mathcal{B}^x$ [Eq. (6.24)] and then transform the required quantities accordingly into the TR invariant basis.

We define the basis change Λ_3 to be the basis change matrix between the TR invariant $\mathcal{B}_2$ [Eq. (2.32)] and the magnetic x–basis $\mathcal{B}^x$ [Eq. (6.24)]. This implies that state $|\phi\rangle_{\mathcal{B}_2}$ given in the TR invariant basis $\mathcal{B}_2$, its components transform according to

$$|\phi\rangle_{\mathcal{B}^x} = \Lambda_3 |\phi\rangle_{\mathcal{B}_2} \ , \tag{6.26}$$

where the basis change matrix Λ_3 is given by

$$\Lambda_3 = \begin{pmatrix} 0 & \frac{1}{\sqrt{2}} & \frac{i}{\sqrt{2}} \\ -i & 0 & 0 \\ 0 & \frac{1}{\sqrt{2}} & -\frac{i}{\sqrt{2}} \end{pmatrix} \ . \tag{6.27}$$

An operator $\hat{\mathrm{O}}_{\mathcal{B}_2}$ given in the TR invariant basis $\mathcal{B}_2$ transforms as

$$\hat{\mathrm{O}}_{\mathcal{B}^x} = \Lambda_3 \hat{\mathrm{O}}_{\mathcal{B}_2} \Lambda_3^\dagger \,, \tag{6.28}$$

in the basis $\mathcal{B}^x$.

In what follows, we start working in the $\mathcal{B}^x$ basis, where everything is simple, since the ground state is one of the basis states and the orthogonal fluctuations can be expressed in terms of the other orthogonal basis states. And, we will later transform the relevant quantities into the TR invariant basis, by considering the inverse of Eq. (6.28). Indeed, the ground state matrix takes the simple form

$$\mathbf{A}_{\mathbf{0}\mathcal{B}^x} = \begin{pmatrix} 1 & 0 & 0 \\ 0 & 0 & 0 \\ 0 & 0 & 0 \end{pmatrix} \,, \tag{6.29}$$

since the ground state is simply the state $|1^x\rangle$ [Eq. (6.23)]. In terms of the director components, we obtain

$$\mathbf{d}^\dagger_{0\mathcal{B}^x} = \begin{pmatrix} 1 \\ 0 \\ 0 \end{pmatrix} \,. \tag{6.30}$$

As explained in Section 2.5, we can generate orthogonal fluctuations by application of the exponential map given in Eq. (2.86). The new state describing the fluctuations around the ground state is given by

$$\mathbf{d}^\dagger(\phi) = \hat{R}(\phi)\mathbf{d}_0^\dagger \,. \tag{6.31}$$

The A matrix transforms according to Eq. (2.88). Only the generators $\hat{\mathcal{A}}^x{}_x$, $\hat{\mathcal{A}}^x{}_y$, $\hat{\mathcal{A}}^x{}_z$, $\hat{\mathcal{A}}^y{}_x$, and $\hat{\mathcal{A}}^z{}_x$ will have non–zero contribution when applied to the ground state matrix [Eq. (6.29)]. Fig. 6.3 represents the action of the generators on the ground state. We can see, for example, that the generator $\hat{\mathcal{A}}^x{}_y$, will create a fluctuation along $|0^x\rangle$, i.e. an $\hat{\mathrm{a}}^\dagger$ boson, and will induce the new state to exhibit some quadrupolar features.

Using the constraint on the trace of A-matrices [Eq. (2.48)], we can disregard the contribution from $\hat{\mathcal{A}}^x{}_x$. We ensure that the trace of A equals unity [Equation 2.57], such that we properly restrict to $su(3)$ and make sure that we are correctly representing a spin-1. We obtain

$$\mathbf{A}(\phi)_{\mathcal{B}^x} = \begin{pmatrix} 1 - \phi_{xy}\phi_{yx} - \phi_{xz}\phi_{zx} & i\phi_{xy} & i\phi_{xz} \\ -i\phi_{yx} & \phi_{xy}\phi_{yx} & \phi_{xz}\phi_{yx} \\ -i\phi_{zx} & \phi_{xy}\phi_{zx} & \phi_{xz}\phi_{zx} \end{pmatrix} \,. \tag{6.32}$$

We can then easily introduce bosonic fluctuations through

$$i\phi_{xy} = \hat{\mathrm{a}} \,, \tag{6.33a}$$
$$-i\phi_{yx} = \hat{\mathrm{a}}^\dagger \,, \tag{6.33b}$$
$$i\phi_{xz} = \hat{\mathrm{b}} \,, \tag{6.33c}$$
$$-i\phi_{zx} = \hat{\mathrm{b}}^\dagger \,. \tag{6.33d}$$

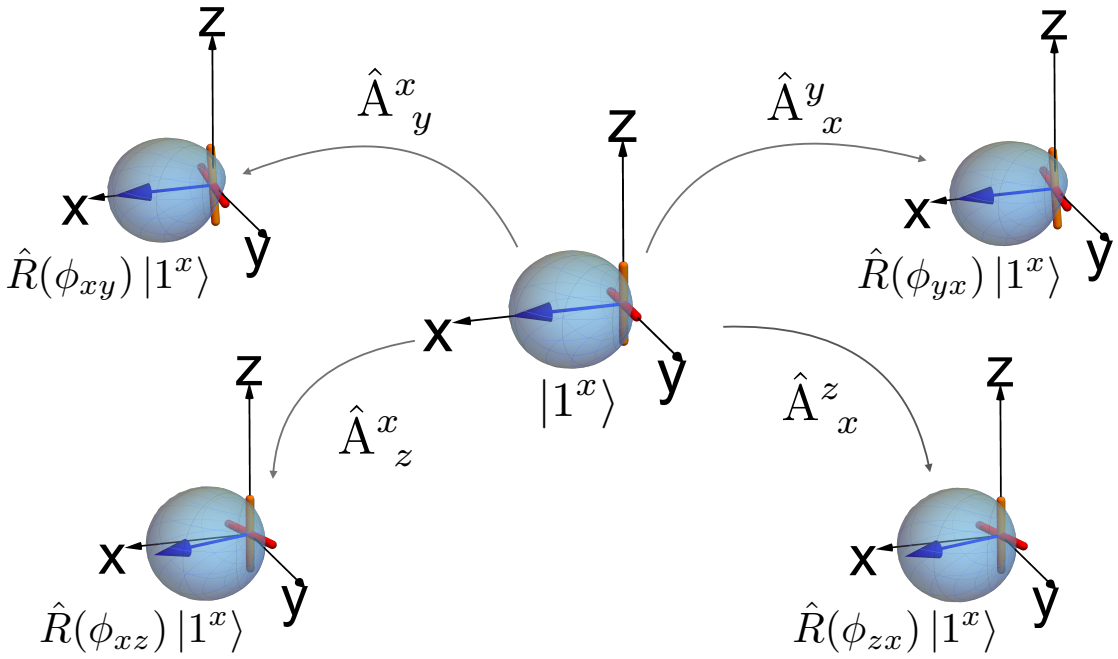

Figure 6.3: Fluctuations created by the generators $\hat{\mathcal{A}}^x{}_y$, $\hat{\mathcal{A}}^x{}_z$, $\hat{\mathcal{A}}^y{}_x$, and $\hat{\mathcal{A}}^z{}_x$, according to Eq. (2.86), for an angle $\phi_{\alpha\beta} = \frac{\pi}{8}$, around the FM ground state given in Eq. (6.23). Figure is reproduced from [201].

We obtain

$$\hat{\mathbf{A}}_{\mathcal{B}^x} = \begin{pmatrix} 1 - \hat{\mathrm{a}}_i^\dagger \hat{\mathrm{a}}_i - \hat{\mathrm{b}}_i^\dagger \hat{\mathrm{b}}_i & \hat{\mathrm{a}}_i & \hat{\mathrm{b}}_i \\ \hat{\mathrm{a}}_i^\dagger & \hat{\mathrm{a}}_i^\dagger \hat{\mathrm{a}}_i & \hat{\mathrm{a}}_i^\dagger \hat{\mathrm{b}}_i \\ \hat{\mathrm{b}}_i^\dagger & \hat{\mathrm{a}}_i \hat{\mathrm{b}}_i^\dagger & \hat{\mathrm{b}}_i^\dagger \hat{\mathrm{b}}_i \end{pmatrix} . \tag{6.34}$$

According to Eq. (6.28), the A matrices expressed in the TR invariant basis $\mathcal{B}_2$ are given by

$$\begin{aligned} \hat{\mathbf{A}}_{B_2} &= \Lambda_3^\dagger \hat{\mathbf{A}}_{\mathcal{B}^x} \Lambda_3 \\ &= \begin{pmatrix} \hat{\mathrm{a}}_i^\dagger \hat{\mathrm{a}}_i & \frac{i}{\sqrt{2}} \hat{\mathrm{a}}_i^\dagger + \frac{i}{\sqrt{2}} \hat{\mathrm{a}}_i^\dagger \hat{\mathrm{b}}_i & -\frac{1}{\sqrt{2}} \hat{\mathrm{a}}_i^\dagger + \frac{1}{\sqrt{2}} \hat{\mathrm{a}}_i^\dagger \hat{\mathrm{b}}_i \\ -\frac{i}{\sqrt{2}} \hat{\mathrm{a}}_i - \frac{i}{\sqrt{2}} \hat{\mathrm{a}}_i \hat{\mathrm{b}}_i^\dagger & \frac{1}{2} + \frac{1}{2} \hat{\mathrm{b}}_i^\dagger + \frac{1}{2} \hat{\mathrm{b}}_i - \frac{1}{2} \hat{\mathrm{a}}_i^\dagger \hat{\mathrm{a}}_i & \frac{i}{2} + \frac{i}{2} \hat{\mathrm{b}}_i^\dagger - \frac{i}{2} \hat{\mathrm{b}}_i - \frac{i}{2} \hat{\mathrm{a}}_i^\dagger \hat{\mathrm{a}}_i - i \hat{\mathrm{b}}_i^\dagger \hat{\mathrm{b}}_i \\ -\frac{1}{\sqrt{2}} \hat{\mathrm{a}}_i + \frac{1}{\sqrt{2}} \hat{\mathrm{a}}_i \hat{\mathrm{b}}_i^\dagger & -\frac{i}{2} - \frac{i}{2} \hat{\mathrm{b}}_i + \frac{i}{2} \hat{\mathrm{b}}_i^\dagger + \frac{i}{2} \hat{\mathrm{a}}_i^\dagger \hat{\mathrm{a}}_i + i \hat{\mathrm{b}}_i^\dagger \hat{\mathrm{b}}_i & \frac{1}{2} - \frac{1}{2} \hat{\mathrm{b}}_i^\dagger - \frac{1}{2} \hat{\mathrm{b}}_i - \frac{1}{2} \hat{\mathrm{a}}_i^\dagger \hat{\mathrm{a}}_i \end{pmatrix} . \end{aligned} \tag{6.35}$$

The next step is to rewrite the Hamiltonian in Eq. (6.16) in terms of the A matrices using the fact that the spin dipole can be rewritten in terms of the A matrices [Eq. (1.67)]. Using Eq. (1.67), the terms of the easy–plane anisotropic Hamiltonian [Eq. (6.19)], in terms of the A-matrices, become

$$\hat{\mathrm{S}}_i^x \hat{\mathrm{S}}_j^x = -(\hat{\mathcal{A}}^y{}_z{}_i - \hat{\mathcal{A}}^z{}_y{}_i)(\hat{\mathcal{A}}^y{}_z{}_j - \hat{\mathcal{A}}^z{}_y{}_j) , \tag{6.36a}$$

$$\hat{\mathrm{S}}_i^y \hat{\mathrm{S}}_j^y = -(\hat{\mathcal{A}}^z{}_x{}_i - \hat{\mathcal{A}}^x{}_z{}_i)(\hat{\mathcal{A}}^z{}_x{}_j - \hat{\mathcal{A}}^x{}_z{}_j) , \tag{6.36b}$$

$$\hat{\mathrm{S}}_i^z \hat{\mathrm{S}}_j^z = (\hat{\mathcal{A}}^x{}_y{}_i - \hat{\mathcal{A}}^y{}_x{}_i)(\hat{\mathcal{A}}^x{}_y{}_j - \hat{\mathcal{A}}^y{}_x{}_j) . \tag{6.36c}$$

For the single ion terms, we use Eq. (1.44) and Eq. (1.68) to rewrite the terms $\hat{\mathrm{S}}_i^{\alpha}\hat{\mathrm{S}}_i^{\alpha}$ of the single–ion anisotropic Hamiltonian [Eq. (6.20)] as a function of the A-matrices, as

$$\hat{\mathrm{S}}_i^x\hat{\mathrm{S}}_i^x = -\frac{2}{3}\hat{\mathcal{A}}_{i\ x}^{x} + \frac{1}{3}\hat{\mathcal{A}}_{i\ y}^{y} + \frac{1}{3}\hat{\mathcal{A}}_{i\ z}^{z} + \frac{2}{3}\,, \tag{6.37a}$$

$$\hat{\mathrm{S}}_i^y\hat{\mathrm{S}}_i^y = -\frac{2}{3}\hat{\mathcal{A}}_{i\ y}^{y} + \frac{1}{3}\hat{\mathcal{A}}_{i\ x}^{x} + \frac{1}{3}\hat{\mathcal{A}}_{i\ z}^{z} + \frac{2}{3}\,, \tag{6.37b}$$

$$\hat{\mathrm{S}}_i^z\hat{\mathrm{S}}_i^z = -\frac{2}{3}\hat{\mathcal{A}}_{i\ z}^{z} + \frac{1}{3}\hat{\mathcal{A}}_{i\ y}^{y} + \frac{1}{3}\hat{\mathcal{A}}_{i\ x}^{x} + \frac{2}{3}\,. \tag{6.37c}$$

Using Eq. (6.36) and Eq. (6.37), the total Hamiltonian [Eq. (6.16)] in terms of the A-matrices then becomes

$$\begin{aligned}\mathcal{H} = \sum_{\langle i,j\rangle}\Big[&-J^{xx}(\hat{\mathcal{A}}_{i\ z}^{y} - \hat{\mathcal{A}}_{i\ y}^{z})(\hat{\mathcal{A}}_{j\ z}^{y} - \hat{\mathcal{A}}_{j\ y}^{z})) \\ &-J^{yy}(\hat{\mathcal{A}}_{i\ x}^{z} - \hat{\mathcal{A}}_{i\ z}^{x})(\hat{\mathcal{A}}_{j\ x}^{z} - \hat{\mathcal{A}}_{j\ z}^{x}) \\ &-J^{zz}(\hat{\mathcal{A}}_{i\ y}^{x} - \hat{\mathcal{A}}_{i\ x}^{y})(\hat{\mathcal{A}}_{j\ y}^{x} - \hat{\mathcal{A}}_{j\ x}^{y})\Big] \\ +\sum_i\Big[&D^{xx}(-\frac{2}{3}\hat{\mathcal{A}}_{i\ x}^{x} + \frac{1}{3}\hat{\mathcal{A}}_{i\ y}^{y} + \frac{1}{3}\hat{\mathcal{A}}_{i\ z}^{z} + \frac{2}{3}) \\ &+D^{yy}(-\frac{2}{3}\hat{\mathcal{A}}_{i\ y}^{y} + \frac{1}{3}\hat{\mathcal{A}}_{i\ x}^{x} + \frac{1}{3}\hat{\mathcal{A}}_{i\ z}^{z} + \frac{2}{3}) \\ &+D^{zz}(-\frac{2}{3}\hat{\mathcal{A}}_{i\ z}^{z} + \frac{1}{3}\hat{\mathcal{A}}_{i\ y}^{y} + \frac{1}{3}\hat{\mathcal{A}}_{i\ x}^{x} + \frac{2}{3})\Big]\,.\end{aligned} \tag{6.38}$$

Inserting Eq. (6.35) into Eq. (6.37), we obtain the single–ion terms as a function of the bosonic operators

$$\begin{aligned}\hat{\mathrm{S}}_i^x\hat{\mathrm{S}}_i^x &= 1 - \hat{\mathrm{a}}_i^{\dagger}\hat{\mathrm{a}}_i\,, \\ \hat{\mathrm{S}}_i^y\hat{\mathrm{S}}_i^y &= \frac{1}{2}(1 + \hat{\mathrm{a}}_i^{\dagger}\hat{\mathrm{a}}_i - \hat{\mathrm{b}}_i^{\dagger} - \hat{\mathrm{b}}_i)\,, \\ \hat{\mathrm{S}}_i^z\hat{\mathrm{S}}_i^z &= \frac{1}{2}(1 + \hat{\mathrm{a}}_i^{\dagger}\hat{\mathrm{a}}_i + \hat{\mathrm{b}}_i^{\dagger} + \hat{\mathrm{b}}_i)\,.\end{aligned} \tag{6.39}$$

We notice that if D^{yy} is not equal to D^{zz}, then the Hamiltonian [Eq. (6.38)] has single bosonic terms, meaning that the state about which we expanded the fluctuations is not the ground state. This is consistent with our previous choice to choose D^{yy} and D^{zz} to be equals [Eq. (6.22)].

After inserting Eq. (6.35) into the total Hamiltonian [Eq. (6.38)], only keeping fluctuations up to 2nd order, and performing a Fourier transform, the Hamiltonian [

Eq. (6.38)] becomes

$$\mathcal{H} = \frac{1}{2}\sum_{\mathbf{k}}\left[\begin{pmatrix}\hat{\mathrm{a}}^{\dagger}_{\mathbf{k}}, & \hat{\mathrm{a}}_{-\mathbf{k}}\end{pmatrix}\begin{pmatrix}A_{\mathbf{k}} & B_{\mathbf{k}}\\ B_{\mathbf{k}} & A_{\mathbf{k}}\end{pmatrix}\begin{pmatrix}\hat{\mathrm{a}}_{\mathbf{k}}\\ \hat{\mathrm{a}}^{\dagger}_{-\mathbf{k}}\end{pmatrix} + \begin{pmatrix}\hat{\mathrm{b}}^{\dagger}_{\mathbf{k}}, & \hat{\mathrm{b}}_{-\mathbf{k}}\end{pmatrix}\begin{pmatrix}C_{\mathbf{k}} & 0\\ 0 & C_{\mathbf{k}}\end{pmatrix}\begin{pmatrix}\hat{\mathrm{b}}_{\mathbf{k}}\\ \hat{\mathrm{b}}^{\dagger}_{-\mathbf{k}}\end{pmatrix}\right] + \frac{1}{2}NzJ^{xx} + N(D^{xx} + D^{\perp}) \,, \tag{6.40}$$

where

$$\begin{aligned} A_{\mathbf{k}} &= -J^{xx}z + \tfrac{1}{2}z(J^{yy}+J^{zz})\gamma(\mathbf{k}) + (D^{\perp} - D^{xx}) \,, \\ B_{\mathbf{k}} &= \tfrac{1}{2}z(J^{zz}-J^{yy})\gamma(\mathbf{k}) \,, \\ C_{\mathbf{k}} &= -2zJ^{xx} \,. \end{aligned} \tag{6.41}$$

In analogy to the FQ case, we need to solve an eigensystem similar to Eq. (4.9). The dispersion relations for $\hat{\mathrm{a}}^{\dagger}_{\mathbf{k}}$ and $\hat{\mathrm{a}}_{\mathbf{k}}$ can be found by imposing them to have bosonic commutation relations [Eq. (C.3)], and diagonalizing

$$\sigma_z\begin{pmatrix}A_{\mathbf{k}} & B_{\mathbf{k}}\\ B_{\mathbf{k}} & A_{\mathbf{k}}\end{pmatrix} = \begin{pmatrix}1 & 0\\ 0 & -1\end{pmatrix}\begin{pmatrix}A_{\mathbf{k}} & B_{\mathbf{k}}\\ B_{\mathbf{k}} & A_{\mathbf{k}}\end{pmatrix} = \begin{pmatrix}A_{\mathbf{k}} & B_{\mathbf{k}}\\ -B_{\mathbf{k}} & -A_{\mathbf{k}}\end{pmatrix} \,, \tag{6.42}$$

where the multiplication by σ_z imposes the bosonic commutation relations for the $\hat{\mathrm{a}}^{\dagger}_{\mathbf{k}}$ excitation. The eigenvalues $\epsilon_{\mathbf{k}}$ are given by

$$\epsilon_{\mathbf{k},1} = +\sqrt{A^2_{\mathbf{k}} - B^2_{\mathbf{k}}} \quad , \quad \epsilon_{\mathbf{k},2} = -\sqrt{A^2_{\mathbf{k}} - B^2_{\mathbf{k}}} \,. \tag{6.43}$$

The dispersion relations for the $\hat{\mathrm{b}}^{\dagger}_{\mathbf{k}}$ and $\hat{\mathrm{b}}_{\mathbf{k}}$ are obtained by diagonalizing

$$\sigma_z\begin{pmatrix}C_{\mathbf{k}} & 0\\ 0 & C_{\mathbf{k}}\end{pmatrix} = \begin{pmatrix}C_{\mathbf{k}} & 0\\ 0 & -C_{\mathbf{k}}\end{pmatrix} \,, \tag{6.44}$$

where σ_z imposes the bosonic commutation relations for the $\hat{\mathrm{b}}^{\dagger}_{\mathbf{k}}$ excitation. The eigenvalues $\epsilon_{\mathbf{k}}$ are given by

$$\epsilon_{\mathbf{k},3} = -C_{\mathbf{k}} \quad , \quad \epsilon_{\mathbf{k},4} = +C_{\mathbf{k}} \,. \tag{6.45}$$

Because the coupling constants are negative, the physical results are

$$\epsilon_{\mathbf{k},1} = +\sqrt{A^2_{\mathbf{k}} - B^2_{\mathbf{k}}} \quad , \quad \epsilon_{\mathbf{k},3} = -C_{\mathbf{k}} = 2z|J^{xx}| \,, \tag{6.46}$$

where $A_{\mathbf{k}}$, $B_{\mathbf{k}}$, and $C_{\mathbf{k}}$ are given in Eq. (6.41).

Following the same procedure as for the FQ state in Section 4.1, we calculate dynamical structure factors for the anisotropic FM case. We start by finding the Bogoliubov transformation that diagonalizes Eq. (6.40). Following the steps given in

Appendix C, we obtain

$$\hat{\mathrm{a}}_{\mathbf{k}} = \frac{1}{\sqrt{\Delta_{\mathbf{k}}^2 - B_{\mathbf{k}}^2}} (\Delta_{\mathbf{k}} \hat{\alpha}_{\mathbf{k}} - B_{\mathbf{k}} \hat{\alpha}_{-\mathbf{k}}^\dagger) \,, \tag{6.47a}$$

$$\hat{\mathrm{a}}_{-\mathbf{k}}^\dagger = \frac{1}{\sqrt{\Delta_{\mathbf{k}}^2 - B_{\mathbf{k}}^2}} (-B_{\mathbf{k}} \hat{\alpha}_{\mathbf{k}} + \Delta_{\mathbf{k}} \hat{\alpha}_{-\mathbf{k}}^\dagger) \,, \tag{6.47b}$$

$$\hat{\mathrm{a}}_{\mathbf{k}}^\dagger = \frac{1}{\sqrt{\Delta_{\mathbf{k}}^2 - B_{\mathbf{k}}^2}} (\Delta_{\mathbf{k}} \hat{\alpha}_{\mathbf{k}}^\dagger - B_{\mathbf{k}} \hat{\alpha}_{-\mathbf{k}}) \,, \tag{6.47c}$$

$$\hat{\mathrm{a}}_{-\mathbf{k}} = \frac{1}{\sqrt{\Delta_{\mathbf{k}}^2 - B_{\mathbf{k}}^2}} (-B_{\mathbf{k}} \hat{\alpha}_{\mathbf{k}}^\dagger + \Delta_{\mathbf{k}} \hat{\alpha}_{-\mathbf{k}}) \,, \tag{6.47d}$$

and

$$\hat{\mathrm{b}}_{\mathbf{k}} = \hat{\beta}_{\mathbf{k}} \,, \tag{6.48a}$$

$$\hat{\mathrm{b}}_{-\mathbf{k}}^\dagger = \hat{\beta}_{-\mathbf{k}}^\dagger \,, \tag{6.48b}$$

$$\hat{\mathrm{b}}_{\mathbf{k}}^\dagger = \hat{\beta}_{\mathbf{k}}^\dagger \,, \tag{6.48c}$$

$$\hat{\mathrm{b}}_{-\mathbf{k}} = \hat{\beta}_{-\mathbf{k}} \,, \tag{6.48d}$$

where $\Delta_{\mathbf{k}}$ is given in Eq. (4.13), and where $A_{\mathbf{k}}$ and $B_{\mathbf{k}}$ are given in Eq. (6.41).

We now follow the calculations outlined in Section 4.2.1 in order to calculate the quantum structure factors. Since we are working in the Bogoliubov representation, the ground state $|\mathrm{GS}\rangle$ is the vacuum state $|\mathrm{vac}\rangle$ for the Bogoliubov bosons. The structure factors are given by Eq. (4.36). We calculate $\langle \mathrm{vac}|\hat{O}_{\mathbf{q}}^{\alpha}|\mu\rangle$ with $|\mu\rangle = \hat{\alpha}_{\mathbf{k}}^\dagger|\mathrm{vac}\rangle \oplus \hat{\beta}_{\mathbf{k}}^\dagger|\mathrm{vac}\rangle$ and $\hat{O}_{\mathbf{q}}^{\alpha} = \hat{\mathrm{S}}_{\mathbf{k}}^{\alpha}$ with $\alpha = x, y, z$, for the dipole structure factor for instance. Using Eq. (1.67), Eq. (1.68) and Eq. (6.35), we can rewrite the spin dipole, the spin quadrupole, and the A-matrix operators in terms of the bosons up to linear order, and after performing a Fourier transform, we can rewrite them in terms of the Bogoliubov bosons using Eq. (6.47) and Eq. (6.48). This allows us to easily calculate the structure factors [Eq. (4.36)].

Using Eq. (4.42), the dynamical spin dipole structure factor, defined by Eq. (I.1), is given by

$$S_{\mathrm{S}}^{\mathsf{FM}}(\mathbf{q}, \omega) = \frac{A_{\mathbf{q}}}{\sqrt{A_{\mathbf{q}}^2 - B_{\mathbf{q}}^2}} \delta(\omega - \epsilon_{\mathbf{q},1}) + S_{\mathrm{S}}^{\mathsf{GS_{FM}}}(\mathbf{q} = 0, \omega) \,. \tag{6.49}$$

The dynamical spin quadrupole structure factor, as given by Eq. (I.17), yields

$$S_{\mathrm{Q}}^{\mathsf{FM}}(\mathbf{q}, \omega) = 2\frac{A_{\mathbf{q}}}{\sqrt{A_{\mathbf{q}}^2 - B_{\mathbf{q}}^2}} \delta(\omega - \epsilon_{\mathbf{q},1}) + 4\delta(\omega - \epsilon_{\mathbf{q},3}) + S_{\mathrm{Q}}^{\mathsf{GS_{FM}}}(\mathbf{q} = 0, \omega) \,. \tag{6.50}$$

The total dynamical factor for the $\hat{\mathcal{A}}$ operators defined in Eq. (I.34) becomes

$$S_{\mathrm{A}}^{\mathsf{FM}}(\mathbf{q}, \omega) = \frac{A_{\mathbf{q}}}{\sqrt{A_{\mathbf{q}}^2 - B_{\mathbf{q}}^2}} \delta(\omega - \epsilon_{\mathbf{q},1}) + \delta(\omega - \epsilon_{\mathbf{q},3}) + S_{\mathrm{A}}^{\mathsf{GS_{FM}}}(\mathbf{q} = 0, \omega) \,, \tag{6.51}$$

where we explicitly summed over the indexes α and β and where the terms of the form $S_{\mathrm{O}}^{\mathsf{GS}_{\mathsf{FM}}}(\mathbf{q}=0,\omega)$ represent the ground state and zero–point energy contribution to the structure factors at $\mathbf{q}=0$, but are not calculated here, for simplicity reasons. For these three results, Eq. (6.49), Eq. (6.50), and Eq. (6.51), we used Eq. (4.13), and $\epsilon_{\mathbf{q},1}$, and $\epsilon_{\mathbf{q},3}$ are given in Eq. (6.46). These results are also identical to results that one can obtain by performing a conventional multi-boson expansion.

Additionally, we check that the sum rule Eq. (2.67) is satisfied, by noticing that the constant terms in Eq. (2.67) would only contribute for $\mathbf{q}=0$ and at equal time, and can therefore be neglected.

In Fig. 6.4, we show results for the dynamical structure factors [Eq. (6.49), Eq. (6.50), and Eq. (6.51)] for the ferromagnetic state for the anisotropic Heisenberg Hamiltonian with single–ion anisotropy [Eq. (6.16)] on the triangular lattice. We first notice that the quadrupolar band $\epsilon_{\mathbf{q},3}$, which corresponds to the $\Delta S=2$ excitation band associated with the $\hat{\beta}_{\mathbf{k}}^{\dagger}$ boson, is gapped and non–dispersive. Because it essentially corresponds to the excitation obtained by applying the lowering operator S^{+} twice, it is quadrupolar in nature and will only contribute to the quadrupolar structure factor channel. Moreover, such a quadrupolar excitation from a FM ground state has a finite energy cost, and it also doesn't have any neighboring quadrupoles to interact with, so it is therefore localized. The isotropic FM Heisenberg case without single–ion anisotropy is presented in Fig. 6.4 (a)–(c). As shown in Fig. 6.4 (d)–(f), we note that the introduction of easy–plane anisotropy with $J^{yy}=J^{zz}\neq J^{xx}$ creates a gap and lifts the dispersion relation according to Eq. (6.46) and Eq. (6.41). In Fig. 6.4 (g)–(i), we see that introducing single–ion anisotropy with $D^{\perp}\neq D^{xx}$ also creates a gap and lifts the dispersion relation again according to Eq. (6.46) and Eq. (6.41). In Fig. 6.4 (j)–(l), we display the interplay of easy-plane and single–ion anisotropy.

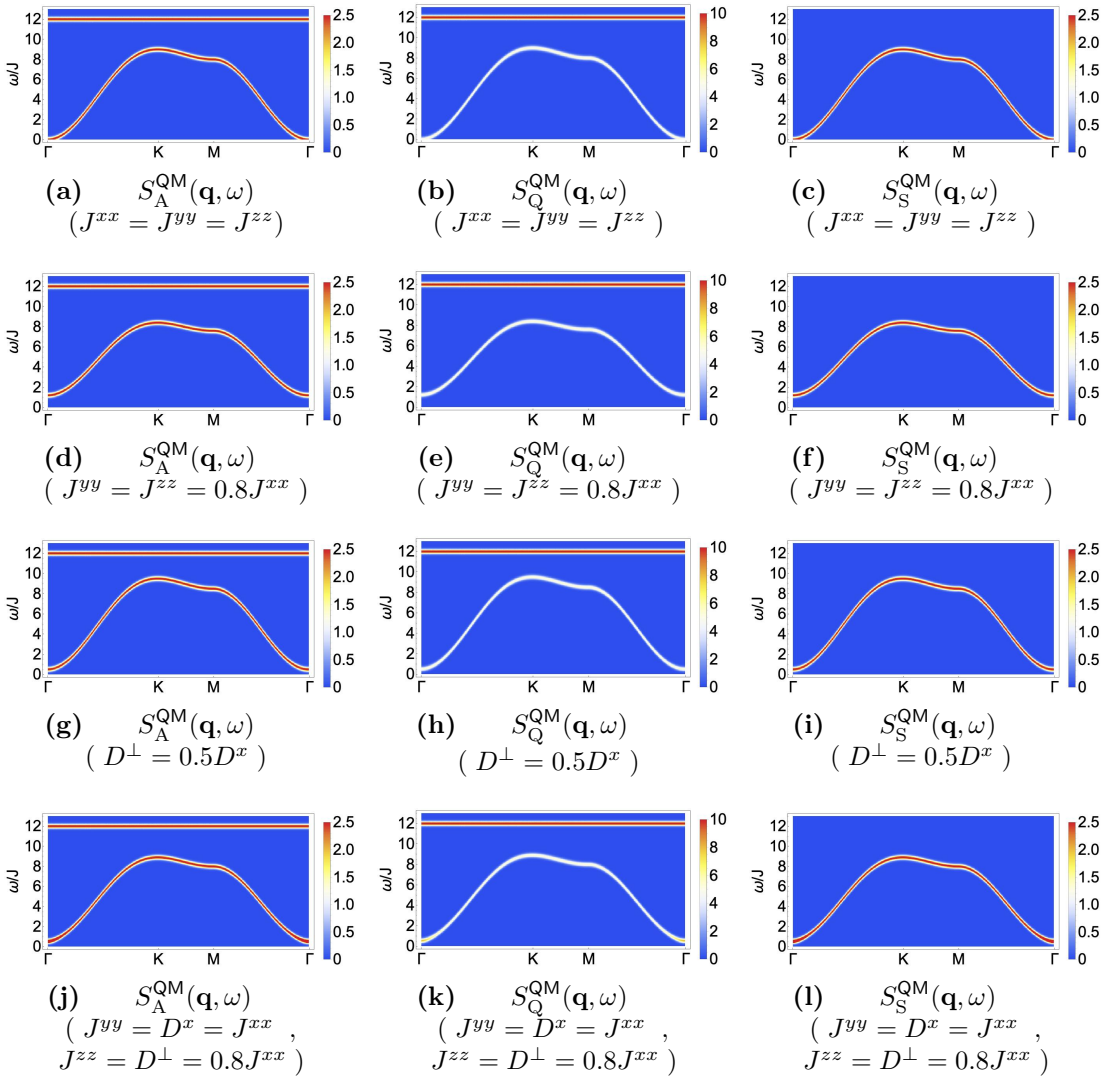

Figure 6.4: Dynamical structure factors predicted by $T=0$ quantum theory of fluctuations for the ferromagnetic (FM) phase of the BBQ model on the triangular lattice (Eq. (1.69)) with J_1 being considered as Heisenberg anisotropic exchange interactions [Eq. (6.19)] and $J_2=0$, and with an additional single ion anisotropic exchange Hamiltonian [Eq. (6.20)]. (a)–(c) Dynamical structure factors for $S_{\rm A}(\mathbf{q},\omega)$ (A-matrices), $S_{\rm Q}(\mathbf{q},\omega)$ (quadrupoles) and $S_{\rm S}(\mathbf{q},\omega)$ (dipoles) obtained for the isotropic FM state of the Heisenberg Hamiltonian [Eq. (6.19)] where $J^{xx}=J^{yy}=J^{zz}=-1$ without any single–ion anisotropy [Eq. (6.20)], $D^{\perp}=D^{x}=0$. (d)–(f) Equivalent results for the easy-plane anisotropic FM state of the Heisenberg Hamiltonian [Eq. (6.19)] where $J^{yy}=J^{zz}=0.8J^{xx}$ and $J^{xx}=-1$ without any single–ion anisotropy [Eq. (6.20)], $D^{\perp}=D^{x}=0$. (g)–(i) Equivalent results for the isotropic FM state of the Heisenberg Hamiltonian [Eq. (6.19)] where $J^{yy}=J^{zz}=J^{xx}=-1$ with single–ion anisotropy [Eq. (6.20)], $D^{\perp}=0.5D^{x}$ and $D^{x}=J^{xx}$. (j)–(l) Equivalent results for the easy-plane anisotropic FM state of the Heisenberg Hamiltonian [Eq. (6.19)] where $J^{zz}=0.8J^{xx}$ and $J^{yy}=J^{xx}=-1$ with single–ion anisotropy [Eq. (6.20)], $D^{\perp}=0.8D^{x}$ and $D^{x}=J^{xx}$. Figures are reproduced from [201]

Chapter 7

Outlook and Conclusion

In the last and seventh Chapter, I complete this Thesis by briefly reviewing the main points addressed throughout the course of this study, and describe two directions that I hope to explore in the future. In Section 7.1, I provide a summary of the results obtained in this Thesis and how they fit in the contextual and current research of interest. Section 7.2 supplies a short discussion about two topics I hope to address in the future. The first topic concerns topological defects in spin nematics as well as spin–1 systems more generally, I link this topic with thermodynamic results that we obtained for the FQ state of the BBQ model on the triangular lattice. The second topic consists of an exploratory generalization of the Self–Consistent Gaussian Approximation (SCGA) method within our $u(3)$ formalism. In Section 7.3, I conclude the Thesis with some final remarks.

7.1 Thesis Panorama

Spin–1 magnets are special. Indeed, in Chapter 1 and Chapter 2, we learned that, besides dipolar degrees of freedom, a spin–1 moment can also carry quadrupolar degrees of freedom on a single site, while retaining quantum fluctuations [87, 131, 180, 183, 250]. This implied that the classical limit $S \to \infty$ commonly taken for a spin–$\frac{1}{2}$ moment as an $O(3)$–vector is not a valid classical limit for a spin–1 moment, despite a spin–1 being considered as more classical than a spin–$\frac{1}{2}$.

For this reason, classical Monte Carlo simulations based on an $O(3)$–vector can not reproduce quadrupolar order nor quadrupolar excitations at the level of a single–site. This might explain why Molecular Dynamics based on an $O(3)$ representation fails at reproducing the low energy features of excitations in the spin–1 pyrochlore material $NaCaNi_2F_7$ as explained in Section 1.3.1 [188, 267]. On the other hand, classical Monte Carlo simulations based on a representation of spin–1 moment as a $\mathbf{d}$ vector allows to access adequately the classical thermodynamics [235] taking into account quadrupolar degrees of freedom. Quantum Monte–Carlo gives a good account of thermodynamic [87, 111] and dynamic [255] properties for quadrupolar orders. But it is restricted to sign–free models, and its dynamics, accessible via analytical continuation, might be problematic for systems with complex excitations. Exact diagonalizing is hampered by finite–size limitations, as the Hilbert space grows rapidly with the number of lattice

sites.

This legates a window for a method that can properly represent a spin–1 moments, describing all its degrees of freedom, guarantying the right classical limit to access classical thermodynamics, and allowing a framework where (semi–)classical dynamics are also available.

In this Thesis, motivated by the ambitions explained above, I have developed a new method to study spin–1 systems. The proposed method allows to access both classical thermodynamics and (semi–)classical dynamics of spin–1 magnets within an analytical theory as well as numerical simulations. I established the validity of our approach by comparison of analytical results with the existing literature for the spin–1 bilinear–biquadratic (BBQ) model on the triangular lattice, as well as through comparison with its corresponding numerical implementation carried out by my collaborators. I also used my method to obtain new interesting findings, among which an explicit relationship between classical finite temperature results and quantum zero–temperature results treated at the (semi–)classical level. This namely allowed to draw a general connection between finite temperature Molecular Dynamics simulations and analytical zero–temperature quantum (semi–classical) results.

The essential attribute of the method presented in this Thesis relies on the choice of representation of spin moments. As explained in Section 2.4, my approach is based on the embedding of the usual $su(3)$ algebra into the $u(3)$ algebra [180]. This allows for a correct and complete description of a spin–1 moment, provides a valid (semi–)classical limit of a spin–1 moments, and treats dipole and quadrupole moments on an equal footing. Additionally, I derived equations of motion for the A–matrices (generators of the $u(3)$ algebra) which take a simple form enabled by the compact structure of the $u(3)$ algebra. Further expansion of the method was obtained through the development of analytical theories of fluctuations in Section 2.5. These can be treated at both the classical and quantum levels.

In addition, I proposed to promote my framework in terms of generators of $U(3)$ and its associated equations of motion into a numerical scheme in order to simulate spin–1 magnets. Within the formalism of A–matrices, a classical Monte-Carlo (u3MC) algorithm as well as a Molecular Dynamics (u3MD) scheme based on the numerical integration of the equations of motion were developed. These methods form a powerful approach for exploring dynamics in spin–1 magnets. The implementation of the numerical simulations has been carried out by my collaborator, Dr. Rico Pohle.

Next, I illustrated my method on the specific ferroquadrupolar (FQ) phase of the spin–1 BBQ model on the triangular lattice in Chapter 3 and Chapter 4. Treated at the classical level, the analytical theory of fluctuations predicted that the excitations form 2 doubly degenerate bands which exhibit either a dipolar or quadrupolar nature [Fig. 3.3 (a)–(c)]. This formed the basis platform from which I developed a low—temperature expansion making predictions for classical thermodynamics properties. These predictions were then compare results for heat capacity $c(T \to 0)$ [Fig. 3.4], the ordered moment $\mathbf{Q}$ [Fig. 3.5], as well as, the equal time structure factors $S_\lambda(\mathbf{q})$ [Fig. 3.6] with u3MC simulation results performed at low temperatures, which all showed a perfect agreement [Section 3.4].

I then show how the fluctuations could be quantized, and how this led to a quantum theory of fluctuations about the FQ ground state. This naturally brought up a descrip-

tion that is shown to be equivalent to an earlier multi–boson approach. This quantum theory of fluctuations was then used to calculate quantum dynamical structure factors for the FQ order [Fig. 4.1 (a)–(c)], which I compared with u3MD simulations in Section 4.3. The u3MD simulations were shown to be able to account well for the quantum (semi–classical) dynamics of the dispersion relations of the quantum excitation around the FQ ground state but failed at reproducing the spectral weight of their structure factors predicted by the $T = 0$ quantum theory.

In Section 5.1, I then delved deeper into the u3MD scheme, showing the reason for the disagreement between "raw" u3MD simulations and $T = 0$ quantum analytical predictions emanates from classical statistics, inherited from the u3MC scheme. I based this observation on an analytical development that accounts for the fluctuations to follow quantum dynamics and be governed by Boltzmann classical statistics. From this followed a simple and general quantum–classical relationship expressed for the structure factors. This result was applied to correct u3MD simulation results for the effect of their classical statistics, in the limit $T \to 0$ [Eq. (5.31)]. Corrected in this manners, u3MD simulations were shown to perfectly reproduce results obtain from the $T = 0$ quantum theory, treated at the (semi–)classical level as discussed in Section 5.3 [Fig. 5.1 and Fig. 5.2].

Finally, I generalized the $U(3)$–approach to systems with spin–anisotropic interactions. Up to this point, I considered the general $SU(2)$–symmetric BBQ model. I showed that my methods, applied to an analytical and numerical treatment, guaranteed a valid representation of a spin–1 moment, by ensuring that the constraints on the trace of the $u(3)$ generators remained preserved by the system. In Chapter 6, I showed that this remains valid in the case of the most general anisotropic model allowed for a spin–1 magnet, asserting a proper and complete description of a spin–1 moment. I illustrated this result by considering the FQ order of the BBQ model with vanishing Heisenberg and anisotropic biquadratic interaction supplemented with single–ion anisotropy. In Section 6.2.2, I showed results for this model, where u3MD simulations corrected for their classical statistics perfectly agree with $T = 0$ quantum analytical theory treated at the (semi–)classical level [Fig. 6.1]. Lastly, in Section 6.3, I presented $T = 0$ quantum analytical theory predictions for the ferromagnetic order of the BBQ model with easy–plane, single–ion anisotropy. This example served not only as an instance for anisotropic models, but also allowed to provide an explicit derivation for orders that are not only of quadrupolar character. Indeed, the representation of the Hamiltonian in terms of the A–matrices is particularly straightforward for quadrupolar types of orders, but is also tractable for systems with dipolar order.

7.2 New Horizons

In this Section, I present interesting areas which I hope to explore in the future. In Section 7.2.1, I explain my interest in investigating further the origin of the peak observed in the specific heat [Fig. 3.4] obtained by u3MC simulation for a FQ state of the BBQ model. I discuss a KT–like phase transition as a possible explanation for the observed behavior of the thermodynamic quantities as seen in u3MD simulations. Additionally, studying topological excitations in spin nematics also allows for the opportunity to

generally model topological defects in spin–1 systems within the $u(3)$ framework.

Lastly, in Section 7.2.2, I explore the generalization of the Self–Consistent Gaussian Approximation (SCGA) in the space of A–matrices. The SCGA provides a useful approach to both ordered and spin liquid phases of magnets, but is commonly based on a classical $O(3)$–vector description of the spin moments. As we know by now, an $O(3)$–vector does not suffice to properly describe a spin–1 moments, as quadrupolar degrees of freedom are not accounted for. Therefore, I investigate, here, the possibility to build an SCGA method for spin–1 systems based on a $u(3)$ description.

7.2.1 Topological Defects in Spin Nematics

As discussed in Section 3.4, the specific heat, obtained from u3MC simulations for the FQ state of the BBQ model on the triangular for a finite–size system, shows a peak at finite temperature, illustrated in Fig. 3.4. The peak sharpens and shifts toward lower temperatures as the size of the system is increased. The temperature of the peak also coincided with the onset of FQ correlations as observes for the ordered moment $\langle \mathbf{Q}^2_{\mathsf{MC}} \rangle$ shown in Fig. 3.5 (a). We further proved that the peak observed in the specific heat is not induced by a conventional phase transition due to the continuous symmetry breaking of the FQ ground state with respect to $SO(3)$ symmetry of the BBQ model. Indeed, a finite temperature phase transition into the FQ ordered ground state in a 2–dimensional lattice would violate the Mermin–Wagner theorem [146]. Concretely, we proved that, in the thermodynamic limit, the ordered moment logarithmically scaled to zero with respect to system size, restoring the Mermin–Wagner theorem.

Here, we discussed a possible explanation for the observed behavior of the thermodynamic quantities as seen in u3MD simulations in terms of a KT–like phase transition. Indeed, the empirical simulation results show a peak in the specific heat. The order parameters showed an onset of ferroquadrupolar correlations at the peak temperatures, without, however, exhibiting long–rang order [Fig. 3.5]. This is very reminiscent of the Kosterlitz-Thouless (KT) phase transition in the 2–dimensional XY-model [121, 122]. In the KT phase transition, the phase transition is due to the unbinding of pair of vortices, when vortices become free moving particles. Additionally, homotopy analysis of the order parameter of the FQ phase implies the possibility for topological defects to appear.

As previously discussed in Section 3.4, a likely explanation for the behavior of the specific heat [cf. Fig. 3.4 in Section 3.4.1] and the ordered moment [see Fig. 3.5 (a) in Section 3.4.2] for the FQ state of the BBQ Hamiltonian [Eq. (2.72)] is the unbinding of pairs of vortices, leading to a topological phase transition. Such a topological phase transition is indeed allowed and can account for the observed data. In the following part, I provide some preliminary analysis that supports this hypothesis.

Vortex and Phase Transition in the FQ state of the BBQ Model

Form homotopy analysis [145], point–like defects are allowed to happen in spin nematics, as previously discussed in Section 1.2.4. This can be seen by considering the order parameter of the FQ state, which is a real director. The order parameter phase is given by real 2-dimensional projective space $\mathbb{RP}^2$ shown in Fig. 1.5. The first homotopy

group is given by [30].

$$\pi_1(\mathbb{RP}^2) = \mathbb{Z}_2 \ , \tag{7.1}$$

previously introduced in Eq. (1.52b) and Eq. (3.103). The fact that the group $\mathbb{Z}_2$ only contains 2 elements, one of which is the identity implies that there are 2 types of defects: a trivial defect, and a topological defect (cf. the discussion in Section 1.2.4). The topological defect is also referred to as $\mathbb{Z}_2$–vortex. This also means that a vortex is its own anti–vortex, as there can only be one type of topological defects. And it is possible for these vortices to mediate a phase transition at finite temperature from a disordered phase into a phase with algebraic correlations.

KT–Argument

The possibility of a topological phase transition into a phase with FQ correlations can be understood by generalizing the usual KT–argument for unbinding to vortices in an XY–magnet

a) Vortex Energy

For simplicity, we assume the directors to lie in the xy–plane. We also consider a purely quadrupolar state, with $\mathbf{S} = 0$, which means that the imaginary part $\mathbf{v}$ is parallel to $\mathbf{u}$, such that $\mathbf{v} = \alpha\mathbf{u}$, with $\alpha \in \mathbb{R}$. The director $\mathbf{d}$ can be parameterized as

$$\mathbf{d} = \frac{1 + i\alpha}{\sqrt{1+\alpha^2}} \begin{pmatrix} \cos(\theta) \\ \sin(\theta) \\ 0 \end{pmatrix} \quad \theta \in [0, \pi] \ . \tag{7.2}$$

We note that it is different from a general director in 3–dimensions. Indeed, here the director is confined to 2 dimensions, and the order parameter is given by half of the circle, namely $\mathbb{RP}^1$. $\mathbb{RP}^1$ is homeomorphic to the circle S^1, and its first homotopy class yields [30]

$$\pi_1(\mathbb{RP}^1) = \mathbb{Z} \ , \tag{7.3}$$

which implies that the vortices are characterized by winding numbers taking on integer values, such that vortices with different winding numbers corresponds to different topological defects, with the subtlety, however, that a 180° rotation brings the director back to itself. Therefore, the winding numbers characterizing the types of defects take on half–integer values

$$k = \pm\frac{1}{2}, \pm 1, \pm\frac{3}{2}, \pm 2, \dots \ . \tag{7.4}$$

The configuration for $\mathbf{d}$ [Eq. (7.2)] plugged into the BBQ Hamiltonian gives an energy of

$$\langle \mathcal{H}_{BBQ} \rangle = \simeq J_2 z N - \frac{J_2 z}{6a^{d-2}} \int \mathrm{d}\mathbf{x} (\boldsymbol{\nabla}\theta(\mathbf{x}))^2 \ , \tag{7.5}$$

where we assumed the angle difference between neighboring sites to be small $(\theta_i - \theta_{i+\delta}) \ll 1$, and where a is the lattice spacing. We see that for our choice of ferro-

quadrupolar coupling constant $J_2 = -|J_2|$, $J_2 < 0$, the Hamiltonian becomes

$$\langle \mathcal{H}_{BBQ} \rangle = -|J_2| z N + \frac{|J_2| z}{6a^{d-2}} \int \mathrm{d}\mathbf{x} (\boldsymbol{\nabla}\theta(\mathbf{x}))^2 \,, \tag{7.6}$$

and that the energy is minimized for configurations of directors with uniform θ. The first term is just the ground state energy $E_0 = J_2 z N$, when all the directors are uniformly aligned with each other. The second term represents the elastic energy from twisting the directors. We denote it by [36],

$$F_{el} = \frac{\rho_s}{2} \int \mathrm{d}\mathbf{x} (\boldsymbol{\nabla}\theta(\mathbf{x}))^2 \,, \tag{7.7}$$

where for the FQ ground state of the BBQ model

$$\rho_s^{\mathsf{FQ}} = \frac{|J_2| z}{3a^{d-2}} \,, \tag{7.8}$$

for the ferroquadrupolar phase of the BBQ model and is identified as the spin–stiffness [36]. Configurations that minimize F_{el} can be found using the Euler-Lagrange equations. This leads to

$$\rho_s \nabla^2 \theta = 0 \,. \tag{7.9}$$

Among all the solutions for θ that satisfies Eq. (7.9), we are interested in the configuration with

$$\theta(\mathbf{r}) = k\phi + \phi_0 \,. \tag{7.10}$$

We choose this solution, because it represents a topological defect with charge k. Indeed considering a configuration, where the spins or the directors can be parametrized by

$$\mathbf{n} = \begin{pmatrix} \cos(k\phi + \phi_0) \\ \sin(k\phi + \phi_0) \end{pmatrix} \,, \tag{7.11}$$

leads to a configuration formed of spins or directors winding around with factor k as we go around a loop enclosing the vortex. The winding number k, or charge of the vortex is given by [36]

$$2\pi k = \oint \mathrm{d}\theta = \int_\Gamma \frac{\mathrm{d}\theta}{\mathrm{d}\alpha} \mathrm{d}\alpha \,, \tag{7.12}$$

where Γ is a contour encircling the vortex, and α a parametrization.

The elastic energy corresponding to this configuration is given by Eq. (7.7). I obtain

$$F_{el} = \rho_s k^2 \pi \log(\frac{R_c}{a}) \,, \tag{7.13}$$

where, as shown on Fig. 7.1, a is the lattice spacing, and R_c is the radius to which extends the vortex. We see that for an infinite system, $R_c \to \infty$, and the energy diverges.

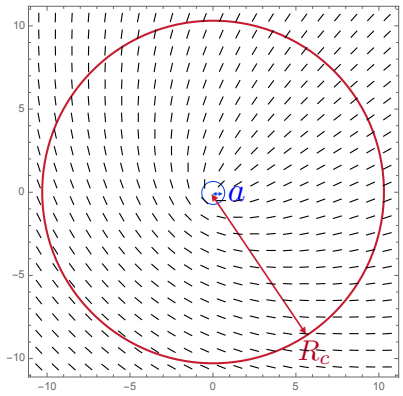

Figure 7.1: Configuration of directors **n** [Eq. (7.11)] in a vortex defined by $k = \frac{1}{2}$ and $\phi_0 = \frac{\pi}{4}$ according to Eq. (7.10) .

b) Vortex Entropy

The vortex entropy can be estimated by

$$S = k_B \log(\frac{\pi R_c^2}{\pi a^2}) \,, \tag{7.14}$$

where $\frac{\pi R_c^2}{\pi a^2}$ represented the number of ways of distributing a vortex of area πa^2 into a system of area πR_c^2. The free energy of a free vortex can be written as

$$\begin{aligned} F &= F_{el} - TS \\ &= \rho_s k^2 \frac{\pi}{2} \log(\frac{R_c^2}{a^2}) - T k_B \log(\frac{R_c^2}{a^2}) \,. \end{aligned} \tag{7.15}$$

The temperature at which a vortex is likely to freely occur is given at $F = 0$, when the free energy changes sign

$$T_c = \frac{\pi \rho_s k^2}{2 k_b} \,. \tag{7.16}$$

For the ferro–quadrupolar phase of the BBQ model [Eq. (3.87)] on the triangular lattice, the spin–stiffness is given by Eq. (7.8), we obtain

$$T_c^{\mathsf{FQ}} = \frac{\pi |J_2| z k^2}{6 k_b} = \frac{\pi}{4} \simeq 0.785398 \,, \tag{7.17}$$

where we used $|J_2| = 1$, $k_B = 1$, $z = 6$ for the triangular lattice, and $k = \pm\frac{1}{2}$ which represents a topological defect with the smallest energy (as higher winding numbers would imply a higher twisting energy).

Eq. (7.17) represents an upper bound limit. Indeed some pair of vortices might appear spontaneously at lower temperatures since such a pair produces a strain that disappears at large enough distances, as can be seen in Fig. 7.2.

We can use Eq. (7.17) to compare with estimations obtained by numerical Monte Carlo simulation. In our case, based on results obtained by u3MC simulation, the temperature transition can be approximated by the temperature at which the peak in

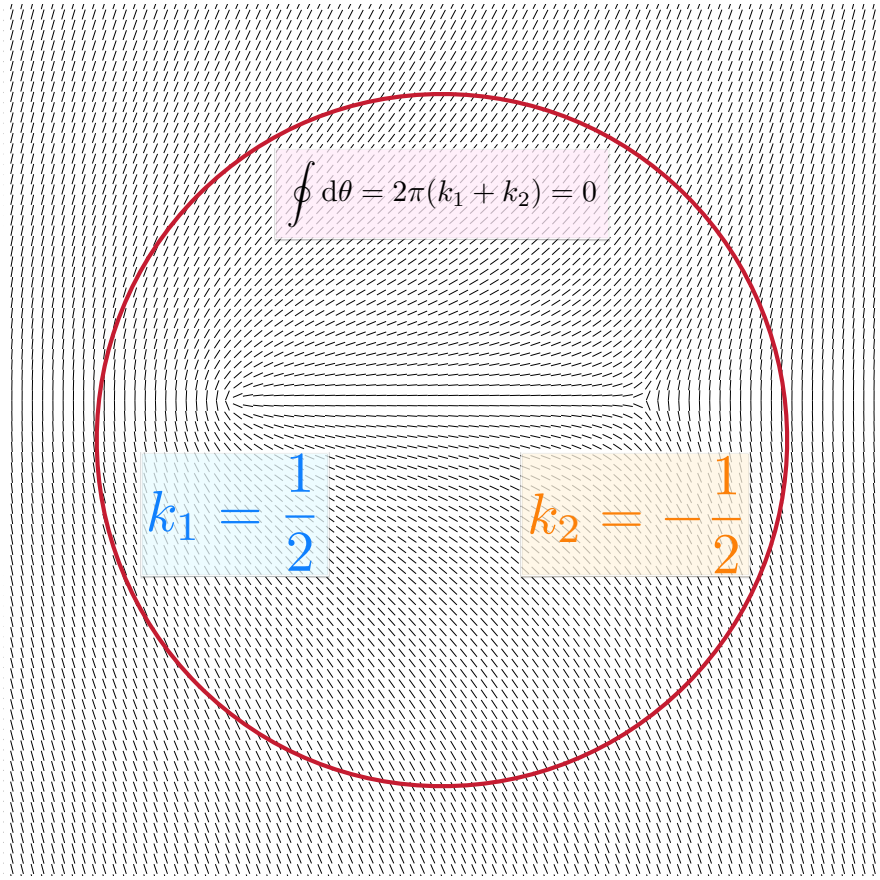

Figure 7.2: Configuration of directors **n** [Eq. (7.11)] in a vortex defined by $k_1 = \frac{1}{2}$, $\phi_0^1 = 0$and $k_2 = \frac{1}{2}$ $\phi_0^2 = \frac{\pi}{2}$ according to Eq. (7.10).

the specific heat occurs. This is estimated by

$$T^*_{\mathsf{FQ}} \simeq 0.43 \,, \tag{7.18}$$

(cf. Section 3.4 and Fig. 3.4) which is consistent with the fact that the prediction obtained by our simple MF analysis represents an upper bound value.

We can also compare with a set of similar results obtained for the XY-model on the square lattice in the case of the KT–transition. A similar approach for the XY–Heisenberg model with dipole spins of length 1 leads to a spin–stiffness [122]

$$\rho_s^{\mathsf{XY}} = \frac{|J|z}{4a^{d-2}} \,, \tag{7.19}$$

which according to Eq. (7.16), leads to a transition temperature

$$T_c^{\mathsf{XY}} = \frac{\pi |J_2| z k^2}{8 k_b} = \frac{\pi}{2} \simeq 1.5708 \,, \tag{7.20}$$

where we used $|J| = 1$, $k_B = 1$, $z = 4$ for the square lattice, and $k = \pm 1$, since for dipolar spins, non–trivial defects have integer winding numbers. Monte–Carlo and

DMRG simulations based on an $O(3)$ representations of spins for the XY–model on the square lattice [20, 44, 89, 96, 118, 120, 175] yield a KT–transition temperature of approximately

$$T^*_{\mathsf{XY}} \simeq 0.893 \; . \tag{7.21}$$

Considering the ratio of the numerical and the MF results obtained for estimates of the transition temperatures for the BBQ and the XY–model, we obtain

$$\frac{T^*_{\mathsf{FQ}}}{T_c^{\mathsf{FQ}}} = 0.55 \; , \qquad \frac{T^*_{\mathsf{XY}}}{T_c^{\mathsf{XY}}} = 0.568 \; . \tag{7.22}$$

We observe that the MF prediction of the transition temperatures T_c for the FQ state and the XY–model are subject to a similar reduction compared to estimations obtained by numerical methods.

From this preliminary analysis, we observe that the formation of a bound state of pairs of solitons is topologically and thermodynamically allowed. As the temperature gets in a close range to the temperature of the peak observed in the specific heat as shown in Fig. 3.4, vortices can form during the Monte Carlo simulation. Additionally, in a snapshot obtained by u3MC simulation shown in Fig. 7.3, we observe that the directors form topological defects such as vortices, similarly to topological defects seen in liquid crystals.

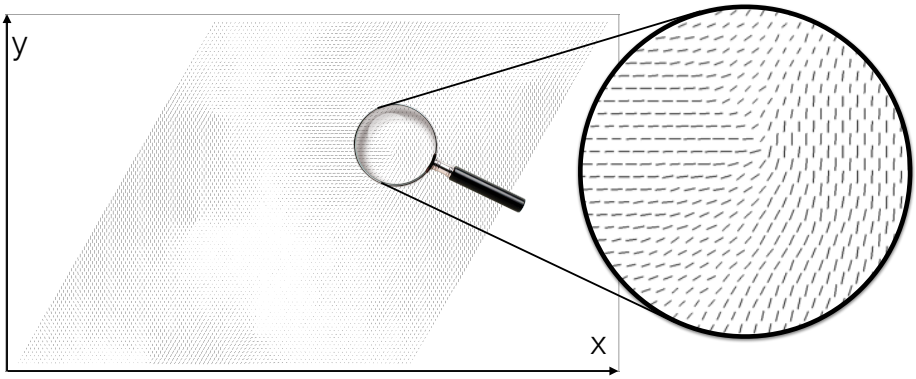

Figure 7.3: Directors in the KT-regime obtained by u3MC Monte Carlo simulations at T=0.036J, described in Section 2.6.1, for the BBQ model [Eq. (2.72)] in the FQ phase. Numerical simulations were carried out by my collaborator Dr. Rico Pohle.

There is therefore good reason to believe that the peak seen in simulation results for the specific heat [Fig. 3.4] is due to a topological phase transition driven by the unbinding of topological defects of the spin nematic state. A sensible starting point to study topological defects in spin–1 magnets in general would be to first investigate the formation of the topological vortices in the context of this topological phase transition. As shown in Fig. 7.3 and Fig. 7.4 (a), we notice that in real space, both topological defects look qualitatively similar, despite being different topological excitations. Indeed in Fig. 7.3, a snapshot of u3MC simulations shows a configuration of directors forming vortices for the FQ order. While in Fig. 7.4, the defects are obtained by imposing proper boundary conditions in the case of the FQ state of the BBQ model [5]. In a KT–like phase transition, the phase transition is due to the unbinding of pair of

vortices, when vortices become free moving particles.

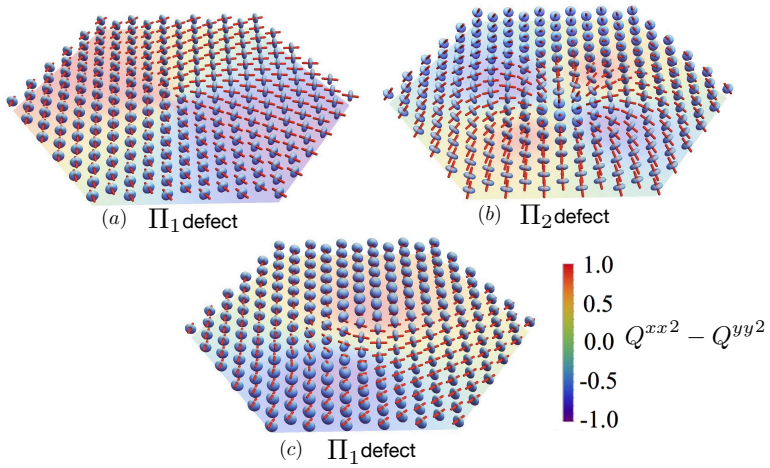

Figure 7.4: Topological defects for a spin–1 system in the FQ phase on the triangular lattice. Directors configuration for a (a) point–like Π_1 topological excitation, (b) Skyrmion–type Π_2 topological excitation, (c) SU(3) Π_2 topological excitation. The background intensities represent the normalized value of the quadrupole component $Q^{xx2} - Q^{yy2}$. Pictures are reproduced from [5].

This topological phase transition of vortices in spin nematics provides us with a good and relatively simple starting point for our investigation. An impressive demonstration of the power of the methods developed in this Thesis is shown in Fig. 7.5. The images Fig. 7.5 (a)–(f) correspond to different time–shots of the time evolution of a system of directors in the FQ phase on the triangular lattice with nematic topological excitations [190]. The intensities corresponds to the total quadrupolar weight $\sum_{\alpha,\beta} Q_i^{\alpha\beta}(t)$ in function of the two spacial variables x and y. Using the u3MC method [Section 2.6.1], the system is thermalized for the FQ phase of the BBQ model on the triangular lattice for parameters given in Eq. (3.87). This is done for a target temperature of $T = 0.01\ J$. The system is time evolved using the equations of motion for the A–matrices [Fig. 1.70], which we numerically integrate using the u3MD scheme introduced in Section 2.6.2. We observe that the two vortices (circled in blue in Fig. 7.5 (a)), get closer and are attracted to each other, while they seem to slightly gravitate around each other. Finally, in Fig. 7.5 (e), they annihilate, and in Fig. 7.5 (f), we can observe some kind of quadrupolar waves emanating from the location where the vortices annihilated. The potential and twisting energy of the vortices seems to be released in some form of quadrupolar radiation. This is very evocative of the gravitational waves induced by two gravitating black holes, which analogy is part of another project [43].

In the future, I plan to generalize our $u(3)$ framework to a description of topological defect in spin–1 systems [190]. To characterize the phase transition, it is useful to use homotopy analysis [145] in order to classify all topological defects of spin–1 systems, and not only topological defects arising in the case of FQ ground state. It would also be useful and interesting to translate all the required quantities such as the spin-stiffness, Berry–curvature, Chern–number within our u(3)–language, starting with generalizing to a director or A-matrix stiffness in order to make it compatible with quadrupolar

systems, as well as dipolar ones. In order to achieve these goals, a Non Linear Sigma Model (nlsm) for the ferroquadrupolar phase of the BBQ model has already been derived [43, 103]. This allows for a hydrodynamic description of the ferroquadrpolar phase of the BBQ model and for determining all the degrees of freedom which play a role in the low energy, long wave-length limits. These form the relevant degrees of freedom to be considered, since we are interested in their small, continuous changes. Moreover, the nlsm is sufficient enough to capture the topological structure of the order parameter space.

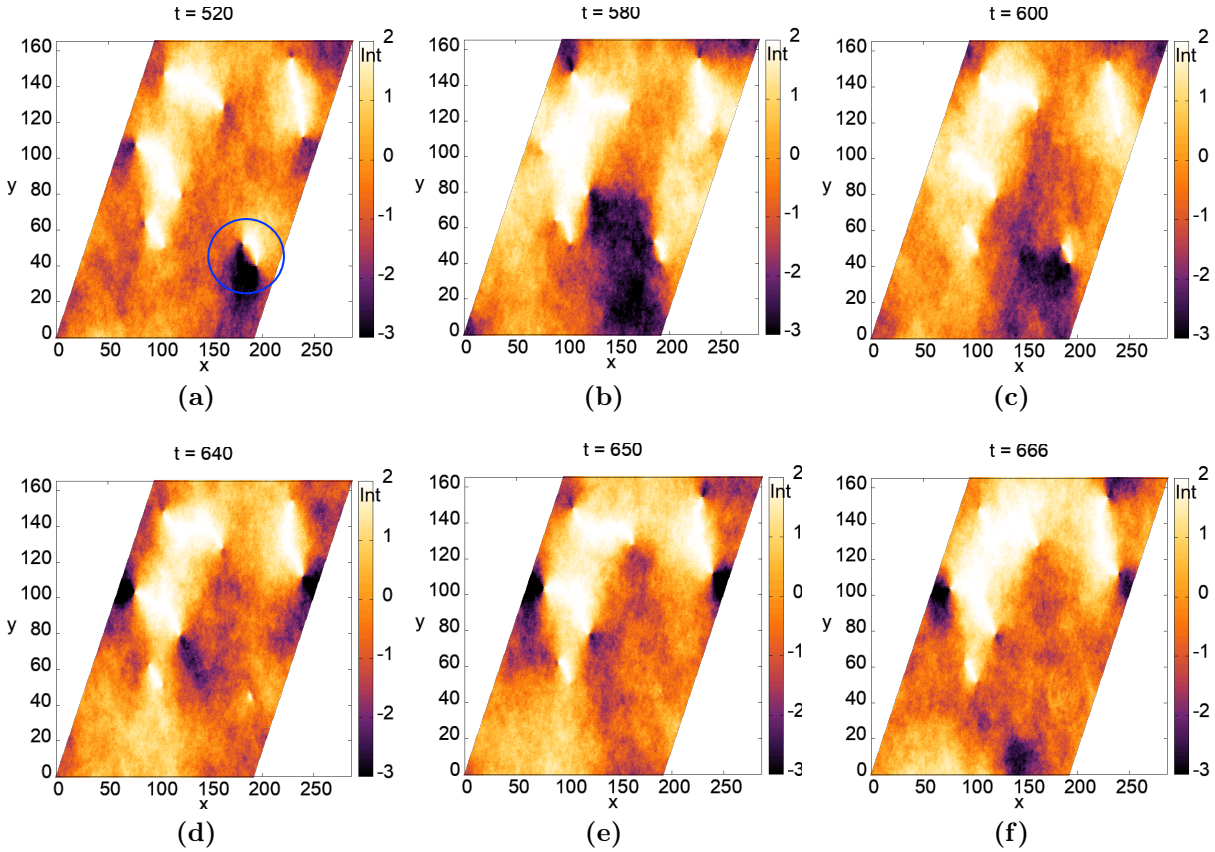

Figure 7.5: (a)-(f) Snapshots at different time during time evolution obtained by u3MD scheme, described in Section 2.6.2, of the BBQ model [Eq. (2.72)] in the FQ phase with topological defects. The x– and y–axis represent the real space variables of the 2 dimensional triangular lattice, and the intensities corresponds to the total quadrupolar weight $\sum_{\alpha,\beta} Q_i^{\alpha\beta}(t)$. Numerical simulations were carried out by my collaborator Dr. Rico Pohle.

Besides this topological phase transition, the time evolution of these topological defects provides a rich and exciting playground for studying spin–1 systems as illustrated in Fig. 7.5. From the earlier work of Hiroaki Ueda, it is known that not all solitons are equivalent, and solitons of higher charges can decay into elementary solitons [252]. Why and how this happens remains a mystery. Expanding our understanding of these aspects using a combination of analytic tools and numerical simulations will definitely

bring insight into their dynamics. Therefore, a generalization of existing theories of interacting vortices made of dipolar spins within our approach will allow for a better understanding of the interaction and dynamics of vortices in quadrupolar systems. Additionally, a general description in terms of the algebra $u(3)$ would enable to access not only systems with quadrupolar type of orders, but also general spin systems which allow for different types of vortices. Well–known concepts such as spin-stiffness, Berry–curvature, Chern–number could be extended to our methodology in order to generally describe defects for spin-1 systems.

An approach consisting in gradually improving complexity seems reasonable, and one may want to start by characterizing single vortex physics first. This could be accessed by looking at structure factors and computing vortex energy and other thermodynamic quantities. The next step is then to investigate the dynamics of a single vortex. This would lead to finally analyzing multi-vortices physics by studying how vortices interact and evolve, as an extension of the single vortex physics requiring the derivation of an effective model.

7.2.2 Generalization to Self-Consistent Gaussian Approximation Within the $u(3)$ Algebra

Here I start by giving a short introduction to the Self-Consistent Gaussian Approximation (SCGA) which is commonly based on $O(3)$ description of dipolar spin and used to compute equal–time structure factors in disordered phases [46, 47, 65–68]. Indeed the SCGA provides a surprisingly powerful tool to extract correlations, especially for classical spin liquid, for which the high-T paramagnetic phase is continuously linked to the low-T spin liquid phase.

Concepts and SCGA for $O(3)$ Spins

Following references [32, 46, 47, 68, 101], I here give a brief outline of the SCGA method for classical $O(3)$–vectors.

We start by assuming that the dipole spin moments interact through an interaction matrix $J^{\alpha\beta}$, such that the Hamiltonian is given by

$$\mathcal{H}_{=} \sum_{\langle i,j \rangle} J^{\alpha\beta} \hat{\mathrm{S}}_i^{\alpha} \hat{\mathrm{S}}_j^{\beta} + E_0 \ , \tag{7.23}$$

that we immediately recognize as the anisotropic Heisenberg model and where E_0 is the ground state energy. We further consider the dipole spin moments as classical spins of fixed length

$$\mathrm{S}_{\mathbf{r}} \cdot \mathrm{S}_{\mathbf{r}} = s^2 \ . \tag{7.24}$$

The essence of the SCGA approach treats the components of the spin vector $\mathrm{S}_{\mathbf{r}}$ as independent variables subject to a constraint on the spin–length which is only enforced on average

$$\langle \sum_{\alpha} \mathrm{S}_{\mathbf{r}}^{\alpha} \mathrm{S}_{\mathbf{r}}^{\alpha} \rangle = s^2 \ . \tag{7.25}$$

This constraint is imposed by the use of a Lagrange multiplier μ. For systems where the interaction of the degrees of freedom takes a quadratic (Gaussian) form, the Lagrange multiplier is found self-consistently through the constraint, as we will see below, and hence the name of the method.

Under these assumptions, we can solve Eq. (7.23) by Fourier transform

$$\hat{\mathrm{S}}_i^\alpha = \frac{1}{\sqrt{N}} \sum_{\mathbf{q}} e^{i\mathbf{q}\mathbf{r}_i} \hat{\mathrm{S}}_{\mathbf{q}}^\alpha \,, \tag{7.26}$$

and write

$$\mathcal{H} = \frac{1}{2} \sum_{\mathbf{q}} \hat{\mathrm{S}}_{-\mathbf{q}}^\alpha J(\mathbf{q})^{\alpha\beta} \hat{\mathrm{S}}_{\mathbf{q}}^\beta + E_0 \,. \tag{7.27}$$

The canonical partition function is defined as

$$Z = \sum_\sigma e^{-\beta \mathcal{H}_\sigma} \,, \tag{7.28}$$

In its continuous version, the canonical partition function is obtained by integrating out the degrees of freedom

$$Z = \int e^{-\beta \mathcal{H}(\vec{s}_{\mathbf{k}})} \mathrm{d}\vec{s}_{\mathbf{k}} \,. \tag{7.29}$$

In order to calculate correlation functions, we introduce a new term to the Hamiltonian $\Delta\mathcal{H}[\mathbf{h}_i]$

$$\Delta\mathcal{H}[\mathbf{h}_i] = -\sum_i h_i^\alpha \hat{\mathrm{S}}_i^\alpha \,, \tag{7.30}$$

where the fictive field $\mathbf{h}$ couples to the dipole moments. Similarly to Section 3.3.3, this allows us to take the appropriate derivative of the free energy with respect to this fictive field and then evaluate the derivative at zero-field. After performing a Fourier transform, Eq. (7.30) yields

$$\Delta\mathcal{H}[\mathbf{h}_\mathbf{q}] = -\sum_{\mathbf{q}} h_{-\mathbf{q}}^\alpha \hat{\mathrm{S}}_{\mathbf{q}}^\alpha \,. \tag{7.31}$$

We introduce a Lagrange multiplier μ such that the constraint Eq. (7.25) is fulfilled.

$$\mu(Ns^2 - \sum_{\mathbf{q}} \sum_\alpha \mathrm{S}_{\mathbf{q}}^\alpha \mathrm{S}_{-\mathbf{q}}^\alpha) = 0 \,. \tag{7.32}$$

By adding the constraint Eq. (7.32) to the total Hamiltonian Eq. (7.27), we have

$$\begin{aligned} \mathcal{H}_\mu &= \frac{1}{2} \sum_{\mathbf{q}} \hat{\mathrm{S}}_{-\mathbf{q}}^\alpha J(\mathbf{q})^{\alpha\beta} \hat{\mathrm{S}}_{\mathbf{q}}^\beta - \mu(N - \sum_{\mathbf{q}} \sum_\alpha \mathrm{S}_{-\mathbf{q}}^\alpha \mathrm{S}_{\mathbf{q}}^\alpha) - \frac{1}{2} \sum_{\mathbf{q}} \left(\mathrm{h}_{-\mathbf{q}}^\alpha \hat{\mathrm{S}}_{\mathbf{q}}^\alpha + \hat{\mathrm{S}}_{-\mathbf{q}}^\alpha \mathrm{h}_{\mathbf{q}}^\alpha \right) + \mathrm{E}_0 \\ &= \frac{1}{2} \sum_{\mathbf{q}} \hat{\mathrm{S}}_{-\mathbf{q}}^\alpha \left(J(\mathbf{q})^{\alpha\beta} + 2\mu\delta^{\alpha\beta} \right) \mathrm{S}_{-\mathbf{q}}^\alpha - \frac{1}{2} \sum_{\mathbf{q}} \left(\mathrm{h}_{-\mathbf{q}}^\alpha \hat{\mathrm{S}}_{\mathbf{q}}^\alpha + \hat{\mathrm{S}}_{-\mathbf{q}}^\alpha \mathrm{h}_{\mathbf{q}}^\alpha \right) - \mu \mathrm{N} + \mathrm{E}_0 \,. \end{aligned} \tag{7.33}$$

We then defined

$$J_\mu(\mathbf{q})^{\alpha\beta} = J(\mathbf{q})^{\alpha\beta} + 2\mu\delta^{\alpha\beta} \ . \tag{7.34}$$

Considering that the total Hamiltonian can fluctuate for any of its degree of freedom $\mathrm{S}^\beta_{\mathbf{q}}$, and treating them as real classical degrees of freedom, the partition function [Eq. (7.29)] becomes

$$Z = e^{-\beta(E_0-\mu s^2 N)} \prod_{\mathbf{q}} \int e^{-\beta\frac{1}{2}\mathrm{S}^\alpha_{-\mathbf{q}}\mathrm{J}_\mu(\mathbf{q})^{\alpha\beta}\mathrm{S}^\beta_{\mathbf{q}}} e^{\frac{1}{2}\beta\left(h^\alpha_{-\mathbf{q}}\hat{\mathrm{S}}^\alpha_{\mathbf{q}} + \hat{\mathrm{S}}^\alpha_{-\mathbf{q}}h^\alpha_{\mathbf{q}}\right)} \mathrm{dS}_{\mathbf{q}} \ , \tag{7.35}$$

where $\mathrm{dS}_{\mathbf{q}} = \prod_\alpha \mathrm{dS}^\alpha_{\mathbf{q}}$ is the integration measure. Using Eq. (F.1e) to calculate the Gaussian integral, we obtain

$$Z = e^{-\beta(E_0-\mu s^2 N)} \prod_{\mathbf{q}} \sqrt{\frac{(2\pi)^n}{\beta^n \mathrm{detJ}_\mu(\mathbf{q})}} e^{\frac{1}{2}\beta h^\alpha_{-\mathbf{q}}[J_\mu(\mathbf{q})^{-1}]^{\alpha\beta}h^\beta_{\mathbf{q}}} \ . \tag{7.36}$$

The associated free energy is then given by

$$F = E_0 - \mu s^2 N - \sum_{\mathbf{q}} \frac{1}{2\beta} \log\left(\frac{(2\pi)^n}{\beta^n \mathrm{detJ}_\mu(\mathbf{q})}\right) - \frac{1}{2}\beta h^\alpha_{-\mathbf{q}}[J_\mu(\mathbf{q})^{-1}]^{\alpha\beta}h^\beta_{\mathbf{q}} \ . \tag{7.37}$$

The average value of $\mathrm{S}^\alpha_{\mathbf{q}}$ is obtained by taking the appropriate derivatives of the free energy with respect to the field $h^\alpha_{\mathbf{q}}$

$$\langle \mathrm{S}^\alpha_{\mathbf{q}} \rangle = - \left.\frac{\partial F}{\partial h^\alpha_{\mathbf{q}}}\right|_{\mathbf{h=0}} = 0 \ , \tag{7.38}$$

and

$$\begin{aligned} \langle \mathrm{S}^\alpha_{\mathbf{q}} \mathrm{S}^\beta_{-\mathbf{q}} \rangle =& - \frac{1}{\beta} \left.\frac{\partial^2 F}{\partial h^\alpha_{\mathbf{q}} \partial h^\beta_{-\mathbf{q}}}\right|_{\mathbf{h=0}} \\ =& \frac{1}{2\beta}[J_\mu(\mathbf{q})^{-1}]^{\alpha\beta} \ , \end{aligned} \tag{7.39}$$

where we used

$$[J_\mu(\mathbf{q})^{-1\,\alpha\beta}] = [J_\mu(\mathbf{q})^{-1}]^{\beta\alpha} \ , \tag{7.40}$$

which encodes the fact that the way a spin on site i interacts with the spin on site j stays invariant if we permute the 2 spins, i.e, spins on different lattice sites commute. And if we take the sum over the diagonal components, we get

$$\begin{aligned} \sum_\alpha \langle \mathrm{S}^\alpha_{\mathbf{q}} \mathrm{S}^\alpha_{-\mathbf{q}} \rangle =& \frac{1}{2\beta} \sum_\alpha ([J_\mu(\mathbf{q})^{-1}]^{\alpha\alpha}) = \frac{1}{2\beta} \mathrm{Tr}(J_\mu(\mathbf{q})^{-1}) \\ =& \frac{1}{2\beta} \sum_\alpha \frac{1}{\omega_\alpha + 2\mu} \ , \end{aligned} \tag{7.41}$$

where ω_α are the eigenvalues of the interaction matrix $J(\mathbf{q})$ defined by Eq. (7.27). We

can use Eq. (7.41) to self-consistently calculate the Lagrange multiplier by considering

$$\frac{1}{N}\sum_{\mathbf{q}}\sum_{\alpha}\mathrm{S}^{\alpha}_{-\mathbf{q}}\mathrm{S}^{\alpha}_{\mathbf{q}}=\sum_{\alpha}\langle\mathrm{S}^{\alpha}_{\mathbf{q}}\mathrm{S}^{\alpha}_{-\mathbf{q}}\rangle=s^2\ , \tag{7.42}$$

and therefore we can write

$$s^2=\frac{1}{2\beta}\sum_{\alpha}\frac{1}{\omega_\alpha+2\mu}\ . \tag{7.43}$$

All we need to do is find a value for μ that satisfies Eq. (7.43), and plug the value found for μ into $J_\mu(\mathbf{q})$ to calculate correlation function through Eq. (7.39).

SCGA for the $u(3)$ Algebra

We here wish to generalize the above method for degrees of freedom of a classical spin–1. As explained in Section 2.3, a spin–1 also possesses quadrupolar besides dipolar degrees of freedom, making to $O(3)$–vector representation incompatible with a complete description of a spin–1. In Section 2.4, we saw that we can use a representation of the algebra $u(3)$ in terms of A–matrices accompanied by a constraint [Eq. (2.57)] to reduce back to the $su(3)$ algebra which properly accounts for a spin–1. The main advantages of working with the A matrices instead of the spin dipole and quadrupole components, besides the fact that the BBQ Hamiltonian written in terms of A matrices only includes quadratric terms in A [Eq. (1.69)], is that they obey simple commutation rules [Eq. (1.66)], making calculation much easier.

Re–Counting Constraints for a Spin–1

This has been discussed in depth in Chapter 2, but we here repeat the important concepts that we need here. Anything that can happen to a spin-1 can be represented by a matrix belonging to the group $SU(3)$, since the Hilbert of a spin—1 is 3–dimensional. The state of a spin-1 can be represented by three complex coefficients [Eq. (2.35)], that we can separate into two 3–dimensional vectors $\mathbf{u}$ and $\mathbf{v}$, which together form the six needed real parameters. For convenience, we rename these coefficients as

$$d^{*\mu}=\mathrm{a}^{\mu}=\mathrm{u}^{\mu}+\mathrm{i}\mathrm{v}^{\mu}\ , \tag{7.44a}$$

$$d_{\mu}=\mathrm{b}_{\mu}=\mathrm{u}_{\mu}-\mathrm{i}\mathrm{v}_{\mu}\ . \tag{7.44b}$$

which consists just in a basis transformation of $\mathbf{u}$ and $\mathbf{v}$ in the complex plane. We still have six real degrees of freedom encoded into two 3–dimensional vectors $\mathbf{a}$ and $\mathbf{b}$, with the constraint

$$\mathbf{ab}=1\ , \tag{7.45}$$

which simply is the normalization of the state [Eq. (2.36)] transcribed in terms of $\mathbf{a}$ and $\mathbf{b}$ such that we are left with five degrees of freedom.

Additionally, there is also the freedom to fix the phase of the state described by the director. This reduces the number of degrees of freedom to four, which are the independent degrees of freedom needed to describe a spin–1 moment.

Counting Constraints for an A–Matrix

We here present how the number of independent degrees of freedom in an A-matrix reduces to four, once all the constraints implied by the properties of the A-matrix are taken into account.

Using Eq. (7.44) and Eq. (2.47), the A-matrix then becomes

$$\langle \mathrm{A} \rangle = \begin{pmatrix} \mathrm{a^x b_x} & \mathrm{a^x b_y} & \mathrm{a^x b_z} \\ \mathrm{a^y b_x} & \mathrm{a^y b_y} & \mathrm{a^y b_z} \\ \mathrm{a^z b_x} & \mathrm{a^z b_y} & \mathrm{a^y b_y} \end{pmatrix} . \tag{7.46}$$

We note that the A-matrix has 9 complex components. This makes a total of 18 real degrees of freedom. But we want to describe a spin-1, which is described by 4 independent degrees of freedom. So we should have additional constraints that restrict the components of the A-matrix such that it does indeed represent a spin-1. The normalization [Eq. (7.45)] simply becomes the trace constraint over the A-matrix

$$TrA = \mathrm{A^x}_{\mathrm{x}} + \mathrm{A^y}_{\mathrm{y}} + \mathrm{A^z}_{\mathrm{z}} = \mathrm{a^x b_x} + \mathrm{a^y b_y} + \mathrm{a^y b_y} = 1 . \tag{7.47}$$

We also notice that because of the form of Eq. (2.46), (and therefore Eq. (7.46)), A is an Hermitian matrix [Eq. (2.49)] and we have

$$\mathrm{A}^{\mu *}_{\ \nu} = \mathrm{A^\nu}_{\ \mu} , \tag{7.48}$$

$$\mathrm{a}^{\mu *} \mathrm{b}^*_\nu = \mathrm{a}^\nu \mathrm{b}_\mu , \tag{7.49}$$

where the last line obvious by construction from the definition of Eq. (7.44) since $\mathrm{a}^{\mu *} = \mathrm{b}_\mu$. In Eq. (7.48), we then need to consider the cases when $\mu = \nu$ and when $\mu \neq \nu$ in order to extract the constraints

$$\begin{array}{lllll} \mu = \nu & \mathrm{A}^{\mu *}_{\ \mu} & = \mathrm{A}^\mu_{\ \mu} & \Rightarrow & \mathrm{Im}(\mathrm{A}^\mu_{\ \mu}) = 0 \quad (\mathrm{A}^\mu_{\ \mu} \in \mathbb{R}) \\ \mu \neq \nu & \mathrm{A}^{\mu *}_{\ \nu} & = \mathrm{A^\nu}_{\ \mu} & \Rightarrow & \mathrm{Re}(\mathrm{A}^{\mu *}_{\ \nu}) = \mathrm{Re}(\mathrm{A^\nu}_{\ \mu}) \ \ \& \ \ \mathrm{Im}(\mathrm{A}^{\mu *}_{\ \nu}) = \mathrm{Im}(\mathrm{A^\nu}_{\ \mu}) . \end{array} \tag{7.50}$$

We note that for $\mu = \nu$ this corresponds to one constraint on the imaginary part, namely enforcing the imaginary part to vanish. This implies that the diagonal elements are all real. While for $\mu \neq \nu$, this corresponds to two constraints, one on the real part, and one on the imaginary part.

Additionally, as can be seen from its definition [Eq. (2.46)], the A–matrix is proportional to a projector operator. A projection P is a linear operator from a vector space V onto itself

$$P : V \to V \text{ such that } \ P^2 = P . \tag{7.51}$$

From here, we can consider the A–matrix as an operator represented in terms of bosonic operators $\mathrm{d}^{\dagger\alpha}\hat{\mathrm{d}}_\beta$ [Eq. (2.66)], or in terms of complex numbers $\mathrm{a}^\alpha \mathrm{b}_\beta$ [Eq. (7.46)], where the difference lie in the fact that the bosonic operators follow bosonic commutation relations [Eq. (2.65)], while **a** and **b** simply commute. We can then show that if we consider the "classical" representation consisting of complex numbers then the A–

matrix is idempotent and is a projection

$$\mathrm{A} = \mathrm{A}.\mathrm{A} \ . \tag{7.52}$$

However, if we consider the A–matrix as an operator represented in terms of bosonic operators $\mathrm{d}^{\dagger\alpha}\hat{\mathrm{d}}_\beta$ [Eq. (2.66)], then A is proportional to an idempotent matrix

$$3\hat{\mathrm{A}} = \hat{\mathrm{A}}.\hat{\mathrm{A}} \ , \tag{7.53}$$

such that $\frac{\hat{\mathrm{A}}}{3}$ is idempotent ($\frac{\hat{\mathrm{A}}}{3}.\frac{\hat{\mathrm{A}}}{3} = \frac{3\hat{\mathrm{A}}}{9} = \frac{\hat{\mathrm{A}}}{3}$). This is because when computing the double product $A.A$, the terms need to be rearranged. This way, one extract the expression of the trace, which then allows to identify the product $A.A$ with $\propto A$. When considering bosons $\mathrm{d}^{\dagger\alpha}$, the terms need to be rearranged by taking care of commutation relations, while no specific care needs to be taken when considering complex numbers. This leads to a factor 3 difference.

Because the SCGA is built around a classical limit, we can neglect commutation relations and assume that the A–matrices consist of complex numbers. Eq. (7.52), written for one component yields

$$\mathrm{A}^\mu{}_\nu = \sum_\kappa \mathrm{A}^\mu{}_\kappa \mathrm{A}^\kappa{}_\nu \ . \tag{7.54}$$

For $\mu = \nu$, writing down the sum over κ explicitly implies

$$\begin{aligned} & \mathrm{A}^\mu{}_\mu = \mathrm{A}^\mu{}_\alpha \mathrm{A}^\alpha{}_\mu + \mathrm{A}^\mu{}_\beta \mathrm{A}^\beta{}_\mu + \mathrm{A}^\mu{}_\mu \mathrm{A}^\mu{}_\mu \\ \Rightarrow \ & \mathrm{A}^\mu{}_\mu \mathrm{A}^\mu{}_\mu - \mathrm{A}^\mu{}_\mu + \sum_{\kappa\neq\mu} \mathrm{A}^\mu{}_\kappa \mathrm{A}^\kappa{}_\mu = 0 \ . \end{aligned} \tag{7.55}$$

Solving the quadratic equation for $\mathrm{A}^\mu{}_\mu$ would imply that the diagonal coefficient can be retrieved from the diagonal ones.

For $\mu \neq \nu$, we have

$$\begin{aligned} & \mathrm{A}^\mu{}_\nu = \mathrm{A}^\mu{}_\alpha \mathrm{A}^\alpha{}_\nu + \mathrm{A}^\mu{}_\nu \mathrm{A}^\nu{}_\nu + \mathrm{A}^\mu{}_\mu \mathrm{A}^\mu{}_\nu \\ \Rightarrow \ & \mathrm{A}^\mu{}_\nu (1 - \mathrm{A}^\mu{}_\mu - \mathrm{A}^\nu{}_\nu) = \mathrm{A}^\mu{}_\alpha \mathrm{A}^\alpha{}_\nu \\ \Rightarrow \ & \mathrm{A}^\mu{}_\nu \mathrm{A}^\alpha{}_\alpha = \mathrm{A}^\mu{}_\alpha \mathrm{A}^\alpha{}_\nu \quad \text{for } \mu \neq \nu \neq \alpha \ , \end{aligned} \tag{7.56}$$

where we use the trace constraint $\mathrm{A}^\mu{}_\mu + \mathrm{A}^\nu{}_\nu + \mathrm{A}^\alpha{}_\alpha = 1$ in the last line. We observe that form Eq. (7.56), we can also extract diagonal components in terms of off-diagonal ones. There is therefore some redundancy in the constraint given in Eq. (7.52). Eq. (7.56) can be rewritten as

$$\mathrm{A}^\mu{}_\nu = \frac{\mathrm{A}^\mu{}_\alpha \mathrm{A}^\alpha{}_\nu}{\mathrm{A}^\alpha{}_\alpha} \ . \tag{7.57}$$

We note that Eq. (7.57) provides then one constraint for each set of $\{\mu, \nu, \alpha\}$ where $\mu \neq \nu \neq \alpha$, and since each of theses are indexed by 3 parameter x, y, or z, knowledge of 2 of the variables within $\{\mu, \nu, \alpha\}$ automatically determines the set. Therefore, we

can simply consider pairs of variable $\{\mu, \nu\}$ such that $\mu \neq \nu$ where each can take on 3 different values, which leads to 6 different possibilities. However, because of the Hermitian nature of the A–matrix [Eq. (7.48)], these 6 constraints are doubly redundant. It follows that we can consider only 3 different pairs $\{\mu, \nu\}$ such that $\mu \neq \nu$ to construct the constraints coming from the fact the A–matrix is idempotent. However, because these constraints are not linear, they actually allow to restrict more than 3 degrees of freedom, namely 4. Indeed, we show that if we assume that we know 4 initial parameters, using the constraints on the trace, the Hermitian property, and the projection property of the A–matrix, we can recover the whole A matrix.

This can be seen by using the 3 constraints for 3 different pairs $\{\mu, \nu\}$ and combing them such that we obtain 3 additional constraints. For concreteness, we could consider as combination of $\{\mu, \nu, \alpha\}$ with $\mu \neq \nu \neq \alpha$, the combinations

$$\{x, y, z\} \quad \mathrm{A}^{\mathrm{x}}{}_{\mathrm{y}}\mathrm{A}^{\mathrm{z}}{}_{\mathrm{z}} = \mathrm{A}^{\mathrm{x}}{}_{\mathrm{z}}\mathrm{A}^{\mathrm{z}}{}_{\mathrm{y}} \ , \tag{7.58a}$$

$$\{x, z, y\} \quad \mathrm{A}^{\mathrm{x}}{}_{\mathrm{z}}\mathrm{A}^{\mathrm{y}}{}_{\mathrm{y}} = \mathrm{A}^{\mathrm{x}}{}_{\mathrm{y}}\mathrm{A}^{\mathrm{y}}{}_{\mathrm{z}} \ , \tag{7.58b}$$

$$\{y, z, x\} \quad \mathrm{A}^{\mathrm{y}}{}_{\mathrm{z}}\mathrm{A}^{\mathrm{x}}{}_{\mathrm{x}} = \mathrm{A}^{\mathrm{y}}{}_{\mathrm{x}}\mathrm{A}^{\mathrm{x}}{}_{\mathrm{z}} \ . \tag{7.58c}$$

We can then combine Eq. (7.58a) and Eq. (7.58b), by extracting $\frac{\mathrm{A}^{\mathrm{x}}{}_{\mathrm{z}}}{\mathrm{A}^{\mathrm{x}}{}_{\mathrm{y}}}$ in both equations and equating their respective expressions. We obtain

$$\begin{aligned} \frac{\mathrm{A}^{\mathrm{x}}{}_{\mathrm{z}}}{\mathrm{A}^{\mathrm{x}}{}_{\mathrm{y}}} &\overset{Eq.\ (7.58a)}{=} \frac{\mathrm{A}^{\mathrm{z}}{}_{\mathrm{z}}}{\mathrm{A}^{\mathrm{z}}{}_{\mathrm{y}}} = \frac{\mathrm{A}^{\mathrm{y}}{}_{\mathrm{z}}}{\mathrm{A}^{\mathrm{y}}{}_{\mathrm{y}}} \overset{Eq.\ (7.58b)}{=} \frac{\mathrm{A}^{\mathrm{x}}{}_{\mathrm{z}}}{\mathrm{A}^{\mathrm{x}}{}_{\mathrm{y}}} \\ \Rightarrow \quad & \mathrm{A}^{\mathrm{y}}{}_{\mathrm{z}}\mathrm{A}^{\mathrm{z}}{}_{\mathrm{y}} = \mathrm{A}^{\mathrm{y}}{}_{\mathrm{y}}\mathrm{A}^{\mathrm{z}}{}_{\mathrm{z}} \ . \end{aligned} \tag{7.59a}$$

Similarly, considering the conjugate transform version of Eq. (7.58a) and Eq. (7.58c), we find

$$\mathrm{A}^{\mathrm{x}}{}_{\mathrm{z}}\mathrm{A}^{\mathrm{z}}{}_{\mathrm{x}} = \mathrm{A}^{\mathrm{x}}{}_{\mathrm{x}}\mathrm{A}^{\mathrm{z}}{}_{\mathrm{z}} \ . \tag{7.59b}$$

Finally, combining Eq. (7.58b) and Eq. (7.58c), we obtain

$$\mathrm{A}^{\mathrm{x}}{}_{\mathrm{y}}\mathrm{A}^{\mathrm{y}}{}_{\mathrm{x}} = \mathrm{A}^{\mathrm{x}}{}_{\mathrm{x}}\mathrm{A}^{\mathrm{y}}{}_{\mathrm{y}} \ . \tag{7.59c}$$

We note that Eq. (7.59a) to Eq. (7.59c), allows to represent the norm of the off-diagonal coefficients in terms of the diagonal ones, which are all real–valued due to the Hermitian property. Therefore, knowing only 4 initial parameters allows to rebuilt the A–matrix.

For instance, this can easily be seen by rewriting the components of A in their complex polar form

$$\mathrm{A}^{\alpha}{}_{\beta} = \mathrm{r}^{\alpha\beta}\mathrm{e}^{\mathrm{i}\phi^{\alpha\beta}} \ , \tag{7.60}$$

and by assuming that we know 2 of the diagonal elements (which are real), let us choose $\mathrm{A}^{\mathrm{x}}{}_{\mathrm{x}} = \mathrm{r}^{\mathrm{xx}}$ and $\mathrm{A}^{\mathrm{y}}{}_{\mathrm{y}} = \mathrm{r}^{\mathrm{yy}}$, as well as the phase of 2 off–diagonal elements ϕ^{xy} and ϕ^{yz}. Using the trace constraint [Eq. (7.47)], we easily obtain the remaining diagonal component $\mathrm{A}^{\mathrm{z}}{}_{\mathrm{z}}$. Then using Eq. (7.59a), we can find the norm of $\mathrm{A}^{\mathrm{y}}{}_{\mathrm{z}}$. Using Eq. (7.59c), we obtain the norm of $\mathrm{A}^{\mathrm{x}}{}_{\mathrm{y}}$. Finally $\mathrm{A}^{\mathrm{x}}{}_{\mathrm{z}}$ can be found using Eq. (7.58a) or Eq. (7.58b).

The A–matrix is then expressed as

$$\mathrm{A} = \begin{pmatrix} r^{xx} & \sqrt{r^{xx}r^{yy}}e^{i\phi^{xy}} & \sqrt{r^{xx}(1-r^{xx}-r^{yy})}e^{i(\phi^{xy}+\phi^{yz})} \\ \sqrt{r^{xx}r^{yy}}e^{-i\phi^{xy}} & r^{yy} & \sqrt{r^{yy}(1-r^{xx}-r^{yy})}e^{i\phi^{yz}} \\ \sqrt{r^{xx}(1-r^{xx}-r^{yy})}e^{i(\phi^{xy}+\phi^{yz})} & \sqrt{r^{yy}(1-r^{xx}-r^{yy})}e^{-i\phi^{yz}} & 1-r^{xx}-r^{yy} \end{pmatrix}, \tag{7.61}$$

in terms of only the 4 initial parameters r^{xx}, r^{yy}, ϕ^{xy} and ϕ^{yz}.

The counting of the number of degrees of freedom is summarized in Table (7.1).

		# Degrees of Freedom	
A-matrix			+18
Trace Constraint	TrA=1		-1
Hermitian Property	$\mathrm{A}^{\mu *}_{\ \ \nu} = \mathrm{A}^{\nu}_{\ \ \mu}$	$\mu = \nu$	-3
		$\mu \neq \nu$	$-2 \times 3 = -6$
Projection Property	$\mathrm{A}^{\mu}_{\ \ \nu}\mathrm{A}^{\alpha}_{\ \ \alpha} = \mathrm{A}^{\mu}_{\ \ \alpha}\mathrm{A}^{\alpha}_{\ \ \nu}$		-4
Total			4

Table 7.1: Constraints counting on the A–matrix describing a spin–1 moment. Naively, an A–matrix contains 18 real degrees of freedom. However, a spin–1 moment is fully characterized by 4 parameters. Here, we show that by accounting for the properties of the A–matrix, in particular, the constraint on the trace, its Hermitian nature, and the fact that it is a projection, reduces back to 4 independent real parameters.

We see by using the properties of the A-matrix, namely, the fact that its trace equals one, that if the complex conjugate of a component equals its conjugate transpose, and that it is a projection, we can restrict the initial 18 real degrees of freedom encompassed within the A-matrix down to 4 real degrees of freedom that are required to describe a spin–1.

The future goal is to derive a numerical implementation of the SCGA for the A–matrix. The BBQ model [Eq. (1.48)] provides a natural starting point, since it is the simpler $SU(2)$ symmetric Hamiltonian for a spin–1 and can easily be restricted to the Heisenberg model by setting $J_2 = 0$. Additionally, we already know its expression in terms of A–matrices. The fact that it is quadratic in $\hat{\mathcal{A}}$ implies that a Gaussian treatment is also applicable. We note that the constraints on the Hermitian property imply 9 linear constraints, dividing the initial 18 degrees of freedom by half. Therefore, we can work with 9 degrees of freedom on which we need to ensure the trace and projection constraints. We can set up these 9 degrees of freedom in a 9–dimensional vector $\hat{\mathrm{T}}_{\mathbf{q}}$, such that we can rewrite the Hamiltonian as

$$\mathcal{H} = \frac{1}{2}\sum_{\mathbf{q}} \hat{\mathrm{T}}^{\alpha}_{-\mathbf{q}} J(\mathbf{q})^{\alpha}_{\beta} \hat{\mathrm{T}}^{\beta}_{\mathbf{q}} \,. \tag{7.62}$$

For instance, we could use as the 9–dimensional vector $\hat{\mathrm{T}}_{\mathbf{q}}$, the following representation

$$\hat{\mathrm{T}}_{\mathbf{q}} = \begin{pmatrix} \hat{\mathcal{A}}^{1}_{\mathbf{q}\ 1} \\ \hat{\mathcal{A}}^{1}_{\mathbf{q}\ 2} \\ \hat{\mathcal{A}}^{1}_{\mathbf{q}\ 3} \\ \hat{\mathcal{A}}^{2}_{\mathbf{q}\ 1} \\ \hat{\mathcal{A}}^{2}_{\mathbf{q}\ 2} \\ \hat{\mathcal{A}}^{2}_{\mathbf{q}\ 3} \\ \hat{\mathcal{A}}^{3}_{\mathbf{q}\ 1} \\ \hat{\mathcal{A}}^{3}_{\mathbf{q}\ 2} \\ \hat{\mathcal{A}}^{3}_{\mathbf{q}\ 3} \end{pmatrix} . \tag{7.63}$$

Whether this is the best choice remains to be determined. What also remains to be understood is how one can self-consistently implement the constraints on the trace and the projection property of the A–matrix. Indeed, an implementation that allows to ensure that the trace is conserved on average and the 3 constraints induced by the idempotent property, should be generalized through the introduction of Lagrange multipliers, similarly to the $O(3)$ case.

7.3 Concluding Remarks

Finally, I would like to emphasize the generality of my approach for describing spin–1 magnets at the (semi)–classical level. Most of the results presented in this Thesis are illustrated for the FQ state of the BBQ model. But, both the analytical classical and quantum theories of fluctuations can be applied to any ordered ground state of a spin–1 system. Additionally, through the generalization of the SCGA method to degrees of freedom of $u(3)$ A–matrices, I am hopeful that this will also enable a valid classical approach for exploring unordered spin–1 systems.

An important result obtained from the analysis between the classical and quantum theories, is the classical–quantum correspondence that links $T = 0$ quantum (semi-classical) prediction with finite temperature classical results or finite u3MD simulation results. This allows to better understand how classical thermal fluctuations can be correct in order be equivalent to quantum fluctuations at $T = 0$. Additionally, it emphasizes the importance of the number of modes available whether a classical or a quantum treatment is considered.

Spin–1 magnets have many interesting properties and spin–1 models have a wide application that also includes for example cold atoms [52, 53, 100, 232, 270] or phenomenological theories of superconducting materials, such as Fe–based superconductors [60, 74, 126, 139, 256]. Taken together, this represents a broad, challenging sets of applications, where the methods developed in this Thesis have the potential to shine light on some very interesting problems.

On the experimental side, the methods developed in this Thesis can be applied to some new and already existing spin–1 materials, such as the triangular–lattice spin–nematic candidate $NiGa_2S_4$ [24, 131, 159, 161, 250, 253], and the pyrochlore spin–liquid candidate $NaCaNi_2F_7$ [188, 267], both discussed in Section 1.3.1.

On the theoretical side, the formalism developed in this thesis has a great potential

at describing properties of spin–1 magnets, and to be generalized to other methods, such as the SCGA. The thermodynamic properties of spin–1 magnets, which can host quadrupoles on a single site, are qualitatively different from spin–$\frac{1}{2}$ systems. For this reason, spin–1 magnets also support different types of orders with interesting topological excitations. They nevertheless remain relatively unexplored, mostly because of the lack of available theoretical tools. This allows for a wide range of applicability of the analytical methods in combination of the u3MC and u3MD methods to provide a powerful tool to investigate the (semi)–classical thermodynamics and dynamic of spin–1 magnets. Additionally, the numerical methods developed in this thesis can also be applied to investigate unordered phases, such as spin–liquids or systems with complex excitations, as well as to explore unusual phase transitions where topological excitations can appear and their associated dynamics, giving access to dynamical properties that until now remained inaccessible. The ordered ground states of the BBQ model have already been shown, for instance, to be able to exhibit topological excitations [63, 78, 102, 103, 260]. Dynamics and thermodynamics of which can be investigated with the methods developed in this Thesis.

The u3MC simulations results shown in this Thesis were obtained using a Metropolis algorithm with a single spin–update. However, more general cluster– [127] or worm–[168] updates could be implemented. Similarly, the u3MD method developed here using a simple 4^{th} order Runge–Kutta algorithm is ripe for technical refinement.

In conclusion, both the analytical and numerical methods developed in this Thesis provide valid and powerful tools to investigate spin–1 magnets. Indeed, the classical and quantum analytical theories of fluctuations, as well as u3MC and u3MD numerical methods introduced in this work provide a reliable and convenient way to explore the classical thermodynamics, and semi–classical dynamics of spin–1 magnets, paving the way for new theories and interpretations of experimental data.

Lastly, I would like to congratulate the reader who made it to this line. This Thesis has been a long journey and I am convinced that we all are happy to see the final point ending this chapter and all the work entailed here, endpoint that will hopefully be the starting point of further interesting research.

Bibliography

[1] I. Affleck and E. H. Lieb. A proof of part of Haldane's conjecture on spin chains. *Letters in Mathematical Physics*, 12(1):57–69, 1986. doi: 10.1007/BF00400304. URL https://doi.org/10.1007/BF00400304.

[2] I. Affleck, T. Kennedy, E. H. Lieb, and H. Tasaki. Rigorous results on valence-bond ground states in antiferromagnets. *Phys. Rev. Lett.*, 59:799–802, Aug 1987. doi: 10.1103/PhysRevLett.59.799. URL https://link.aps.org/doi/10.1103/PhysRevLett.59.799.

[3] I. Affleck, T. Kennedy, E. H. Lieb, and H. Tasaki. Valence bond ground states in isotropic quantum antiferromagnets. *Communications in Mathematical Physics*, 115(3):477–528, 1988. doi: 10.1007/BF01218021. URL https://doi.org/10.1007/BF01218021.

[4] Y. Akagi, M. Udagawa, and Y. Motome. Hidden Multiple-Spin Interactions as an Origin of Spin Scalar Chiral Order in Frustrated Kondo Lattice Models. *Phys. Rev. Lett.*, 108:096401, Feb 2012. doi: 10.1103/PhysRevLett.108.096401. URL https://link.aps.org/doi/10.1103/PhysRevLett.108.096401.

[5] Y. Akagi, H. Ueda, and N. Shannon. unpublished.

[6] M. Akaki, D. Yoshizawa, A. Okutani, T. Kida, J. Romhányi, K. Penc, and M. Hagiwara. Direct observation of spin-quadrupolar excitations in $Sr_2CoGe_2O_7$ by high-field electron spin resonance. *Phys. Rev. B*, 96:214406, Dec 2017. doi: 10.1103/PhysRevB.96.214406. URL https://link.aps.org/doi/10.1103/PhysRevB.96.214406.

[7] Y. Amari. private communication.

[8] P. W. Anderson. Antiferromagnetism. Theory of Superexchange Interaction. *Phys. Rev.*, 79:350–356, Jul 1950. doi: 10.1103/PhysRev.79.350. URL https://link.aps.org/doi/10.1103/PhysRev.79.350.

[9] P. W. Anderson and H. Hasegawa. Considerations on Double Exchange. *Phys. Rev.*, 100:675–681, Oct 1955. doi: 10.1103/PhysRev.100.675. URL https://link.aps.org/doi/10.1103/PhysRev.100.675.

[10] A. Andreev and I. Grishchuk. Spin Nematics. *JETP*, 87:467–475, 1984. URL http://www.jetp.ac.ru/cgi-bin/e/index/e/60/2/p267?a=list.

[11] G. B. Arfken and H. J. Weber. *Mathematical Methods for Physicists – International Edition*. Academic Press, INC, 4th edition, 1995. ISBN 0-12-059816-7.

[12] Aristotle. *On the Soul*. Aeterna Press, London, 2015/10/26 2015. ISBN 978-1785167362.

[13] A. Auerbach. *Interacting Electrons and Quantum Magnetism*. Springer, 1994.

[14] P. Balla. The Equation of Motion Method for Spin Systems with Multipolar Hamiltonians. Master's thesis, Budapest University of Technology and Economics, 2014.

[15] A. Banerjee, J. Yan, J. Knolle, C. A. Bridges, M. B. Stone, M. D. Lumsden, D. G. Mandrus, D. A. Tennant, R. Moessner, and S. E. Nagler. Neutron scattering in the proximate quantum spin liquid α–$RuCl_3$. *Science*, 356(6342):1055–1059, 2022/06/12 2017. doi: 10.1126/science.aah6015. URL `https://doi.org/10.1126/science.aah6015`.

[16] S. K. Banerjee and B. M. Moskowitz. *Ferrimagnetic Properties of Magnetite*, pages 17–41. Springer US, Boston, MA, 1985. ISBN 978-1-4613-0313-8. doi: 10.1007/978-1-4613-0313-8_2. URL `https://doi.org/10.1007/978-1-4613-0313-8_2`.

[17] M. M. S. Barbeau, M. Eckstein, M. I. Katsnelson, and J. H. Mentink. Optical control of competing exchange interactions and coherent spin-charge coupling in two-orbital Mott insulators. *SciPost Phys.*, 6:27, 2019. doi: 10.21468/SciPostPhys.6.3.027. URL `https://scipost.org/10.21468/SciPostPhys.6.3.027`.

[18] M. Barma. Phonon-induced phase transition in a classical Heisenberg chain. *Phys. Rev. B*, 12:2710–2715, Oct 1975. doi: 10.1103/PhysRevB.12.2710. URL `https://link.aps.org/doi/10.1103/PhysRevB.12.2710`.

[19] V. G. Bar'yakhtar, V. I. Butrim, A. K. Kolezhuk, and B. A. Ivanov. Dynamics and relaxation in spin nematics. *Phys. Rev. B*, 87:224407, Jun 2013. doi: 10.1103/PhysRevB.87.224407. URL `https://link.aps.org/doi/10.1103/PhysRevB.87.224407`.

[20] M. J. S. Beach, A. Golubeva, and R. G. Melko. Machine learning vortices at the kosterlitz-thouless transition. *Phys. Rev. B*, 97:045207, Jan 2018. doi: 10.1103/PhysRevB.97.045207. URL `https://link.aps.org/doi/10.1103/PhysRevB.97.045207`.

[21] F. Becca and S. Sorella. *Quantum Monte Carlo Approaches for Correlated Systems*. Cambridge University Press, 2017. doi: 10.1017/9781316417041.

[22] O. Benton. *unpublished*.

[23] R. N. Bhatt and K. Yang. Non-Heisenberg couplings and ferromagnetic instability in a random antiferromagnetic spin-1 chain. *Journal of Applied Physics*, 83(11): 7231–7233, 2022/05/19 1998. doi: 10.1063/1.367612. URL `https://doi.org/10.1063/1.367612`.

[24] S. Bhattacharjee, V. B. Shenoy, and T. Senthil. Possible ferro-spin nematic order in $NiGa_2S_4$. *Phys. Rev. B*, 74:092406, Sep 2006. doi: 10.1103/PhysRevB.74.092406. URL https://link.aps.org/doi/10.1103/PhysRevB.74.092406.

[25] S. Bieri, M. Serbyn, T. Senthil, and P. A. Lee. Paired chiral spin liquid with a Fermi surface in $S = 1$ model on the triangular lattice. *Phys. Rev. B*, 86:224409, Dec 2012. doi: 10.1103/PhysRevB.86.224409. URL https://link.aps.org/doi/10.1103/PhysRevB.86.224409.

[26] F. Bloch. Über die Quantenmechanik der Elektronen in Kristallgittern. *Zeitschrift für Physik*, 52(7):555–600, 1929. doi: 10.1007/BF01339455. URL https://doi.org/10.1007/BF01339455.

[27] M. Blume and Y. Hsieh. Biquadratic Exchange and Quadrupolar Ordering. *Journal of Applied Physics*, 40:1249, 1969.

[28] N. Bohr. I. On the constitution of atoms and molecules. *The London, Edinburgh, and Dublin Philosophical Magazine and Journal of Science*, 26(151):1–25, 07 1913. doi: 10.1080/14786441308634955. URL https://doi.org/10.1080/14786441308634955.

[29] R. J. Boyd. A quantum mechanical explanation for Hund's multiplicity rule. *Nature*, 310(5977):480–481, 1984. doi: 10.1038/310480a0. URL https://doi.org/10.1038/310480a0.

[30] G. E. Bredon. *Topology and Geometry*. Graduate texts in mathematics. Springer-Verlag, 1993. ISBN 9783540979265. URL https://books.google.co.jp/books?id=vsSjQgAACAAJ.

[31] J. Z. Buchwald. *From Maxwell to microphysics : aspects of electromagnetic theory in the last quarter of the nineteenth century*. 1985. ISBN 0226078825 9780226078823 0226078833 9780226078830.

[32] B. Canals and D. Garanin. Spin Liquid Phase in the Pyrochlore Antiferromagnet. *Canadian Journal of Physics - CAN J PHYS*, 79:1323–1331, 12 2001. doi: 10.1139/cjp-79-11-12-1323.

[33] B. Canals and C. Lacroix. Pyrochlore Antiferromagnet: A Three-Dimensional Quantum Spin Liquid. *Phys. Rev. Lett.*, 80:2933, 1998. URL https://journals.aps.org/prl/abstract/10.1103/PhysRevLett.80.2933.

[34] B. Canals and C. Lacroix. Quantum spin liquid: The Heisenberg antiferromagnet on the three-dimensional pyrochlore lattice. *Phys. Rev. B*, 61:1149, 2000. URL https://journals.aps.org/prb/abstract/10.1103/PhysRevB.61.1149.

[35] G. Catarina and J. Fernández-Rossier. Hubbard model for spin-1 Haldane chains. *Phys. Rev. B*, 105:L081116, Feb 2022. doi: 10.1103/PhysRevB.105.L081116. URL https://link.aps.org/doi/10.1103/PhysRevB.105.L081116.

[36] P. M. Chaikin and T. Lubensky. *Principle of Condensed Matter Physics*. Cambridge University Press, 2000.

[37] S. Chandrasekhar. *Liquid Crystals*. Cambridge University Press, 2 edition, 1992. doi: 10.1017/CBO9780511622496.

[38] G. Chen, M. Hermele, and L. Radzihovsky. Frustrated Quantum Critical Theory of Putative Spin-Liquid Phenomenology in $6H-\mathrm{B}-\mathrm{Ba_3NiSb_2O_9}$. *Phys. Rev. Lett.*, 109:016402, Jul 2012. doi: 10.1103/PhysRevLett.109.016402. URL https://link.aps.org/doi/10.1103/PhysRevLett.109.016402.

[39] X. Chen, Z.-C. Gu, Z.-X. Liu, and X.-G. Wen. Symmetry protected topological orders and the group cohomology of their symmetry group. *Phys. Rev. B*, 87: 155114, Apr 2013. doi: 10.1103/PhysRevB.87.155114. URL https://link.aps.org/doi/10.1103/PhysRevB.87.155114.

[40] J. G. Cheng, G. Li, L. Balicas, J. S. Zhou, J. B. Goodenough, C. Xu, and H. D. Zhou. High-Pressure Sequence of $\mathrm{Ba_3NiSb_2O_9}$ Structural Phases: New $S = 1$ Quantum Spin Liquids Based on $\mathrm{Ni^{2+}}$. *Phys. Rev. Lett.*, 107:197204, Nov 2011. doi: 10.1103/PhysRevLett.107.197204. URL https://link.aps.org/doi/10.1103/PhysRevLett.107.197204.

[41] G.-W. Chern, K. Barros, Z. Wang, H. Suwa, and C. D. Batista. Semiclassical dynamics of spin density waves. *Phys. Rev. B*, 97:035120, Jan 2018. doi: 10.1103/PhysRevB.97.035120. URL https://link.aps.org/doi/10.1103/PhysRevB.97.035120.

[42] A. L. Chernyshev and M. E. Zhitomirsky. Spin waves in a triangular lattice antiferromagnet: Decays, spectrum renormalization, and singularities. *Phys. Rev. B*, 79:144416, Apr 2009. doi: 10.1103/PhysRevB.79.144416. URL https://link.aps.org/doi/10.1103/PhysRevB.79.144416.

[43] L. Chojnacki, R. Pohle, H. Yan, Y. Akagi, and N. Shannon. unpublished.

[44] S. G. Chung. Essential finite-size effect in the two-dimensional XY model. *Phys. Rev. B*, 60:11761–11764, Oct 1999. doi: 10.1103/PhysRevB.60.11761. URL https://link.aps.org/doi/10.1103/PhysRevB.60.11761.

[45] C. Cohen-Tannoudji, P. Davies, D. Betts, B. Diu, F. Laloë, B. Dui, S. Hemley, N. Ostrowsky, and D. Ostrowsky. *Quantum Mechanics*. Number v. 1 in A Wiley - Interscience publication. Wiley, 1977. ISBN 9780471164333. URL https://books.google.co.jp/books?id=iHcpAQAAMAAJ.

[46] P. H. Conlon and J. T. Chalker. Spin Dynamics in Pyrochlore Heisenberg Antiferromagnets. *Phys. Rev. Lett.*, 102:237206, Jun 2009. doi: 10.1103/PhysRevLett.102.237206. URL https://link.aps.org/doi/10.1103/PhysRevLett.102.237206.

[47] P. H. Conlon and J. T. Chalker. Absent pinch points and emergent clusters: Further neighbor interactions in the pyrochlore Heisenberg antiferromagnet. *Phys. Rev. B*, 81:224413, Jun 2010. doi: 10.1103/PhysRevB.81.224413. URL https://link.aps.org/doi/10.1103/PhysRevB.81.224413.

[48] P. Corboz, A. M. Läuchli, K. Totsuka, and H. Tsunetsugu. Spontaneous trimerization in a bilinear-biquadratic $S = 1$ zig-zag chain. *Phys. Rev. B*, 76:220404, Dec 2007. doi: 10.1103/PhysRevB.76.220404. URL https://link.aps.org/doi/10.1103/PhysRevB.76.220404.

[49] E. Coronado, B. S. Tsukerblat, and R. Georges. *Exchange Interactions I: Mechanisms*, pages 65–84. Springer Netherlands, Dordrecht, 1996. ISBN 978-94-017-2319-0. doi: 10.1007/978-94-017-2319-0_3. URL https://doi.org/10.1007/978-94-017-2319-0_3.

[50] S. H. Curnoe. Quantum spin configurations in $Tb_2Ti_2O_7$. *Phys. Rev. B*, 75: 212404, Jun 2007. doi: 10.1103/PhysRevB.75.212404. URL http://link.aps.org/doi/10.1103/PhysRevB.75.212404.

[51] D. Dahlbom, H. Zhang, C. Miles, X. Bai, C. D. Batista, and K. Barros. Geometric integration of classical spin dynamics via a mean-field Schrödinger equation, 2022. URL https://arxiv.org/abs/2204.07563.

[52] L. de Forges de Parny, H. Yang, and F. Mila. Anderson Tower of States and Nematic Order of Spin-1 Bosonic Atoms on a 2D Lattice. *Phys. Rev. Lett.*, 113: 200402, Nov 2014. doi: 10.1103/PhysRevLett.113.200402. URL https://link.aps.org/doi/10.1103/PhysRevLett.113.200402.

[53] E. Demler and F. Zhou. Spinor Bosonic Atoms in Optical Lattices: Symmetry Breaking and Fractionalization. *Phys. Rev. Lett.*, 88:163001, Apr 2002. doi: 10.1103/PhysRevLett.88.163001. URL https://link.aps.org/doi/10.1103/PhysRevLett.88.163001.

[54] P. Dirac. *The Principles of Quantum Mechanics*. Comparative Pathobiology - Studies in the Postmodern Theory of Education. Clarendon Press, 1981. ISBN 9780198520115. URL https://books.google.co.jp/books?id=XehUpGiM6FIC.

[55] P. A. M. Dirac. Quantum mechanics of many-electron systems. *Proc. R. Soc. Lond.*, (A):123714–733, 1929. URL https://doi.org/10.1098/rspa.1929.0094.

[56] I. Dzyaloshinsky. A thermodynamic theory of "weak" ferromagnetism of antiferromagnetics. *Journal of Physics and Chemistry of Solids*, 4(4):241–255, 1958. ISSN 0022-3697. doi: https://doi.org/10.1016/0022-3697(58)90076-3. URL https://www.sciencedirect.com/science/article/pii/0022369758900763.

[57] D. J. Earl and M. W. Deem. Parallel tempering: Theory, applications, and new perspectives. *Phys. Chem. Chem. Phys.*, 7:3910–3916, 2005. doi: 10.1039/B509983H. URL http://dx.doi.org/10.1039/B509983H.

[58] B. Fak, S. Bieri, E. Canévet, L. Messio, C. Payen, M. Viaud, C. Guillot-Deudon, C. Darie, J. Ollivier, and P. Mendels. Evidence for a spinon Fermi surface in the triangular $S = 1$ quantum spin liquid $Ba_3NiSb_2O_9$. *Phys. Rev. B*, 95:060402, Feb 2017. doi: 10.1103/PhysRevB.95.060402. URL `https://link.aps.org/doi/10.1103/PhysRevB.95.060402`.

[59] P. Fazekas. *Lecture Notes on Electron Correlation and Magnetism*. WORLD SCIENTIFIC, 1999. doi: 10.1142/2945. URL `https://www.worldscientific.com/doi/abs/10.1142/2945`.

[60] R. M. Fernandes, A. V. Chubukov, and J. Schmalian. What drives nematic order in iron-based superconductors? *Nature Physics*, 10:97 EP –, 01 2014. URL `http://dx.doi.org/10.1038/nphys2877`.

[61] R. P. Feynman, R. B. Leighton, and M. Sands. *The Feynman lectures on physics Vol. 3, Vol. 3,*. Addison-Wesley, Reading, Mass., 1965. ISBN 9780201021189 0201020149 9780201020144 0201021188.

[62] M. J. Freiser. Ordered States of a Nematic Liquid. *Phys. Rev. Lett.*, 24:1041–1043, May 1970. doi: 10.1103/PhysRevLett.24.1041. URL `https://link.aps.org/doi/10.1103/PhysRevLett.24.1041`.

[63] E. G. Galkina, B. A. Ivanov, O. A. Kosmachev, and Y. A. Fridman. Two-dimensional solitons in spin nematic states for magnets with an isotropic exchange interaction. *Low Temperature Physics*, 41(5):382–389, 2022/03/17 2015. doi: 10.1063/1.4921470. URL `https://doi.org/10.1063/1.4921470`.

[64] Y.-H. Gao, X.-P. Yao, F.-Y. Li, and G. Chen. Spin-1 pyrochlore antiferromagnets: Theory, model, and materials' survey. *Frontiers of Physics*, 15(6):63201, 2020. doi: 10.1007/s11467-020-0974-4. URL `https://doi.org/10.1007/s11467-020-0974-4`.

[65] D. A. Garanin. The 1/D expansion for low-dimensional classical magnets. *Journal of Statistical Physics*, 74(1):275–311, 1994. doi: 10.1007/BF02186815. URL `https://doi.org/10.1007/BF02186815`.

[66] D. A. Garanin. The 1/D expansion for classical magnets: Low-dimensional models with magnetic field. *Journal of Statistical Physics*, 83(5):907–931, 1996. doi: 10.1007/BF02179549. URL `https://doi.org/10.1007/BF02179549`.

[67] D. A. Garanin. Self-consistent Gaussian approximation for classical spin systems: Thermodynamics. *Phys. Rev. B*, 53:11593–11605, May 1996. doi: 10.1103/PhysRevB.53.11593. URL `https://link.aps.org/doi/10.1103/PhysRevB.53.11593`.

[68] D. A. Garanin and B. Canals. Classical spin liquid: Exact solution for the infinite-component antiferromagnetic model on the kagomé lattice. *Phys. Rev. B*, 59:443–456, Jan 1999. doi: 10.1103/PhysRevB.59.443. URL `https://link.aps.org/doi/10.1103/PhysRevB.59.443`.

[69] J. S. Gardner, M. J. P. Gingras, and J. E. Greedan. Magnetic pyrochlore oxides. *Rev. Mod. Phys.*, 82:53–107, Jan 2010. doi: 10.1103/RevModPhys.82.53. URL https://link.aps.org/doi/10.1103/RevModPhys.82.53.

[70] M. Gen, T. Nomura, D. I. Gorbunov, S. Yasin, P. T. Cong, C. Dong, Y. Kohama, E. L. Green, J. M. Law, M. S. Henriques, J. Wosnitza, A. A. Zvyagin, V. O. Cheranovskii, R. K. Kremer, and S. Zherlitsyn. Magnetocaloric effect and spin-strain coupling in the spin-nematic state of $LiCuVO_4$. *Phys. Rev. Research*, 1: 033065, Oct 2019. doi: 10.1103/PhysRevResearch.1.033065. URL https://link.aps.org/doi/10.1103/PhysRevResearch.1.033065.

[71] W. Gerlach and O. Stern. Der experimentelle Nachweis der Richtungsquantelung im Magnetfeld. *Zeitschrift für Physik*, 9(1):349–352, 1922. doi: 10.1007/BF01326983. URL https://doi.org/10.1007/BF01326983.

[72] W. Gerlach and O. Stern. Das magnetische Moment des Silberatoms. *Zeitschrift für Physik*, 9(1):353–355, 1922. doi: 10.1007/BF01326984. URL https://doi.org/10.1007/BF01326984.

[73] T. Gilbert. A phenomenological theory of damping in ferromagnetic materials. *IEEE Transactions on Magnetics*, 40(6):3443–3449, 2004. doi: 10.1109/TMAG.2004.836740.

[74] S.-S. Gong, W. Zhu, D. N. Sheng, and K. Yang. Possible nematic spin liquid in spin-1 antiferromagnetic system on the square lattice: Implications for the nematic paramagnetic state of FeSe. *Phys. Rev. B*, 95:205132, May 2017. doi: 10.1103/PhysRevB.95.205132. URL https://link.aps.org/doi/10.1103/PhysRevB.95.205132.

[75] J. B. Goodenough. Theory of the Role of Covalence in the Perovskite-Type Manganites $[La, M(II)]MnO_3$. *Phys. Rev.*, 100:564–573, Oct 1955. doi: 10.1103/PhysRev.100.564. URL https://link.aps.org/doi/10.1103/PhysRev.100.564.

[76] J. B. Goodenough. *Magnetism and the chemical bond.* Interscience Publishers, New York, 1963.

[77] J. B. Goodenough and A. L. Loeb. Theory of Ionic Ordering, Crystal Distortion, and Magnetic Exchange Due to Covalent Forces in Spinels. *Phys. Rev.*, 98:391–408, Apr 1955. doi: 10.1103/PhysRev.98.391. URL https://link.aps.org/doi/10.1103/PhysRev.98.391.

[78] T. Grover and T. Senthil. Non-Abelian Spin Liquid in a Spin-One Quantum Magnet. *Phys. Rev. Lett.*, 107:077203, Aug 2011. doi: 10.1103/PhysRevLett.107.077203. URL https://link.aps.org/doi/10.1103/PhysRevLett.107.077203.

[79] M. Hagiwara, K. Katsumata, I. Affleck, B. I. Halperin, and J. P. Renard. Observation of S=1/2 degrees of freedom in an S=1 linear-chain Heisenberg antiferromagnet. *Phys. Rev. Lett.*, 65:3181–3184, Dec 1990. doi: 10.1103/PhysRevLett.65.3181. URL https://link.aps.org/doi/10.1103/PhysRevLett.65.3181.

[80] M. Hagiwara, L. Svistov, T. Fujita, H. Yamaguchi, S. Kimura, K. Omura, A. Prokofiev, A. Smirnov, and Z. Honda. Possibility of the field-induced spin-nematic phase in $LiCuVO_4$. *Journal of Physics: Conference Series*, 320:012049, 09 2011. doi: 10.1088/1742-6596/320/1/012049.

[81] E. Hairer, G. Wanner, and S. P. Nørsett. *Solving Ordinary Differential Equations I – Nonstiff Problems*. Springer Berlin Heidelberg, 1993. ISBN 978-3-540-78862-1.

[82] F. Haldane. Continuum dynamics of the 1-D Heisenberg antiferromagnet: Identification with the O(3) nonlinear sigma model. *Physics Letters A*, 93(9): 464–468, 1983. ISSN 0375-9601. doi: https://doi.org/10.1016/0375-9601(83)90631-X. URL https://www.sciencedirect.com/science/article/pii/037596018390631X.

[83] F. D. M. Haldane. Nonlinear Field Theory of Large-Spin Heisenberg Antiferromagnets: Semiclassically Quantized Solitons of the One-Dimensional Easy-Axis Néel State. *Phys. Rev. Lett.*, 50:1153–1156, Apr 1983. doi: 10.1103/PhysRevLett.50.1153. URL https://link.aps.org/doi/10.1103/PhysRevLett.50.1153.

[84] F. D. M. Haldane. Nobel Lecture: Topological quantum matter. *Rev. Mod. Phys.*, 89:040502, Oct 2017. doi: 10.1103/RevModPhys.89.040502. URL https://link.aps.org/doi/10.1103/RevModPhys.89.040502.

[85] J. Hamilton. *A Life of Discovery: Michael Faraday, Giant of the Scientific Revolution*. Random House, 2002. ISBN 9781400060160. URL https://books.google.co.jp/books?id=EEOCpSVu2wQC.

[86] K. Harada and N. Kawashima. Loop Algorithm for Heisenberg Models with Biquadratic Interaction and Phase Transitions in Two Dimensions. *Journal of the Physical Society of Japan*, 70(1):13–16, 2022/05/08 2001. doi: 10.1143/JPSJ.70.13. URL https://doi.org/10.1143/JPSJ.70.13.

[87] K. Harada and N. Kawashima. Quadrupolar order in isotropic Heisenberg models with biquadratic interaction. *Phys. Rev. B*, 65:052403, Jan 2002. doi: 10.1103/PhysRevB.65.052403. URL https://link.aps.org/doi/10.1103/PhysRevB.65.052403.

[88] R. J. Harrison, R. E. Dunin-Borkowski, and A. Putnis. Direct imaging of nanoscale magnetic interactions in minerals. *Proceedings of the National Academy of Sciences*, 99(26):16556–16561, 2022/06/12 2002. doi: 10.1073/pnas.262514499. URL https://doi.org/10.1073/pnas.262514499.

[89] M. Hasenbusch. The two-dimensional XY model at the transition temperature: a high-precision Monte Carlo study. *Journal of Physics A: Mathematical and*

General, 38(26):5869–5883, jun 2005. doi: 10.1088/0305-4470/38/26/003. URL https://doi.org/10.1088/0305-4470/38/26/003.

[90] W. Heisenberg. Zur theorie des ferromagnetismus. *Zeitschrift für Physik*, 49(9): 619–636, 1928. doi: 10.1007/BF01328601. URL https://doi.org/10.1007/BF01328601.

[91] W. Heitler and F. London. Wechselwirkung neutraler Atome und homöopolare Bindung nach der Quantenmechanik. *Zeitschrift für Physik*, 44(6):455–472, 1927. doi: 10.1007/BF01397394. URL https://doi.org/10.1007/BF01397394.

[92] C. L. Henley. Power-law spin correlations in pyrochlore antiferromagnets. *Phys. Rev. B*, 71:014424, Jan 2005. doi: 10.1103/PhysRevB.71.014424. URL http://link.aps.org/doi/10.1103/PhysRevB.71.014424.

[93] C. L. Henley. The "Coulomb Phase" in Frustrated Systems. *Annu. Rev. Condens. Matter Phys.*, 1:179–2010, 2010. doi: 10.1146/annurev-conmatphys-070909-104138. URL http://www.annualreviews.org/doi/10.1146/annurev-conmatphys-070909-104138.

[94] K. Hirakawa and H. Kadowaki. The ground states and phase transitions in the two-dimensional triangular lattice antiferromagnets. *Physica B+C*, 136(1):335–340, 1986. ISSN 0378-4363. doi: https://doi.org/10.1016/S0378-4363(86)80086-9. URL https://www.sciencedirect.com/science/article/pii/S0378436386800869. Neutron Scattering.

[95] M. Hoffmann and S. Blügel. Systematic derivation of realistic spin models for beyond-Heisenberg solids. *Phys. Rev. B*, 101:024418, Jan 2020. doi: 10.1103/PhysRevB.101.024418. URL https://link.aps.org/doi/10.1103/PhysRevB.101.024418.

[96] Y.-D. Hsieh, Y.-J. Kao, and A. W. Sandvik. Finite-size scaling method for the Berezinskii–Kosterlitz–Thouless transition. *Journal of Statistical Mechanics: Theory and Experiment*, 2013(09):P09001, sep 2013. doi: 10.1088/1742-5468/2013/09/p09001. URL https://doi.org/10.1088%2F1742-5468%2F2013%2F09%2Fp09001.

[97] J. Hubbard and B. H. Flowers. Electron correlations in narrow energy bands. II. The degenerate band case. *Proceedings of the Royal Society of London. Series A. Mathematical and Physical Sciences*, 277(1369):237–259, 1964. doi: 10.1098/rspa.1964.0019. URL https://royalsocietypublishing.org/doi/abs/10.1098/rspa.1964.0019.

[98] K. Hwang, T. Dodds, S. Bhattacharjee, and Y. B. Kim. Three-dimensional nematic spin liquid in a stacked triangular lattice 6H-B structure. *Phys. Rev. B*, 87:235103, Jun 2013. doi: 10.1103/PhysRevB.87.235103. URL https://link.aps.org/doi/10.1103/PhysRevB.87.235103.

[99] Y. Imai, K. Nawa, Y. Shimizu, W. Yamada, H. Fujihara, T. Aoyama, R. Takahashi, D. Okuyama, T. Ohashi, M. Hagihala, S. Torii, D. Morikawa, M. Terauchi, T. Kawamata, M. Kato, H. Gotou, M. Itoh, T. J. Sato, and K. Ohgushi. Zigzag magnetic order in the Kitaev spin-liquid candidate material $RuBr_3$ with a honeycomb lattice. *Phys. Rev. B*, 105:L041112, Jan 2022. doi: 10.1103/PhysRevB.105.L041112. URL https://link.aps.org/doi/10.1103/PhysRevB.105.L041112.

[100] A. Imambekov, M. Lukin, and E. Demler. Spin-exchange interactions of spin-one bosons in optical lattices: Singlet, nematic, and dimerized phases. *Phys. Rev. A*, 68:063602, Dec 2003. doi: 10.1103/PhysRevA.68.063602. URL https://link.aps.org/doi/10.1103/PhysRevA.68.063602.

[101] S. V. Isakov, K. Gregor, R. Moessner, and S. L. Sondhi. Dipolar Spin Correlations in Classical Pyrochlore Magnets. *Phys. Rev. Lett.*, 93:167204, Oct 2004. doi: 10.1103/PhysRevLett.93.167204. URL http://link.aps.org/doi/10.1103/PhysRevLett.93.167204.

[102] B. A. Ivanov and R. S. Khymyn. Soliton dynamics in a spin nematic. *Journal of Experimental and Theoretical Physics*, 104(2):307–318, Apr 2007. ISSN 1090-6509. doi: 10.1134/S106377610702015X. URL https://doi.org/10.1134/S106377610702015X.

[103] B. A. Ivanov and A. K. Kolezhuk. Effective field theory for the $S = 1$ quantum nematic. *Phys. Rev. B*, 68:052401, Aug 2003. doi: 10.1103/PhysRevB.68.052401. URL https://link.aps.org/doi/10.1103/PhysRevB.68.052401.

[104] B. A. Ivanov, R. S. Khymyn, and A. K. Kolezhuk. Pairing of Solitons in Two-Dimensional $S = 1$ Magnets. *Phys. Rev. Lett.*, 100:047203, Jan 2008. doi: 10.1103/PhysRevLett.100.047203. URL https://link.aps.org/doi/10.1103/PhysRevLett.100.047203.

[105] H. Jones. *Groups, Representations and Physics*. CRC Press, 2020. ISBN 9781420050295. URL https://books.google.co.jp/books?id=0vNp8Df5XukC.

[106] A. Joshi, M. Ma, F. Mila, D. N. Shi, and F. C. Zhang. Elementary excitations in magnetically ordered systems with orbital degeneracy. *Phys. Rev. B*, 60:6584–6587, Sep 1999. doi: 10.1103/PhysRevB.60.6584. URL https://link.aps.org/doi/10.1103/PhysRevB.60.6584.

[107] D. A. S. Kaib, K. Riedl, A. Razpopov, Y. Li, S. Backes, I. Mazin, and R. Valenti. Electronic and magnetic properties of the RuX_3 (X=Cl, Br, I) family: Two siblings – and a cousin?, 2022. URL https://arxiv.org/abs/2203.01626.

[108] J. Kanamori. Superexchange interaction and symmetry properties of electron orbitals. *Journal of Physics and Chemistry of Solids*, 10(2):87–98, 1959. ISSN 0022-3697. doi: https://doi.org/10.1016/0022-3697(59)90061-7. URL https://www.sciencedirect.com/science/article/pii/0022369759900617.

[109] T. Kasuya. A Theory of Metallic Ferro- and Antiferromagnetism on Zener's Model. *Progress of Theoretical Physics*, 16(1):45–57, 07 1956. ISSN 0033-068X. doi: 10.1143/PTP.16.45. URL https://doi.org/10.1143/PTP.16.45.

[110] J. Katriel and R. Pauncz. *Theoretical Interpretation of Hund's Rule*, volume 10, pages 143–185. Academic Press, 1977. ISBN 0065-3276. doi: https://doi.org/10.1016/S0065-3276(08)60580-8. URL https://www.sciencedirect.com/science/article/pii/S0065327608605808.

[111] R. K. Kaul. Spin nematic ground state of the triangular lattice $S = 1$ biquadratic model. *Phys. Rev. B*, 86:104411, Sep 2012. doi: 10.1103/PhysRevB.86.104411. URL https://link.aps.org/doi/10.1103/PhysRevB.86.104411.

[112] R. K. Kaul, R. G. Melko, and A. W. Sandvik. Bridging Lattice-Scale Physics and Continuum Field Theory with Quantum Monte Carlo Simulations. *Annual Review of Condensed Matter Physics*, 4(1):179–215, 2022/05/08 2013. doi: 10.1146/annurev-conmatphys-030212-184215. URL https://doi.org/10.1146/annurev-conmatphys-030212-184215.

[113] H. Kawamura. Z_2-vortex order of frustrated Heisenberg antiferromagnets in two dimensions. *Journal of Physics: Conference Series*, 320:012002, sep 2011. doi: 10.1088/1742-6596/320/1/012002. URL https://doi.org/10.1088/1742-6596/320/1/012002.

[114] H. Kawamura and M. Kikuchi. Free-vortex formation and topological phase transitions of two-dimensional spin systems. *Phys. Rev. B*, 47:1134–1137, Jan 1993. doi: 10.1103/PhysRevB.47.1134. URL https://link.aps.org/doi/10.1103/PhysRevB.47.1134.

[115] H. Kawamura and S. Miyashita. Phase Transition of the Two-Dimensional Heisenberg Antiferromagnet on the Triangular Lattice. *Journal of the Physical Society of Japan*, 53(12):4138–4154, 1984. doi: 10.1143/JPSJ.53.4138. URL https://doi.org/10.1143/JPSJ.53.4138.

[116] H. Kawamura and A. Yamamoto. Vortex-Induced Topological Transition of the Bilinear–Biquadratic Heisenberg Antiferromagnet on the Triangular Lattice. *Journal of the Physical Society of Japan*, 76(7):073704, 2007. URL https://doi.org/10.1143/JPSJ.76.073704.

[117] H. Kawamura, A. Yamamoto, and T. Okubo. Z_2-Vortex Ordering of the Triangular-Lattice Heisenberg Antiferromagnet. *Journal of the Physical Society of Japan*, 79(2):023701, 2022/05/01 2010. doi: 10.1143/JPSJ.79.023701. URL https://doi.org/10.1143/JPSJ.79.023701.

[118] J.-K. Kim. Phase transition in the two-dimensional classical xy model. *Physics Letters A*, 223(4):261–266, 1996. doi: https://doi.org/10.1016/S0375-9601(96)00740-2. URL https://www.sciencedirect.com/science/article/pii/S0375960196007402.

[119] Y. Kohama, H. Ishikawa, A. Matsuo, K. Kindo, N. Shannon, and Z. Hiroi. Possible observation of quantum spin-nematic phase in a frustrated magnet. *Proceedings of the National Academy of Sciences*, 116(22):10686–10690, 2019. ISSN 0027-8424. doi: 10.1073/pnas.1821969116. URL https://www.pnas.org/content/116/22/10686.

[120] Y. Komura and Y. Okabe. Large-scale monte carlo simulation of two-dimensional classical xy model using multiple gpus. *Journal of the Physical Society of Japan*, 81(11):113001, 2022/06/09 2012. doi: 10.1143/JPSJ.81.113001. URL https://doi.org/10.1143/JPSJ.81.113001.

[121] J. M. Kosterlitz and D. J. Thouless. Long range order and metastability in two dimensional solids and superfluids. (Application of dislocation theory). *Journal of Physics C: Solid State Physics*, 5(11):L124–L126, jun 1972. doi: 10.1088/0022-3719/5/11/002. URL https://doi.org/10.1088/0022-3719/5/11/002.

[122] J. M. Kosterlitz and D. J. Thouless. Ordering, metastability and phase transitions in two-dimensional systems. *Journal of Physics C: Solid State Physics*, 6(7):1181–1203, apr 1973. doi: 10.1088/0022-3719/6/7/010. URL https://doi.org/10.1088/0022-3719/6/7/010.

[123] H. Kramers. L'interaction entre les atomes magnétogènes dans un cristal paramagnétique. *Physica*, 1(1):182–192, 1934. ISSN 0031-8914. doi: https://doi.org/10.1016/S0031-8914(34)90023-9. URL https://www.sciencedirect.com/science/article/pii/S0031891434900239.

[124] B. M. Kreutz. Mediterranean Contributions to the Medieval Mariner's Compass. *Technology and Culture*, 14(3):367–383, 1973. ISSN 0040165X, 10973729. URL http://www.jstor.org/stable/3102323.

[125] J. W. Krizan and R. J. Cava. $NaCaNi_2F_7$: A frustrated high-temperature pyrochlore antiferromagnet with $S = 1\,Ni^{2+}$. *Phys. Rev. B*, 92:014406, Jul 2015. doi: 10.1103/PhysRevB.92.014406. URL https://link.aps.org/doi/10.1103/PhysRevB.92.014406.

[126] H.-H. Lai, W.-J. Hu, E. M. Nica, R. Yu, and Q. Si. Antiferroquadrupolar Order and Rotational Symmetry Breaking in a Generalized Bilinear-Biquadratic Model on a Square Lattice. *Phys. Rev. Lett.*, 118:176401, Apr 2017. doi: 10.1103/PhysRevLett.118.176401. URL https://link.aps.org/doi/10.1103/PhysRevLett.118.176401.

[127] D. P. Landau and K. Binder. *A Guide to Monte Carlo Simulations in Statistical Physics*. Cambridge University Press, 4 edition, 2014. doi: 10.1017/CBO9781139696463.

[128] L. Landau and E. Lifshitz. *Quantum Mechanics: Non-Relativistic Theory*. Course of theoretical physics. Elsevier Science, 1991. ISBN 9780750635394. URL https://books.google.co.jp/books?id=J9ui6KwC4mMC.

[129] L. Landau and E. Lifshitz. *Statistical Physics: Volume 5*. Number v. 5. Elsevier Science, 2013. ISBN 9780080570464. URL https://books.google.co.jp/books?id=VzgJN-XPTRsC.

[130] L. D. Landau and E. M. Lifshitz. *Quantum Mechanics (Non-relativistic Theory*. Butterworth–Heineman, Oxford, 3rd edition, 1977. ISBN 008016739.

[131] A. Läuchli, F. Mila, and K. Penc. Quadrupolar Phases of the $S = 1$ Bilinear-Biquadratic Heisenberg Model on the Triangular Lattice. *Phys. Rev. Lett.*, 97: 087205, Aug 2006. doi: 10.1103/PhysRevLett.97.087205. URL http://link.aps.org/doi/10.1103/PhysRevLett.97.087205.

[132] P. A. Lee, N. Nagaosa, and X.-G. Wen. Doping a Mott insulator: Physics of high-temperature superconductivity. *Rev. Mod. Phys.*, 78:17–85, Jan 2006. doi: 10.1103/RevModPhys.78.17. URL https://link.aps.org/doi/10.1103/RevModPhys.78.17.

[133] D. S. Levine and M. Head-Gordon. Clarifying the quantum mechanical origin of the covalent chemical bond. *Nature Communications*, 11(1):4893, 2020. doi: 10.1038/s41467-020-18670-8. URL https://doi.org/10.1038/s41467-020-18670-8.

[134] I. N. Levine. *Quantum chemistry*. Seventh edition. Boston : Pearson, [2014], 2014. URL https://search.library.wisc.edu/catalog/9910167862202121.

[135] P. Li, G.-M. Zhang, and S.-Q. Shen. SU(3) bosons and the spin nematic state on the spin-1 bilinear-biquadratic triangular lattice. *Phys. Rev. B*, 75:104420, Mar 2007. doi: 10.1103/PhysRevB.75.104420. URL https://link.aps.org/doi/10.1103/PhysRevB.75.104420.

[136] X. Li, H. Yu, F. Lou, J. Feng, M.-H. Whangbo, and H. Xiang. Spin Hamiltonians in Magnets: Theories and Computations. *Molecules*, 26(4), 2021. ISSN 1420-3049. doi: 10.3390/molecules26040803. URL https://www.mdpi.com/1420-3049/26/4/803.

[137] E. Lieb, T. Schultz, and D. Mattis. Two soluble models of an antiferromagnetic chain. *Annals of Physics*, 16(3):407–466, 1961. ISSN 0003-4916. doi: https://doi.org/10.1016/0003-4916(61)90115-4. URL https://www.sciencedirect.com/science/article/pii/0003491661901154.

[138] Z.-X. Liu, Y. Zhou, and T.-K. Ng. Possibility of $S = 1$ spin liquids with fermionic spinons on triangular lattices. *Phys. Rev. B*, 81:224417, Jun 2010. doi: 10.1103/PhysRevB.81.224417. URL https://link.aps.org/doi/10.1103/PhysRevB.81.224417.

[139] C. Luo, T. Datta, and D.-X. Yao. Spin and quadrupolar orders in the spin-1 bilinear-biquadratic model for iron-based superconductors. *Phys. Rev. B*, 93: 235148, Jun 2016. doi: 10.1103/PhysRevB.93.235148. URL https://link.aps.org/doi/10.1103/PhysRevB.93.235148.

[140] A. H. MacDonald, S. M. Girvin, and D. Yoshioka. $\frac{t}{U}$ expansion for the Hubbard model. *Phys. Rev. B*, 37:9753–9756, Jun 1988. doi: 10.1103/PhysRevB.37.9753. URL https://link.aps.org/doi/10.1103/PhysRevB.37.9753.

[141] G. Marsaglia. Choosing a Point from the Surface of a Sphere. *The Annals of Mathematical Statistics*, 43(2):645–646, 1972.

[142] R. Masui and K. Totsuka. Electric and Magnetic Properties of Higher-Spin Kondo-Heisenberg Models at Strong Coupling, 2022. URL https://arxiv.org/abs/2202.03708.

[143] V. M. Matveev. Quantum quadrupolar magnetism and phase transitions in the presence of biquadratic exchange. *JETP*, 38:813, 1974.

[144] J. C. Maxwell. VIII. A dynamical theory of the electromagnetic field. *Philosophical Transactions of the Royal Society of London*, 155:459–512, 1865. doi: 10.1098/rstl.1865.0008. URL https://royalsocietypublishing.org/doi/abs/10.1098/rstl.1865.0008.

[145] N. D. Mermin. The topological theory of defects in ordered media. *Rev. Mod. Phys.*, 51:591–648, Jul 1979. doi: 10.1103/RevModPhys.51.591. URL https://link.aps.org/doi/10.1103/RevModPhys.51.591.

[146] N. D. Mermin and H. Wagner. Absence of Ferromagnetism or Antiferromagnetism in One- or Two-Dimensional Isotropic Heisenberg Models. *Phys. Rev. Lett.*, 17:1133–1136, Nov 1966. doi: 10.1103/PhysRevLett.17.1133. URL https://link.aps.org/doi/10.1103/PhysRevLett.17.1133.

[147] N. Metropolis, A. W. Rosenbluth, M. N. Rosenbluth, A. H. Teller, and E. Teller. Equation of State Calculations by Fast Computing Machines. *The Journal of Chemical Physics*, 21(6):1087–1092, 1953. URL https://doi.org/10.1063/1.1699114.

[148] F. Michaud, F. Vernay, and F. Mila. Theory of inelastic light scattering in spin-1 systems: Resonant regimes and detection of quadrupolar order. *Phys. Rev. B*, 84:184424, Nov 2011. doi: 10.1103/PhysRevB.84.184424. URL https://link.aps.org/doi/10.1103/PhysRevB.84.184424.

[149] W. Miiller, M. Christensen, A. Khan, N. Sharma, R. B. Macquart, M. Avdeev, G. J. McIntyre, R. O. Piltz, and C. D. Ling. $YCa_3(VO)_3(BO_3)_4$: A Kagomé Compound Based on Vanadium(III) with a Highly Frustrated Ground State. *Chemistry of Materials*, 23(5):1315–1322, 03 2011. doi: 10.1021/cm1034003. URL https://doi.org/10.1021/cm1034003.

[150] F. Mila and F.-C. Zhang. On the origin of biquadratic exchange in spin 1 chains. *The European Physical Journal B - Condensed Matter and Complex Systems*, 16 (1):7–10, 2000. doi: 10.1007/s100510070242. URL https://doi.org/10.1007/s100510070242.

[151] R. Moessner and J. T. Chalker. Low-temperature properties of classical geometrically frustrated antiferromagnets. *Phys. Rev. B*, 58:12049–12062, 1998. URL http://link.aps.org/doi/10.1103/PhysRevB.58.12049.

[152] R. Moessner and J. T. Chalker. Properties of a Classical Spin Liquid: The Heisenberg Pyrochlore Antiferromagnet. *Phys. Rev. Lett.*, 80:2929–2932, 1998. URL http://link.aps.org/doi/10.1103/PhysRevLett.80.2929.

[153] M. Moreno-Cardoner, H. Perrin, S. Paganelli, G. De Chiara, and A. Sanpera. Case study of the uniaxial anisotropic spin-1 bilinear-biquadratic Heisenberg model on a triangular lattice. *Phys. Rev. B*, 90:144409, Oct 2014. doi: 10.1103/PhysRevB.90.144409. URL https://link.aps.org/doi/10.1103/PhysRevB.90.144409.

[154] T. Moriya. Anisotropic Superexchange Interaction and Weak Ferromagnetism. *Phys. Rev.*, 120:91–98, Oct 1960. doi: 10.1103/PhysRev.120.91. URL https://link.aps.org/doi/10.1103/PhysRev.120.91.

[155] T. Moriya. New Mechanism of Anisotropic Superexchange Interaction. *Phys. Rev. Lett.*, 4:228–230, Mar 1960. doi: 10.1103/PhysRevLett.4.228. URL https://link.aps.org/doi/10.1103/PhysRevLett.4.228.

[156] N. F. Mott. The Basis of the Electron Theory of Metals, with Special Reference to the Transition Metals. *Proceedings of the Physical Society. Section A*, 62(7): 416–422, jul 1949. doi: 10.1088/0370-1298/62/7/303. URL https://doi.org/10.1088/0370-1298/62/7/303.

[157] N. F. Mott and R. Peierls. Discussion of the paper by de Boer and Verwey. *Proceedings of the Physical Society*, 49(4S):72–73, aug 1937. doi: 10.1088/0959-5309/49/4s/308. URL https://doi.org/10.1088/0959-5309/49/4s/308.

[158] P. Nahin. Maxwell's grand unification. *IEEE Spectrum*, 29(3):45–, 1992. doi: 10.1109/6.123329.

[159] S. Nakatsuji, Y. Nambu, H. Tonomura, O. Sakai, S. Jonas, C. Broholm, H. Tsunetsugu, Y. Qiu, and Y. Maeno. Spin Disorder on a Triangular Lattice. *Science*, 309(5741):1697–1700, 2005. ISSN 0036-8075. doi: 10.1126/science.1114727. URL http://science.sciencemag.org/content/309/5741/1697.

[160] S. Nakatsuji, H. Tonomura, K. Onuma, Y. Nambu, O. Sakai, Y. Maeno, R. T. Macaluso, and J. Y. Chan. Spin Disorder and Order in Quasi-2D Triangular Heisenberg Antiferromagnets: Comparative Study of $FeGa_2S_4$, $Fe_2Ga_2S_5$, and $NiGa_2S_4$. *Phys. Rev. Lett.*, 99:157203, Oct 2007. doi: 10.1103/PhysRevLett.99.157203. URL https://link.aps.org/doi/10.1103/PhysRevLett.99.157203.

[161] Y. Nambu, S. Nakatsuji, and Y. Maeno. Coherent Behavior and Nonmagnetic Impurity Effects of Spin Disordered State in $NiGa_2S_4$. *Journal of the Physical Society of Japan*, 75(4):043711, 2006. URL https://doi.org/10.1143/JPSJ.75.043711.

[162] Y. Nambu, M. Ichihara, Y. Kiuchi, S. Nakatsuji, and Y. Maeno. Synthesis and characterization of the quasi-two-dimensional triangular antiferromagnets $Ni_{1x}M_xGa_2S_4$ (M=Mn, Fe, Co, Zn). *Journal of Crystal Growth*, 310(7):1881–1885, 2008. ISSN 0022-0248. URL https://doi.org/10.1016/j.jcrysgro.2007.11.222.

[163] Y. Nambu, S. Nakatsuji, Y. Maeno, E. K. Okudzeto, and J. Y. Chan. Spin Dependent Impurity Effects on the 2D Frustrated Magnetism of $NiGa_2S_4$. *Phys. Rev. Lett.*, 101:207204, Nov 2008. doi: 10.1103/PhysRevLett.101.207204. URL https://link.aps.org/doi/10.1103/PhysRevLett.101.207204.

[164] Y. Nambu, R. T. Macaluso, T. Higo, K. Ishida, and S. Nakatsuji. Structural properties of the two-dimensional triangular antiferromagnet $NiGa_2S_4$. *Phys. Rev. B*, 79:214108, Jun 2009. doi: 10.1103/PhysRevB.79.214108. URL https://link.aps.org/doi/10.1103/PhysRevB.79.214108.

[165] Y. Nambu, J. S. Gardner, D. E. MacLaughlin, C. Stock, H. Endo, S. Jonas, T. J. Sato, S. Nakatsuji, and C. Broholm. Spin Fluctuations from Hertz to Terahertz on a Triangular Lattice. *Phys. Rev. Lett.*, 115:127202, Sep 2015. doi: 10.1103/PhysRevLett.115.127202. URL https://link.aps.org/doi/10.1103/PhysRevLett.115.127202.

[166] J. Needham and L. Wang. *Science and civilisation in China. Vol. 4, Pt. 2, Vol. 4, Pt. 2,*. Cambridge University Press, Cambridge, 1965.

[167] W. D. Nesse. *Introduction to mineralogy*. Oxford University Press, New York, 2000. ISBN 0195106911 9780195106916.

[168] M. E. J. Newman and G. T. Barkema. *Monte Carlo Methods in Statistical Physics*. Clarendon Press, 1999.

[169] D. Ni, X. Gui, K. M. Powderly, and R. J. Cava. Honeycomb-Structure RuI_3, A New Quantum Material Related to α–$RuCl_3$. *Advanced Materials*, 34(7):2106831, 2022/06/12 2022. doi: https://doi.org/10.1002/adma.202106831. URL https://doi.org/10.1002/adma.202106831.

[170] A. Niazi, S. L. Bud'ko, D. L. Schlagel, J. Q. Yan, T. A. Lograsso, A. Kreyssig, S. Das, S. Nandi, A. I. Goldman, A. Honecker, R. W. McCallum, M. Reehuis, O. Pieper, B. Lake, and D. C. Johnston. Single-crystal growth, crystallography, magnetic susceptibility, heat capacity, and thermal expansion of the antiferromagnetic $S = 1$ chain compound CaV_2O_4. *Phys. Rev. B*, 79:104432, Mar 2009. doi: 10.1103/PhysRevB.79.104432. URL https://link.aps.org/doi/10.1103/PhysRevB.79.104432.

[171] I. Niesen and P. Corboz. A tensor network study of the complete ground state phase diagram of the spin-1 bilinear-biquadratic Heisenberg model on the square lattice. *SciPost Phys.*, 3:030, 2017. doi: 10.21468/SciPostPhys.3.4.030. URL https://scipost.org/10.21468/SciPostPhys.3.4.030.

[172] I. Niesen and P. Corboz. Emergent Haldane phase in the $S = 1$ bilinear-biquadratic Heisenberg model on the square lattice. *Phys. Rev. B*, 95:180404, May 2017. doi: 10.1103/PhysRevB.95.180404. URL https://link.aps.org/doi/10.1103/PhysRevB.95.180404.

[173] I. Niesen and P. Corboz. Ground-state study of the spin-1 bilinear-biquadratic Heisenberg model on the triangular lattice using tensor networks. *Phys. Rev. B*, 97:245146, Jun 2018. doi: 10.1103/PhysRevB.97.245146. URL https://link.aps.org/doi/10.1103/PhysRevB.97.245146.

[174] J. Oitmaa and C. J. Hamer. $S = 1$ bilinear biquadratic spin model on the square lattice: A series expansion study. *Phys. Rev. B*, 87:224431, Jun 2013. doi: 10.1103/PhysRevB.87.224431. URL https://link.aps.org/doi/10.1103/PhysRevB.87.224431.

[175] P. Olsson. Monte Carlo analysis of the two-dimensional XY model. II. Comparison with the Kosterlitz renormalization-group equations. *Phys. Rev. B*, 52: 4526–4535, Aug 1995. doi: 10.1103/PhysRevB.52.4526. URL https://link.aps.org/doi/10.1103/PhysRevB.52.4526.

[176] F. P. Onufrieva. Low–temperature properites of spin systems with tensor order parameters. *Zh. Eksp. Teor. Fiz.*, 89:2270, 1985.

[177] A. Orlova, E. L. Green, J. M. Law, D. I. Gorbunov, G. Chanda, S. Krämer, M. Horvatić, R. K. Kremer, J. Wosnitza, and G. L. J. A. Rikken. Nuclear Magnetic Resonance Signature of the Spin-Nematic Phase in $LiCuVO_4$ at High Magnetic Fields. *Phys. Rev. Lett.*, 118:247201, Jun 2017. doi: 10.1103/PhysRevLett.118.247201. URL https://link.aps.org/doi/10.1103/PhysRevLett.118.247201.

[178] M. Oshikawa, M. Yamanaka, and I. Affleck. Magnetization Plateaus in Spin Chains: "Haldane Gap" for Half-Integer Spins. *Phys. Rev. Lett.*, 78:1984–1987, Mar 1997. doi: 10.1103/PhysRevLett.78.1984. URL https://link.aps.org/doi/10.1103/PhysRevLett.78.1984.

[179] T. Oyamada, K. Hongo, Y. Kawazoe, and H. Yasuhara. Unified interpretation of Hund's first and second rules for 2p and 3p atoms. *The Journal of Chemical Physics*, 133(16):164113, 2022/05/15 2010. doi: 10.1063/1.3488099. URL https://doi.org/10.1063/1.3488099.

[180] N. Papanicolaou. Unusual phases in quantum spin-1 systems. *Nuclear Physics B*, 305(3):367 – 395, 1988. ISSN 0550-3213. doi: https://doi.org/10.1016/0550-3213(88)90073-9. URL http://www.sciencedirect.com/science/article/pii/0550321388900739.

[181] W. Pauli. Exclusion Principle and Quantum Mechanics. *Nobel Lecture*, 1946. URL https://www.nobelprize.org/prizes/physics/1945/pauli/lecture/.

[182] W. Pauli. *General Principles of Quantum Mechanics*. Springer-Verlag, 1980. ISBN 9783540098423. URL https://books.google.co.jp/books?id=A84NAQAAIAAJ.

[183] K. Penc and A. M. Läuchli. *Spin Nematic Phases in Quantum Spin Systems*, pages 331–362. Springer Berlin Heidelberg, Berlin, Heidelberg, 2011. ISBN 978-3-642-10589-0. doi: 10.1007/978-3-642-10589-0_13. URL https://doi.org/10.1007/978-3-642-10589-0_13.

[184] D. Pesin and L. Balents. Mott physics and band topology in materials with strong spin–orbit interaction. *Nature Physics*, 6(5):376–381, 2010. doi: 10.1038/nphys1606. URL https://doi.org/10.1038/nphys1606.

[185] W. Pfeifer. *The Lie Algebras su(N): An Introduction*. Birkhäuser Basel, 2003. ISBN 9783764324186. URL https://books.google.co.jp/books?id=xoHWEPENKNEC.

[186] O. Pieper, B. Lake, A. Daoud-Aladine, M. Reehuis, K. Prokeνs, B. Klemke, K. Kiefer, J. Q. Yan, A. Niazi, D. C. Johnston, and A. Honecker. Magnetic structure and interactions in the quasi-one-dimensional antiferromagnet CaV_2O_4. *Phys. Rev. B*, 79:180409, May 2009. doi: 10.1103/PhysRevB.79.180409. URL https://link.aps.org/doi/10.1103/PhysRevB.79.180409.

[187] A. Pires. Dynamics of the ferroquadrupolar phase of the S=1 bilinear–biquadratic model on the triangular lattice. *Solid State Communications*, 196:24–27, 2014. ISSN 0038-1098. doi: https://doi.org/10.1016/j.ssc.2014.07.015. URL https://www.sciencedirect.com/science/article/pii/S0038109814003020.

[188] K. W. Plumb, H. J. Changlani, A. Scheie, S. Zhang, J. W. Krizan, J. A. Rodriguez-Rivera, Y. Qiu, B. Winn, R. J. Cava, and C. L. Broholm. Continuum of quantum fluctuations in a three-dimensional S = 1 Heisenberg magnet. *Nature Physics*, 15(1):54–59, 2019. doi: 10.1038/s41567-018-0317-3. URL https://doi.org/10.1038/s41567-018-0317-3.

[189] R. Pohle, H. Yan, and N. Shannon. Theory of $Ca_{10}Cr_7O_{28}$ as a bilayer breathing-kagome magnet: Classical thermodynamics and semiclassical dynamics. *Phys. Rev. B*, 104:024426, Jul 2021. doi: 10.1103/PhysRevB.104.024426. URL https://link.aps.org/doi/10.1103/PhysRevB.104.024426.

[190] R. Pohle, Y. Akagi, K. Remund, and N. Shannon. Dynamics of ferroquadrupolar order near a topological phase transition. in preparation.

[191] F. Pollmann, E. Berg, A. M. Turner, and M. Oshikawa. Symmetry protection of topological phases in one-dimensional quantum spin systems. *Phys. Rev. B*, 85:075125, Feb 2012. doi: 10.1103/PhysRevB.85.075125. URL https://link.aps.org/doi/10.1103/PhysRevB.85.075125.

[192] K. Y. Povarov, V. K. Bhartiya, Z. Yan, and A. Zheludev. Thermodynamics of a frustrated quantum magnet on a square lattice. *Phys. Rev. B*, 99:024413, Jan

2019. doi: 10.1103/PhysRevB.99.024413. URL https://link.aps.org/doi/10.1103/PhysRevB.99.024413.

[193] B. Pradines, L. Lacombe, N. Guihéry, and N. Suaud. Study of the Electronic Structure of $NiGa_2S_4$ and Extraction of the Spin Hamiltonian Parameters from Ab Initio Calculations. *European Journal of Inorganic Chemistry*, 2018(3-4):503–508, 2018. doi: https://doi.org/10.1002/ejic.201700974. URL https://chemistry-europe.onlinelibrary.wiley.com/doi/abs/10.1002/ejic.201700974.

[194] W. H. Press, S. A. Teukolsky, W. T. Vetterling, and B. P. Flannery. *Numerical Recipes 3rd Edition: The Art of Scientific Computing*. Cambridge University Press, New York, NY, USA, 3rd edition, 2007. ISBN 0521880688, 9780521880688.

[195] J. A. Quilliam, F. Bert, A. Manseau, C. Darie, C. Guillot-Deudon, C. Payen, C. Baines, A. Amato, and P. Mendels. Gapless quantum spin liquid ground state in the spin-1 antiferromagnet 6HB-$Ba_3NiSb_2O_9$. *Phys. Rev. B*, 93:214432, Jun 2016. doi: 10.1103/PhysRevB.93.214432. URL https://link.aps.org/doi/10.1103/PhysRevB.93.214432.

[196] A. P. Ramirez. Strongly Geometrically Frustrated Magnets. *Annual Review of Materials Science*, 24(1):453–480, 2022/05/04 1994. doi: 10.1146/annurev.ms.24.080194.002321. URL https://doi.org/10.1146/annurev.ms.24.080194.002321.

[197] A. P. Ramirez, G. P. Espinosa, and A. S. Cooper. Elementary excitations in a diluted antiferromagnetic Kagomé lattice. *Phys. Rev. B*, 45:2505–2508, Feb 1992. doi: 10.1103/PhysRevB.45.2505. URL https://link.aps.org/doi/10.1103/PhysRevB.45.2505.

[198] A. P. Ramirez, B. Hessen, and M. Winklemann. Entropy Balance and Evidence for Local Spin Singlets in a Kagomé-Like Magnet. *Phys. Rev. Lett.*, 84:2957–2960, Mar 2000. doi: 10.1103/PhysRevLett.84.2957. URL https://link.aps.org/doi/10.1103/PhysRevLett.84.2957.

[199] J. G. Rau and M. J. Gingras. Frustrated Quantum Rare-Earth Pyrochlores. *Annual Review of Condensed Matter Physics*, 10(1):357–386, 2019. doi: 10.1146/annurev-conmatphys-022317-110520. URL https://doi.org/10.1146/annurev-conmatphys-022317-110520.

[200] K. Remund. Semi–classical Equations of Motion for Quantum Spin Nematics. Master's thesis, Ecole Polytechnique Federal Lausanne, 2015.

[201] K. Remund, R. Pohle, Y. Akagi, J. Romhányi, and N. Shannon. Semi-classical simulation of spin-1 magnets. *Phys. Rev. Research*, 4:033106, Aug 2022. doi: 10.1103/PhysRevResearch.4.033106. URL https://link.aps.org/doi/10.1103/PhysRevResearch.4.033106.

[202] M. A. Ruderman and C. Kittel. Indirect Exchange Coupling of Nuclear Magnetic Moments by Conduction Electrons. *Phys. Rev.*, 96:99–102, Oct 1954. doi: 10.1103/PhysRev.96.99. URL https://link.aps.org/doi/10.1103/PhysRev.96.99.

[203] E. Rutherford. The scattering of α and β particles by matter and the structure of the atom. *The London, Edinburgh, and Dublin Philosophical Magazine and Journal of Science*, 21(125):669–688, 05 1911. doi: 10.1080/14786440508637080. URL https://doi.org/10.1080/14786440508637080.

[204] J. R. Rydberg. *Recherches sur la constitution des spectres d'émission des éléments chimiques*, volume Band 23 No 11 of *Kungliga vetenskapsakademiens handlingar*. Kungliga Vetenskapsakademien, 1890.

[205] J. J. Sakurai and J. Napolitano. *Modern quantum mechanics*. 2021. ISBN 9781108587280 1108587283. URL https://doi.org/10.1017/9781108587280.

[206] A. M. Samarakoon, A. Banerjee, S.-S. Zhang, Y. Kamiya, S. E. Nagler, D. A. Tennant, S.-H. Lee, and C. D. Batista. Comprehensive study of the dynamics of a classical Kitaev spin liquid. *Phys. Rev. B*, 96:134408, Oct 2017. doi: 10.1103/PhysRevB.96.134408. URL https://link.aps.org/doi/10.1103/PhysRevB.96.134408.

[207] T. E. Saunders and J. T. Chalker. Spin Freezing in Geometrically Frustrated Antiferromagnets with Weak Disorder. *Phys. Rev. Lett.*, 98:157201, Apr 2007. doi: 10.1103/PhysRevLett.98.157201. URL https://link.aps.org/doi/10.1103/PhysRevLett.98.157201.

[208] U. Schollwöck. The density-matrix renormalization group. *Rev. Mod. Phys.*, 77:259–315, Apr 2005. doi: 10.1103/RevModPhys.77.259. URL https://link.aps.org/doi/10.1103/RevModPhys.77.259.

[209] U. Schollwöck, T. Jolicœur, and T. Garel. Onset of incommensurability at the valence-bond-solid point in the $S = 1$ quantum spin chain. *Phys. Rev. B*, 53:3304–3311, Feb 1996. doi: 10.1103/PhysRevB.53.3304. URL https://link.aps.org/doi/10.1103/PhysRevB.53.3304.

[210] F. Schwabl. *Quantum Mechanics, Fourth Edition*. Springer Berlin, Heidelberg, 01 2007. ISBN 978-3-540-71932-8. doi: 10.1007/978-3-540-71933-5. URL https://doi.org/10.1007/978-3-540-71933-5.

[211] J. Schwichtenberg. *Physics from Symmetry*. Undergraduate Lecture Notes in Physics. Springer International Publishing, 2017. ISBN 9783319666303. URL https://books.google.co.jp/books?id=zS8xswEACAAJ.

[212] U. F. P. Seifert and L. Savary. Phase diagrams and excitations of anisotropic $S = 1$ quantum magnets on the triangular lattice, 2022. URL https://arxiv.org/abs/2203.13490.

[213] T. Senthil. Symmetry-Protected Topological Phases of Quantum Matter. *Annual Review of Condensed Matter Physics*, 6(1):299–324, 2022/05/15 2015. doi: 10.1146/annurev-conmatphys-031214-014740. URL https://doi.org/10.1146/annurev-conmatphys-031214-014740.

[214] M. Serbyn, T. Senthil, and P. A. Lee. Exotic $S = 1$ spin-liquid state with fermionic excitations on the triangular lattice. *Phys. Rev. B*, 84:180403, Nov 2011. doi: 10.1103/PhysRevB.84.180403. URL https://link.aps.org/doi/10.1103/PhysRevB.84.180403.

[215] M. Serbyn, T. Senthil, and P. A. Lee. Overscreened Kondo fixed point in $S = 1$ spin liquid. *Phys. Rev. B*, 88:024419, Jul 2013. doi: 10.1103/PhysRevB.88.024419. URL https://link.aps.org/doi/10.1103/PhysRevB.88.024419.

[216] R. Shankar. *Principles of quantum mechanics*. Plenum Press, New York, 1994. ISBN 0306447908 9780306447907.

[217] N. Shannon, B. Schmidt, K. Penc, and P. Thalmeier. Finite temperature properties and frustrated ferromagnetism in a square lattice Heisenberg model. *Eur. Phys. J. B*, 38(4):599–616, 4 2004. URL https://doi.org/10.1140/epjb/e2004-00156-3.

[218] N. Shannon, K. Penc, and Y. Motome. Nematic, vector-multipole, and plateau-liquid states in the classical $O(3)$ pyrochlore antiferromagnet with biquadratic interactions in applied magnetic field. *Phys. Rev. B*, 81:184409, May 2010. doi: 10.1103/PhysRevB.81.184409. URL http://link.aps.org/doi/10.1103/PhysRevB.81.184409.

[219] R. W. Sharples. *Alexander of Aphrodisias: Quaestiones 2.16-3.15*. Bloomsbury Academic, London, 2014/11/07/ 1994. ISBN 978-1-4725-5168-9. doi: 10.5040/9781472551689. URL http://www.bloomsburycollections.com/book/alexander-of-aphrodisias-quaestiones-2-16-3-15/.

[220] I. Shim and J. P. Dahl. A new interpretation of Hund's first rule. *Theoretica chimica acta*, 48(2):165–174, 1978. doi: 10.1007/PL00020709. URL https://doi.org/10.1007/PL00020709.

[221] R. Shindou and T. Momoi. $SU(2)$ slave-boson formulation of spin nematic states in $S = \frac{1}{2}$ frustrated ferromagnets. *Phys. Rev. B*, 80:064410, Aug 2009. doi: 10.1103/PhysRevB.80.064410. URL http://link.aps.org/doi/10.1103/PhysRevB.80.064410.

[222] R. Shindou, S. Yunoki, and T. Momoi. Projective studies of spin nematics in a quantum frustrated ferromagnet. *Phys. Rev. B*, 84:134414, Oct 2011. doi: 10.1103/PhysRevB.84.134414. URL http://link.aps.org/doi/10.1103/PhysRevB.84.134414.

[223] R. Shindou, S. Yunoki, and T. Momoi. Dynamical spin structure factors of quantum spin nematic states. *Phys. Rev. B*, 87:054429, Feb 2013. doi: 10.1103/

PhysRevB.87.054429. URL https://link.aps.org/doi/10.1103/PhysRevB.87.054429.

[224] Y. Shirata, H. Tanaka, T. Ono, A. Matsuo, K. Kindo, and H. Nakano. Quantum Magnetization Plateau in Spin-1 Triangular-Lattice Antiferromagnet $Ba_3NiSb_2O_9$. *Journal of the Physical Society of Japan*, 80(9):093702, 2011. doi: 10.1143/JPSJ.80.093702. URL https://doi.org/10.1143/JPSJ.80.093702.

[225] L. Shu-hua. *Origine de la Boussole 11. Aimant et Boussole.* Isis 45 (2), 1954.

[226] H. J. Silverstein, R. Sinclair, A. Sharma, Y. Qiu, I. Heinmaa, A. Leitmäe, C. R. Wiebe, R. Stern, and H. Zhou. Naturally tuned quantum critical point in the $S = 1$ kagomé $YCa_3(VO)_3(BO_3)_4$. *Phys. Rev. Materials*, 2:044006, Apr 2018. doi: 10.1103/PhysRevMaterials.2.044006. URL https://link.aps.org/doi/10.1103/PhysRevMaterials.2.044006.

[227] M. Skoulatos, F. Rucker, G. J. Nilsen, A. Bertin, E. Pomjakushina, J. Ollivier, A. Schneidewind, R. Georgii, O. Zaharko, L. Keller, C. Rüegg, C. Pfleiderer, B. Schmidt, N. Shannon, A. Kriele, A. Senyshyn, and A. Smerald. Putative spin-nematic phase in $BaCdVO(PO_4)_2$. *Phys. Rev. B*, 100:014405, Jul 2019. doi: 10.1103/PhysRevB.100.014405. URL https://link.aps.org/doi/10.1103/PhysRevB.100.014405.

[228] A. Smerald. *Theory of the nuclear magnetic* $1/T_1$ *relaxation rate in conventional and unconventional magnets.* Springer Theses, 2013.

[229] A. Smerald and N. Shannon. Theory of spin excitations in a quantum spin-nematic state. *Phys. Rev. B*, 88:184430, Nov 2013. doi: 10.1103/PhysRevB.88.184430. URL http://link.aps.org/doi/10.1103/PhysRevB.88.184430.

[230] A. Smerald and N. Shannon. Theory of NMR $1/T_1$ relaxation in a quantum spin nematic in an applied magnetic field. *Phys. Rev. B*, 93:184419, May 2016. doi: 10.1103/PhysRevB.93.184419. URL https://link.aps.org/doi/10.1103/PhysRevB.93.184419.

[231] A. Smerald, H. T. Ueda, and N. Shannon. Theory of inelastic neutron scattering in a field-induced spin-nematic state. *Phys. Rev. B*, 91:174402, May 2015. doi: 10.1103/PhysRevB.91.174402. URL http://link.aps.org/doi/10.1103/PhysRevB.91.174402.

[232] D. M. Stamper-Kurn and M. Ueda. Spinor Bose gases: Symmetries, magnetism, and quantum dynamics. *Rev. Mod. Phys.*, 85:1191–1244, Jul 2013. doi: 10.1103/RevModPhys.85.1191. URL https://link.aps.org/doi/10.1103/RevModPhys.85.1191.

[233] J. Stillwell. *Naive Lie Theory.* Undergraduate Texts in Mathematics. Springer New York, 2008. ISBN 9780387782157. URL https://books.google.co.jp/books?id=SuR5OAgxyDIC.

[234] C. Stock, S. Jonas, C. Broholm, S. Nakatsuji, Y. Nambu, K. Onuma, Y. Maeno, and J.-H. Chung. Neutron-Scattering Measurement of Incommensurate Short-Range Order in Single Crystals of the $S = 1$ Triangular Antiferromagnet $NiGa_2\mathbf{S}_4$. *Phys. Rev. Lett.*, 105:037402, Jul 2010. doi: 10.1103/PhysRevLett.105.037402. URL https://link.aps.org/doi/10.1103/PhysRevLett.105.037402.

[235] E. M. Stoudenmire, S. Trebst, and L. Balents. Quadrupolar correlations and spin freezing in $S = 1$ triangular lattice antiferromagnets. *Phys. Rev. B*, 79:214436, Jun 2009. doi: 10.1103/PhysRevB.79.214436. URL https://link.aps.org/doi/10.1103/PhysRevB.79.214436.

[236] K. Suzuki and K. Hattori. Ground-State Phase Diagram of the S = 1 One-Dimensional Kondo Lattice Model with a Uniaxial Anisotropy under Transverse Fields. *Journal of the Physical Society of Japan*, 88(2):024707, 2022/06/06 2019. doi: 10.7566/JPSJ.88.024707. URL https://doi.org/10.7566/JPSJ.88.024707.

[237] K. Suzuki and K. Hattori. Superconducting Correlations in the One-Dimensional Kondo Lattice Models under Magnetic Fields. *Journal of the Physical Society of Japan*, 89(3):034703, 2022/06/06 2020. doi: 10.7566/JPSJ.89.034703. URL https://doi.org/10.7566/JPSJ.89.034703.

[238] R. H. Swendsen and J.-S. Wang. Replica Monte Carlo Simulation of Spin-Glasses. *Phys. Rev. Lett.*, 57:2607–2609, Nov 1986. doi: 10.1103/PhysRevLett.57.2607. URL https://link.aps.org/doi/10.1103/PhysRevLett.57.2607.

[239] M. Taillefumier, J. Robert, C. L. Henley, R. Moessner, and B. Canals. Semiclassical spin dynamics of the antiferromagnetic Heisenberg model on the kagome lattice. *Phys. Rev. B*, 90:064419, Aug 2014. doi: 10.1103/PhysRevB.90.064419. URL https://link.aps.org/doi/10.1103/PhysRevB.90.064419.

[240] J. Takano and H. Tsunetsugu. Theory of Impurity Effects on the Spin Nematic State. *Journal of the Physical Society of Japan*, 80(9):094707, 2011. doi: 10.1143/JPSJ.80.094707. URL https://doi.org/10.1143/JPSJ.80.094707.

[241] S. Takayoshi, K. Totsuka, and A. Tanaka. Symmetry-protected topological order in magnetization plateau states of quantum spin chains. *Phys. Rev. B*, 91:155136, Apr 2015. doi: 10.1103/PhysRevB.91.155136. URL https://link.aps.org/doi/10.1103/PhysRevB.91.155136.

[242] K. Takubo, T. Mizokawa, J.-Y. Son, Y. Nambu, S. Nakatsuji, and Y. Maeno. Unusual Superexchange Pathways in an NiS_2 Triangular Lattice with Negative Charge-Transfer Energy. *Phys. Rev. Lett.*, 99:037203, Jul 2007. doi: 10.1103/PhysRevLett.99.037203. URL https://link.aps.org/doi/10.1103/PhysRevLett.99.037203.

[243] A. Tanaka, K. Totsuka, and X. Hu. Geometric phases and the magnetization process in quantum antiferromagnets. *Phys. Rev. B*, 79:064412, Feb

2009. doi: 10.1103/PhysRevB.79.064412. URL https://link.aps.org/doi/10.1103/PhysRevB.79.064412.

[244] K. Tanaka, Y. Yokoyama, and C. Hotta. Origin of Biquadratic Exchange Interactions in a Mott Insulator as a Driving Force of Spin Nematic Order. *Journal of the Physical Society of Japan*, 87(2):023702, 2022/05/10 2018. doi: 10.7566/JPSJ.87.023702. URL https://doi.org/10.7566/JPSJ.87.023702.

[245] O. Tchernyshyov and G.-W. Chern. *Spin-Lattice Coupling in Frustrated Antiferromagnets*, pages 269–291. Springer Berlin Heidelberg, Berlin, Heidelberg, 2011. ISBN 978-3-642-10589-0. doi: 10.1007/978-3-642-10589-0_11. URL https://doi.org/10.1007/978-3-642-10589-0_11.

[246] S. Thompson. *... Michael Faraday, His Life and Work*. Century science series. Cassell, limited, 1901. URL https://books.google.co.jp/books?id=HKf5g3qYYz8C.

[247] T. A. Tóth, A. M. Läuchli, F. Mila, and K. Penc. Three-Sublattice Ordering of the SU(3) Heisenberg Model of Three-Flavor Fermions on the Square and Cubic Lattices. *Phys. Rev. Lett.*, 105:265301, Dec 2010. doi: 10.1103/PhysRevLett.105.265301. URL https://link.aps.org/doi/10.1103/PhysRevLett.105.265301.

[248] T. A. Tóth, A. M. Läuchli, F. Mila, and K. Penc. Competition between two- and three-sublattice ordering for $S = 1$ spins on the square lattice. *Phys. Rev. B*, 85:140403, Apr 2012. doi: 10.1103/PhysRevB.85.140403. URL https://link.aps.org/doi/10.1103/PhysRevB.85.140403.

[249] S. Trebst and C. Hickey. Kitaev materials. *Physics Reports*, 950:1–37, 2022. ISSN 0370-1573. doi: https://doi.org/10.1016/j.physrep.2021.11.003. URL https://www.sciencedirect.com/science/article/pii/S0370157321004051. Kitaev materials.

[250] H. Tsunetsugu and M. Arikawa. Spin Nematic Phase in S=1 Triangular Antiferromagnets. *J. Phys. Soc. Jpn*, 75(8):083701, 2006. doi: 10.1143/JPSJ.75.083701. URL http://dx.doi.org/10.1143/JPSJ.75.083701.

[251] H. T. Ueda and T. Momoi. Nematic phase and phase separation near saturation field in frustrated ferromagnets. *Phys. Rev. B*, 87:144417, Apr 2013. doi: 10.1103/PhysRevB.87.144417. URL http://link.aps.org/doi/10.1103/PhysRevB.87.144417.

[252] H. T. Ueda, Y. Akagi, and N. Shannon. Quantum solitons with emergent interactions in a model of cold atoms on the triangular lattice. *Phys. Rev. A*, 93:021606, Feb 2016. doi: 10.1103/PhysRevA.93.021606. URL https://link.aps.org/doi/10.1103/PhysRevA.93.021606.

[253] M. E. Valentine, T. Higo, Y. Nambu, D. Chaudhuri, J. Wen, C. Broholm, S. Nakatsuji, and N. Drichko. Impact of the Lattice on Magnetic Properties

and Possible Spin Nematicity in the $S = 1$ Triangular Antiferromagnet $NiGa_2S_4$. *Phys. Rev. Lett.*, 125:197201, Nov 2020. doi: 10.1103/PhysRevLett.125.197201. URL https://link.aps.org/doi/10.1103/PhysRevLett.125.197201.

[254] J. Villain. Insulating spin glasses. *Zeitschrift für Physik B Condensed Matter*, 33 (1):31–42, 1979. doi: 10.1007/BF01325811. URL https://doi.org/10.1007/BF01325811.

[255] A. Völl and S. Wessel. Spin dynamics of the bilinear-biquadratic $S = 1$ Heisenberg model on the triangular lattice: A quantum Monte Carlo study. *Phys. Rev. B*, 91:165128, Apr 2015. doi: 10.1103/PhysRevB.91.165128. URL https://link.aps.org/doi/10.1103/PhysRevB.91.165128.

[256] Z. Wang, W.-J. Hu, and A. H. Nevidomskyy. Spin Ferroquadrupolar Order in the Nematic Phase of FeSe. *Phys. Rev. Lett.*, 116:247203, Jun 2016. doi: 10.1103/PhysRevLett.116.247203. URL https://link.aps.org/doi/10.1103/PhysRevLett.116.247203.

[257] G. H. Wannier. Antiferromagnetism. The Triangular Ising Net. *Phys. Rev.*, 79: 357–364, Jul 1950. doi: 10.1103/PhysRev.79.357. URL https://link.aps.org/doi/10.1103/PhysRev.79.357.

[258] S. R. White and I. Affleck. Spectral function for the $S = 1$ Heisenberg antiferromagetic chain. *Phys. Rev. B*, 77:134437, Apr 2008. doi: 10.1103/PhysRevB.77.134437. URL https://link.aps.org/doi/10.1103/PhysRevB.77.134437.

[259] S. M. Winter, Y. Li, H. O. Jeschke, and R. Valentí. Challenges in design of Kitaev materials: Magnetic interactions from competing energy scales. *Phys. Rev. B*, 93:214431, Jun 2016. doi: 10.1103/PhysRevB.93.214431. URL https://link.aps.org/doi/10.1103/PhysRevB.93.214431.

[260] C. Xu, F. Wang, Y. Qi, L. Balents, and M. P. A. Fisher. Spin Liquid Phases for Spin-1 Systems on the Triangular Lattice. *Phys. Rev. Lett.*, 108:087204, Feb 2012. doi: 10.1103/PhysRevLett.108.087204. URL https://link.aps.org/doi/10.1103/PhysRevLett.108.087204.

[261] Y. Yamamoto. *Ancient Greece: The Science of Magnetism is Born*, chapter Chapter 1, pages 3–38. 2018. doi: 10.1142/9789813223776_0001. URL https://www.worldscientific.com/doi/abs/10.1142/9789813223776_0001.

[262] C. Zener. Interaction Between the d Shells in the Transition Metals. *Phys. Rev.*, 81:440–444, Feb 1951. doi: 10.1103/PhysRev.81.440. URL https://link.aps.org/doi/10.1103/PhysRev.81.440.

[263] C. Zener. Interaction between the d-Shells in the Transition Metals. II. Ferromagnetic Compounds of Manganese with Perovskite Structure. *Phys. Rev.*, 82: 403–405, May 1951. doi: 10.1103/PhysRev.82.403. URL https://link.aps.org/doi/10.1103/PhysRev.82.403.

[264] H. Zhang and C. D. Batista. Classical spin dynamics based on SU(N) coherent states. *Phys. Rev. B*, 104:104409, Sep 2021. doi: 10.1103/PhysRevB.104.104409. URL https://link.aps.org/doi/10.1103/PhysRevB.104.104409.

[265] H. Zhang, Z. Wang, D. Dahlbom, K. Barros, and C. D. Batista. CP^2 Skyrmions and Skyrmion Crystals in Realistic Quantum Magnets, 2022. URL https://arxiv.org/abs/2203.15248.

[266] L. Zhang, Y.-Q. Zhang, P. Zhang, L. Zhao, M. Guo, and J. Tang. Single-Molecule Magnet Behavior Enhanced by Synergic Effect of Single-Ion Anisotropy and Magnetic Interactions. *Inorganic Chemistry*, 56(14):7882–7889, 07 2017. doi: 10.1021/acs.inorgchem.7b00625. URL https://doi.org/10.1021/acs.inorgchem.7b00625.

[267] S. Zhang, H. J. Changlani, K. W. Plumb, O. Tchernyshyov, and R. Moessner. Dynamical Structure Factor of the Three-Dimensional Quantum Spin Liquid Candidate $NaCaNi_2F_7$. *Phys. Rev. Lett.*, 122:167203, Apr 2019. doi: 10.1103/PhysRevLett.122.167203. URL https://link.aps.org/doi/10.1103/PhysRevLett.122.167203.

[268] H. H. Zhao, C. Xu, Q. N. Chen, Z. C. Wei, M. P. Qin, G. M. Zhang, and T. Xiang. Plaquette order and deconfined quantum critical point in the spin-1 bilinear-biquadratic Heisenberg model on the honeycomb lattice. *Phys. Rev. B*, 85:134416, Apr 2012. doi: 10.1103/PhysRevB.85.134416. URL https://link.aps.org/doi/10.1103/PhysRevB.85.134416.

[269] S. Zhao, P. Dalmas de Réotier, A. Yaouanc, D. E. MacLaughlin, J. M. Mackie, O. O. Bernal, Y. Nambu, T. Higo, and S. Nakatsuji. Spin dynamics and spin freezing in the triangular lattice antiferromagnets $FeGa_2S_4$ and $NiGa_2S_4$. *Phys. Rev. B*, 86:064435, Aug 2012. doi: 10.1103/PhysRevB.86.064435. URL https://link.aps.org/doi/10.1103/PhysRevB.86.064435.

[270] T. Zibold, V. Corre, C. Frapolli, A. Invernizzi, J. Dalibard, and F. Gerbier. Spin-nematic order in antiferromagnetic spinor condensates. *Phys. Rev. A*, 93:023614, Feb 2016. doi: 10.1103/PhysRevA.93.023614. URL https://link.aps.org/doi/10.1103/PhysRevA.93.023614.

Appendix A

Spin Fluctuation Probability

In this Appendix, I detail how the spin fluctuation probabilities drawn in Fig. 1.3, Fig. 2.1, Fig. 3.1, Fig. 3.2, Fig. 6.2, and Fig. 6.3 are calculated.

Fluctuations around a given state $|\alpha\rangle$ can be calculated by computing its spin fluctuation probability, defined as the spatial probability distribution of the overlapping between the state $|\alpha\rangle$ and the spin coherent state $|\Omega\rangle$. The spin coherent state $|\Omega\rangle$ is obtained by applying a rotation operator in 3 dimensions defined by the angles θ and ϕ on the m=1 state $|1\rangle$:

$$|\Omega\rangle = \mathcal{R}(\theta, \phi)|1\rangle \ . \tag{A.1}$$

The spin coherent state represents then a spin pointing in the direction defined by the angles θ and ϕ. In the case of a spin–1, the spin coherent state is expressed as:

$$|\Omega\rangle = \frac{1+\cos\theta}{2}e^{-i\phi}|1\rangle + \frac{\sin\theta}{\sqrt{2}}|0\rangle + \frac{1-\cos\theta}{2}e^{-i\phi}|\overline{1}\rangle \ . \tag{A.2}$$

The spin fluctuation probability of the state $|\alpha\rangle$ is defined as the norm of the scalar product with the spin coherent state:

$$P(\theta, \phi)_{|\alpha\rangle} = |\langle\alpha|\Omega\rangle|^2 \ . \tag{A.3}$$

Appendix B

Properties of A–Matrices

Here, I present the fundamental properties of the "A-matrix". It follows from the definition in Eq. (2.46) that the A–object is mathematically a (1,1)-tensor, but for simplicity, I might usually refer to it as a matrix. In this Appendix, I also give the detailed explanations accompanying the symmetry analysis of the BBQ Model [Eq. (1.69)] that I discuss at the end of Section 2.4.4.

B.1 Properties of a Single A–Matrix

First, I present how Eq. (2.62) is obtained. Eq. (2.62) tells us how an object like $\hat{\mathcal{A}}^{\alpha}{}_{\beta}$ would transform under a general linear transformation Λ. To this end, as explained in Section 2.4.3, we consider a general linear transformation $\Lambda : V \to V$, such that $\det\Lambda \neq 0$, so that Λ is invertible, and we define

$$\tilde{\Lambda} = \Lambda^{-1^T} \ . \tag{B.1}$$

Under such a transformation, the basis vector $\mathbf{e}_i$ of the vector space V will transform according to

$$\overline{\mathbf{e}}_i = \tilde{\Lambda}_i{}^j \mathbf{e}_j \ . \tag{B.2}$$

Since the vector $\mathbf{v} = v^i \mathbf{e}_i$ is a mathematical object which existence does not depend on the basis, the components v^i should transform according to

$$\overline{v}^i = \Lambda^i{}_j v^j \ , \tag{B.3}$$

such that the vector $\mathbf{v} = \overline{v}^i \overline{\mathbf{e}}_i = v^i \mathbf{e}_i$ stays invariant. It is then also possible to introduce the dual basis $\{\mathbf{e}^{\star i}\}$ of the dual vector space $V^\star$. The basis vectors can be defined by the relations

$$e^{\star i}(e_j) = \delta^i_j \ . \tag{B.4}$$

Any element $\mathbf{v}^\star$ of $V^\star$ can be decomposed as

$$\mathbf{v}^\star = v^\star_i \mathbf{e}^{\star i} \ , \tag{B.5}$$

where the components $v_i^\star$ are simply given by the value of the function $\mathbf{v}^\star$ on the basis vector $\mathbf{e}_i$ of V

$$v_i^\star = \mathbf{v}^\star(\mathbf{e}_i) \ . \tag{B.6}$$

Under a general transformation Λ on the basis vectors $\mathbf{e}_i$, the dual basis vectors $\mathbf{e}^{\star i}$ will transform according to

$$\overline{\mathbf{e}}^{\star i} = \Lambda^i{}_j \mathbf{e}^{\star j} \ , \tag{B.7}$$

in order to preserve Eq. (B.4). And the component $v_i^\star$ will transform as

$$\overline{v}_i^\star = \tilde{\Lambda}_i{}^j v_j^\star \ . \tag{B.8}$$

Finally, under such a general transformation Λ, the component of an object like $\hat{\mathcal{A}}^\alpha{}_\beta$, which is actually a (1,1)-tensor, will transform as stated in Eq. (2.62).

B.2 Properties of Quadratric Terms of A–Matrices

Here, I show how the products of two objects $\hat{\mathcal{A}}^\alpha{}_\beta$ would transform under a linear transformation, in order to analyze the symmetry properties of the BBQ Hamiltonian rewritten in terms of $\hat{\mathcal{A}}$ -"matrices" [Eq. (1.69)]. Again, I emphasize that the object $\hat{\mathcal{A}}^\alpha{}_\beta$ is mathematically a tensor, but for simplicity, I might sometimes refer to them as matrices.

Going back to Eq. (1.69), it can easily be seen that the first term $\hat{\mathcal{A}}_i^\alpha{}_\beta \hat{\mathcal{A}}_j^\beta{}_\alpha$ is $U(3)$ symmetric because both indexes α and β are contravariant on one site and covariant on the other. The $\hat{\mathcal{A}}_i^\alpha{}_\beta \hat{\mathcal{A}}_j^\beta{}_\alpha$ will therefore stay invariant under a transformation $U \in U(3)$, for which we have

$$U \in U(3) \ : \ \ UU^\dagger = U^\dagger U = \mathbb{I} \quad \Rightarrow \quad U^\dagger = U^{-1} \ . \tag{B.9}$$

Indeed, under a $U(3)$ symmetry, the first term will transform as

$$\begin{aligned}
(\hat{\mathcal{A}}_i^\alpha{}_\beta)^\mu{}_\nu (\hat{\mathcal{A}}_j^\beta{}_\alpha)^\nu{}_\mu \rightarrow & U^\mu{}_\gamma U^{\dagger\kappa}{}_\nu (\hat{\mathcal{A}}_i^\alpha{}_\beta)^\gamma{}_\kappa U^\nu{}_\eta U^{\dagger\lambda}{}_\mu (\hat{\mathcal{A}}_j^\beta{}_\alpha)^\eta{}_\lambda \\
= & \, U^\mu{}_\gamma U^{\dagger\lambda}{}_\mu U^\nu{}_\eta U^{\dagger\kappa}{}_\nu (\hat{\mathcal{A}}_i^\alpha{}_\beta)^\gamma{}_\kappa (\hat{\mathcal{A}}_j^\beta{}_\alpha)^\eta{}_\lambda \\
= & \, \delta_\gamma{}^\lambda \delta_\eta{}^\kappa (\hat{\mathcal{A}}_i^\alpha{}_\beta)^\gamma{}_\kappa (\hat{\mathcal{A}}_j^\beta{}_\alpha)^\eta{}_\lambda \\
= & \, (\hat{\mathcal{A}}_i^\alpha{}_\beta)^\gamma{}_\kappa (\hat{\mathcal{A}}_j^\beta{}_\alpha)^\kappa{}_\gamma \ .
\end{aligned} \tag{B.10}$$

The second term in Eq. (1.69), on the other hand, is not $U(3)$ symmetric, but it is $O(3)$ symmetric. We can see that under a $U(3)$ transformation, it transforms as:

$$\begin{aligned}
(\hat{\mathcal{A}}_i^\alpha{}_\beta)^\mu{}_\nu (\hat{\mathcal{A}}_j^\alpha{}_\beta)^\mu{}_\nu \rightarrow & U^\mu{}_\gamma U^{\dagger\kappa}{}_\nu (\hat{\mathcal{A}}_i^\alpha{}_\beta)^\gamma{}_\kappa U^\mu{}_\eta U^{\dagger\lambda}{}_\nu (\hat{\mathcal{A}}_j^\alpha{}_\beta)^\eta{}_\lambda \\
= & \, U^\mu{}_\gamma U^\mu{}_\eta U^{\dagger\lambda}{}_\nu U^{\dagger\kappa}{}_\nu (\hat{\mathcal{A}}_i^\alpha{}_\beta)^\gamma{}_\kappa (\hat{\mathcal{A}}_j^\alpha{}_\beta)^\eta{}_\lambda \ .
\end{aligned} \tag{B.11}$$

Clearly, this is not invariant under a $U(3)$ transformation, but it is under a $O(3)$

transformation. If $U = O \in O(3)$, we have

$$O \in O(3) \;:\; OO^T = O^T O = \mathbb{I} \quad \Rightarrow \quad O^T = O^{-1} \,, \tag{B.12}$$

and under a $O(3)$ transformation, it transforms as:

$$\begin{aligned}(\hat{\mathcal{A}}_i^{\alpha}{}_{\beta})^{\mu}{}_{\nu}(\hat{\mathcal{A}}_j^{\alpha}{}_{\beta})^{\mu}{}_{\nu} \rightarrow & O^{\mu}{}_{\gamma}O^{\mu}{}_{\eta}O^{T\lambda}{}_{\nu}O^{T\kappa}{}_{\nu}(\hat{\mathcal{A}}_i^{\alpha}{}_{\beta})^{\gamma}{}_{\kappa}(\hat{\mathcal{A}}_j^{\alpha}{}_{\beta})^{\eta}{}_{\lambda} \\ &= O^{T}{}_{\gamma}{}^{\mu}O^{\mu}{}_{\eta}O^{T\lambda}{}_{\nu}O_{\nu}{}^{\kappa}(\hat{\mathcal{A}}_i^{\alpha}{}_{\beta})^{\gamma}{}_{\kappa}(\hat{\mathcal{A}}_j^{\alpha}{}_{\beta})^{\eta}{}_{\lambda} \\ &= \delta_{\gamma\eta}\delta^{\kappa\lambda}(\hat{\mathcal{A}}_i^{\alpha}{}_{\beta})^{\gamma}{}_{\kappa}(\hat{\mathcal{A}}_j^{\alpha}{}_{\beta})^{\eta}{}_{\lambda} \\ &= (\hat{\mathcal{A}}_i^{\alpha}{}_{\beta})^{\gamma}{}_{\kappa}(\hat{\mathcal{A}}_j^{\alpha}{}_{\beta})^{\gamma}{}_{\kappa} \,. \end{aligned} \tag{B.13}$$

The Hamiltonian is therefore overall $O(3)$ symmetric, indeed both terms are invariant under an $O(3)$ symmetry. And in the case of $J_1 = J_2$, the second term in Eq. (1.69) vanishes, and the Hamiltonian is $U(3)$ symmetric. Therefore, working in $U(3)$ does not change the global symmetry of the Hamiltonian, since $o(3) \simeq su(2)$, and there is an homomorphism from $SU(2)$ into $O(3)$. However, the locally augmented $SU(3)$ symmetry of the Hamiltonian when $J_1 = J_2$ is enlarged from $SU(3)$ to $U(3)$. However, because of the constraint on the $\mathcal{A}_i$–matrices [Eq. (2.73)], the $U(3)$ symmetry is broken down to $SU(3)$.

The Hamiltonian can be rewritten in a more general form as

$$\mathcal{H}_{\mathsf{BBQ}} = \sum_{\langle i,j \rangle} J^{\alpha\mu}_{\beta\nu} \hat{\mathcal{A}}_i^{\alpha}{}_{\beta} \hat{\mathcal{A}}_j^{\mu}{}_{\nu} \,, \tag{B.14}$$

with

$$J = \begin{pmatrix} \begin{pmatrix} J_2 & 0 & 0 \\ 0 & 0 & 0 \\ 0 & 0 & 0 \end{pmatrix} & \begin{pmatrix} 0 & J_2 - J_1 & 0 \\ J_1 & 0 & 0 \\ 0 & 0 & 0 \end{pmatrix} & \begin{pmatrix} 0 & 0 & J_2 - J_1 \\ 0 & 0 & 0 \\ J_1 & 0 & 0 \end{pmatrix} \\ \begin{pmatrix} 0 & J_1 & 0 \\ J_2 - J_1 & 0 & 0 \\ 0 & 0 & 0 \end{pmatrix} & \begin{pmatrix} 0 & 0 & 0 \\ 0 & J_2 & 0 \\ 0 & 0 & 0 \end{pmatrix} & \begin{pmatrix} 0 & 0 & 0 \\ 0 & 0 & J_2 - J_1 \\ 0 & J_1 & 0 \end{pmatrix} \\ \begin{pmatrix} 0 & 0 & J_1 \\ 0 & 0 & 0 \\ J_2 - J_1 & 0 & 0 \end{pmatrix} & \begin{pmatrix} 0 & 0 & 0 \\ 0 & 0 & J_1 \\ 0 & J_2 - J_1 & 0 \end{pmatrix} & \begin{pmatrix} 0 & 0 & 0 \\ 0 & 0 & 0 \\ 0 & 0 & J_2 \end{pmatrix} \end{pmatrix} . \tag{B.15}$$

The indexes α and β correspond respectively to the line and the row of the table that assigns the designated matrix, whose components are then given by μ and ν. For example,

$$J^{1\mu}_{2\nu} = \begin{pmatrix} 0 & J_2 - J_1 & 0 \\ J_1 & 0 & 0 \\ 0 & 0 & 0 \end{pmatrix} \quad , \quad J^{12}_{21} = J_1 \quad , \quad J^{11}_{22} = J_2 - J_1 \,. \tag{B.16}$$

The symmetries of the Hamiltonian are now hidden in the symmetries of the tensor $J^{\alpha\mu}_{\beta\nu}$. Firstly, we see that the Hamiltonian is $O(3)$ symmetric, because the repeated summed indexes are always either covariant or contravariant. The tensor is also symmetric under the exchange $\alpha\beta \leftrightarrow \mu\nu$

$$J^{\alpha\mu}_{\beta\nu} = J^{\mu\alpha}_{\nu\beta} \,. \tag{B.17}$$

Eq. (B.17) expresses the fact that there is actually a tensor product between the two

operators $\hat{\mathcal{A}}_{i\ \beta}^{\alpha}$ and $\hat{\mathcal{A}}_{j\ \nu}^{\mu}$ acting on different sites. We also have $\alpha \leftrightarrow \nu$ with $\beta \leftrightarrow \mu$ together, which is just relabeling the indexes.

In the case of $J_1 = J_2$, the tensor is also symmetric under the exchanges $\alpha \leftrightarrow \mu$ and $\beta \leftrightarrow \nu$ or both

$$J_{\beta\nu}^{\alpha\mu} = J_{\beta\nu}^{\mu\alpha} = J_{\nu\beta}^{\alpha\mu} \ . \tag{B.18}$$

It is also symmetric under the exchanges $\beta \leftrightarrow \mu$ and $\alpha \leftrightarrow \nu$

$$J_{\beta\nu}^{\alpha\mu} = J_{\mu\nu}^{\alpha\beta} = J_{\beta\alpha}^{\nu\mu} = J_{\mu\alpha}^{\nu\beta} \ , \tag{B.19}$$

in which case, it can easily be seen that the Hamiltonian is $U(3)$ invariant, since every index is now summed covariantly.

Appendix C

Bogolioubov Transformation

Here I show how the Bogoliubov transformation used in Section 4.1 is performed.

A Bogolioubov transformation consists in finding new bosons $\hat{\mathrm{v}}_{\mathbf{k}}^{\dagger\alpha}$ and $\hat{\mathrm{v}}_{\mathbf{k}\alpha}$ expressed in terms of the bosons $\hat{\mathrm{w}}_{\mathbf{k}}^{\dagger\alpha}$ and $\hat{\mathrm{w}}_{\mathbf{k}\alpha}$ [Eq. (4.6b)] , such that they diagonalize the Hamiltonian

$$\mathcal{H}_{\mathsf{BBQ}} \sim \sum_{\mathbf{k}} \epsilon_{\mathbf{k}} \hat{\mathbf{v}}_{\mathbf{k}}^{\dagger} \hat{\mathbf{v}}_{\mathbf{k}} \ . \tag{C.1}$$

Let us assume that the components are given by

$$\begin{aligned} \hat{\mathrm{v}}_{\mathbf{k}\alpha} =& U_{\mathbf{k}_\alpha}{}^{\beta} \hat{\mathrm{w}}_{\mathbf{k}\beta} \ , \\ \hat{\mathrm{v}}_{\mathbf{k}}^{\dagger\alpha} =& \hat{\mathrm{w}}_{\mathbf{k}}^{\dagger\beta} U_{\mathbf{k}\beta}^{\dagger}{}^{\alpha} \ , \end{aligned} \tag{C.2}$$

where $U_{\mathbf{k}}$ is, in our case, the transformation from the basis made out of bosons expressed by time-reversal basis states to the basis in which the Hamiltonian is diagonal. Requiring them to have bosonic commutation relations [Eq. (4.7)], leads to

$$\begin{aligned} \left[\hat{\mathrm{v}}_{\mathbf{k}\alpha}, \hat{\mathrm{v}}_{\mathbf{q}}^{\dagger\beta}\right] &= \left[U_{\mathbf{k}_\alpha}{}^{\gamma} \hat{\mathrm{w}}_{\mathbf{k}\gamma}, U_{\mathbf{q}\eta}^{\dagger}{}^{\beta} \hat{\mathrm{w}}_{\mathbf{q}}^{\dagger\eta}\right] \\ &= U_{\mathbf{k}_\alpha}{}^{\gamma} U_{\mathbf{q}\eta}^{\dagger}{}^{\beta} \left[\hat{\mathrm{w}}_{\mathbf{k}\gamma}, \hat{\mathrm{w}}_{\mathbf{q}}^{\dagger\eta}\right] \\ &= U_{\mathbf{k}_\alpha}{}^{\gamma} U_{\mathbf{q}\eta}^{\dagger}{}^{\beta} \gamma_{0\gamma}{}^{\eta} \delta_{\mathbf{kq}} \overset{!}{=} \gamma_{0\alpha}{}^{\beta} \delta_{\mathbf{kq}} \\ \Rightarrow \quad & U_{\mathbf{k}_\alpha}{}^{\gamma} \gamma_{0\gamma}{}^{\eta} U_{\mathbf{k}\eta}^{\dagger}{}^{\beta} = \gamma_{0\alpha}{}^{\beta} \\ \Rightarrow \quad & \gamma_{0\gamma}{}^{\eta} U_{\mathbf{k}\eta}^{\dagger}{}^{\beta} \gamma_{0\beta}^{\alpha} = U_{\mathbf{k}}^{-1}{}_{\gamma}^{\alpha} \ , \end{aligned} \tag{C.3}$$

where γ_0 is defined in Eq. (4.8), and where we used the fact that

$$\gamma_0 = \gamma_0{}^{-1} \ . \tag{C.4}$$

In the compact form, Eq. (C.3) becomes

$$\gamma_0 U_{\mathbf{k}}^{\dagger} \gamma_0 = U_{\mathbf{k}}^{-1} \ . \tag{C.5}$$

We see that the transformation $U_{\mathbf{k}}$ is not unitary, $U_{\mathbf{k}}^{-1} \neq U_{\mathbf{k}}^{\dagger}$, and that we shall use Eq. (C.5) to find the inverse transformation.

Inverting Eq. (C.2) and plugging it into the Hamiltonian leads us to look for a

transformation $U_{\mathbf{k}}$ such that $U_{\mathbf{k}}\ \gamma_0 M_{\mathbf{k}} U_{\mathbf{k}}^{-1}$ is diagonal. If we define $D_{\mathbf{k}}$ as being a diagonal matrix, we can write

$$\begin{aligned} & U_{\mathbf{k}}\ \gamma_0 M_{\mathbf{k}} U_{\mathbf{k}}^{-1} = D_{\mathbf{k}} \\ \Rightarrow \quad & {\gamma_0}_\nu{}^\alpha M_{\mathbf{k}\alpha}{}^\beta U_{\mathbf{k}}^{-1}{}_\beta{}^i = U_{\mathbf{k}}^{-1}{}_\nu{}^i D_{\mathbf{k}i}^i \ \text{ for i} = 1,2,3,4\ , \end{aligned} \tag{C.6}$$

where we see that $U_{\mathbf{k}}^{-1}{}_\nu{}^i$ is an eigenvector of $\gamma_0 M_{\mathbf{k}}$ with eigenvalue $D_{\mathbf{k}i}^i$. Eq. (C.6) is rewritten as Eq. (4.9) in the main text. This means that we need to diagonalize $\gamma_0 M_{\mathbf{k}}$ and that the corresponding eigenvectors are the column of the matrix $U_{\mathbf{k}}^{-1}$.

Finding the Bogolioubov transformation reduces then to find the eigenvalues and eigenvectors of the system in Eq. (4.9). Since Eq. (4.9) consists of twice the same system, we only need to solve it once, and we only consider

$$\sigma_z m_{\mathbf{k}} e_i = \epsilon_{\mathbf{k},i} e_i \quad i = 1,2\ , \tag{C.7}$$

where

$$\sigma_z = \begin{pmatrix} 1 & 0 \\ 0 & -1 \end{pmatrix} \quad , \quad m_{\mathbf{k}} = \begin{pmatrix} A_{\mathbf{k}} & -B_{\mathbf{k}} \\ B_{\mathbf{k}} & -A_{\mathbf{k}} \end{pmatrix}\ , \tag{C.8}$$

and where σ_z plays the role of γ_0 but for the two independent subsystems for $\left(\hat{\mathrm{a}}_{-\mathbf{k}},\ \ \hat{\mathrm{a}}_{\mathbf{k}}^\dagger\right)$ and $\left(\hat{\mathrm{b}}_{-\mathbf{k}},\ \ \hat{\mathrm{b}}_{\mathbf{k}}^\dagger\right)$. The eigenvalues $\epsilon_{\mathbf{k},1/2}$ of $\sigma_z m_{\mathbf{k}}$ are given in Eq. (4.11). The eigenvectors are given by

$$e_1 \ = \begin{pmatrix} \alpha_1 \\ 1 \end{pmatrix} \quad , \quad e_2 \ = \begin{pmatrix} \alpha_2 \\ 1 \end{pmatrix}\ , \tag{C.9}$$

in the basis $\{\hat{\mathrm{a}}_{\mathbf{k}}, \hat{\mathrm{a}}_{-\mathbf{k}}^\dagger\}$ and where we define

$$\alpha_i = -\frac{A_{\mathbf{k}} + \epsilon_{\mathbf{k},i}}{B_{\mathbf{k}}}\ . \tag{C.10}$$

The columns of the matrix $U_{\mathbf{k}}^{-1}$ are given by the eigenvectors

$$U_{\mathbf{k}}^{-1} \ = \begin{pmatrix} \alpha_1 & \alpha_2 \\ 1 & 1 \end{pmatrix}\ . \tag{C.11}$$

Using Eq. (C.5), we can calculate $U_{\mathbf{k}}$ as follows:

$$U_{\mathbf{k}} \ = \sigma_z U_{\mathbf{k}}^{\dagger -1}\ \sigma_z = \begin{pmatrix} \alpha_1 & -1 \\ -\alpha_2 & 1 \end{pmatrix}\ . \tag{C.12}$$

Using Eq. (C.2), the new bosons that diagonalize the Hamiltonian are given by

$$\hat{\alpha}_{\mathbf{k}} = \hat{\mathrm{v}}_{\mathbf{k}1} = {U_{\mathbf{k}}}_1{}^1 \hat{\mathrm{w}}_{\mathbf{k}1} + {U_{\mathbf{k}}}_1{}^2 \hat{\mathrm{w}}_{\mathbf{k}2} = \alpha_1 \hat{\mathrm{a}}_{\mathbf{k}} - \hat{\mathrm{a}}_{-\mathbf{k}}^\dagger\ , \tag{C.13a}$$

$$\hat{\alpha}_{-\mathbf{k}}^\dagger = \hat{\mathrm{v}}_{\mathbf{k}2} = {U_{\mathbf{k}}}_2{}^1 \hat{\mathrm{w}}_{\mathbf{k}1} + {U_{\mathbf{k}}}_2{}^2 \hat{\mathrm{w}}_{\mathbf{k}2} = -\alpha_2 \hat{\mathrm{a}}_{\mathbf{k}} + \hat{\mathrm{a}}_{-\mathbf{k}}^\dagger\ , \tag{C.13b}$$

$$\hat{\alpha}_{\mathbf{k}}^\dagger = \hat{\mathrm{v}}_{\mathbf{k}}^{\dagger 1} = \hat{\mathrm{w}}_{\mathbf{k}}^{\dagger 1} U_{\mathbf{k}1}^{\dagger\ 1} + \hat{\mathrm{w}}_{\mathbf{k}}^{\dagger 2} U_{\mathbf{k}2}^{\dagger\ 1} = \alpha_1 \hat{\mathrm{a}}_{\mathbf{k}}^\dagger - \hat{\mathrm{a}}_{-\mathbf{k}}\ , \tag{C.13c}$$

$$\hat{\alpha}_{-\mathbf{k}} = \hat{\mathrm{v}}_{\mathbf{k}}^{\dagger 2} = \hat{\mathrm{w}}_{\mathbf{k}}^{\dagger 1} U_{\mathbf{k}1}^{\dagger\ 2} + \hat{\mathrm{w}}_{\mathbf{k}}^{\dagger 2} U_{\mathbf{k}2}^{\dagger\ 2} = -\alpha_2 \hat{\mathrm{a}}_{\mathbf{k}}^\dagger + \hat{\mathrm{a}}_{-\mathbf{k}}\ . \tag{C.13d}$$

For instance, we note that we should have $\hat{\mathrm{v}}_{\mathbf{k}1} = \hat{\mathrm{v}}^{\dagger 2}_{-\mathbf{k}}$ i.e $\hat{\alpha}_{\mathbf{k}}(\mathbf{k}) = \hat{\alpha}_{-\mathbf{k}}(-\mathbf{k})$. However, we see that it is not the case

$$\hat{\mathrm{v}}_{\mathbf{k}1} = \alpha_1 \hat{\mathrm{a}}_{\mathbf{k}} - \hat{\mathrm{a}}^{\dagger}_{-\mathbf{k}} \neq -\alpha_2 \hat{\mathrm{a}}^{\dagger}_{-\mathbf{k}} + \hat{\mathrm{a}}_{\mathbf{k}} = \hat{\mathrm{v}}^{\dagger 2}_{-\mathbf{k}} \, . \tag{C.14}$$

For it to be the case, we see that we need the matrix element of the transformation to be

$$U_{\mathbf{k}1}{}^{1} = U^{\dagger\ 2}_{-\mathbf{k}2} \, , \tag{C.15a}$$
$$U_{\mathbf{k}1}{}^{2} = U^{\dagger\ 2}_{-\mathbf{k}1} \, . \tag{C.15b}$$

To solve this issue, we can assume that we can multiply the eigenvectors by some parameters, a and b for instance, such that Eq. (C.15) is satisfied

$$e_1 \ = a \begin{pmatrix} \alpha_1 \\ 1 \end{pmatrix} \quad , \quad e_2 \ = b \begin{pmatrix} \alpha_2 \\ 1 \end{pmatrix} . \tag{C.16}$$

$U^{-1}_{\mathbf{k}}$ becomes

$$U^{-1}_{\mathbf{k}} \ = \begin{pmatrix} a\alpha_1 & b\alpha_2 \\ a & b \end{pmatrix} . \tag{C.17}$$

Using Eq. (C.5), we can calculate $U_{\mathbf{k}}$ as follows:

$$U_{\mathbf{k}} \ = \sigma_z U^{\dagger -1}_{\mathbf{k}} \ \sigma_z = \begin{pmatrix} a\alpha_1 & -a \\ -b\alpha_2 & b \end{pmatrix} . \tag{C.18}$$

We also have

$$U^{\dagger}_{\mathbf{k}} \ = \begin{pmatrix} a\alpha_1 & -b\alpha_2 \\ -a & b \end{pmatrix} . \tag{C.19}$$

Note that the coefficients α_1 and α_2 depend on $\mathbf{k}$ through $\epsilon_{\mathbf{k}}$,but we dropped the dependency in $\mathbf{k}$ for α_1 and α_2. Using the fact that $\epsilon_{\mathbf{k}} = \epsilon_{-\mathbf{k}}$, Eq. (C.15) implies

$$\begin{array}{rcl} U_{\mathbf{k}1}{}^{1} & = & U^{\dagger\ 2}_{-\mathbf{k}2} \, , \\ a\alpha_1 & = & b \, , \\ a\frac{-A_{\mathbf{k}} - \sqrt{A^2_{\mathbf{k}} - B^2_{\mathbf{k}}}}{B_{\mathbf{k}}} & = & b \, , \\ \frac{a}{-B_{\mathbf{k}}} & = & \frac{b}{A_{\mathbf{k}} + \sqrt{A^2_{\mathbf{k}} - B^2_{\mathbf{k}}}} \, , \end{array} \tag{C.20a}$$

and

$$\begin{array}{rcl} U_{\mathbf{k}1}{}^{2} & = & U^{\dagger\ 2}_{-\mathbf{k}1} \, , \\ -b\alpha_2 & = & -a \, , \\ -b\frac{-A_{\mathbf{k}} + \sqrt{A^2_{\mathbf{k}} - B^2_{\mathbf{k}}}}{B_{\mathbf{k}}} & = & -a \, , \\ \frac{b}{-B_{\mathbf{k}}} & = & \frac{-a}{-A_{\mathbf{k}} + \sqrt{A^2_{\mathbf{k}} - B^2_{\mathbf{k}}}} \, . \end{array} \tag{C.20b}$$

We see that if we multiply the last line of Eq. (C.20b) by $\frac{-B_{\mathbf{k}}}{A_{\mathbf{k}}+\sqrt{A_{\mathbf{k}}^2-B_{\mathbf{k}}^2}}$ we get

$$\frac{-B_{\mathbf{k}}}{A_{\mathbf{k}}+\sqrt{A_{\mathbf{k}}^2-B_{\mathbf{k}}^2}}\frac{b}{-B_{\mathbf{k}}}=\frac{-B_{\mathbf{k}}}{A_{\mathbf{k}}+\sqrt{A_{\mathbf{k}}^2-B_{\mathbf{k}}^2}}\frac{-a}{-A_{\mathbf{k}}+\sqrt{A_{\mathbf{k}}^2-B_{\mathbf{k}}^2}}\,, \tag{C.21a}$$

$$\Rightarrow \quad \frac{b}{A_{\mathbf{k}}+\sqrt{A_{\mathbf{k}}^2-B_{\mathbf{k}}^2}}=\frac{a}{-B_{\mathbf{k}}}\,. \tag{C.21b}$$

We note that Eq. (C.21b) is exactly the same condition as in the last line of Eq. (C.20a). This makes sense, because the 1$^{\text{st}}$condition, namely ${U_{\mathbf{k}1}}^1 = {U^\dagger}^2_{-\mathbf{k}2}$ is correlated the the second one ${U_{\mathbf{k}1}}^2 = {U^\dagger}^2_{-\mathbf{k}1}$, as the components ${U_{\mathbf{k}1}}^1$, ${U_{\mathbf{k}1}}^2$ are not independent, as they need to be eigenvectors, and nor are the components ${U^\dagger}^2_{-\mathbf{k}2}$, ${U^\dagger}^2_{-\mathbf{k}1}$. This means that we can choose

$$a=-B_{\mathbf{k}}\,, \tag{C.22}$$

$$b=A_{\mathbf{k}}+\sqrt{A_{\mathbf{k}}^2-B_{\mathbf{k}}^2}\,. \tag{C.23}$$

In this case, the eigenvectors become

$$e_1 \;=\begin{pmatrix}\Delta_{\mathbf{k}}\\ -B_{\mathbf{k}}\end{pmatrix}\quad,\quad e_2\;=\begin{pmatrix}-B_{\mathbf{k}}\\ \Delta_{\mathbf{k}}\end{pmatrix}, \tag{C.24}$$

where $\Delta_{\mathbf{k}}$ is given Eq. (4.13). And the transformation matrix becomes

$$U_{\mathbf{k}}^{-1}\;=\begin{pmatrix}\Delta_{\mathbf{k}} & -B_{\mathbf{k}}\\ -B_{\mathbf{k}} & \Delta_{\mathbf{k}}\end{pmatrix}\,. \tag{C.25}$$

Using Eq. (C.5), we can calculate $U_{\mathbf{k}}$ as follows:

$$U_{\mathbf{k}}\;=\sigma_z U_{\mathbf{k}}^{\dagger-1}\,\sigma_z=\begin{pmatrix}\Delta_{\mathbf{k}} & B_{\mathbf{k}}\\ B_{\mathbf{k}} & \Delta_{\mathbf{k}}\end{pmatrix}\,. \tag{C.26}$$

And its complex conjugate yields

$$U_{\mathbf{k}}^{\dagger}\;=\begin{pmatrix}\Delta_{\mathbf{k}} & B_{\mathbf{k}}\\ B_{\mathbf{k}} & \Delta_{\mathbf{k}}\end{pmatrix}\,. \tag{C.27}$$

Using Eq. (C.2), the new bosons, which diagonalize the Hamiltonian, are given by

$$\hat{\alpha}_{\mathbf{k}}=\hat{\mathrm{v}}_{\mathbf{k}1}={U_{\mathbf{k}1}}^1\hat{\mathrm{w}}_{\mathbf{k}1}+{U_{\mathbf{k}1}}^2\hat{\mathrm{w}}_{\mathbf{k}2}=\Delta_{\mathbf{k}}\hat{\mathrm{a}}_{\mathbf{k}}+B_{\mathbf{k}}\hat{\mathrm{a}}^\dagger_{-\mathbf{k}}\,, \tag{C.28a}$$

$$\hat{\alpha}^\dagger_{-\mathbf{k}}=\hat{\mathrm{v}}_{\mathbf{k}2}={U_{\mathbf{k}2}}^1\hat{\mathrm{w}}_{\mathbf{k}1}+{U_{\mathbf{k}2}}^2\hat{\mathrm{w}}_{\mathbf{k}2}=B_{\mathbf{k}}\hat{\mathrm{a}}_{\mathbf{k}}+\Delta_{\mathbf{k}}\hat{\mathrm{a}}^\dagger_{-\mathbf{k}}\,, \tag{C.28b}$$

$$\hat{\alpha}^\dagger_{\mathbf{k}}=\hat{\mathrm{v}}^{\dagger 1}_{\mathbf{k}}=\hat{\mathrm{w}}^{\dagger 1}_{\mathbf{k}}{U^\dagger}^1_{\mathbf{k}1}+\hat{\mathrm{w}}^{\dagger 2}_{\mathbf{k}}{U^\dagger}^1_{\mathbf{k}2}=\Delta_{\mathbf{k}}\hat{\mathrm{a}}^\dagger_{\mathbf{k}}+B_{\mathbf{k}}\hat{\mathrm{a}}_{-\mathbf{k}}\,, \tag{C.28c}$$

$$\hat{\alpha}_{-\mathbf{k}}=\hat{\mathrm{v}}^{\dagger 2}_{\mathbf{k}}=\hat{\mathrm{w}}^{\dagger 1}_{\mathbf{k}}{U^\dagger}^2_{\mathbf{k}1}+\hat{\mathrm{w}}^{\dagger 2}_{\mathbf{k}}{U^\dagger}^2_{\mathbf{k}2}=B_{\mathbf{k}}\hat{\mathrm{a}}^\dagger_{\mathbf{k}}+\Delta_{\mathbf{k}}\hat{\mathrm{a}}_{-\mathbf{k}}\,. \tag{C.28d}$$

We see that, now, we indeed have $\hat{\mathrm{v}}_{\mathbf{k}1}=\hat{\mathrm{v}}^{\dagger 2}_{-\mathbf{k}}$, i.e., $\hat{\alpha}_{\mathbf{k}}(\mathbf{k})=\hat{\alpha}_{-\mathbf{k}}(-\mathbf{k})=\hat{\alpha}_{\mathbf{k}}$. However, we still need to normalize the new bosons. Indeed, they should also satisfy bosonic

commutation relations

$$\begin{aligned}\left[\hat{\alpha}_{\mathbf{k}}, \hat{\alpha}_{\mathbf{k}}^{\dagger}\right] &= \left[\frac{1}{\sqrt{N}}(\Delta_{\mathbf{k}}\hat{\mathrm{a}}_{\mathbf{k}} + B_{\mathbf{k}}\hat{\mathrm{a}}_{-\mathbf{k}}^{\dagger}), \frac{1}{\sqrt{N}}(\Delta_{\mathbf{k}}\hat{\mathrm{a}}_{\mathbf{k}}^{\dagger} + B_{\mathbf{k}}\hat{\mathrm{a}}_{-\mathbf{k}})\right] \\ &= \frac{1}{N}(\Delta_{\mathbf{k}}^2\left[\hat{\mathrm{a}}_{\mathbf{k}}, \hat{\mathrm{a}}_{\mathbf{k}}^{\dagger}\right] + B_{\mathbf{k}}^2\left[\hat{\mathrm{a}}_{-\mathbf{k}}^{\dagger}, \hat{\mathrm{a}}_{-\mathbf{k}}\right]) \\ &= \frac{1}{N}(\Delta_{\mathbf{k}}^2 - B_{\mathbf{k}}^2) \stackrel{!}{=} 1 \\ \Rightarrow \quad N &= \Delta_{\mathbf{k}}^2 - B_{\mathbf{k}}^2 \,. \end{aligned} \tag{C.29}$$

Finally, the normalized transformation matrix becomes

$$U_{\mathbf{k}} = \frac{1}{\sqrt{\Delta_{\mathbf{k}}^2 - B_{\mathbf{k}}^2}} \begin{pmatrix} \Delta_{\mathbf{k}} & B_{\mathbf{k}} \\ B_{\mathbf{k}} & \Delta_{\mathbf{k}} \end{pmatrix} \,. \tag{C.30}$$

The inverse [Eq. (C.5)] holds

$$U_{\mathbf{k}}^{-1} = \sigma_z U_{\mathbf{k}}^{\dagger} \sigma_z = \frac{1}{\sqrt{\Delta_{\mathbf{k}}^2 - B_{\mathbf{k}}^2}} \begin{pmatrix} \Delta_{\mathbf{k}} & -B_{\mathbf{k}} \\ -B_{\mathbf{k}} & \Delta_{\mathbf{k}} \end{pmatrix} \,. \tag{C.31}$$

By inverting the Bogolibov transformation [Eq. (C.2)], we can express the old bosons in terms of the new Bogolibov bosons using Eq. (C.31),

$$\hat{\mathrm{a}}_{\mathbf{k}} = \hat{\mathrm{w}}_{\mathbf{k}1} = U_{\mathbf{k}}^{-1}{}_1{}^{\beta}\hat{\mathrm{v}}_{\mathbf{k}\beta} = \frac{1}{\sqrt{\Delta_{\mathbf{k}}^2 - B_{\mathbf{k}}^2}}(\Delta_{\mathbf{k}}\hat{\alpha}_{\mathbf{k}} - B_{\mathbf{k}}\hat{\alpha}_{-\mathbf{k}}^{\dagger}) \,, \tag{C.32a}$$

$$\hat{\mathrm{a}}_{-\mathbf{k}}^{\dagger} = \hat{\mathrm{w}}_{\mathbf{k}2} = U_{\mathbf{k}}^{-1}{}_2{}^{\beta}\hat{\mathrm{v}}_{\mathbf{k}\beta} = \frac{1}{\sqrt{\Delta_{\mathbf{k}}^2 - B_{\mathbf{k}}^2}}(-B_{\mathbf{k}}\hat{\alpha}_{\mathbf{k}} + \Delta_{\mathbf{k}}\hat{\alpha}_{-\mathbf{k}}^{\dagger}) \,, \tag{C.32b}$$

$$\hat{\mathrm{a}}_{\mathbf{k}}^{\dagger} = \hat{\mathrm{w}}_{\mathbf{k}}^{\dagger 1} = \hat{\mathrm{v}}_{\mathbf{k}}^{\dagger\beta}U_{\mathbf{k}}^{\dagger -1}{}_{\beta}{}^{1} = \frac{1}{\sqrt{\Delta_{\mathbf{k}}^2 - B_{\mathbf{k}}^2}}(\Delta_{\mathbf{k}}\hat{\alpha}_{\mathbf{k}}^{\dagger} - B_{\mathbf{k}}\hat{\alpha}_{-\mathbf{k}}) \,, \tag{C.32c}$$

$$\hat{\mathrm{a}}_{-\mathbf{k}} = \hat{\mathrm{w}}_{\mathbf{k}}^{\dagger 2} = \hat{\mathrm{v}}_{\mathbf{k}}^{\dagger\beta}U_{\mathbf{k}}^{\dagger -1}{}_{\beta}{}^{1} = \frac{1}{\sqrt{\Delta_{\mathbf{k}}^2 - B_{\mathbf{k}}^2}}(-B_{\mathbf{k}}\hat{\alpha}_{\mathbf{k}}^{\dagger} + \Delta_{\mathbf{k}}\hat{\alpha}_{-\mathbf{k}}) \,. \tag{C.32d}$$

For the other part of the Hamiltonian containing the $\hat{\mathrm{b}}^{\dagger}$ bosons, the problem is exactly the same, and therefore, we can just use the solutions we found above. The eigenvalues $\epsilon_{\mathbf{k},3}$ and $\epsilon_{\mathbf{k},4}$ associated to the Bogoliubov bosons for the $\left(\hat{\mathrm{b}}_{-\mathbf{k}}, \ \hat{\mathrm{b}}_{\mathbf{k}}^{\dagger}\right)$ subsystem are given by Eq. (4.11). To express the old bosons in terms of the new Bogoliubov

bosons, we can just use Eq. (C.32):

$$\hat{\mathrm{b}}_{\mathbf{k}} = \frac{1}{\sqrt{\Delta_{\mathbf{k}}^2 - B_{\mathbf{k}}^2}}(\Delta_{\mathbf{k}}\hat{\beta}_{\mathbf{k}} - B_{\mathbf{k}}\hat{\beta}_{-\mathbf{k}}^\dagger) \,, \tag{C.33a}$$

$$\hat{\mathrm{b}}_{-\mathbf{k}}^\dagger = \frac{1}{\sqrt{\Delta_{\mathbf{k}}^2 - B_{\mathbf{k}}^2}}(-B_{\mathbf{k}}\hat{\beta}_{\mathbf{k}} + \Delta_{\mathbf{k}}\hat{\beta}_{-\mathbf{k}}^\dagger) \,, \tag{C.33b}$$

$$\hat{\mathrm{b}}_{\mathbf{k}}^\dagger = \frac{1}{\sqrt{\Delta_{\mathbf{k}}^2 - B_{\mathbf{k}}^2}}(\Delta_{\mathbf{k}}\hat{\beta}_{\mathbf{k}}^\dagger - B_{\mathbf{k}}\hat{\beta}_{-\mathbf{k}}) \,, \tag{C.33c}$$

$$\hat{\mathrm{b}}_{-\mathbf{k}} = \frac{1}{\sqrt{\Delta_{\mathbf{k}}^2 - B_{\mathbf{k}}^2}}(-B_{\mathbf{k}}\hat{\beta}_{\mathbf{k}}^\dagger + \Delta_{\mathbf{k}}\hat{\beta}_{-\mathbf{k}}) \,. \tag{C.33d}$$

There is a constant term coming from the Bogoliubov transformation [Eq. (C.32) and Eq. (C.33)]. For the bosons $\hat{\mathrm{a}}_{\pm\mathbf{k}}^\dagger, \hat{\mathrm{a}}_{\pm\mathbf{k}}$ it holds:

$$-A_{\mathbf{k}} + \sqrt{A_{\mathbf{k}}^2 - B_{\mathbf{k}}^2} = -A_{\mathbf{k}} + \epsilon_{\mathbf{k},1} \,, \tag{C.34a}$$

and for the bosons $\hat{\mathrm{b}}_{\pm\mathbf{k}}^\dagger, \hat{\mathrm{b}}_{\pm\mathbf{k}}$:

$$-A_{\mathbf{k}} + \sqrt{A_{\mathbf{k}}^2 - B_{\mathbf{k}}^2} = -A_{\mathbf{k}} + \epsilon_{\mathbf{k},3} \,, \tag{C.34b}$$

where we use Eq. (4.11).

After performing the Bogolibov transformation, the Hamiltonian becomes

$$\mathcal{H} = E_0 + \frac{1}{2}\sum_{\mathbf{k}} \left[\epsilon_{\mathbf{k},1}\hat{\alpha}_{\mathbf{k}}^\dagger\hat{\alpha}_{\mathbf{k}} + \epsilon_{\mathbf{k},1}\hat{\alpha}_{-\mathbf{k}}^\dagger\hat{\alpha}_{-\mathbf{k}} - A_{\mathbf{k}} + \epsilon_{\mathbf{k},1} + \epsilon_{\mathbf{k},3}\hat{\beta}_{\mathbf{k}}^\dagger\hat{\beta}_{\mathbf{k}} + \epsilon_{\mathbf{k},3}\hat{\beta}_{-\mathbf{k}}^\dagger\hat{\beta}_{-\mathbf{k}} - A_{\mathbf{k}} + \epsilon_{\mathbf{k},3}\right] \,, \tag{C.35}$$

that we can rewrite as

$$\mathcal{H} = E_0 + \sum_{\mathbf{k}} \left[\epsilon_{\mathbf{k},1}(\hat{\alpha}_{\mathbf{k}}^\dagger\hat{\alpha}_{\mathbf{k}} + \frac{1}{2}) + \epsilon_{\mathbf{k},3}(\hat{\beta}_{\mathbf{k}}^\dagger\hat{\beta}_{\mathbf{k}} + \frac{1}{2}) - A_{\mathbf{k}}\right] \,, \tag{C.36}$$

where E_0 is given in Eq. (3.14). Eq. (C.36) is given in the main text by Eq. (4.15), where we used the fact that $\epsilon_{\mathbf{k},1} = \epsilon_{\mathbf{k},3}$ [Eq. (4.11)], since they are the eigenvalues of an identical problem.

Appendix D

Conventions for the Triangular Lattice

In this Appendix, I present the convention used to describe the triangular lattice and its reciprocal space. The real space lattice vectors, linking a single site unit cell to another, are chosen as

$$\mathbf{a} = \begin{pmatrix} 1 \\ 0 \end{pmatrix} \; ; \quad \mathbf{b} = \tfrac{1}{2} \begin{pmatrix} 1 \\ \sqrt{3} \end{pmatrix} . \tag{D.1}$$

The associated vectors in reciprocal space are given by

$$\mathbf{k}_a = \tfrac{2\pi}{\sqrt{3}} \begin{pmatrix} \sqrt{3} \\ -1 \end{pmatrix} \; ; \quad \mathbf{k}_b = \tfrac{2\pi}{\sqrt{3}} \begin{pmatrix} 0 \\ 2 \end{pmatrix} . \tag{D.2}$$

We define the points along the irreducible wedge in reciprocal space to be

$$\mathbf{\Gamma} = \begin{pmatrix} 0 \\ 0 \end{pmatrix} \; ; \quad \mathbf{K} = \tfrac{4\pi}{3} \begin{pmatrix} 1 \\ 0 \end{pmatrix} \; ; \quad \mathbf{M} = \tfrac{\pi}{\sqrt{3}} \begin{pmatrix} \sqrt{3} \\ 1 \end{pmatrix} . \tag{D.3}$$

The vectors δ linking the 6 neighboring sites are given by

$$\begin{gathered} \delta = \begin{pmatrix} 1 \\ 0 \end{pmatrix} \; ; \quad \tfrac{1}{2} \begin{pmatrix} 1 \\ \sqrt{3} \end{pmatrix} \; ; \quad \tfrac{1}{2} \begin{pmatrix} -1 \\ \sqrt{3} \end{pmatrix} \; ; \\ \begin{pmatrix} -1 \\ 0 \end{pmatrix} \; ; \quad \tfrac{1}{2} \begin{pmatrix} -1 \\ -\sqrt{3} \end{pmatrix} \; ; \quad \tfrac{1}{2} \begin{pmatrix} 1 \\ -\sqrt{3} \end{pmatrix} . \end{gathered} \tag{D.4}$$

For the triangular lattice, the coordination number and the geometrical factor given in Eq. (3.18) yield

$$z = 6 \quad ; \quad \gamma_{\triangleleft}(\mathbf{k}) = \tfrac{1}{3}(\cos(k_x) + 2\cos(\tfrac{k_x}{2})\cos(\tfrac{\sqrt{3}k_y}{2})) . \tag{D.5}$$

The numerical simulations presented in this Thesis are all performed on a cluster of sites defined by the real space basis vectors given by Eq. (D.1) and scaled by L, such that $N = L^2$ is the number of lattice sites, with periodic boundary conditions.

Appendix E

Numerical Simulation of Spin–1

For completeness, I here provide details about the numerical implementation of our method which has been implemented by my collaborator Dr. Rico Pohle.

E.1 u3MC

We here show the evidence that the generalised Marsaglia approach proposed in Eq. (2.120), which randomly generates the variable $x_1, \cdots, x_6$ on a 5-dimensional sphere points, properly and independently selects them.

As illustrated in Fig. E.1, the second moment $\langle x_m^2 \rangle$ of each variable $x_1, \cdots, x_6$ [Eq. (2.120)] converges towards 1/6 (middle black solid line) as the number of points $N_{dot} \to \infty$, proving that the x_m are uncorrelated. The central–limit theorem requires the statistical errors in function of N_{dot}, to decrease as $1/\sqrt{N_{dot}}$. This behaviour is indicated by the dashed lines.

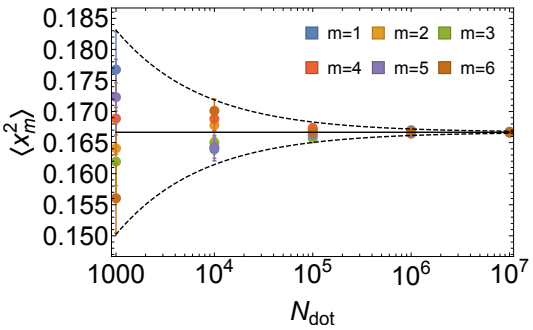

Figure E.1: Statistical independence of points randomly generated a 5–dimensional sphere, using Eq. (2.120). The second moment $\langle x_m^2 \rangle$ of the variables x_m, $m = 1, ..., 6$ is plotted as a function of the number of points, N_{dot} and converges towards $\langle x_m^2 \rangle \to 1/6$ (middle black solid line) as $N_{\text{dot}} \to \infty$. Statistical errors respect the central–limit theorem and decrease as $1/\sqrt{N_{\text{dot}}}$ (dashed lines). Sampling was performed by my collaborator Dr. Rico Pohle. Figure is reproduced from [201].

E.1.1 Phase Diagram and Comparison with Published Results

We first benchmark our method, by carrying out u3MC simulations for the spin–1 BBQ model Eq. (2.68) on a triangular lattice, and comparing the obtained thermodynamic properties with published results [131, 229, 235]. Results for the heat capacity are shown in Fig. E.2, with parameters $J_1 = 1$, $J_2 = -1.5$, in accordance with earlier work [235]. For these parameters, mean–field calculations [Figure 1.11] predict an antiferromagnetic (AFM) ground state with 3–sublattice order, close to a phase boundary with ferroquadrupolar (FQ) order [131, 229]. Simulation for the heat capacity in the space of $\mathcal{A}$–matrices [cf. Section 2.6.1], shows a two peaks structure. One peak is located around $T \approx 0.5\ J_1$, corresponding to the onset of FQ fluctuations, and another one $T \approx 0.3\ J_1$ corresponding to the onset of AFM fluctuations. For comparison, we have additionally carried out similar simulations for $\mathbf{d}$–vectors, following the sSU(3) approach of Stoudenmire *et al.* [235]. These results are also shown in Fig. E.2, and we find quantitative agreement between the two methods within statistical errors. This analysis has also been extended to obtain a complete finite–temperature phase diagram for the BBQ model, which was previously presented in Fig. 1.13. Results are shown for a linear dimension $L = 48$ [N=2304 spins] of the cluster. The onset of the correlations as the temperature is decreased corresponds to the peak found in the heat capacity as a function of

$$J_1 = J\cos\theta\ ,\ J_2 = J\cos\theta\ . \tag{E.1}$$

The nature of each phase is determined by using the equal–time structure factors $S_{\mathcal{S}}(\mathbf{q})$ and $S_{\mathcal{Q}}(\mathbf{q})$ [Eq. (2.124)]. Fig. E.3 shows results for structure factors evaluated at given ordering vectors, for a temperature $T/J = 0.01$.

The correlations found by the u3MC method at low temperature exactly correspond to the four known mean–field ground states [131, 229], as illustrated in Fig. 1.11. As previously noted by Stoudenmire *et al.* [235], FQ order corresponds to a secondary order parameter within the coplanar AFM ground state. Consistent with this, for $\theta \lesssim -\frac{\pi}{4}$ the onset of FQ fluctuations occurs at a higher temperature than the onset of AFM fluctuations (cf. results for $\theta \approx -0.313\ \pi$ in Fig. E.2).

We also note that similar behaviour occurs in a range of parameters $\theta \sim \pi/2$, near the border between FM and AFQ phases, where the onset of FM fluctuations occurs at a higher temperature than the onset of AFQ fluctuations. However, an interpretation in terms of a secondary order–parameter is here not possible. Nevertheless, we note that the single–sublattice phase dominates at higher temperatures. We infer that the entropy of fluctuations about the FM ground state is higher than the entropy of fluctuations about the AFQ ground state, presumably because of the k^2 dispersion of the FM excitations.

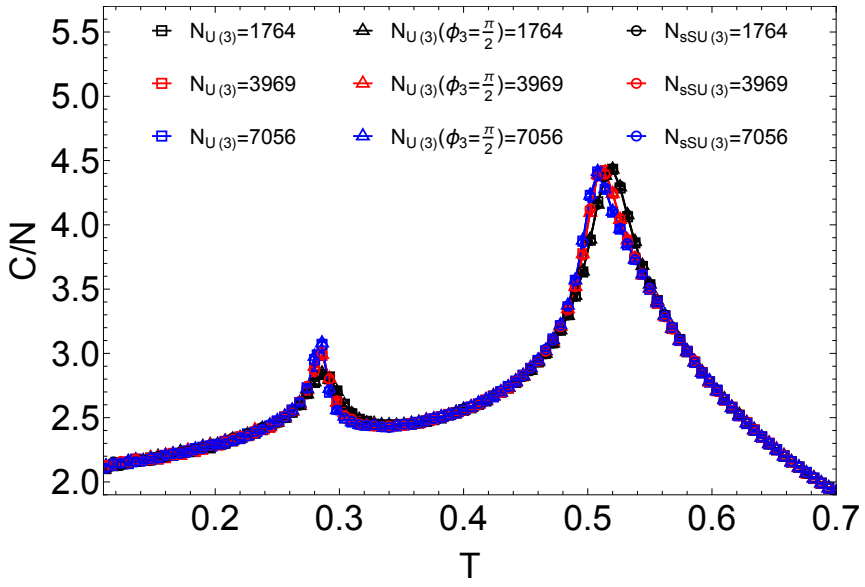

Figure E.2: Comparison of the $U(3)$ Monte Carlo (u3MC) method with published results for the spin–1 bilinear—biquadratic (BBQ) model on the triangular lattice for parameters $J_1 = 1$, $J_2 = -1.5$, which corresponds to the AFM phase [Fig. 1.11]. Specific heat C/N shows a double–peak structure. Results obtained from MC simulation, based on a $u(3)$ matrices, $\hat{\mathcal{A}}^{\alpha}_{\beta}$ description, for an u3MC update based on a 5–dimensional sphere [Eq. (2.120)] and 4–dimensional sphere by eliminating the gauge freedom on the phase [Eq. (2.120) with Eq. (2.122)] are represented by squares and triangles symbols, respectively. u3MC simulations were performed by my collaborator Dr. Rico Pohle. While, circles correspond to results from "sSU(3)" MC simulations in the space of the complex vector $\mathbf{d}$, following Stoudenmire *et al.*. The three different approaches agree within statistical errors. Figure is reproduced from [201].

Between dipolar and quadrupolar phases, the phase boundaries follow the well defined "vertical" behaviour as shown as solid red lines in Fig. 1.13, which corresponds to the two $SU(3)$ points. This is consistent with the $SU(3)$ symmetry of the ground–state manifolds, which contains both a dipolar and a quadrupolar nature. And the $SU(3)$ symmetry of the ground–state manifolds is being preserved up to temperature associated with the onset of correlations, T^*. This allows for the exciting possibility of finding exotic topological phase transitions at T^*, corresponding to topological defects specifically associated to the $SU(3)$ points [104, 252]. This interesting topic is left aside for future studies.

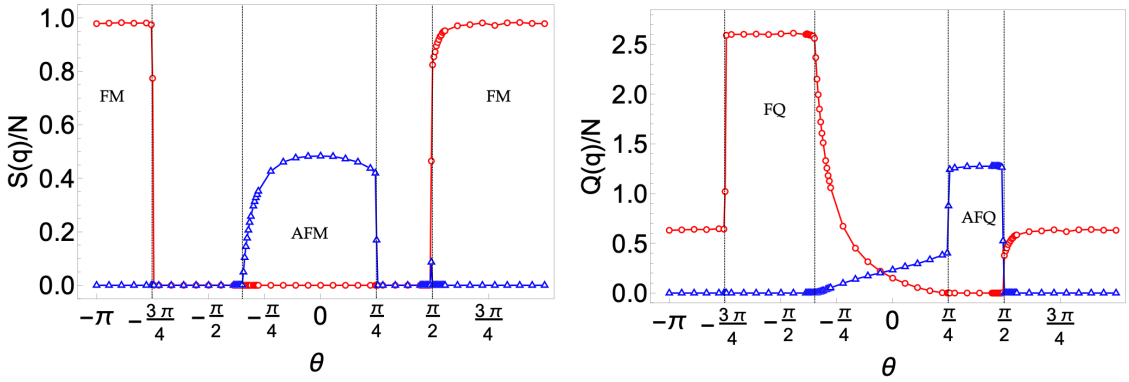

(a) Dipolar structure factor $S_{\mathrm{S}}(\mathbf{q})$ **(b)** Quadrupolar structure factor $S_{\mathrm{Q}}(\mathbf{q})$

Figure E.3: Phases occurring in the spin–1 BBQ model on a triangular lattice at finite temperature, as found in classical Monte Carlo simulation in the space of $u(3)$ matrices (u3MC). (a) Dipolar structure factor $S_{\mathrm{S}}(\mathbf{q})$ [Eq. (2.124)], representing ferromagnetic (FM) correlations for $\mathbf{q} = \Gamma$ (red circles) and 3–sublattice antiferromagnetic (AFM) correlations for $\mathbf{q} = K$ (blue triangles). (b) Quadrupolar structure factor $S_{\mathrm{Q}}(\mathbf{q})$ [Eq. (2.124)], showing ferroquadrupolar (FQ) correlations for $\mathbf{q} = \Gamma$ (red circles) and 3–sublattice antiferroquadrupolar (AFQ) correlations for $\mathbf{q} = K$ (blue triangles). Simulations of Eq. (1.48) were performed using the u3MC method described in Section 2.6.1, for a system size with linear dimension $L = 48$ ($N = 2304$ spins), at a temperature $T = 0.01\ J$ and for the FQ phase with parameters given by Eq. (E.1). The phases found are in direct correspondence with known results for the mean–field ground state [131, 183, 229], summarised in Fig. 1.11. In each case, the temperature associated with the onset of fluctuations corresponds to the peak found in specific heat, cf. Fig. 1.13. Simulations were carried out by my collaborator Dr. Rico Pohle. Figures are reproduced from [201].

E.2 Molecular Dynamics Simulations Within $u(3)$ Framework

Here I provide additional details about the practical implementation of the "u3MD" approach introduced in Section 2.6.2.

E.2.1 Implementation of u3MD Update

We iteratively apply the RK–4–integration

$$\{\mathcal{A}^{\alpha}_{i,\beta}(t)\} \mapsto \{\mathcal{A}^{\alpha}_{i,\beta}(t + \delta t_{\mathsf{RK}})\} + \mathcal{O}(\delta t^{5}_{\mathsf{RK}}) \,, \tag{E.2}$$

which generates a time series for $\{\mathcal{A}^{\alpha}_{i,\beta}(t)\}$. The errors associated with the RK–integration are controlled by the size of δt_{RK}. A single RK update is defined through numerical integration of Eq. (2.74) for every component of every spin in the lattice. The results are saved for every 20^{th} global update. This allows to work with manageable data size and to maintain sufficient precision in the numerical integration scheme.

The stored data then generates a time series

$$\{\mathcal{A}^{\alpha}_{\beta}(i,t_n)\}\ , \quad t_n = n\ \delta t\ , \quad n = 1 \ldots N_{\mathsf{t}}\ , \tag{E.3}$$

where δt is the size of the effective time step and where N_t is the total number of stored time steps. The size of the effective time step, δt, determines the highest frequency that we can resolve to

$$\delta t = \frac{2\pi}{\omega_{\mathsf{max}}}\ . \tag{E.4}$$

And the duration of the simulation

$$\Delta t = N_t\ \delta t\ , \tag{E.5}$$

determines the energy–resolution

$$\delta\omega = \frac{2\pi}{\Delta t}\ , \tag{E.6}$$

where we choose to work in units such that $\hbar = 1$.

Practically, we set a typical length of time–series corresponding to

$$N_t = 1600\ , \tag{E.7}$$

and a time–step

$$\delta t \approx 0.4\ J^{-1}\ , \tag{E.8}$$

such that the time–interval used in RK integration for an individual spin is

$$\delta t_{\mathsf{RK}} \equiv \delta t/20 \approx 0.02\ J^{-1}\ . \tag{E.9}$$

This choice of parameters allows us to resolve excitations with energy up to

$$\omega_{\mathsf{max}} \approx 16\ J\ , \tag{E.10}$$

which is twice as large as the maximum energy for excitations of the FQ state as shown in Fig. 1.14, with parameters

$$(J = 1, \theta = -\frac{\pi}{2}) \Rightarrow (J_1 = 0.0, J_2 = -1.0)\ . \tag{E.11}$$

The corresponding energy resolution

$$\delta\omega \approx 10^{-2}\ J\ , \tag{E.12}$$

is shown to be sufficient in order to resolve fine–structure in dynamical structure factors described below. As previously mentioned, the validity of our MD approach relies on the preservation of the trace of the $\mathcal{A}$–matrices [Eq. (2.73)] and the conservation of the total energy of the system $E[\mathcal{A}_i]$ [Eq. (2.117)].

First, we examine the constraint on spin–length. As explained in Section 2.4.5, the structure of the EoM [Eq. (2.74)] guarantees that the spin–length constraint is preserved throughout the time evolution, such that, as long as the initial configuration $\{\hat{\mathcal{A}}_i^{\alpha}{}_{\beta}(t=0)\}$ satisfies the spin–length constraint

$$\text{Tr } \hat{\mathcal{A}}_i \equiv 1 \; \forall \; i \in (1 \ldots \text{N}) \; , \tag{E.13}$$

the constraint will remain satisfied at all times. In Fig. 2.2 (a), we indeed note that, up to numerical precision, the trace of $\mathcal{A}_i$ is conserved. Simulations were done for a duration corresponding to $N_t = 5000$. Therefore, simulations of any feasible duration, continue to properly describe spin–1 moments.

Secondly, we look into the conservation of energy. RK–integration does not conserve energy. The size of the RK time step, δt_{RK}, gives out the rate at which the error builds up. And, by ensuring that δt_{RK} is sufficiently small, we can keep the errors in energy bounded. From Fig. 2.2 (b), we can see that the error in energy produced over simulations of duration $N_t = 5000$ is $\approx 0.03\ J$. This means that one "MD step", which consists in scanning the entire lattice using the RK–4 algorithm, accumulates an error in the total energy of order $\sim 10^{-6}\ J$. This is sufficiently small to make sure that the energy is adequately conserved for simulations of practical duration, i.e. $N_t = 1600$, $\Delta t \approx 1600 \times \delta t = 640\ J^{-1}$.

E.2.2 Calculation of Dynamical Structure Factors

Time evolution of the equations of motions enables us to obtain a time series $\{\mathcal{A}^{\alpha}_{\beta}(i, t_n)\}$. Investigating the associated dynamics can be done by directly drawing the spin configurations and animating their evolution [190], or by computing dynamical structure factors of the form

$$S_{\lambda}(\mathbf{q}, t_n) = \left\langle \sum_{\alpha\beta} \left(m_{\lambda}{}^{\alpha}{}_{\beta}(\mathbf{q}, t_n) \right)^* m_{\lambda}{}^{\alpha}{}_{\beta}(\mathbf{q}, 0) \right\rangle \; , \tag{E.14}$$

with $\lambda = S, Q, A$ (similarly to the equal–time structure factor defined in Eq. (2.124)). where for dynamical structure factor for $\mathcal{A}$–matrices, we define

$$m_A{}^{\alpha}{}_{\beta}(\mathbf{q}, t_n) = \frac{1}{\sqrt{N}} \sum_{i=1}^{N} e^{i\mathbf{r}_i \mathbf{q}} \mathcal{A}_i^{\alpha}{}_{\beta}(t_n) \, , \tag{E.15}$$

(similarly to the time–independent moment Eq. (2.125)). For dipole– $m_S{}^{\alpha}{}_{\alpha}(\mathbf{q}, t)$ and quadrupole–moments $m_Q{}^{\alpha}{}_{\beta}(\mathbf{q}, t)$, we can obtain equivalent expressions by extension of Eq. (2.126) and Eq. (2.127).

In order to compare with experiments, it is usually more convenient to work with the time Fourier transformed structure factors

$$S_{\lambda}(\mathbf{q}, \omega_m) = \frac{1}{\sqrt{N_t}} \sum_{n=1}^{N_t} e^{i\omega_m t_n} \; S_{\lambda}(\mathbf{q}, t_n) \; , \tag{E.16}$$

where ω_m and $\mathbf{q}$ are discrete

$$\omega_m = m\ \delta\omega\ , \quad m = 0 \ldots N_{\mathrm{t}} - 1\ . \tag{E.17}$$

Additionally, we multiply the time–series entries used to compute Eq. (E.16) by a Gaussian envelope centered at $t_n = \Delta t/2$. This allows to avoid numerical artefacts (Gibbs phenomenon) due to discontinuities at $t = 0$ and $t = \Delta t$ [11]. We then evaluate the dynamical structure factor as expressed in Eq. (2.130) and Eq. (2.131), where Eq. (2.131) is computed by Fast Fourier transform (FFT) [194]. The Gaussian envelope multiplication is performed using

$$\overline{g}(t_n) = \frac{\delta t}{\delta\omega_n}\frac{\sigma}{\sqrt{2\pi}} e^{-\frac{\sigma^2}{2}(t_n - \Delta t/2)^2}\ , \tag{E.18}$$

and takes in a dimensional factor $\delta t/\delta\omega$ associated with integrals. We choose the value of σ such that the full–width half maximum (FWHM) of $\overline{g}(t_n)$ is $\approx \Delta t$. The introduction of the Gaussian envelope in time is equivalent to a convolution of $S_\lambda(\mathbf{q}, \omega)$ with a Gaussian in frequency space, with

$$\mathrm{FWHM} = 2\sqrt{2\ln 2} \times \sigma\ , \tag{E.19}$$

which is approximately equal to $\delta\omega$, and which determines the ultimate energy resolution of the results. Structure factors are then calculated by averaging over 500 independent time–series, each originated from separate initial states drawn from classical MC simulation.

Appendix F

Useful Gaussian Integrals

Here, I present useful Gaussian integrals that are used to calculate partition functions for the analytic derivations. Namely the following one–dimensional Gaussian integrals are used

$$\int e^{-\frac{1}{2}ax^2}\mathrm{d}x = \sqrt{\frac{2\pi}{a}}\ , \tag{F.1a}$$

$$\int e^{-\frac{1}{2}ax^2}e^{\pm bx}\mathrm{d}x = \sqrt{\frac{2\pi}{a}}e^{\frac{b^2}{2a}}\ , \tag{F.1b}$$

$$\int e^{-\frac{1}{2}ax^2}e^{\pm ibx}\mathrm{d}x = \sqrt{\frac{2\pi}{a}}e^{-\frac{b^2}{2a}}\ . \tag{F.1c}$$

These can be generalized to a multi-dimensions integral with a source term

$$\int e^{-\frac{1}{2}x_iA_{ij}x_j+B_ix_i}\mathrm{d}\vec{x} = \sqrt{\frac{(2\pi)^n}{\det A}}e^{\frac{1}{2}\vec{B}^TA^{-1}\vec{B}}\ , \tag{F.1d}$$

or more generally,

$$\int e^{-\frac{1}{2}x_iA^i{}_jx^j+B^T_{1,i}x^i+x_iB^i_2}\mathrm{d}\vec{x} = \sqrt{\frac{(2\pi)^n}{\det A}}e^{2\vec{B}^T_1A^{-1}\vec{B}_2}\ , \tag{F.1e}$$

where n is the dimension of the matrix $\mathbf{A}$. Below, I provide a proof of Eq. (F.1e).

Proof: We assume $\mathbf{A}$ to be a real symmetric $n\times n$-matrix. This means that $\mathbf{A}$ is orthogonally diagonalizable, i.e., it is similar to a diagonal matrix $\mathbf{D} = \mathrm{diag}(d^1{}_1,\ldots,d^n{}_n)$

$$\mathbf{A} = \mathbf{SDS}^{-1}\ , \tag{F.2}$$

and the $n\times n$ basis change matrix $\mathbf{S}$ is orthogonal. The basis change matrix $\mathbf{S}$ then satisfies

$$\mathbf{S}^T = \mathbf{S}^{-1}\ , \tag{F.3}$$

and the old coordinates are related to the new ones by

$$\vec{x} = \mathbf{S}\vec{y}\,, \tag{F.4a}$$
$$\vec{x}^T = \vec{y}\mathbf{S}^T\,, \tag{F.4b}$$
$$\mathrm{d}\vec{x} = \det\mathbf{S}\mathrm{d}\vec{y} = \mathrm{d}\vec{y}\,, \tag{F.4c}$$

where in the last line we used the fact that the Jacobian matrix of the map $\vec{x}(\vec{y}) \to \mathbf{S}\vec{y}$ is the matrix $\mathbf{S}$ itself, and that its determinant is 1, since it is an orthogonal matrix. The term in the exponential in Eq. (F.1e) then becomes

$$E := -\frac{1}{2}\vec{x}^T\mathbf{A}\vec{x} + \vec{B}_1^T\vec{x} + \vec{x}^T\vec{B}_2 \tag{F.5a}$$
$$= -\frac{1}{2}\vec{y}^T\mathbf{D}\vec{y} + \vec{B}_1^T\mathbf{S}\vec{y} + \vec{y}^T\mathbf{S}^{-1}\vec{B}_2\,. \tag{F.5b}$$

If we expand, we obtain:

$$E = \sum_i \left[-\frac{1}{2}y_i d^i{}_i y^i + \sum_\alpha \left(B^T_{1,\alpha}S^\alpha{}_i y^i + y_i(S^{-1})^i{}_\alpha B^\alpha_2\right)\right]\,, \tag{F.5c}$$

where we used the fact that $\mathbf{D}$ is a diagonal matrix. For the i^{th} term, we can complete the square as

$$\begin{aligned}
&-\frac{1}{2}y_i d^i{}_i y^i + \sum_\alpha \left(B^T_{1,\alpha}S^\alpha{}_i y^i + y_i(S^{-1})^i{}_\alpha B^i_2\right)\\
&= -\frac{1}{2}d^i_i(y_i - \frac{2}{d^i{}_i}\sum_\alpha B^T_{1,\alpha}S^\alpha{}_i)(y^i - \frac{2}{d^i_i}\sum_\beta (S^{-1})^i{}_\beta B^\beta_2) + 2\sum_\alpha\sum_\beta B^T_{1,\alpha}S^\alpha{}_i\frac{1}{d^i_i}(S^{-1})^i{}_\beta B^\beta_2\,.
\end{aligned} \tag{F.6}$$

Using again the fact that $d^i{}_i$ is the i^{th} diagonal term of $\mathbf{D}$, and inverting Eq. (F.2), we can rewrite $\frac{1}{d^i_i}$ as

$$\frac{1}{d^i_i} = (D^{-1})^i{}_i = \sum_{\mu,\nu}(S^{-1})^i{}_\mu(A^{-1})^\mu{}_\nu(S)^\nu{}_i\,. \tag{F.7}$$

Performing the variable change as

$$z_i = y_i - \frac{2}{d^i{}_i}\sum_\alpha B^T_{1,\alpha}S^\alpha{}_i\,, \tag{F.8a}$$
$$z^i = y^i - \frac{2}{d^i_i}\sum_\beta (S^{-1})^i{}_\beta B^\beta_2\,, \tag{F.8b}$$
$$\mathrm{d}\vec{z} = \mathrm{d}\vec{y}\,, \tag{F.8c}$$

inserting Eq. (F.7) into the last term of Eq. (F.6), and summing over all the compo-

nents, we obtain

$$E = -\frac{1}{2}\vec{z}^{T}\mathbf{D}\vec{z} + 2\vec{B}_1^{T}(\mathbf{A}^{-1})\vec{B}_2 \; . \tag{F.9a}$$

We now have the product of n Gaussian integrals of the form of Eq. (F.1a)

$$\begin{aligned}\int e^{-\frac{1}{2}x_i A^i{}_j x^j + B^T_{1,i}x^i + x_i B^i_2}\mathrm{d}\vec{x} &= \left[\prod_i \int e^{-\frac{1}{2}z_i d^i{}_i z^i}\mathrm{d}z_i\right] e^{2\vec{B}_1^{T}(\mathbf{A}^{-1})\vec{B}_2} \\ &= \sqrt{\frac{(2\pi)^n}{\prod_i d^i{}_i}}\, e^{2\vec{B}_1^{T}(\mathbf{A}^{-1})\vec{B}_2} \; .\end{aligned} \tag{F.10}$$

We then use the fact that

$$\det\mathbf{A} = \det\mathbf{S}\det\mathbf{D}\det\mathbf{S}^{-1} = \det\mathbf{D} = \prod_i d^i{}_i \; , \tag{F.11}$$

to obtain Eq. (F.1e).

Appendix G

Classical Structure Factors

In this Appendix, I provide details of the calculation of the equal time structure factors derived within the low–temperature classical analytic theory of fluctuations presented in Section 3.3.

Details for the classical structure factors at $\mathbf{q} \neq 0$ can be found in Appendix G.1 for dipole moments , in Appendix G.3 for quadrupole moments, and in Appendix G.5 for A–matrices . For the ground state contribution at $\mathbf{q} = 0$ which consists in taking into account up to quadratic order in the expansion of fluctuations, the general steps of the calculation are given in Section 3.3.4. The details for the classical structure factors at $\mathbf{q} = 0$ are provided in Appendix G.2 for the dipole moments, in Appendix G.4 for the quadrupole moments, in Appendix G.6 for the A–matrices.

G.1 Dipole Moments: Classical Structure Factor for $\mathbf{q} \neq 0$

First, we consider the structure factor for dipole moments of spin

$$S_{\mathrm{S}}^{\mathsf{CL}}(\mathbf{q}) \;=\; \sum_{\alpha} \langle \hat{\mathrm{S}}_{\mathbf{q}}^{\alpha} \hat{\mathrm{S}}_{-\mathbf{q}}^{\alpha} \rangle \; . \tag{G.1}$$

The relevant source term is

$$\Delta\mathcal{H}[h_{i,\beta}^{\alpha}] \;=\; -\sum_{i,\lambda} h_{i,\beta}^{\alpha} \delta_{\alpha\beta} \hat{\mathrm{S}}_{i,\lambda}^{\beta} \; . \tag{G.2}$$

According to Eq. (1.67) and using Eq. (3.10), we can express the spin dipole components in function of the fluctuations. Considering fluctuation terms up to 1$^{\mathrm{st}}$ order and using Eq. (3.25), the spin dipole moments in terms of the fluctuations diagonalizing the BBQ Hamiltonian are given by Eq. (3.36). Retaining terms linear in the fluctuations, we

obtain

$$\begin{aligned} \hat{\mathrm{S}}_i^x &= -\sqrt{2} v_{4,i} \ , \\ \hat{\mathrm{S}}_i^y &\simeq 0 \ , \\ \hat{\mathrm{S}}_i^z &= \sqrt{2} v_{2,i} \ . \end{aligned} \tag{G.3}$$

After performing a Fourier transform, the change in the Hamiltonian due to $\Delta\mathcal{H}[h_{i,\beta}^{\alpha}]$ [Eq. (G.2)] yields

$$\Delta\mathcal{H}[\mathbf{h}_{\mathbf{q}}] = -\sum_{\mathbf{q}} \left[\frac{\sqrt{2}}{2} h_{\mathbf{q}}^z v_{-\mathbf{q},2} + \frac{\sqrt{2}}{2} h_{-\mathbf{q}}^z v_{\mathbf{q},2} - \frac{\sqrt{2}}{2} h_{\mathbf{q}}^x v_{-\mathbf{q},4} - \frac{\sqrt{2}}{2} h_{-\mathbf{q}}^x v_{\mathbf{q},4} \right] \ ,$$

and according to Eq. (3.68), we get

$$\tilde{C}[\mathbf{h}_{\mathbf{q}}] = 0 \ , \tag{G.4}$$

where we neglected 2^{nd} order terms in fluctuations, since they only contribute for $\mathbf{q} = 0$, and

$$\begin{aligned} \tilde{\mathbf{N}}_1[\mathbf{h}_{\mathbf{q}}]^T &= \left(0, \quad \tfrac{\sqrt{2}}{2} h_{\mathbf{q}}^z, \quad 0, \quad -\tfrac{\sqrt{2}}{2} h_{\mathbf{q}}^x \right) \ , \\ \tilde{\mathbf{N}}_2[\mathbf{h}_{-\mathbf{q}}] &= \begin{pmatrix} 0 \\ \frac{\sqrt{2}}{2} h_{-\mathbf{q}}^z \\ 0 \\ -\frac{\sqrt{2}}{2} h_{-\mathbf{q}}^x \end{pmatrix} \ . \end{aligned} \tag{G.5}$$

According to Eq. (3.64), the first moments are given by the first derivative of $\tilde{C}[\mathbf{h}_{\mathbf{q}}]$ [Eq. (G.4)] with respect to the fictive field $\mathbf{h}$. We get

$$\langle S_{\mathbf{q}}^x \rangle = \langle S_{\mathbf{q}}^z \rangle = 0 \ . \tag{G.6}$$

The total structure factor for the dipole moment is given by Eq. (G.1), and using Eq. (3.74), Eq. (3.75), and Eq. (G.5), we obtain

$$S_{\mathrm{S}}^{\mathsf{CL}}(\mathbf{q} \neq 0) = \frac{2}{\beta\omega_{\mathbf{q},2}} + \frac{2}{\beta\omega_{\mathbf{q},4}} + \mathcal{O}(T^2) = \frac{4}{\beta\omega_{\mathbf{q}}^-} + \mathcal{O}(T^2) \ , \tag{G.7}$$

where we used Eq. (3.22b). Its spectral decomposition [Eq. (3.73)] becomes

$$S_{\mathrm{S}}^{\mathsf{CL}}(\mathbf{q} \neq 0, \omega) = \frac{4}{\beta\omega_{\mathbf{q}}^-} \delta(\omega - \omega_{\mathbf{q}}^-) + \mathcal{O}(T^2) \ . \tag{G.8}$$

G.2 Dipole Moments: Classical Structure Factor at $\mathbf{q} = 0$

We now consider the dipole structure factor at the origin of the reciprocal space called the Γ–point. We consider the structure factor for the spin dipole moments

$$S_{\mathrm{S}}^{\mathsf{CL}}(\mathbf{q}=0) \;=\; \sum_{\alpha} \langle \hat{\mathrm{S}}^{\alpha}_{\mathbf{q}=0} \hat{\mathrm{S}}^{\alpha}_{\mathbf{q}=0} \rangle \; . \tag{G.9}$$

We follow the procedure depicted in Section 3.3.4. The relevant source term for dipole moments is given by Eq. (G.2), which we need to rewrite in a similar form as Eq. (3.77). We use Eq. (3.10) and Eq. (1.67) to express the dipole moments in terms of the fluctuations ϕ, which is given by Eq. (3.12). We insert Eq. (3.12) into Eq. (G.2) and keep terms up to second order in fluctuations. We use Eq. (3.13)–Eq. (3.16) for the BBQ Hamiltonian. Then, for the total Hamiltonian given in Eq. (3.51), written in the form of Eq. (3.77), we obtain

$$M_{\mathbf{k}}[\mathbf{h}_{\mathbf{q}=0}] = \begin{pmatrix} A_{\mathbf{k}} & -B_{\mathbf{k}} & 0 & \frac{i}{\sqrt{N}} h^{y}_{\mathbf{q}=0,y} \\ -B_{\mathbf{k}} & A_{\mathbf{k}} & -\frac{i}{\sqrt{N}} h^{y}_{\mathbf{q}=0,y} & 0 \\ 0 & \frac{i}{\sqrt{N}} h^{y}_{\mathbf{q}=0,y} & A_{\mathbf{k}} & -B_{\mathbf{k}} \\ -\frac{i}{\sqrt{N}} h^{y}_{\mathbf{q}=0,y} & 0 & -B_{\mathbf{k}} & A_{\mathbf{k}} \end{pmatrix} , \tag{G.10}$$

$$\begin{aligned} \mathbf{N}_1[\mathbf{h}_{\mathbf{k}}]^T &= \tfrac{1}{2} \left(-h^{z}_{\mathbf{k},z}, \;\; -h^{z}_{\mathbf{k},z}, \;\; h^{x}_{\mathbf{k},x}, \;\; h^{x}_{\mathbf{k},x} \right) \; , \\ \mathbf{N}_2[\mathbf{h}_{-\mathbf{k}}] &= \tfrac{1}{2} \begin{pmatrix} -h^{z}_{-\mathbf{k},z} \\ -h^{z}_{-\mathbf{k},z} \\ h^{x}_{-\mathbf{k},x} \\ h^{x}_{-\mathbf{k},x} \end{pmatrix} \; , \end{aligned} \tag{G.11}$$

$$C[\mathbf{h}_{\mathbf{k}}] = 0 \; . \tag{G.12}$$

We diagonalize Eq. (G.10) to obtain the eigenmodes. We find

$$\begin{aligned} \omega^{+}_{\mathbf{k}}[\mathbf{h}_{\mathbf{q}=0}] &= \omega_{\mathbf{k},1}[\mathbf{h}_{\mathbf{q}=0}] = \omega_{\mathbf{k},3}[\mathbf{h}_{\mathbf{q}=0}] \\ &= A_{\mathbf{k}} + \sqrt{\left(\frac{h^{y}_{0,y}}{\sqrt{N}} \right)^{2} + B^{2}_{\mathbf{k}}} \; , \end{aligned} \tag{G.13a}$$

$$\begin{aligned} \omega^{-}_{\mathbf{k}}[\mathbf{h}_{\mathbf{q}=0}] &= \omega_{\mathbf{k},2}[\mathbf{h}_{\mathbf{q}=0}] = \omega_{\mathbf{k},4}[\mathbf{h}_{\mathbf{q}=0}] \\ &= A_{\mathbf{k}} - \sqrt{\left(\frac{h^{y}_{0,y}}{\sqrt{N}} \right)^{2} + B^{2}_{\mathbf{k}}} \; . \end{aligned} \tag{G.13b}$$

We now can calculate the spin dipole moments through Eq. (3.82), where we use Eq. (G.12), and Eq. (G.13), and where for the last term, we simply invert Eq. (G.10) and multiply by the vectors in Eq. (G.11). We obtain

$$\langle S^{x}_{\mathbf{q}=0} \rangle = \langle S^{y}_{\mathbf{q}=0} \rangle = \langle S^{z}_{\mathbf{q}=0} \rangle = 0 \; . \tag{G.14}$$

For the square dipole moments, we use Eq. (3.83). We find

$$\langle S^x_{\mathbf{q}=0} S^x_{\mathbf{q}=0}\rangle = \frac{2}{\beta}\frac{1}{A_{\mathbf{q}=0}-B_{\mathbf{q}=0}} = \frac{2}{\beta}\frac{1}{\omega_0^-} , \tag{G.15a}$$

$$\langle S^y_{\mathbf{q}=0} S^y_{\mathbf{q}=0}\rangle = 0 , \tag{G.15b}$$

$$\langle S^z_{\mathbf{q}=0} S^z_{\mathbf{q}=0}\rangle = \frac{2}{\beta}\frac{1}{A_{\mathbf{q}=0}-B_{\mathbf{q}=0}} = \frac{2}{\beta}\frac{1}{\omega_0^-} , \tag{G.15c}$$

where we used Eq. (3.22).

Finally, we calculate the dipole structure factor at the Γ–point given by Eq. (G.9). We get

$$S_{\mathrm{S}}^{\mathsf{CL}}(\mathbf{q}=0) \;=\; \frac{4}{\beta}\frac{1}{\omega_0^-} + \mathcal{O}(T^2) . \tag{G.16}$$

Because the $\mathbf{q}=0$ contributions are coming from the ground state and happen for $\omega = 0$, the spectral representation of Eq. (G.16) yields

$$S_{\mathrm{S}}^{\mathsf{CL}}(\mathbf{q}=0,\omega) \;=\; \frac{4}{\beta}\frac{1}{\omega_0^-}\delta(\omega) + \mathcal{O}(T^2) . \tag{G.17}$$

Combining Eq. (G.7) and Eq. (G.16), we get Eq. (3.85). And considering their respective spectral representation Eq. (G.8) and Eq. (G.17), we obtain Eq. (3.86).

G.3 Quadrupole Moments: Classical Structure Factor for $\mathbf{q} \neq 0$

Next, we consider the structure factor for quadrupole moments of spin

$$S_{\mathrm{Q}}^{\mathsf{CL}}(\mathbf{q}) \;=\; \sum_{\alpha\beta} \langle \hat{\mathrm{Q}}^{\alpha\beta}_{\mathbf{q}} \hat{\mathrm{Q}}^{\beta\alpha}_{-\mathbf{q}}\rangle , \tag{G.18}$$

where the scalar contraction implied by the sum on α, β respects $SU(2)$ symmetry. In this case the source term is

$$\Delta\mathcal{H}[\mathbf{h}_i] = -\sum_i h^{\alpha}_{i,\beta}\hat{\mathrm{Q}}^{\alpha\beta}_i . \tag{G.19}$$

The quadrupole components $\hat{\mathrm{Q}}^{\alpha\beta}_i$ in the function of the classical fluctuations can be found using Eq. (1.68) and Eq. (3.10). This is given by Eq. (3.35), where we keep terms up to linear order in the fluctuations. Using Eq. (3.25), we can express $\Delta\mathcal{H}[\mathbf{h}_i]$ in terms of the fluctuations that diagonalize the BBQ Hamiltonian. After performing a Fourier transform, and rewriting the Hamiltonian in the form of Eq. (3.68), we get

$$\tilde{C}[\mathbf{h}_{\mathbf{q}}] = \sqrt{N}\left(-\frac{4}{3}h^{yy}_{\mathbf{q}} + \frac{2}{3}(h^{xx}_{\mathbf{q}} + h^{zz}_{\mathbf{q}})\right) , \tag{G.20}$$

where we neglected 2nd order terms in fluctuations, since they only contribute for $\mathbf{q} = 0$, and

$$\tilde{\mathbf{N}}_1[\mathbf{h_q}]^T = \left(0, \quad \tfrac{i\sqrt{2}}{2}\xi^1_{\mathbf{q}}, \quad 0, \quad -\tfrac{i\sqrt{2}}{2}\xi^1_{\mathbf{q}}\right) ,$$
$$\tilde{\mathbf{N}}_2[\mathbf{h_{-q}}] = \begin{pmatrix} 0 \\ \frac{i\sqrt{2}}{2}\xi^1_{-\mathbf{q}} \\ 0 \\ -\frac{i\sqrt{2}}{2}\xi^1_{-\mathbf{q}} \end{pmatrix} , \tag{G.21}$$

where

$$\xi^1_{\mathbf{q}} = (h^{xy}_{\mathbf{q}} + h^{yx}_{\mathbf{q}}) \quad , \quad \xi^2_{\mathbf{q}} = (h^{yz}_{\mathbf{q}} + h^{zy}_{\mathbf{q}}) . \tag{G.22}$$

The total quadrupole structure factor is given by Eq. (G.18). According to Eq. (3.74) and Eq. (3.75), and using Eq. (G.21), we obtain

$$S^{\mathsf{CL}}_{\mathrm{Q}}(\mathbf{q} \neq 0) = \frac{4}{\beta\omega_{\mathbf{q},1}} + \frac{4}{\beta\omega_{\mathbf{q},3}} + \mathcal{O}(T^2) = \frac{8}{\beta\omega^+_{\mathbf{q}}} + \mathcal{O}(T^2) , \tag{G.23}$$

where we used Eq. (3.22a). Its spectral decomposition [Eq. (3.73)] becomes

$$S^{\mathsf{CL}}_{\mathrm{Q}}(\mathbf{q} \neq 0, \omega) = \frac{8}{\beta\omega^+_{\mathbf{q}}}\delta(\omega - \omega^+_{\mathbf{q}}) + \mathcal{O}(T^2) . \tag{G.24}$$

G.4 Quadrupole Moments: Classical Structure Factor at $\mathbf{q} = 0$

We now consider the quadrupole structure factor at the Γ–point, which is defined as

$$S^{\mathsf{CL}}_{\mathrm{Q}}(\mathbf{q} = 0) \;=\; \sum_{\alpha\beta} \langle \hat{\mathrm{Q}}^{\alpha\beta}_{\mathbf{q}=0} \hat{\mathrm{Q}}^{\beta\alpha}_{\mathbf{q}=0} \rangle . \tag{G.25}$$

We follow the same procedure as depicted in Section 3.3.4. The relevant source term for quadrupole moments is given by Eq. (G.19). We use Eq. (3.16) for the BBQ Hamiltonian as well as Eq. (3.10) and Eq. (1.68) to express Eq. (G.19) up to second order in terms of the fluctuations. For the total Hamiltonian given by Eq. (3.51),written in the form of Eq. (3.77), we obtain

$$M_{\mathbf{k}}[\mathbf{h}_{\mathbf{q}=0}] = \begin{pmatrix} A_{\mathbf{k}} + \alpha_1 & -B_{\mathbf{k}} & 0 & \beta_1 \\ -B_{\mathbf{k}} & A_{\mathbf{k}} + \alpha_1 & \beta_1 & 0 \\ 0 & \beta_1 & A_{\mathbf{k}} + \alpha_2 & -B_{\mathbf{k}} \\ \beta_1 & 0 & -B_{\mathbf{k}} & A_{\mathbf{k}} + \alpha_2 \end{pmatrix} , \tag{G.26}$$

$$\mathbf{N}_1[\mathbf{h_k}]^T = \tfrac{-i}{2}\left(-\xi^1_{\mathbf{k}}, \quad \xi^1_{\mathbf{k}}, \quad \xi^2_{\mathbf{k}}, \quad -\xi^2_{\mathbf{k}}\right) ,$$
$$\mathbf{N}_2[\mathbf{h_{-k}}] = \tfrac{i}{2}\begin{pmatrix} -\xi^1_{-\mathbf{k}} \\ \xi^1_{-\mathbf{k}} \\ \xi^2_{-\mathbf{k}} \\ -\xi^2_{-\mathbf{k}} \end{pmatrix} , \tag{G.27}$$

$$C[\mathbf{h}_{\mathbf{q}=0}] = \sqrt{N}\left(\frac{4}{3}h^y_{\mathbf{q}=0,y} - \frac{2}{3}(h^x_{\mathbf{q}=0,x} + h^z_{\mathbf{q}=0,z})\right) , \tag{G.28}$$

where we define

$$\begin{gathered}\alpha_1 = \tfrac{2}{\sqrt{N}}(h^x_{\mathbf{q}=0,x} - h^y_{\mathbf{q}=0,y}) , \quad \alpha_2 = \tfrac{2}{\sqrt{N}}(h^z_{\mathbf{q}=0,z} - h^y_{\mathbf{q}=0,y}) , \\ \beta_1 = \tfrac{1}{\sqrt{N}}(h^x_{\mathbf{q}=0,z} + h^z_{\mathbf{q}=0,x}) , \\ \xi^1_{\mathbf{k}} = (h^x_{\mathbf{k},y} + h^y_{\mathbf{k},x}) \quad , \quad \xi^2_{\mathbf{k}} = (h^y_{\mathbf{k},z} + h^z_{\mathbf{k},y}) .\end{gathered} \tag{G.29}$$

We diagonalize Eq. (G.26) to obtain the eigenmodes. We find

$$\omega_{\mathbf{k},1}[\mathbf{h}_{\mathbf{q}=0}] = A_{\mathbf{k}} + B^2_{\mathbf{k}} + \frac{1}{2}(\alpha_+ + \Delta) , \tag{G.30a}$$

$$\omega_{\mathbf{k},2}[\mathbf{h}_{\mathbf{q}=0}] = A_{\mathbf{k}} - B^2_{\mathbf{k}} + \frac{1}{2}(\alpha_+ + \Delta) , \tag{G.30b}$$

$$\omega_{\mathbf{k},3}[\mathbf{h}_{\mathbf{q}=0}] = A_{\mathbf{k}} + B^2_{\mathbf{k}} + \frac{1}{2}(\alpha_+ - \Delta) , \tag{G.30c}$$

$$\omega_{\mathbf{k},4}[\mathbf{h}_{\mathbf{q}=0}] = A_{\mathbf{k}} - B^2_{\mathbf{k}} + \frac{1}{2}(\alpha_+ - \Delta) , \tag{G.30d}$$

where

$$\alpha_+ = \alpha_1 + \alpha_2 \quad , \quad \Delta = \sqrt{(\alpha_1 - \alpha_2)^2 + 4\beta_1^2} . \tag{G.31}$$

Finally, we use Eq. (3.82) and Eq. (3.83) to compute the quadrupole structure factor at the Γ–point given by Eq. (G.25). When calculating Eq. (3.82) and Eq. (3.83), we use Eq. (G.28) and Eq. (G.30), and for the last term, we simply invert Eq. (G.26) and multiply by the vectors expressed in Eq. (G.27). We obtain

$$S^{\mathsf{CL}}_{\mathrm{Q}}(\mathbf{q}=0) \;=\; \frac{8}{\beta}\frac{1}{\omega_0^+} + \frac{8}{3}N - \frac{8}{\beta}\sum_{\mathbf{k}}\left[\frac{1}{\omega^+_{\mathbf{k}}} + \frac{1}{\omega^-_{\mathbf{k}}}\right] + \mathcal{O}(T^2) . \tag{G.32}$$

However, we note that at the Γ–point, $\omega_0^+ = 0$. Therefore, in order to get rid of confounding divergent terms, we rewrite the quadrupole structure factor as

$$S^{\mathsf{CL}}_{\mathrm{Q}}(\mathbf{q}=0) \;=\; -\frac{8}{\beta}\frac{1}{\omega_0^-} + \frac{8}{3}N - \frac{8}{\beta}\sum_{\mathbf{k}\neq 0}\left[\frac{1}{\omega^+_{\mathbf{k}}} + \frac{1}{\omega^-_{\mathbf{k}}}\right] + \mathcal{O}(T^2) . \tag{G.33}$$

Because the $\mathbf{q} = 0$ contributions are coming from the ground state and happen for

$\omega = 0$, the spectral representation of Eq. (G.33) yields

$$\begin{aligned} S_{\mathrm{Q}}^{\mathsf{CL}}(\mathbf{q}=0,\omega) &= -\frac{8}{\beta}\frac{1}{\omega_0^-}\delta(\omega) + \frac{8}{3}N\delta(\omega) \\ &\quad -\frac{8}{\beta}\sum_{\mathbf{k}\neq 0}\left[\frac{1}{\omega_{\mathbf{k}}^+}+\frac{1}{\omega_{\mathbf{k}}^-}\right]\delta(\omega) + \mathcal{O}(T^2)\ . \end{aligned} \tag{G.34}$$

Combining Eq. (G.23) and Eq. (G.33), we obtain Eq. (3.89). Considering their respective spectral representation given by Eq. (G.24) and Eq. (G.34), we obtain Eq. (3.91).

G.5 A-matrices: Classical Structure Factor $\mathbf{q} \neq 0$

The matrix $\hat{\mathcal{A}}^{\alpha}{}_{\beta}$ is the most fundamental object describing the spins, and their structure factors is defined by

$$S_{\mathrm{A}}^{\mathsf{CL}}(\mathbf{q}) = \sum_{\alpha\beta}\langle \hat{\mathcal{A}}^{\alpha}_{\mathbf{q}\ \beta}\hat{\mathcal{A}}^{\beta}_{-\mathbf{q}\ \alpha}\rangle\ . \tag{G.35}$$

We note that the sum on the contracted indices α, β preserves the full $U(3)$ symmetry of the representation. The corresponding source term is

$$\Delta\mathcal{H}[\mathbf{h}_i] = -\sum_i h^{\alpha}_{i,\beta}\hat{\mathcal{A}}^{\alpha}_{i\ \beta}\ . \tag{G.36}$$

The components of the A matrix $\hat{\mathcal{A}}^{\alpha}_{i\ \beta}$ in terms of the classical fluctuations are given in Eq. (3.10). After expressing them as a function of the fluctuations that diagonalize the BBQ Hamiltonian [Eq. (3.25)], we obtain Eq. (3.34), where we keep terms up to linear order in the fluctuations. After performing a Fourier transform, and rewriting the total Hamiltonian [Eq. (3.51)] according to Eq. (3.68), we get

$$\tilde{C}[\mathbf{h}_{\mathbf{q}}] = \sqrt{N}h^{yy}_{\mathbf{q}}\ , \tag{G.37}$$

where we neglected 2^{nd} order terms in fluctuations, since they only contribute for $\mathbf{q} = 0$,

$$\begin{aligned} \tilde{\mathbf{N}}_1[\mathbf{h}_{\mathbf{q}}]^T &= \left(\tfrac{i\sqrt{2}}{2}\xi^1_{\mathbf{q}},\ \ \tfrac{i\sqrt{2}}{2}\xi^1_{\mathbf{q}},\ \ -\tfrac{i\sqrt{2}}{2}\xi^2_{\mathbf{q}}\ \ -\tfrac{i\sqrt{2}}{2}\xi^2_{\mathbf{q}}\right)\ , \\ \tilde{\mathbf{N}}_2[\mathbf{h}_{-\mathbf{q}}] &= \begin{pmatrix} \frac{i\sqrt{2}}{2}\xi^1_{-\mathbf{q}} \\ \frac{i\sqrt{2}}{2}\xi^1_{-\mathbf{q}} \\ -\frac{i\sqrt{2}}{2}\xi^2_{-\mathbf{q}} \\ -\frac{i\sqrt{2}}{2}\xi^2_{-\mathbf{q}} \end{pmatrix}\ , \end{aligned} \tag{G.38}$$

where

$$\xi^1_{\mathbf{q}} = (h^{xy}_{\mathbf{q}} + h^{yx}_{\mathbf{q}}) \quad , \quad \xi^2_{\mathbf{q}} = (h^{yz}_{\mathbf{q}} + h^{zy}_{\mathbf{q}})\ . \tag{G.39}$$

The total structure factor for A matrices is obtained by computing Eq. (G.35).

According to Eq. (3.75), and Eq. (3.74), and using Eq. (G.38), we obtain

$$\begin{aligned} S_{\mathrm{A}}^{\mathsf{CL}}(\mathbf{q}\neq 0) =& \frac{1}{\beta\omega_{\mathbf{q},1}} + \frac{1}{\beta\omega_{\mathbf{q},2}} + \frac{1}{\beta\omega_{\mathbf{q},3}} + \frac{1}{\beta\omega_{\mathbf{q},4}} + \mathcal{O}(T^2) \\ =& \frac{2}{\beta\omega_{\mathbf{q}}^{+}} + \frac{2}{\beta\omega_{\mathbf{q}}^{-}} + \mathcal{O}(T^2)\ , \end{aligned} \tag{G.40}$$

where we used Eq. (3.22). Its spectral decomposition is given by

$$\begin{aligned} S_{\mathrm{A}}^{\mathsf{CL}}(\mathbf{q}\neq 0,\omega) =& \frac{2}{\beta\omega_{\mathbf{q}}^{+}}\delta(\omega-\omega_{\mathbf{q}}^{+}) + \frac{2}{\beta\omega_{\mathbf{q}}^{-}}\delta(\omega-\omega_{\mathbf{q}}^{-}) \\ &+ \mathcal{O}(T^2)\ . \end{aligned} \tag{G.41}$$

Again replacing the eigenvalues by their expressions given in Eq. (3.22), we have

$$\begin{aligned} S_{\mathrm{A}}^{\mathsf{CL}}(\mathbf{q}\neq 0,\omega) =& \frac{2}{\beta}\frac{1}{A_{\mathbf{q}}+B_{\mathbf{q}}}\delta(\omega-\omega_{\mathbf{q}}^{+}) \\ &+ \frac{2}{\beta}\frac{1}{A_{\mathbf{q}}-B_{\mathbf{q}}}\delta(\omega-\omega_{\mathbf{q}}^{-}) \\ &+ \mathcal{O}(T^2)\ . \end{aligned} \tag{G.42}$$

G.6 A-Matrices: Classical Structure Factor at $\mathbf{q}=0$

We now consider the structure factor for the A–matrix at the Γ–point, which is defined as

$$S_{\mathrm{A}}^{\mathsf{CL}}(\mathbf{q}=0) \;=\; \sum_{\alpha\beta}\langle \hat{\mathcal{A}}^{\alpha}_{\mathbf{q}=0\ \beta}\hat{\mathcal{A}}^{\beta}_{\mathbf{q}=0\ \alpha}\rangle\ . \tag{G.43}$$

Again, we follow the procedure depicted in Section 3.3.4. The relevant source term for dipole moments is given by Eq. (G.36). We use Eq. (3.16) for the BBQ Hamiltonian as well as Eq. (3.10) to express Eq. (G.36) up to second order in terms of the fluctuations. For the total Hamiltonian given in Eq. (3.51), and written in the form of Eq. (3.77), we obtain

$$M_{\mathbf{k}}[\mathbf{h}_{\mathbf{q}=0}] = \begin{pmatrix} A_{\mathbf{k}}-\alpha_1 & -B_{\mathbf{k}} & 0 & -\beta_1 \\ -B_{\mathbf{k}} & A_{\mathbf{k}}-\alpha_1 & -\beta_2 & 0 \\ 0 & -\beta_1 & A_{\mathbf{k}}-\alpha_2 & -B_{\mathbf{k}} \\ -\beta_2 & 0 & -B_{\mathbf{k}} & A_{\mathbf{k}}-\alpha_2 \end{pmatrix}\ , \tag{G.44}$$

$$\begin{aligned} \mathbf{N}_1[\mathbf{h}_{\mathbf{k}}]^T &= \tfrac{i}{2}\begin{pmatrix} -h^x_{\mathbf{k},y}, & h^y_{\mathbf{k},x}, & h^y_{\mathbf{k},z}, & -h^z_{\mathbf{k},y} \end{pmatrix}\ , \\ \mathbf{N}_2[\mathbf{h}_{-\mathbf{k}}] &= \tfrac{-i}{2}\begin{pmatrix} -h^y_{\mathbf{k},x} \\ h^x_{\mathbf{k},y} \\ h^z_{\mathbf{k},y} \\ -h^y_{\mathbf{k},z} \end{pmatrix}\ , \end{aligned} \tag{G.45}$$

$$C[\mathbf{h}_{\mathbf{q}=0}] = -\sqrt{N} h^y_{\mathbf{q}=0,y} \ , \tag{G.46}$$

where we defined

$$\begin{aligned} \alpha_1 = \tfrac{1}{\sqrt{N}}(h^x_{\mathbf{q}=0,x} - h^y_{\mathbf{q}=0,y}) \ , \quad \alpha_2 = \tfrac{1}{\sqrt{N}}(h^z_{\mathbf{q}=0,z} - h^y_{\mathbf{q}=0,y}) \ , \\ \beta_1 = \tfrac{1}{\sqrt{N}} h^z_{\mathbf{q}=0,x} \ , \quad \beta_2 = \tfrac{1}{\sqrt{N}} h^x_{\mathbf{q}=0,z} \ . \end{aligned} \tag{G.47}$$

We diagonalize Eq. (G.26) to obtain the eigenmodes. We find

$$\omega_{\mathbf{k},1}[\mathbf{h}_{\mathbf{q}=0}] = A_{\mathbf{k}} - \frac{1}{2}(\alpha_+ - \Delta^-) \ , \tag{G.48a}$$

$$\omega_{\mathbf{k},2}[\mathbf{h}_{\mathbf{q}=0}] = A_{\mathbf{k}} - \frac{1}{2}(\alpha_+ + \Delta^-) \ , \tag{G.48b}$$

$$\omega_{\mathbf{k},3}[\mathbf{h}_{\mathbf{q}=0}] = A_{\mathbf{k}} - \frac{1}{2}(\alpha_+ - \Delta^+) \ , \tag{G.48c}$$

$$\omega_{\mathbf{k},4}[\mathbf{h}_{\mathbf{q}=0}] = A_{\mathbf{k}} - \frac{1}{2}(\alpha_+ + \Delta^+) \ , \tag{G.48d}$$

where

$$\begin{aligned} \alpha_+ &= \alpha_1 + \alpha_2 \ , \\ \Delta^- &= \sqrt{\alpha_-^2 + 4(B_{\mathbf{k}}^2 + \beta_1\beta_2 - \sqrt{B_{\mathbf{k}}^2(\alpha_-^2 + \beta_-^2)})} \ , \\ \Delta^+ &= \sqrt{\alpha_-^2 + 4(B_{\mathbf{k}}^2 + \beta_1\beta_2 + \sqrt{B_{\mathbf{k}}^2(\alpha_-^2 + \beta_-^2)})} \ , \end{aligned} \tag{G.49}$$

with

$$\begin{aligned} \alpha_- &= \alpha_1 - \alpha_2 \ , \\ \beta_- &= \beta_1 - \beta_2 \ . \end{aligned} \tag{G.50}$$

Finally, we use Eq. (3.83) and Eq. (3.82) to compute the structure factor for the A–matrix at the Γ–point given by Eq. (G.43). When calculating Eq. (3.83) and Eq. (3.82), we use Eq. (G.46) and Eq. (G.48), and for the last term, we simply invert Eq. (G.44) and multiply by the vectors in Eq. (G.45). We obtain

$$\begin{aligned} S_{\mathrm{A}}^{\mathsf{CL}}(\mathbf{q} = 0) = \frac{2}{\beta}\left[\frac{1}{\omega_0^+} + \frac{1}{\omega_0^-}\right] \\ + N - \frac{2}{\beta}\sum_{\mathbf{k}}\left[\frac{1}{\omega_{\mathbf{k}}^+} + \frac{1}{\omega_{\mathbf{k}}^-}\right] + \mathcal{O}(T^2) \ . \end{aligned} \tag{G.51}$$

Again, just as for the quadrupole structure factor, we note that at the Γ–point, $\omega_0^+ = 0$. Therefore, in order to get rid of confounding divergent terms, we rewrite the structure

factor as

$$S_{\mathrm{A}}^{\mathsf{CL}}(\mathbf{q}=0) = N - \frac{2}{\beta}\sum_{\mathbf{k}\neq 0}\left[\frac{1}{\omega_{\mathbf{k}}^{+}} + \frac{1}{\omega_{\mathbf{k}}^{-}}\right] + \mathcal{O}(T^2)\ . \tag{G.52}$$

Because the $\mathbf{q} = 0$ contributions are coming from the ground state and happen for $\omega = 0$, the spectral representation of Eq. (G.52) yields

$$\begin{aligned} S_{\mathrm{A}}^{\mathsf{CL}}(\mathbf{q}=0,\omega) &= N\delta(\omega) \\ &\quad -\frac{2}{\beta}\sum_{\mathbf{k}\neq 0}\left[\frac{1}{\omega_{\mathbf{k}}^{+}} + \frac{1}{\omega_{\mathbf{k}}^{-}}\right]\delta(\omega) + \mathcal{O}(T^2)\ . \end{aligned} \tag{G.53}$$

Combining Eq. (G.40) and Eq. (G.52), we obtain Eq. (3.93). Considering their respective spectral representation given by Eq. (G.41) and Eq. (G.53), we obtain Eq. (3.94).

Appendix H

System Size Dependence of the Ordered Moment

In this Appendix, I present the details of the manufacturing of Section 3.4.2. More precisely, I explain how the simulation data for the ordered moment is fitted and how I calculated the ordered moment to extract its scaling behaviour with respect of system size, using the prediction obtained from the low temperature classical analytical theory [Section 3.3].

In Table (H.1), I show the temperature intervals on which the corresponding ordered parameters values are used for the fits of the slope $\alpha(L)$ of the ordered parameters in Fig. 3.5 (a), for different system sizes.

System size L	T_{min}	T_{max}
L=12	0.01	0.100177
L=24	0.01	0.100177
L=48	0.0252403	0.100177
L=96	0.0343658	0.100177

Table H.1: Temperature intervals used for fitting the parameter $\alpha(L)$ according to Eq. (3.108).

I also present here how the ordered moments as expressed by Eq. (3.99) and presented in Fig. 3.5 (b) are calculated. In order to compute Eq. (3.99), a sum in k–space needs to be performed. I here also show that the sum scales logarithmically with the system size L by explicitly calculating the coefficient μ corresponding to the logarithmic behavior [Eq. (H.6)]. To do this, I calculate the sum numerically for different system sizes L and fit it according to Eq. (H.6) (as shown by the orange line in Fig. 3.5 (b)). Additionally, I also transform the sum into an integral and extract the logarithmic scaling behavior.

In order to perform the sum in reciprocal space appearing in the analytical prediction of the order moment given in Eq. (3.99), the Brillouin zone is turned into a parallelogram of area $\frac{8\pi}{\sqrt{3}}$, as it is spanned by the reciprocal vectors $\mathbf{K}_a$ and $\mathbf{K}_b$ given in Eq. (D.2). We then discretize it into $N = L^2$ tiles of dimension δA given by

$$\delta\mathbf{k}_a = \tfrac{1}{L}\mathbf{K}_a \quad , \quad \delta\mathbf{k}_b = \tfrac{1}{L}\mathbf{K}_b \, , \tag{H.1}$$

such that

$$\delta A = \frac{8\pi^2}{\sqrt{3}L^2} \, . \tag{H.2}$$

In order to compare the logarithmic behaviour of the sum in Eq. (3.99) over reciprocal vectors performed numerically with the analytical logarithmic behaviour, we consider

$$\frac{1}{N}\sum_{\mathbf{k}} I_{\mathbf{k}} \Rightarrow N\delta A \sum_{k_x,k_x} I_{\mathbf{k}} = \int I_{\mathbf{k}} \mathrm{d}\mathbf{k} \, . \tag{H.3}$$

We can now sum over the k–space numerically, or integrate analytically.

In Eq. (H.3), we take as integrant the term expressed as a sum in the result obtained in Eq. (3.99), as we wish to compute the temperature–dependent part of the ordered moment given in Eq. (3.99)

$$\frac{1}{N}\sum_{\mathbf{k}} I_{\mathbf{k}} = \frac{8}{N}\sum_{\mathbf{k}\neq 0}\left[\frac{1}{\omega^{+}_{\mathbf{k}}} + \frac{1}{\omega^{-}_{\mathbf{k}}}\right] \, . \tag{H.4}$$

Using Eq. (3.22), we obtain

$$I_{\mathbf{k}} = \frac{16 A_{\mathbf{k}}}{\epsilon^2_{\mathbf{k},1}} \, , \tag{H.5}$$

where $\epsilon_{\mathbf{k},1}$ is given in Eq. (4.11). We then compute the discrete sum numerically according to Eq. (H.3) for the different system sizes, including the ones given in Table (H.1). When performing the sum, we also avoid the origin $\mathbf{k} = (0,0)$, where $\epsilon_{\mathbf{k},1}$ vanishes, (indeed, $\gamma(0) = 1$, and according to Eq. (3.17), $A_0 = B_0$) and which is not included in the sum of Eq. (3.99) . For a specific system size, we then get a number as the result of the discrete sum obtained for that specific system size. These numbers are plotted as the red dots in Fig. 3.5 (b) as a function of the system size.

According to Eq. (3.108), we assume that the system size dependency should be of the form

$$-\left.\frac{\mathrm{d}S^{CL}_{\mathrm{Q}}(\mathbf{q}=\Gamma)}{\mathrm{d}T}\right|_{T=0} = \frac{1}{N}\sum_{\mathbf{k}} I_{\mathbf{k}} \sim \; C + \mu\log(L) + \frac{\nu}{L} + \frac{\xi}{L^2} \, . \tag{H.6}$$

We use Eq. (H.6) to fit the results obtained by computing the discrete sum in Eq. (H.3), i.e, the red dots in Fig. 3.5 (b). The fit is shown in in Fig. 3.5 (b) by the orange line.

Additionally, we want to investigate how accurate the discrete sum is, compared to the integration, and how it depends on system size. If we consider the integral version in 2–dimensions for polar coordinates, we can cut off to some small $k_s = \frac{4\pi}{\sqrt{3}L}$ in order to avoid the origin $\mathbf{k} = (0,0)$ as follows:

$$\int I_{\mathbf{k}} \mathrm{d}\mathbf{k} = 2\pi \int_{k_s}^{k_f} I_{\mathbf{k}} k \mathrm{d}k \, . \tag{H.7}$$

For the FQ state, where we chose, $J_1 = 0.0$ and $J_2 = -1.0$, the coefficients $A_{\mathbf{k}}$ and $B_{\mathbf{k}}$

[Eq. (3.17)] and the dispersion relation $\epsilon_{\mathbf{k},1}$ [Eq. (4.11)] become

$$\begin{aligned} A_{\mathbf{k}} &= z \ , \\ B_{\mathbf{k}} &= -z\gamma(\mathbf{k}) \ , \\ \epsilon_{\mathbf{k}}^2 &= z^2(1-\gamma(\mathbf{k})^2) \ . \end{aligned} \tag{H.8}$$

For the triangular lattice, the geometrical factor is given by Eq. (D.5), and for sufficiently small values of k, we can use the Taylor expansion on it. We obtain

$$\gamma(\mathbf{k}) \simeq 1 - \frac{1}{4}(k_x^2 + k_y^2) = 1 - \frac{1}{4}k^2 \ , \tag{H.9a}$$

$$\epsilon_{\mathbf{k}}^2 \simeq z^2 \frac{1}{2} k^2 \ , \tag{H.9b}$$

$$I_{\mathbf{k}} = \frac{16 A_{\mathbf{k}}}{\epsilon_{\mathbf{k},1}^2} \simeq \frac{16z}{z^2 \frac{1}{2} k^2} = \frac{32}{zk^2} \ , \tag{H.9c}$$

$$2\pi \int_{k_s}^{k_f} I_{\mathbf{k}} k \mathrm{d}k \simeq 2\pi \int_{k_s}^{k_f} \frac{32}{zk^2} k \mathrm{d}k \ . \tag{H.9d}$$

Since $z = 6$ for the triangular lattice, we have

$$\begin{aligned} &\frac{2\pi 16}{3} \int_{k_s}^{k_f} \frac{1}{k} \mathrm{d}k = \frac{2\pi 16}{3} (\log(k_f) - \log(k_s)) \ , \\ &= \frac{2\pi 16}{3} \log(L) + \frac{2\pi 16}{3} \log(k_f) - \frac{2\pi 16}{3} \log(\frac{4\pi}{\sqrt{3}}) \ , \end{aligned} \tag{H.10}$$

where in the last line, we used the fact that we chose the cut–off according to $k_s = \frac{4\pi}{\sqrt{3}L}$. Before we fit the sum with the expression given by Eq. (H.6), we need to account for correction coming from the tiling of the k-space as explained in Eq. (H.3). Therefore, we need to divide by

$$\delta A * N = \frac{8\pi^2}{\sqrt{3}} \ . \tag{H.11}$$

From Eq. (H.6), we can obtain the value for the coefficient μ for Eq. (H.10), which we can compare with the fit from the values of the sum calculated numerically as shown in Fig. 3.5 (b) :

$$\mu_{ana} = \frac{\frac{2\pi 16}{3}}{\frac{8\pi^2}{\sqrt{3}}} = \frac{4}{\sqrt{3}\pi} = 0.735 \quad , \quad \mu_{num} = 0.735 \ . \tag{H.12}$$

Appendix I

Dynamical Structure Factors Within Zero–Temperature Quantum Theory

In this appendix, I provide the details of the method used to calculate the zero–temperature quantum structure factors in Section 4.2.

In Section 4.2.1, I presented how to calculate dynamical structure factors at finite energy through the explicit calculation of matrix elements within the quantum theory of fluctuations. Here, I provide details about its application to dipole moments [Appendix I.1], quadrupole moments [Appendix I.3], and A–matrices [Appendix I.5], which are summarized in the main text in Section 4.2.3, Section 4.2.4, and Section 4.2.5, respectively.

In Section 4.2.2, I explain how the calculation for the static structure factors ($\omega = 0$) can also be computed through functional derivatives of the ground–state energy, in order to account for the ground–state and zero–point energy contribution at $\mathbf{q} = 0$. Here, I show calculations for the dipole moments [Appendix I.2], quadrupole moments [Appendix I.4], and A–matrices [Appendix I.6].

I.1 Dipole Moments: Quantum Structure Factor at General Values of q

We consider first the spin dipole dynamical structure factor

$$S_{\mathrm{S}}^{\mathsf{QM}}(\mathbf{q},\omega) = \int_{-\infty}^{\infty} \frac{\mathrm{d}t}{2\pi} e^{i\omega t} \sum_{\mu} \langle \hat{\mathrm{S}}_{\mathbf{q}}^{\mu}(t) \hat{\mathrm{S}}_{-\mathbf{q}}^{\mu}(0) \rangle \ . \tag{I.1}$$

Substituting Eq. (4.4) in the expression for spin operators, Eq. (1.67), and keeping terms to linear order, we find

$$\hat{\mathrm{S}}_i^x \simeq i(\hat{\mathrm{b}}_i^{\dagger} - \hat{\mathrm{b}}_i) \ , \tag{I.2a}$$

$$\hat{\mathrm{S}}_i^y \simeq 0 \ , \tag{I.2b}$$

$$\hat{\mathrm{S}}_i^z \simeq -i(\hat{\mathrm{a}}_i^{\dagger} - \hat{\mathrm{a}}_i) \ . \tag{I.2c}$$

Performing a Fourier transform and using the Bogoliubov transformation Eq. (4.12), we can express these as

$$\hat{\mathrm{S}}^x_{\mathbf{q}} \simeq i\xi_{\mathsf{S}}(\mathbf{q})(\hat{\beta}^\dagger_{-\mathbf{q}} - \hat{\beta}_{\mathbf{q}}) \,, \tag{I.3a}$$

$$\hat{\mathrm{S}}^y_{\mathbf{q}} \simeq 0 \,, \tag{I.3b}$$

$$\hat{\mathrm{S}}^z_{\mathbf{q}} \simeq -i\xi_{\mathsf{S}}(\mathbf{q})(\hat{\alpha}^\dagger_{-\mathbf{q}} - \hat{\alpha}_{\mathbf{q}}) \,, \tag{I.3c}$$

where $\xi_{\mathsf{S}}(\mathbf{q})$ is the coherence factor

$$\xi_{\mathsf{S}}(\mathbf{q}) = \frac{\Delta_{\mathbf{q}} + B_{\mathbf{q}}}{\sqrt{\Delta^2_{\mathbf{q}} - B^2_{\mathbf{q}}}} \,. \tag{I.4}$$

Using Eq. (4.42), we can then calculate the structure factor for dipole moments as

$$S^{\mathsf{QM}}_{\mathrm{S}}(\mathbf{q},\omega) = \sum_{\mu,\mathbf{k}} \left| \langle n_{\mathbf{k}} | \hat{\mathrm{S}}^\mu_{\mathbf{q}} | 0 \rangle \right|^2 \delta(\omega - \omega_{n_{\mathbf{k}}}) + S^{\mathsf{GS}}_{\mathrm{S}}(\mathbf{q}=0,\omega) \,, \tag{I.5}$$

where $|0\rangle$ is the FQ ground state [Eq. (3.4)], and

$$|n_{\mathbf{k}}\rangle = \hat{\alpha}^\dagger_{\mathbf{k}}|0\rangle \otimes \hat{\beta}^\dagger_{\mathbf{k}}|0\rangle \,, \tag{I.6}$$

represents the first excited states where $\otimes$ implies a direct product, as the bosons $\hat{\alpha}^\dagger_{\mathbf{q}}$ and $\hat{\beta}^\dagger_{\mathbf{q}}$ are independent. By using Eq. (I.6), we account for the 1^{st} excited states and we therefore disregard the ground state and zero-point energy contribution to the structure factors, which is expressed by the term $S^{\mathsf{GS}}_{\mathrm{O}}(\mathbf{q}=0,\omega)$ in Eq. (I.5).

Finally, we find

$$S^{\mathsf{QM}}_{\mathrm{S}}(\mathbf{q},\omega) = 2\xi_{\mathsf{S}}(\mathbf{q})^2\delta(\omega - \epsilon(\mathbf{q})) + S^{\mathsf{GS}}_{\mathrm{S}}(\mathbf{q}=0,\omega) \tag{I.7a}$$

$$= 2\frac{\sqrt{A_{\mathbf{q}} + B_{\mathbf{q}}}}{\sqrt{A_{\mathbf{q}} - B_{\mathbf{q}}}}\delta(\omega - \epsilon(\mathbf{q})) + S^{\mathsf{GS}}_{\mathrm{S}}(\mathbf{q}=0,\omega) \,, \tag{I.7b}$$

where we used Eq. (I.4) and Eq. (4.13) in the last line. Detailed calculations for $\mathbf{q}=0$ contributions to the dipole moment structure factor can be found in Appendix I.2. More precisely, $S^{\mathsf{GS}}_{\mathrm{S}}(\mathbf{q}=0,\omega)$ is given by Eq. (I.16), which combined with Eq. (I.7b) gives the total quantum structure factor for the dipole moments expressed in Eq. (4.71).

I.2 Dipole Moments: Contribution of the Ground State to the Quantum Structure Factor at $\mathbf{q}=0$

We consider the structure factor at $\mathbf{q}=0$ for dipole moments of spin

$$S^{\mathsf{GS}}_{\mathrm{S}}(\mathbf{q}=0) \;=\; \sum_\alpha \langle \hat{\mathrm{S}}^\alpha_{\mathbf{q}=0} \hat{\mathrm{S}}^\alpha_{-\mathbf{q}=0} \rangle_{T=0} \,. \tag{I.8}$$

The relevant source term is given by Eq. (G.2). According to Eq. (1.67) and using Eq. (4.4), we can express Eq. (G.2) in function of fluctuations orthogonal to the FQ ground state [Eq. (3.2)]. Considering fluctuation terms up to 2$^{\text{nd}}$ order, we have

$$\begin{aligned} \hat{\mathrm{S}}_i^x &= -i(\hat{\mathrm{b}}_i - \hat{\mathrm{b}}_i^\dagger) \, , \\ \hat{\mathrm{S}}_i^y &= i(\hat{\mathrm{a}}_i^\dagger \hat{\mathrm{b}}_i - \hat{\mathrm{a}}_i \hat{\mathrm{b}}_i^\dagger) \, , \\ \hat{\mathrm{S}}_i^z &= -i(\hat{\mathrm{a}}_i^\dagger - \hat{\mathrm{a}}_i) \, . \end{aligned} \tag{I.9}$$

After performing a Fourier transform, and considering the source term Hamiltonian $\Delta\mathcal{H}[h^\alpha_{i,\beta}]$ [Eq. (G.2)] at $\mathbf{q} = 0$, we have

$$\begin{aligned} \Delta\mathcal{H}[\mathbf{h_q}] = &- \sum_{\mathbf{q}} \left[i h^x_{-\mathbf{q}} (\hat{\mathrm{b}}^\dagger_{\mathbf{q}} - \hat{\mathrm{b}}_{\mathbf{q}}) - i h^z_{-\mathbf{q}} (\hat{\mathrm{a}}^\dagger_{\mathbf{q}} - \hat{\mathrm{a}}_{\mathbf{q}}) \right] \delta_{\mathbf{q},0} \\ &- \sum_{\mathbf{k}} \frac{i}{\sqrt{N}} h^y_{\mathbf{q}=0} (\hat{\mathrm{a}}^\dagger_{\mathbf{k}} \hat{\mathrm{b}}_{\mathbf{k}} - \hat{\mathrm{a}}_{\mathbf{k}} \hat{\mathrm{b}}^\dagger_{\mathbf{k}}) \, . \end{aligned} \tag{I.10}$$

And using Eq. (4.5) for the BBQ Hamiltonian, the total Hamiltonian [Eq. (3.51)] in terms of the bosons takes the same form as in Eq. (4.50), where $M_{\mathbf{k}}[\mathbf{h}_{\mathbf{q}=0}]$ is given by

$$M_{\mathbf{k}}[\mathbf{h}_{\mathbf{q}=0}] = \begin{pmatrix} A_{\mathbf{k}} & -B_{\mathbf{k}} & -\frac{i}{\sqrt{N}} h^y_{\mathbf{q}=0} & 0 \\ -B_{\mathbf{k}} & A_{\mathbf{k}} & 0 & \frac{i}{\sqrt{N}} h^y_{\mathbf{q}=0} \\ \frac{i}{\sqrt{N}} h^y_{\mathbf{q}=0} & 0 & A_{\mathbf{k}} & -B_{\mathbf{k}} \\ 0 & -\frac{i}{\sqrt{N}} h^y_{\mathbf{q}=0} & -B_{\mathbf{k}} & A_{\mathbf{k}} \end{pmatrix} \, , \tag{I.11a}$$

where $A_{\mathbf{k}}$ and $B_{\mathbf{k}}$ are given in Eq. (3.17) and where $\mathbf{N}[\mathbf{h_k}]$ is given by

$$\mathbf{N}[\mathbf{h_k}] = i \begin{pmatrix} h^z_{-\mathbf{k}} \\ -h^z_{\mathbf{k}} \\ -h^x_{-\mathbf{k}} \\ h^x_{\mathbf{k}} \end{pmatrix} \, , \tag{I.11b}$$

and where $C[\mathbf{h}_{\mathbf{q}=0}]$ holds

$$C[\mathbf{h}_{\mathbf{q}=0}] = 0 \, . \tag{I.11c}$$

Following the procedure depicted in Section 4.1 and detailed in Appendix C, we perform a Bogoliubov transformation. The eigenvalues $\epsilon_{\mathbf{k},\lambda}$ are given by

$$\epsilon_{\mathbf{k},1}[\mathbf{h}_{\mathbf{q}=0}] = -\epsilon_{\mathbf{k},2} = +\sqrt{A^2_{\mathbf{k}} - B^2_{\mathbf{k}}} + \frac{1}{\sqrt{N}} h^y_{\mathbf{q}=0} \, , \tag{I.12a}$$

$$\epsilon_{\mathbf{k},3}[\mathbf{h}_{\mathbf{q}=0}] = -\epsilon_{\mathbf{k},4} = +\sqrt{A^2_{\mathbf{k}} - B^2_{\mathbf{k}}} - \frac{1}{\sqrt{N}} h^y_{\mathbf{q}=0} \, . \tag{I.12b}$$

After performing the Bogoliubov transformation, the Hamiltonian can be rewritten as

follows:

$$\mathcal{H} = E_0 + \Delta E_0[\mathbf{h}_{\mathbf{q}=0}] + \sum_{\mathbf{k}} \left[\epsilon_{\mathbf{k},1}[\mathbf{h}_{\mathbf{q}=0}] \hat{\alpha}^\dagger_{\mathbf{k}} \hat{\alpha}_{\mathbf{k}} + \epsilon_{\mathbf{k},3}[\mathbf{h}_{\mathbf{q}=0}] \hat{\beta}^\dagger_{\mathbf{k}} \hat{\beta}_{\mathbf{k}} \right] , \tag{I.13}$$

where $C[\mathbf{h}_{\mathbf{q}=0}]$ is disregarded since it is null [Eq. (I.11c)], and where $\Delta E_0[\mathbf{h}_{\mathbf{q}=0}]$ is the zero–point energy

$$\Delta E_0[\mathbf{h}_{\mathbf{q}=0}] \;=\; \frac{1}{2} \sum_{\mathbf{k}} \left[\epsilon_{\mathbf{k},1}[\mathbf{h}_{\mathbf{q}=0}] + \epsilon_{\mathbf{k},3}[\mathbf{h}_{\mathbf{q}=0}] \right] . \tag{I.14}$$

According to Eq. (4.64), the ground state contribution to the first moments yield

$$\langle S^x_{\mathbf{q}} \rangle_{T=0} = \langle S^z_{\mathbf{q}} \rangle_{T=0} = 0 , \tag{I.15a}$$

$$\langle S^y_{\mathbf{q}} \rangle_{T=0} = \frac{1}{2} \sum_{\mathbf{k}} \left[\frac{1}{\sqrt{N}} - \frac{1}{\sqrt{N}} \right] = 0 . \tag{I.15b}$$

And according to Eq. (4.65) and Eq. (I.8), the spin dipole structure factor at $\mathbf{q} = 0$ yields

$$S^{\mathsf{GS}}_{\mathrm{S}}(\mathbf{q} = 0) \;=\; 0 . \tag{I.16}$$

Indeed, the ground state is quadrupolar and does not break time–reversal symmetry. Therefore, at zero temperature, the contribution of quantum fluctuations from the zero–point energy should average to zero for the spin dipole moments. The spectral representation of Eq. (I.16) is then also trivially null. Combining Eq. (I.7b) and Eq. (I.16), we obtain Eq. (4.71).

I.3 Quadrupole Moments: Quantum Structure Factor at General Values of q

We now consider the dynamical structure factor associated with quadrupole moments

$$S^{\mathsf{QM}}_{\mathrm{Q}}(\mathbf{q}, \omega) = \int_{-\infty}^{\infty} \frac{\mathrm{d}t}{2\pi} e^{i\omega t} \sum_{\mu\nu} \langle \hat{\mathrm{Q}}^{\mu\nu}_{\mathbf{q}}(t) \hat{\mathrm{Q}}^{\mu\nu}_{-\mathbf{q}}(0) \rangle . \tag{I.17}$$

Following the same steps as for the spin–structure factor, we use Eq. (4.4) to express the quadupole components up to linear order in Eq. (1.68). We find

$$\hat{\mathbf{Q}}_i \cong \begin{pmatrix} \frac{2}{3} & -\hat{\mathrm{a}}^\dagger_i - \hat{\mathrm{a}}_i & 0 \\ -\hat{\mathrm{a}}^\dagger_i - \hat{\mathrm{a}}_i & -\frac{4}{3} & -\hat{\mathrm{b}}^\dagger_i - \hat{\mathrm{b}}_i \\ 0 & -\hat{\mathrm{b}}^\dagger_i - \hat{\mathrm{b}}_i & \frac{2}{3} \end{pmatrix} . \tag{I.18}$$

An equivalent calculation of matrix elements in the Bogoliubov basis [Eq. (4.12)] yields

$$\hat{\mathbf{Q}}_{\mathbf{q}} \cong \begin{pmatrix} \frac{2}{3}\sqrt{N}\delta(\mathbf{q}) & \xi_{\mathsf{Q}}(\mathbf{q})(\hat{\alpha}^{\dagger}_{-\mathbf{q}} + \hat{\alpha}_{\mathbf{q}}) & 0 \\ \xi_{\mathsf{Q}}(\mathbf{q})(\hat{\alpha}^{\dagger}_{-\mathbf{q}} + \hat{\alpha}_{\mathbf{q}}) & -\frac{4}{3}\sqrt{N}\delta(\mathbf{q}) & \xi_{\mathsf{Q}}(\mathbf{q})(\hat{\beta}^{\dagger}_{-\mathbf{q}} + \hat{\beta}_{\mathbf{q}}) \\ 0 & \xi_{\mathsf{Q}}(\mathbf{q})(\hat{\beta}^{\dagger}_{-\mathbf{q}} + \hat{\beta}_{\mathbf{q}}) & \frac{2}{3}\sqrt{N}\delta(\mathbf{q}) \end{pmatrix} , \tag{I.19}$$

where N is the number of sites and where $\xi_{\mathsf{Q}}(\mathbf{q})$ is the coherence factor for quadrupoles defined as

$$\xi_{\mathsf{Q}}(\mathbf{q}) = \frac{B_{\mathbf{q}} - \Delta_{\mathbf{q}}}{\sqrt{\Delta_{\mathbf{q}}^2 - B_{\mathbf{q}}^2}} . \tag{I.20}$$

Using Eq. (4.42), we can then calculate the structure factor for quadrupole moments as defined in Eq. (I.17). We obtain

$$S_{\mathrm{Q}}^{\mathsf{QM}}(\mathbf{q},\omega) = 4\xi_{\mathsf{Q}}(\mathbf{q})^2\delta(\omega - \epsilon(\mathbf{q})) + S_{\mathrm{Q}}^{\mathsf{GS}}(\mathbf{q}=0,\omega) \tag{I.21a}$$

$$= 4\frac{\sqrt{A_{\mathbf{q}} - B_{\mathbf{q}}}}{\sqrt{A_{\mathbf{q}} + B_{\mathbf{q}}}}\delta(\omega - \epsilon(\mathbf{q})) + S_{\mathrm{Q}}^{\mathsf{GS}}(\mathbf{q}=0,\omega) , \tag{I.21b}$$

where we used Eq. (I.20) and Eq. (4.13) in the last line.

Detailed calculations for $\mathbf{q} = 0$ contributions to the quadrupole moment structure factor can be found in Appendix I.4. More precisely, $S_{\mathrm{Q}}^{\mathsf{GS}}(\mathbf{q}=0,\omega)$ is given by Eq. (I.32), which combined with Eq. (I.21) gives the total quantum structure factor for the quadrupole moments expressed in Eq. (4.78).

I.4 Quadrupole Moments: Contribution of the Ground State to the Quantum Structure Factor at $\mathbf{q} = 0$

We now consider the quadrupole structure factor at the Γ–point, which is defined as

$$S_{\mathrm{Q}}^{\mathsf{GS}}(\mathbf{q}=0) \;=\; \sum_{\alpha\beta} \langle \hat{\mathrm{Q}}^{\alpha\beta}_{\mathbf{q}=0} \hat{\mathrm{Q}}^{\beta\alpha}_{\mathbf{q}=0} \rangle_{T=0} . \tag{I.22}$$

We follow the same procedure as depicted in Section 4.2.2. The relevant source term for quadrupole moments is given by Eq. (G.19). We can express Eq. (G.19) up to second order in terms of the bosons by using Eq. (4.4) and Eq. (1.68). We use Eq. (4.5) for the BBQ Hamiltonian. For the total Hamiltonian given by Eq. (3.51), written in the form of Eq. (4.50), we find that $M_{\mathbf{k}}[\mathbf{h}_{\mathbf{q}=0}]$ is given by

$$M_{\mathbf{k}}[\mathbf{h}_{\mathbf{q}=0}] = \begin{pmatrix} A_{\mathbf{k}} + \alpha_1 & -B_{\mathbf{k}} & \beta_1 & 0 \\ -B_{\mathbf{k}} & A_{\mathbf{k}} + \alpha_1 & 0 & \beta_1 \\ \beta_1 & 0 & A_{\mathbf{k}} + \alpha_2 & -B_{\mathbf{k}} \\ \beta_1 & 0 & -B_{\mathbf{k}} & A_{\mathbf{k}} + \alpha_2 \end{pmatrix} , \tag{I.23a}$$

that $\mathbf{N}[\mathbf{h}_\mathbf{k}]$ is given by

$$\mathbf{N}[\mathbf{h}_\mathbf{k}] = \begin{pmatrix} \xi^1_{-\mathbf{k}} \\ \xi^1_{\mathbf{k}} \\ \xi^2_{-\mathbf{k}} \\ \xi^2_{-\mathbf{k}} \end{pmatrix} , \tag{I.23b}$$

and that $C[\mathbf{h}_{\mathbf{q}=0}]$ holds

$$C[\mathbf{h}_{\mathbf{q}=0}] = \sqrt{N} \left(\frac{4}{3} h^y_{\mathbf{q}=0,y} - \frac{2}{3} (h^x_{\mathbf{q}=0,x} + h^z_{\mathbf{q}=0,z}) \right) , \tag{I.23c}$$

with $A_\mathbf{k}$ and $B_\mathbf{k}$ being given in Eq. (3.17) and with the following definitions

$$\begin{aligned} \alpha_1 = \tfrac{2}{\sqrt{N}} (h^x_{\mathbf{q}=0,x} - h^y_{\mathbf{q}=0,y}) , \quad \alpha_2 = \tfrac{2}{\sqrt{N}} (h^z_{\mathbf{q}=0,z} - h^y_{\mathbf{q}=0,y}) , \\ \beta_1 = \tfrac{1}{\sqrt{N}} (h^x_{\mathbf{q}=0,z} + h^z_{\mathbf{q}=0,x}) , \\ \xi^1_\mathbf{k} = (h^x_{\mathbf{k},y} + h^y_{\mathbf{k},x}) \quad , \quad \xi^2_\mathbf{k} = (h^y_{\mathbf{k},z} + h^z_{\mathbf{k},y}) . \end{aligned} \tag{I.24}$$

Following the procedure depicted in Section 4.1 and detailed in Appendix C, we perform a Bogoliubov transformation. The eigenvalues $\epsilon_{\mathbf{k},\lambda}$ are given by

$$\begin{aligned} &\epsilon_{\mathbf{k},1}[\mathbf{h}_{\mathbf{q}=0}] = -\epsilon_{\mathbf{k},2}[\mathbf{h}_{\mathbf{q}=0}] = \\ &\sqrt{A^2_\mathbf{k} - B^2_\mathbf{k} + \beta_1^2 + \frac{1}{2}\left(\alpha_1^2 + \alpha_2^2\right) + A_\mathbf{k}\alpha^+ - \Delta \left(A_\mathbf{k} + \frac{\alpha^+}{2} \right)} , \end{aligned} \tag{I.25a}$$

$$\begin{aligned} &\epsilon_{\mathbf{k},3}[\mathbf{h}_{\mathbf{q}=0}] = -\epsilon_{\mathbf{k},4}[\mathbf{h}_{\mathbf{q}=0}] = \\ &\sqrt{A^2_\mathbf{k} - B^2_\mathbf{k} + \beta_1^2 + \frac{1}{2}\left(\alpha_1^2 + \alpha_2^2\right) + A_\mathbf{k}\alpha^+ + \Delta \left(A_\mathbf{k} + \frac{\alpha^+}{2} \right)} , \end{aligned} \tag{I.25b}$$

where α^+ and Δ are defined in Eq. (G.31). After performing the Bogoliubov transformation, the Hamiltonian can be rewritten as follows:

$$\begin{aligned} \mathcal{H} =& E_0 + \Delta E_0[\mathbf{h}_{\mathbf{q}=0}] + C[\mathbf{h}_{\mathbf{q}=0}] \\ &+ \left[\sum_\mathbf{k} \epsilon_{\mathbf{k},1}[\mathbf{h}_{\mathbf{q}=0}] \hat{\alpha}^\dagger_\mathbf{k} \hat{\alpha}_\mathbf{k} + \epsilon_{\mathbf{k},3}[\mathbf{h}_{\mathbf{q}=0}] \hat{\beta}^\dagger_\mathbf{k} \hat{\beta}_\mathbf{k} \right] , \end{aligned} \tag{I.26}$$

where $C[\mathbf{h}_{\mathbf{q}=0}]$ is given in Eq. (I.23c), and where $\Delta E_0[\mathbf{h}_{\mathbf{q}=0}]$ is the zero–point energy and yields

$$\Delta E_0[\mathbf{h}_{\mathbf{q}=0}] \;=\; \frac{1}{2} \sum_\mathbf{k} \left[\epsilon_{\mathbf{k},1}[\mathbf{h}_{\mathbf{q}=0}] + \epsilon_{\mathbf{k},3}[\mathbf{h}_{\mathbf{q}=0}] \right] . \tag{I.27}$$

According to Eq. (4.64), the ground state contribution to the first moments yield

$$\langle Q^{xx}_{\mathbf{q}=0}\rangle_{T=0} = -\frac{2}{3}\sqrt{N} + \frac{1}{\sqrt{N}}\sum_{\mathbf{k}}\left[\frac{A_{\mathbf{k}}}{\sqrt{A^2_{\mathbf{k}} - B^2_{\mathbf{k}}}}\right] , \tag{I.28a}$$

$$\langle Q^{xy}_{\mathbf{q}=0,y}\rangle_{T=0} = \langle Q^{yx}_{\mathbf{q}=0}\rangle_{T=0} = 0 , \tag{I.28b}$$

$$\langle Q^{xz}_{\mathbf{q}=0,z}\rangle_{T=0} = \langle Q^{zx}_{\mathbf{q}=0}\rangle_{T=0} = 0 , \tag{I.28c}$$

$$\langle Q^{yy}_{\mathbf{q}=0,y}\rangle_{T=0} = \frac{4}{3}\sqrt{N} - \frac{1}{\sqrt{N}}\sum_{\mathbf{k}}\left[\frac{2A_{\mathbf{k}}}{\sqrt{A^2_{\mathbf{k}} - B^2_{\mathbf{k}}}}\right] , \tag{I.28d}$$

$$\langle Q^{yz}_{\mathbf{q}=0,z}\rangle_{T=0} = \langle Q^{zy}_{\mathbf{q}=0}\rangle_{T=0} = 0 , \tag{I.28e}$$

$$\langle Q^{zz}_{\mathbf{q}=0}\rangle_{T=0} = -\frac{2}{3}\sqrt{N} + \frac{1}{\sqrt{N}}\sum_{\mathbf{k}}\left[\frac{A_{\mathbf{k}}}{\sqrt{A^2_{\mathbf{k}} - B^2_{\mathbf{k}}}}\right] . \tag{I.28f}$$

Before calculating the structure factor, we note that, as given in Eq. (I.28), the first quadrupole moments consist of two terms with different scaling behaviour with respect to the parameter we expand fluctuations about, which is the length of the spin s. Indeed, similarly to multi-bosons expansion, or its linear spin-wave version with Holstein–Primakoff bosons or Schwinger bosons in the case of a $su(2)$ representation of the spin, we assume the fluctuations to be sufficiently small compared to the spin length s. In other words, $C[\mathbf{h}_{\mathbf{q}=0}]$ from Eq. (I.23c) and the eigenvalues in Eq. (I.25) scale with s as

$$C[\mathbf{h}_{\mathbf{q}=0}] \sim s h^{\mu}_{\mathbf{q}=0\mu} , \tag{I.29a}$$

$$\epsilon_{\mathbf{k},\lambda}[\mathbf{h}_{\mathbf{q}=0}] \sim s\sqrt{Const. + \frac{h^{\mu}_{\mathbf{q}=0\mu}}{s^2} + \frac{\mathcal{O}(\mathbf{h}^2_{\mathbf{q}=0})}{s^2}} . \tag{I.29b}$$

Their derivatives with respect to $h^{\mu}_{\mathbf{q}=0,\mu}$ that enters the quadrupole moments [Eq. (4.64)] yield

$$\left.\frac{C[\mathbf{h}_{\mathbf{q}=0}]}{\partial h^{\mu}_{\mathbf{q}=0,\mu}}\right|_{\mathbf{h}=\mathbf{0}} \sim s , \tag{I.30a}$$

$$\left.\frac{\partial\epsilon_{\mathbf{k},\lambda}[\mathbf{h}_{\mathbf{q}=0}]}{\partial h^{\mu}_{\mathbf{q}=0,\mu}}\right|_{\mathbf{h}=\mathbf{0}} \sim \frac{s}{\sqrt{Const.}}\left.\frac{\partial\frac{h^{\mu}_{\mathbf{q}=0\mu}}{s^2}}{\partial h^{\mu}_{\mathbf{q}=0,\mu}}\right|_{\mathbf{h}=\mathbf{0}} \sim \frac{1}{s} .$$

This implies that the scaling behaviour of the first quadrupole moments goes as

$$\langle Q^{\mu\mu}_{\mathbf{q}=0}\rangle_{T=0} \sim s + \frac{1}{s} , \tag{I.31}$$

where s is the length of the spin. We now argue that because our approximation is valid up to linear order in $\frac{1}{s}$, i.e., second order in fluctuations, we can disregard $\frac{1}{s^2}$ terms. $\frac{1}{s^2}$ terms are physical but should not enter into our level of approximation. Indeed, one would expect additional contributions to the $\frac{1}{s^2}$ term coming from higher orders

in perturbation theory. However, we do not take these into account here and simply consider terms up to $\frac{1}{s}$. According to Eq. (4.65) and Eq. (I.22), the spin quadrupole structure factor at $\mathbf{q} = 0$ yields

$$S_{\mathsf{Q}}^{\mathsf{GS}}(\mathbf{q}=0) \;=\; \frac{8}{3}N - 8\sum_{\mathbf{k}}\left[\frac{A_{\mathbf{k}}}{\sqrt{A_{\mathbf{k}}^2 - B_{\mathbf{k}}^2}}\right] + \mathcal{O}(\frac{1}{s^2})\;. \tag{I.32}$$

Its spectral representation is given by

$$S_{\mathsf{Q}}^{\mathsf{GS}}(\mathbf{q}=0,\omega) \;=\; \left(\frac{8}{3}N - 8\sum_{\mathbf{k}}\left[\frac{A_{\mathbf{k}}}{\sqrt{A_{\mathbf{k}}^2 - B_{\mathbf{k}}^2}}\right]\right)\delta(\omega) + \mathcal{O}(\frac{1}{s^2})\;. \tag{I.33}$$

Combining Eq. (I.21) and Eq. (I.33), we obtain Eq. (4.78).

I.5 A–Matrices : Quantum Structure Factors at General Values of q

The most fundamental objects in our theory are not dipoles or quadrupoles, but the A–matrices which describe the quantum state of the spin–1 moment. It is therefore useful to introduce a dynamical structure factor

$$S_{\mathsf{A}}^{\mathsf{QM}}(\mathbf{q},\omega) = \int_{-\infty}^{\infty}\frac{\mathrm{d}t}{2\pi}e^{i\omega t}\sum_{\mu\nu}\langle\hat{\mathcal{A}}^{\mu}{}_{\nu}(t)\hat{\mathcal{A}}^{\nu}{}_{\mu}(0)\rangle\;. \tag{I.34}$$

Neglecting 2^{nd}order and higher terms, Eq. (4.4) becomes

$$\hat{\mathbf{A}}_i \simeq \begin{pmatrix} 0 & \hat{\mathrm{a}}_i^{\dagger} & 0 \\ \hat{\mathrm{a}}_i & 1 & \hat{\mathrm{b}}_i \\ 0 & \hat{\mathrm{b}}_i^{\dagger} & 0 \end{pmatrix}\;. \tag{I.35}$$

Once again we can use the Bogoliubov basis [Eq. (4.12)] to find

$$\hat{\mathbf{A}}_{\mathbf{q}} \cong \begin{pmatrix} 0 & \xi_{\mathsf{A}}^{-}(\mathbf{q})\hat{\alpha}_{-\mathbf{q}}^{\dagger} - \xi_{\mathsf{A}}^{+}(\mathbf{q})\hat{\alpha}_{\mathbf{q}} & 0 \\ -\xi_{\mathsf{A}}^{+}(\mathbf{q})\hat{\alpha}_{-\mathbf{q}}^{\dagger} + \xi_{\mathsf{A}}^{-}(\mathbf{q})\hat{\alpha}_{\mathbf{q}} & \sqrt{N}\delta_{\mathbf{q},0} & -\xi_{\mathsf{A}}^{+}(\mathbf{q})\hat{\beta}_{-\mathbf{q}}^{\dagger} + \xi_{\mathsf{A}}^{-}(\mathbf{q})\hat{\beta}_{\mathbf{q}} \\ 0 & \xi_{\mathsf{A}}^{-}(\mathbf{q})\hat{\beta}_{-\mathbf{q}}^{\dagger} - \xi_{\mathsf{A}}^{+}(\mathbf{q})\hat{\beta}_{\mathbf{q}} & 0 \end{pmatrix}\;, \tag{I.36}$$

where N is the number of sites and $\xi_{\mathsf{A}}^{+}(\mathbf{q})$ and $\xi_{\mathsf{A}}^{-}(\mathbf{q})$ are the coherence factors for A–matrices defined as

$$\xi_{\mathsf{A}}^{+}(\mathbf{q}) = \frac{\xi_{\mathsf{S}}(\mathbf{q}) + \xi_{\mathsf{Q}}(\mathbf{q})}{2}\;, \tag{I.37a}$$

$$\xi_{\mathsf{A}}^{-}(\mathbf{q}) = \frac{\xi_{\mathsf{S}}(\mathbf{q}) - \xi_{\mathsf{Q}}(\mathbf{q})}{2}\;, \tag{I.37b}$$

where $\xi_{\mathsf{S}}(\mathbf{q})$ and $\xi_{\mathsf{Q}}(\mathbf{q})$ are defined in Eq. (I.4) and Eq. (I.20) respectively.

Using Eq. (4.42), we can then calculate the structure factor for quadrupole moments

as defined in Eq. (I.34). We obtain

$$S_{\mathrm{A}}^{\mathsf{QM}}(\mathbf{q},\omega) = 2(\xi_{\mathsf{A}}^{+}(\mathbf{q})^2 + \xi_{\mathsf{A}}^{-}(\mathbf{q})^2)\delta(\omega-\epsilon(\mathbf{q})) + S_{\mathrm{A}}^{\mathsf{GS}}(\mathbf{q}=0,\omega) \tag{I.38a}$$

$$= \frac{1}{2}(\xi_{\mathsf{S}}(\mathbf{q})^2 + \xi_{\mathsf{Q}}(\mathbf{q})^2)\delta(\omega-\epsilon(\mathbf{q})) + S_{\mathrm{A}}^{\mathsf{GS}}(\mathbf{q}=0,\omega) \tag{I.38b}$$

$$= 2\frac{A_{\mathbf{q}}}{\sqrt{A_{\mathbf{q}}^2 - B_{\mathbf{q}}^2}}\delta(\omega-\epsilon(\mathbf{q})) + S_{\mathrm{A}}^{\mathsf{GS}}(\mathbf{q}=0,\omega)\ , \tag{I.38c}$$

where we used Eq. (I.37) in the second line and Eq. (I.20), Eq. (I.4) and Eq. (4.13) in the last line. Detailed calculations for $\mathbf{q} = 0$ contributions to the A–matrix structure factor can be found in Appendix I.6. More precisely, $S_{\mathrm{A}}^{\mathsf{GS}}(\mathbf{q}=0,\omega)$ is given by Eq. (I.39), which combined with Eq. (I.38c) gives the total quantum structure factor for the A-matrices expressed in Eq. (4.86).

We also note that written in the form that includes the coherence factors, the sum rule [Eq. (3.96)] for $\mathbf{q} \neq 0$ is easily verified.

I.6 A-matrices: Contribution of the Ground State to the Quantum Structure Factor at $\mathbf{q} = 0$

For the quantum zero temperature structure factor for the A–matrices at $\mathbf{q} = 0$, we make use of the sum rule given in Eq. (3.96). This leads to

$$\begin{aligned} S_{\mathrm{A}}^{\mathsf{GS}}(\mathbf{q}=0) &= \frac{1}{4}S_{\mathrm{Q}}^{\mathsf{GS}}(\mathbf{q}=0) + \frac{1}{2}S_{\mathrm{S}}^{\mathsf{GS}}(\mathbf{q}=0) + \frac{1}{3}N\delta_{\mathbf{q},0} \\ &= N - 2\sum_{\mathbf{k}}\left[\frac{A_{\mathbf{k}}}{\sqrt{A_{\mathbf{k}}^2 - B_{\mathbf{k}}^2}}\right] + \mathcal{O}(\frac{1}{s^2})\ , \end{aligned} \tag{I.39}$$

where we used Eq. (I.16) and Eq. (I.32). Its spectral representation yields

$$S_{\mathrm{A}}^{\mathsf{GS}}(\mathbf{q}=0,\omega) = \left(N - 2\sum_{\mathbf{k}}\left[\frac{A_{\mathbf{k}}}{\sqrt{A_{\mathbf{k}}^2 - B_{\mathbf{k}}^2}}\right]\right)\delta(\omega) + \mathcal{O}(\frac{1}{s^2})\ . \tag{I.40}$$

Combining Eq. (I.38c) with Eq. (I.40) gives the total quantum structure factor for the A-matrices expressed in Eq. (4.86).